

General Disclaimer

One or more of the Following Statements may affect this Document

- This document has been reproduced from the best copy furnished by the organizational source. It is being released in the interest of making available as much information as possible.
- This document may contain data, which exceeds the sheet parameters. It was furnished in this condition by the organizational source and is the best copy available.
- This document may contain tone-on-tone or color graphs, charts and/or pictures, which have been reproduced in black and white.
- This document is paginated as submitted by the original source.
- Portions of this document are not fully legible due to the historical nature of some of the material. However, it is the best reproduction available from the original submission.

(NASA-CR-151948) THE DEVELOPMENT OF
ADVANCED AUTOMATIC FLARE AND DECRAB FOR
POWERED LIFT SHORT HAUL AIRCRAFT USING A
MICROWAVE LANDING SYSTEM (Lear Siegler,
Inc., Los Angeles, Calif.) 278 p HC A13/MF G3/05

N77-23093

A01

Unclas

28864



**Lear Siegler, Inc.
Astronics Division**

NASA CR-151948

THE DEVELOPMENT
OF
ADVANCED AUTOMATIC FLARE AND DECRAB
FOR
POWERED LIFT SHORT HAUL AIRCRAFT
USING A MICROWAVE LANDING SYSTEM

April 1977

By

Geert Gevaert
Ben Feinreich



Prepared Under Contract Number
NAS2-9068

By

LEAR SEIGLER, INC./ASTRONICS DIVISION

For

AMES RESEARCH CENTER
NATIONAL AERONAUTICS AND SPACE ADMINISTRATION

3171 SOUTH BUNDY DRIVE
SANTA MONICA, CA. 90406
AREA CODE 213 391-7211

NASA CR-151948

**THE DEVELOPMENT OF
ADVANCED AUTOMATIC FLARE AND DECRAB
FOR POWERED LIFT SHORT HAUL AIRCRAFT
USING A MICROWAVE LANDING SYSTEM**

April 1977

By

**Geert Gevaert
Ben Feinreich**

Distribution of this report is provided in the interest of
information exchange. Responsibility for the contents
resides in the author or organization that prepared it.

**Prepared under Contract No. NAS2-9068 by
LEAR SIEGLER INC., ASTRONICS DIVISION,
Santa Monica, California 90406**

For

**AMES RESEARCH CENTER
NATIONAL AERONAUTICS AND SPACE ADMINISTRATION**

FORWARD

This report presents the results of studies conducted by the Astronics Division of Lear Siegler, Inc. (LSi) at Santa Monica, California, for the NASA Ames Research Center, Moffett Field, California, under contract number NAS2-9068. The NASA technical monitor was D. Watson, FSN Branch. LSi technical guidance was provided by L. Lykken, Analysis and Software Section Head.

We wish to acknowledge the fruitful discussions and helpful suggestions provided by Gordon Hardy, Don Smith and Del Watson of NASA ARC and Bill Hindson of NAE. The analytical design and simulation effort which provided the basis of the lateral portion of this report was capably performed by Jim Shannon.

ABSTRACT

Advanced automatic flare and decrab control laws have been developed for future powered lift STOL aircraft and are described in this report. The NASA C-8A Augmentor Wing Vehicle was used as the aircraft model and the automatic landing control laws are being implemented and flight tested on that aircraft. The control laws provide excellent longitudinal and lateral axes landing performance and safety which is compatible with the FAA Category IIIA CTOL certification requirements. The system is also designed for use with Microwave Landing System equipment.

The recommended system was selected from a number of candidate systems that were investigated during this study. The longitudinal control laws utilize the throttle for flight path control and use the direct lift augmentor flap chokes for flight path augmentation. The elevator is used to control airspeed during the approach phase and to enhance path control during the flare. The forward slip maneuver was selected over the flat decrab technique for runway alignment because it can effectively handle the large crab angles obtained at STOL approach speeds.

Performance evaluation of selected system configurations has been obtained over the total landing environment, and limitations have been defined. Critical failure modes have been evaluated. Pilot display concepts are defined, and in-flight experiments are proposed.

TABLE OF CONTENTS

	<u>Page</u>
1.0 INTRODUCTION	1-1
1.1 Objectives	1-1
1.2 Ground Rules	1-2
1.3 Tasks	1-3
2.0 SUMMARY OF RESULTS AND RECOMMENDATIONS	2-1
2.1 Summary of Results	2-1
2.2 Recommendations	2-3
3.0 THE RECOMMENDED SYSTEM	3-1
3.1 Pitch Landing System	3-1
3.2 Lateral Landing System	3-4
4.0 PERFORMANCE EVALUATION	4-1
4.1 Pitch Performance Requirements	4-1
4.2 Lateral Performance Requirements	4-3
4.3 Evaluation Techniques	4-3
5.0 GLIDESLOPE TRACK AND FLARE	5-1
5.1 Candidate Control Algorithms	5-1
5.2 Tradeoff Criteria	5-2
5.3 System Optimization	5-3
5.4 Performance	5-16
5.5 Off-Nominal Conditions	5-29
5.6 Failure Effects	5-35
5.7 Limitations	5-38
5.8 Display Concepts	5-41

	<u>Page</u>
6.0 LOCALIZER TRACK AND RUNWAY ALIGNMENT	6-1
6.1 Candidate Control Algorithms	6-1
6.2 Tradeoff Criteria	6-9
6.3 System Optimization	6-10
6.4 Performance	6-25
6.5 Off-Nominal Conditions	6-34
6.6 Failure Effects	6-39
6.7 Limitations	6-41
6.8 Display Concepts	6-41
7.0 SENSOR TRADEOFFS	7-1
7.1 Longitudinal Axis	7-1
7.2 Lateral Axis	7-4
8.0 RECOMMENDED EXPERIMENTS	8-1
8.1 NASA Simulator Tests	8-2
8.2 Flight Tests	8-3
APPENDIX A SIMULATION DEFINITION	A-1
A-1 Airframe Dynamics	A-1
A-2 Control System Dynamics	A-2
A-3 Geometry and Sensors	A-13
A-4 MLS Disturbance Models	A-19
A-5 Atmospheric Disturbance Models	A-19
APPENDIX B GLIDESLOPE TRACK AND FLARE RESULTS	B-1
APPENDIX C LOCALIZER TRACK AND ALIGN RESULTS	C-1
APPENDIX D ADVANCED VS. CONVENTIONAL CONTROL LAW COMPARISON	D-1
D-1 Longitudinal landing system	D-1
D-2 Lateral Landing System	D-5

LIST OF FIGURES

<u>Figure</u>	<u>Title</u>	<u>Page</u>
3-1	Pitch Landing System - Control Laws	3-2
3-2	Pitch Landing System Filters	3-3
3-3	Lateral Landing System - Roll Block Diagram	3-6
3-4	Lateral Landing System - Yaw Block Diagram	3-7
4-1	STOL Runway Geometry	4-1
5-1	Pitch Control Strategies	5-1
5-2	Effect of Crossfeed and Reduced Speed Gain	5-4
5-3	Throttle to Elevator Crossfeed vs. Reduced K_u	5-5
5-4	Pitch Flare Initiation Altitude Variation	5-8
5-5	Flare Command Profile	5-8
5-6	Effect of Sink Rate Command	5-10
5-7	Effect of Flare Altitude	5-10
5-8	Segmented Flare Profile	5-12
5-9	Pitch Step Responses with Gain Variation	5-14
5-10	Effect of Throttle Gain Variation	5-15
5-11	Landing Time History: No Wind	5-17
5-12A	Landing Time Histories: Wind Shears	5-18
5-12B	Landing Time Histories: Wind Shears	5-19
5-13	Sink Rate vs. Altitude Profiles	5-20
5-14	Touchdown Sink Rate Distribution	5-24
5-15	Touchdown Range Distribution	5-25
5-16	Touchdown Pitch Attitude Distribution	5-26
5-17	Distribution of Beam Deviations at Approach Window	5-27

<u>Figure</u>	<u>Title</u>	<u>Page</u>
5-18	Effect of Wind Shear Spikes	5-28
5-19	Effect of Glide Slope Angle Variations	5-30
5-20	Effect of Aircraft Weight Variation	5-31
5-21	Terrain Step Geometry	5-31
5-22	Effect of Terrain Steps	5-32
5-23	Effect of Ground Effect Variations	5-33
5-24	Effect of Throttle Hysteresis	5-34
5-25	Effect of Throttle Dynamics	5-34
5-26	Effect of Limited Beam Hardovers	5-36
5-27	Wind Shear Profile	5-39
5-28	Limiting Wind Levels	5-39
5-29	Effect of RPM Retardation Limit	5-40
6-1	Flat Decrab Simplified Block Diagram	6-2
6-2	Forward Slip Simplified Block Diagram	6-3
6-3	Align Entry Candidate Systems	6-5
6-4	Rudder Bias Generation Tradeoff	6-6
6-5	Wing Down Compensation Candidates	6-7
6-6	Lateral Position, Rate, and Acceleration Candidates	6-8
6-7	Flat Decrab and Forward Slip Stochastic Performance Summary	6-11
6-8	Touchdown Attitude Distribution for Flat Decrab and Forward Slip	6-13
6-9	Flat Decrab (#A) Response in Deterministic Winds	6-14
6-10	Rate Limited Forward Slip (#B) Response in Deterministic Winds	6-15
6-11	Effect of Align Entry Techniques	6-17

<u>Figure</u>	<u>Title</u>	<u>Page</u>
6-12	Model Referenced Forward Slip (#E) Response in Deterministic Disturbances	6-18
6-13	Effect of Rudder Bias and Lateral Acceleration Usage on Landing Performance	6-20
6-14	Effect of Rate Signal Variations on Landing Performance	6-21
6-15	Touchdown Lateral Distance Distribution	6-28
6-16	Touchdown Lateral Rate Distribution	6-29
6-17	Touchdown Heading Error Distribution	6-30
6-18	Touchdown Bank Angle Distribution	6-31
6-19	Lateral Window Deviation Distribution	6-32
6-20	ΔY_{TD} (ft) Due to Deterministic Variations	6-35
6-21	Effect of Deterministic Variations on \dot{Y} , ψ , and ϕ_{TD}	6-36
6-22	ΔY Window (ft) Due to Deterministic Variations	6-37
6-23	Effect of Approach Speed Variation On (#E) Landing Performance	6-39
7-1	Airspeed Complementary Filter	7-1
7-2	Altitude Rate Filter	7-2
7-3	Beam Deviation Filter	7-3
7-4	Acceleration Augmented Complementary Filter	7-5
7-5	Unaugmented Lateral Filter	7-5
7-6	Accelerometer Derived Rate	7-6
7-7	Heading Augmented Lateral Filter	7-6
7-8	Acceleration Derivation	7-7
7-9	Crosswind Estimation	7-8

LIST OF TABLES

<u>Table</u>	<u>Title</u>	<u>Page</u>
2-I	Landing Performance Overview	2-2
4-I	Performance Requirements	4-2
5-I	Pitch Performance Summary	5-21
5-II	Pitch Deterministic Disturbances	5-22
5-III	Pitch Activity Summary	5-23
5-IV	Pitch Attitude Hardover Effects Summary	5-37
5-V	Pitch Sensor Failure Detectability	5-42
6-I	Lateral Performance Summary	6-27
6-II	Lateral Deterministic Disturbance Effects	6-33
6-III	Lateral RMS Activity Summary	6-34
6-IV	Lateral Failure Response Summary	6-40

SYMBOLS

a_x	Longitudinal acceleration
a_y	Lateral acceleration
a_z	Normal acceleration
b	Wing span
C	Aerodynamic nondimensional coefficient
\bar{c}	Mean aerodynamic chord
e	Naperian base
g	Acceleration due to gravity
h	Altitude
h_G	Landing gear height above the runway
h_{CG}	Aircraft center of gravity height above the runway
Δh	Altitude deviation from glide slope beam
I_x	Roll moment of inertia
I_y	Pitch moment of inertia
I_z	Yaw moment of inertia
I_{xz}	Product of inertia
K	Gain; constant
L	Sum of aerodynamic and thrust roll moments divided by roll moment of inertia
L_λ	$\partial L / \partial \lambda$ where $\lambda = v, \beta, p, r,$ or δ

M	Sum of aerodynamic and thrust pitch moments divided by pitch moment of inertia
M_λ	$\partial M / \partial \lambda$ where $\lambda = u, w, \alpha, q, \text{ or } \delta$
N	Sum of aerodynamic and thrust yaw moments divided by yaw moment of inertia
N_λ	$\partial N / \partial \lambda$ where $\lambda = v, \beta, p, r, \text{ or } \delta$
P	Probability
p	Roll rate
q	Pitch rate
R	Range measured from GPIIP
r	Yaw rate
S	Wing reference area
s	Laplace operator
TD	Time delay
t	Time
U_0	Nominal approach airspeed
U_A	Aerodynamic velocity
U_I	Inertial velocity
U_{WIND}	Downtrack wind velocity
u	Velocity perturbation along x-axis
V_{WIND}	Crosstrack wind velocity

W	Aircraft weight
W_{WIND}	Vertical wind velocity
w	Velocity perturbation along z-axis
$WINDV$	Total wind speed
X_{TD}	Touchdown distance measured from GPIP
X	Sum of aerodynamic and thrust forces along x-axis divided by vehicle mass
X_{λ}	$\partial X / \partial \lambda$ where $\lambda = u, w, \alpha, \text{ or } \delta$
$Y, \Delta Y$	Lateral deviation from extended runway centerline
Y	Sum of aerodynamic and thrust forces along y-axis divided by vehicle mass
Y_{λ}	$\partial Y / \partial \lambda$ where $\lambda = \beta, v, p, r, \text{ or } \delta$
Z	Sum of aerodynamic and thrust forces along z-axis divided by vehicle mass
Z_{λ}	$\partial Z / \partial \lambda$ where $\lambda = u, w, \alpha, \text{ or } \delta$
α	Angle of attack
β	Sideslip angle
γ	Flight path angle
Δ	Deviation
δ	Control deflection; specialized by subscripts
δ_T	Throttle
δ_{CH}	Choke
δ_e	Elevator
δ_n	Nozzle
δ_w	Wheel

δ_a	Aileron
δ_{sp}	Spoiler
δ_R	Rudder
ζ	Damping ratio
θ	Pitch attitude
μ	Mean
σ	Standard deviation; RMS value of stochastic disturbances
σ_u	Downtrack turbulence level
σ_v	Crosstrack turbulence level
σ_w	Vertical turbulence level
σ_p	Equivalent roll rate turbulence level
σ_r	Equivalent yaw rate turbulence level
σ_{EL}	Elevation noise level
σ_{AZ}	Azimuth noise level
σ_{BN}	Beam noise level
τ	Time constant
ϕ	Roll attitude
ψ	Heading
ω	Frequency

SUBSCRIPTS

A	Aerodynamic
B	Body axes
BL	Blended
C	Command (appears mostly as superscript)
CG	Center of gravity

DR	Dutch roll
err	Error
F, f	Filter output
FL	Flare
G	Landing gear
GE	Ground effect
I	Integrator
I	Inertial
m	Metric
o	Initial (trim) value
P	Predict
ph	Phugoid
R	Roll mode; Runway axes
RA	Radar Altimeter
s	Spiral mode
sp	Short period mode
TD	Touchdown
WINDOW 100	Value at the 30.5m (100 ft.) approach window

ACRONYMS AND ABBREVIATIONS

AC	Advisory Circular
ALN	Align
AMST	Advanced Medium STOL Transport
Aug	Augmentor
Az	Azimuth

CF	Crossfeed
CMD	Command
CTOL	Conventional Takeoff and Landing
DCB	Decrab
DME	Distance Measuring Equipment
EADI	Electronic Attitude and Director Indicator
FSCG	Longitudinal Center of Gravity Fuselage Station
GPIP	Glide Path Intercept Point
GS	Glide Slope
HSI	Horizontal Situation Indicator
HUD	Heads Up Display
HW	Headwind
HWS	Headwind and Shear
HYST	Hysteresis
ITP	Intended Touchdown Point
LOC	Localizer
MFD	Multi-function Display
MLS	Microwave Landing System
QSRA	Quiet STOL Research Aircraft
RMS	Root Mean Square
RSS	Root Sum Square
SGN	Sign
SHR	Shear
SOW	Statement of Work
STOL	Short Takeoff and Landing

STOLAND	The automatic landing system that is currently implemented on the Aug. Wing Vehicle
TRK	Track
TW	Tailwind
TWS	Tailwind and Shear
WLCG	Vertical Center of Gravity Water Line
WO	Washout
WR	Window requirements: deviation allowed at the approach window
XF	Crossfeed
Y/D	Yaw Damper

REFERENCES

- 7-1 "Microwave Landing System Study - Landing Performance Effects of MLS Multipath Disturbances", LSi SA-74.087, 27 November, 1974.
- 7-2 "Microwave Landing System Study - Flare Control", LSi ADR-769, 16 August, 1972.
- A-1 W.B. Cleveland, R.F. Vomaske, and S.R.M. Sinclair, "Augmentor Wing Jet STOL Research Aircraft Simulation Model", NASA TMX 62149, April, 1972.
- A-2 R.K. Heffley, R.L. Stapleford, R.C. Rumold and J.M. Lehman, "A STOL Airworthiness Investigation Using a Simulation of an Augmentor Wing Transport", NASA TMX 62396, October, 1974.
- A-3 F. Newman and D.N. Warner, Jr., "A STOL Terminal Area Navigation System", NASA TMX 62348, May, 1974
- A-4 "Automatic Landing Systems", FAA AC20-57A, 12 January, 1971.
- A-5 G.Gevaert, L. Lykken, N. Shah, "A Simulation Program for Category III Autoland Certification", 1972 Summer Computer Simulation Conference Paper, San Diego, CA.
- A-6 N. Shah, G. Gevaert, L. Lykken, "The Effect of Aircraft Environment on Category III Autoland Performance and Safety," AIAA Paper No. 72-811, August, 1972.
- A-7 "Microwave Landing System Study - Area Navigation Impact on Autopilots", LSi ADR-765, 4 March, 1974.

1.0 INTRODUCTION

The Astronics Division of Lear Siegler, Inc. (LSI) performed this study to develop advanced automatic flare and decrab systems for powered lift short haul aircraft under contract to NASA Ames Research Center as part of the STOL Operating System Experiments. The study results are documented in this report.

The study objectives, ground rules, and tasks are outlined in this introductory section, with the pertinent simulation data summarized in Appendix A. A summary of the results and a description of the recommended advanced flare and decrab systems are provided in Sections 2.0 and 3.0. The performance evaluation methods, sensor tradeoffs, and recommended in-flight experiments are presented as Section 4, 7 and 8. The rest of the results are split by axis, with longitudinal results discussed in Section 5 with backup data in Appendix B, and the lateral results in Section 6 supported by the data in Appendix C.

1.1 Objectives

The basic purpose of this study was to define advanced concepts for automatic flare and decrab guidance and control for a multiple controller powered lift STOL vehicle. Key areas addressed by this study were:

1. Best means to utilize the multiple controllers (throttle, elevator, chokes, spoilers, nozzles, rudder, ailerons) available on a powered lift STOL aircraft to optimize landing performance.
2. Provision of effective path control despite throttle system limitations.
3. Design of the runway alignment maneuver to effectively handle the large crab angles associated with STOL Aircraft operation.
4. MLS signal usage, including Elevation 2 considerations.
5. Tradeoff of sensor usage versus performance to define a minimum equipment complement for Cat. IIIA operation.
6. Performance evaluation over the total landing environment for the best candidate systems.

7. Definition of landing system limitations.
8. Recommended in-flight experiments to validate these concepts.

1.2 Ground Rules

The following ground rules were applied to this study.

1. The airframe to be selected has to be representative of the next generation of powered-lift short haul aircraft concepts. Originally, aircraft as the USAF AMST or NASA QSRA or a composite vehicle having the basic features of those aircraft were among the candidates. The Aug. Wing Vehicle was selected since it is representative of powered-lift short haul STOL aircraft and it is immediately available for testing.
2. The MODILS system installed at Crows Landing was used as the MLS model in these studies. However, the use of the Elevation 2 flare scanner was also considered.
3. In the glide slope and localizer track phase, the aircraft is assumed stabilized in the STOL configuration on the beam. Nominal glide slope angle of 7.50 and approach speed of 65 kts. have been used, but the performance impact of deviations from this nominal approach case were considered. Landing is on a 30.5 x 610 m (100 x 2,000 ft.) runway as defined in Section 4.
4. Performance evaluation of the proposed system is to be made for various levels of gust disturbances, wind shear, instrumentation errors and noise. Analytical methods as well as unpiloted simulation are to be used in the evaluation (evaluation techniques are discussed in Section 4).
5. Gust disturbances, wind shears, instrumentation errors per FAA requirements were considered (see description in Appendix A).
6. The proposed control laws have to be compatible with existing Aug. Wing flight control hardware and software so that no major modifications are required for their implementation. Safety features have to be included, taking into account the non-redundant structure of the existing experimental system.
7. The flare and decrab trajectory followed by the automated system should be close to that which would be flown by the vehicle when under piloted control.

1.3 Tasks

In this study, the following tasks were specifically addressed.

1. STOL automatic landing state-of-the-art review: Applicable FAA, NASA and MLS documents were reviewed, especially in the areas of landing safety and performance, and design criteria, ground rules, and requirements applicable to this study were extracted. Also, reports and literature regarding STOL landing studies and experiments have been reviewed.
2. Vehicle selection and preparation of a data package: The Aug. Wing Vehicle was selected, as mentioned previously. Data regarding air-frame dynamics, sensors, controls, avionics system and limitations were assembled into a comprehensive data book. A summary is provided in Appendix A.
3. Selection of candidate control laws: Candidate control laws were selected based on LSi's landing system design experience with CTOL and unconventional (space shuttle) aircraft, and taking into account characteristics that are peculiar to STOL:
 - a. Available controls.
 - b. Path controller dynamic limitations.
 - c. Poor handling qualities.
 - d. High sensitivity to wind disturbances.
 - e. High rate of descent.
 - f. High touchdown accuracy requirement.
4. Trade-offs leading to the definition of a recommended system: Trade studies have been conducted to select the best system candidate giving consideration to the design ground rules and requirements, complexity and ease of implementation. A key factor in these tradeoff studies was the use of high speed repetitive operation hybrid computer simulations to obtain statistical landing performance data for many control system/disturbance condition combinations.
5. Performance evaluation and definition of limitations: Performance data on selected system configurations was obtained over the total landing environment including winds, shears, turbulence, sensor errors and noise, and off-nominal conditions such as approach speed, glide slope angle and weight variations. Landing system limitations were defined, including wind disturbance magnitudes, sensor errors, control dynamics and authority. Landing performance requirements are met as long as those limitations are not exceeded.

6. Critical failure mode evaluation: Failures were simulated and their impact on vehicle motion and landing performance was assessed.
7. Pilot display concept definition: The display required for the management of the proposed automatic landing system and flight trajectory parameters was conceptually defined.
8. Proposition of experiments: Experiments to evaluate the advanced automatic landing system in flight are proposed.
9. Documentation of results: Study results were documented in monthly progress reports and in this final report.

2.0 SUMMARY OF RESULTS AND RECOMMENDATIONS

2.1 Summary of Results

The recommended advanced landing system for a powered lift STOL aircraft is defined in Section 3 of this report. This system provides excellent longitudinal and lateral landing performance compatible with FAA Cat. IIIA landing requirements. A summary of the SOW defined design goals and actual landing performance is given in Table 2-1. This indicates that all performance requirements are satisfied, even in the limiting stochastic disturbance case, with moderate control activity similar to typical CTOL aircraft during automatic landing.

The recommended system is the best tradeoff among the many candidate configurations investigated during this study. The control law algorithms can be readily implemented in the existing Aug. Wing digital autopilot.

The recommended longitudinal system is a three control configuration in which the direct lift chokes are used to augment throttle response for flight path control, thus minimizing the impact of throttle nonlinearities on landing performance. The $\pm 0.1g$ direct lift authority is adequate to handle limiting stochastic disturbance levels. Elevator is used to maintain airspeed control in the approach and to enhance path control in the flare.

The forward slip alignment used in the recommended lateral landing system effectively handles the large crab angles obtained at STOL approach speeds. A 23 knot crosswind limit can be tolerated, which is significantly higher than the FAA recommended 15 knot wind limit. A major benefit of the forward slip align technique is the insensitivity to maneuver timing variations caused by the large changes in inertial speed which are possible in varying longitudinal wind conditions. A model referenced align entry is used, with crab angle reduction commanded as a function of altitude. This alignment initiation technique is used to provide maximum adaptability to varying lateral and longitudinal winds, eliminate rapid control motions, and minimize undesirable heading or roll attitude overshoots near the ground.

Varying wind conditions are the major contributor to longitudinal landing dispersion, while MLS disturbances and deterministic variations are secondary. The $\pm 0.17^\circ$ one sigma azimuth bias which is associated with the

TABLE 2-I LANDING PERFORMANCE OVERVIEW

<u>Parameter</u>	<u>2σ Requirement</u>	<u>Actual</u>
\dot{h}_{TD} m/sec (fps)	< 1.83 (6.0)	1.49 (4.9)
X_{TD} m (ft)	$\pm 60.96 (\pm 200)$	+48.77 (+160) -30.48 (-100)
Δh_{window} m (ft)	$\pm 3.66 (\pm 12)$	$\pm 1.16 (\pm 3.8)$
θ_{TD} deg	---	± 1.4
Y_{TD} m(ft)	$\pm 4.57 (\pm 15)$	$\pm 2.68 (\pm 8.8)$
ΔY_{window} m (ft)	$\pm 7.62 (\pm 25)$	$\pm 2.21 (\pm 7.25)$
$\Delta \psi_{TD}$ deg	---	± 2.1
ϕ_{TD} deg	---	± 1.8
<u>RMS Activity</u>		
δT (%)		.8
δCH (%)		12.0
δe ($^{\circ}$)		1.2
δw ($^{\circ}$)		3.4
δR ($^{\circ}$)		2.0

- Notes: 1. All data is given for limiting stochastic wind and beam disturbance levels.
2. Requirements are those defined in the SOW.

MODILS system induces as much lateral touchdown position dispersion as limiting wind levels. The 0.06° bias typically associated with MLS systems would relegate azimuth bias to a secondary contributor to dispersions.

A two control pitch landing system was also defined. This configuration employs the elevator to augment path response rather than direct lift chokes. Although acceptable performance can be realized, there is a strong dependence on throttle nonlinearities and increased control and aircraft activity.

An alternate lateral landing system was also defined for usage in a vehicle without a cross track acceleration signal. This system uses roll attitude and rudder position to derive a pseudo acceleration for filter augmentation and wing down compensation. Landing dispersions and control activities are slightly worse than with the recommended system. Additionally, some dependence on flight condition results from the fact that flight condition dependent aircraft dynamics parameters are used as constants in the computation of the pseudo acceleration. Nevertheless, adequate landing performance is provided by this configuration.

A performance comparison between the recommended advanced control system and the conventional landing system that is currently implemented on the Aug. Wing vehicle is provided in Appendix D. The results show that the performance improvement is dramatic. This comparison illustrates the superiority of an integrated closed loop glide slope and flare system over one which makes extensive use of open loop predictor commands. The lateral performance improvement shows the superiority of the forward slip alignment over a flat decrab system which is much more sensitive to the large variations in maneuver timing associated with STOL aircraft operation.

2.2 Recommendations

The recommended longitudinal and lateral landing system algorithms, which are presented in Section 3, are being incorporated in the Aug. Wing Vehicle autopilot software and verified on NASA's simulator, and they will be tested in flight. We believe that this system will provide excellent automatic landings on a routine basis.

Several other areas are recommended for further investigation:

1. The use of nozzles for direct drag control promises much better performance, especially for speed control and touchdown range dispersion minimization.
2. Optimization of navigation filters could yield significant performance improvement.
3. The use of elevation 2 MLS information would allow a more innovative solution to the flare problem.

4. For this multiple control vehicle, a decoupled approach may be beneficial both from an automatic landing viewpoint and for normal flight using flight director guidance.
5. The impact of MLS noise and bias characteristics should be investigated further, particularly as they affect lateral guidance and the possible use as a radar altimeter replacement.
6. In this study, the system was designed for Cat. IIIA operation - an effective rollout guidance system should be designed to provide zero visibility capability.
7. Studies should also be performed to define STOL landing requirements analogous to those spelled out in FAA AC 20-57A and 120-28 and 29 for CTOL aircraft automatic landing system certification.

3.0 THE RECOMMENDED SYSTEM

The recommended advanced longitudinal and lateral automatic landing system for the Aug. Wing STOL aircraft is defined in this section. This system provides landing performance compatible with Cat. IIIA landing requirements. A detailed system description follows.

3.1 Pitch Landing System

The choke augmented recommended configuration utilizes elevator for pitch and airspeed control and throttles, augmented by the direct lift augmentor flap chokes, for flight path control. The block diagram of the system is shown as Figures 3-1 and 3-2. A two control variant, in which elevator and throttle only are used, is presented and discussed in Appendix B.

This recommended landing system requires only a minimum sensor complement consisting of glide slope deviation (Δh), radar altitude (h_{RA}), airspeed (U_A), pitch gyro which provides both attitude (θ) and derived rate ($\dot{\theta}$), and runway axis vertical and longitudinal accelerations (\ddot{h}_R , \ddot{x}_R) obtained from a three axis accelerometer. An airspeed complementary filter is used in generating the feedback airspeed signal (U_A) by blending raw airspeed with longitudinal acceleration, as shown in Figure 3-2. An altitude rate filter blends radar altimeter derived sink rate (\dot{h}_{RA}) with washed out vertical acceleration to generate a blended sink rate signal, \dot{h}_{BL} . Smoothed altitude deviation (Δh_f) is obtained from the rate and position limited first order filter shown. (Sensor tradeoffs are discussed in Section 7).

In the glide slope track phase, a beam proportional signal is fed to the throttle and chokes and beam integral fed to the throttle only, with damping provided by vertical acceleration and rate derived by integration of washed out vertical acceleration. Radar altimeter derived sink rate is not used prior to the flare, as it is added and subtracted downstream and upstream of the flare gain scheduler which has unity gain above flare altitude. This is done to avoid the noise induced in the radar altimeter derived sink rate by terrain irregularities. Pitch rate and pitch attitude feedbacks to elevator constitute a pitch inner loop into which airspeed error commands are channeled.

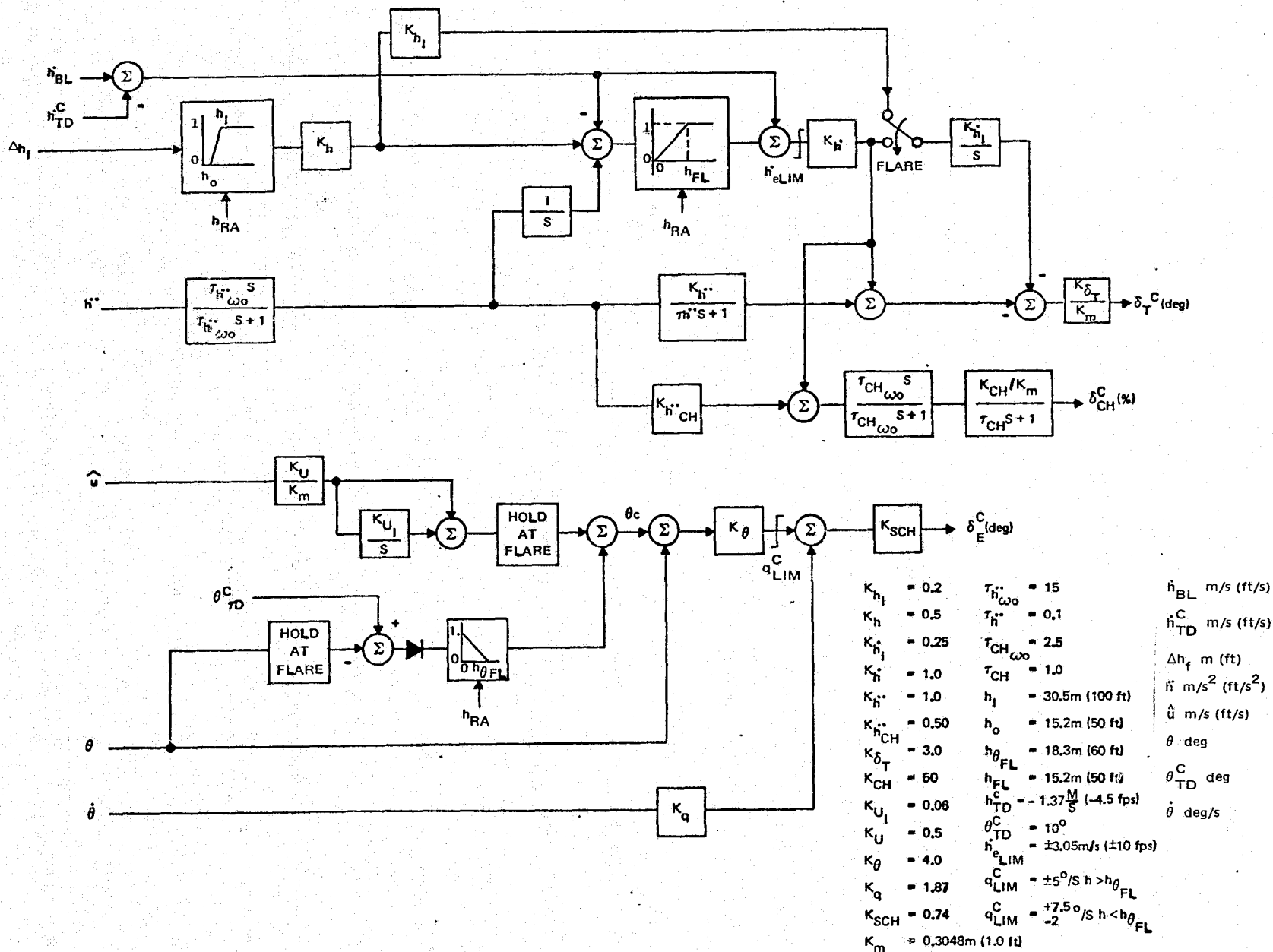


Figure 3-1. Pitch Landing System - Control Laws

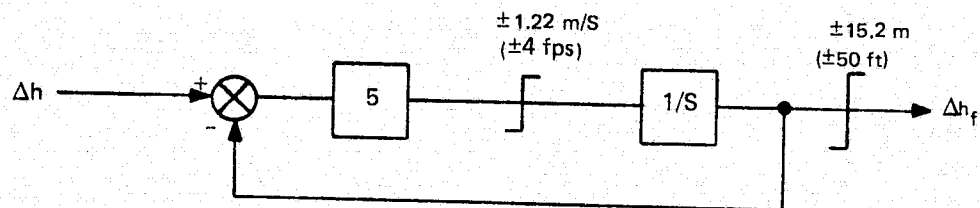
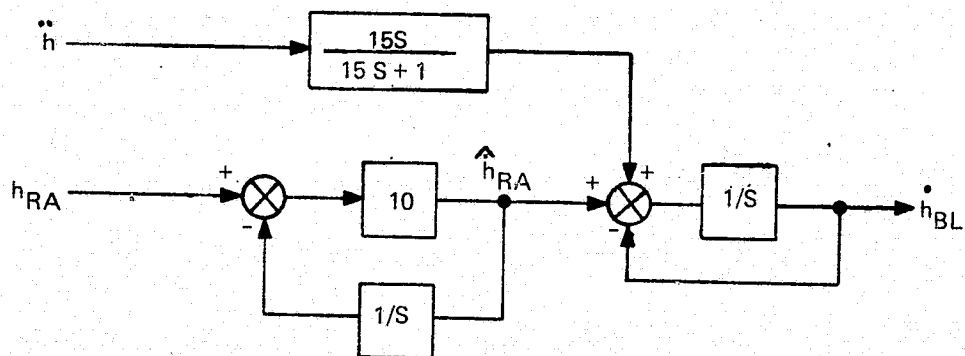
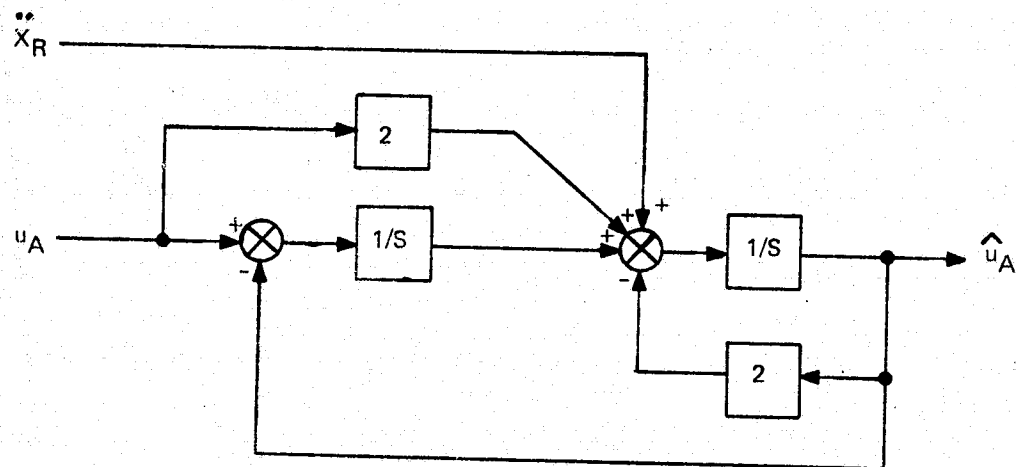


Figure 3-2. Pitch Landing System Filters

Throttles, chokes and elevators are used for flare. As beam deviation is phased out between 30.5m (100 ft.) and 15.2m (50 ft.) altitude, the aircraft attempts to maintain its mean descent rate. At 18.3m (60 ft.), the airspeed signal to elevator is frozen and a pitch up command is introduced, increasing linearly with decreasing altitude, attaining ten degrees attitude command at zero altitude. At 15.2m (50 ft.), the flare scheduler starts decreasing gain, phasing out the acceleration derived sink rate and phasing in the radar altimeter derived blended sink rate. This produces a sink rate command that decreases linearly with altitude, from the prevailing pre-flare value to the final touchdown sink rate command of 1.37 m/s (4.5 fps). This exponential flare law has a time constant inversely proportional to the pre-flare sink rate, thus minimizing touchdown range dispersions due to changes in ground speed caused by winds and approach speed variations.

The throttle integrator input is switched from beam deviation to sink rate error at 15.2m (50 ft.). Thus vertical acceleration and the proportional and integral of sink rate error move the throttle to control the flare. A different blend of vertical acceleration and sink rate error is channeled to the chokes to augment flight path control and minimize limit cycling tendencies due to throttle system nonlinearities. The choke command is passed through a 2.5 second washout in order to eliminate thrust trim changes, maintaining full choke authority for corrections at frequencies that are too high to be effectively handled by the throttle. The choke command is also passed through a one second low pass filter to reduce high frequency noise.

Four limiters are incorporated in the system in order to moderate the impact of sensor hardovers and large stochastic variations. The vertical acceleration signal is washed out to eliminate sensor bias effects. Excellent beam track and flare performance are obtained with the recommended system as shown in subsection 5.4.

3.2 Lateral Landing System

The sensitivity to external disturbances and large crab angles typical of STOL aircraft places severe demands on the design of the automatic landing system. The accurate control of aircraft position and heading required just prior to touchdown makes the runway alignment the most critical phase of the lateral landing control problem. The recommended automatic landing system defined in Figures 3-3 and 3-4 utilizes a forward slip runway alignment technique to provide precise control of aircraft state through touchdown. The major advantages provided over a typical flat decrab system are:

1. Early alignment initiation with no abrupt transients or commands, thus facilitating pilot monitoring and instilling confidence in system performance.
2. Performance is insensitive to the large longitudinal wind induced timing variations typical of STOL approach flight.

3. Closed loop lateral position control through touchdown is largely responsible for the noted lateral dispersion immunity to timing variations.
4. The model reference align trajectory provides minimal overshoot of runway heading or the steady bank angle required for wing down compensation, improving pilot acceptability and passenger comfort.
5. The fully closed loop control without predict inputs provides landing performance which is relatively insensitive to aircraft and disturbance variations.
6. Crosswinds up to 23 knots at 7.62m (25 ft.) are tolerated.

During localizer track, filtered beam error and integral of raw deviation command aircraft banks to maintain the approach track, with a combination of filtered beam rate and lagged, washed out cross track acceleration for path damping. A position correction for MLS antenna location is used. The 30/sec roll rate limited bank command signal with 5° authority is adequate for localizer track and align operation in limiting wind conditions. The normal roll attitude and rate inner loop stabilization is used, with a slow integration to maintain trim. In yaw, the washed out sum of roll command and yaw rate augment the vehicle's yaw damping and provide turn coordination, with some help from the lateral accelerometer.

At the 45.72m (150 ft.) align altitude, the align model reference heading trajectory is switched into the yaw axis. This reference heading command is reduced from the course datum error existing at alignment initiation to two degrees between 45.72 and 15.24m (150 and 50 ft.), yielding an alignment rate which is a function of both initial heading error and aircraft sink rate. The course datum error from the reference trajectory is integrated to maintain the steady rudder required during the alignment. This proportional plus integral command is limited to 12.5° of rudder, which adequately compensates for more than 20 knot steady crosswind and allows sufficient additional rudder motion to maintain yaw damper authority for this basically unstable vehicle. At 15.24m (50 ft.), the yaw integral is switched from model error to raw course datum to smoothly remove the remaining 2° of heading error. For very small crosswinds requiring less than 2° crab angle, the alignment is handled entirely by the raw course datum proportional plus integral paths. In the roll axis, the beam computations are maintained to guide the vehicle along the desired horizontal path, with increased pseudo cross track rate gains for better control. A one second roll washout limited to 5° of bank is inserted along with cross track acceleration to provide wing down compensation. The 5° alignment limit is ample for steady crosswind levels higher than the FAA limiting case, and minimizes the potential for large touchdown bank angles. If the limit is exceeded, the vehicle will maintain a small crab angle.

An alternate configuration described in Section 6 and Appendix C is recommended for general usage where an accurate cross track acceleration signal is not available. Its structure is very similar, with cross track acceleration replaced by a pseudo acceleration derived from roll attitude and rudder position, thus eliminating the need for a lateral accelerometer. Landing performance with this system is only slightly degraded.

Figure 3-3. Lateral Landing System — Roll Block Diagram

Figure 3-4. Lateral Landing System – Yaw Block Diagram

4.0 PERFORMANCE EVALUATION

Performance requirements for this advanced automatic landing system study are defined in this section. Techniques used in the evaluation of expected performance are also described here.

4.1 Pitch Performance Requirements

Longitudinal performance requirements are summarized in Table 4-I.

The assumed STOL port runway geometry is shown in Figure 4-1.

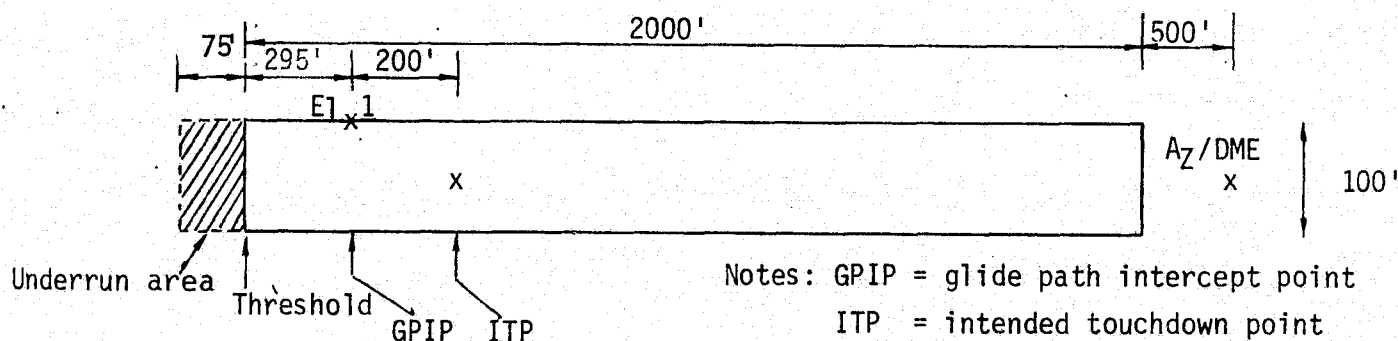


Figure 4-1. STOL Runway Geometry

If the STOL field geometry were scaled for glide path angle from CTOL geometry defined in ICAO Annex 14, then the standard 349m (1145 ft.) threshold length would become 420 ft. for a 7.5° glide path. This seems excessive and a better rationale for defining threshold length may be the threshold crossing height. Assuming that a 9.144m (30 ft.) threshold crossing height is desired, this translates into a 89.916m (295 ft.) threshold length for the Aug. Wing vehicle geometry on a nominal approach. A 60.96m (200 ft.) under-run area assumed for a CTOL runway would yield 22.35m (73.3 ft.) STOL port under-run area. Thus, the land short 10⁻⁶ requirement would become 112.776m (370 ft.) before the GPIP. The land long boundary should be based on required ground roll distance to stop the vehicle after touchdown. Assuming

TABLE 4-I. PERFORMANCE REQUIREMENTS

<u>Parameter</u>	<u>μ</u>	<u>2σ</u>	<u>10^{-6}</u>
Longitudinal:			
$-\dot{h}_{TD}$ m/s (fps)	1.22 (4)	<1.83 (6)	<3.05 (10)
X_{TD} m (ft) beyond GPIIP	61 (200)	± 61 (± 200)	<283.2 (929) >-112.8 (-370)
θ_{TD} deg	5	---	<15 >-1
Δh_{window} m (ft.)	0	± 3.66 (± 12)	---
Lateral:			
Y_{TD} m (ft)	---	<4.57 (15.0)	<9.07 (29.75)
\dot{Y}_{TD} m/s (fps)	---	---	<3.05 (10.0)
$\Delta \psi_{TD}$ deg	---	---	<10.0
ϕ_{TD} deg	---	± 5.6	<20.0
ΔY_{window} m (ft.)	---	± 7.62 (± 25.0)	---

Notes:

1. The specified mean and 2σ requirements are design goals, while the 10^{-6} requirements are based on the safe landing boundaries for the Aug. Wing vehicle.
2. For lateral axis, means should all be zero when evaluated over the total environment.
3. Δh_{window} and ΔY_{window} are vertical and lateral tracking error at the 30.48m (100 ft.) approach window.

a 60 kt. touchdown with 0.2g deceleration capability, the distance required to attain a complete stop is 236.5m (776 ft.), thus defining the maximum touchdown point as 283.2m (929 ft.) beyond the GPIP for a 609.6m (2000 ft.) runway.

4.2 Lateral Performance Requirements

These are summarized in Table 4-I. Most of these requirements were specified by NASA in the SOW or are determined by vehicle constraints. The allowed lateral landing dispersion was specified as $\pm 4.57\text{m}$ (15 ft.) in the SOW. However, the FAA AC20-57A requirement for not landing any closer than five feet to runway edge effectively specifies that for the Aug. Wing vehicle on a 100 foot runway, the probability of exceeding 29.75 feet of lateral deviation at touchdown must be less than 10^{-6} , which is equivalent to a 2 sigma dispersion of 12.1 feet. Applying the above 29.75 ft. constraint to lateral deviation during rollout, the touchdown heading error becomes 10° . This is based on the assumption that lateral rate just after touchdown is approximately equal to $U_0/57.3$ times the touchdown course error, and that a correcting lateral acceleration of 0.2 g's is applied to arrest the lateral velocity. The corresponding 2 sigma value for $\Delta\psi_{TD}$ is 4.16 degrees. The touchdown bank angle requirement is based on aircraft geometry. Wing contact for a typical projected production STOL aircraft occurs at approximately 20.0 degrees of bank. Since wing contact at touchdown must have $<10^{-9}$ occurrence probability, the 2σ dispersion for ϕ_{TD} must be less than 5.6 degrees. For landings in 15 knot limiting winds per AC-20-57A, a nominal TD bank angle at $U_0 = 70$ kt. is 3.20 degrees. For a Gaussian distribution, a 10^{-9} probability corresponds to about 6 sigma, thus allowing $20-3.2 = 16.8$ degrees ϕ_{TD} variation on a 6 sigma basis, or a 2σ dispersion of $\pm 5.6^\circ$.

The touchdown crosstrack velocity limit is normally dependent on touchdown bank angle. For conservatism, we considered a one gear touchdown limit of 3.048 m/s (10 fps) as a 10^{-6} requirement.

4.3 Evaluation Techniques

To obtain a total population estimate of automatic landing system fault free performance, it is normal to determine the effect of all disturbances, acting separately and in combination, on the landing performance indication parameters for the whole spectrum of disturbance levels. Three basic steps are involved:

1. The disturbance models under consideration must be defined and statistically described, including correlation between disturbances. Normally, deterministic variations are independent, but for atmospheric disturbances, a given wind level also specifies the associated shears and gust intensities. Models used are defined in Appendix A.

2. A functional relationship is then established between the exceedance distributions of the performance parameters and the disturbances. This was done using a hybrid simulation, with deterministic variations treated separately and the stochastic atmospheric and beam disturbance effects obtained simultaneously from high speed repetitive operation (10 times real time) with performance parameter exceedances recorded on counters.
3. The overall probability distributions for the performance parameters of interest may then be obtained by convolving the individual effects by a multiple integration of the conditional probability distributions over the disturbance space. In general, this requires an N^{th} order integration for N disturbances. In fact, various simplifications were made for both pitch and lateral performance parameters to reduce computational requirements. For example, in pitch the performance effects of the deterministic disturbances can be considered linearly independent, and thus the combined effect is the root sum square of the individual effects. These effects were combined with the distributions due to limiting level of stochastic disturbances to obtain a conservative estimate of the total population distribution function for the parameters of interest. A complete performance evaluation requires that statistical data be obtained for several levels of stochastic disturbances, both individually and in conjunction with significant deterministic variations. These results are then combined to yield a 2σ landing performance assessment over the total environment for the final system. Our past experience has indicated that a good estimate of 2σ performance variations can be obtained by using only 1 or 2 disturbance levels, and this technique was used to evaluate performance of landing system tradeoff candidates to enable selection of the optimum design.

The landing performance indicators are \dot{h} , x , θ , y , \dot{y} , ϕ , and $\Delta\psi$ at touchdown, with a measure of beam tracking provided by horizontal and vertical deviation from the beam center lines at the 30.5m (100 ft.) window.

5.0 GLIDESLOPE TRACK AND FLARE

5.1 Candidate Control Algorithms

The flight variables to be controlled in the glideslope track and flare phases are flight path, airspeed and pitch attitude. Elevator, throttles, augmentor flap chokes, nozzles and spoilers are controls that are available on the C-8A Augmentor Wing Aircraft for possible control of the longitudinal flight variables. Spoilers were not considered for pitch control. Control strategies that were evaluated in this study are shown in Figure 5-1.

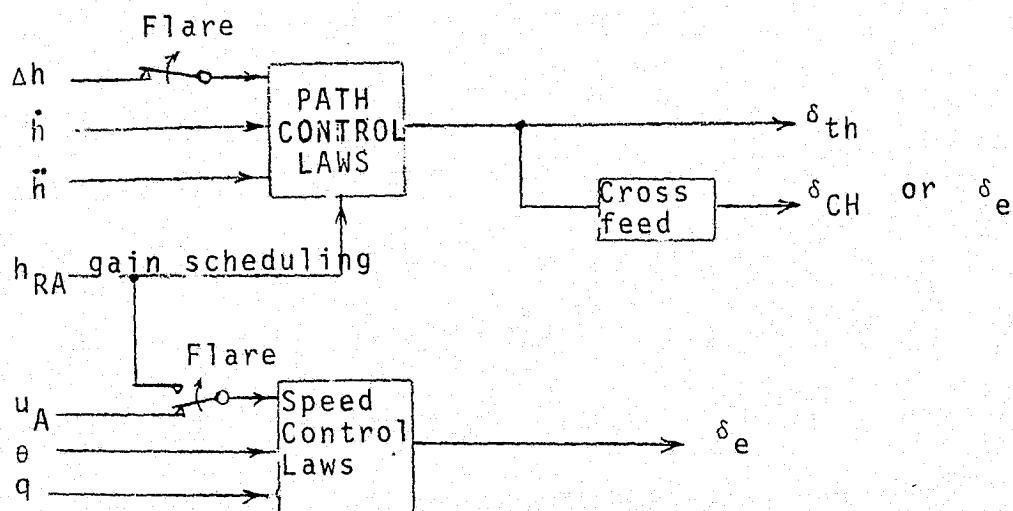


Figure 5-1. Pitch Control Strategies

In a CTOL airplane, throttles and elevator may be used interchangeably to control flight path and airspeed. In a powered lift STOL having an almost vertical thrust vector, throttles would make a very poor speed control. Therefore the throttles were considered for flight path control only, with speed and pitch attitude to be controlled by the elevator.

Control of flight path with throttles only is strongly influenced by the poor dynamic response and nonlinearities such as hysteresis which are typical

of thrust control systems. Two techniques were considered to augment the path response. In the two control scheme a path crossfeed to elevator was studied. Another alternative was to use a direct lift augmentation controller. The chokes that control internal flow through the augmentor flaps were the direct lift element that was evaluated.

The use of nozzles as direct drag control has not been evaluated in this study. This control seems to have a promising potential and it is therefore recommended to include it in a subsequent study.

In addition to the controller strategies discussed, two different flare control algorithm philosophies were considered. In one, essentially open loop throttle and elevator predict commands are inserted at flare to yield the desired flare trajectory for the nominal, no disturbance landing case. Then closed loop control is added to compensate for disturbances and to maintain the aircraft on the desired trajectory. Usually the predict commands are functions of some of the common deterministic disturbances (as approach speed, weight, path angle) to improve performance in those cases. The other philosophy, which is exemplified by the recommended landing system, utilizes closed loop control throughout the flare to compensate for both deterministic and stochastic disturbances. Performance data for both approaches is included in the appendices.

5.2 Tradeoff Criteria

Following is a list of considerations that were taken into account in the tradeoff between the various candidate control configurations:

1. Performance in disturbances, mainly consisting of steady wind and shear, turbulence, and MLS beam noise. The important landing performance indicators are touchdown sink rate, range, and pitch attitude, maneuver margin, and deviation from the beam at the 30.5 m (100 ft) approach window. Each candidate system has to meet the performance requirements defined in Section 4.
2. Excursions in the presence of disturbances of both the controlled variables (deviation from the glideslope beam, sink rate, normal acceleration, airspeed, pitch attitude) and the control activity. When comparing system configurations that meet the performance requirements, a system that yields smaller RMS excursions of controlled variables and control deflections is preferred. In many cases, tighter tracking may be traded for increased control activity.
3. Pilot acceptability and monitoring compatibility. Systems are designed to be compatible with manual control techniques and not to include any unexpected or confusing inputs. Maneuvers that are executed in a manner allowing time for pilot detection of abnormalities are preferred.

4. Ride quality. Configurations that attenuate aircraft acceleration and attitude responses to disturbances are preferred. Also, abrupt or other types of maneuvers which produce excessive accelerations or pitch rates are undesirable.
5. Sensitivity of the system to tolerances, errors and off-nominal conditions.
6. Response to MLS and other sensor failures.
7. Minimum system complexity consistent with the performance requirements.

5.3 System Optimization

The recommended pitch control laws evolved from the tradeoff studies that are described in this subsection. The main subjects that have been treated are:

1. Path Response Augmentation
2. Pitch Flare
3. Path Flare Profile
4. Gain Variations

A discussion of each topic follows.

Path Response Augmentation

The recommended longitudinal landing system is a three control configuration, utilizing throttle with choke augmentation to control flight path, and elevator to control pitch attitude and airspeed. A detailed description was provided in Section 3.

A two control variant, in which the chokes are not employed as an active control, has also been evaluated. In this Elevator Augmented Configuration, the basic assignments of throttle for path control and elevator for speed control were not changed. Both unaugmented throttle and path to elevator crossfeed were evaluated and compared. Crossfeed was implemented such that the airplane would pitch up in response to an increase of sink rate (polarity opposite to that required to decouple speed from path). The crossfeed very significantly reduces the tendency of the airplane to get blown above the beam and to land long, as summarized in Figure 5-2. It also reduces touchdown sink rate dispersion. A reduction in throttle activity is observed with the crossfeed, as indicated in the activity traces of Figure 5-3. The performance improvement is obtained at the cost of a small airspeed tracking degradation

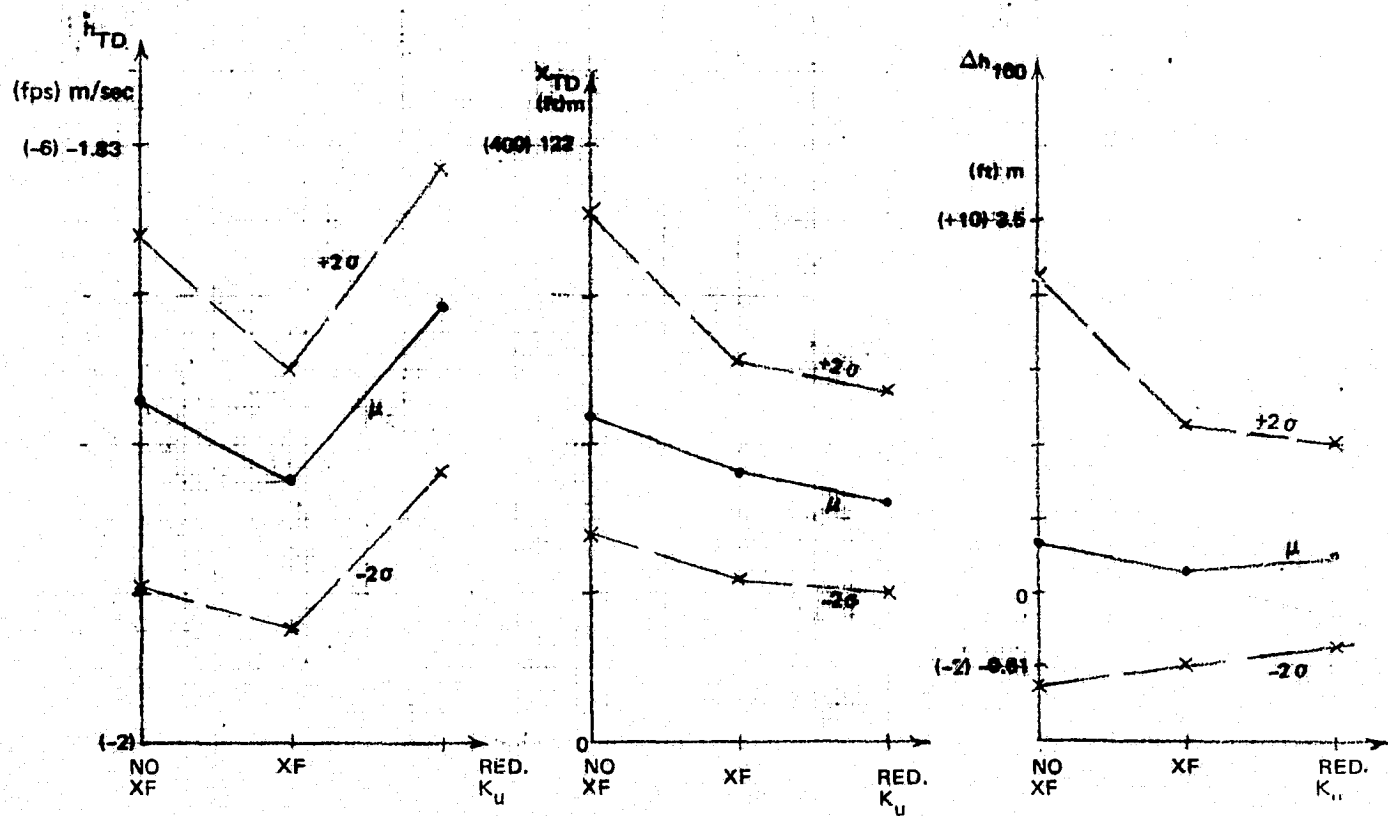


Figure 5-2. Effect of Crossfeed and Reduced Speed Gain

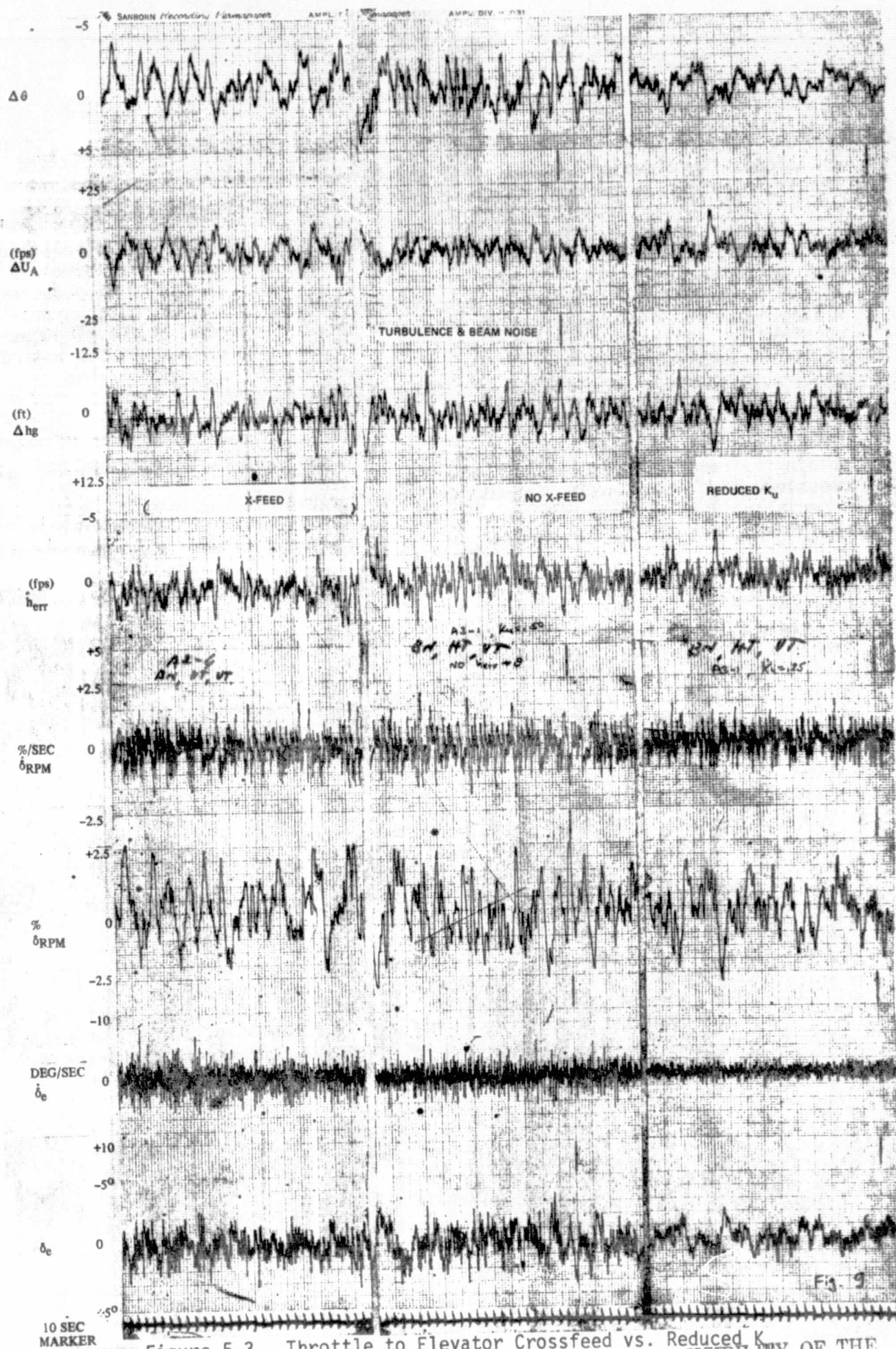


Figure 5-3. Throttle to Elevator Crossfeed vs. Reduced K_u

and an increase in elevator rate activity. This is plausible as without the crossfeed, the elevator controls only speed, whereas with the crossfeed, it reacts to both airspeed and sink rate errors.

The main benefit of the crossfeed for path control is manifested relatively infrequently, affecting the lower-than-10% probability region. This suggests that deviations above the MLS beam or long landings are related to exceedances of the throttle's lift reduction capability where the crossfeed helps by providing negative acceleration through the elevator. Consequently, it might be possible to utilize the crossfeed only when the throttle approaches its retard limit, thereby retaining most of the performance improvement without the continuous increase in elevator (and column) rate activity.

In the Choke Augmented Throttle Configuration, chokes rather than elevator provide the augmentation required to overcome the throttle shortcomings and obtain the required performance. However, it appears that a path to elevator crossfeed when the throttle is near its limits would also be beneficial, especially if choke authority is limited. No detailed investigation of this option was made during our study.

Pitch Flare

In a CTOL airplane, both glideslope track and flare are accomplished mainly by the elevator. In the recommended STOL control laws, the elevator is used to control airspeed in the approach. However, since speed control may be relaxed in the flare, pitch attitude can be used to enhance flare profile control. Three techniques were evaluated as follows:

1. Predictor Commands

One example of this technique is currently implemented on the Augmentor Wing Airplane. A pitch up command is slowed in at flare initiate, with magnitude based on initial pitch attitude, aircraft weight, and approach speed. In addition, the pitch command is modified to provide closed loop control about the desired flare trajectory, with no closed loop throttle control until very near touchdown. Landing performance with this system is not good, as described in Appendix D. This technique can provide good landing performance if the predict commands are varied extensively as a function of aircraft and disturbance states. Some simple variations were attempted, resulting in marginally acceptable landings at best. In fact, for this approach to be effective, the predictor commands would need such extensive adaptation to initial state as to be essentially closed loop. Thus, all further effort was concentrated on closed loop type flare control laws.

2. Throttle Flare

In this technique, flare is accomplished by the throttle, with the elevator controlling airspeed to obtain a controlled deceleration throughout the flare. Although acceptable sink rate and range performance were obtained, the touchdown pitch attitude variations were excessive since attitude is not directly controlled in this method. Landing safety requirements on θ_{\max} and θ_{\min} , designed to prevent tail scraping or nose-wheel-first touchdowns, cannot be met as pitch attitude control is essentially open loop with rotation proportional to flare duration. This procedure does not provide good adaptation to wind variations since in tail wind the initial pitch attitude is low and the flare is abrupt, resulting in little rotation, whereas in head wind the high initial pitch attitude and long flare duration result in a large rotation.

3. Throttle and Elevator Flare

In this technique, airspeed commands to the elevator are frozen at flare initiate, and a pitch attitude command is inserted as the following function of altitude:

$$\Delta\theta^C = \left[\theta_{TD}^C - \theta(h = h_{\theta FL}) \right] \left(1 - \frac{h}{h_{\theta FL}} \right) \quad h \leq h_{\theta FL}$$

This closed loop pitch flare command serves to regulate rotation rate as a function of sink rate, thus responding to sink rate changes caused by external disturbances. Since $\Delta\theta^C$ amplitude is a function of pre-flare average wind or sink rate, this pitch command increases rotation for tail wind and reduces it for head wind. This reduces pitch dispersions, land short and floating probabilities, and throttle demand at flare regardless of wind condition.

In comparison to the throttle flare technique, the throttle-and-elevator flare resulted in improvement in touchdown spreads of 30% in sink rate, 25% in range, and 35% in pitch attitude, all in the $\pm 1\sigma$ region. Improvement outside of the 1σ region was even more pronounced. Therefore, a pitch command that is a function of altitude is recommended in the final configuration.

Variations in the value of θ_{TD}^C were studied. Performance was found to be insensitive to a few degrees of such variations and a value of 10° was chosen based on considerations of having a reasonable amount of rotation throughout the flare and touching down at a convenient pitch attitude that is sufficiently far from both upper and lower pitch attitude limits.

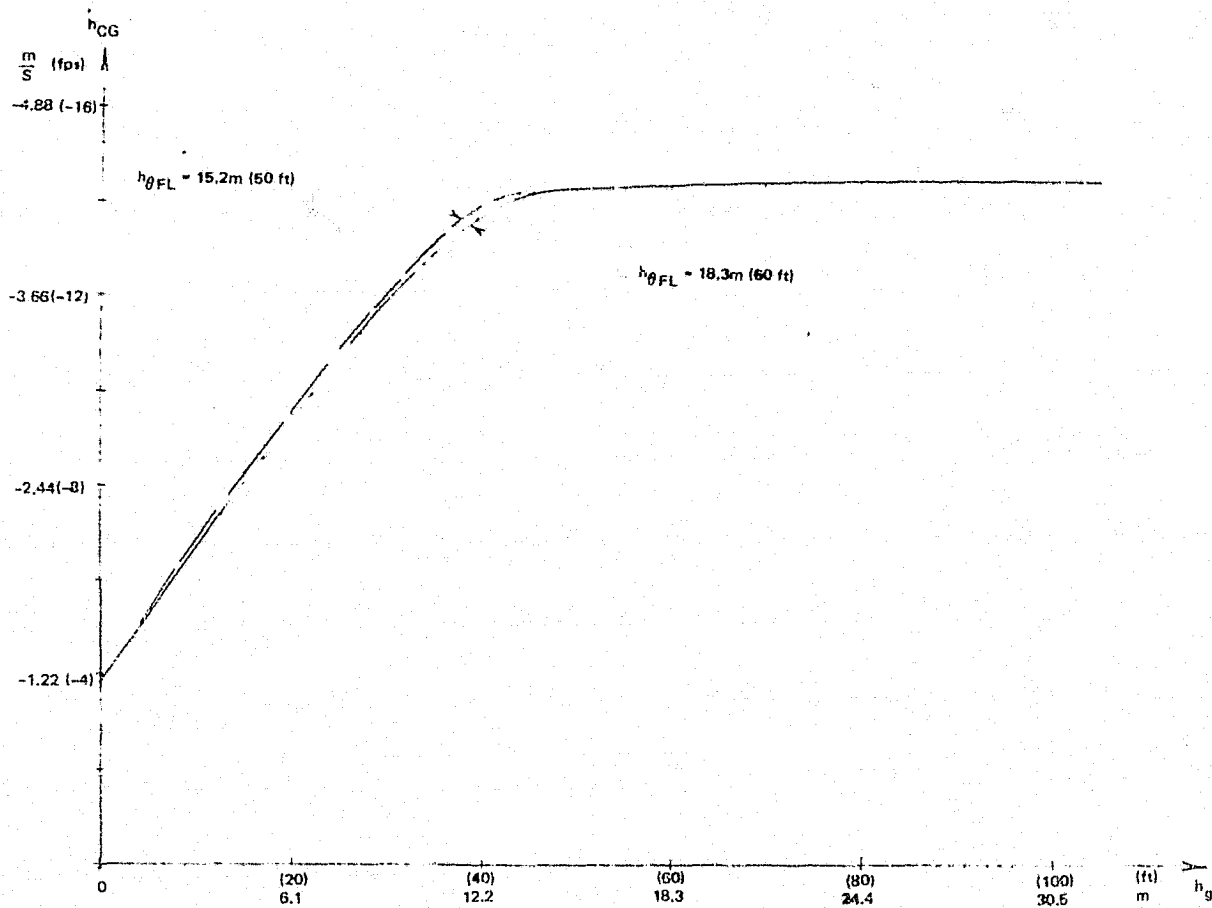


Figure 5-4. Pitch Flare Initiation Altitude Variation

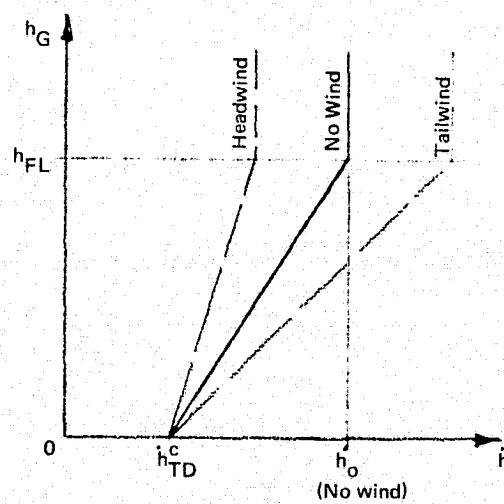


Figure 5-5. Flare Command Profile

Variations in timing of the pitch flare with respect to throttle flare initiation were also studied. An early pitch flare initiation provides some lead on rotation that serves to overcome the n_z/q lag, thus affecting the initial throttle and choke demand at flare initiate. Sink rate reduction starts slightly earlier and is smoother with the advanced pitch flare, as shown in Figure 5-4. No significant impact on landing performance was recorded when pitch flare initiation altitude was changed from 12.2 m (40 ft) to 18.3 m (60 ft) while the throttle flare initiation was kept at 15.2 m (50 ft). However, it is recommended to initiate pitch flare at 18.3 m (60 ft) in order to minimize throttle and choke demand in nominal flares.

Path Flare Profile

The recommended pitch landing system utilizes the flare command profile shown in Figure 5-5. h_0 is the airplane's pre-flare sink-rate. Flare altitude, (h_{FL}), and the touchdown sink rate command (\dot{h}_{TD}^C) are constant. In the recommended system, $h_{FL} = 15.2$ m (50 ft) and $\dot{h}_{TD}^C = -1.37$ m/s (-4.5 fps). For a flare loop with adequate band width, the linear variation of sink rate command with altitude results in an exponential flare, with time constant equal to the slope of the shown flare line. The initial sink rate changes with winds and approach speeds resulting in variation of slope as shown in Figure 5-5 for three wind conditions. For a given glide path angle, a higher initial sink rate corresponds with a higher forward velocity, and thus the shortened flare time constant compensates for variations in inertial speed to minimize range dispersion.

The following variations of this profile have been evaluated:

1. Touchdown Sink-Rate Command

Touchdown sink rate command values of 0.91, 1.37, 1.83 m/s (3, 4.5 and 6 ft/sec) were evaluated. The results are shown in Figure 5-6. Smaller range dispersions are associated with the higher sink rate commands.

A value of $\dot{h}_{TD}^C = -1.37$ m/s (-4.5 ft/sec) has been chosen as being a good compromise since it provides acceptable range dispersion along with a sufficiently low probability for high touchdown sink rates.

2. Flare Altitude

Variations in flare initiation altitude from 15.2 m to 12.2 m (50 to 40 ft) were studied with results summarized in Figure 5-7. The lower flare altitude reduces both touchdown sink rate and range dispersions. However, the probability of hard landings tends to increase and the

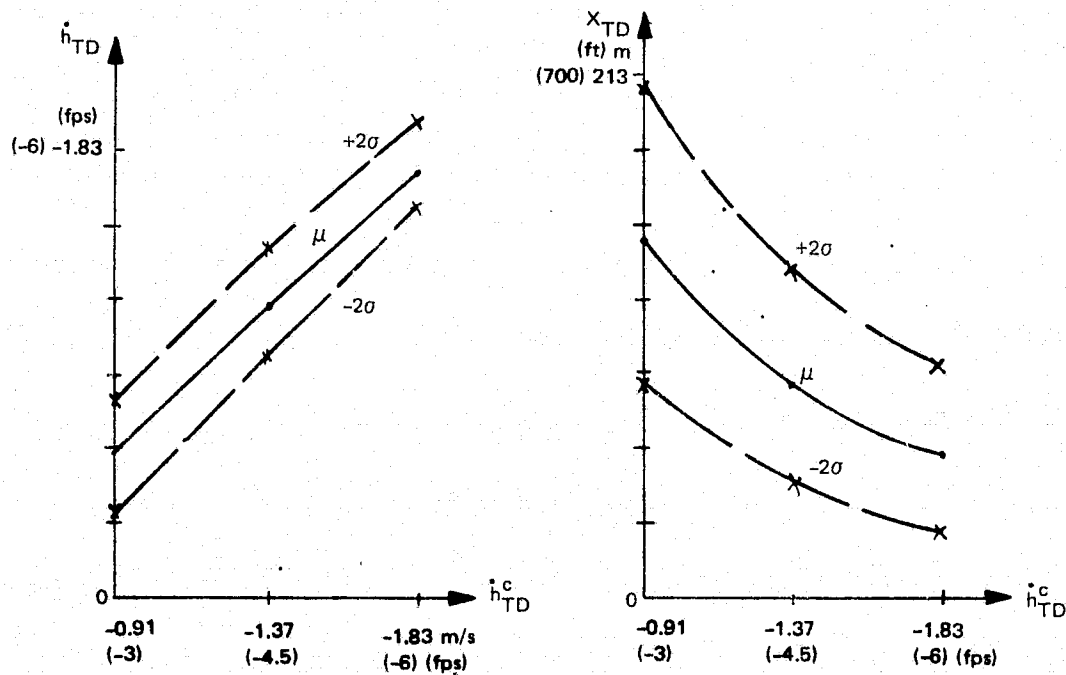


Figure 5-6. Effect of Sink-Rate Command

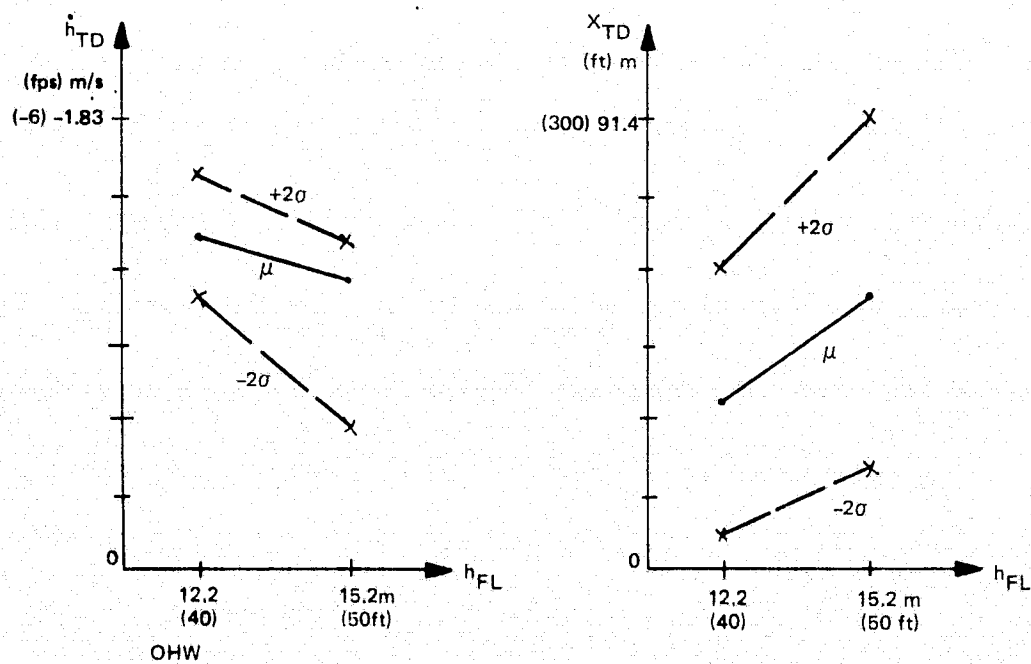


Figure 5-7. Effect of Flare Altitude

flare becomes more abrupt with attendant higher normal acceleration transient. The time interval between flare initiation and touchdown is reduced by about 20% which raises a question with respect to pilot acceptability of a 12.2 m (40 ft) flare initiation altitude. All those problems seem to outweigh the improvement in range performance and a 15.2 m (50 ft) altitude is recommended for flare initiation.

3. Variable Flare Altitude

Flare initiation altitude variation as a function of pre-flare sink rate was also examined. A flare initiation algorithm was defined by:

$$h_{FL} = -2.5 \dot{h}_0 + 2.29 \text{ in metric units}$$

$$(h_{FL} = -2.5 \dot{h}_0 + 7.5 \text{ in English units})$$

This resulted in flare initiation at 15.2 m (50 ft) in limiting tail wind, and 7.62 m (25 ft) in limiting head wind. In deterministic winds and shears, this yielded 40% reduced range dispersion, with a 0.91 m/sec (3 fps) sink rate command. However, the added system complexity and the adverse implications on pilot monitoring led to the abandonment of this method in favor of an increased touchdown sink rate command.

4. Variable \dot{h}_{TD}^C

Variable touchdown sink rate command as a function of pre-flare sink rate was investigated, with $\dot{h}_{TD}^C = K\dot{h}_0$ for K varying between 0.10 and 0.30. This simple algorithm yielded range dispersions that were worse than with the constant \dot{h}_{TD}^C , because the large wind induced variation of initial sink rate for STOL approaches yielded a very soft touchdown command for headwinds. Further studies should consider an algorithm of the form:

$$\dot{h}_{TD}^C = \dot{h}_1^C + K\dot{h}_0$$

5. Segmented Flare Command Profile

The nominal flare command profile shown in Figure 5-5 calls for a step in vertical acceleration at flare initiation, resulting in a relatively large sink rate error. In an attempt to reduce this error, a two segment flare was implemented, with a higher first segment altitude to allow shallower slopes as shown in Figure 5-8. However, this modification failed to either produce any significant reduction of \dot{h}_{err} or favorably affect landing performance. The segmented flare command was therefore discarded.

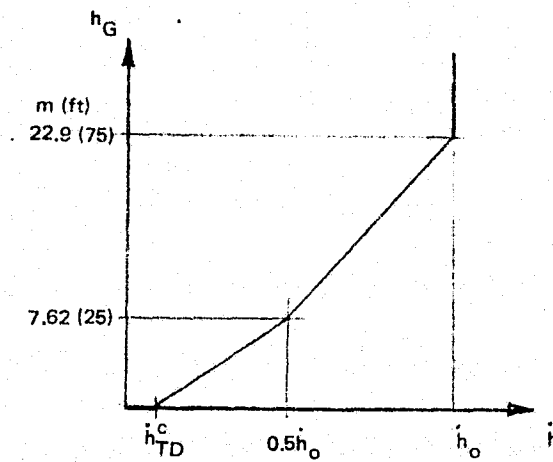


Figure 5-8. Segmented Flare Profile

Gain Variations

The effect of gain variations on system operation and performance was studied quite extensively. The gains defined in the recommended configuration provided the best performance subject to the design criteria. Three of the gain variations have particularly interesting implications, and these may require attention in further simulation and flight-test work.

1. Airspeed to Elevator Gain

The use of elevator in airspeed control introduces undesired coupling into path control. When the airplane encounters a forward gust, the increase in lift causes an upward acceleration. The airspeed feedback commands pitch up, in order to counter the sensed increase of airspeed. The pitch up motion increases the upward acceleration which is a disturbance to path tracking.

The speed gain of $K_u = 1.64$ degrees pitch attitude per m/s of airspeed (0.50 per fps) has been established in flight tests that have been conducted on the Augmentor Wing aircraft prior to this study. A reduction of airspeed gain was considered during optimization of the Elevator Augmented throttle configuration. Figures 5-2 and 3 show that, in the two-control configuration, halving the speed gain results in about the same performance improvement that is obtained by crossfeeding sink rate error to elevator. Moreover, Figure 5-3 shows that with $K_u = 0.82$ deg/m/s (0.25 deg/fps), control and pitch activity are significantly reduced, with a minimal speed variation increase about equivalent to that induced by the crossfeed.

Thus a speed gain reduction from the 0.5 value used in the recommended system (Figure 3-1) might be beneficial both in terms of performance and activity. Final tuning of this gain should be done in flight tests as it is important to base it on the actual speed excursions that result so as to maintain the required lift margin. An alternate approach would be to use nozzles for speed control.

2. Pitch Attitude Gain

The mean pitch attitude decreases by 2° when the ground effect magnitude is doubled (see Section 5.5). The feasibility of an increase in pitch gains has been studied, aimed at the reduction of this sensitivity. Pitch attitude time histories with gain variations are shown in Figure 5-9. The response with $K_\theta = 8$ and $K_q = 3.8$, which are twice the nominal gains, looks good and does not exhibit any problem. Statistical performance data has also been taken with the increased pitch attitude gain, showing essentially the same spreads that were measured with the nominal pitch gain. Statistical results for touchdown pitch attitude with nominal and doubled gains show no difference in spread, although the mean pitch attitude with the higher gains is closer to the commanded 10 degrees.

The evaluation indicates that an increase of pitch gains is possible. However, the nominal gain is retained in the recommended system. The decision whether or not to change these gains might be best made during flight tests, based on the real impact of ground effect induced moments on touchdown attitude.

3. Throttle Gain Variations

The effects of throttle gain variations on landing performance of the recommended configuration are shown in Figure 5-10. There is a significant performance improvement with increased throttle gain, especially in headwinds when the choke washout is fast compared to the flare time. When the gain is increased from half to double the nominal value, the 3σ touchdown sink rate dispersion is reduced by a drastic 70% in headwind and by 35% in tailwind, along with a significant reduction in probability of hard landings. Touchdown range dispersion is reduced by 19% with headwind and 26% with tailwind, with floating tendency reduced by 24.4 m (80 ft) at the 3σ level. Since the throttle gain margin is nominally greater than ten, stability is not adversely affected by a moderate throttle gain increase. Activity in disturbances is also improved with an increased throttle gain, as discussed in subsection 5.4.

Further evaluation of throttle gain increase is recommended in NASA's simulator and in flight. If the actual throttle dynamics exhibit more stiction or hysteresis than our model, the increased throttle gain would be even more beneficial.

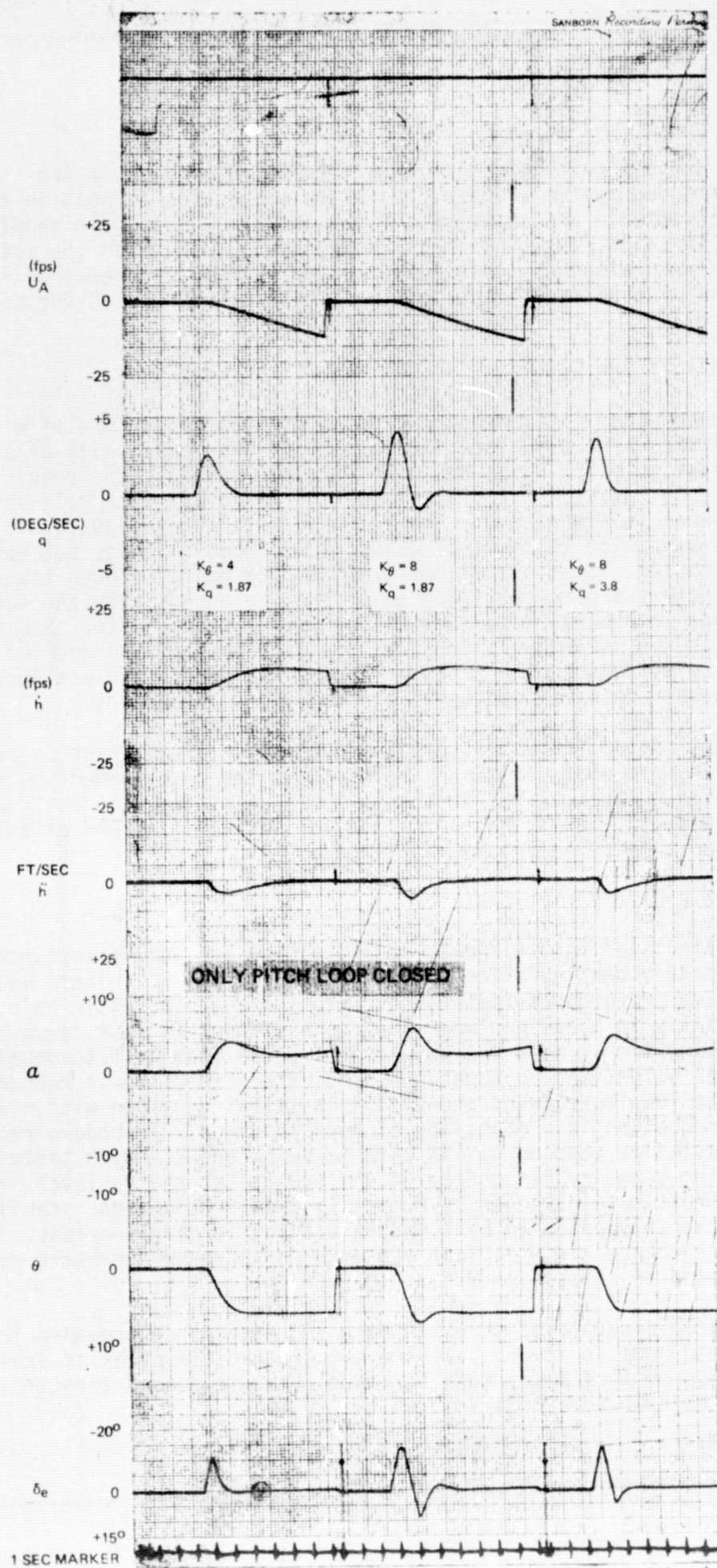


Figure 5-9. Pitch Step Responses with Gain Variation

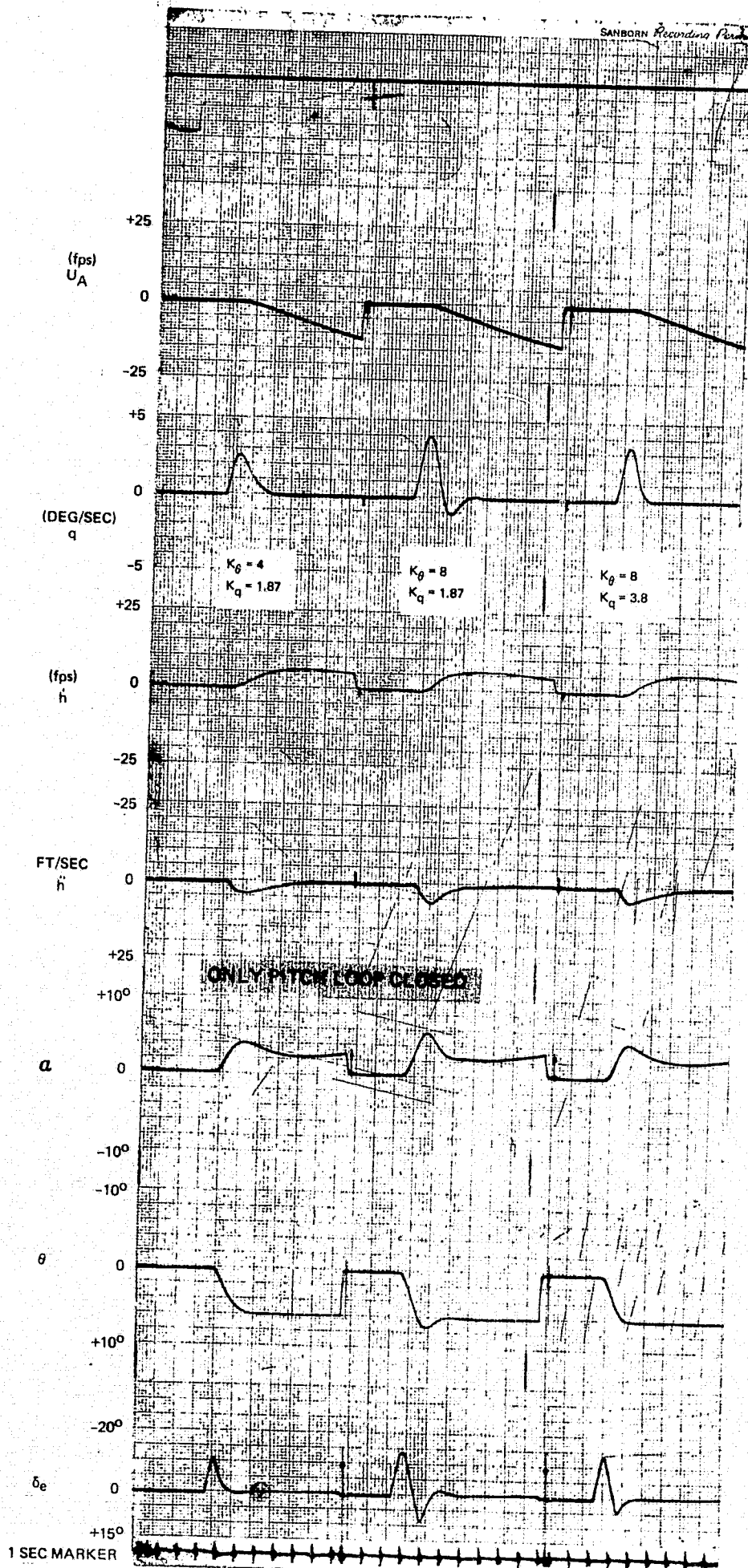
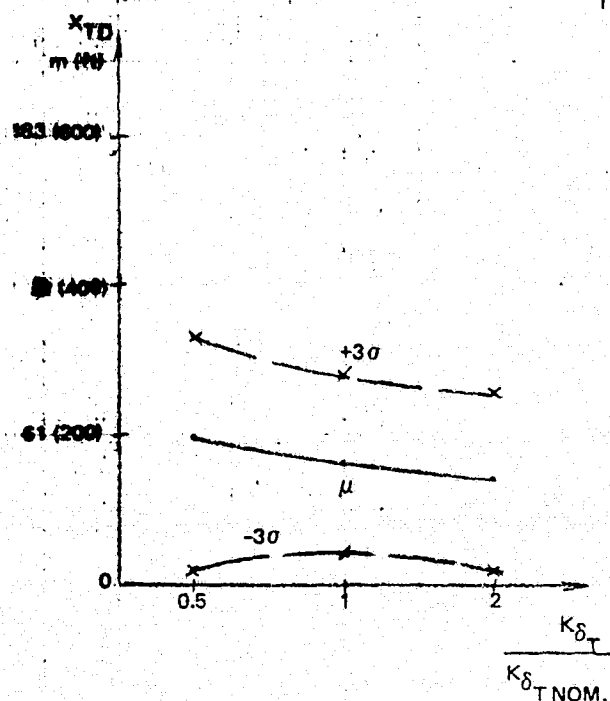
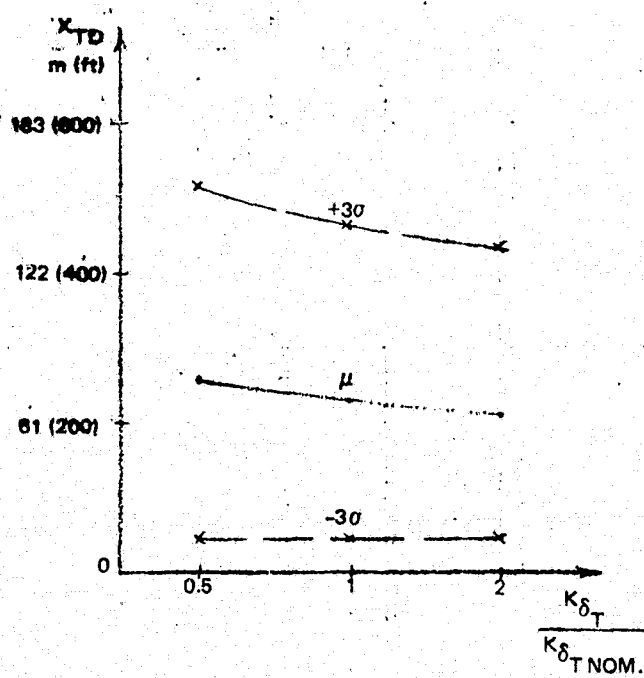
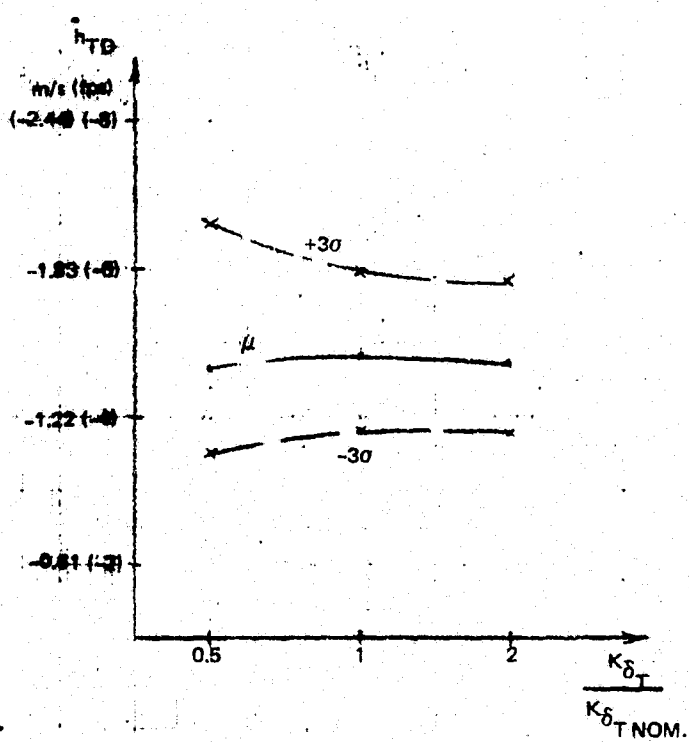
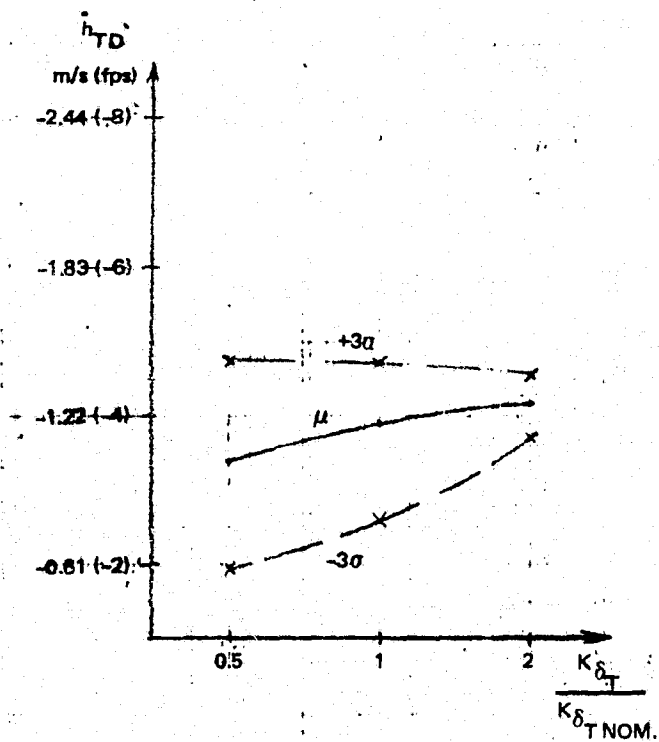


Figure 5-9. Pitch Step Responses with Gain Variation



12.9 m/s (25 kt) HWS

5.15 m/s (10 kt) TWS

Figure 5-10. Effect of Throttle Gain Variation

5.4 Performance

A summary of pitch landing performance is presented in this subsection. The more detailed performance data are presented in Appendix B.

Landing Performance

Landing time histories and sink rate versus altitude profiles for the pitch landing system are included in this section. For the no disturbance landing time history (Figure 5-11), no deviation from the glideslope is observed prior to the flare. A smooth reduction of sink rate from the approach value of 4.36 m/sec (14.3 fps) to the touchdown value of about 1.22 m/sec (4 fps) is performed throughout the flare. In the absence of disturbances, almost no throttle and only small choke deflection is obtained with the flare almost uniquely performed by pitch rotation. Landings in deterministic wind and shear (shown in Figure 5-12) result in small deviations from the glideslope and noticeable throttle and choke deflections. However, only small deviations in touchdown sink rate, range and pitch attitude are obtained. The smooth reduction of sink rate through the flare and the tight touchdown sink rate control achieved by this system are clearly shown in the flare profiles of Figure 5-13.

The probability distributions for average performance of the recommended system are shown as Figures 5-14 through 5-17 with a summary presented in Table 5-I. All landing performance requirements are satisfied. For conservatism, all stochastic performance data was obtained in limiting headwind and tailwind (12.9 m/s, -5.15 m/s, +25 kt, -10 kt), and the corresponding shear (0.169 m/s/m, 0.0676 m/s/m, 10 kt/100', 4 kt/100') and turbulence levels ($\sigma_u = 1.92$ m/s 6.3 fps, $\sigma_w = 0.762$ m/s 2.5 fps), without accounting for their ($\approx 1\%$) occurrence probabilities. These results are shown by solid lines in the figures. The dashed lines show the added effect of various deterministic disturbances listed in Table 5-II, and thus these curves represent the total population expected landing performance.

Activity in Disturbances

Activity in disturbances comprising limiting turbulence and beam noise is summarized in Table 5-III. The middle column corresponds to the recommended system whereas the other two show the effects of throttle gain variations. With the nominal gain, beam tracking is very good with a 1σ value at 20% of the 30.5 m (100') window requirement. Airspeed variation is only 3.6% of the nominal airspeed, resulting in excellent maintenance of the maneuver margin. Pitch attitude excursions are moderate. Throttle activity is moderate, with a 1σ value of 0.8% compared to the authority limit of 3% (retard). Throttle rate activity is only 10% of the 4.4%/sec rpm rate limit. Elevator and choke activities look acceptable.

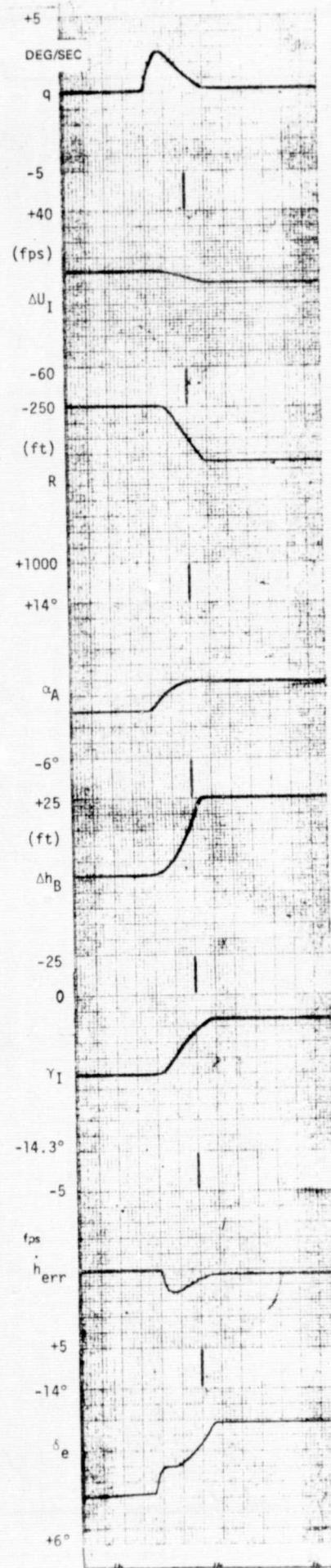
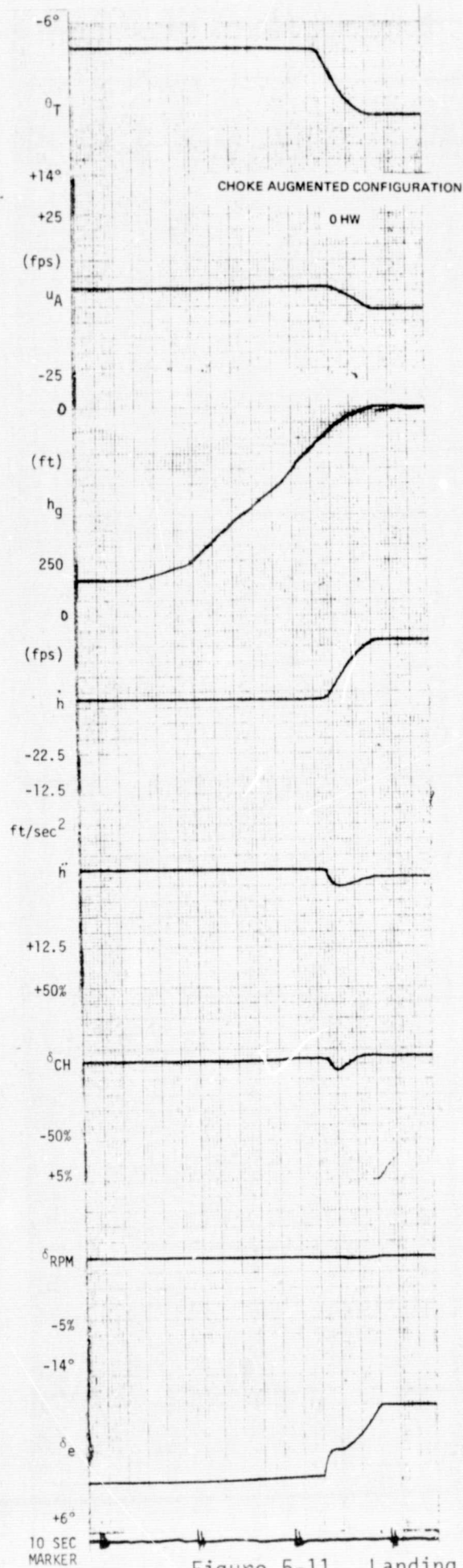


Figure 5-11. Landing Time History: No Wind

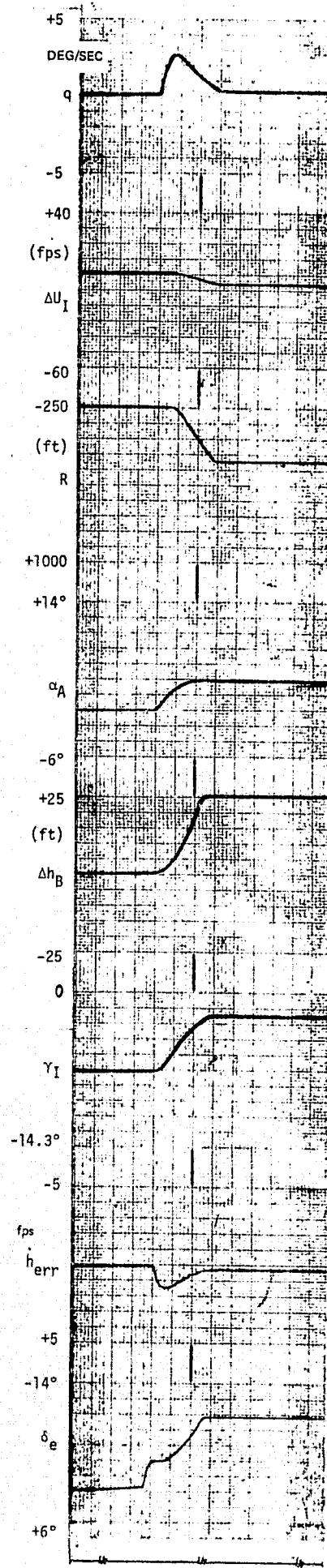
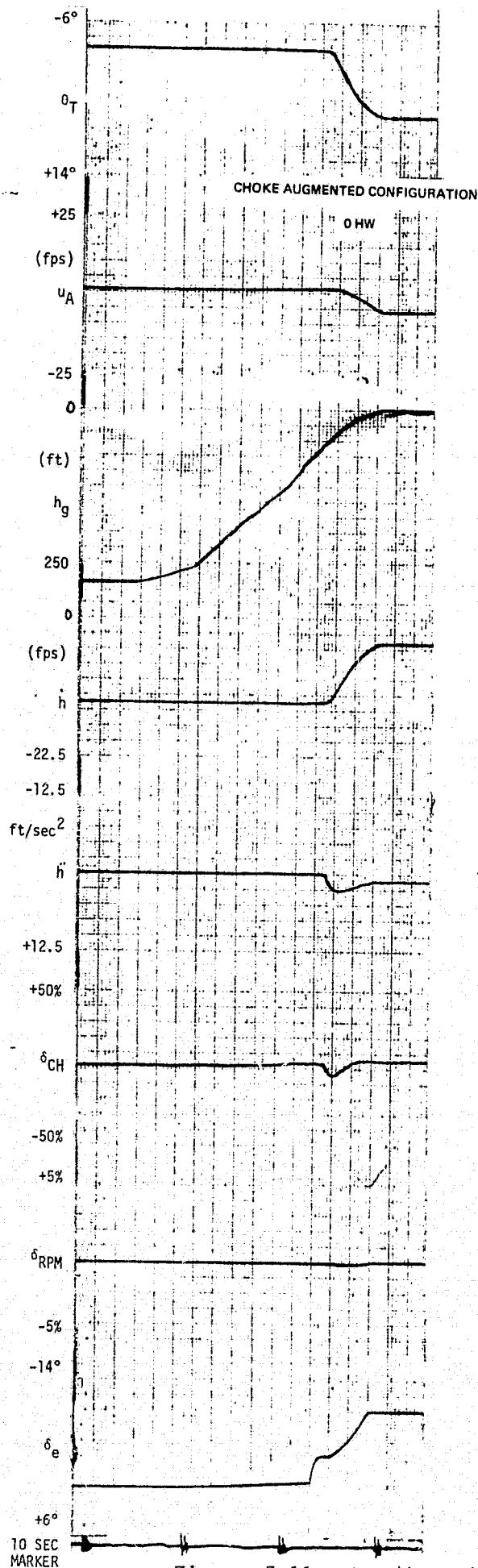


Figure 5-11. Landing Time History: No Wind

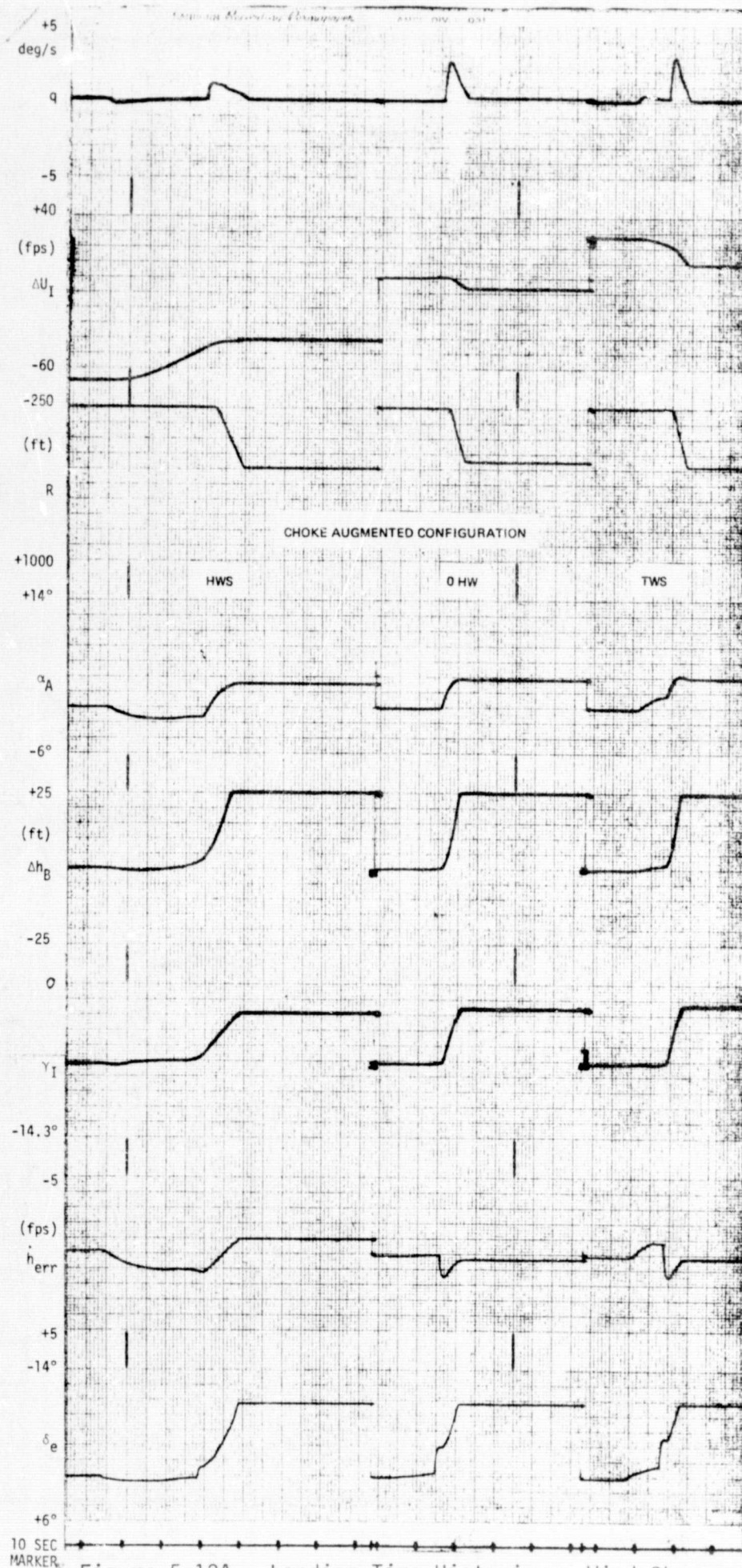


Figure 5-12A. Landing Time Histories: Wind Shears

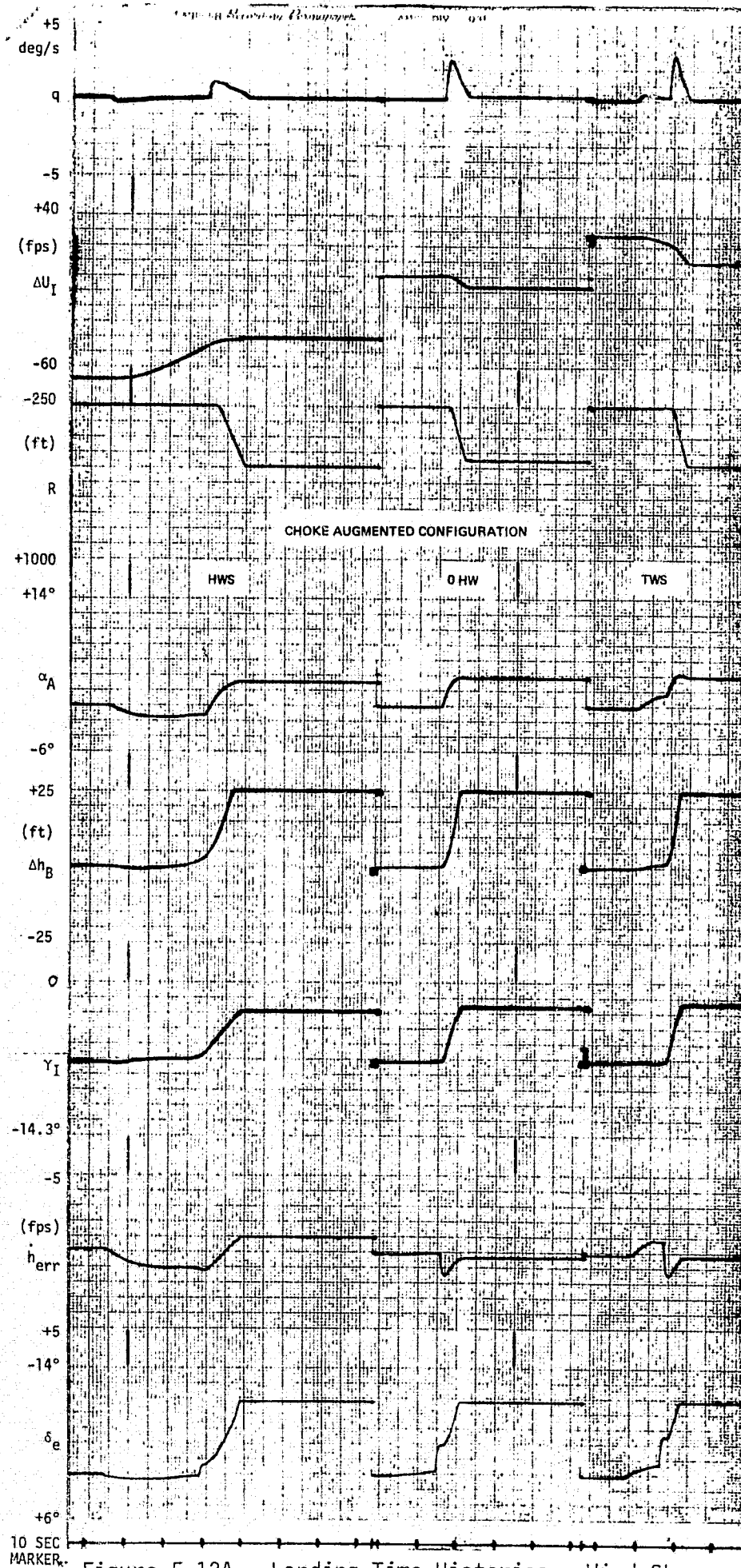
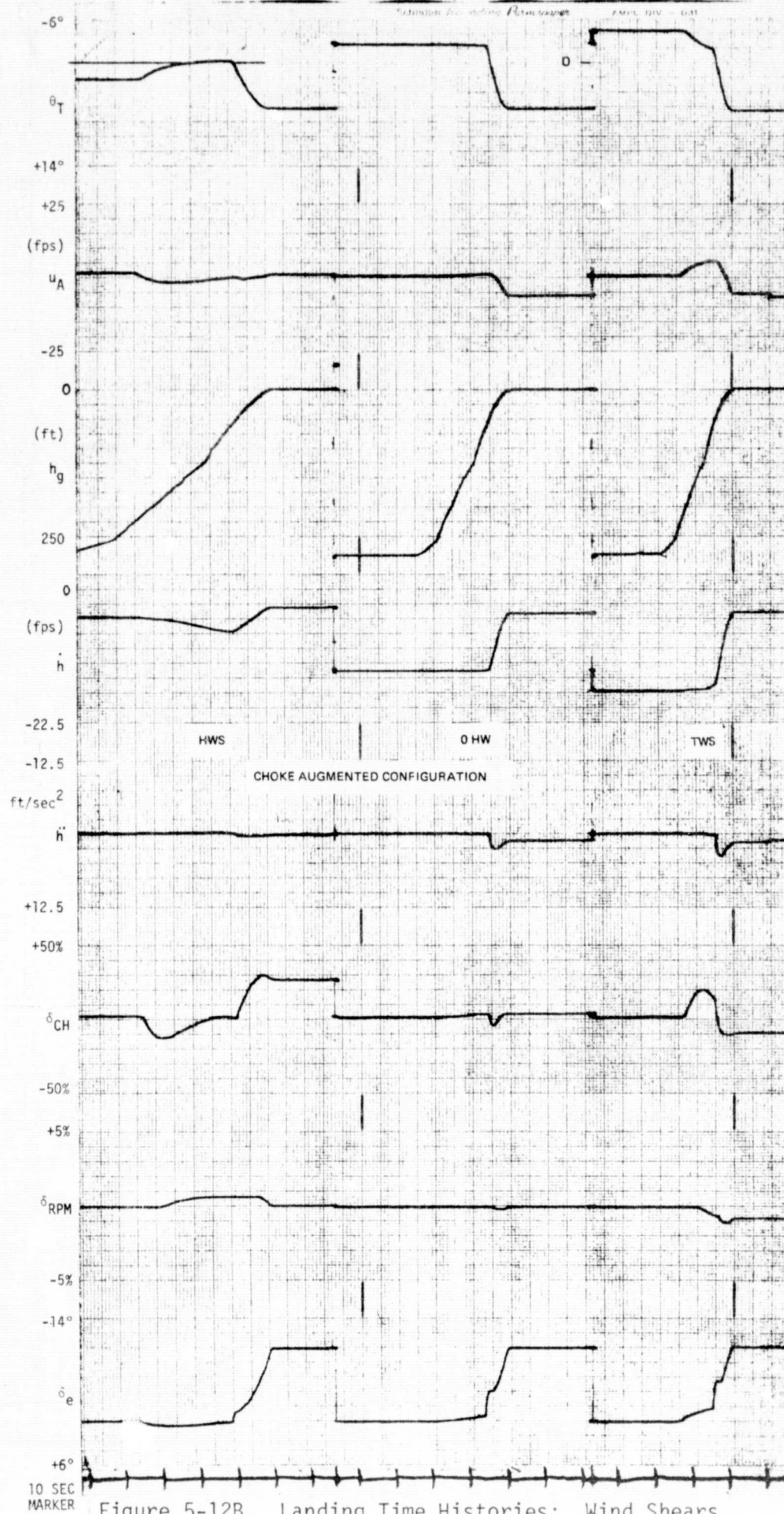


Figure 5-12A. Landing Time Histories: Wind Shears



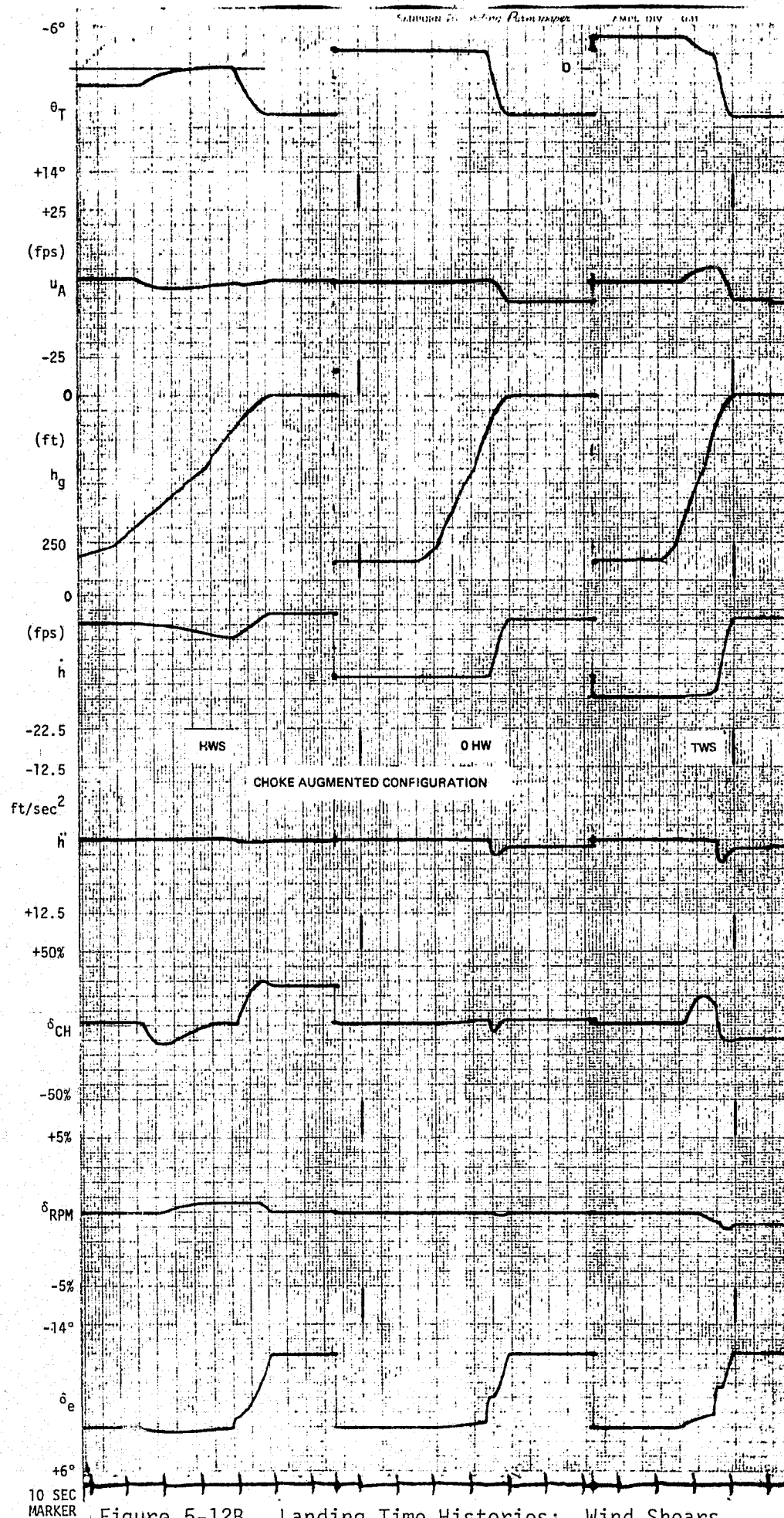


Figure 5-12B. Landing Time Histories: Wind Shears

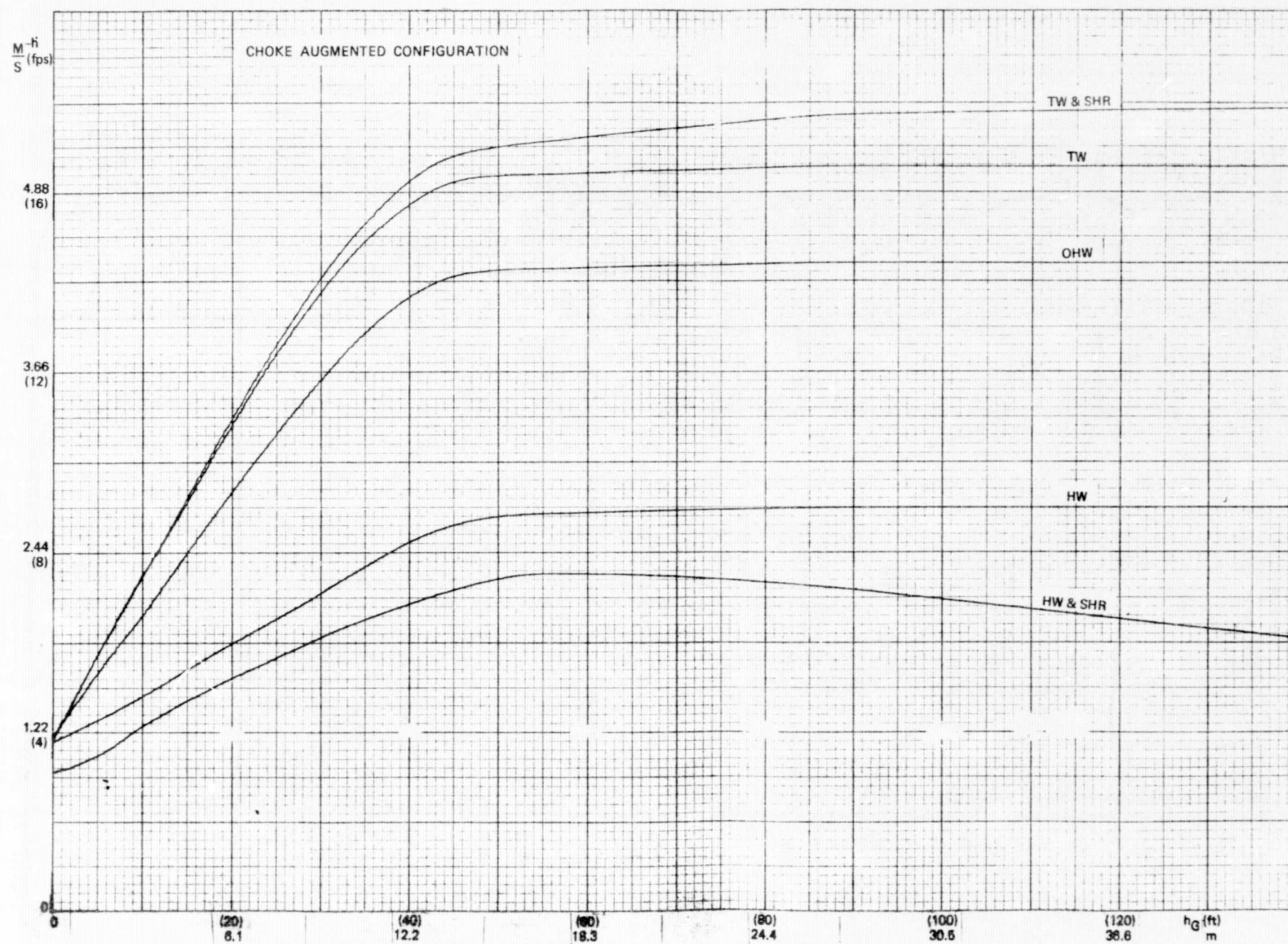


Figure 5-13. Sink Rate vs. Altitude Profiles

TABLE 5-I. PITCH PERFORMANCE SUMMARY

<u>Variable</u>		<u>Requirement</u>	<u>Actual</u>
\dot{h}_{TD}	μ	1.22 (4)	1.22 (4)
m (fps)	2σ	<1.83 (6)	1.62 (5.3)
	10^{-6}	<3.05 (10)	2.16 (7.1)
X_{TD}	μ	61 (200)	67 (220)
m(ft) beyond GPIIP	2σ	± 61 (200)	+51.8 (170) -30.5 (100)
	10^{-6}	<283.2 (929)	210 (690)
		>-112.8 (-370)	- 9.1 (-30)
θ_{TD} (deg)	μ	5	6.7
	2σ	-	+1.4 -2.2
	10^{-6}	<15	10
		>-1	1
Δh_{window}	μ	0	0.61 (2)
m (ft.)	2σ	$\pm 3.66 (\pm 12)$	$\pm 1.43 (\pm 4.7)$

Notes:

1. This table defines total population landing performance, including stochastic and deterministic disturbance effects.
2. Deterministic disturbances are: Winds and shears, glide slope angle, threshold length variation, beam offset, radar altimeter bias, and aircraft weight and approach speed variation.
3. Stochastic disturbances are:

limiting turbulence	$\sigma_u = 1.92$ m/s (6.3 fps)
	$\sigma_w = 0.76$ m/s (2.5 fps)
beam noise	$\sigma_{BN} = 0.07^\circ$
4. The specified mean and 2σ requirements are design goals, while the 10^{-6} requirements are based on the safe landing boundaries for the Aug. Wing vehicle.
5. Δh_{window} is vertical tracking error at the 30.5m (100 ft.) approach window.

TABLE 5-II. PITCH DETERMINISTIC DISTURBANCES

<u>Disturbance</u>	<u>Magnitude</u>	<u>Probability Level</u>
Glide Slope Angle Variation	1.5°	3 σ
Runway Threshold Variation	20m(65.6 ft)	4.5 σ
Glide Slope Beam Offset	1.83m (6 ft)	4.5 σ
Radio Altimeter Bias	0.457m (1.5ft)	2 σ
Aircraft Weight Variation	35584N(8000 lbs)	4.5 σ

- 1) Normal distribution assumed.
- 2) Glide-slope beam offset includes equivalent beam integrator bias and ramps downstream of the integrator.

TABLE 5-III. PITCH ACTIVITY SUMMARY (RMS)

$K_{\delta T}$	<u>Half</u>	<u>Nominal</u>	<u>Double</u>
$\Delta \dot{h}$, m/s (fps)	0.244 (0.8)	0.244 (0.8)	0.244 (0.8)
$\Delta h/W.R.$	0.2	0.2	0.17
u/U_0	0.044	0.036	0.033
θ , deg.	2	1.4	1.2
δ_{RPM} , %	0.8	0.8	0.8
$\dot{\delta}_{RPM}$, %/sec	0.2	0.4	0.6
δ_e , deg.	1.2	1.2	1.2
δ_{CH} , %	17	12	10

Notes:

1. W.R. is the 30.5m (100 ft.) window requirement, equal to 3.66m (12 ft.).
2. Results shown are in the beam tracking phase.
3. Limiting turbulence and beam noise were used, with:

$$\sigma u = 1.92 \text{ m/sec (6.3 fps)}$$

$$\sigma w = 0.762 \text{ m/sec (2.5 fps)}$$

$$\sigma_{BN} = 0.07^0$$

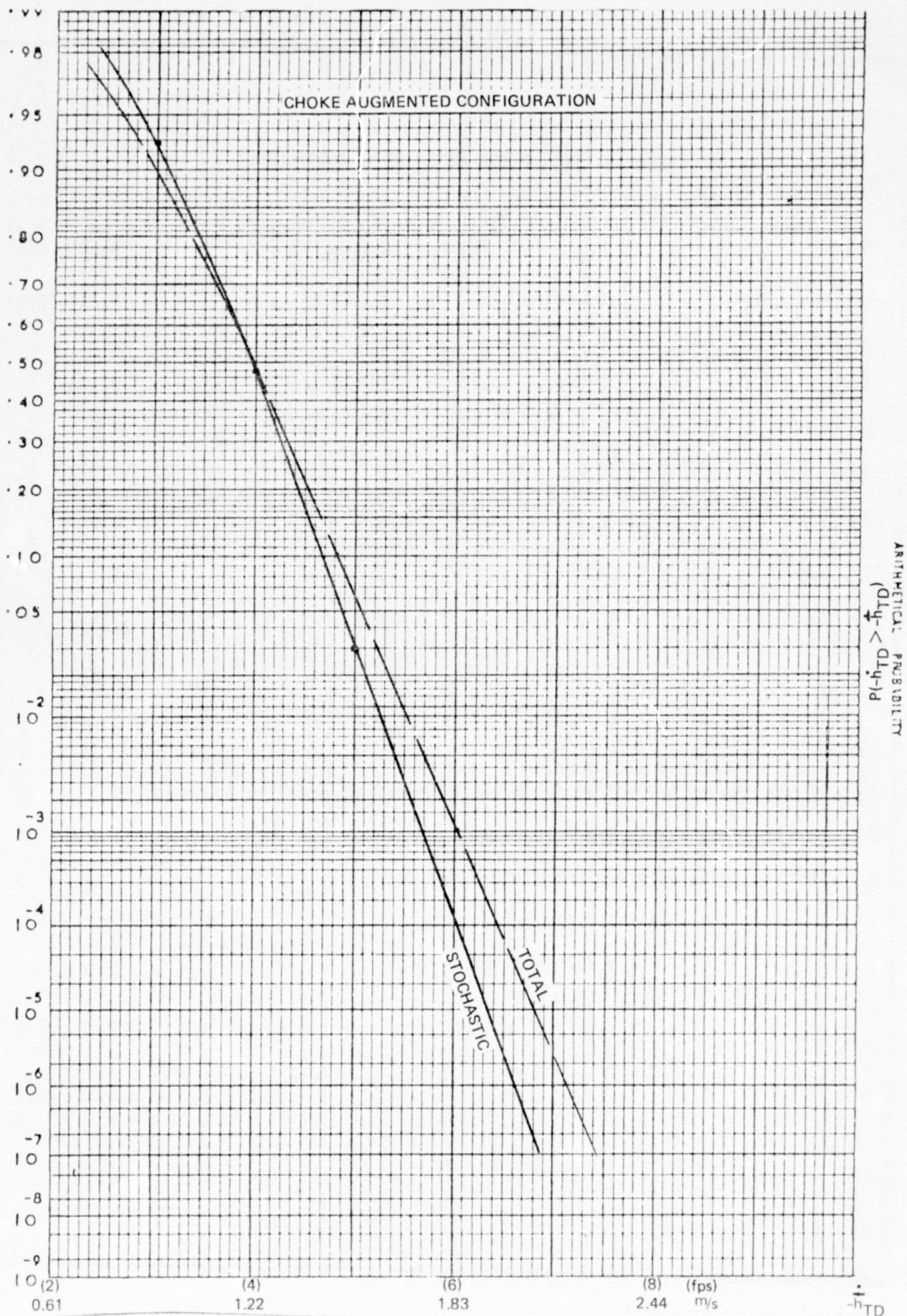


Figure 5-14. Touchdown Sink Rate Distribution

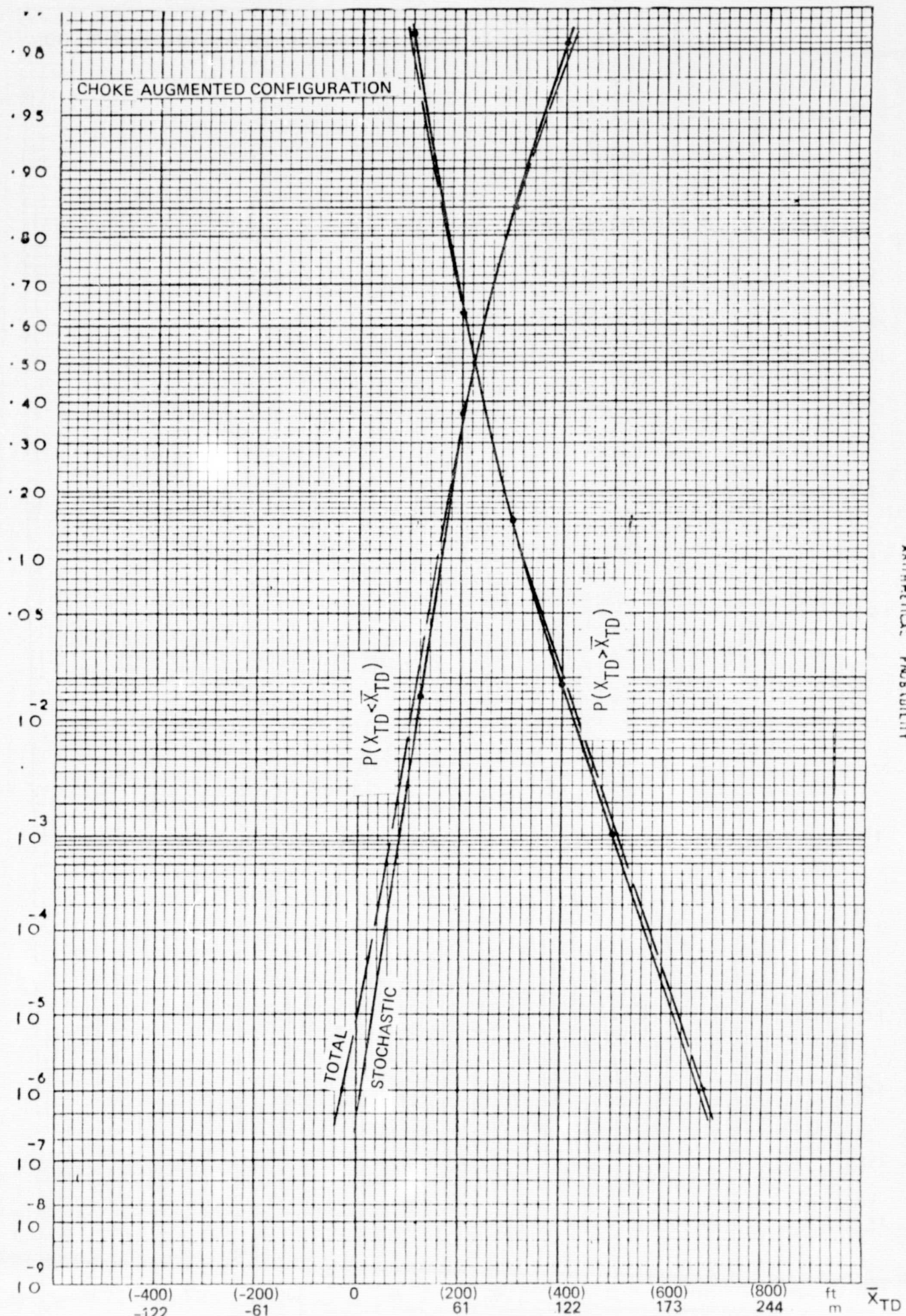


Figure 5-15. Touchdown Range Distribution

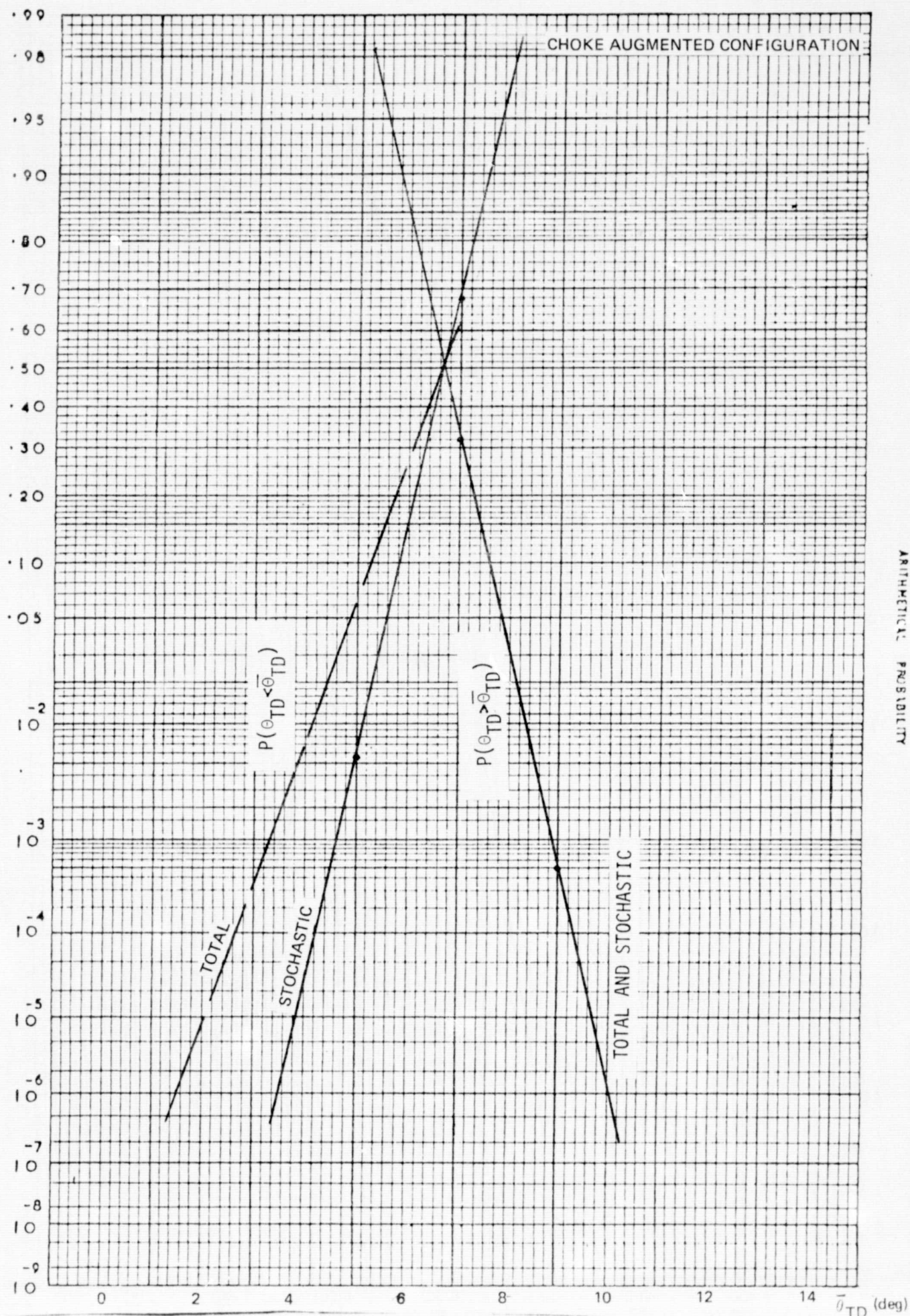


Figure 5-16. Touchdown Pitch Attitude Distribution

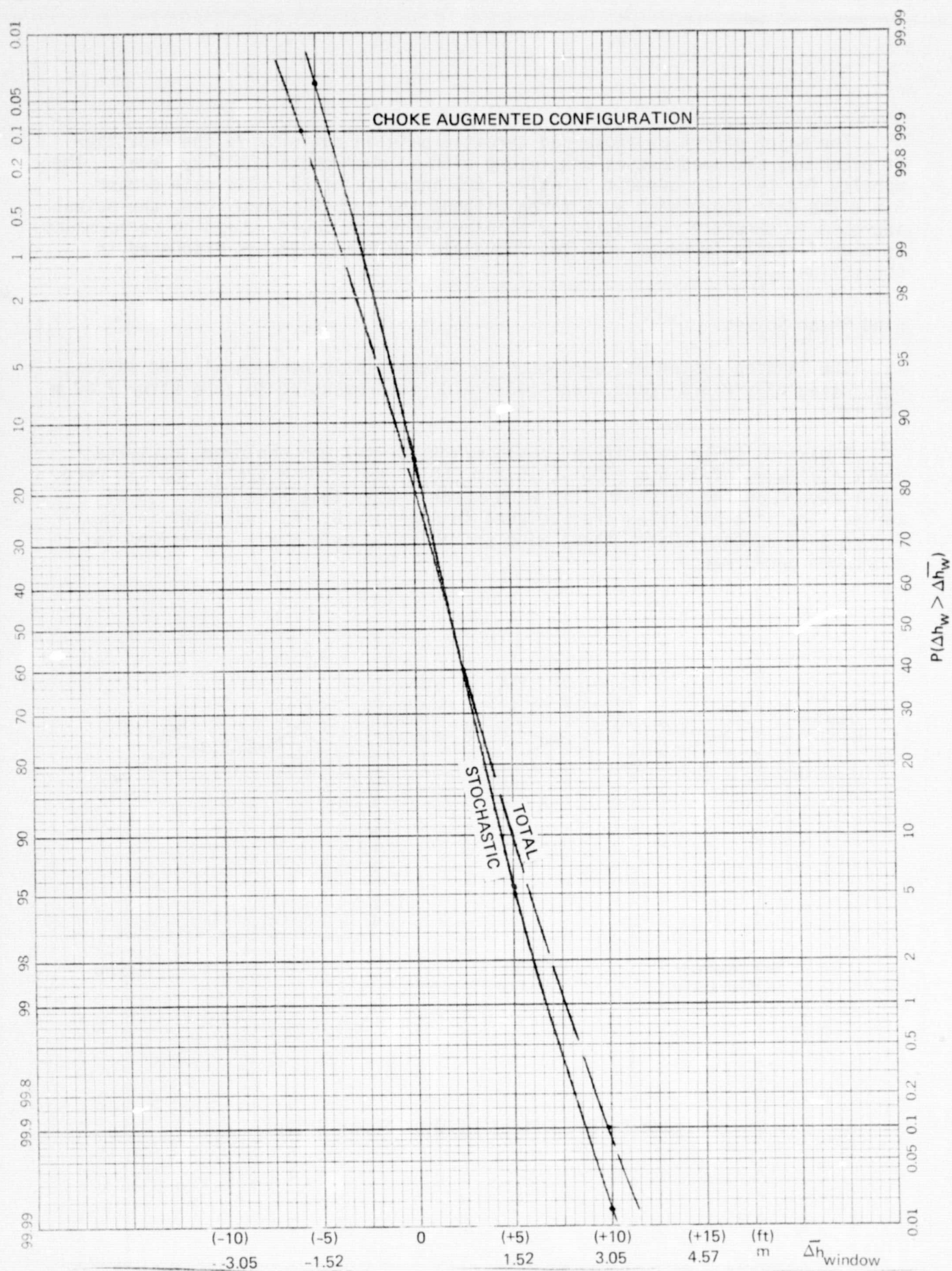


Figure 5-17. Distribution of Beam Deviation at Approach Window

The major effect of increased throttle gain on activity is the reduction of pitch and airspeed excursions, along with a lower choke activity level. The penalty for this improvement is only a 50% increase of throttle rate demand. Since the data shown here were taken without the throttle dead zone, the actual increase in throttle rate activity is expected to be lower. Landing performance is significantly improved with the increased throttle gain, as discussed in subsection 5.3.

Wind Shear Spikes

The landing system was subjected to deterministic horizontal wind spikes, consisting of a 0.676 1/sec shear (40 kt/100 ft) reversing to zero after 7.62 m (25 ft).

A maximum spike velocity of ± 5.15 m/s (± 10 kts) was employed, centered about altitudes of 30.5 m (100'), 15.2 m (50'), and 7.62 m (25'). Spikes were superimposed on the deterministic wind shear models that have been used regularly. The time histories are included in Appendix B. As indicated in the Figure 5-18 summary chart, these wind spikes cause only small variations in touchdown performance.

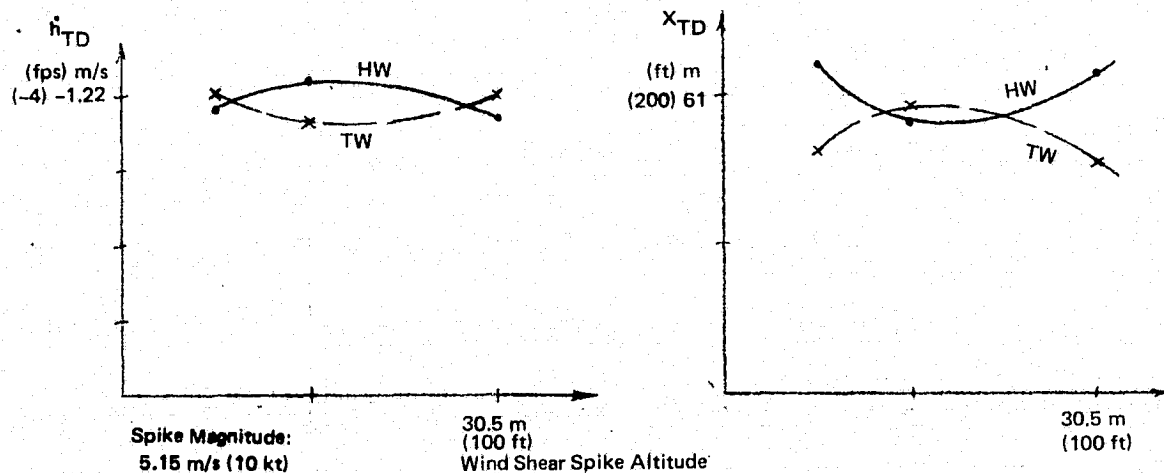


Figure 5-18. Effect of Wind Shear Spikes

5.5 Off-Nominal Conditions

The impact of the following off-nominal conditions on performance has been studied, and the results are presented in this section.

1. Approach glideslope angle variations
2. Heavy weight flight condition
3. Terrain irregularities
4. Ground effect variations
5. Throttle model variations

Discussion of each of those conditions follows.

Approach Glideslope Angle Variations

Performance with 6° and 9° approach glideslope was evaluated and compared to the nominal 7.5° . The results are shown in Figure 5-19.

Increasing the glideslope from 6° to 9° results in an increase in the mean touchdown sink rate. The lowest sink rate spread is observed at 7.5° , and it is larger for both 6° and 9° . The probability of exceeding 10 fps is smaller than 10^{-6} for both 6° and 9° glideslopes. The effect of increased glideslope angle on touchdown range is to reduce both mean and spread. However, the land short and long requirements are met for glide path angles between 6 and 9 degrees. Although performance with 6° or 9° glide path angles is somewhat degraded with respect to the nominal 7.5° , the touchdown sink rate, range, and pitch attitude requirements remain satisfied. However, there is a trend toward nosegear first touchdowns with the 9° glideslope angle. The flare attitude command (θ_{TD}^c) should be adjusted as a function of nominal glide path angle to eliminate this problem.

Heavy Weight Flight Condition

A gross airplane weight of 177929N (40,000 lbs) and 33.5 m/s (65 kts) trim approach speed have been utilized as the nominal flight condition. The off-nominal condition study included a flight condition based on 213515N (48,000 lbs) gross weight and 37.6 m/s (73 kts) approach speed. Stability derivatives for both flight conditions are tabulated in Appendix A.

Landing performance is summarized in Figure 5-20. Sink rate is shown in 5.15 m/s (10 kts) tailwind shear as this is the worst case for hard landings. Range is shown in 12.9 m/s (25 kts) headwind shear as this is the worst case for floating. The two sigma touchdown sink rate value increases slightly, from 1.57 to 1.62 m/s (5.15 to 5.3 fps), for the heavy weight flight condition. Range spread is increased from 91.4 to 103.6 m (300 to 340 ft). Performance requirements are met despite this slight degradation.

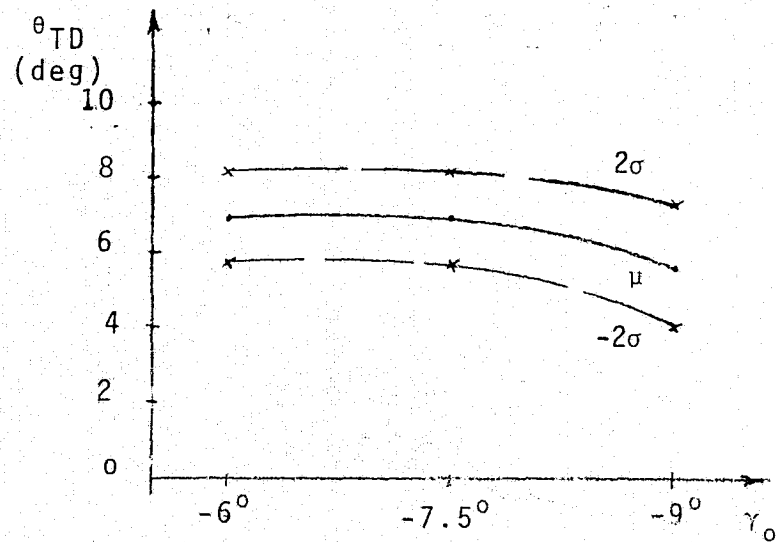
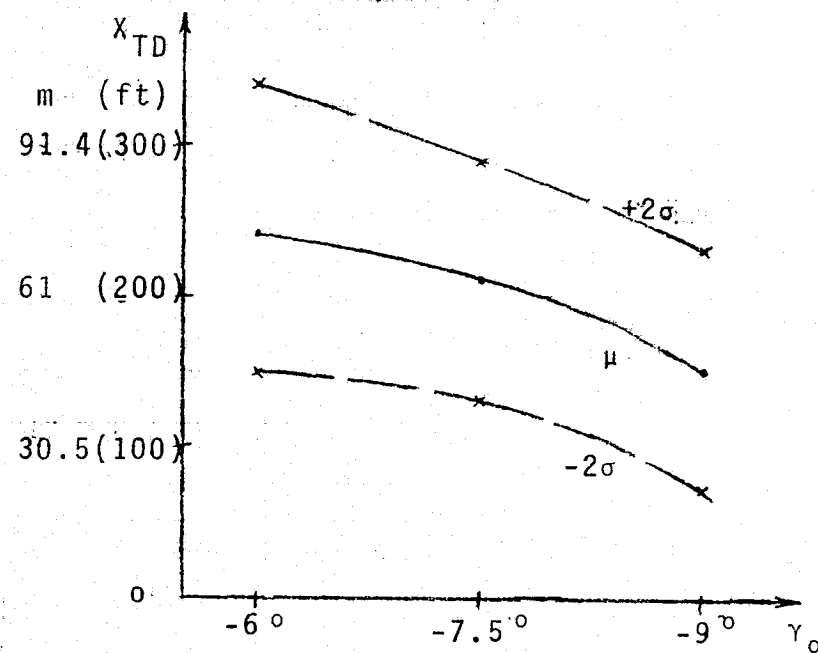
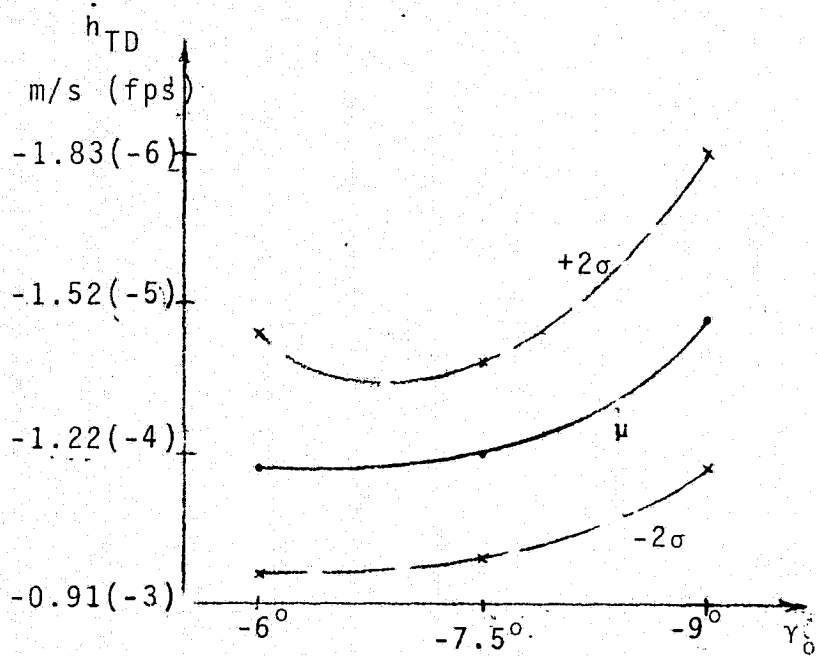


Figure 5-19. Effect of Glideslope Angle Variations

REPRODUCIBILITY OF THE
ORIGINAL PAGE IS POOR

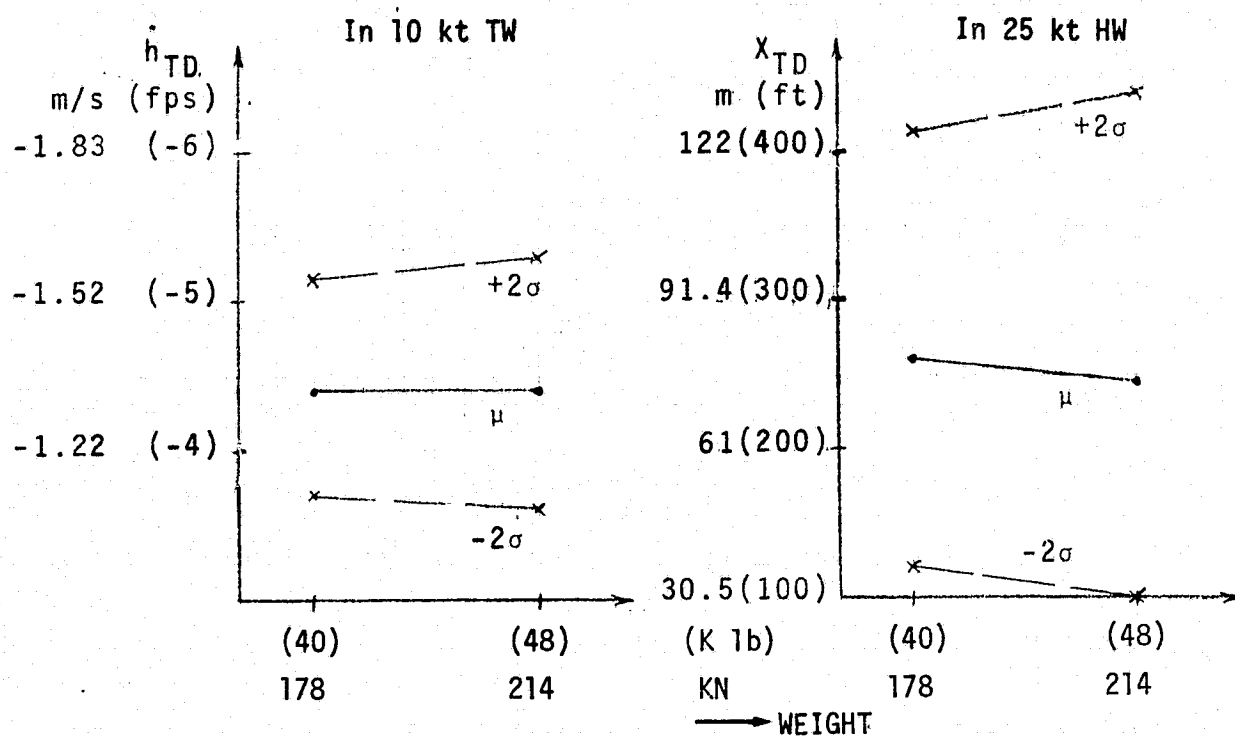


Figure 5-20. Effect of Aircraft Weight Variation

Terrain Irregularities

The impact of terrain geometry as shown in Figure 5-21 has been studied.

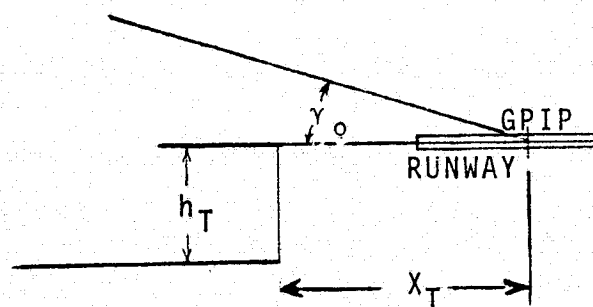


Figure 5-21. Terrain Step Geometry

This type of terrain shape affects the landing by causing a step in radio altimeter output, along with a transient in the derived altitude rate. Based on CTOL runway requirements, a value of 107 m (350 ft) was chosen for X_T , resulting in the step being inserted at a gear height above the runway of about 12.2 m (40 ft). Terrain step amplitudes (h_T) of 0, 6.1, 9.1 and 15.2 m (0, 20, 30, 50 ft) were evaluated. Figure 5-22 summarizes the impact on touchdown results.

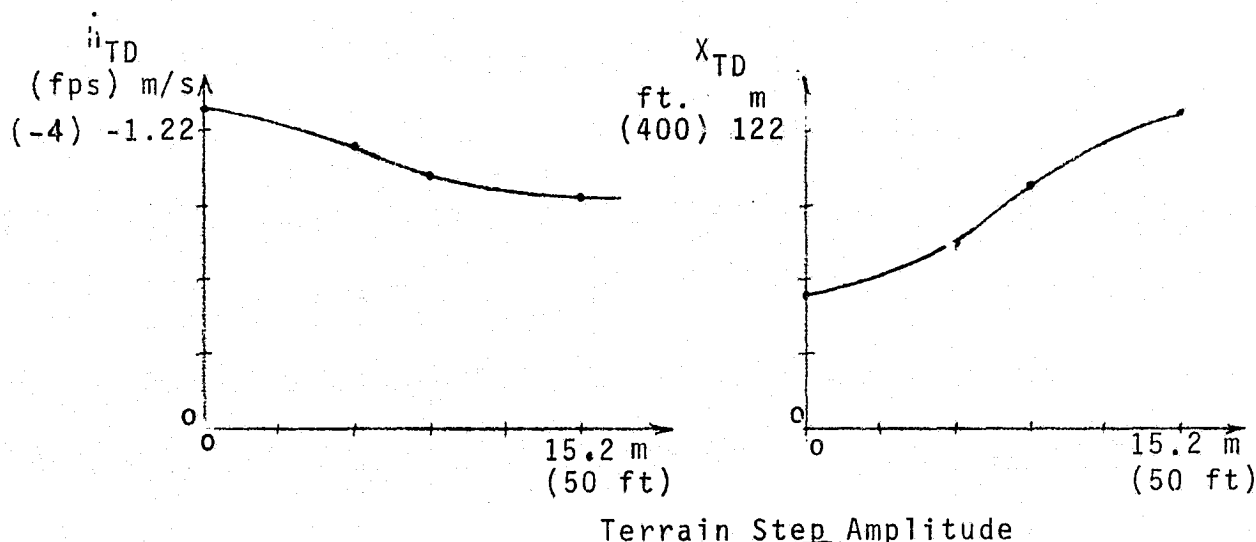


Figure 5-22. Effect of Terrain Steps

It may be concluded that even the 15.2 m (50') step has only a modest impact on landing performance, despite the associated 0.3 g vertical acceleration spike, and landing is completed within the required range and sink rate.

Ground Effect Variations

The pitch equations of motion used in this study included a ground effect as defined in Appendix A.

Landings in which ground effect was varied from zero to twice its nominal value were performed in order to evaluate the sensitivity of the system to such variations.

Figure 5-23 summarizes the effect of ground effect variations on touchdown performance in limiting turbulence.

The increased ground effect reduces the mean touchdown sink rate as expected from the increase in lift. Longer touchdown ranges are associated with the lower sink rates. Pitch attitude is reduced by about 2 degrees for each quantum increase of ground effect. This reduction results from the increased nose down pitching moment.

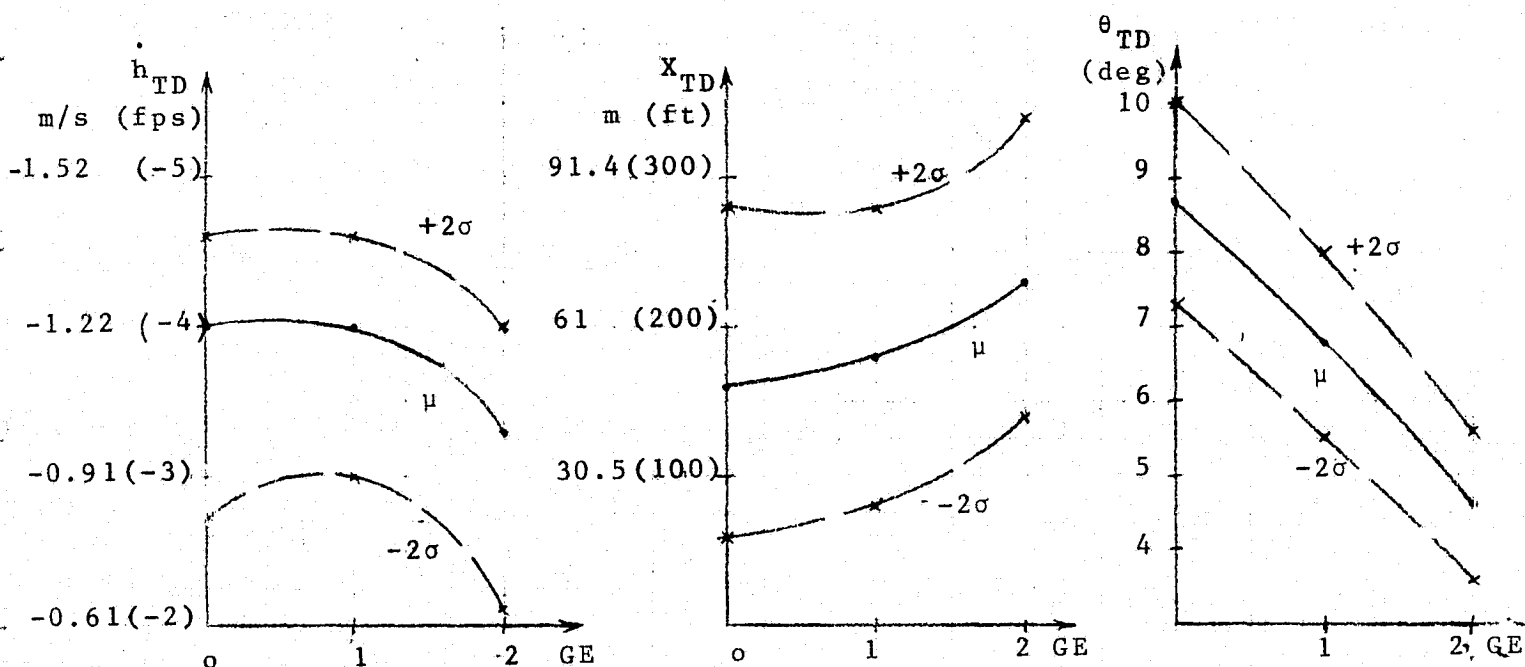


Figure 5-23. Effect of Ground Effect Variations

If the pitching moment ground effect turns out in flight tests to be stronger than nominally assumed, better control over touchdown pitch attitude may be obtained by increasing K_θ and K_q as discussed in Section 5.3. However, a stronger lift increase may warrant a reduction of pitch flare command in order to minimize floating.

Throttle Model Variations

The nominal throttle model that has been used in this study included $\pm 0.7\%$ RPM hysteresis. Variations of hysteresis amplitude and a different model including a 0.5 second delay were studied. The nominal model and the variations are described in Appendix A. The effect of the various models on performance is discussed here.

Figure 5-24 shows the effect of throttle hysteresis on landing performance, and Figure 5-25 compares results with $\pm 0.7\%$ hysteresis versus the 0.5 sec time delay model. Spreads are increased with the increase of hysteresis. The time delay model yields a lower mean sink rate and slightly reduced spread; in addition, the system's gain margin is lower than with the $\pm 0.7\%$ hysteresis. Thus, the throttle gain margins noted in flight should be used as a basis for selecting the final throttle gain.

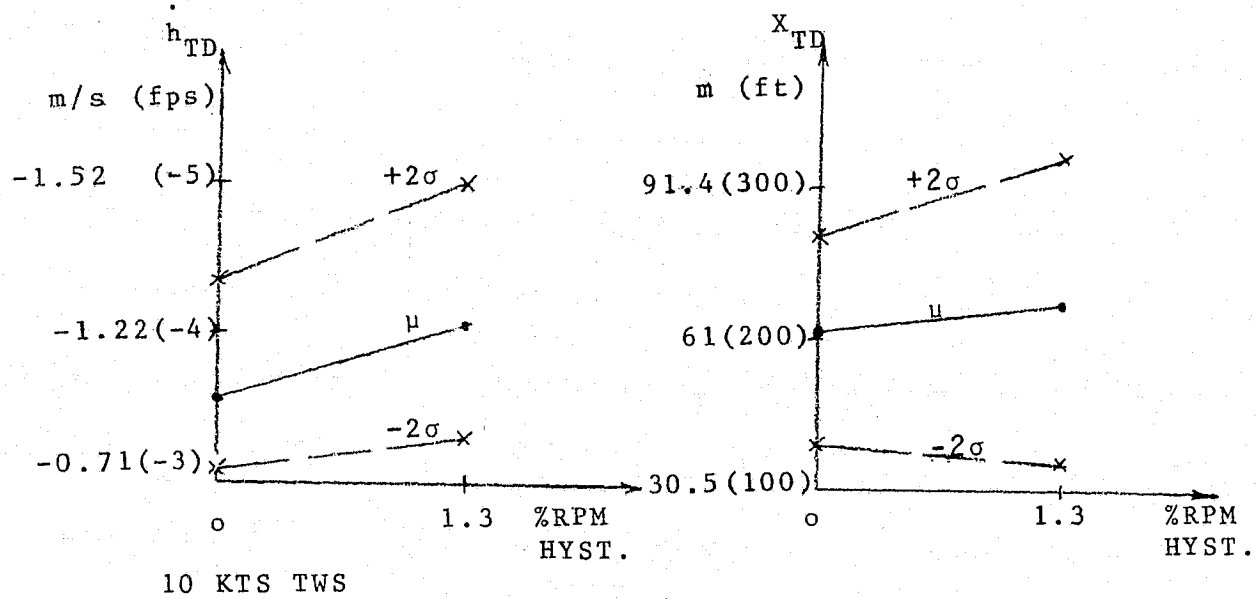


Figure 5-24. Effect of Throttle Hysteresis

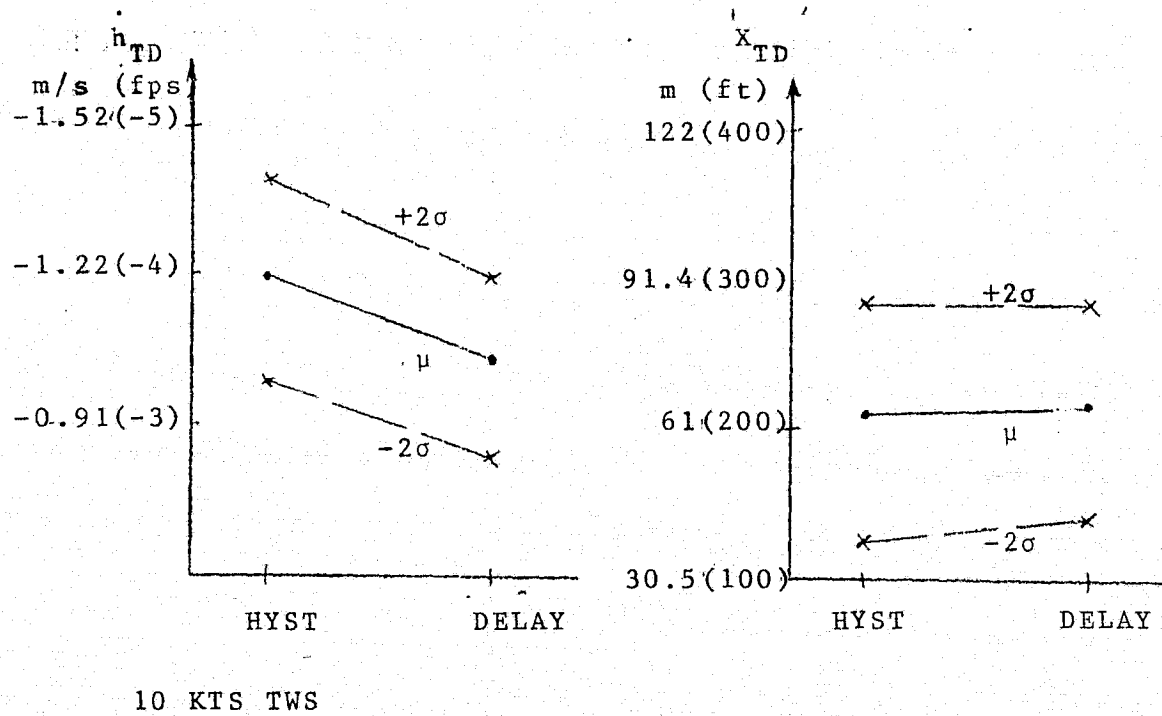


Figure 5-25. Effect of Throttle Dynamics

5.6 Failure Effects

Failures were introduced at various points in the system during landing approach in order to evaluate their impact. Detailed description follows:

MLS Beam

Limited hardovers of the beam error signal (Δh_b) were introduced at altitudes of 152, 61, and 30.5 m (500', 200' and 100'). The hardovers were limited to 15.2 m (50 ft) since that is the recommended Δh_b limit during glideslope track. With the recommended \dot{h}_{err} limit of ± 3 m/s (± 10 fps) and $K_h = 0.5$, these hardovers saturate \dot{h}_{err} such that larger hardover magnitudes would not result in more violent deviations.

Results are summarized in Figure 5-26 and time histories are shown in Appendix B. Pilot intervention is necessary to prevent a landing that is either very hard or short when the failure is applied at 152 or 61 m (500' or 200'). The low vertical acceleration allows sufficient time for recovery. The rate limit in the Δh filter is designed to slow down deviations resulting from failures of this type. Further improvement may be achieved by the use of a complementary beam filter, blending Δh and \dot{h} - then a beam failure indication may be used to switch the failed signal out, continuing to estimate Δh by a double integration of \dot{h} for a limited time in which corrective action may be taken.

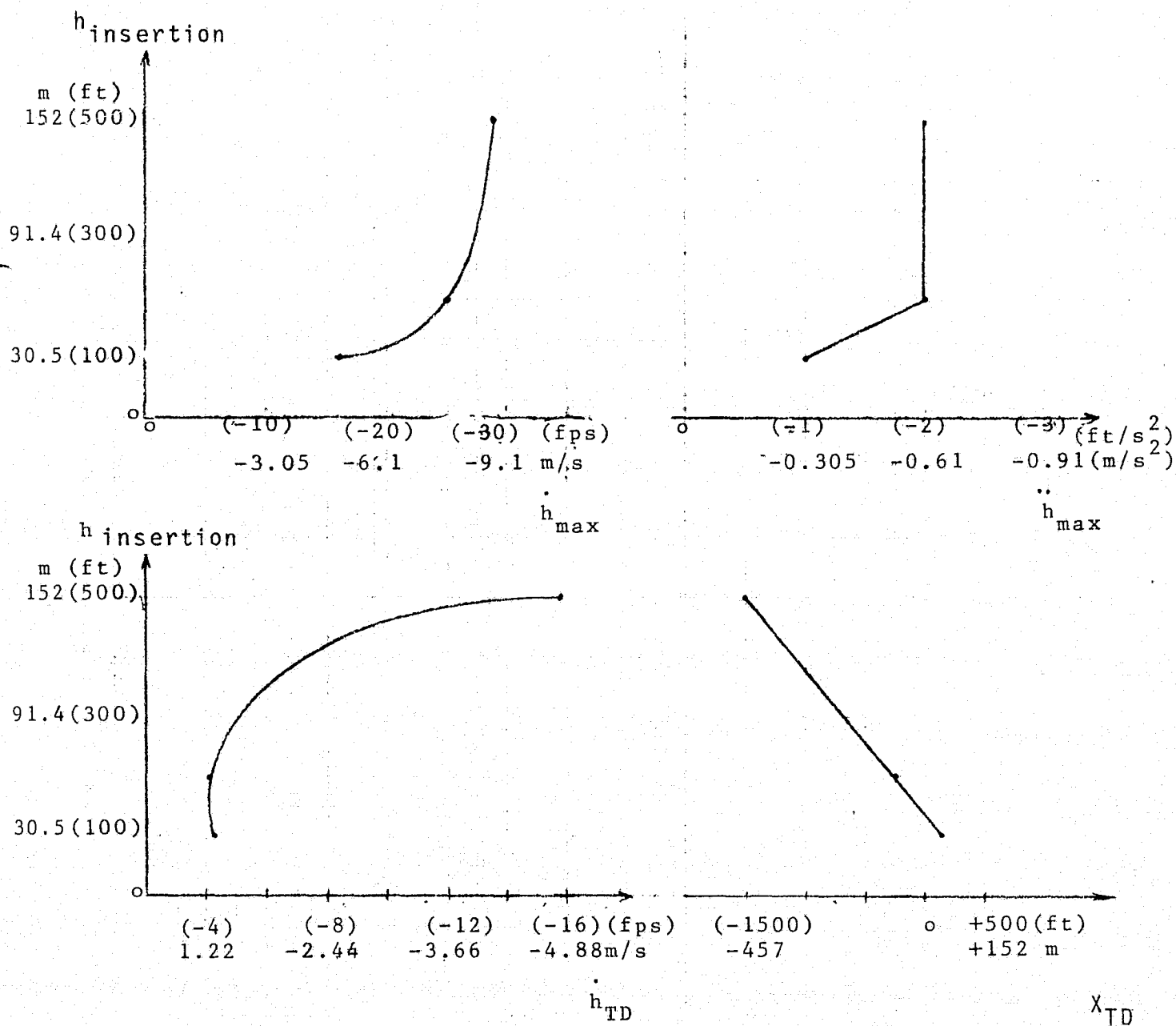
Pilot intervention is not required when the failure occurs at or below 30 m (100') as both touchdown sink rate and range are well within the acceptable boundaries.

Radar Altimeter Hardover

A radar altimeter hardover of 305 m (1000') magnitude was inserted at a gear height of 15.2 m (50'). Radar altimeter derived sink rate is used in the flare, and its altitude signal is used for flare initiation switching and gain scheduling. The failure induced rate of climb signal would cause aircraft controls to reduce lift - however, the radar altimeter controlled gain scheduler eliminates the faulty \dot{h}_{RA} from the system once the indicated radar altitude exceeds 15.2 m (50'). The net result is no flare and the airplane maintains its 4.42 m/s (14.5 fps) sink rate until it impacts the runway 8.38 m (27.5 ft) ahead of the GPIIP.

This is therefore a critical failure, requiring pilot intervention to prevent a hard landing.

A time history is shown in Appendix B.



NOTE: Hardovers of 15.2m (50 ft) were inserted at $h_{insertion}$ altitude.

Figure 5-26. Effect of Limited Beam Hardovers

The use of a vertical complementary filter in which h_{RA} and \ddot{h} are blended to compute h and \dot{h} may be useful in protecting against radar altimeter failures. Since a radar altimeter failure indication is typically available, the vertical filter can be mechanized such that the faulty h_{RA} signal is switched out and h and \dot{h} are estimated through integrations of \ddot{h} . As this would be done only during the time interval required for flaring, it is expected to result in a near nominal landing.

Normal Accelerometer

A hardover of 0.5g magnitude at 152m altitude (500 ft.) results in an increase of sink rate at 1.22 m/sec² (4 ft./sec.²). A maximum sink rate of 9.14 m/sec (30 fps) is attained unless the pilot intervenes. This failure becomes critical if it occurs at an altitude of 15.2m (50 ft.), as sink rate increases from 5.4 m/sec (14 fps) to 6.1 m/sec (20 fps) at touchdown within two seconds. An open of the normal accelerometer results in a mild instability. When it occurs at 152m (500 ft.), a slowly diverging oscillation results. At 15.2m (50 ft.), without pilot intervention, touchdown occurs at $\dot{h} = -0.76$ m/sec (-2.5 fps), $X = 163$ m (535 ft.).

Pitch Attitude

The effects of pitch attitude hardovers are summarized in Table 5-IV. Failures were evaluated without the pitch rate limiter shown in Figure 3-1.

TABLE 5-IV. PITCH ATTITUDE +20° HARDOVER EFFECTS SUMMARY

Failure altitude m (ft)	152 (500)	15.2 (50)
Extreme pitch attitude (deg)	-20	-20
Extreme angle of attack (deg)	-20	-20
Max sink rate m/s (fps)	5.8 (19)	4.9 (16)
Max vertical acceleration m/sec ² (ft/sec ²)	-1.52 (-5)	0.914 (-3)
Time to reach max sink rate (secs)	2	2.5

This failure is critical, especially at 15.2m (50 ft.). A rate limiter of $\pm 50^\circ/\text{sec}$ above 15.2m (50 ft.) and $+7.50^\circ, -20^\circ$ below 15.2m (50 ft.) on pitch rate (as shown in Figure 3-1) is incorporated in order to slow down development of failure transients.

Pitch attitude open at 152m (500 ft.) does not present any problem. The airplane keeps tracking the glide slope, flares and touches down at $\dot{h} = -1.19 \text{ m/s}$ (-3.9 fps), $X = 76.2\text{m}$ (250 ft.).

Pitch Rate

Pitch rate failures are not critical. Pitch damping is, of course, reduced; however, the airplane lands at reasonable sink rate and range.

Time histories are shown in Appendix B.

5.7 Limitations

In order that the required performance be obtained, some limitations have to be imposed on operational conditions and system elements. These limitations are discussed in this section.

Winds, Shear, and Turbulence

An integrated atmospheric disturbance model was used in this study. The total mean wind level (WINDV) also defines the horizontal gust amplitudes while the mean downwind (U) and crosswind (V) components determine the shear levels. A fixed level of vertical turbulence is used, as specified in FAA AC 20-57A. A more detailed wind model is presented as Figure A-11 in Appendix A.

For most of the stochastic longitudinal landing performance evaluation, limiting levels of total wind and downwind were used, with associated turbulence and shear. These limiting levels were 12.9 m/sec (25 kt) total wind, +12.9 m/sec (+25 kt) headwind, and -5.15 m/sec (-10 kt) tailwind. For these mean wind levels, the corresponding turbulence and shears are:

Vertical turbulence $\sigma_w = 0.76 \text{ m/sec}$ (2.54 fps)

Horizontal turbulence $\sigma_u = 0.15 \text{ WINDV}$

Shear gradient $K_s = 0.0131 \text{ 1/m}$ (0.004 1/ft.)

or Headwind shear = 0.169 1/sec (10 kt/100 ft.)

Tailwind shear = 0.0676 1/sec (4 kt/100 ft.)

Statistical landing performance was evaluated with increased levels of total wind and downwind to determine the maximum wind levels which could be effectively handled by the landing system. For both headwind and tailwind, the first landing criteria to be violated was $X_{TD} > 283\text{m}$ (929 ft.) on a 10^{-6} basis. Thus the longitudinal landing system provides effective touch-down control for headwinds to 15.4 m/sec (30 kt) with 30 kt total wind and tailwinds to 8.7 m/sec (17 kt) with 17 kt total wind. As discussed in Section 6, a 7.7 m/sec (15 kt) crosswind limit was defined for the lateral landing system. These limiting wind levels are summarized pictorially in Figure 5-28.

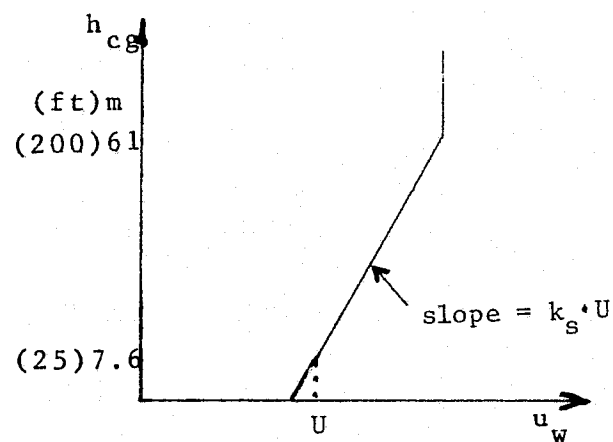


Figure 5-27. Wind Shear Profile

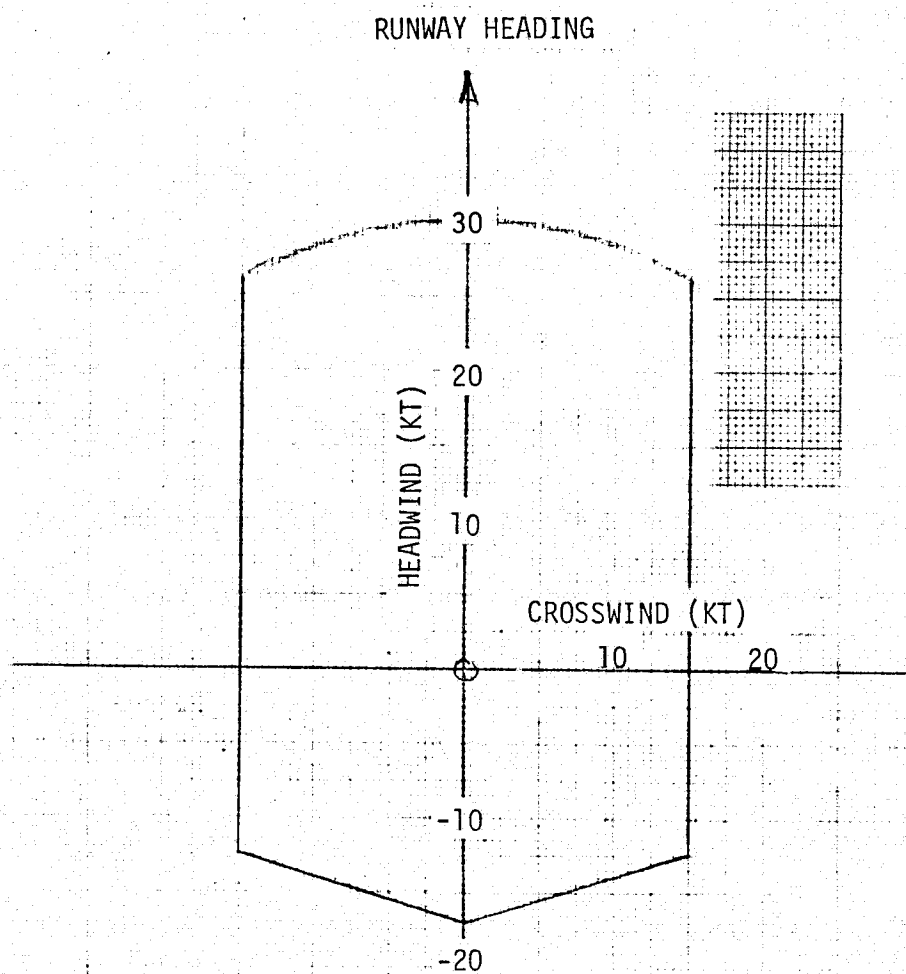


Figure 5-28. Limiting Wind Levels

Throttle Authority and Dynamics

Nominal values of +4.5 percent RPM (increase) or -3 percent RPM (decrease) were assumed throughout this study. Those values correspond to +0.31 and -0.21g normal acceleration in the nominal 33.5 m/s (65 Kts) flight condition. No problem seems to be caused by the upper limit as indicated by the tight sink rate control that is obtained and the absence of bends towards high sink rates in the probability distribution plots. However, the limited lift reduction capability gives rise to a floating tendency as shown in Figure 5-29. For the occasional large headwind gusts, sink rate is reduced below the commanded value; then the throttle/choke combination has insufficient authority to overcome the wind-induced excess lift, thus yielding a very long touchdown.

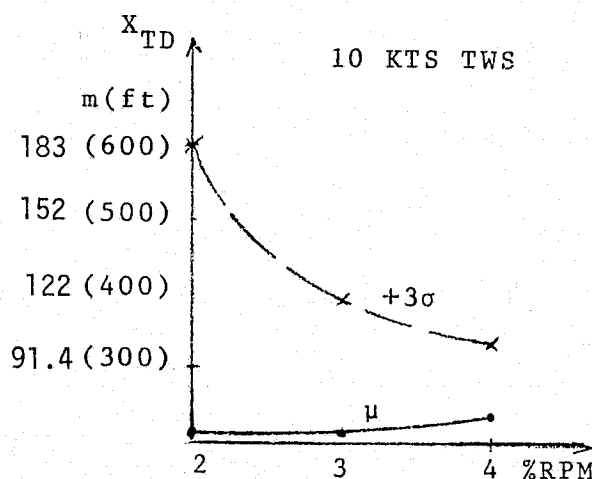


Figure 5-29. Effect of RPM Retardation Limit

A 3 percent RPM reduction limit is sufficient for the performance requirements to be met. With a 2 percent limit the probability for $X_{TD} > 1000$ ft. exceeds the required value of 10^{-6} in a 5.15 m/s (10 Kts) tailwind shear and turbulence corresponding to 12.9 m/s (25 Kts) of total wind.

The nominal throttle and engine dynamic model used in this study is described in Appendix A. The throttle is the major flight path controller, assisted by the DLC chokes. This leads to a situation in which a significant degradation in throttle and engine dynamics may result in performance degradation or even instability.

Approach Glide Slope Angle

The effect of varying the nominal 7.5° glide slope to 6° or 9° is discussed in Section 5.5. However, one of the results constitutes an operational limitation and is therefore reiterated here. With a six degree glide

slope, 5.15 m/s (10 Kts) tailwind, and turbulence corresponding to 12.9 m/s (25 Kts) total wind, the probability of $X_{TD} > 1000$ ft. is barely below 10^{-6} . Therefore six degrees is the shallowest glideslope with which performance requirements are met. This floating tendency occurs only at the low probability region of the distribution curve. The 2σ requirements are comfortably met with the six degree slope in 5.15 m/s (10 Kts) tailwind. As discussed in section 5-5, an adaptive flare attitude command [$\theta_{TD}^C = f(\gamma_0)$] would also tend to minimize floating for shallower glide path angles and thus ameliorate this limitation.

5.8 Display Concepts

The main objective of the display during an automatic landing approach is to help the pilot monitor the operation of the autopilot. In the event of a failure, the display should help the pilot in making a decision to take over command of the airplane, and in identifying the required corrective control action.

The nature and complexity of the display should be closely related to the safety and redundancy scheme of the flight control system. In a fail operational system, in which the pilot is not required to intervene even after a failure has occurred, a very simple failure annunciator may be sufficient. However, in a nonredundant system such as the present experimental Augmentor Wing Autopilot, a more elaborate display is necessary.

A simple display that could be easily implemented in the Augmentor Wing instrumentation is suggested. Monitoring of system errors is the basic idea. System errors in the glide slope tracking phase are deviation from the glide slope, and speed error. The existing EADI is equipped with path deviation and speed error indicators and both signals are directly available in the autopilot. Most autopilot or sensor malfunctions should result in an unusual increase in error which the pilot should be able to detect.

At the flare altitude, the advanced control laws call for a linear reduction of sink rate with altitude. Since the existing EADI displays actual flight path angle, it is suggested to include an additional bar that will represent the commanded flight path angle. The position of this bar will be computed on the basis of the autopilot \dot{h}_{err} signal. The vertical displacement between the two bars will represent the flight path error, and an autopilot or sensor failure will cause this displacement to increase. Also the position of the γ^C bar will provide a natural indication of system performance since it should be close to the actual glide path bar prior to the flare and thereafter move gradually up as altitude decreases to touchdown. Critical sensor failures will cause a drastic change in this pattern which should be readily detected by the pilot.

Potentially hazardous sensor hardovers (Δh_B , \ddot{h} , θ , u) will cause a large error and thus be readily detected on the display. However, there are some potentially hazardous failures which require different means of detection. A passive beam failure will not be detected on the display since beam error would constantly be at zero. This failure may be detected by the deviation from the nominal flight path angle. Radar altimeter hardover prevents flare and is not readily detectable on the display since γ error is constantly zero. Detection of this failure may be accomplished through pilot constant monitoring of the radar altimeter indication or automatically by the use of a monitor comparing baro altitude with radar altitude. Both signals will have to be washed out and lagged to avoid offset and terrain irregularities from tripping this monitor. A pitch attitude passive failure may lead to excessive rotation in the flare and it may not be readily detected on the display. The pilot has to monitor angle of attack in order to be able to detect this problem. An airspeed passive failure may cause an airspeed departure which will not be detectable on the display. Pilot monitoring of raw airspeed should be used to eliminate this situation. The detectability of all above mentioned failures is summarized in Table 5-V.

The detection problems discussed here exemplify the inherent difficulties of in-line monitoring without having redundancy in sensor information.

TABLE 5-V. SENSOR FAILURE DETECTABILITY

<u>Sensor</u>	<u>Failure</u>	<u>Hazard</u>	<u>Detection</u>
Δh_B	H.O.	Critical @ $h > 150$ ft	Yes
	Passive	Bad	No
h_{RA}	H.O.	Critical	No
	Passive	O.K.	No
\ddot{h}	H.O.	Critical	Yes
	Passive	Mild	Yes
θ	H.O.	Critical	Yes
	Passive	Bad (Over rotation)	No
q	H.O.	O.K.	No
	Passive	O.K.	No
u	H.O.	Critical	Yes
	Passive	Bad	No

Additional information that should be considered for display is engine RPM situation with respect to the autopilot authority limits, and the DLC chokes position with respect to their limits. This will help the pilot determine whether the system moves the controls in the right direction, as indicated by the error signals. It will also indicate the limiting of RPM which may be a factor in a pilot's decision to assume control.

The display concepts that have been discussed so far were of the type pertaining to the present state of the aircraft and autoland system. Various predictions may be made through computations based on present data, and these may also be candidates for display. Predictions that may be useful include:

1. Predicted sink rate at touchdown, based on current altitude, sink rate, vertical acceleration, and estimated external disturbances.
2. Predicted touchdown point, based on the previously computed sink rate time history, current position, ground speed, and estimated external disturbances.
3. Compute sink rate at touchdown assuming that a large predetermined fraction of the lift increase capability currently available is applied. Sound go-around alarm when this sink rate turns out to be larger than a predetermined limit.

6.0 LOCALIZER TRACK AND RUNWAY ALIGNMENT

For good lateral automatic landing performance, the runway alignment maneuver must be initiated with the aircraft stabilized on beam centerline. Thus the design of a stable, tight localizer track mode is a necessary prerequisite to defining an advanced automatic decrab control system. Even for close in curved path approaches, the capture algorithm will place the aircraft on the localizer sufficiently early to allow transients to settle. Since the capture will have no impact on landing performance, it is not considered in this study. For Category IIIA landings, automatic roll-out guidance is not required, and it also is not included in this study.

6.1 Candidate Control Algorithms

6.1.1 Runway Alignment

During the critical last few seconds before touchdown, the aircraft's heading must be aligned with the runway, with touchdown on the centerline at a low, controlled roll attitude and side velocity to preclude hazard potential and promote passenger comfort. On the Augmentor Wing Vehicle, two controllers are available: the rudder for yaw control and the wheel which provides roll control through a fixed combination of aileron, choke, and spoiler deflection. For runway alignment the essential tradeoff was between the flat decrab and forward slip maneuvers.

The runway alignment algorithm currently implemented in the Aug Wing vehicle is typical of the flat decrab systems. A simplified diagram is included as figure 6-1. Prior to runway alignment, lateral position error, rate, and acceleration are processed to generate the roll command, while the rudder provides yaw damping and turn coordination, and course datum error is not directly utilized. When the align mode is initiated just a few seconds before touchdown (4.88m or 16 ft. of radar altitude in this instance), the following sequence is initiated:

1. The localizer computations to roll are opened, thus no longer providing closed loop beam guidance.

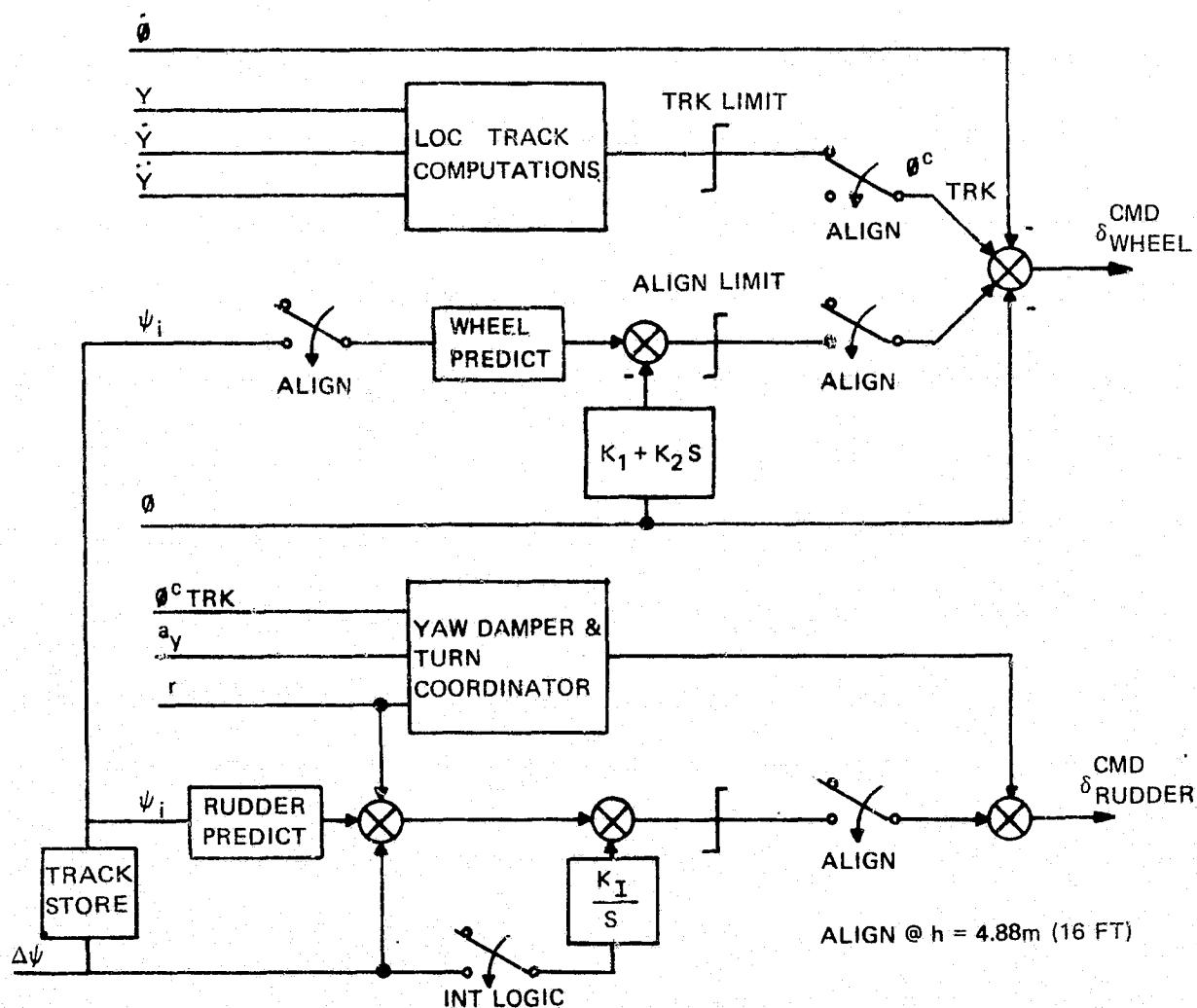


Figure 6-1. FLAT DECRAb Simplified Block Diagram

2. An open loop rudder predict command based on memorized prealign course error is immediately inserted, along with an open loop wheel predict command and higher roll attitude and rate gains in an attempt to cancel rudder induced rolling moments and cross-track acceleration.
3. In addition, proportional plus delayed integral course datum error is inserted into the rudder to improve heading control, with increased yaw rate gain to maintain stability.

As expected from the preponderance of open loop commands typical of the flat decrab system, initiation timing and variations in aircraft/wind states can significantly impact landing performance.

A simplified block diagram of the forward slip system is shown as figure 6-2. Prior to alignment, the localizer track law is identical to the other system. The noncritical timing of the forward slip allows initiation at a comfortable altitude (45.72m or 150 ft in this case), causing the following sequence:

1. The localizer computations to roll are maintained to provide closed loop beam control through touchdown.
2. The course datum error signal, processed to provide a controlled heading error trajectory, provides high gain proportional plus integral commands to the rudder to effect the alignment.
3. Cross-track acceleration modifies the roll command to provide the wing-down attitude required to cancel the wind-induced side force.

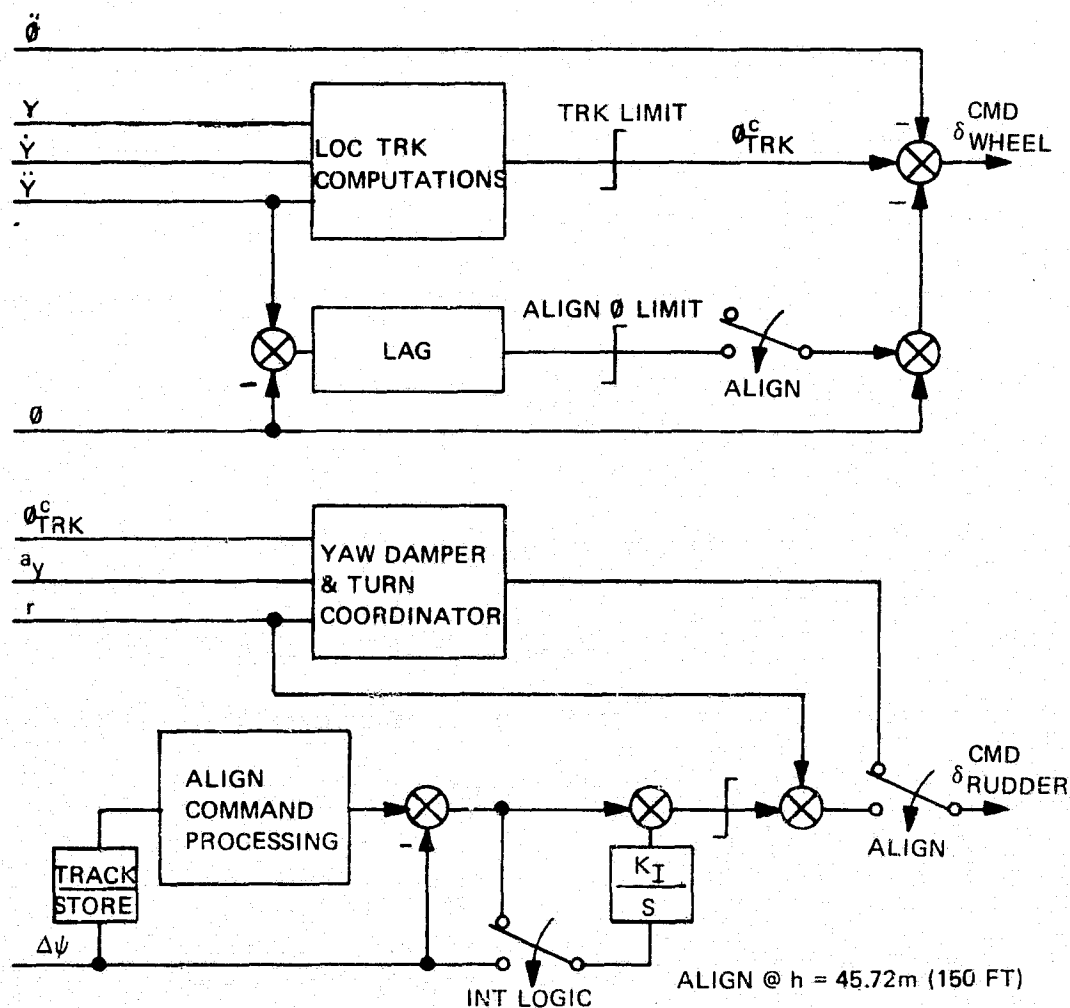


Figure 6-2. FORWARD SLIP Simplified Block Diagram

4. Closed loop control of both beam deviation and course datum error is used throughout the align maneuver.
5. Since abrupt yaw corrections are not performed, no open loop predict terms are required to augment the basic system closed loop bandwidth.

The alignment initiation timing is not critical, and touchdown performance is less dependent on vehicle and wind variations.

Once the preferred runway alignment technique was selected, several minor algorithm variations were considered to optimize landing performance. Three further tradeoffs were considered:

1. A rate limited align entry versus a reference heading trajectory, as indicated in figure 6-3.
2. Computed crosswind to provide a rudder predict term versus the closed loop control which became practical with the use of a reference heading trajectory, as shown in figure 6-4.
3. Rudder crossfeed versus cross-track acceleration (figure 6-5) to maintain the required wing down compensation during the forward slip maneuver.

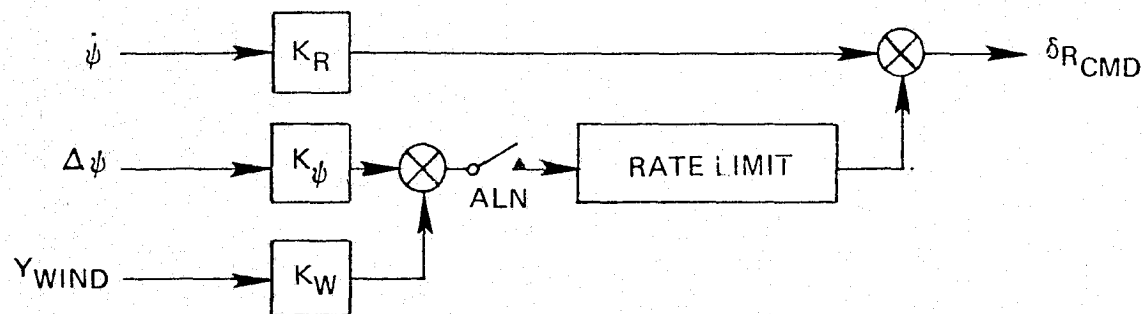
6.1.2 Localizer Track

Although a stable, tight localizer track phase is desired prior to alignment, its impact on landing performance is not as direct. Thus, less emphasis was given to beam track tradeoffs, and only two areas were considered:

1. Derivation of lateral position and rate signals from acceleration augmented MLS versus unaugmented MLS versus accelerometer derived rate, as shown in figure 6-6.
2. Use of roll attitude and rudder to eliminate the lateral accelerometer.

All these tradeoffs are discussed in detail in section 6.3 and Appendix C, along with some relatively minor system variations which can also impact automatic landing performance.

RATE LIMITED ENTRY



REFERENCE HEADING TRAJECTORY

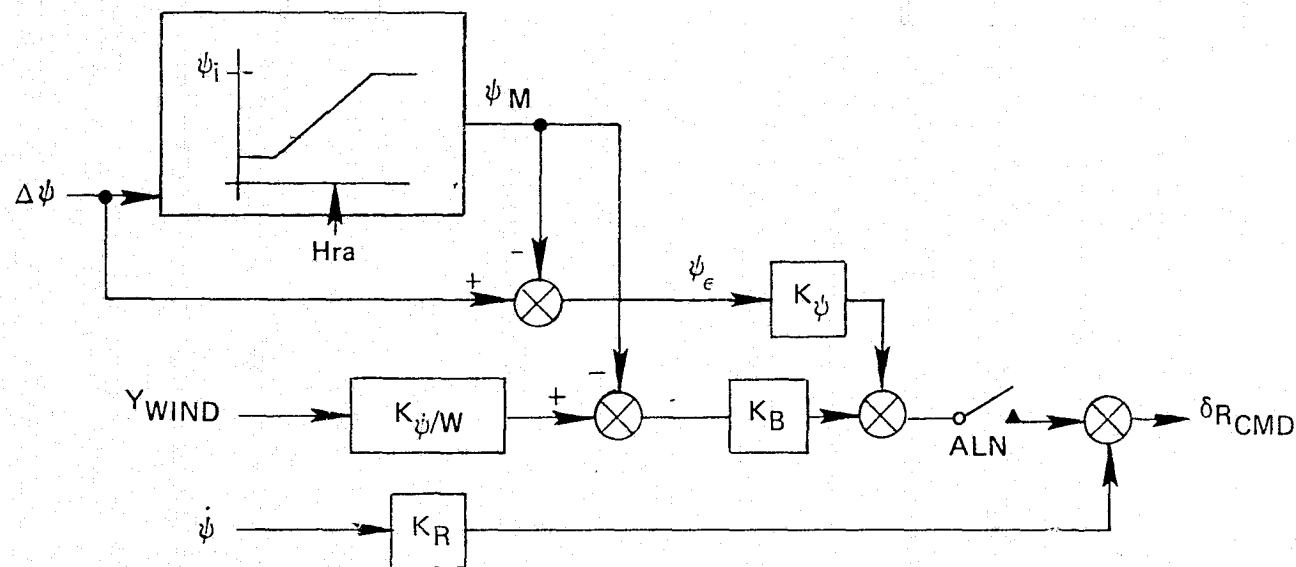
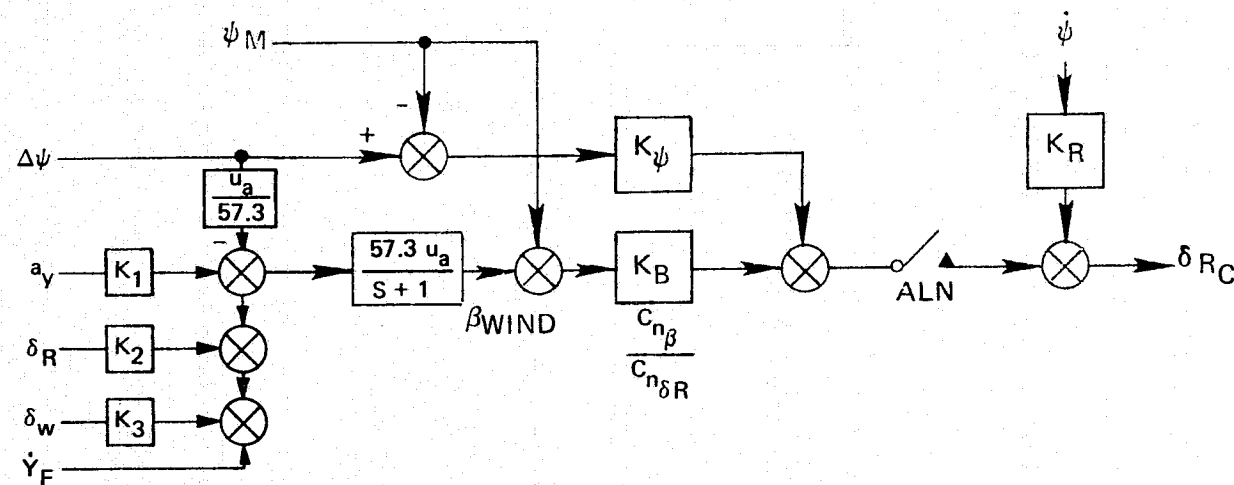


Figure 6-3. Align Entry Candidate Systems

RUDDER BIAS FROM COMPUTED CROSSWIND



CLOSED LOOP RUDDER CONTROL

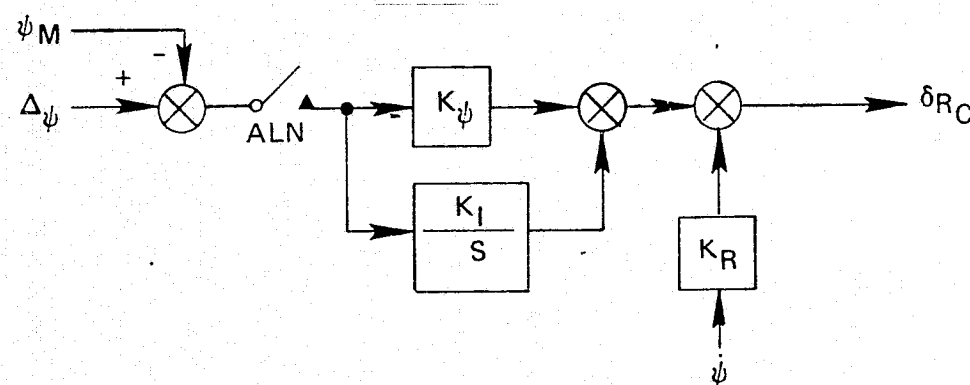


Figure 6-4. Rudder Bias Generation Tradeoff

ACCELEROMETER REFERENCED ROLL CONTROL VS. RUDDER CROSSFEED

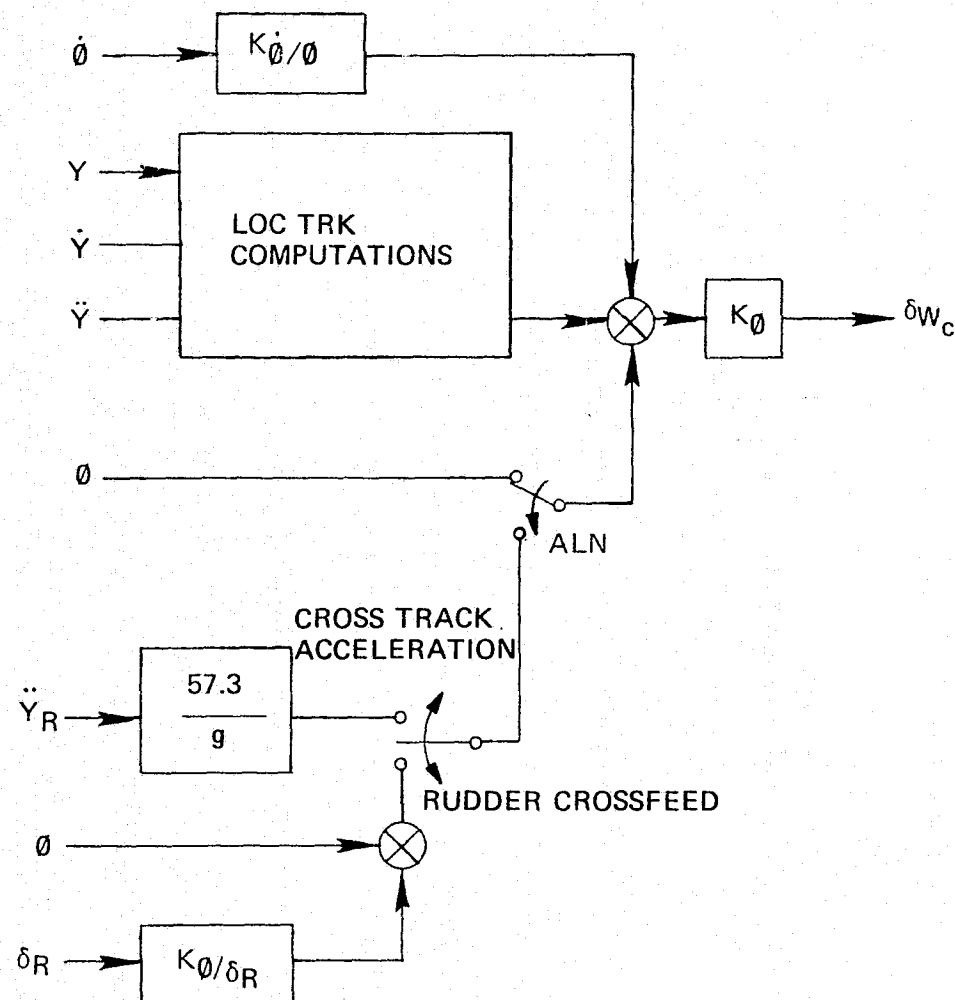


Figure 6-5. Wing Down Compensation Candidates

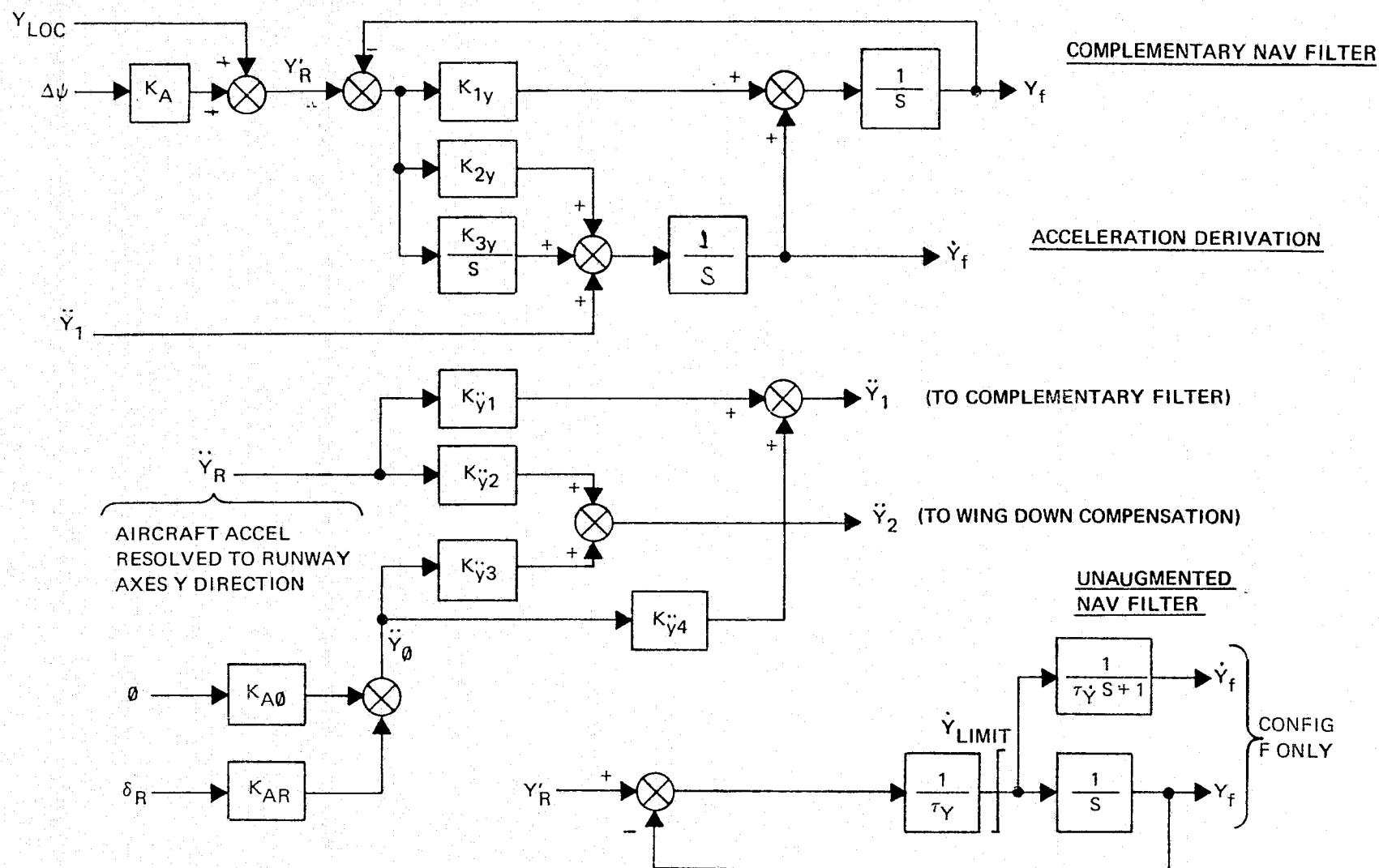


Figure 6-6. Lateral Position, Rate, and Acceleration Candidates

6.2 TRADEOFF CRITERIA

Many factors were considered during the extensive tradeoff studies which led to the recommended system definition. These performance evaluation criteria are discussed below.

1. Landing performance in stochastic and deterministic disturbances is the main indicator of system adequacy. The important lateral landing performance indicators are lateral displacement, velocity, drift angle, and roll attitude at touchdown, and beam deviation at the 30.48m (100 ft) approach window. Each candidate system must meet the performance requirements defined in section 4 under the disturbance conditions specified in Appendix A.
2. Control surface activity in stochastic atmospheric and MLS disturbances should be minimized, especially in the frequency range beyond the bandwidth of the landing system.
3. Sensitivity of the system to tolerances, errors and off-nominal conditions are to be a design consideration, since an appreciable performance degradation due to these variations could yield noticeably degraded landing performance over the "total population" environment.
4. Pilot acceptability and monitoring compatibility. The landing system should be compatible with manual control techniques and should not yield any unexpected or confusing control inputs, with maneuvers executed to allow time for effective pilot monitoring or override as required. Three items are of specific interest during runway alignment from a pilot preference viewpoint: maneuver initiation prior to decision altitude allows a safe early evaluation of the alignment, overshoot of the runway heading during decrab should be avoided, and overshoot of the bank angle required to provide the crosswind compensation should not occur.
5. Response (or susceptibility) to engine failure and MLS failures will be considered. As a minimum, the landing system should not aggravate engine out performance and should minimize the effects of any single sensor failure.
6. Ride quality is of considerable importance in commercial aircraft. Configurations that attenuate aircraft acceleration, rate, and attitude responses to atmospheric disturbances are preferred. Also, abrupt or other types of maneuvers which produce significant accelerations or attitude changes are undesirable.

One quantitative index of performance to be used will be RMS response of roll attitude and lateral acceleration to turbulence and beam noise inputs.

7. System complexity should be avoided unless a very definite performance improvement can be shown to result from the additional complexity. Such tradeoffs will be identified as possible options.

6.3 SYSTEM OPTIMIZATION

The tradeoffs that led to the recommended lateral landing system are described in this section. A detailed description of the seventeen different configurations that were statistically evaluated is given in Appendix C. These variations fall under the following seven categories.

1. Runway alignment configuration
2. Align entry command
3. Rudder bias generation
4. Wing down compensation
5. Crosstrack rate derivation
6. Lateral acceleration
7. Other variations (antenna location, gains, washouts)

In the following discussion, frequent reference is made to the system variations defined in Appendix C.

Runway Alignment Configuration

The runway alignment algorithm currently implemented in the Aug Wing vehicle was used as a representative example of a flat decrab configuration. This is an apt choice, since this control law has been optimized for the Aug Wing vehicle peculiarities and will provide a baseline against which to compare forward slip align performance. This basic tradeoff was made early in the program, with configurations A and B representing the flat decrab and the basic forward slip respectively. The conclusions drawn from the comparison were reconfirmed later with configurations R and P which are updated and refined versions of the flat decrab and forward slip techniques.

The performance of the flat decrab and forward slip align system was evaluated in limiting (15 knot) crosswind, shear, turbulence and MLS disturbance levels as defined in Appendix A, for longitudinal mean winds of 0, +25, and -10 knots. The resulting touchdown distributions of the critical landing performance indicators (Y , \dot{Y} , $\Delta\psi$, θ) for these two configurations is summarized in figure 6-7. Since the localizer track law is essentially the same, the beam deviation at the approach (30.48m or 100 ft) window is nearly identical for both systems. However, lateral deviation, lateral rate, and heading error

FLAT DECRAB (#R)

FORWARD SLIP (#D)

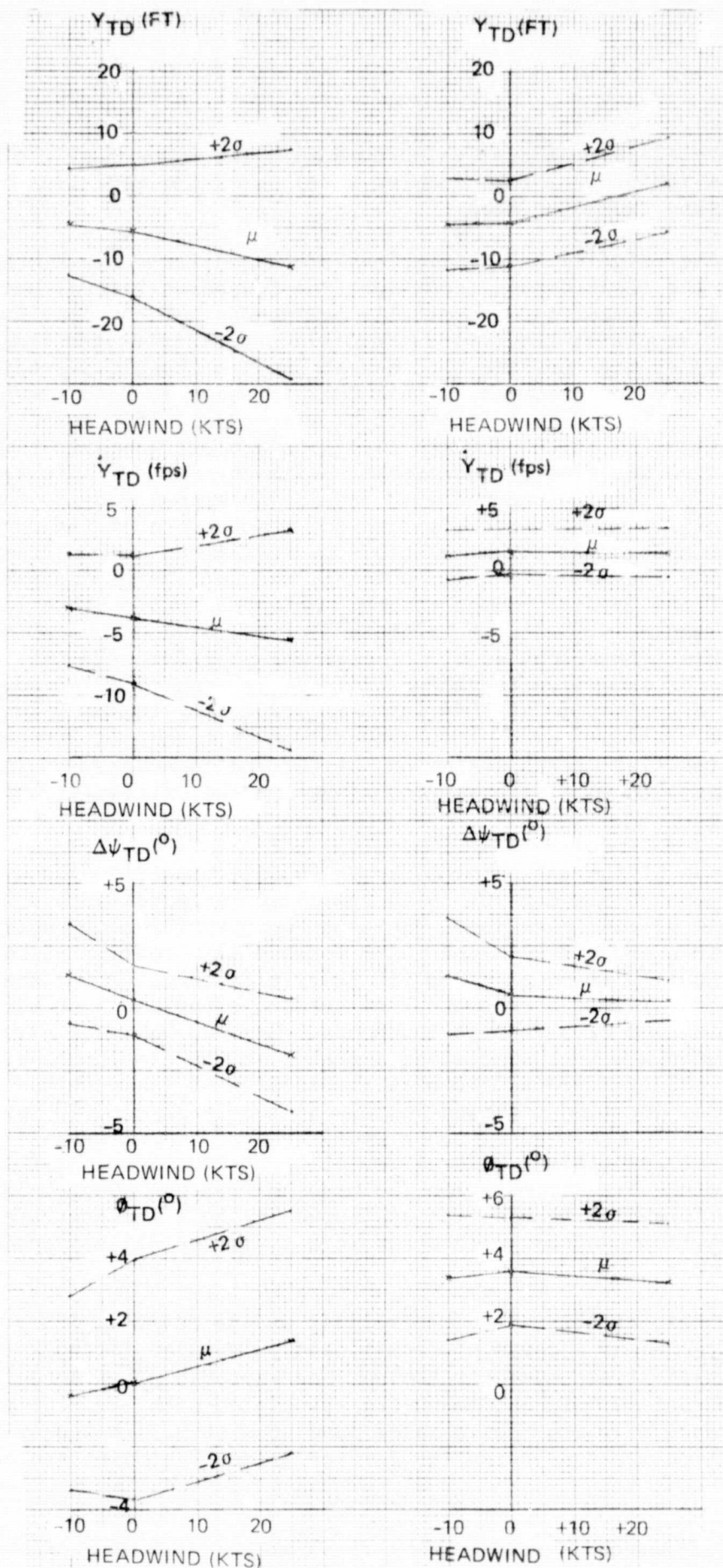


Figure 6-7. Flat Decrab & Forward Slip Stochastic Performance Summary
6-11

REPRODUCIBILITY OF THE
PAGE IS POOR

at touchdown are all significantly improved with the forward slip alignment (by more than a factor of 2 for headwind case) as is the variation of touchdown roll attitude about the mean.

Several other significant conclusions are drawn from this stochastic landing data. For the forward slip technique, the touchdown lateral position and rate variations are small and essentially independent of the longitudinal wind condition which regulates the vertical profile and dictates the timing of the alignment maneuver; however, the flat decrab shows a drastic degradation in landing performance for headwind, with a 200% increase in 2σ dispersion (10.97m or 36 ft) compared to the zero longitudinal wind case. This demonstrates the relative insensitivity of the forward slip to alignment maneuver timing, in direct contrast to the flat decrab system. With the forward slip system, touchdown heading dispersion is reduced with increasing headwind since the longer time in align allows accurate acquisition and maintenance of the runway heading. In tailwinds, improvements may be possible by initiating the mode somewhat earlier or increasing the course datum gain, but this was not deemed desirable or necessary in view of the good alignment accuracy obtained. Although a larger mean touchdown bank angle is needed to maintain the wing down compensation in the forward slip case, variations about the mean are significantly reduced. Thus the probability of excessive touchdown attitude is dramatically reduced (by several orders of magnitude at 10^0), as demonstrated by the bank angle distribution curve of figure 6-8. This degradation in touchdown performance with headwinds for the flat decrab system points out the inadequacy of the open loop predict terms to cope with varying winds and the criticality of the align maneuver timing.

A comparison of the alignment maneuver in deterministic wind disturbances is given in figures 6-9 and 6-10. Although these responses were obtained with the early (A and B) configurations, the align maneuvers are characteristic of the flat decrab and rate-limited-entry forward slip configurations. For the flat decrab, the initiation at 4.88m (16 ft) yields abrupt wheel and rudder responses with relatively good control of heading error and poor control of lateral deviation and rate through touchdown. One run was made with no termination at touchdown, thus simulating a change in the time profile from align to touchdown — this yielded a dead beat acquisition of the required runway heading while lateral position diverged rapidly at nearly 3m/sec (10 fps). The rate limited forward slip produced smoother wheel and rudder motions, to yield good heading alignment and minimal lateral deviation at touchdown, at the expense of some (28%) wing down compensation and heading (7%) overshoot. The data obtained without landing termination at touchdown shows the accurate heading and lateral position control which makes this system relatively insensitive to timing variations.

Based on these results, the forward slip was selected as the preferred runway alignment technique because of significantly improved touchdown performance, relative insensitivity to maneuver timing, and improved pilot acceptability by avoiding the abrupt last second maneuvers associated with the flat decrab. In summary, a forward slip provides a safer landing system. Thus only the forward slip configuration was considered for further tradeoff studies and optimization.

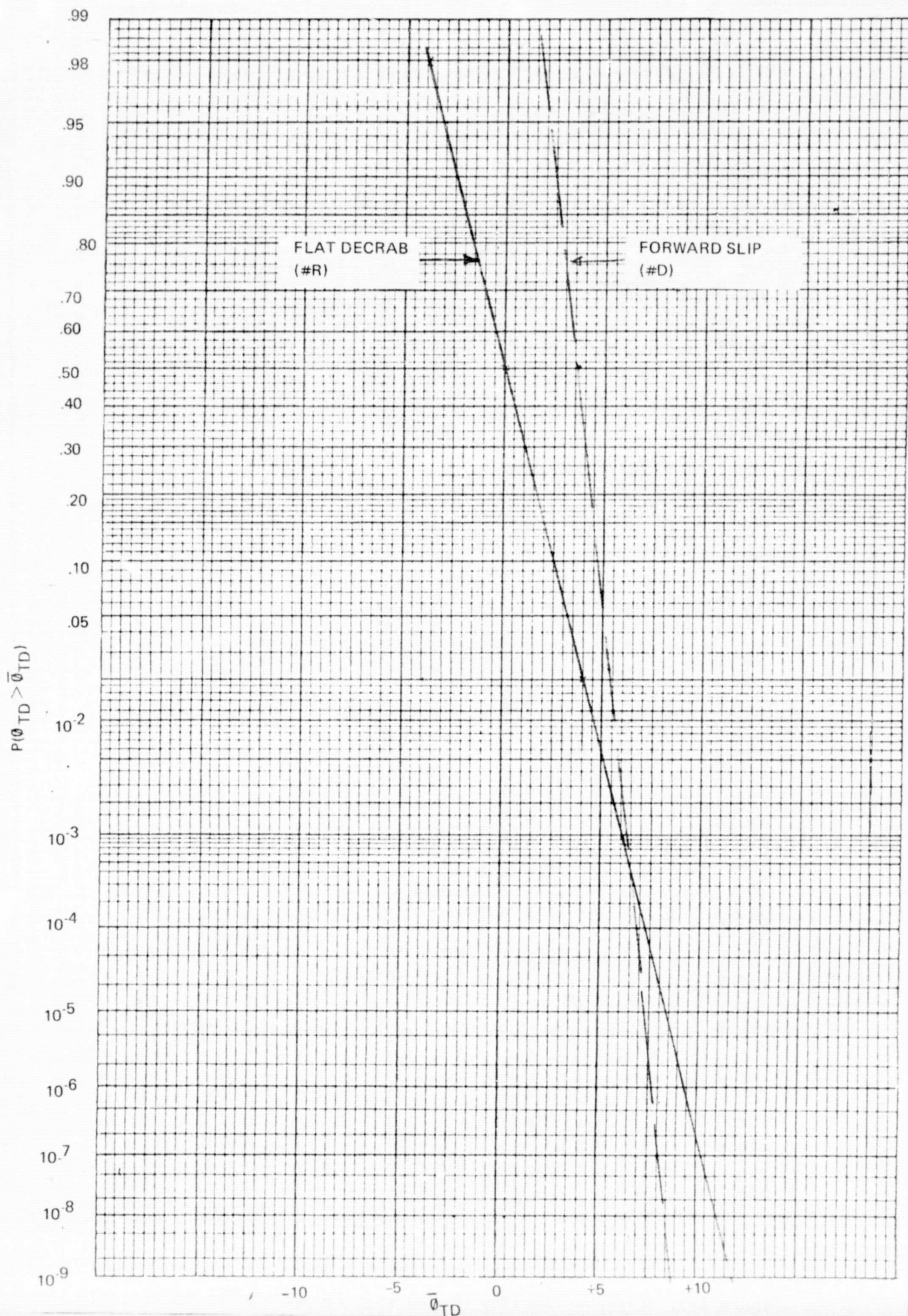


Figure 6-8. Touchdown Attitude Distribution for Flat Decrab & Forward Slip

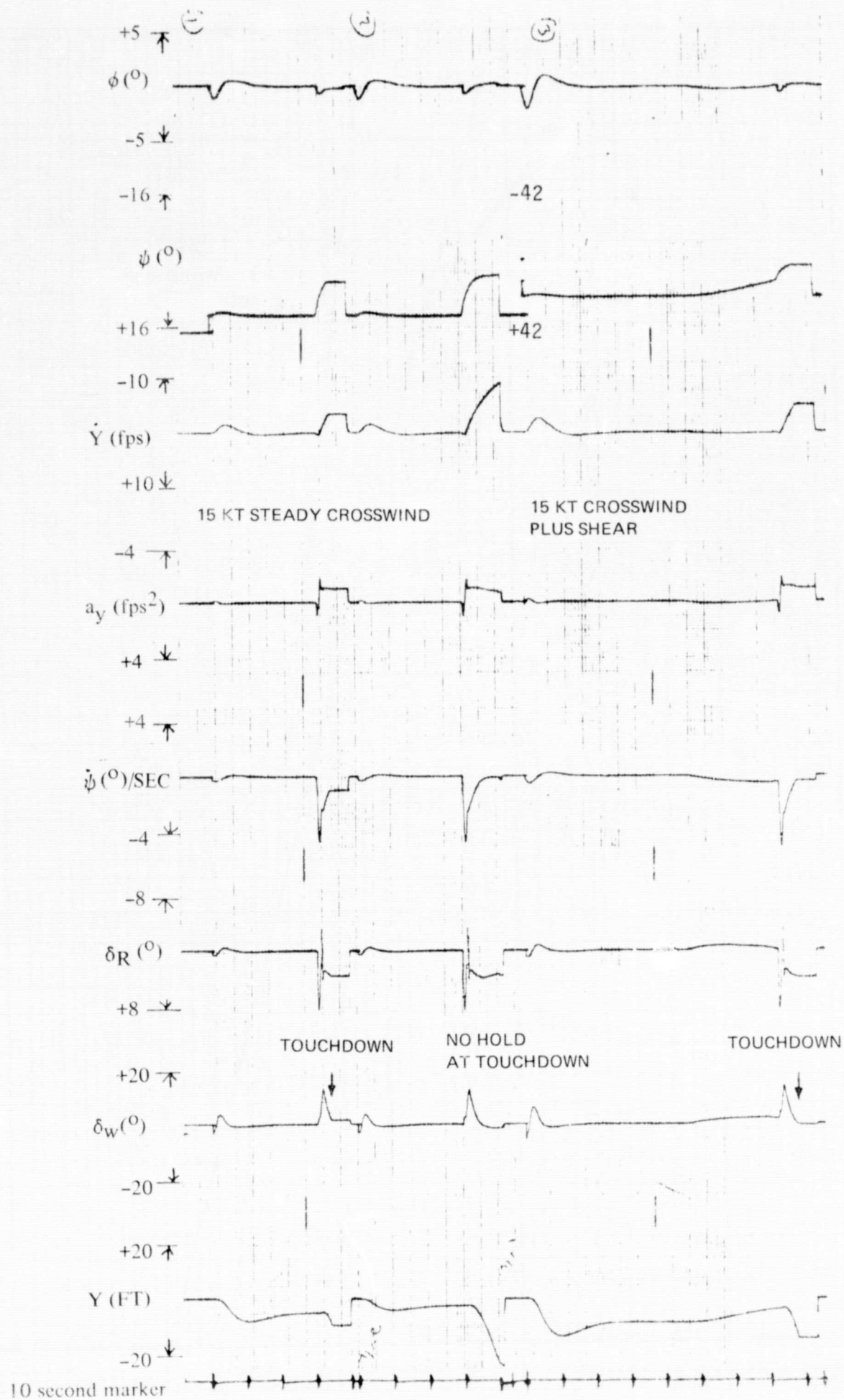


Figure 6-9. Flat Decrab (#A) Response in Deterministic Winds

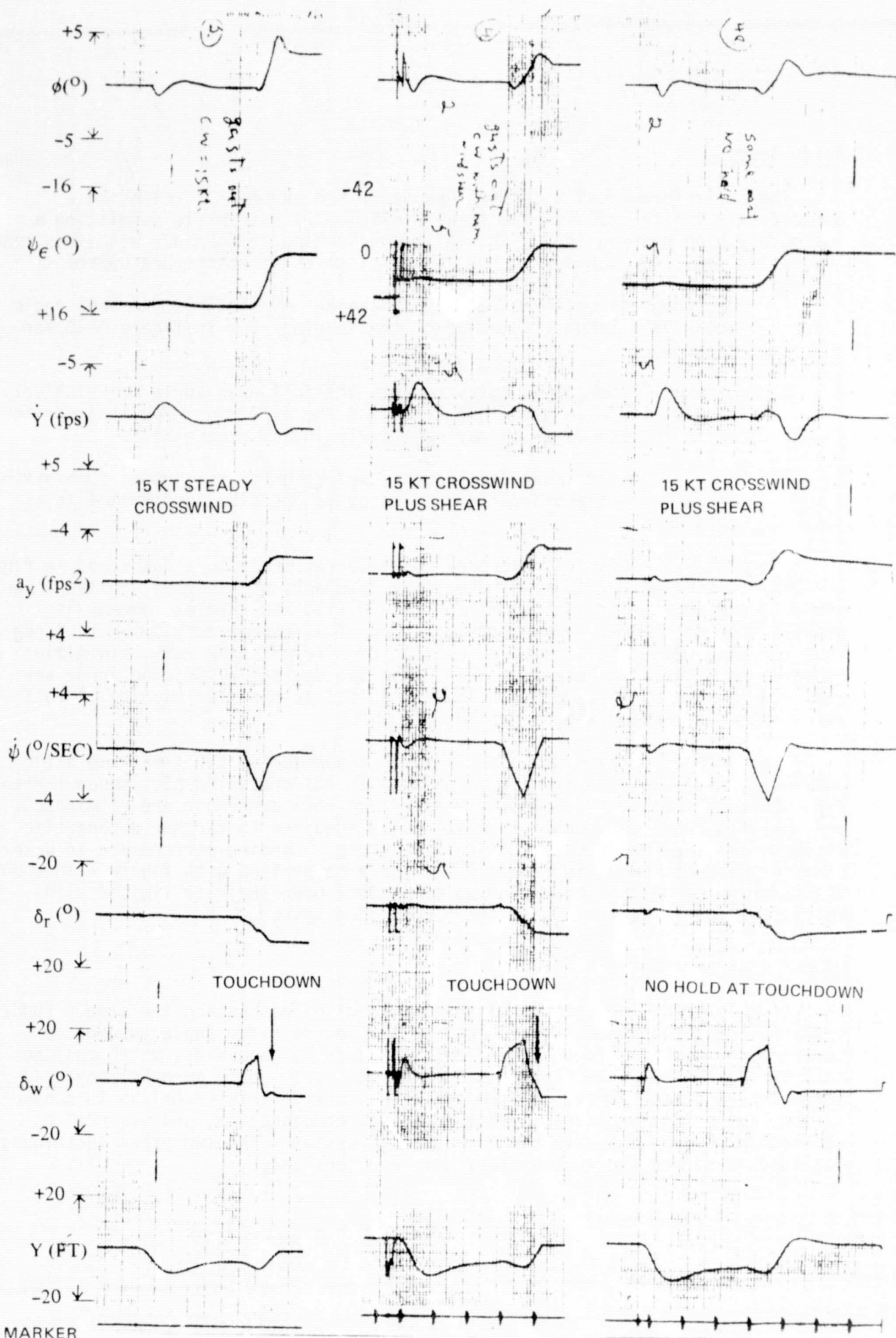


Figure 6-10. Rate Limited Forward Slip (#B) Response in Deterministic Winds

Align Entry

The basic forward slip control law described above (#B) relies on a command rate limiter to slow the forward slip entry rate while permitting a reasonably high heading loop gain. Although landing performance with this configuration satisfies the design requirements, three drawbacks are apparent:

1. Overshoot of both the reference heading and steady state bank angle occur on a large percentage of the landings (as in figure 6-10 for example).
2. A rate limited align entry removes the full crab angle at relatively high altitude in headwinds, yielding the full wing down attitude for up to 10 seconds which may negatively impact ride quality.
3. In a high wind shear environment, selection of the proper combination of rate limit and heading/rate gains to optimize performance is difficult.

The altitude scheduled reference course error trajectory described in figure 6-3 was implemented to eliminate these drawbacks of the rate limited align entry. Between 45.72m and 15.24m (150 and 50 ft), the heading command is reduced from the course datum error existing at alignment initiation to 2 degrees. Thus the alignment rate becomes a function of aircraft sink rate, minimizing maneuver abruptness in headwinds. The last two degrees of heading error are smoothly integrated to zero below 15.24m (50 ft) to minimize heading or roll overshoots due to wind shear and other factors.

A comparison of bank angle and heading trajectories for these two align entry alternates is given in figure 6-11 in 15 kts crosswind plus shear. With the reference trajectory, both the heading and roll overshoot are eliminated, and the zero heading error is asymptotically acquired to further desensitize performance to align maneuver timing variations. Landing performance in deterministic winds is shown in figure 6-12, and a comparison with figure 6-10 shows the superiority of the model heading trajectory over the rate limited align entry, and justifies its use in the recommended system.

Rudder Bias Generation

In this study, we considered three methods of generating the steady rudder required for the alignment maneuver. As the course datum angle is reduced toward zero, a slideslip of equivalent magnitude is generated, which must be held by the rudder. The flat decrab candidate system used an open loop rudder predict term based on heading error at align entry. This technique is subject to the limitations inherent in most open loop compensation, and was not considered in conjunction with the forward slip system. The two other techniques outlined in figure 6-4 were evaluated more extensively.

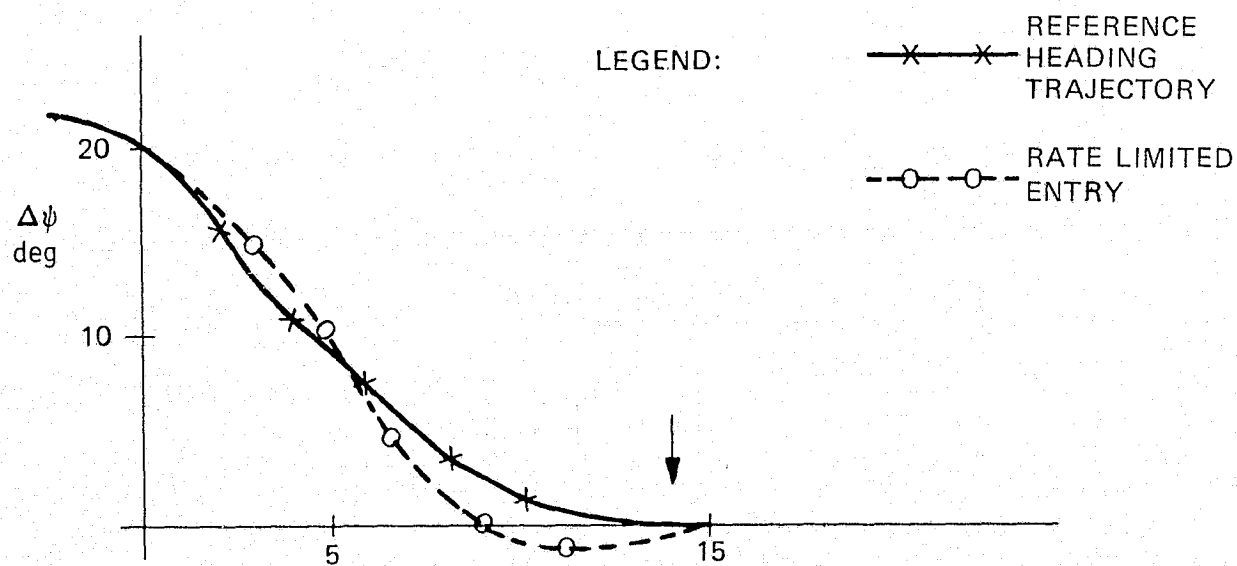
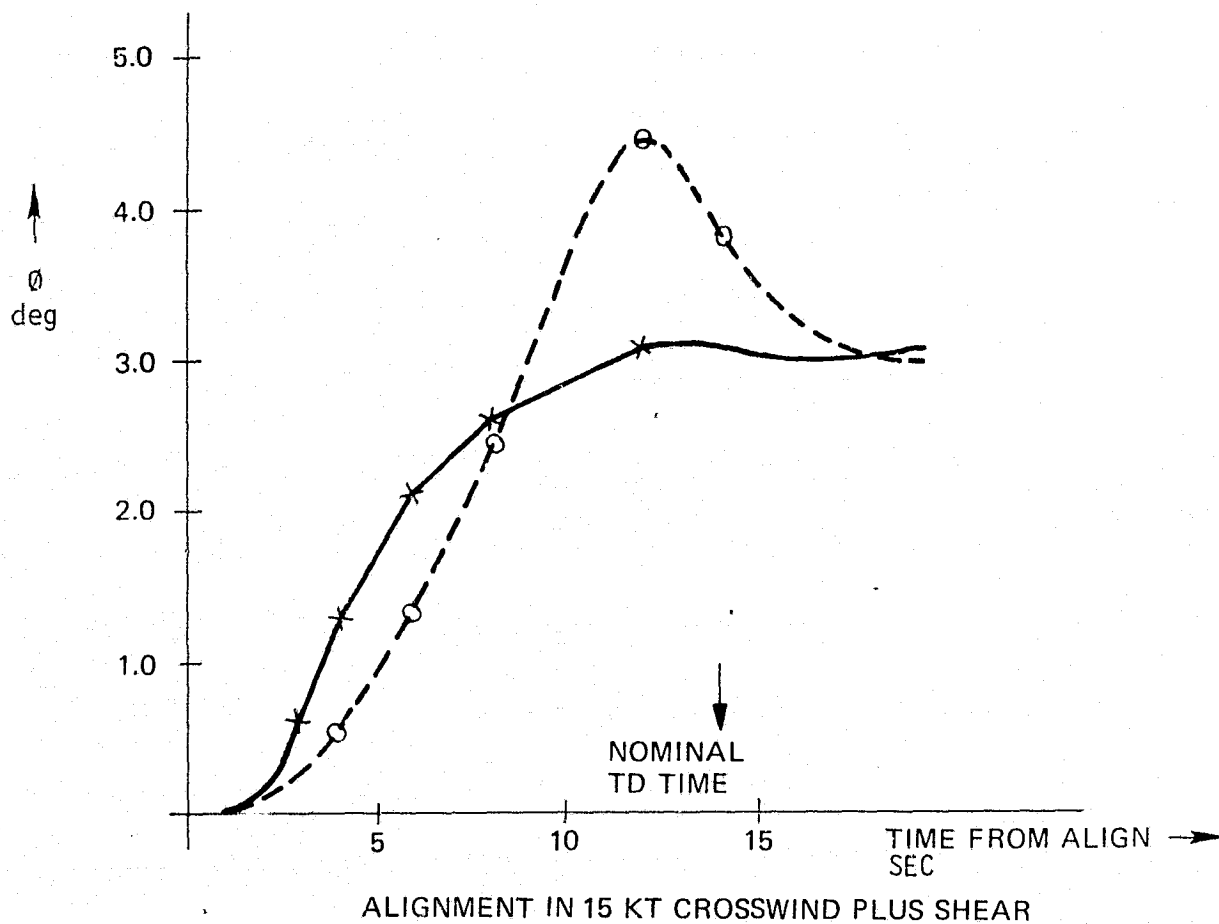


Figure 6-11. Effect of Align Entry Techniques

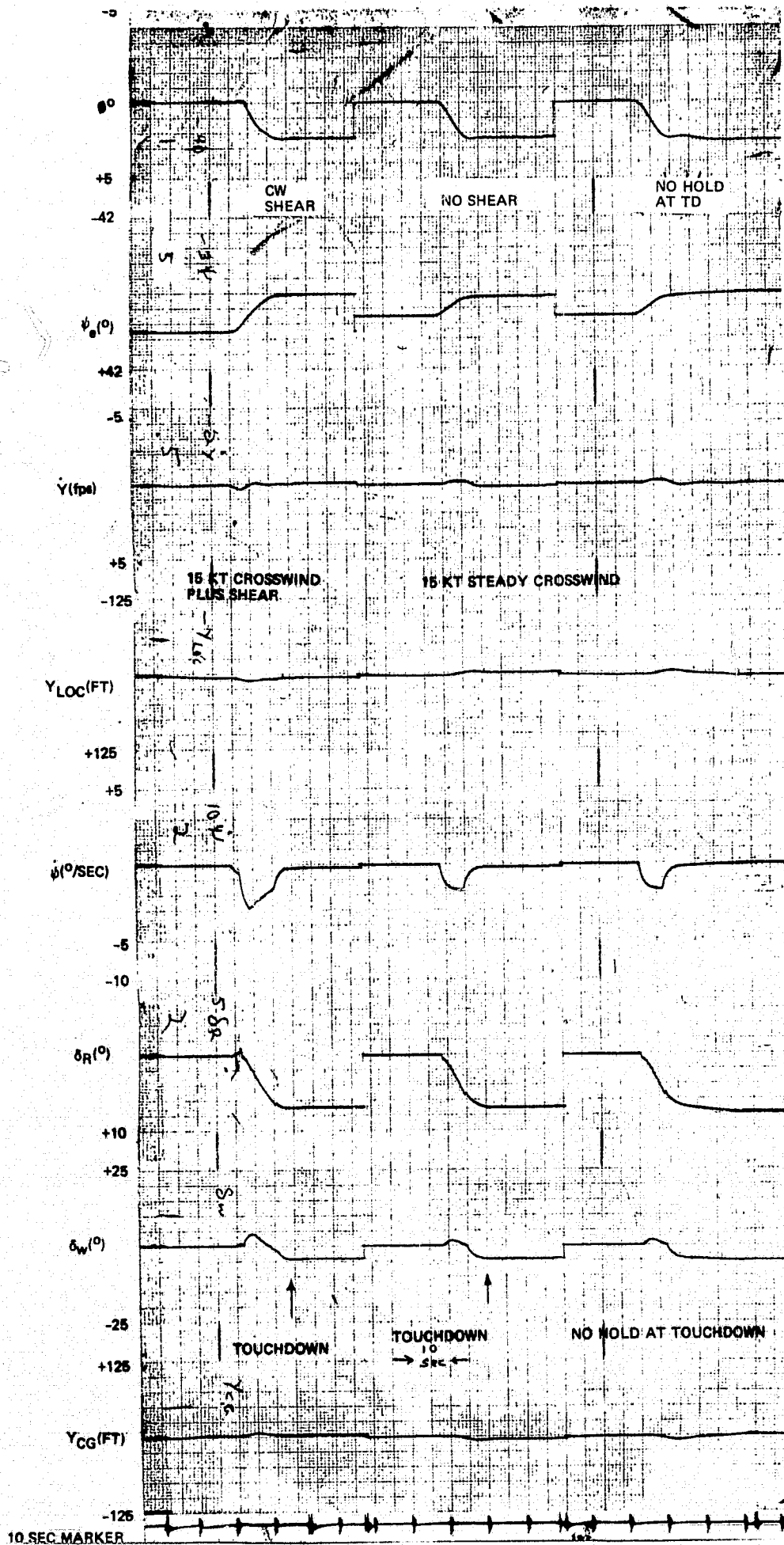


Figure 6-12. Model Reference Forward Slip (#E) Response in Deterministic Disturbances

In the initial forward slip configuration, the steady state rudder required during alignment was obtained from a crosswind estimate. The crosswind is determined from course datum error, filtered cross track velocity, and a priori knowledge of the dominant sideforce stability derivatives to select K_1 through K_3 in the expressions

$$\dot{Y}_{wind} \approx -U_0 (\Delta\psi + \beta) + \dot{Y}_F$$

$$\beta \approx K_1 a_y + K_2 \delta_R + K_3 \delta_w$$

The estimated crosswind angle ($\beta_{wind} = \frac{\dot{Y}_{wind}}{U_a}$) is modified by the ratio of

$C_{n\beta}/C_{n\delta R}$ to hold the required steady state rudder. Although this method yielded good performance for the Aug Wing vehicle, it has two significant drawbacks: the computation is fairly complex, and it requires a priori knowledge of K_1 through K_3 , the $C_{n\beta}/C_{n\delta R}$ ratio, and their variations with flight conditions.

A closed loop rudder control system was defined to maintain the steady rudder, which would inherently compensate for wind and vehicle variations. With the heading reference trajectory align entry, the aircraft is able to track the model trajectory with only small errors, thus allowing the use of high gain integral terms to provide the required steady rudder during the alignment. Although the improvement in stochastic landing performance is small for the nominal configuration (as indicated by comparing C and D in figure 6-13), this system does not require a priori knowledge of stability derivatives and is inherently adaptive to aircraft and disturbance state variations. The reduction in system complexity is readily apparent from figure 6-4. Thus the closed loop rudder bias generation was incorporated in the recommended system.

Wing Down Compensation

For the flat decrab system, a shaped open loop bank command is inserted at align to minimize the roll transient due to the align rudder kick. The roll compensation amplitude is a function of the pre-align course datum error. This open loop roll compensation was not investigated with the forward slip.

For the forward slip landing system, two alternate methods of providing wing down compensation were investigated, one using crosstrack acceleration and the other pseudo acceleration. In the Aug Wing vehicle, crosswind acceleration is obtained by resolving the three accelerometer outputs into runway axes. For the recommended system, washed out crosstrack acceleration (\dot{Y}_R) is used for complementary filtering of the MLS position and rate signals and for wing down compensation, which yields configuration D and provides very good landing performance. For configuration J, a pseudo crosstrack acceleration was generated by $\dot{Y}_\phi = g\phi + K_{AR} \cdot \delta_R$, where K_{AR} has some flight condition dependency. This pseudo acceleration was used only for wing down compensation, while \dot{Y}_R was retained for the complementary filter. As noted in figure 6-14 for zero

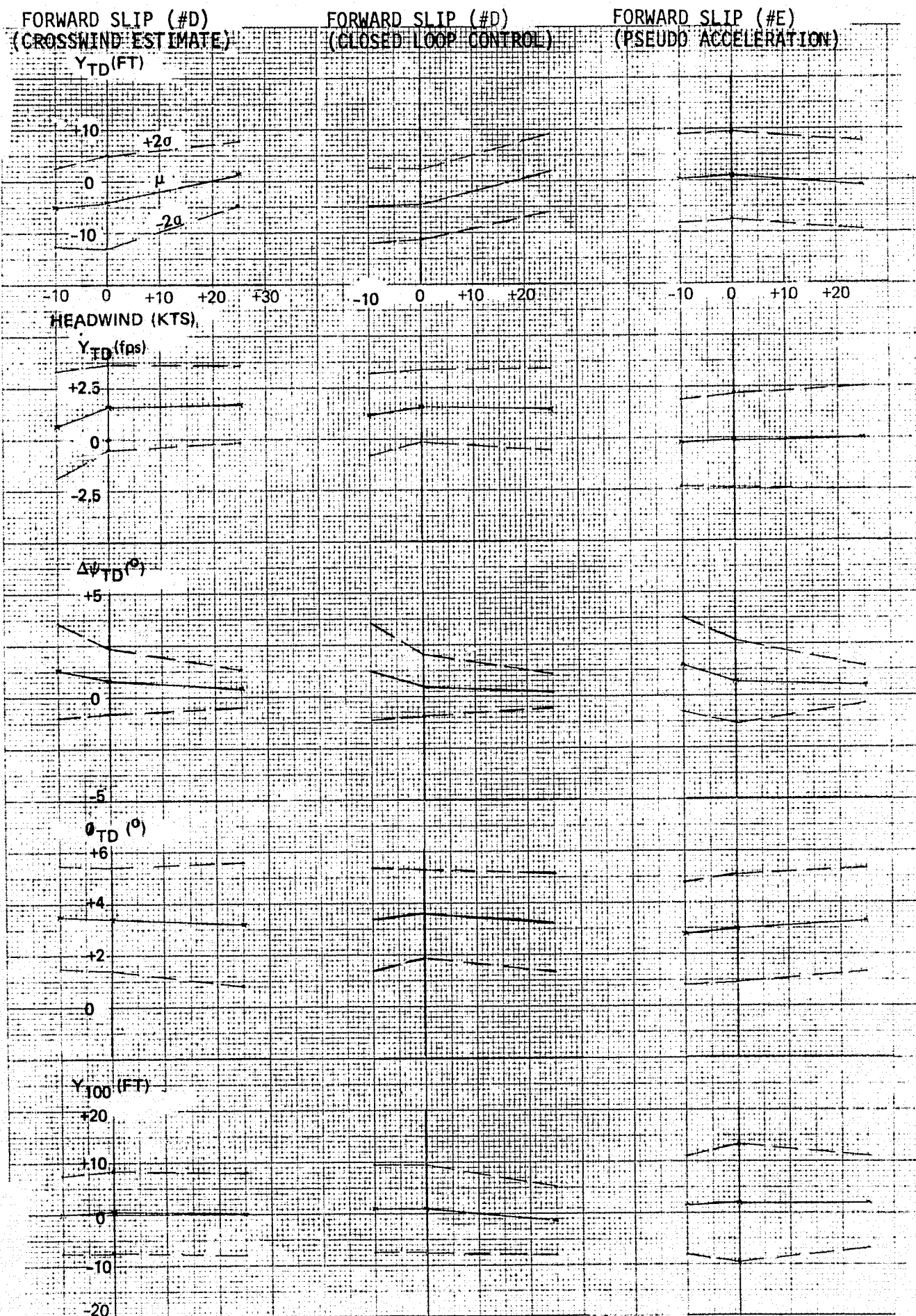


Figure 6-13. Effect of Rudder Bias & Lateral Acceleration Usage on Landing Performance

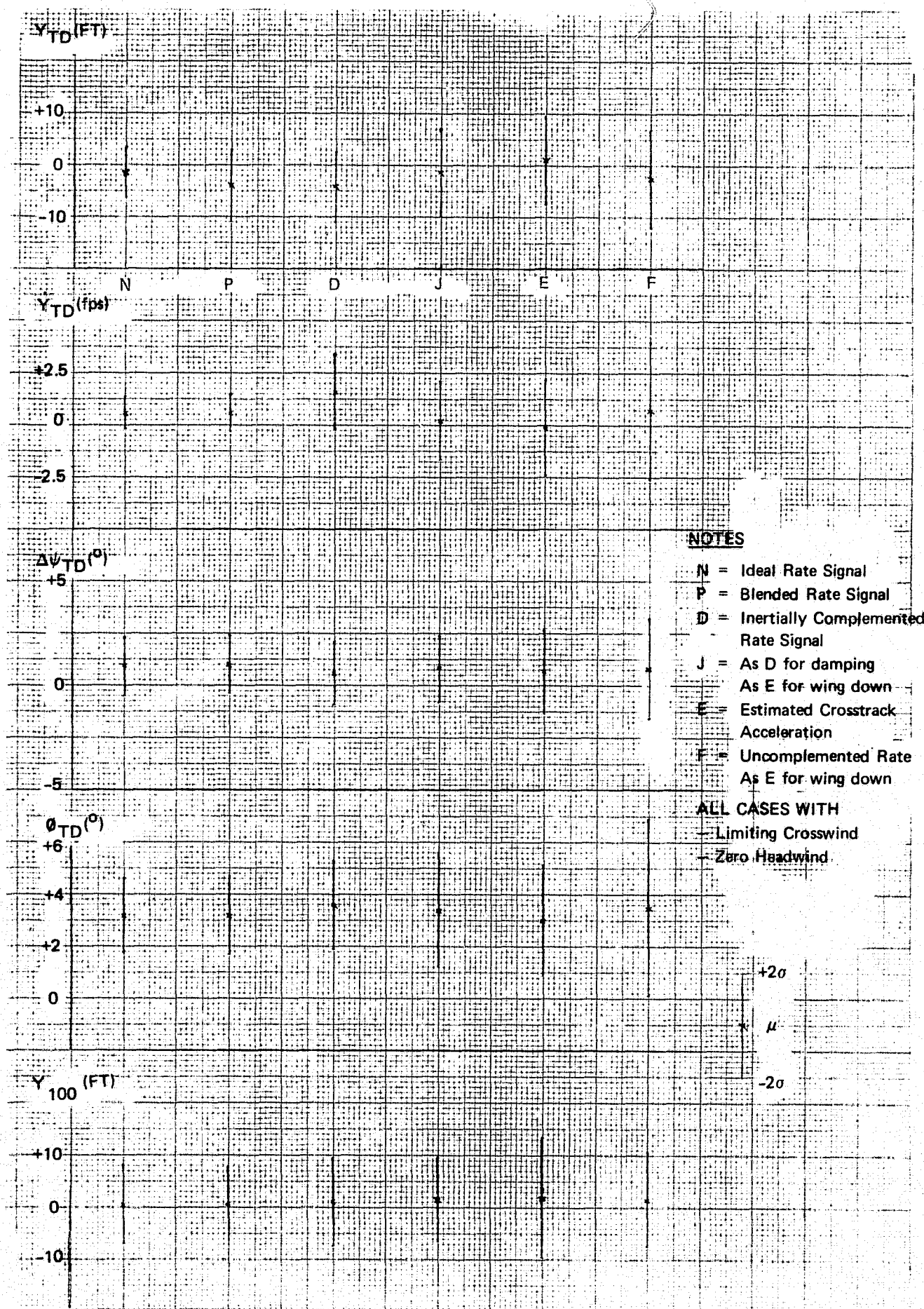


Figure 6-14. Effect of Rate Signal Variations on Landing Performance

headwind, all touchdown performance indicators show slightly increased dispersions compared to D, but still well within the requirements. Although the use of roll plus rudder to replace crosstrack acceleration in the wing down computation provides acceptable performance, it has two disadvantages: there is no reduction in sensors, since crosstrack acceleration is retained for the lateral filter complementation, and it does require rudder position; also the K_{AR} gain must be carefully selected based on a priori knowledge of the aircraft, and may require gain scheduling for proper operation. Thus the use of crosstrack acceleration for wing down compensation is preferable if available; otherwise, crosstrack acceleration should be entirely eliminated from the landing system to provide the benefit of reduced sensors.

Position and Rate Signal

The qualities unique to a STOL vehicle have little bearing on localizer track performance. Since the localizer tracking function both precedes and is part of the runway alignment mode, it is of unavoidable interest in any study of the runway alignment maneuver.

Conducting the localizer tracking task to a precision necessary to permit low visibility approach and landing has proven in the past to be mostly a problem of coping with poor quality localizer deviation data. Lateral position data is usually extractable at a usable quality by using lightly filtered, range corrected beam data with little or no augmentation. For path stability, some signal representative of rate of closure to the beam center must also be acquired. Early systems intended for certification with Cat. I or lower quality beams used course error signal as a rate term, with beam standoff in crosswind minimized by washing out the heading signal and using a beam deviation integral term. The existence of a changing wind (shear) further complicates the problem since the relationship between heading change and position rate change is no longer valid. Another technique is to use lagged roll as a damping term. Since roll angle is proportional to lateral acceleration in a coordinated turn, lagged roll as an approximation to integral of acceleration is a reasonable representation of lateral deviation rate. Again, errors are introduced by changing winds which effectively "uncoordinate" the airplane somewhat. This technique is sensitive to offsets of the gyro signal (mechanical or electrical) since, to be representative of integration, the roll lag filter must have a time constant on the order of 20 seconds or more and have a correspondingly high steady state gain.

In this study, we considered several alternate means of generating smoothed position and rate signals. In the baseline forward slip system (Configuration D), the crosstrack acceleration signal available in the Aug Wing vehicle inertially complements the MLS position data to provide smoothed position and rate outputs from the navigation filter. This inertially complemented system provides good beam tracking and align performance, and will be used as the basis of comparison for the other tradeoff configurations.

Since the advent of MLS promises reduced noise content compared to ILS, a configuration (F) was defined which uses unaugmented beam filtering to provide the lateral position and rate signals. A 4.57m/sec (15 fps) rate limited position filter was used, with 0.5 second time constants on both the position and rate signals, to provide a suitable compromise between noise suppression and stability considerations. Although surface activity was comparable to the augmented nav filter system, beam tracking performance was notably degraded, with about 50% increased Y and \emptyset variations and nearly doubled Y excursions. Since this configuration would be used only if the crosstrack acceleration was unavailable, the wing down signal incorporates pseudo acceleration from bank angle and rudder. As noted in figure 6-14, touchdown lateral rate and bank angle dispersions are significantly increased, with some degradation in position and heading control. Thus an unaugmented beam filter is not recommended for use with this quality (characteristic of MODILS) of azimuth guidance signal.

The derived crosstrack acceleration signal considered for wing down compensation was also considered as an inertial acceleration replacement in the complementary nav filter, yielding a landing system (E) which is independent of crosstrack acceleration. Roll and lateral rate variations were only slightly degraded (less than 15%) with equivalent surface activity. The landing performance summaries with this system are presented in figures 6-13 and 6-14. Performance is notably improved over the unaugmented filter case (F), and is almost the equal of the base line system regardless of the longitudinal wind condition. Since this configuration yields acceptable landing performance and track activity, it is the recommended system for general usage where a crosstrack acceleration signal is not available.

To determine the impact of the rate signal quality on landing performance, we considered a configuration (N) which is unachievable in reality, using perfect lateral rate for track damping. Heading performance is substantially improved, with lateral dispersion 70% of the baseline system, and only 50% of the touchdown rate variations. Thus choice of the lateral rate signal has significant performance impact.

Since rate signal quality significantly impacts landing performance, further tradeoffs were conducted to define a blended rate configuration (P). Here 25% of the rate is obtained from the nav filter and 75% (after align) obtained from washed out lagged crosstrack acceleration to minimize the effects of higher frequency azimuth signal irregularities. As noted in figure 6-14, this system approaches the performance of the ideal rate configuration (N), resulting in landing performance better than the baseline system. Another variation was investigated, with the same gains but using pseudo acceleration rather than the crosstrack acceleration signal. The resultant touchdown dispersions in lateral position and rate were nearly doubled, probably because the pseudo acceleration signal has significant lower frequency errors. For the Aug Wing vehicle with its accurate crosstrack acceleration signal, the inertially blended rate configuration (P) provides the best landing performance and it is recommended for implementation.

An accelerometer derived rate signal was briefly considered. However, if a lateral acceleration signal is available, it can be better used to provide wing down compensation and complement the position information as for the baseline system. Thus derivation of the rate signal from acceleration only would be of limited benefit.

Lateral Acceleration

The tradeoff on lateral acceleration has been discussed in several previous sections, but it will be summarized here. On the Aug Wing vehicle, the availability of an accurate crosstrack acceleration signal provides effective filtering of the MLS position signal, formation of an accurate blended lateral rate, and a good acceleration signal for wing down compensation, all of which are used in the recommended forward slip system (P) to provide excellent beam tracking and touchdown performance.

For general usage on a vehicle which does not have high quality lateral acceleration, the derived acceleration configuration (E) is recommended. The first attempt to derive acceleration used ϕ , δ_R , and r , but inclusion of the yaw acceleration term (derived from filtered yaw rate) caused gross instability to occur in the closed loop control mode. Thus we used

$$\ddot{Y}_\phi = K_\phi \cdot \phi + K_{AR} \cdot \delta_R$$

which appears sufficiently accurate for both nav filter complementation and wing down compensation. During loc track, the rudder signal is not necessary since the aircraft is essentially at zero sideslip angle. During the alignment maneuver, the rudder input is necessary to account for the crosstrack acceleration due to sideslip angle. Several limitations are noted below.

The adequacy of this approximation is dependent on the magnitude of wind-shear encountered and the bandwidth of the navigation filter used to produce the lateral rate signal (\dot{y}_f) for path control damping. At the maximum wind-shear simulated and with the existing nav filter gains, the performance is acceptable. When pseudo acceleration as defined above is used, the constant K_{AR} must be determined from a priori knowledge of the ratio $\beta/\delta_R \cdot a_y/\beta$, which is relatively constant for the Aug Wing vehicle for 60 to 70 knot approach speeds. In general, however, it may be necessary to schedule this rudder gain. Additionally, aircraft asymmetry considerations may require a relatively fast washout on rudder, reducing the approximation fidelity at low frequencies. Thus it must be stressed that the rate term cannot rely too heavily on the inertial component at lower frequencies (as in configuration Q) unless the acceleration signal is accurately represented.

Other Variations

Several other relatively minor tradeoffs were considered. Elimination of the antenna location correction term shifts the nominal touchdown point slightly, and requires some additional maneuvering during alignment which is noticeable in deterministic wind conditions. However, touchdown statistics are not significantly affected, and thus the antenna correction term is mainly esthetically justified.

Based on gyro and accelerometer error analysis, it is beneficial to use an acceleration washout in the control algorithm. A 50 second time constant is adequate to minimize offsets while retaining the required low frequency bandwidth for effective wing down compensation, lateral rate derivation, and nav filter augmentation. The landing performance impact on the recommended configuration is negligible. In fact, landing statistics obtained with a 10 second washout (K) show minimal performance degradation.

Several gain variations were considered. Detailed results are presented in Appendix C, with a brief summary included here. A 50% reduced roll attitude gain (I) yields increased dispersions in beam tracking parameters and degraded landing performance, especially for roll attitude and lateral rate at touchdown. Although reduced lateral rate gain at align yield some reduction in wheel activity, it yields almost 50% increased touchdown position dispersions. A doubled position integral gain somewhat degrades stability and landing performance slightly, while providing some increased immunity from gyro and accelerometer offsets. Since the offset induced landing inaccuracies are acceptable with the nominal system, an increase in integral gain could not be justified.

6.4 PERFORMANCE

A performance summary of the recommended lateral landing system is presented here, with the detailed supporting data included in Appendix C. Four performance aspects are considered:

1. Landing performance in stochastic disturbances only
2. Landing performance over the total landing environment
3. Deterministic variations and off-nominal conditions
4. Localizer track activity in stochastic disturbances

Landing Performance

The landing performance of the recommended lateral landing system (P) is summarized in Table 6-I both for stochastic disturbances only and over the total landing environment. This data was obtained with limiting atmospheric and MLS disturbance levels, with averaged limiting longitudinal winds and shears, without accounting for the low occurrence probability of these disturbance levels, and thus it represents a conservative estimate of landing performance. With one exception, landing performance is excellent, satisfying all the design goals and FAA automatic landing requirements by wide margins. Although the lateral touchdown dispersion due to limiting stochastic disturbances is less than 67% of the design requirement, the large azimuth bias attributed to the MODILS system yields 79% of the allowable dispersion by itself, resulting in a 0.686m (2.25 ft) exceedance of the 10^{-6} landing requirement on a total population basis.

The probability distributions for these landing parameters are presented in figures 6-15 to 6-19, with the solid lines representing the performance averaged over limiting headwind and tailwind in stochastic disturbances only, and the dashed lines providing the total population landing performance which includes the effects of all significant deterministic variations.

Deterministic Variations

Many deterministic variations were considered during this study. Those which significantly impact lateral landing performance are listed in Table 6-II along with their effect on the aircraft performance indication parameters, with a more complete discussion given in the next section.

Except for azimuth bias, the performance impact of these deterministic variations is relatively small compared to atmospheric disturbance induced landing dispersions. However, the lateral displacement error at the intended touchdown point due to the $\pm 0.17^\circ$ one sigma azimuth bias is larger than the dispersion due to all other sources combined. With the upcoming MLS guidance system, an azimuth bias of only 0.06° is expected, yielding a total population two sigma dispersion of 3.27m (10.74 ft), which is well within the design guidelines.

Activity in Disturbances

A summary of aircraft state variations and control activity in limiting stochastic turbulence levels is given in Table 6-III. Three configurations are presented: P, the recommended system with blended lateral rate signal, D with runway axis lateral acceleration, and E with pseudo lateral acceleration derived from roll angle and rudder position.

TABLE 6-I. LATERAL PERFORMANCE SUMMARY

PARAMETER	REQUIREMENT	ACTUAL	
		STOCHASTIC ONLY	TOTAL POPULATION
Y_{TD} m (ft)	μ —	-0.396 (-1.31)	-0.396 (-1.3)
	2σ <4.57 (15.0)	-3.048 (-10.0)	-5.334 (-17.5)
	10^{-6} <9.07 (29.75)	-6.279 (-20.6)	-9.754 (-32.0)
\dot{Y}_{TD} m/sec (fps)	μ —	+0.152 (+0.5)	+0.152 (+0.5)
	2σ —	$\pm(0.305)$ (± 1.0)	± 0.381 (± 1.25)
	10^{-6} <3.048 (10.0)	0.853 (2.8)	1.067 (3.5)
$\Delta\psi_{TD}$	μ —	+0.9	+0.9
	2σ —	± 2.1	± 2.7
	10^{-6} <10	+6.0	+7.6
ϕ_{TD} deg	μ —	+3.3	+3.3
	2σ —	± 1.8	± 1.9
	10^{-6} <20.0	+7.6	+7.9
ΔY_{window} m (ft)	μ —	+0.152 (+0.5)	+0.152 (+0.5)
	2σ 7.62 (± 25.0)	± 2.21 (± 7.25)	± 2.972 (± 9.75)

- NOTES:
1. This table defines both stochastic only and total population landing performance, where the latter includes deterministic disturbance effects.
 2. Only those requirements specified in SOW or dictated by aircraft/geometry limitations are listed.
 3. For lateral axis, means should all be zero when evaluated over the total environment. Since actual results are presented for limiting wind from the right, significant mean values are obtained.
 4. ΔY_{window} is lateral tracking error at the 30.48m (100 ft) approach window.
 5. For conservatism, results are presented for limiting crosswind, shear, turbulence, and MLS noise levels for averaged limiting headwind and tailwind conditions, without accounting for the $\approx 4\%$ probability of occurrence of these limiting atmospheric disturbances.
 6. Deterministic variations included in total population distributions are MLS azimuth bias, course datum error, accelerometer and gyro errors, and approach speed variations.

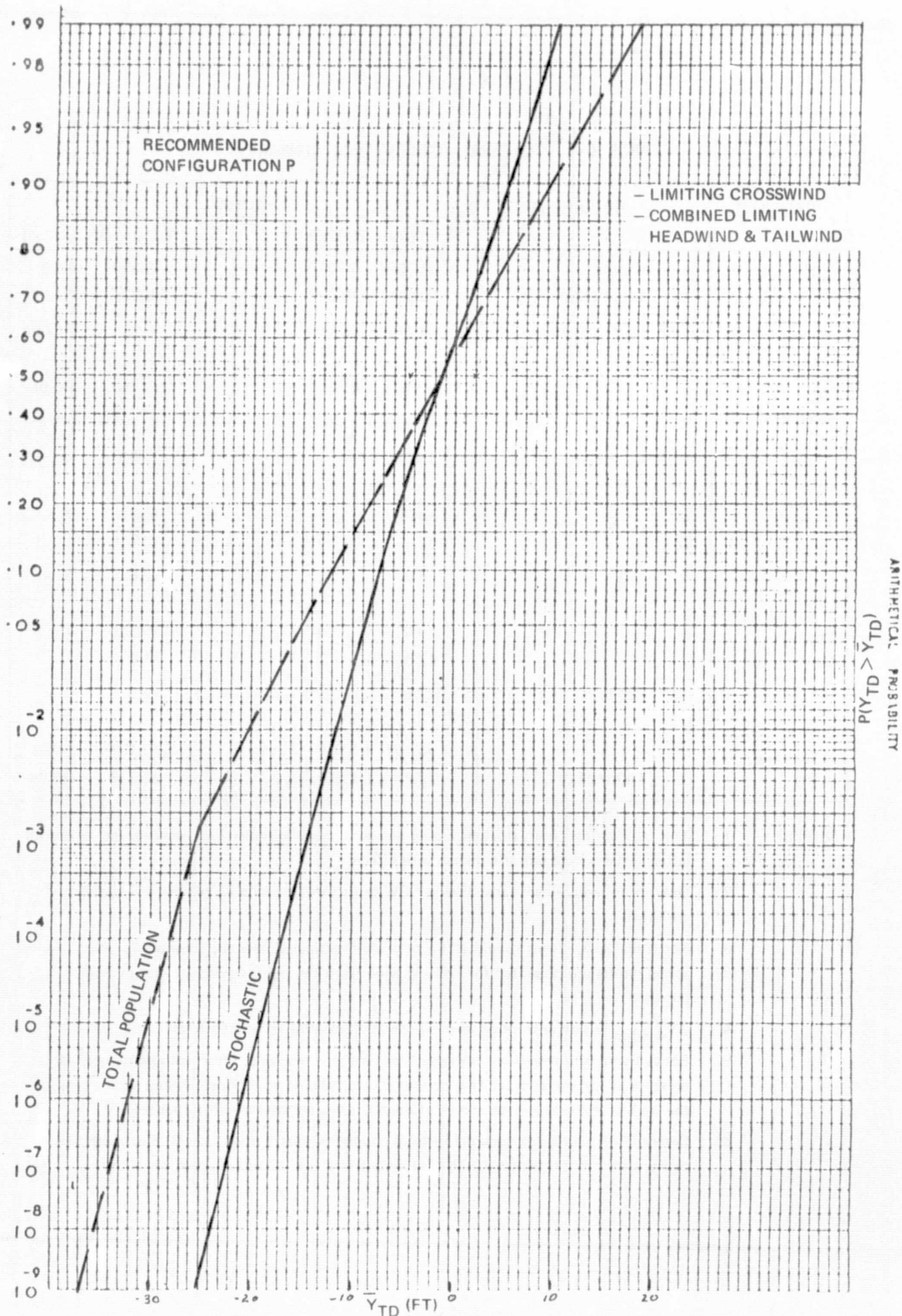


Figure 6-15. Touchdown Lateral Distance Distribution

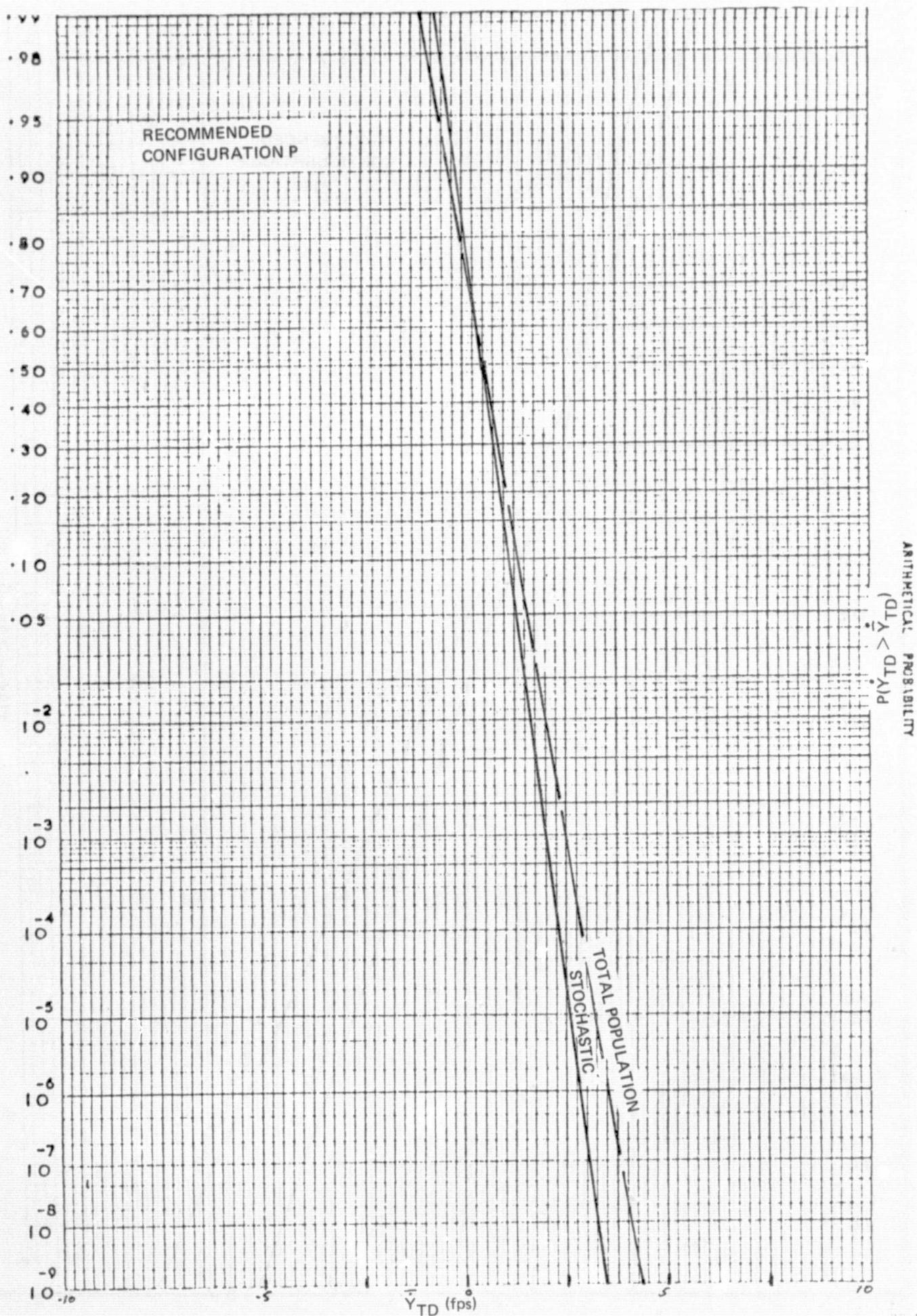


Figure 6-16. Touchdown Lateral Rate Distribution

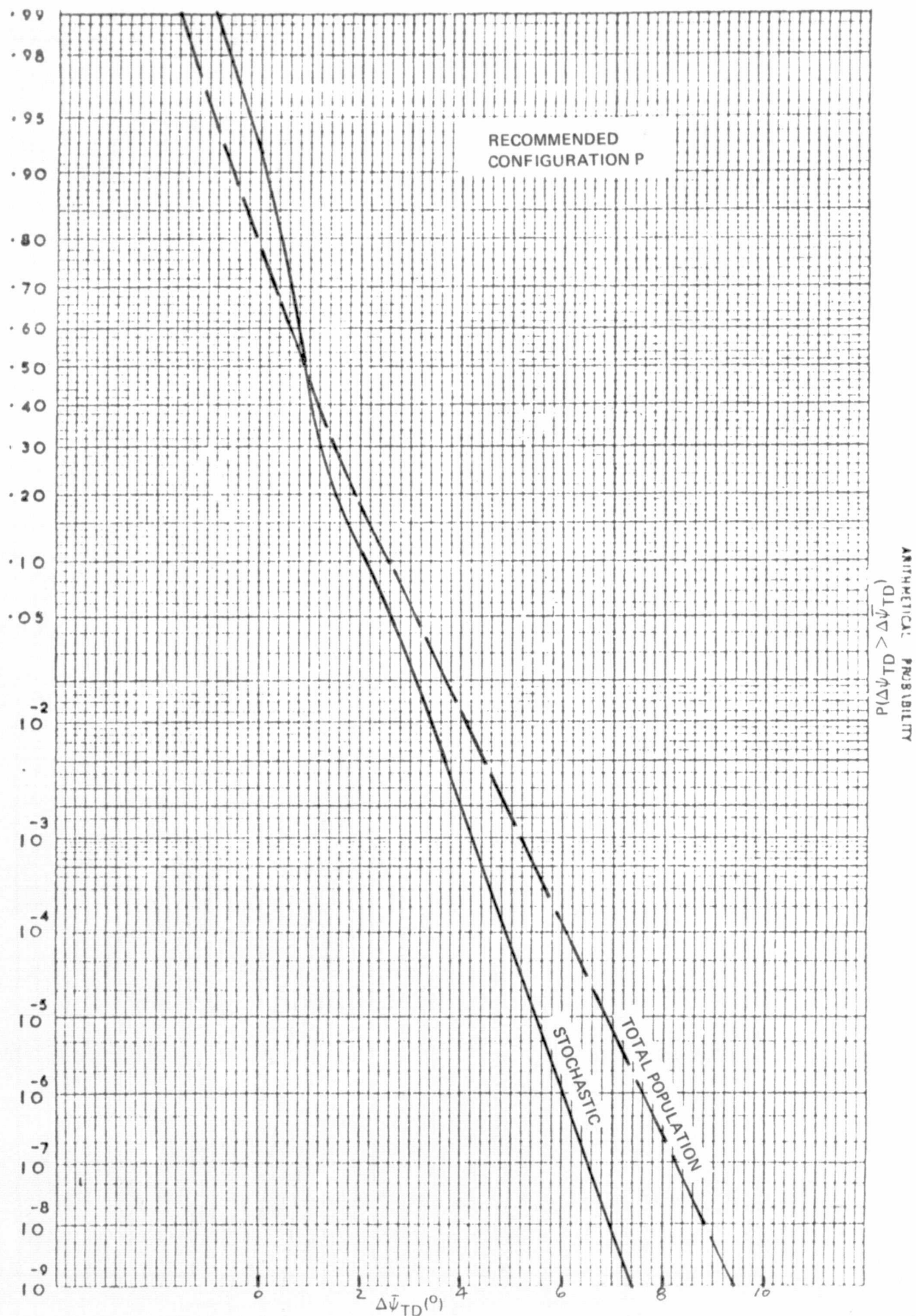


Figure 6-17. Touchdown Heading Error Distribution

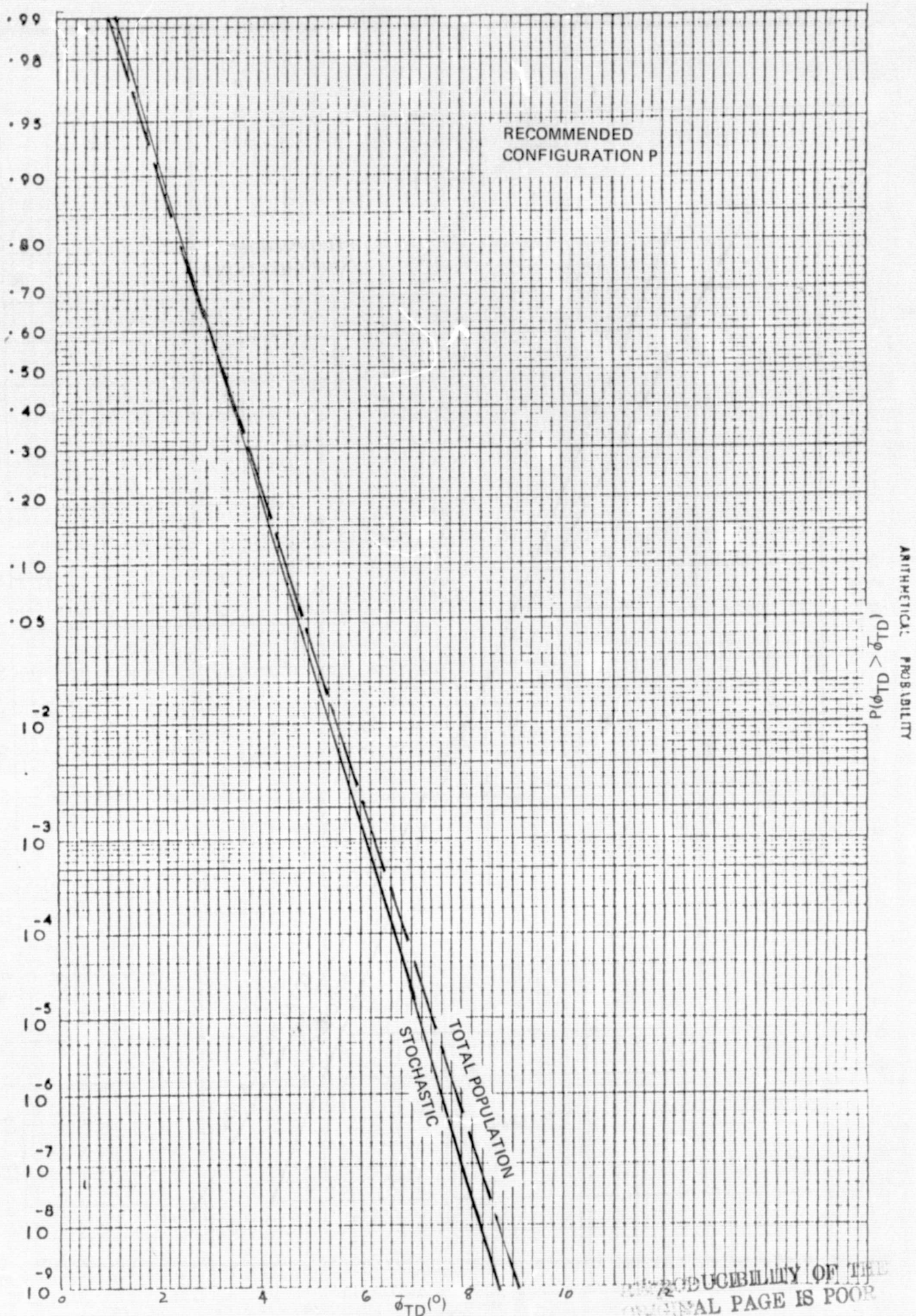


Figure 6-18. Touchdown Bank Angle Distribution

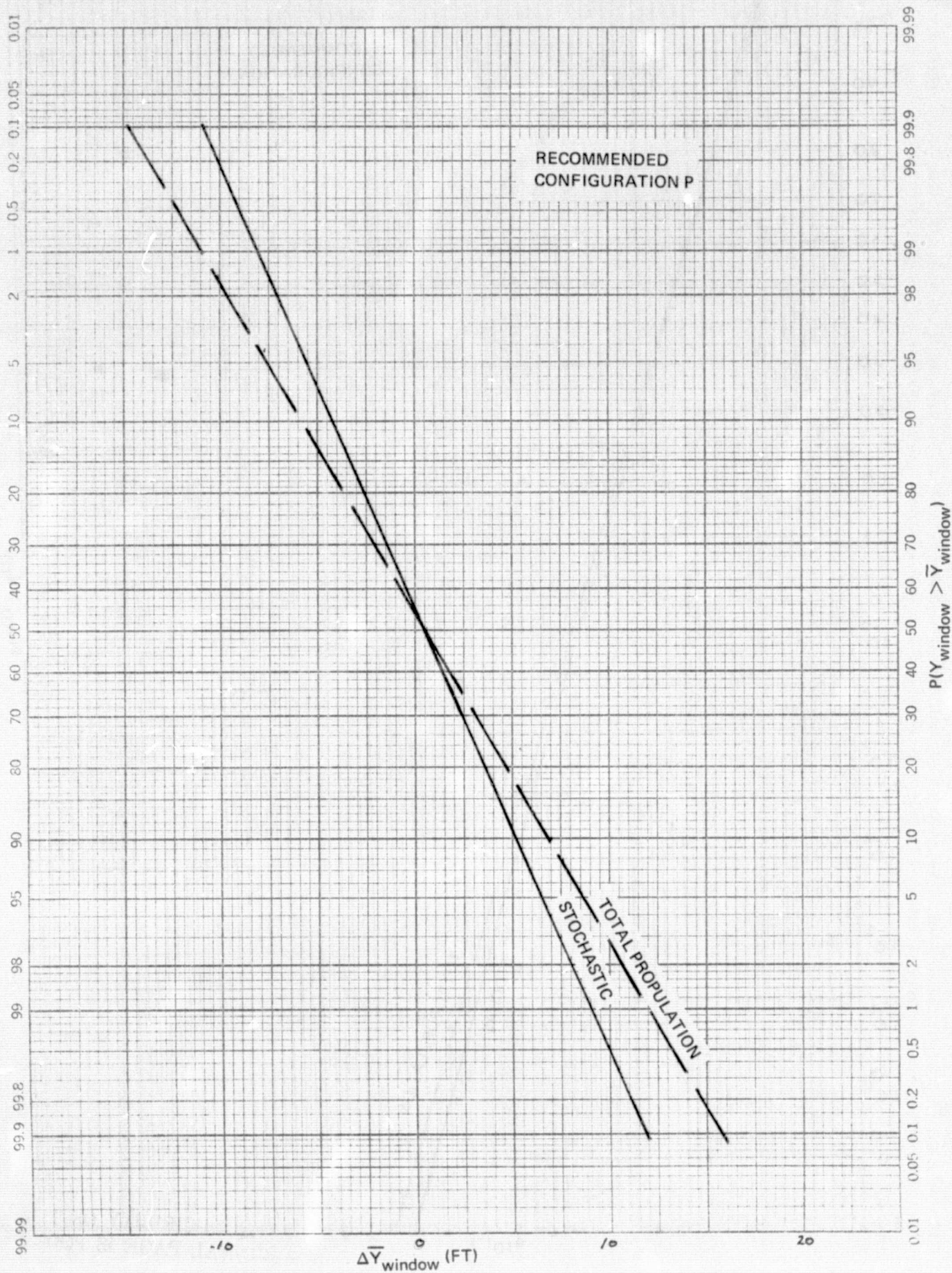


Figure 6-19. Lateral Window Deviation Distribution

TABLE 6-II. LATERAL DETERMINISTIC DISTURBANCE EFFECTS

DISTURBANCE	STANDARD DEVIATION	CUTOFF	ΔY_{TD}	$\Delta \dot{Y}_{TD}$	$\Delta \psi_{TD}$	$\Delta \phi_{TD}$	ΔY_{window}
1. Azimuth Bias	0.17°	@ 3σ	1.81m (5.93 ft)	—	—	—	2.5m (8.2 ft) *
2. Course Datum Error	0.889°	No	0.12m (0.39 ft)	0.10m/sec (0.34 fps)	0.89°	0.24°	0.12m (0.39 ft)
3. Accelerometer Errors	0.00228g	No	0.80m (2.64 ft)	—	—	0.23°	0.80m (2.64 ft)
4. Vertical Gyro Errors	0.173°	No	0.59m (1.95 ft)	—	—	0.17°	0.59m (1.95 ft)
5. Approach Speed Variations	1.0 ft	No	0.18m (0.6 ft)	0.015m/sec (0.05 fps)	0.19°	0.08°	0.15m (0.5 ft)

- NOTES:
1. Normal distributions are assumed for all deterministic variations, and performance effects are for 1σ disturbance levels.
 2. Azimuth bias distribution is cut off at 3σ level since it is assumed that the near field monitor would detect variations of more than 0.5° .
 3. Accelerometer and gyro errors depend on dynamics, and the equivalent worst case value is indicated.
 4. The azimuth distribution is assumed normal to the cutoff point, and no cutoff is used on the other distributions for conservatism.
 5. Blank entries indicate no significant contribution due to that disturbance.
 6. The ΔY_{window} due to azimuth bias (*) does not contribute to window accuracy since it is measured with respect to the beam, not extended runway center line.
 7. These results are graphically presented in Figures 6-20 through 6-22.

TABLE 6-III. LATERAL RMS ACTIVITY SUMMARY

CONFIGURATION	\bar{Y} m (ft)	$\dot{\bar{Y}}$ m/sec (fps)	ϕ deg	δ_w deg	δ_R deg
(P) Blended Rate	0.94 (3.1)	0.17 (0.55)	0.95	3.4	2.0
(D) Inertial Acceleration	1.04 (3.4)	0.32 (1.05)	1.05	3.8	2.0
(E) Pseudo Acceleration	1.52 (5.0)	0.35 (1.15)	1.2	3.6	1.8

- NOTES: 1. All data was obtained during localizer track.
 2. All data represents RMS response to limiting stochastic wind and beam disturbances.

The blended lateral rate signal in the recommended system provides substantially reduced beam position and rate activity without a wheel activity penalty. The pseudo acceleration system recommended for general usage suffers a noticeable beam track performance penalty, due mainly to errors in the acceleration signals used in the beam complementary filter. In all cases, wheel activity is on a par with typical modern CTOL aircraft during localizer track, while rudder activity is somewhat larger.

In summary, the recommended system provides landing performance compatible with Cat IIIA landing requirements. With the MODILS system, azimuth bias is the major contributor to lateral touchdown dispersion. Aircraft and control activity levels are typical of current CTOL automatic landing systems.

6.5 OFF-NOMINAL CONDITIONS

The off-nominal conditions and deterministic system errors which were considered in this study include:

1. MLS guidance system errors
2. Sensor errors
3. Off-nominal approach conditions.

Those variations which significantly contribute to landing dispersion are discussed further. The probability distribution plots of the variations induced by these deterministic disturbances are included as Figures 6-20 through 6-22.

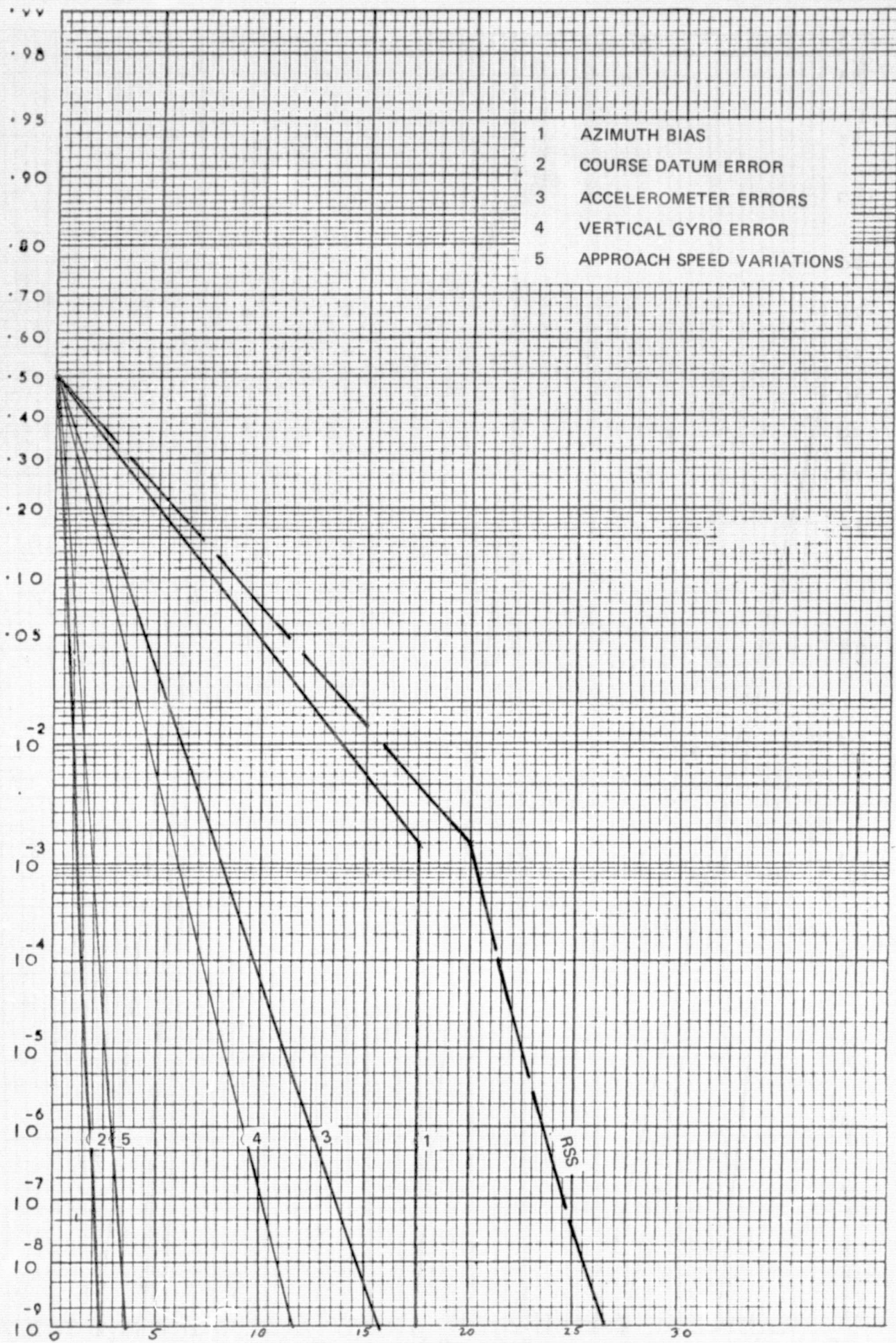


Figure 6-20. ΔY_{TD} (ft) Due to Deterministic Variation

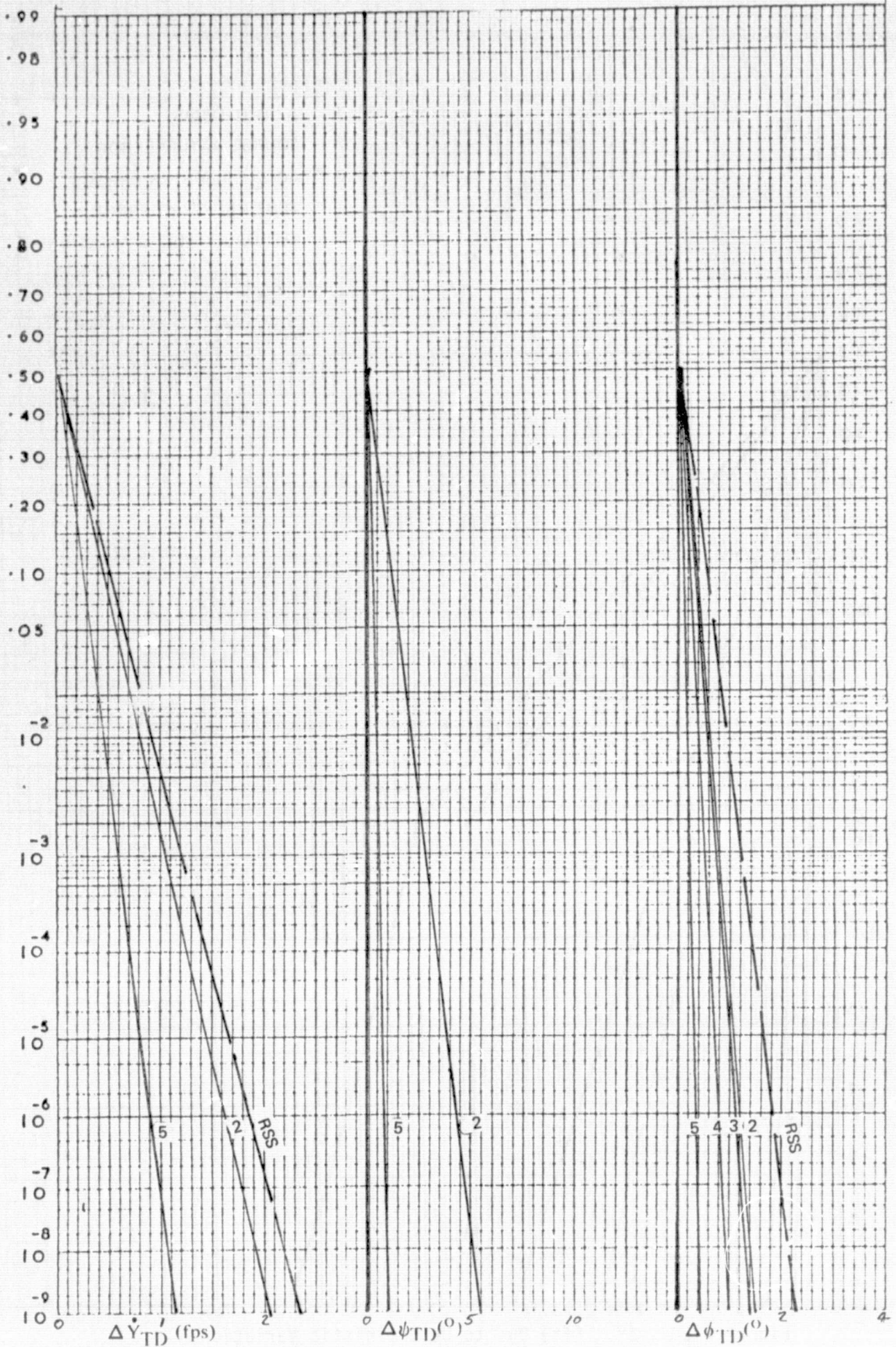


Figure 6-21. Effect of Deterministic Variations on \dot{Y} , ψ , & ϕ_{TD}

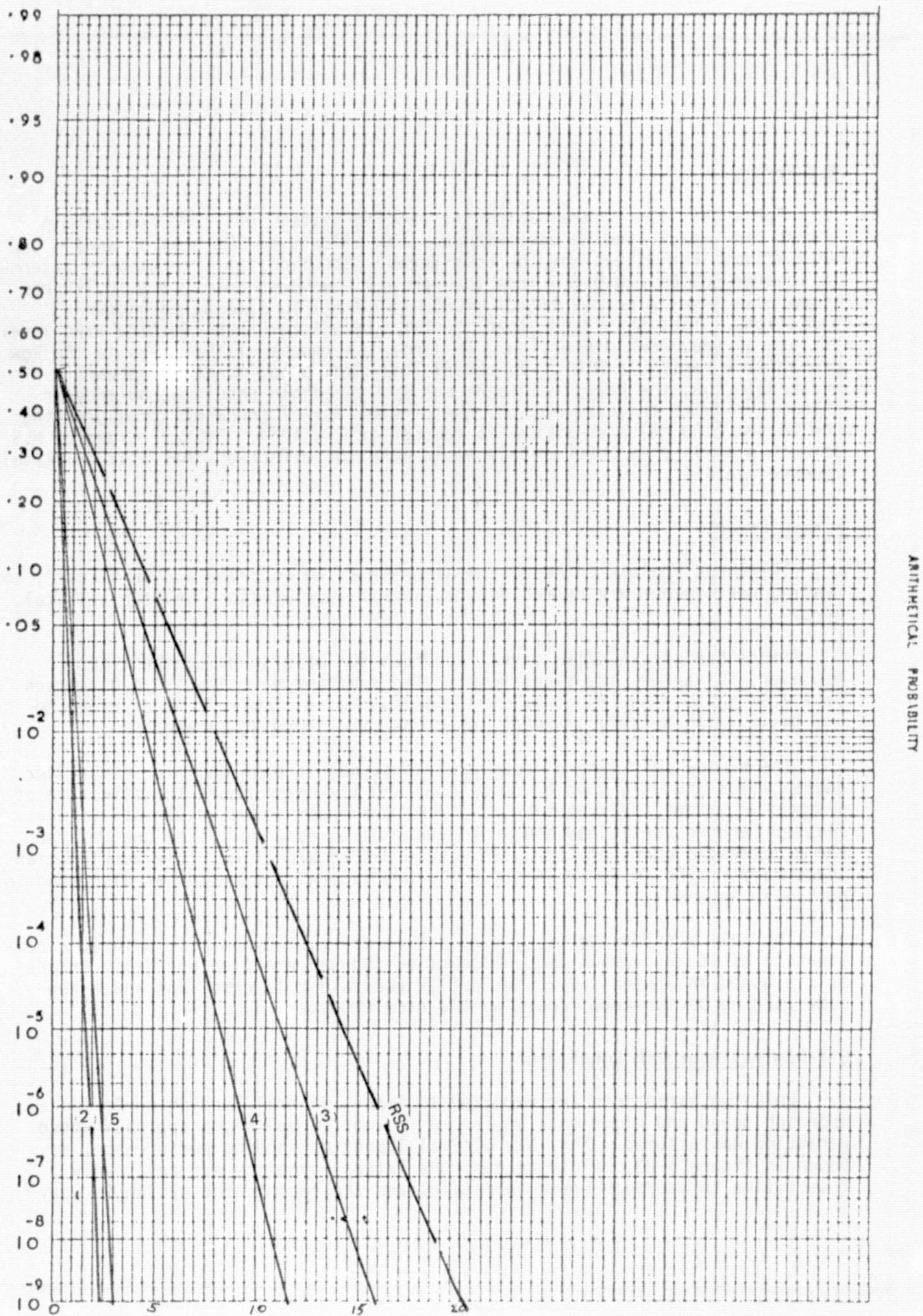


Figure 6-22. ΔY_{Window} (ft) Due to Deterministic Variations

MLS Errors

For a Cat IIIA lateral automatic landing system, only DME and azimuth errors can impact landing performance. The effects of DME bias is small, and only azimuth variations need be considered. Assuming that the azimuth antenna is located 609.6m (2000 ft) from the nominal touchdown point, the $\pm 0.17^\circ$ one sigma bias level directly yields $\pm 1.81\text{m}$ (5.93 ft) 1σ lateral touchdown variations. Thus this term alone is more significant than limiting wind levels on lateral touchdown dispersion. To limit the impact of this bias in the low probability region, a 0.5° 3σ cutoff level was used, since it appears reasonable that the near field beam monitor threshold should be no greater than 0.5° . With this assumption, the probability of one wheel transgressing the 30.48m (100 ft) wide runway is reduced to 2×10^{-8} . Typical expected MLS azimuth bias is only 0.06° , which would make the effect of this bias relatively inconsequential.

Sensor Errors

The three sensors on board the aircraft which contribute significantly to landing performance are course datum, lateral acceleration, and the vertical gyro.

Since the course datum signal provides the main input to the align maneuver, its errors are significant. The expected accuracy is ± 4.0 degrees on a 4.5σ basis. As expected, it yields touchdown misalignment on a one to one basis, with relatively small impact on other landing parameters.

The runway axis lateral acceleration signal is used both for nav filter augmentation and wing down compensation, and its error characteristics are of a dynamic nature. The equivalent offset was found to be $\pm 0.01g$ 4.5σ . The induced landing variations are very dependent on landing system design; for the recommended configuration with washed out acceleration, this acceleration inaccuracy yields $\pm 0.8\text{m}$ (2.64 ft) one sigma lateral dispersion as discussed in detail in Appendix C.

The roll attitude vertical gyro errors are also dynamic in nature, a combination of steady errors and acceleration induced erection and drift errors as discussed in Appendix C. The $\pm 0.173^\circ$ equivalent 1σ error has about the same landing performance impact as the accelerometer.

Off-Nominal Approach Conditions

Only two variations are expected to impact lateral landing performance, approach speed and glide path angle. A ± 5 knot (4.5σ) sigma approach speed variation was assumed. This has minimal impact on landing performance, as shown in figure 6-23, mainly because the lateral dynamics are relatively insensitive to approach speed variations and the recommended system is very

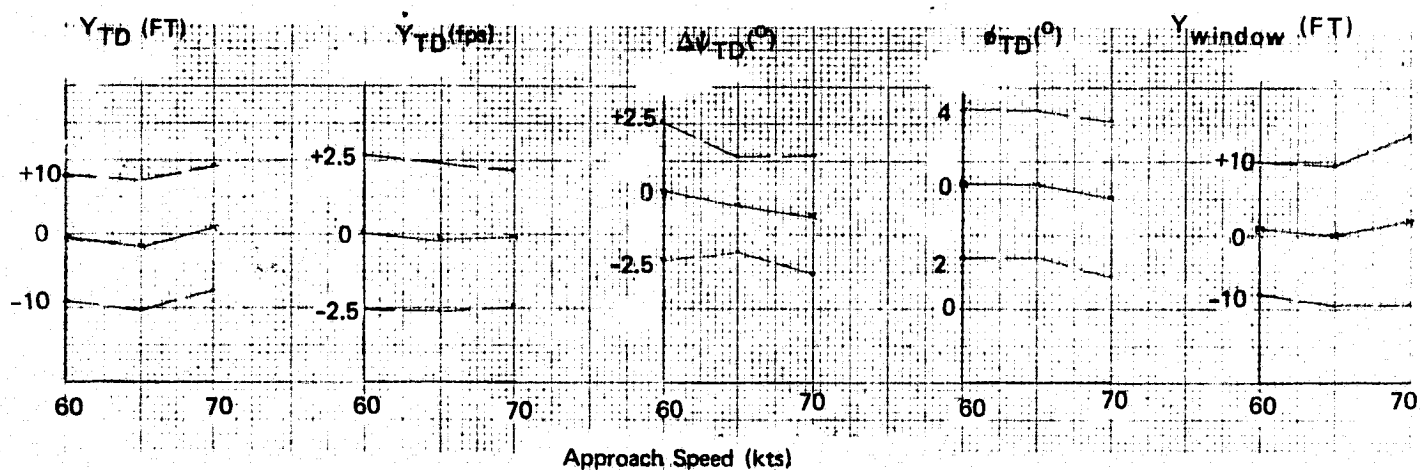


Figure 6-23. Effect of Approach Speed Variation on (#E) Landing Performance

tolerant of alignment timing variations resulting from the speed change. This tolerance to align maneuver timing changes also makes the lateral performance insensitive to approach angle variations.

6.6 FAILURE EFFECTS

A significant consideration of any autoland system design is its response to possible failures. Effects of internal failures can be handled with varying degrees of success by monitoring devices and redundant elements. Other failures external to the system must be considered also, preferably during the system design phase. Of particular interest is the response of the system to engine failure and to failure of the MLS ground station.

Table 6-IV lists results of simulation data comparing the response due to these two failures of system D with inertial acceleration, E with pseudo acceleration, and the flat decrab system (R). Data on the recommended system (P) is not included, but it would be even less sensitive to these failures than D due to the blended lateral rate signal.

Engine failure was simulated by applying a roll axis moment equal to twice the magnitude of hot thrust roll moment per engine. The moment was supplied through a 1.5 second lag to account for engine response to loss of fuel. The doubling factor was introduced to represent an increased thrust from the remaining engine that would be commanded upon recognition of the loss of one engine. The single engine rolling moment due to hot thrust was determined to be approximately 111,909 N-m (82,540 ft-lbs). Yaw moment due to hot thrust was determined to be negligible at the 80 degree nozzle angle.

Localizer failure was simulated by applying a step voltage of magnitude large enough to saturate the localizer deviation input (30.48m, or 100 feet linear deviation). No significant differences in response to localizer failure

TABLE 6-IV. LATERAL FAILURE RESPONSE SUMMARY

FAILURE	MODE	CONFIG.	PEAK ϕ DEG	TIME SEC	DEVIATION m (ft)	RATE m/sec (fps)
Engine	Align	E	2.3	9.2	15.24 (50)	3.05 (10.0)
				5.0	4.57 (15)	1.83 (6.0)
Engine	Align	D	1.3	14.0	15.24 (50)	1.31 (4.3)
				5.0	3.05 (10)	1.22 (4.0)
Engine	Loc Trk	E	2.5	9.0	15.24 (50)	2.90 (9.5)
				5.0	4.57 (15)	1.98 (6.5)
Engine	Loc Trk	D	2.1	9.6	15.24 (50)	2.74 (9.0)
				5.0	4.57 (15)	1.83 (6.0)
Engine	Loc Trk	R	4.0	6.8	15.24 (50)	5.49 (18.0)
				5.0	7.62 (25)	3.05 (10.0)
Loc Hardover	Loc Trk	R		8.0	15.24 (50)	5.03 (16.5)
				5.0	3.66 (12)	2.44 (8.0)
Loc Hardover	Loc Trk	E		8.4	15.24 (50)	4.57 (15.0)
				5.0	3.51 (11.5)	2.44 (8.0)
Loc Hardover	Align	E		8.8	15.24 (50)	4.27 (14.0)
				5.0	3.05 (10)	1.98 (6.5)
Loc Hardover	Align	D		8.8	15.24 (50)	4.57 (15.0)
				5.0	3.05 (10)	1.98 (6.5)

- NOTES:
1. Configuration D is inertial acceleration forward slip system
E is pseudo acceleration forward slip system
R is flat decrab sytem.
 2. Failure immunity would be better with recommended system (P) due to the additional inertially derived rate term.

was noted between the three configurations. However, the recommended configurations would show less sensitivity to loc hardovers because of the additional lateral acceleration derived rate term.

There is a notable difference in response to engine failure. In particular, the rate of buildup of deviation resulting from engine failure is much slower for the forward slip configurations, mainly due to acceleration and roll gain differences compared to the flat decrab system.

6.7 LIMITATIONS

All aircraft certified for automatic landing have limitations based on aircraft-peculiar characteristics. Of most interest to the present study is the determination of the maximum crab angle which can be allowed and therefore of the maximum crosswind capability. An obvious limitation on crab angle is that determined by rudder authority. With the aug wing aircraft, a 12.5 degree rudder align command limit was established allowing operation in crosswind up to 23 knots at ground level for nominal airspeed of 70 knots. However, with the large azimuth bias characteristic of the MODILS system, the maximum crosswind should be limited to 15 knots.

The accuracy of the rate damping term and of the lateral acceleration term used for wing down compensation have a pronounced effect on lateral dispersion when a large slip angle is necessary. With the recommended configuration for the Aug Wing vehicle (P), no additional limitation is necessary. Similarly, the general usage system (E) needs no additional constraint unless the subject aircraft has a wider range of landing speeds — in that case, the accuracy of the \ddot{y} approximation would have to be carefully assessed under the operating extremes.

6.8 DISPLAY CONCEPTS

The basic lateral automatic landing display philosophy is similar to that discussed in Section 5.8 for pitch. The main objective of the display during and automatic landing approach is to help the pilot monitor the operation of the autopilot. The nature and complexity of the display should be closely related to the safety and redundancy scheme of the flight control system. In a fail operational system, a very simple failure annunciator may be sufficient, while more elaborate displays are necessary for the non-redundant Augmentor Wing vehicle.

During a fully automatic landing, data suitable for display falls into two categories:

1. Data relating the present "state" of the aircraft and autoland system.
2. Data pertinent to anticipated future conditions if the approach continues, and data pertinent to anticipated future conditions if the approach is discontinued.

The first category includes both raw data (MLS deviations, radio altitude, sink rate, airspeed, course error, and attitude) and processed data such as "approach gate," flight path angle, and flight director commands. The second category is more unconventional and would include such things as projected touchdown conditions and projected go-around altitude loss or lateral deviation.

In formulating a display concept, the first guideline should be to provide only useful information which does not unnecessarily add to the pilot workload. Furthermore, it is highly desirable to formulate the displays to give a clear and unmistakable indication when pilot intervention is required.

Since the pilot's role during automatic landing is to supervise the operation and take over control only if absolutely necessary, then the display concept should attempt to assist him in deciding whether operation is acceptable or whether intervention is required. The display role is to a certain extent dependent on the level of monitoring built into the flight control system. Assuming the use of a multiple channel system with comparison type monitoring, then the display of flight director commands may be unnecessary or unwanted. His attention may better be directed toward assessing the overall performance.

For the lateral-directional axis during the runway alignment maneuver, important parameters are the lateral position, the roll angle, and the course error. The approach gate and the horizon currently provide information relative to the first two parameters with course datum error on the HSI. With the potential for increased crab angle associated with STOL aircraft, it is advisable to provide further information on heading such as superimposing a line indicative of the programmed aircraft heading on the aircraft symbol in the MFD or EADI.

A projection of probable landing conditions which accounts for observed external disturbances could be very valuable. The development of such concepts is a sizeable task and should be begun only after some agreement is reached as to exactly what information is needed and what action is to be taken by the pilot when presented with the data. Furthermore, a display concept with the capability of advising pilot intervention without necessarily having detected a system failure is quite argumentative, and in any event requires stringent precautions against giving false warning due to a display system failure.

7.0 SENSOR TRADEOFFS

Various combinations of sensors were considered in this landing system study in order to provide a performance versus equipment complement tradeoff for STOL vehicles. The considerations given in this section are based on the current study results and previous work performed in these areas. Included are inertially augmented navigation and control filters, unaugmented signal filtering, accelerometer tradeoffs, Elevation 2 system considerations, and wind estimation.

7.1 LONGITUDINAL AXIS

Use of Navigation Filters

The airspeed signal for speed control through the elevator is obtained by complementary filtering of raw airspeed with longitudinal acceleration as shown in Figure 7-1. This reduces the effect of gust induced airspeed variations without introducing lag. No attempt was made to optimize the complementary filter break frequency in this study.

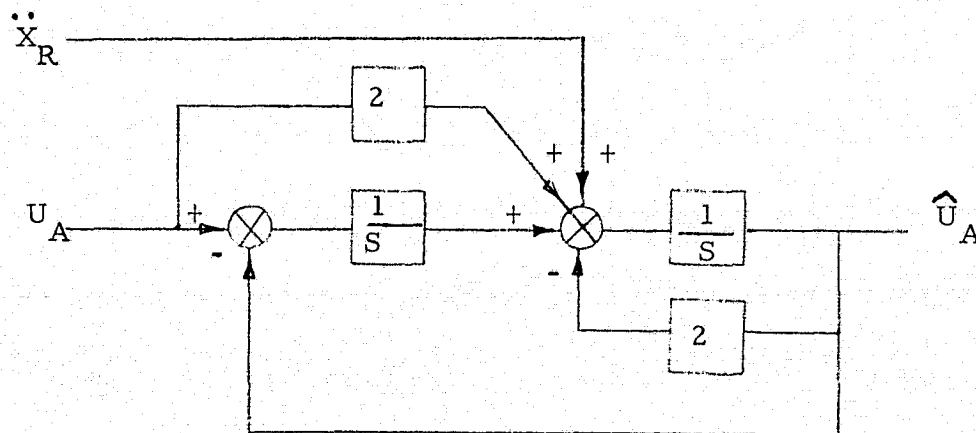


Figure 7-1. Airspeed Complementary Filter

This filter significantly reduces the pitch attitude and elevator activity by attenuating the high frequency horizontal gust induced airspeed variations in the raw air data signals. To obtain acceptable levels of activity without such a filter, the speed loop gains would be reduced, thus degrading the airspeed control and maneuver margin accuracy. In addition, the filter slows the effect of airspeed hardover failures through use of acceleration feedback and the 1 second effective second order lag time.

The Vertical Rate signal required in the glideslope and flare algorithms is generated in two distinct manners. During glideslope track, a radar altimeter derived rate signal tends to be noisy due to approach terrain variations; a smooth rate signal for path damping is obtained by integrating washed out vertical acceleration. Near the runway threshold the approach terrain gradient is more controlled, and an accurate closure rate with respect to the runway is required for accurate touchdown. Thus for flare, altitude rate as derived from the radar altimeter is phased in. Radar altitude is differentiated with a 0.1 second time constant, and the derived rate is complementary filtered with vertical acceleration as shown in Figure 7-2, to minimize the effect of high frequency noise on the derived rate signal and damp failure transients through the use of the vertical acceleration signal. A vertical filter mechanization analogous to the lateral navigation filter shown in the next section could also be used. Since the filter implemented in our simulation yielded adequate tracking and noise suppression, no alternatives were investigated during this study.

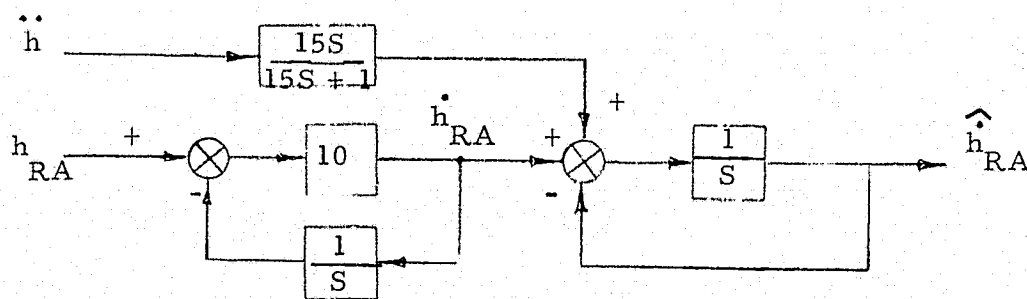


Figure 7-2. Altitude Rate Filter

For the beam deviation signal obtained from MLS information, a simple rate limited first order filter as shown in figure 7-3 is used to attenuate high frequency beam noise, limit hardover transient effects, and minimize the effects of the multipath disturbances described in Reference 7-1. Although this implementation yields acceptable beam noise induced control activity, the effect of MLS signal quantization and other irregularities could be substantially reduced by complementary filtering with vertical acceleration in a manner analogous to the lateral beam filter.

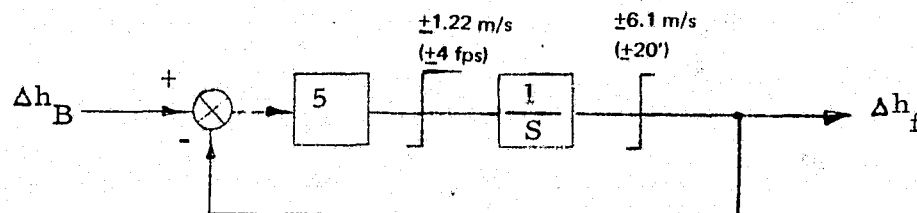


Figure 7-3. Beam Deviation Filter

Accelerometers

Linear accelerometers were used in all three axes which is consistent with the Aug Wing equipment complement. These accelerations were then transformed through aircraft Euler angles to yield longitudinal, vertical, and lateral accelerations in runway referenced axes for use in the navigation filters. For a STOL aircraft landing system which does not have the computational power provided by a digital autopilot, the longitudinal and normal accelerometers alone could be used for the pitch control system, with a simplified axis transformation. This would still yield the benefits of a complementary air-speed filter and adequate vertical acceleration accuracy for effective rate filtering and aircraft damping.

In the recommended longitudinal landing system, the longitudinal accelerometer is used for both airspeed filtering and derivation of runway referenced vertical acceleration. This accelerometer could be inclined to sense forward acceleration for the nominal approach condition, with only a small touchdown performance penalty. A revised speed control law would allow elimination of this accelerometer, yielding some increase in activity or a degradation in speed tracking but with negligible impact on touchdown sink rate and range accuracy.

However, a vertical acceleration signal is an integral part of the longitudinal landing system, contributing significantly to both its performance and integrity. It should preferably be the second derivative of altitude, but a non-resolved normal accelerometer output could also be used at some performance penalty. Vertical acceleration, as used in the recommended system, has four major advantages:

1. It provides altitude rate damping during glideslope track, independent of radar altitude, barometric source, or MLS irregularities or redundancies.
2. Acceleration is ideal for complementary filtering of both altitude rate required during flare and beam error during glideslope track.
3. As a feedback to the direct lift chokes it provides gust alleviation.
4. Its use in the control algorithm aids damping and reduces the detrimental effects of other sensor failures.

Elevation 2 Considerations

The azimuth and elevation MLS system provide the wide coverage sector consistent with the steep descents and close in maneuvering associated with efficient STOL airport operation. In this study, these guidance signals are used as a direct replacement for ILS type information, with the path filters tailored for the MLS noise characteristics. In previous studies (Reference 7-2), the suitability of MLS-derived altitude rate and acceleration signals for CTOL landing systems was also evaluated. A good rate signal was obtained only if inertially augmented complementary filters were used. Due to MLS noise characteristics, the derived acceleration signal was not useable.

The flare elevation 2 system is a higher accuracy MLS system located down the runway to provide more precise coverage through flare. The elevation 2 system and associated DME provide altitude accuracies similar to current radar altimeters, and thus would directly replace the on-board radar altimeter and provide flare quality altitude rate if acceleration-augmented. One possible deficiency is lack of runway slope information which is inherent in radar altimeters. As described in Reference 7-2, the elevation 2 system also could be used to define an inertially fixed flare trajectory rather than the h/\dot{h} profile used in our recommended system. Thus performance wise, the elevation 2 scanner could replace the radar altimeter and provide altitude rate. However, disturbance characteristics prevent derivation of effective longitudinal or vertical accelerations.

When MLS information is used for more than a mere replacement for ILS signals, both ground based and airborne system redundancy is an important consideration. In an ILS system, signal outage and switching transients lasting several seconds typically can be tolerated because guidance inputs are filtered or rate limited and basic path damping is provided by on-board sensors, while the flare system is independent of glideslope information. If MLS derived altitude and rate signals are used to replace radar altimeter and altitude rate sensors, then guidance signal outage will directly affect vehicle stability and control, and prolonged erroneous signals could not be tolerated. Thus adequate airborne and ground based MLS system redundancy would be required for CAT III landing operation.

7.2 LATERAL AXIS

The lateral landing algorithm requires cross track error, rate, and acceleration. Several means of generating these signals were evaluated in this study.

Navigation Filters

Four alternates for generating smoothed position error and rate were considered. The recommended lateral landing system uses a rate signal obtained from both the acceleration augmented complementary filter of Figure 7-4 and lagged acceleration of Figure 7-6. This three state filter

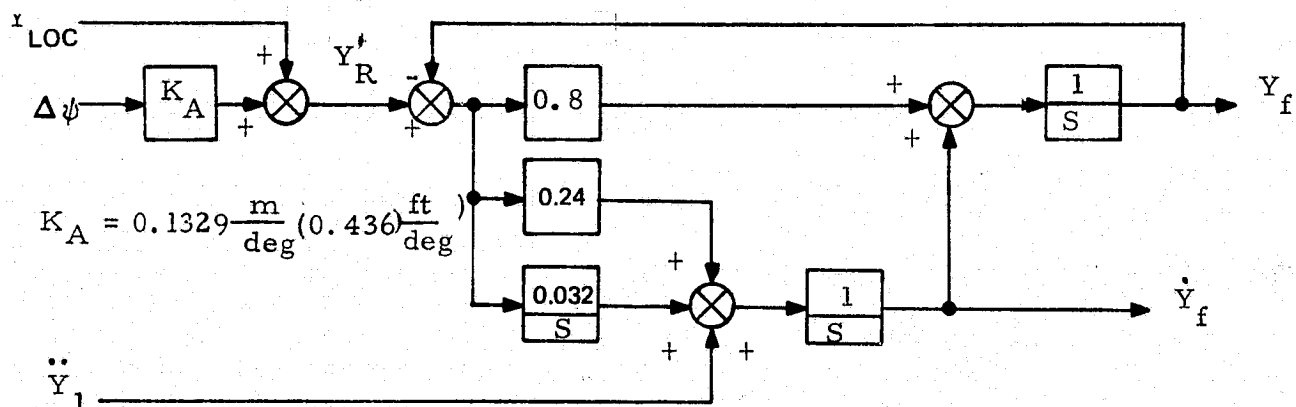


Figure 7-4. Acceleration Augmented Complementary Filter

provides smoothed position and rate signals from the raw MLS data and cross track acceleration, with inherent accelerometer bias compensation.

The runway referenced acceleration which is used in the complementation is discussed in more detail later. Its use helps minimize localizer failure transients, especially if failure logic and/or a track error limit is used to reconfigure the filter to a dead reckoning mode after failures. The filtered outputs yield tight localizer tracking without excessive control activity.

A simplified lateral landing system was also evaluated during our study, using the unaugmented beam position and rate filter shown in Figure 7-5. To maintain localizer track stability and bandwidth, only 0.5 second filtering is used. Since the MLS noise has a bandwidth of 0.25 rad/sec, this filter provides simplicity at the expense of increased activity and MLS failure susceptibility. An alternate pseudo rate signal can be obtained from washed out, lagged acceleration as shown in Figure 7-6. This rate signal provides adequate damping without inducing excessive activity. However, since lateral acceleration is required, the previously described complementary filter can be implemented with little increase in computation complexity and with substantial benefit both in stability, activity, and path tracking. A lagged roll system

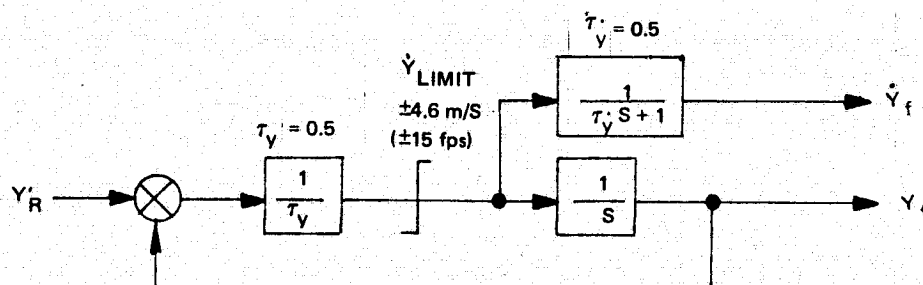


Figure 7-5. Unaugmented Lateral Filter

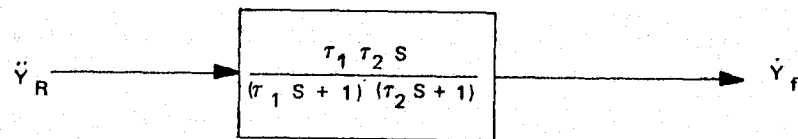


Figure 7-6. Accelerometer Derived Rate

could also be used instead of beam rate, but it is usually quite susceptible to roll gyro errors. If a crosstrack acceleration signal is not available, heading augmented rate filter could be used. A typical implementation is shown in Figure 7-7. This filter uses washed out course datum to provide a smooth rate output, with no complementation of position information. Both wind shear and the alignment maneuver input erroneous lateral steering information in the critical few seconds before touchdown. Thus this filter was not further considered in this study.

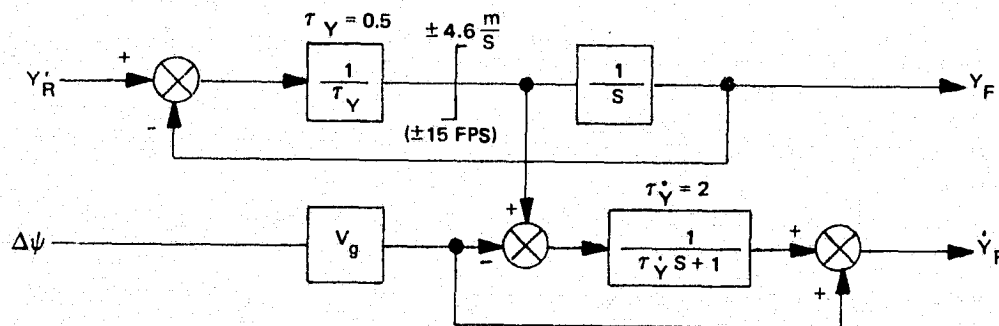


Figure 7-7. Heading Augmented Lateral Filter

Acceleration

The selection of the runway axis lateral acceleration signal for use in the navigation filter and control law involved tradeoff studies between the three candidates shown in Figure 7-8. For the Aug Wing vehicle, the computational power of the digital autopilot allows body-to-runway transformation of the three strapdown accelerometers to provide runway axis crosstrack acceleration. This implementation ($K_{\ddot{Y}_1} = K_{\ddot{Y}_2} = 1$, $K_{\ddot{Y}_3} = K_{\ddot{Y}_4} = 0$) provides the crosstrack acceleration required for both complementary filtering and wing down compensation.

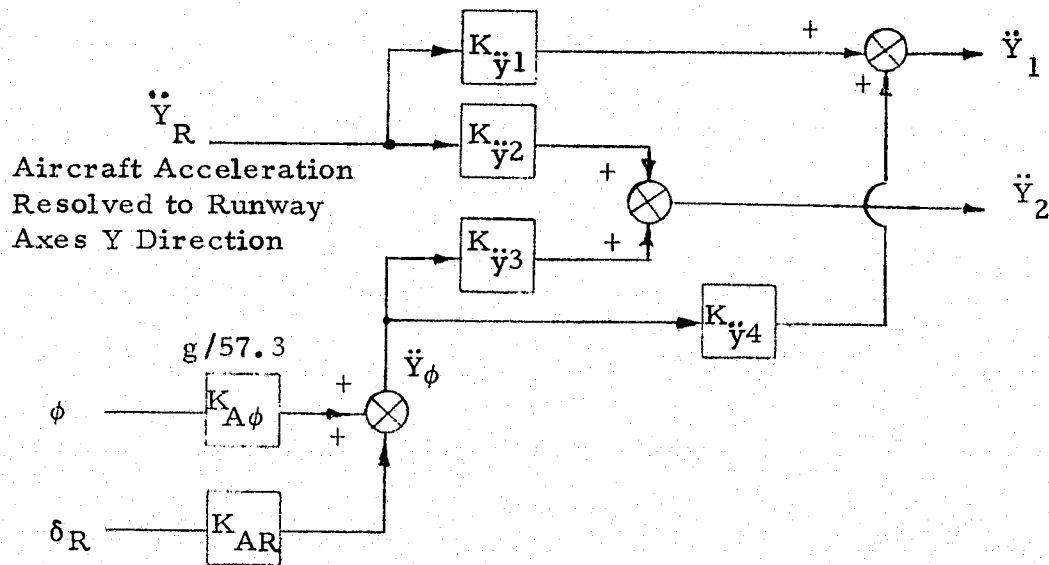


Figure 7-8. Acceleration Derivation

In a minimum sensor system, derived acceleration can be used for both filtering and control ($K_{\ddot{Y}1} = K_{\ddot{Y}2} = 0$, $K_{\ddot{Y}3} = K_{\ddot{Y}4} = 1$).

An approximation of earth axis lateral acceleration is obtained from roll attitude and rudder position, two signals which are already available in the autopilot. The roll term assumes coordinated turns during localizer track, with the rudder term required as a measure of side acceleration due to side slip during runway alignment. The rudder input should not include the trim position, and it may need to be gain scheduled if substantially different flight conditions fall within the approach flight envelope. For the Aug Wing vehicle, the derivation of crosstrack acceleration yielded acceptable landing performance.

Wind Estimation

Some of the runway alignment techniques investigated require a crosswind estimate for proper operation. Several methods were considered. An integrated INS system inherently provides wind data, but it was not available on the Aug Wing vehicle. Alternately, the wind could be navigation filter derived. However, it was felt most vehicles may not have the inertially referenced navigation filters, and thus a wind estimation technique was used that relies entirely on normal autopilot inputs, as shown in Figure 7-9.

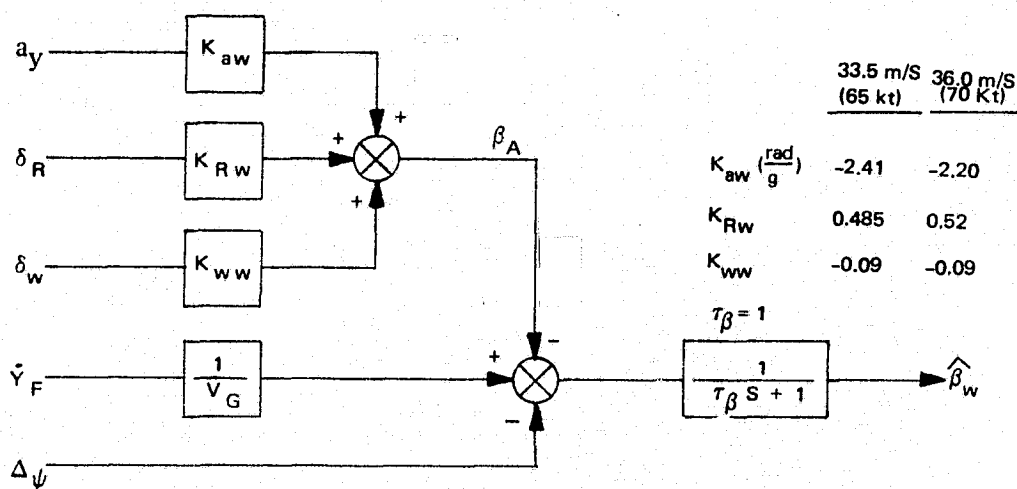


Figure 7-9. Crosswind Estimation

Basically, this involved expressing aerodynamic sideslip angle as a function of lateral acceleration and surface positions and inertial crab angle as a function of relative heading and side velocity to yield a side wind estimate. As can be seen from the gain table, the wind estimate is relatively insensitive to flight condition variations.

8.0 RECOMMENDED EXPERIMENTS

The control laws defined in this study are directly applicable to the Augmentor Wing aircraft operated by NASA Ames Research Center. In support of flight test, ARC also operates a total system simulator capable of both automatic and piloted operation. This simulator provides an efficient means to validate the recommended control law implementation, verify performance, define operational limits, and investigate failure susceptibility. This will enhance confidence in the advanced decrab and flare control algorithms and provide a data base for the subsequent aircraft test flights.

The ARC simulator has better fidelity than LSI's simulations in three areas:

1. It includes the actual digital flight control hardware and software.
2. The non-linear aerodynamics and equation of motion are solved to simulate airframe dynamics. Linearized, small perturbation equations were used in this study.
3. The simulator cockpit provides the displays and controls necessary for piloted operation, allowing pilot interaction and evaluation of the new landing control system during both normal and abnormal operation.

The essential differences between the simulator and aircraft are:

1. The lack of visual and motion cues.
2. No real actuators or sensors are included.
3. Some uncertainty in aerodynamics, especially ground proximity effects and controller characteristics.

Thus both simulator and flight test experiments are recommended to qualify the advanced landing control algorithms.

Statistical performance data collection involving a large number of automatic landings is most readily performed in the LSI hybrid simulation, and those results are included in this report. The investigation of system limitations, control activity, pilot acceptance, sensitivity to variations, and failure effects may be efficiently carried out in NASA's simulator, in addition to a limited number of statistical data runs. Flight tests will allow correlation with the simulations and evaluation or verification of other areas such as pilot acceptance and ride quality. The outline for recommended NASA simulator and in flight experiments is delineated in this section.

Simulator and in flight validation and correlation is recommended for both the Choke Augmented and Elevator Augmented pitch landing configurations. This more extensive effort is recommended for pitch since the airframe dynamics are significantly dependent on choke bias and controller usage, and there are substantial differences between the two configurations. In the lateral-directional axes, however, only wheel and rudder controls are used, and performance is mainly control law dependent. Therefore, it is felt that inflight verification of one configuration is sufficient for establishing airframe dynamics correlation, and simulation results may be relied on for configuration comparison.

8.1 NASA SIMULATOR TESTS

1. The recommended control laws should be implemented in the Augmentor Wing simulator software and verified. Step responses and calm air landing time histories should be produced and compared to results obtained in the LSI simulation. The effect of deterministic winds, shears, and low altitude wind reversals must be evaluated to complete the system verification.
2. A limited sample of landings performed on the NASA simulator in random wind disturbances can be used to validate LSI's predicted stochastic performance results and provide a data base for flight test performance correlation.
3. Sensitivity to variations of approach speed, weight, center of gravity, temperature, and glide slope angle should be evaluated. Off nominal conditions like terrain irregularities and sensor offsets may be simulated.
4. Failures should be inserted in the NASA simulator with a pilot at the controls, and their effect should be evaluated. This would supplement the work that has been done in the identification of critical failures.
5. Based on the results of the previously mentioned tests, the expected landing system limitations will be defined, along with recommended recovery techniques if these boundaries are transgressed.

8.2 FLIGHT TESTS

The major evaluation effort should be performed in simulation. The main objective of flight tests should be verification of the simulations and performing experiments in areas where simulator fidelity may be inadequate. To minimize in-flight hazard potential and instill confidence in landing system performance, all experiments should be preceded by simulator evaluation. Flight tests should be designed to evaluate the systems well within their operational envelopes, with the simulator used in the exploration of areas close to the performance boundaries.

1. Verification of beam track and flare in calm air. Step responses and time histories should be obtained for correlation with the simulator.
2. A limited effort should be directed at the performance of landings in measured wind conditions. Actual wind profiles should be recorded to enhance correlation.
3. Some of the variations in approach speed, weight, and glide slope angle may justify flight verification.
4. Failures may be inserted in flight to expand the simulator results if it is safe to do so.
5. Correlation and evaluation of both Choke Augmented and Elevator Augmented configurations should be performed during the flight test phase.

APPENDIX A
SIMULATION DEFINITION

LIST OF FIGURES AND TABLES

<u>Figure</u>	<u>Title</u>	<u>Page</u>
A-1	Longitudinal Airframe Step Responses	A-7
A-2	Longitudinal Airframe Step Responses	A-8
A-3	Free Airframe Step Gust Responses	A-9
A-4	Lateral Airframe Response at 65 Knots	A-10
A-5	Longitudinal Actuator Models	A-11
A-6	Throttle Model Including Delay	A-12
A-7	Throttle Step Responses	A-12
A-8	Lateral Directional Actuator Models	A-13
A-9	Airplane Geometry	A-14
A-10	Wind Shear Spike Profile	A-18
A-11	MODILS Error Models	A-19
A-12	Standard Wind Model	A-20
A-13	Altitude Profile Generation	A-21
A-14	Typical Altitude Profiles	A-22
<u>Table</u>	<u>Title</u>	<u>Page</u>
A-I	Longitudinal Equations of Motion	A-3
A-II	Longitudinal Stability Derivatives	A-4
A-III	Lateral Directional Equations of Motion	A-5
A-IV	Lateral Directional Stability Derivatives	A-6
A-V	Physical Data for Landing Configuration	A-16
A-VI	Sensor Characteristics	A-17

APPENDIX A

SIMULATION DEFINITION

The nonpiloted simulation of the C-8A Augmentor Wing Jet STOL Research Aircraft (AWJSRA) and its automatic landing system are defined in this appendix. This simulation definition includes:

1. Airframe Dynamics
2. Control Dynamics
3. Geometry and Sensors
4. MLS Noise Model
5. Wind Models

A-1 AIRFRAME DYNAMICS

The nominal flight condition for this study is defined below. For this weight, the approach speed was conservatively selected slower than the speed required for the maneuver margin, especially with chokes deployed.

	<u>No Chokes</u>		<u>Chokes</u>
Weight	177929N	(40,000 lb)	
Speed	33.47 m/sec	(65 Kt)	
α	0.0906 rad	(5.19 ⁰)	0.1012 rad (5.8 ⁰)
γ	-0.1309 rad	(-7.5 ⁰)	
RPM	92%		94%
Flaps	1.134 rad	(65 ⁰)	
Nozzles	1.309 rad	(75 ⁰)	1.396 rad (80 ⁰)

A-1.1 Equations of Motion

The normal set of uncoupled, linearized, small perturbation aerodynamic equations of motion were used as documented in Tables A-I and III. The aircraft equations and stability derivatives incorporated in the separate longitudinal and lateral landing simulations are described in detail, along with representative time responses.

A-1.2 Stability Derivatives

These data were obtained from References A-1 and A-2. Two flight conditions were used during the longitudinal studies and three flight cases for the lateral studies. The stability axes dimensional derivatives and other pertinent data are included in Tables A-II and A-IV.

A-1.3 Airframe Response Characteristics

Characteristic roots for the nominal 33.47 m/sec (65 Kt) approach case are given below.

Longitudinal:	$\zeta_{sp} = 0.976$	$\omega_{sp} = 1.004 \text{ 1/sec}$
	$\zeta_{ph} = 0.230$	$\omega_{ph} = 0.1883 \text{ 1/sec}$
Lateral:	$\zeta_{DR} = 0.291$	$\omega_{DR} = 0.931 \text{ 1/sec}$
	$\tau_S = -4.68 \text{ sec}$	$\tau_R = 1.44 \text{ sec}$

For the nominal flight condition, the longitudinal free aircraft responses are shown in Figures A-1 and 2 for step elevator, choke, throttle, and nozzle inputs, and in Figure A-3 for u and α gust inputs. The lateral aircraft response to p and r initial conditions and wheel and rudder step inputs are included as Figure A-4.

A-2 CONTROL SYSTEM DYNAMICS

For the Aug Wing vehicle, control surface aerodynamic and inertia loads were sufficiently small that acceleration limits and detailed actuator models were not required. Thus only important nonlinearities as hysteresis and rate and position limits were included in this study. The simplified actuator models are described in this section.

A-2.1 Longitudinal Control System

The elevator, throttle, choke, and nozzle actuator models are presented as Figure A-5. Spoilers and flaps were not used as control elements in longitudinal landing studies. A 30% choke bias is used, to give a $\pm 0.1 \text{ g}$ direct lift capability.

TABLE A-I. LONGITUDINAL EQUATIONS OF MOTION

$$\dot{u} = X_u \cdot u_A + X_w \cdot w_A - g \cos \gamma_O \cdot \theta + [\Delta X_{GE} + \Delta X_{aGE} \cdot a] \cdot HF \\ + X_{\delta e} \cdot \delta_e + X_{\delta RPM} \cdot \delta_{RPM} + X_{\delta N} \cdot \delta_N + X_{\delta CH} \cdot \delta_{CH}$$

$$\dot{w} = Z_u \cdot u_A + Z_w \cdot \dot{w} + Z_w \cdot w_A + (U_O + Z_q) \cdot q - g \sin \gamma_O \cdot \theta + [\Delta Z_{GE} + \Delta Z_{aGE} \cdot a] \cdot HF \\ + Z_{\delta e} \cdot \delta_e + Z_{\delta RPM} \cdot \delta_{RPM} + Z_{\delta N} \cdot \delta_N + Z_{\delta CH} \cdot \delta_{CH}$$

$$\dot{q} = M_u \cdot u_A + M_{\dot{w}} \cdot \dot{w} + M_w \cdot w_A + M_q \cdot q + [\Delta M_{GE} + \Delta M_{aGE} \cdot a] \cdot HF \\ + M_{\delta e} \cdot \delta_e + M_{\delta RPM} \cdot \delta_{RPM} + M_{\delta N} \cdot \delta_N + M_{\delta CH} \cdot \delta_{CH}$$

$$\ddot{h} = U_I (q - \dot{a}) + \sin \gamma_O \cdot \dot{u}$$

$$\dot{h} = U_I \cdot \gamma_I$$

$$\dot{a} = \dot{w}/U_O, a_A = w_A/U_O$$

$$U_I = U_O + u_A - u_{WIND}$$

$$\gamma_I = \theta_T - a_T$$

$$a_T = a_O + a_A - a_{WIND}$$

$$\theta_T = \theta_O + \theta$$

$$HF = e^{-(hg/h_{GE})}$$

u_A, w_A, a_A are incremental aerodynamic values about trim

θ is incremental pitch attitude about trim.

The subscripts o and τ indicate trim and total values respectively.

The subscript I indicates inertial quantity.

TABLE A-II. LONGITUDINAL STABILITY DERIVATIVES

Parameter	Units	Nominal Flight Condition		Heavy Weight	
W	N (lb)	177929.	(40000.)	213515.	(48000.)
U ₀	m/sec (kt)	33.47	(65.)	37.59	(73.)
α_0 (with chokes)	radians (deg)	.1012	(5.8)	.1012	(5.8)
RPM (with chokes)	%	94.	(94.)	94.	(94.)
I _y	kg-m ² (slug-ft ²)	280656.	(207000.)	336781.	(248400.)
X _u	1/sec	-.068	(-.068)	-.062	(-.062)
Z _u	1/sec	-.281	(-.281)	-.223	(-.223)
M _u	1/m-sec (1/ft-sec)	-.00115	(-.00035)	.00012	(+.000036)
Z _w	1	-.013	(-.013)	-.0092	(-.0092)
M _w	1/m (1/ft)	-.0121	(-.0037)	-.0082	(-.0025)
X _w	1/sec	.136	(.136)	.110	(.110)
Z _w	1/sec	-.505	(-.505)	-.478	(-.478)
M _w	1/m-sec (1/ft-sec)	-.0148	(-.0045)	-.0234	(-.00713)
Z _q	m/sec (ft/sec)	0.0	(0.0)	0.0	(0.0)
M _q	1/sec	-1.08	(-1.08)	-.967	(-.967)
X _{δe}	m/sec ² (ft/sec ²)	0.0	(0.0)	0.0	(0.0)
Z _{δe}	m/sec ² (ft/sec ²)	-1.676	(-5.5)	-1.743	(-5.72)
M _{δe}	1/sec ²	-1.56	(-1.56)	-1.59	(-1.59)
X _{δRPM}	m/sec ² -% (ft/sec ² -%)	.0049	(.0161)	.0309	(.1015)
Z _{δRPM}	m/sec ² -% (ft/sec ² -%)	-.6767	(-2.22)	-.5456	(-1.79)
M _{δRPM}	1/sec ² -%	.0081	(.0081)	.0048	(.0048)
X _{δN}	m/sec ² (ft/sec ²)	-1.1247	(-3.69)		
Z _{δN}	m/sec ² (ft/sec ²)	-.1076	(-.353)		
M _{δN}	1/sec ²	-2.865	(-2.865)		
X _{δCH}	m/sec ² -% (ft/sec ² -%)	.00112	(.00369)	.00118	(.00387)
Z _{δCH}	m/sec ² -% (ft/sec ² -%)	.03344	(.1097)	.03511	(.1152)
M _{δCH}	1/sec ² -%	-.00026	(-.00026)	-.00027	(-.00027)
ΔX _{GE}	m/sec ² (ft/sec ²)	.5471	(1.795)	.5745	(1.885)
ΔZ _{GE}	m/sec ² (ft/sec ²)	-.5468	(-1.794)	-.5741	(-1.884)
ΔM _{GE}	1/sec ²	-.1855	(-.1855)	-.1948	(-.1948)
ΔX _{αGE}	m/sec ² (ft/sec ²)	1.0442	(3.426)	1.0964	(3.597)
ΔZ _{αGE}	m/sec ² (ft/sec ²)	3.4808	(11.42)	3.6548	(11.99)
ΔM _{αGE}	1/sec ²	-.935	(-.935)	-.982	(-.982)
h _{GE}	m (ft)	4.572	(15.0)	4.572	(15.0)

NOTE: 1. All derivatives are given in stability axes.
2. All angles are in radians unless otherwise noted.

TABLE A-III. LATERAL DIRECTIONAL EQUATIONS OF MOTION

$$U_O \cdot \dot{\beta} = Y_p \cdot p_A + a_o \cdot U_O \cdot p + Y_r \cdot r_A - U_O \cdot r + Y_\beta \cdot \beta_A + g \cos \theta_O \cdot \phi$$

$$+ Y_{\delta R} \cdot \delta_R + Y_{\delta A} \cdot \delta_A + Y_{\delta SP} \cdot \delta_{SP} + Y_{\delta CH} \cdot \delta_{CH}$$

$$\dot{p} = L_p \cdot p_A + \frac{I_{xz}}{I_x} \cdot \dot{r} + L_r \cdot r_A + L_\beta \cdot \dot{\beta} + L_\beta \cdot \beta_A$$

$$+ L_{\delta R} \cdot \delta_R + L_{\delta A} \cdot \delta_A + L_{\delta SP} \cdot \delta_{SP} + L_{\delta CH} \cdot \delta_{CH}$$

$$\dot{r} = N_p \cdot p_A + \frac{I_{xz}}{I_z} \cdot \dot{p} + N_r \cdot r_A + N_\beta \cdot \beta + N_\beta \cdot \beta_A$$

$$+ N_{\delta R} \cdot \delta_R + N_{\delta A} \cdot \delta_A + N_{\delta SP} \cdot \delta_{SP} + N_{\delta CH} \cdot \delta_{CH}$$

$$\begin{bmatrix} p \\ r \end{bmatrix}_B = \begin{bmatrix} \cos a_O & -\sin a_O \\ \sin a_O & \cos a_O \end{bmatrix} \begin{bmatrix} p \\ r \end{bmatrix}_s$$

Body axes rates

$$\dot{\phi} = p_B + \tan \theta_O \cdot r_B$$

Euler rates

$$\dot{\psi} = r_B$$

$$a_y = U_O (\dot{\beta} + r_B) - g \phi$$

Lateral acceleration

$$\ddot{Y}_R = \cos \Delta \psi \cdot (a_y + g \phi)$$

Runway crosstrack acceleration

$$\beta_A = \beta + \beta_{WIND}$$

$$\Delta \psi = \psi - \psi_{RUNWAY}$$

δ_A , δ_{SP} , and δ_{CH} indicate differential deflections, with chokes given in %.

The A and o subscripts denote aerodynamic and trim quantities respectively.

The B subscript denotes body axes quantities.

The subscript I indicates inertial quantity.

TABLE A-IV. LATERAL DIRECTIONAL STABILITY DERIVATIVES

Parameter	Units	Slow Flight Condition		Nominal Flight Condition		Fast Flight Condition	
U_0	m/sec (kts)	30.9	(60.)	33.5	(65.)	36.0	(70.)
α_0	rad (deg)	.123	(7.07)	.0906	(5.19)	.0541	(3.1)
RPM	%	91.4		91.0		90.8	
I_X	kg-m ² (slug-ft ²)	350966.	(258857.)	352448.	(259950.)	355227.	(262000.)
I_Z	kg-m ² (slug-ft ²)	604894.	(446143.)	603412.	(445050.)	601175.	(443400.)
I_{XZ}	kg-m ² (slug-ft ²)	18350.	(13534.)	26642.	(19650.)	35712.	(26340.)
Y_p/U_0		- .138		- .1046		- .0677	
Y_r/U_0		.024		.0236		.0240	
$Y_{\dot{\beta}}/U_0$	1/sec	- .118		- .1216		- .124	
L_p	1/sec	- .579		- .612		- .6504	
L_r	1/sec	.908		.863		.842	
$L_{\dot{\beta}}$	1/sec	- .0049		- .0068		- .0089	
$L_{\dot{\beta}}$	1/sec ²	0.0		0.0		0.0	
N_p	1/sec	- .219		- .2064		- .1907	
N_r	1/sec	- .278		- .285		- .256	
$N_{\dot{\beta}}$	1/sec	.024		.0255		.0272	
$N_{\dot{\beta}}$	1/sec ²	.430		.510		.596	
$Y_{\delta R}/U_0$	1/sec	.055		.0593		.064	
$L_{\delta R}$	1/sec ²	.141		.206		.293	
$N_{\delta R}$	1/sec ²	- .670		- .7754		- .895	
$Y_{\delta A}/U_0$	1/sec	- .0050		- .0052		- .0055	
$L_{\delta A}$	1/sec ²	.737		.695		.677	
$N_{\delta A}$	1/sec ²	- .038		- .060		- .037	
$Y_{\delta SP}/U_0$	1/sec	- .0090		- .0095		- .010	
$L_{\delta SP}$	1/sec ²	.273		.280		.321	
$N_{\delta SP}$	1/sec ²	- .0036		- .0058		0.0	
$Y_{\delta CH}/U_0$	1/sec-%	- .0000524		- .0000559		- .0000524	
$L_{\delta CH}$	1/sec ² -%	.00363		.00428		.00337	
$N_{\delta CH}$	1/sec ² -%	.00001		.000063		.00014	

NOTE: 1. All derivatives and inertias are given in stability axes:
2. All angles are in radians unless otherwise noted.

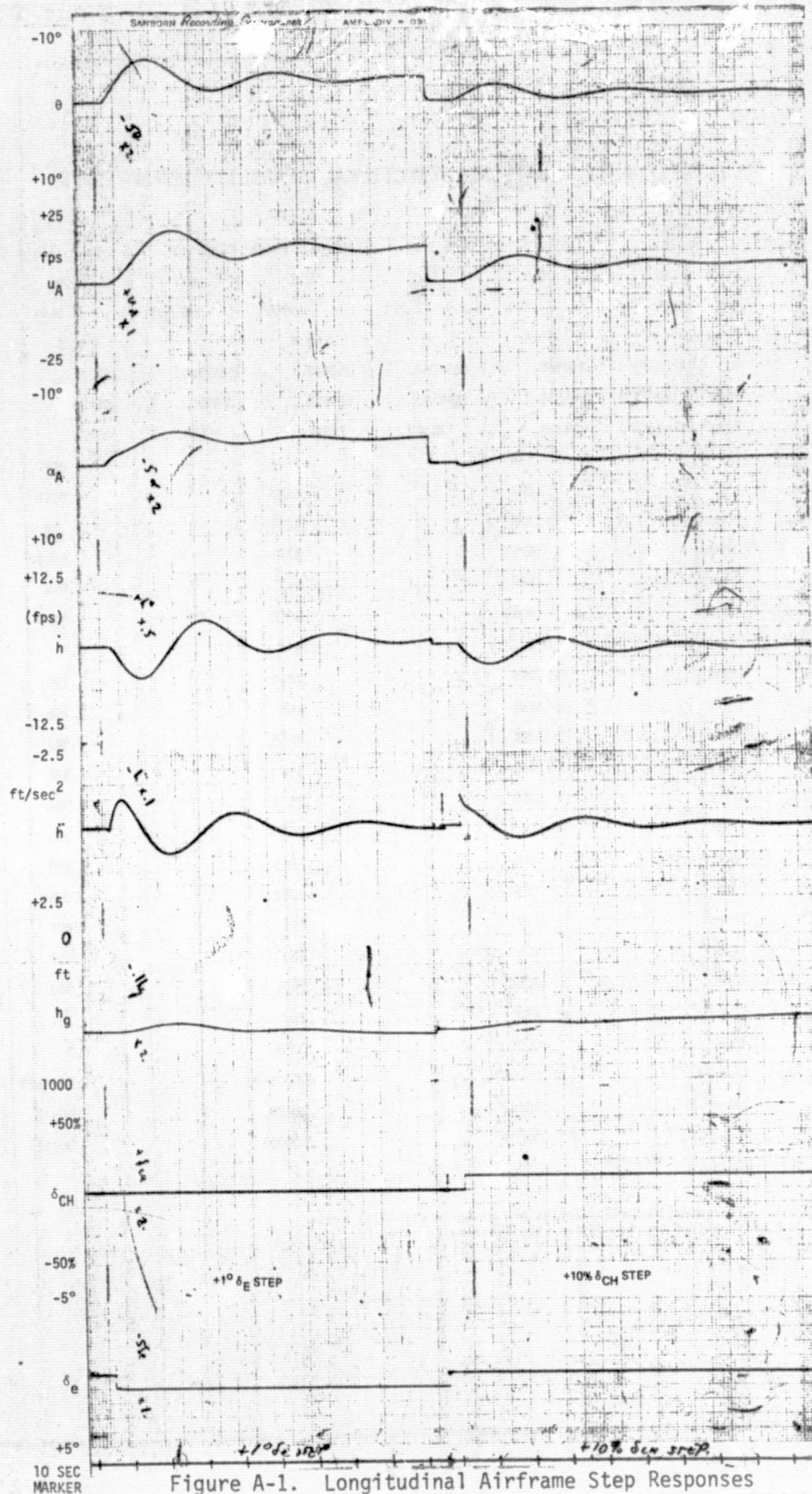


Figure A-1. Longitudinal Airframe Step Responses

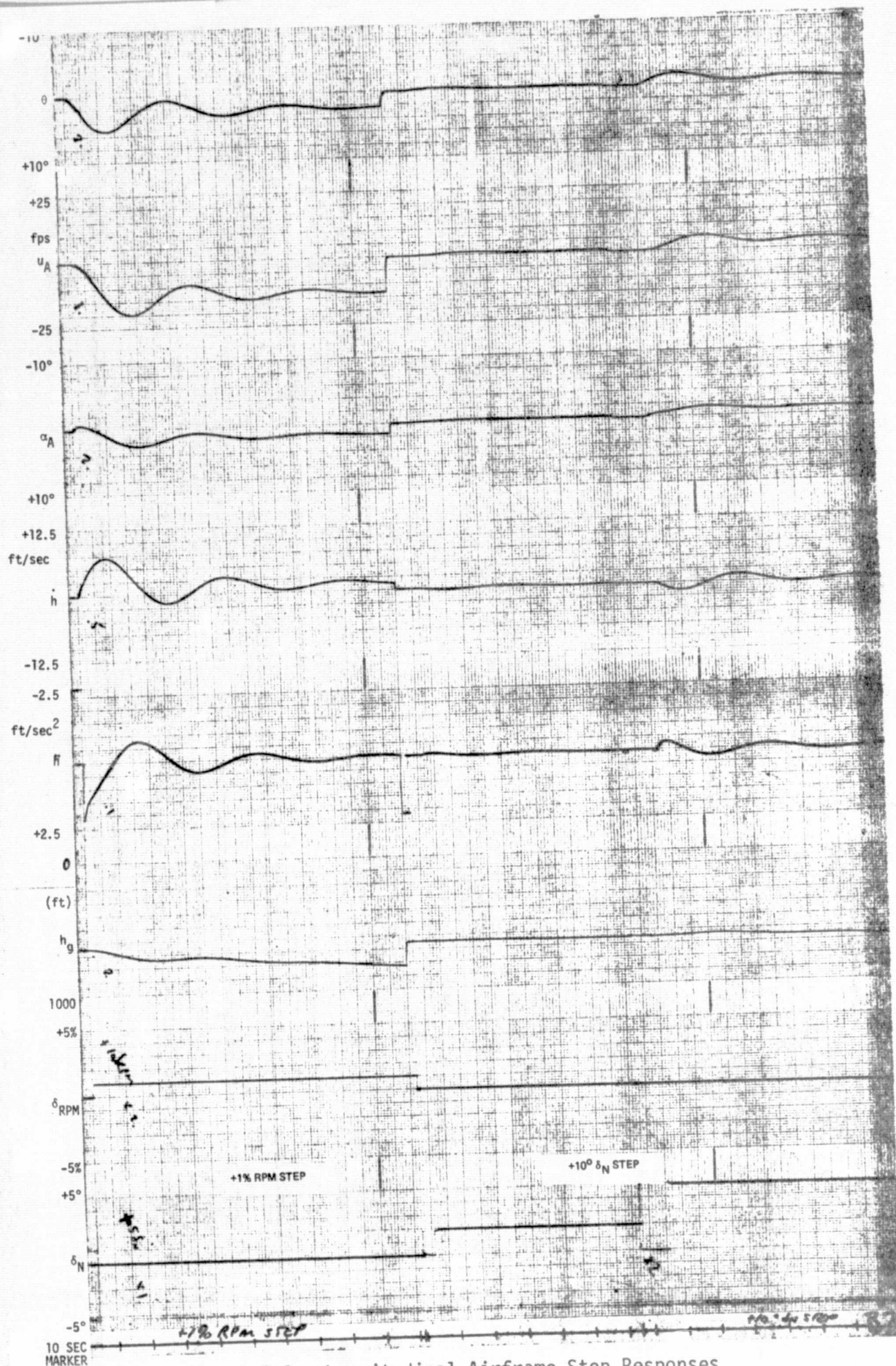


Figure A-2. Longitudinal Airframe Step Responses

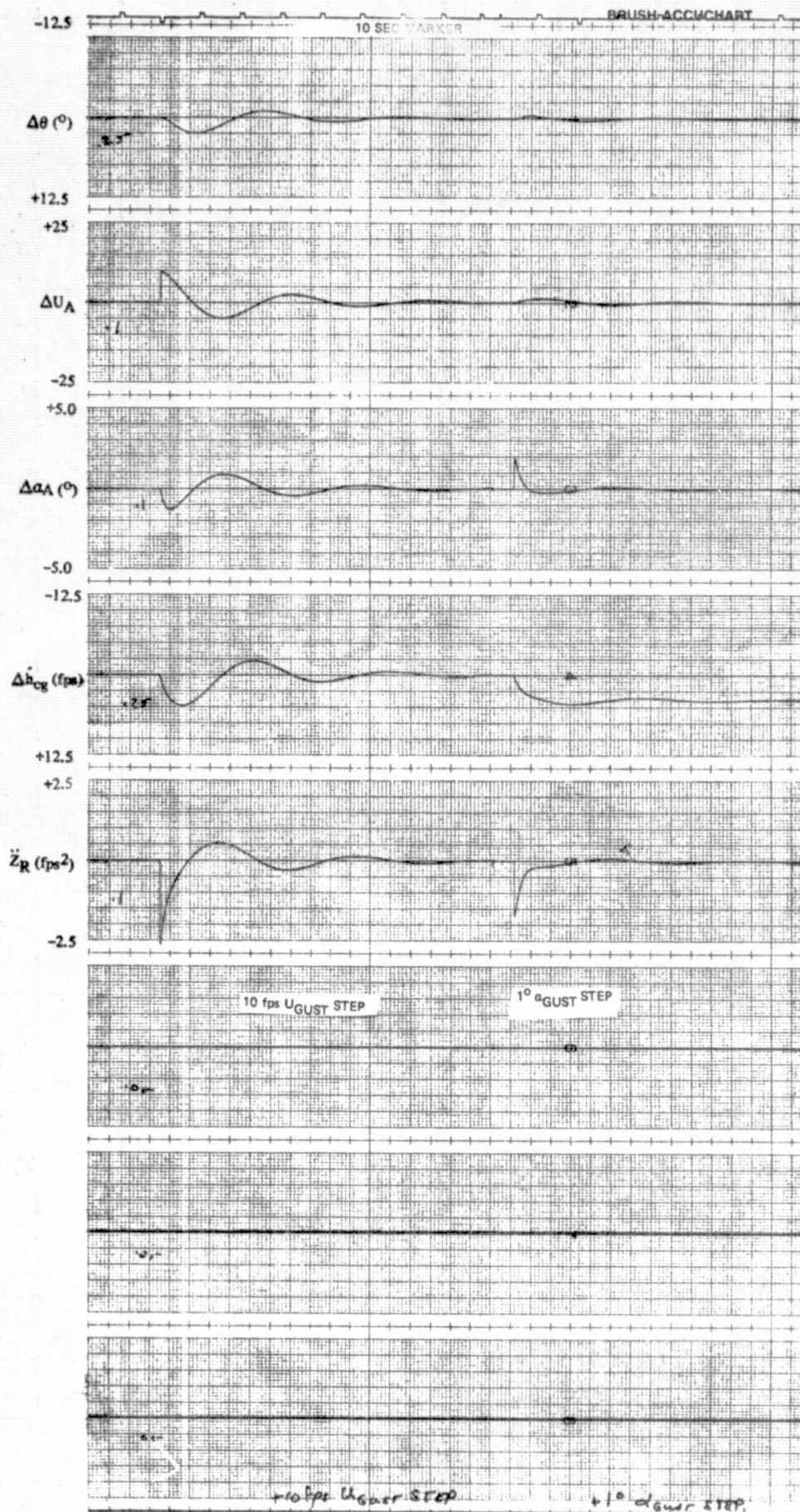


Figure A-3. Free Airframe - Step Gust Responses

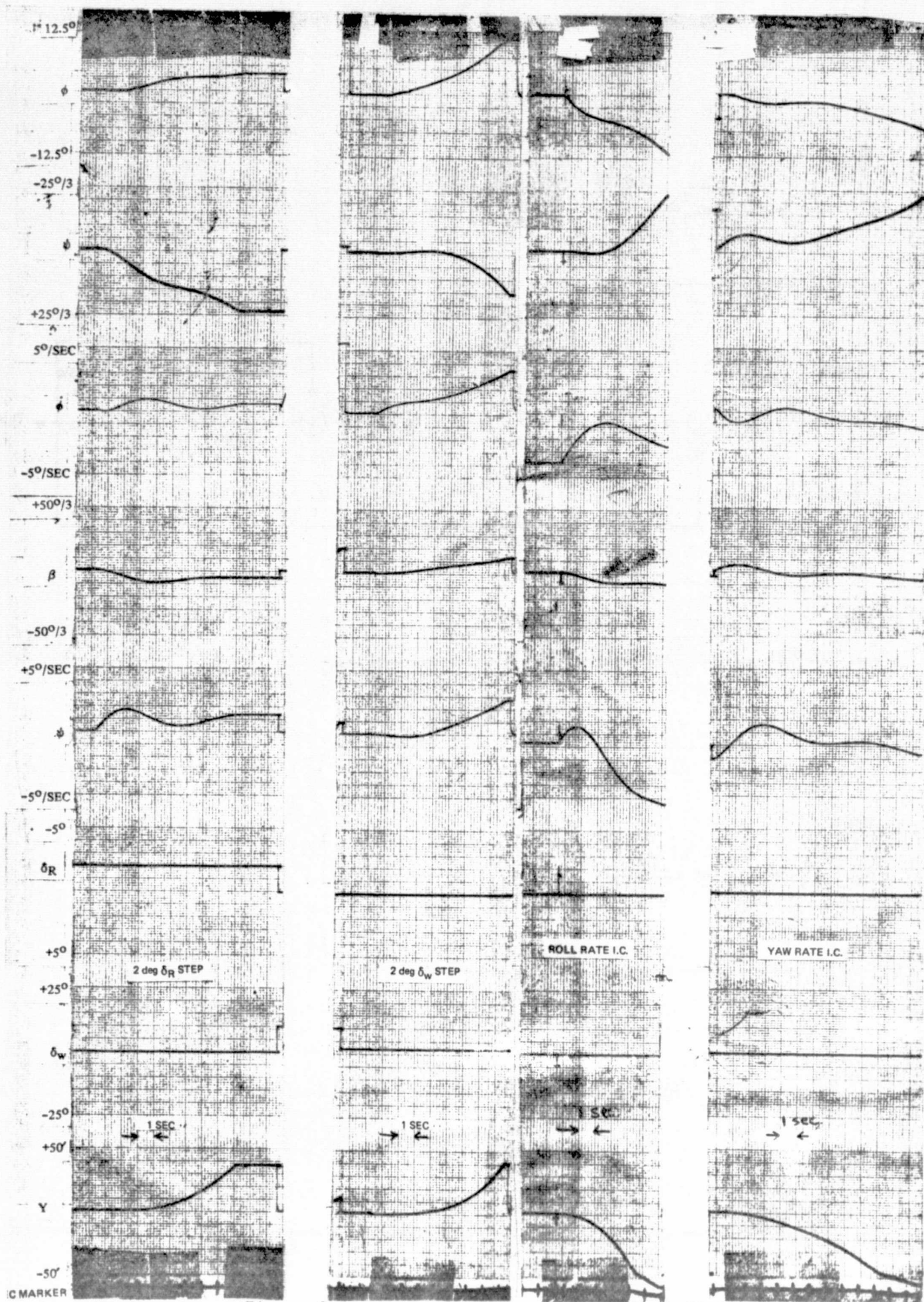


Figure A-4. Lateral Airframe Response at 65 Kts

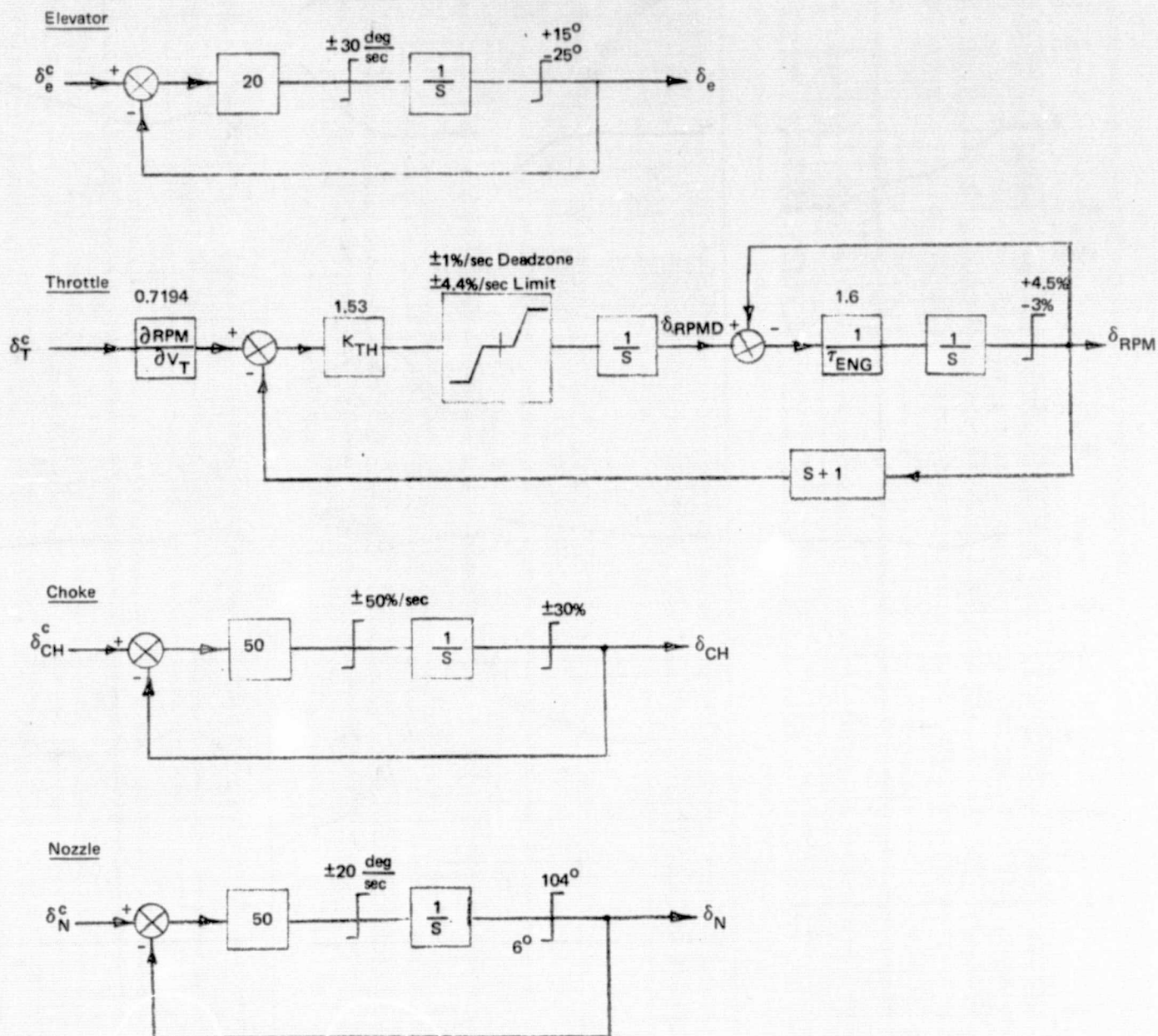


Figure A-5. Longitudinal Actuator Models

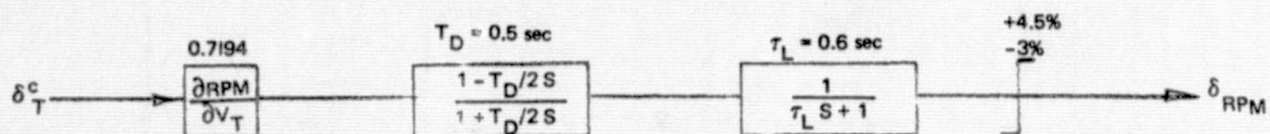


Figure A-6. Throttle Model Including Delay

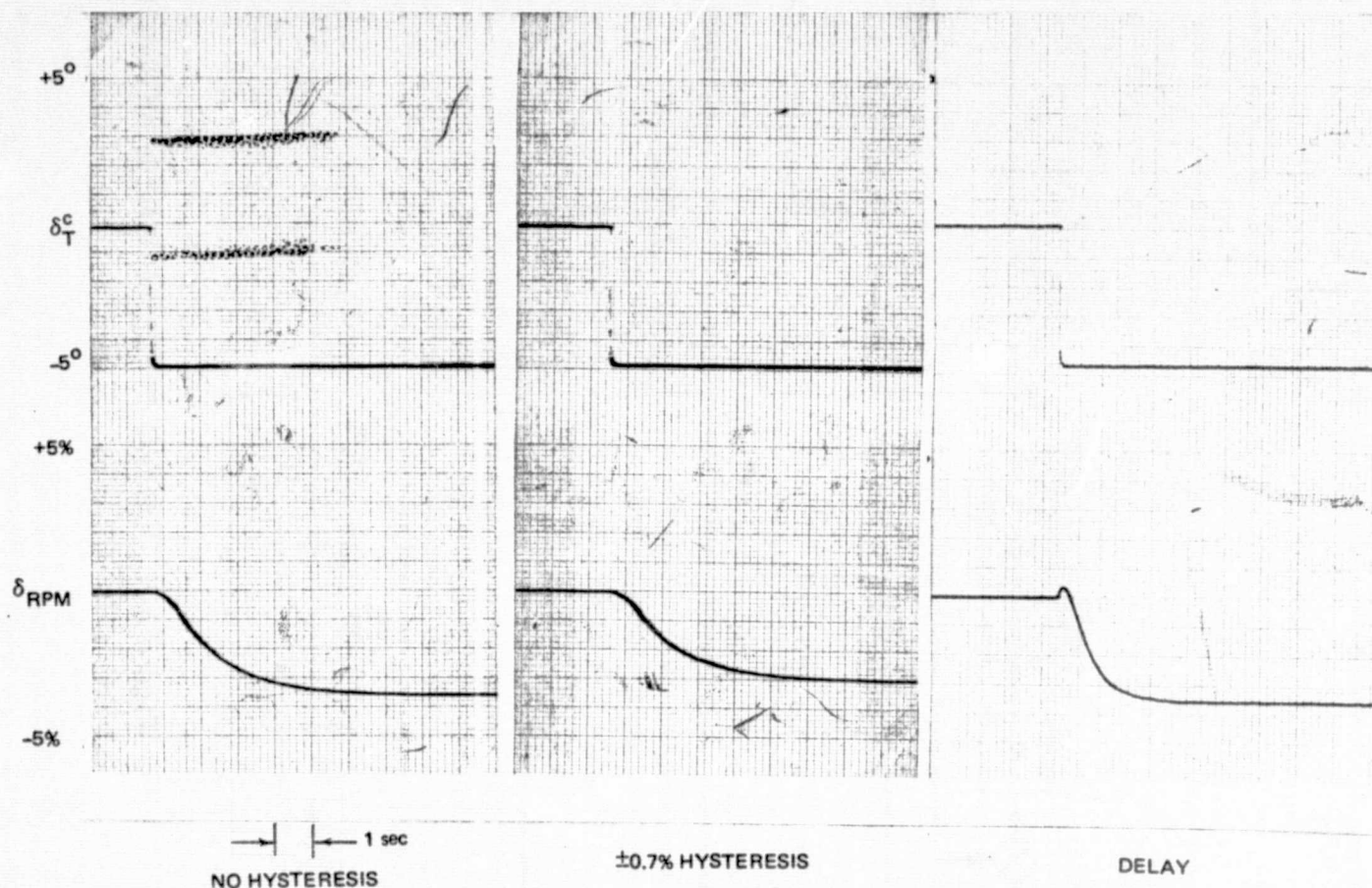


Figure A-7. Throttle Step Responses

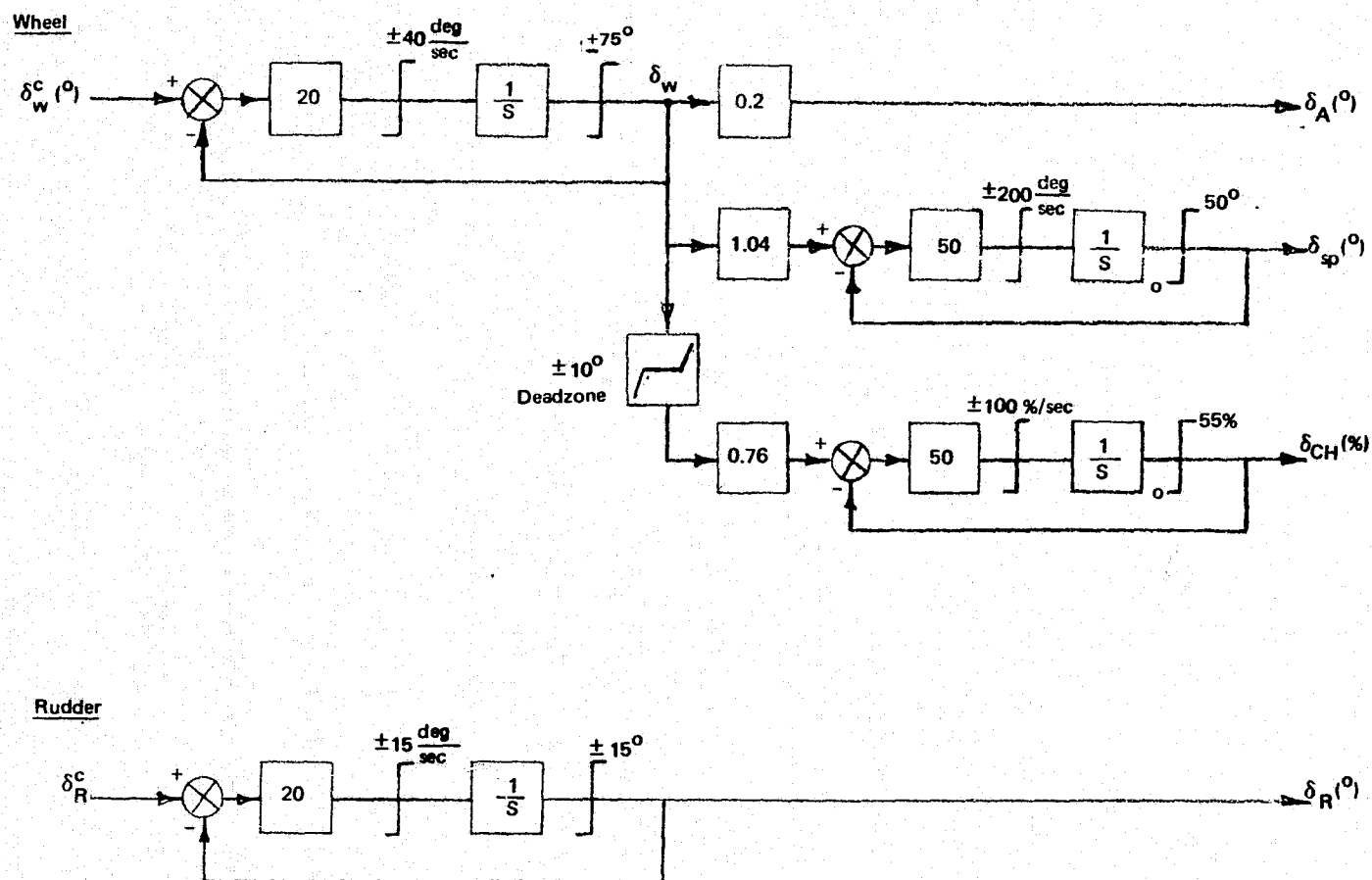


Figure A-8. Lateral-Directional Actuator Models

Throttle Model Variations

The nominal throttle model shown in Figure A-5 includes 1.4% total RPM hysteresis. The impact of doubled hysteresis on landing performance was also considered. Based on Aug Wing flight test data, a different model was developed, consisting of cascaded 0.5 sec time delay and 0.6 sec engine lag. The simulation implementation is given as Figure A-6. Step responses of the nominal model with and without hysteresis, and of the delay model are shown in Figure A-7. This indicates that our nominal model attains 50% of the command in 1.5 sec versus 0.9 sec for the delay model. Thus the nominal model provides a conservative approximation of actual throttle response characteristics.

A-2.2 Lateral Directional Control System

The wheel, rudder, aileron, spoiler, and choke models are shown in Figure A-8, along with the roll control nonlinearities. The spoiler and choke actuator dynamics were omitted during our studies with negligible loss of fidelity since the wheel actuator dynamics and limits are more constraining.

A-3 GEOMETRY AND SENSORS

A-3.1 Sensor Geometry

The relative geometry of the gear, c.g., and MLS antenna are illustrated in Figure A-9. The gear and MLS receiver location are expressed in terms of cg height above the runway by the expressions:

$$\begin{aligned} h_G &= h_{cg} - Z_G \cos \theta + X_G \sin \theta & X_{REC} &= 7.62\text{m (25.0 ft)} \\ h_{REC} &= h_{cg} - Z_{REC} \cos \theta + X_{REC} \sin \theta & Z_{REC} &= 1.524\text{m (5.0 ft)} \end{aligned}$$

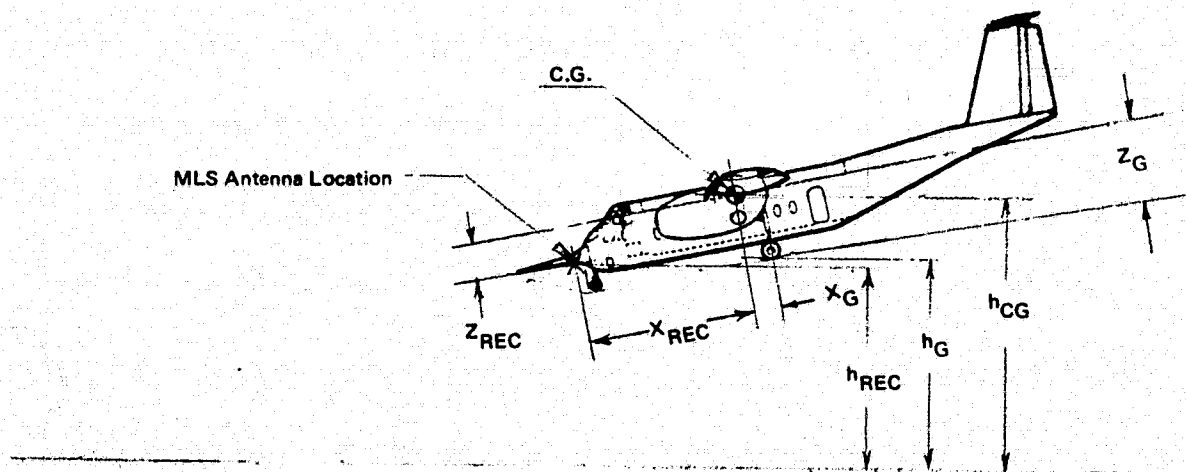


Figure A-9. Airplane Geometry

The three axis accelerometers are located near the cg. Since offset location corrections are included in the acceleration signal processing, the sensors were assumed to be cg mounted for this study. The radar altimeter antennae are located very near the gear fuselage station and calibrated for the gear length. The rate gyros were assumed to be oriented with the fuselage reference line. Barometric altitude and rate are not used in the landing control laws and thus were not included in the simulation.

A-3.2 Physical Data

The weight, inertia, and dimensions of the Aug Wing vehicle in landing configuration are given in Table A-V. The gear geometry is also presented. This geometry defines the following absolute touchdown constraints for the Aug Wing vehicle:

$$\begin{aligned} \theta_{\min} &= -1^{\circ} & \theta_{\max} &= +15.1^{\circ} \text{ gear compressed} & |\phi|_{\max} &= 28^{\circ} \\ & & &= +17.0^{\circ} \text{ gear extended} & & \end{aligned}$$

A-3.3 Sensor Models

Only those sensors whose dynamics or errors impact landing performance are discussed in this section. Also, only the errors which affect landing performance are included — e.g. accelerometer biases are not included since the signals are washed out. The properties of the sensors which impact landing performance are summarized in Table A-VI.

Although MLS yields discrete information at 5 scans per second for elevation and azimuth guidance and 40 per second for DME, we used continuous position inputs during our studies. During our previous glideslope and localizer track MLS studies reported in Reference A-7, it was determined that these update rates provided control activity and landing performance identical to a continuous guidance signal, especially if beam filtering is used. Although we used continuous position signals to limit simulation complexity, the actual MLS error models defined below were included to maintain fidelity in the results.

A-4 MLS DISTURBANCE MODELS

In this study, the MODILS error models were used, with data obtained from Reference A-3. The azimuth, elevation, and DME error amplitudes and spectral characteristics are given in Figure A-11. It should be noted that the effect of DME inaccuracies is small with respect to the angular errors during the final approach.

TABLE A-V. PHYSICAL DATA FOR LANDING CONFIGURATION

GEAR GEOMETRY

	<u>Nose</u>	<u>Right</u>	<u>Left</u>
X_G	7.285 (23.9)	-1.183 (-3.88)	-1.183 (-3.88)
Y_G	0.0	4.648 (15.25)	-4.648 (-15.25)
Z_G	3.383 (11.1)	3.383 (11.1)	3.383 (11.1)
$Z_{\text{Compression}}$.253 (0.83)	.311 (1.02)	.311 (1.02)

AIRCRAFT DIMENSIONS

W	177929	N	(40,000. lb)
I_X	359295	Kg-m^2	(265,000. slug-ft ²)
I_Y	280656	Kg-m^2	(207,000. slug-ft ²)
I_Z	596565	Kg-m^2	(440,000. slug-ft ²)
I_{XZ}	48810	Kg-m^2	(36,000. slug-ft ²)
S_{wing}	80.36	m^2	(865. ft ²)
$S_{\text{Hor. Tail}}$	21.65	m^2	(233. ft ²)
$S_{\text{Vert. Tail}}$	14.12	m^2	(152. ft ²)
b	24.00	m	(78.75 ft)
\bar{C}	3.78	m	(12.4 ft)
FSCG	866.65	cm.	(341.2 in)
WLCG	454.66	cm.	(179.0 in)

NOTE: Gear Geometry is expressed in meters (feet)

TABLE A-VI. SENSOR CHARACTERISTICS

<u>Sensor</u>	<u>Dynamics</u>	<u>Errors</u>
Radar Altimeter	$\frac{1}{.1S + 1}$	Bias - ± 1.03 m (3.4 ft)
GS/LOC Receiver	$\frac{1}{.1S + 1}$	Figure A-10
Vertical Gyro		Verticality - $\pm .6^\circ$ False erection - $\pm 1.0^\circ$
Accelerometers		Cross axis sensitivity .01
Course Datum		Equivalent Bias - $\pm 4.0^\circ$

NOTE: All errors are given as 4.5σ values

A-5 ATMOSPHERIC DISTURBANCE MODELS

In these landing studies, both a standard atmospheric disturbance model and specific deterministic wind inputs were considered. The final performance determination was based on the standard disturbance model.

A-5.1 Standard Wind Model

The basic wind model used for approach and landing is closely patterned after the standard FAA wind model specified in AC-20-57A (Reference A-4) and described more fully in References A-5 and 6. The total wind level also determines the turbulence amplitudes, while the shear corresponds to the headwind and crosswind components. A summary of the standard wind model is shown as Figure A-12.

For this study, winds were assumed to be in earth local level axes and transformed into aircraft axes. Headwinds and tailwinds were taken to be equiprobable. No pitch rate gusts were used, since their effects are negligibly small compared to horizontal and vertical turbulence. Uncorrelated white noise generators were used for longitudinal, lateral, vertical, and roll rate gusts. A random turbulence intensity with an exceedance probability of 0.01 was selected as a design condition for this study. This corresponds to 1.92 m/s (6.3 fps) RMS longitudinal and lateral turbulence, and 0.77 m/s (2.54 fps) RMS vertical turbulence.

A-5.2 Wind Shear Spikes

In some cases, the aircraft was subjected to wind shear spikes as shown in Figure A-10. This allowed evaluation of the impact of shear gradients much larger than the standard wind model.

Maximum spike velocities (U_{sp}) of ± 5.15 m/sec (10 kt) were inserted, centered about h_{sp} . The spikes were superimposed on the regular shear model to determine the most sensitive combination of wind reversals at various altitudes.

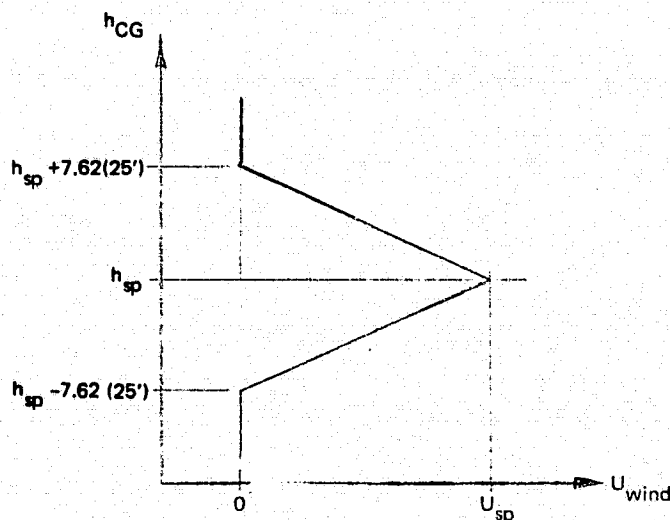
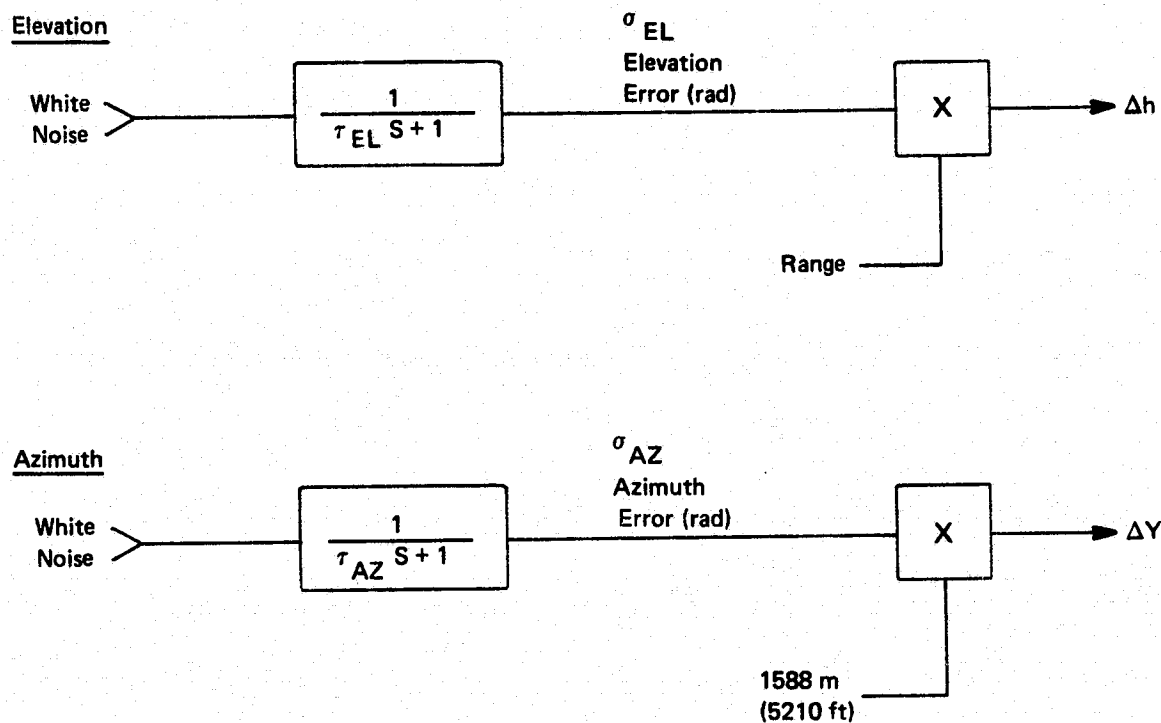
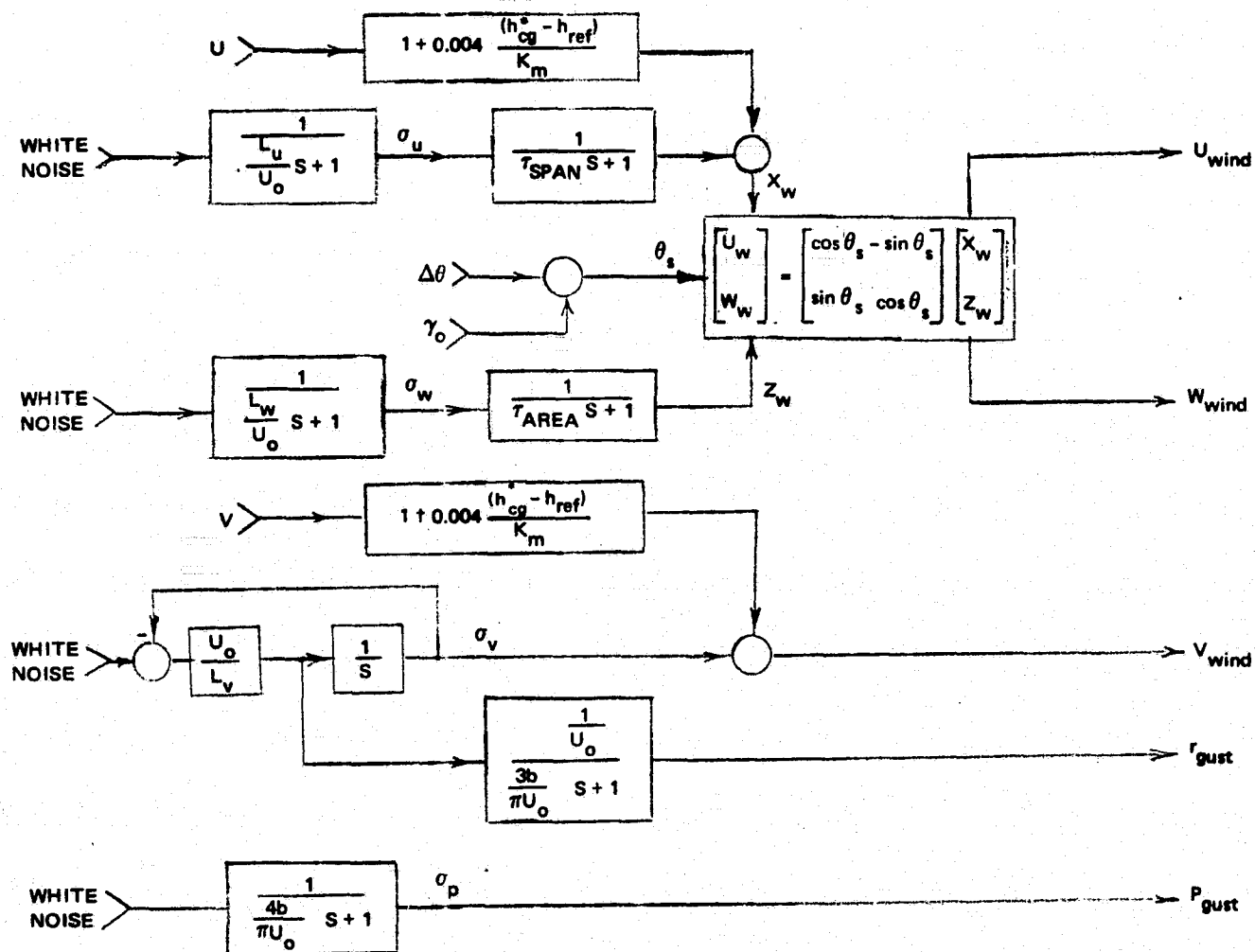


Figure A-10. Wind Shear Spike Profile
A-18



	τ	σ Noise	σ Bias
Elevation	10.0	.07°	.05°
Azimuth	4.0	.03°	.17°
DME	-----	12.2m (40.0 ft)	6.1m (20.0 ft)

Figure A-11. MODILS Error Models



	u	v	w	p
L (SCALE LENGTH)	182.88m (600 ft)	182.88m (600 ft)	9.14m (30 ft)	—
$\tau_{SPAN, AREA}$	$\frac{33.5 K_m}{U_o}$	—	$\frac{25.89 K_m}{U_o}$	—
σ	0.15WINDV	0.15V	$0.773 \frac{m}{sec} (1.5 \text{ kt})$	$0.00853 \frac{\sigma_w}{K_m} \frac{rad}{sec}$
Mean Wind Limit	+12.88 +25 kt -5.15 m/sec -10 kt	$\pm 7.73 \text{ m/sec } (\pm 15 \text{ kt})$	—	—
Prob of Exceedance	1%	4.5%	—	—

h_{cg}^* = CG Height (200 ft maximum)

h_{ref} = Wind Reference Altitude = 7.62m (25 ft)

K_m = Metric Constant = 0.34m (1.0 ft) for metric (English) units

b = Wing Span = 24.0m (78.75 ft)

U_o = Approach speed = 33.48m/sec (109.85 fps)

U = Down Wind Speed; V = Crosswind Speed; WINDV = Total Wind Speed (25 kt Limit)

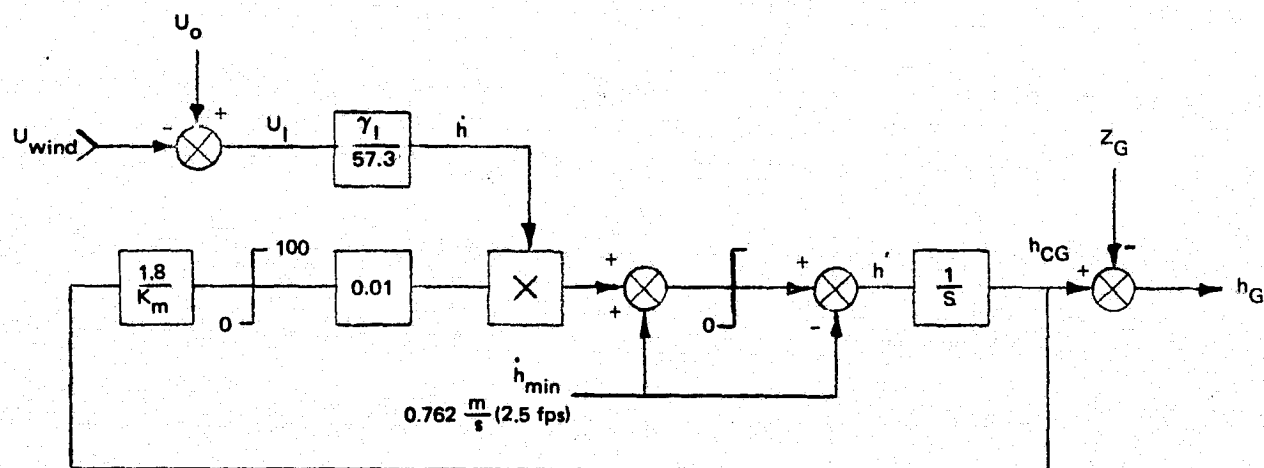
Figure A-12. Standard Wind Model

A-5.3 Altitude Profiles for Lateral Landings

Since the time between align initiate and touchdown can have a significant impact on landing performance, the effect of longitudinal winds and shears on lateral performance was included in the simulation.

A simplified flare model was constructed, with the altitude trajectory varying with inertial velocity and flare time constant in a manner very similar to the actual pitch approach and flare control system. The altitude profile generator block diagram is given as Figure A-13, with sample profiles for limiting headwind and tailwind shown in Figure A-14.

This altitude trajectory is used to drive the sidewind shear and the align model, and to indicate touchdown. Thus the proper relationship is maintained between altitude and time for all downwind conditions, to allow realistic determination of lateral landing performance.



K_m = metric constant = 0.3048 (1.0) for metric (English) units.

Z_G = 3.383m (11.1 ft)

Figure A-13. Altitude Profile Generation

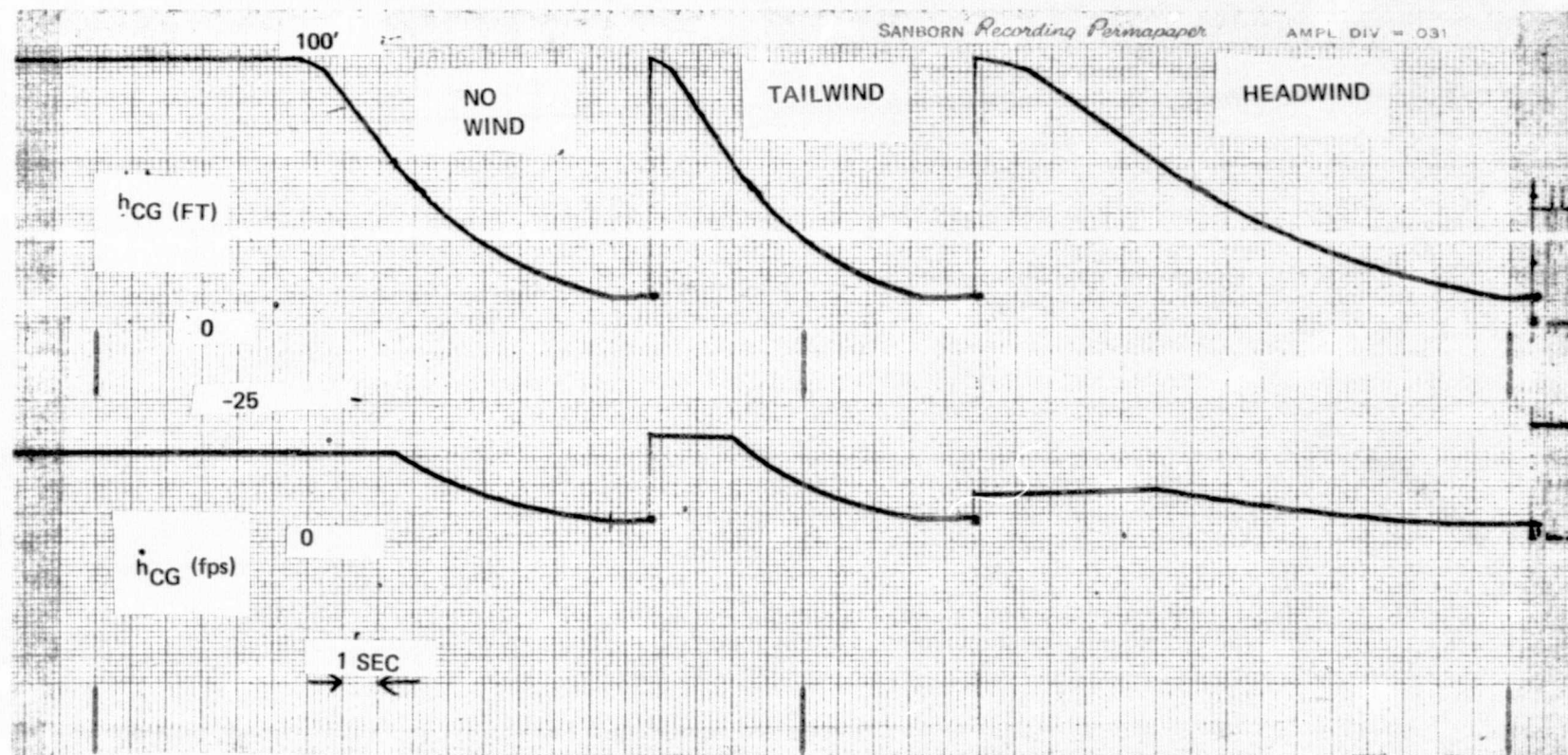


Figure A-14. Typical Altitude Profiles

APPENDIX B

GLIDE SLOPE TRACK AND FLARE RESULTS

ELEVATOR AUGMENTED CONFIGURATION

<u>Figure</u>	<u>Title</u>	<u>Page</u>
B-1	Elevator Augmented Configuration Block Diagram	B-2
B-2A	Landing Time History: No Wind	B-4
B-2B	Landing Time Histories: Wind Shears	B-5
B-2C	Landing Time Histories: Wind Shears	B-6
B-3	Sink Rate Vs. Altitude Profiles	B-7
B-4	Touchdown Sink Rate Distribution	B-10
B-5	Touchdown Range Distribution	B-11
B-6	Touchdown Pitch Attitude Distribution	B-12
B-7	Vertical Window Deviation Distribution	B-13

TIME HISTORIES

<u>Figure</u>	<u>Title</u>	<u>Page</u>
B-8	Wind Shear Spikes at 100'	B-15
B-9	Wind Shear Spikes at 100' and 50'	B-16
B-10	Wind Shear Spikes at 50'	B-17
B-11	Wind Shear Spikes at 25'	B-18
B-12	Wind Shear Spikes at 25'	B-19
B-13	Terrain Steps	B-20
B-14	Ground Effect Variations	B-21
B-15	Failure Time Histories — Accelerometer and Beam	B-22
B-16	Failure Time Histories — Radar Altimeter	B-23
B-17	Failure Time Histories — Radar Altimeter and Accelerometer	B-24
B-18	Failure Time Histories — Pitch Attitude	B-25
B-19	Failure Time Histories — Pitch Rate	B-26

<u>Figure</u>	<u>Title</u>	<u>Page</u>
B-20	\dot{h} and Δh Step Responses — Choke Configuration, with δ_{TH} Hyst.	B-27
B-21	\dot{h} and Δh Step Responses — Choke Configuration, no δ_{TH} Hyst.	B-28
B-22	\dot{h} and Δh Step Responses — Elevator Configuration	B-29

ACTIVITY IN DISTURBANCES

<u>Figure</u>	<u>Configuration</u>	<u>σ_u</u>		<u>σ_w</u>		<u>σ_{BN}</u>	<u>Page</u>
B-23	Choke	6.28	&	2.5	&	0.07^0	B-30
B-24	Choke $K_T = 1.4$	6.28		2.5		0.07^0	B-31
	$K_T = 3$	6.28		2.5		0.07^0	B-31
	$K_T = 6$	6.28		2.5		0.07^0	
B-25	Choke	6.28	&	2.5	&	0.07^0	
		-		-		0.07^0	B-32
B-26	Choke	6.28		-		-	
		-		2.5		-	B-33
B-27	Choke	3.1	&	1.2	&	0.035^0	
		3.1		-		-	B-34
B-28	Choke	-		1.2		-	
		-		-		0.035^0	B-35
B-29	No Choke, Elevator XF	6.28		2.5		0.07^0	
	No XF	6.28		2.5		0.07^0	
	Reduced Ku	6.28		2.5		0.07^0	B-36
B-30	No Choke, XF	6.28		-		-	
	No XF	6.28		-		-	
	Reduced Ku	6.28		-		-	B-37
B-31	No Choke, XF	-		2.5		-	
	No XF	-		2.5		-	
	Reduced Ku	-		2.5		-	B-38
B-32	No Choke, XF	-		-		0.07^0	
	No XF	-		-		0.07^0	
	Reduced Ku	-		-		0.07^0	B-39

PROBABILITY DISTRIBUTIONS

<u>Figure</u>	<u>Title</u>	<u>Parameter</u>	<u>Configuration</u>	<u>Page</u>
B-33	Wind Variations	\dot{h}	Choke Aug.	B-40
B-34	Wind Variations	χ	Choke Aug.	B-41
B-35	Wind Variations	θ	Choke Aug.	B-42
B-36	Wind Variations	Δh_{100}	Choke Aug.	B-43
B-37	Wind Variations	α	Choke Aug.	B-44
B-38	Wind Variations	u	Choke Aug.	B-45
B-39	Sink Rate Dispersion Due to Off-Nominal Conditions	\dot{h}	Choke Aug.	B-46
B-40	Range Dispersion Due to Off-Nominal Conditions	χ	Choke Aug.	B-47
B-41	Pitch Dispersion Due to Off-Nominal Conditions	θ	Choke Aug.	B-48
B-42	Effect of Beam Offset on Glide Slope Tracking	Δh_B	Choke Aug.	B-49
B-43	Wind Variations	\dot{h}	Elevator Aug.	B-50
B-44	Wind Variations	χ	Elevator Aug.	B-51
B-45	Wind Variations	θ	Elevator Aug.	B-52
B-46	Wind Variations	Δh_{100}	Elevator Aug.	B-53
B-47	Wind Variations	α	Elevator Aug.	B-54
B-48	Wind Variations	u	Elevator Aug.	B-55
B-49	Elevator Aug. vs. Reduced Ku	\dot{h}	Elevator Aug.	B-56
B-50	Elevator Aug. vs. Reduced Ku	χ	Elevator Aug.	B-57
B-51	Elevator Aug. vs. Reduced Ku	Δh_{100}	Elevator Aug.	B-58
B-52	Flare Altitude Variations	\dot{h}	Choke Aug.	B-59
B-53	Flare Altitude Variations	χ	Choke Aug.	B-60

<u>Figure</u>	<u>Title</u>	<u>Parameter</u>	<u>Configuration</u>	<u>Page</u>
B-54	Touchdown Sink Rate Command Variations (HW)	\dot{h}	Choke Aug.	B-61
B-55	Touchdown Sink Rate Command Variations (TW)	\dot{h}	Choke Aug.	B-62
B-56	Touchdown Sink Rate Command Variations	X	Choke Aug.	B-63
B-57	Pitch Gain Variations	θ	Choke Aug.	B-64
B-58	Throttle Gain Variations (TW)	\dot{h}	Choke Aug.	B-65
B-59	Throttle Gain Variations (HW)	\dot{h}	Choke Aug.	B-66
B-60	Throttle Gain Variations (TW)	X	Choke Aug.	B-67
B-61	Throttle Gain Variations (HW)	X	Choke Aug.	B-68
B-62	Aircraft Weight Variations	\dot{h}	Choke Aug.	B-69
B-63	Aircraft Weight Variations	X	Choke Aug.	B-70
B-64	Ground Effect Variations	\dot{h}	Choke Aug.	B-71
B-65	Ground Effect Variations	X	Choke Aug.	B-72
B-66	Ground Effect Variations	θ	Choke Aug.	B-73
B-67	RPM Limit Variations	X	Choke Aug.	B-74
B-68	Throttle Model Variations	\dot{h}	Choke Aug.	B-75
B-69	Throttle Model Variations	X	Choke Aug.	B-76

<u>Table</u>	<u>Title</u>	<u>Page</u>
B-I	Pitch Landing Performance Summary	B-8
B-II	Activity Summary (RMS)	B-9

APPENDIX B

GLIDE SLOPE TRACK AND FLARE RESULTS

This appendix presents the Elevator Augmented Throttle version of the pitch control laws in which the DLC chokes are not used as an active control. Also shown are the supplementary data on which Section 5 results and summary figures are based.

B-1. ELEVATOR AUGMENTED CONFIGURATION

The recommended system configuration presented in Section 3 is based on a three control technique using throttle, chokes and elevator. Another configuration, using throttle and elevator only, is presented here. The two control technique allows a high degree of commonality between the automatic system and manual control, thus simplifying pilot monitoring of the system's operation.

The Elevator Augmented Configuration (Figure B-1) utilizes similar control algorithms. The major difference is the crossfeed of sink rate error to the elevator rather than chokes. Additional differences between the configurations are:

1. A lead-lag compensation network is introduced in the throttle path of the Elevator Augmented Configuration.
2. The following gain changes:

	K_{δ_T}	K_h	$K_{\dot{h}}$	K_q
Chokes	3.0	1.0	1.0	1.87
Elevator	1.4	0.5	0.375	4.0

The effect of the reduction of K_{δ_T} and K_h in the Elevator Augmented Configuration is to reduce the throttle gain by a factor of four. However, the lead-lag network raises the gain by the same factor at frequencies higher than 0.1 rps. Consequently, the low frequency throttle gain of the Elevator Augmented Configuration is one fourth of the Choke Augmented Configuration's throttle gain, but both configurations have the same throttle gain at frequencies above 0.1 rps. The lead lag is required in order to minimize path limit cycle.

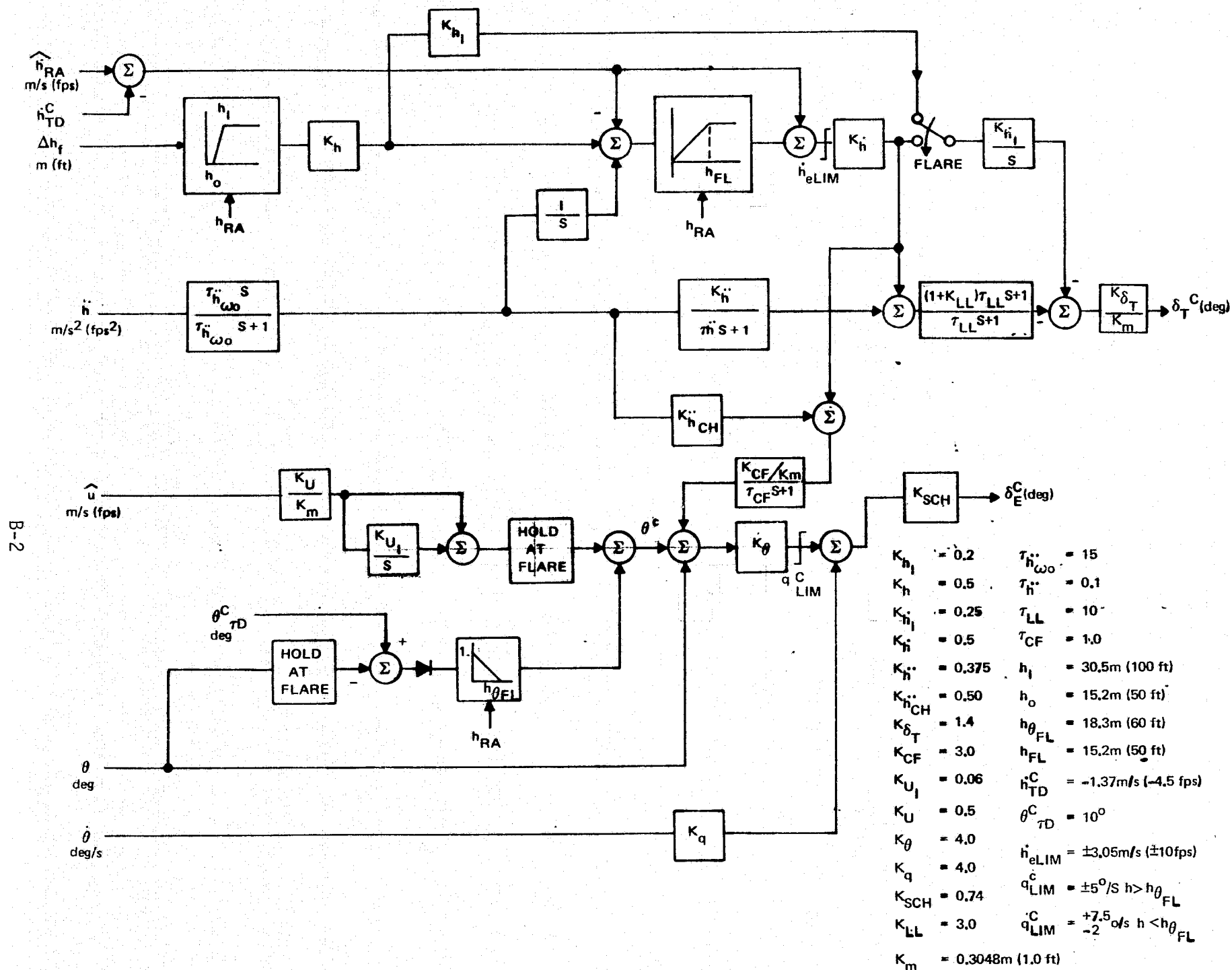


Figure B-1. Elevator Augmented Configuration Block Diagram

Landing time histories and \dot{h} versus h traces for the Elevator Augmented Configuration are shown as Figures B-2 and B-3. The traces are very similar to those shown in Subsection 5.4 for the Choke Augmented Configuration.

A landing performance summary comparing the Choke and Elevator Augmented Configurations with the requirements is shown in Table B-I. Range and sink-rate performance of the Elevator Augmented Configuration are better than those obtained with the Choke Augmented Configuration. However, the results shown for Choke Augmentation were obtained with half the recommended throttle gain. An increased throttle gain improves performance as shown in Subsection 5.3. Furthermore, the highest possible throttle gain has been employed with the Elevator Augmented Configuration in order to achieve the performance shown, whereas a wide gain margin has been retained in the Choke Configuration. The low margins of the Elevator Augmented Configuration may necessitate a gain reduction if phase lag in the airplane turns out to be worse than in our simulation due to digital mechanization or hardware non-linearities. Also, the possibility of using flight path to elevator cross-feed in the Choke Augmented Configuration has not been evaluated in detail in this study; however, it is felt that this technique might improve sink rate and range performance.

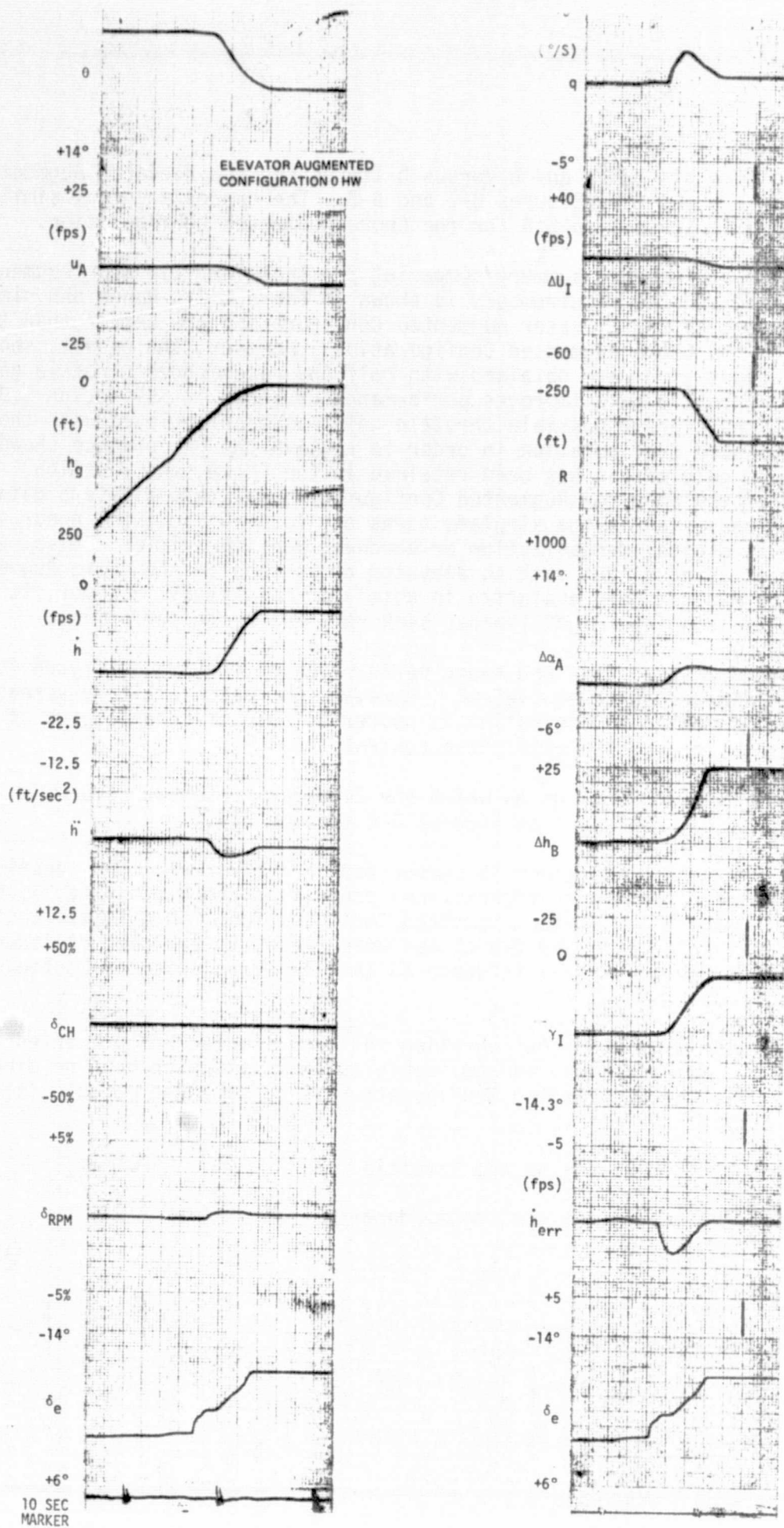
The touchdown sink rate and range performance of the two configurations should be considered to be equivalent. However, the pitch attitude spread in the Elevator Augmented Configuration is poorer because of interference of flight path to elevator cross-feed with pitch control.

Probability distributions on which the Elevator Augmented column in Table B-I is based, are shown as Figures B-4 through B-7.

The activity in disturbances is summarized in Table B-II. The conspicuous difference between the two configurations, other than choke activity, is the increased throttle rate with the Elevator Augmented Configuration. This is attributable to the absence of gust alleviation by the chokes which leads to a higher reliance on the throttle. Also, speed control is worse in the Elevator Augmented Configuration because of the crossfeed.

The Elevator Augmented Configuration has been studied and presented here because the two control technique may be applicable to vehicles which have no direct lift capability. The Choke Augmented Configuration is recommended because it achieves equivalent performance with

1. Reduced dependence on the throttle.
2. Reduced path limit cycling tendency.



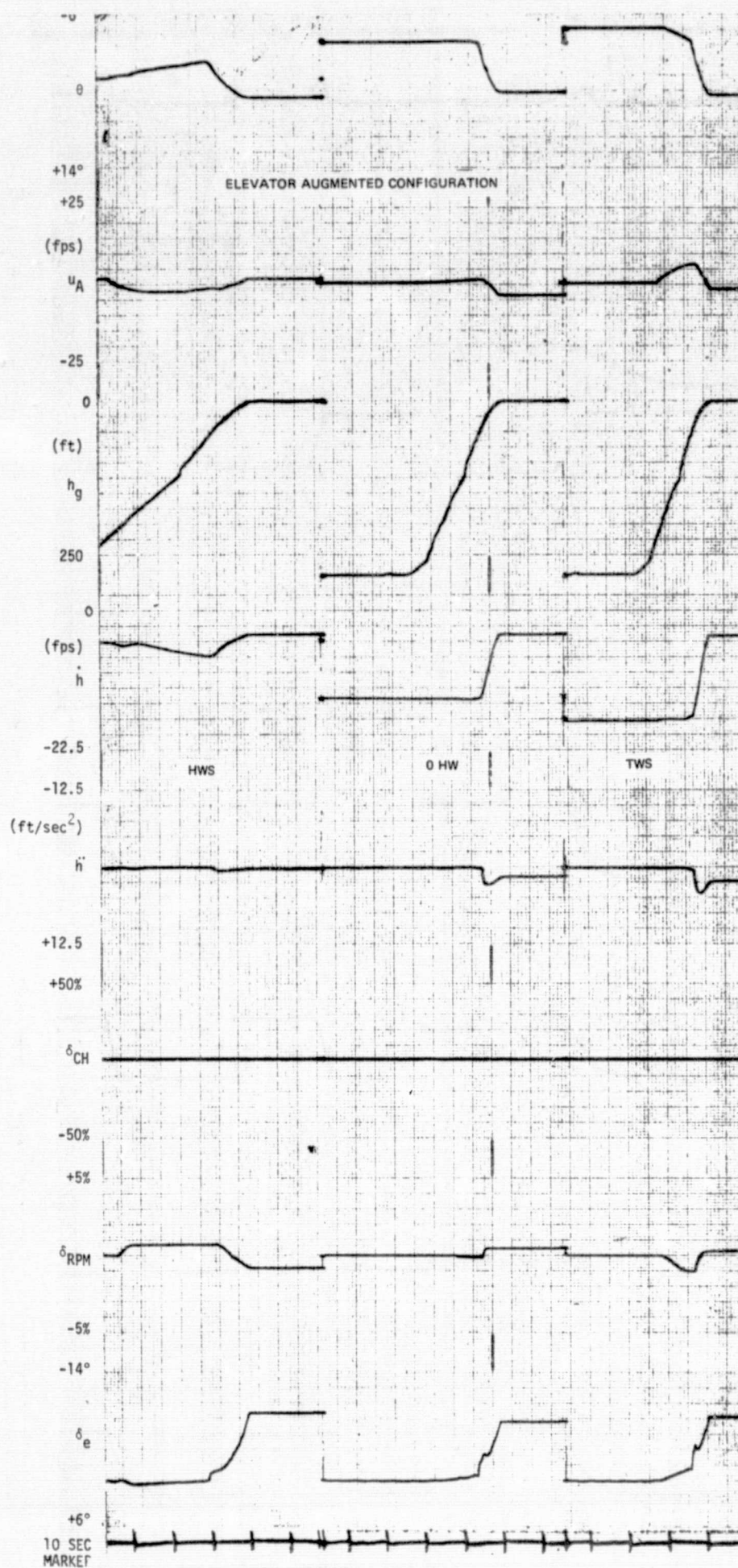


Figure B-2B. Landing Time Histories: Wind Shears

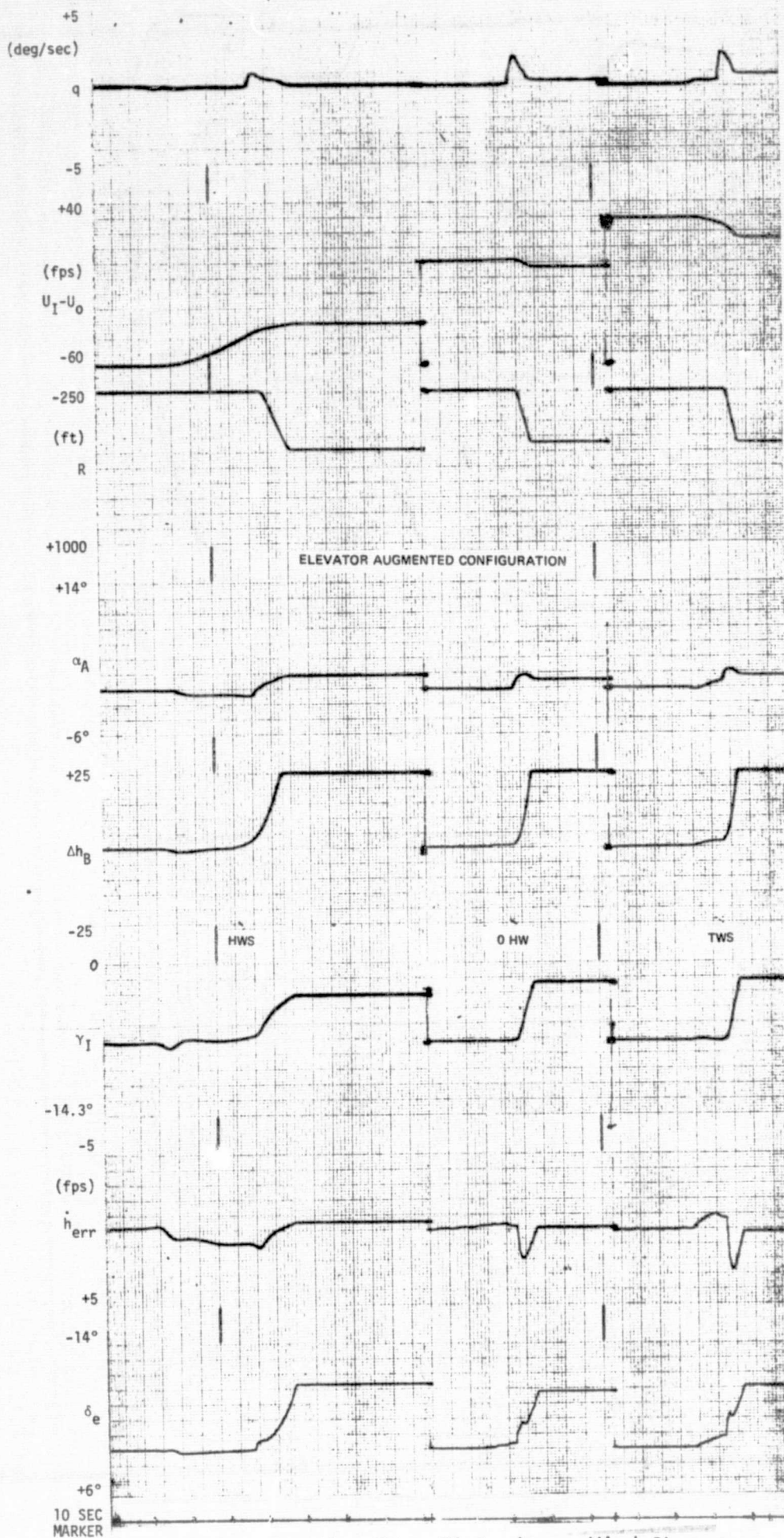


Figure B-2C. Landing Time Histories: Wind Shears

B-7

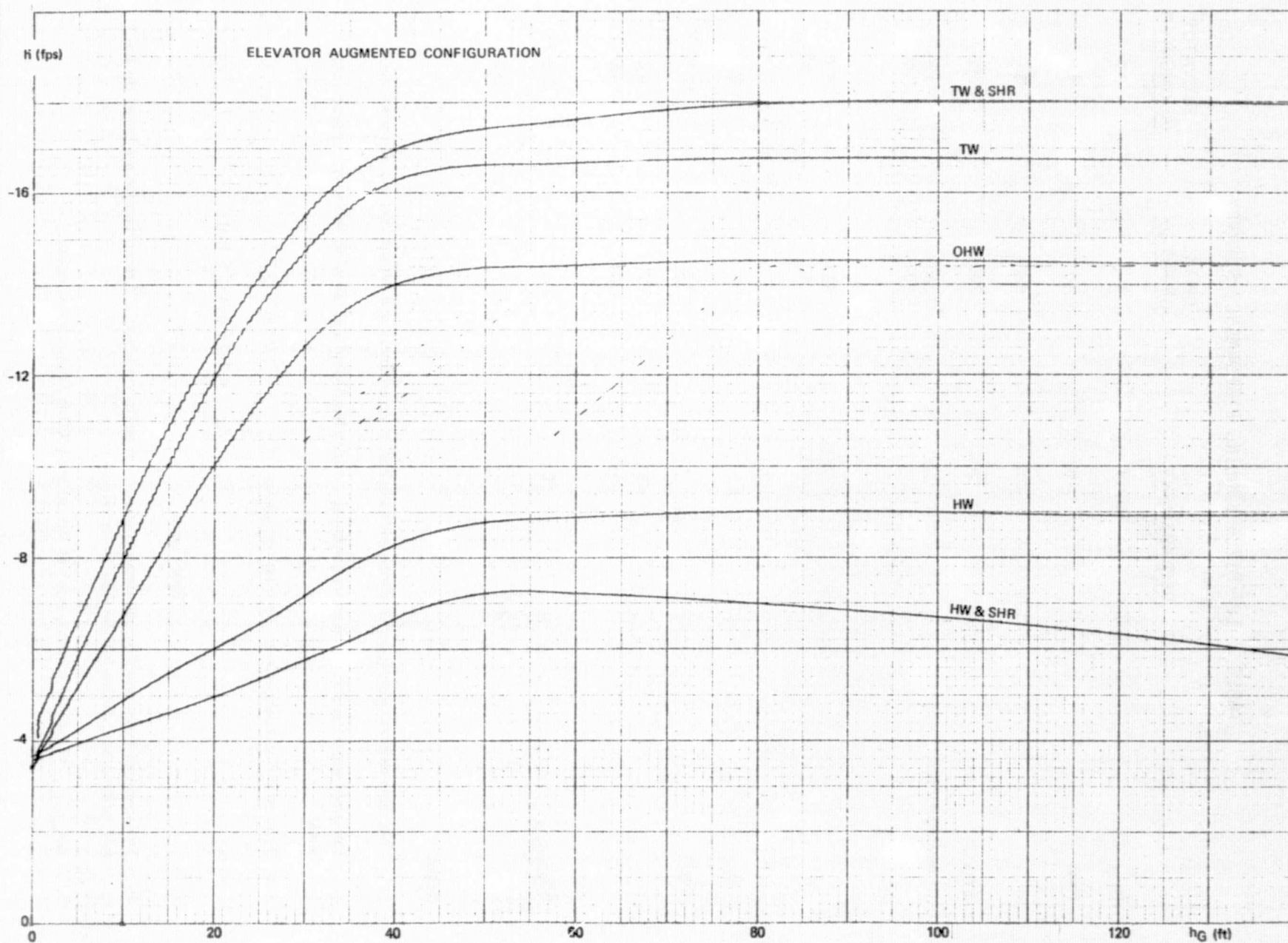


Figure B-3. Sink Rate vs. Altitude Profiles

TABLE B-I. PITCH LANDING PERFORMANCE SUMMARY

	<u>REQUIREMENT</u>		<u>CHOKE AUGMENTED</u>	<u>ELEVATOR AUGMENTED</u>
\dot{h}_{TD}	μ	4	4	3.7
(fps)	2σ	<6	5.1	4.6
	10^{-6}	<10	6.6	6
X_{TD}	μ	200	220	200
(ft beyond GPIP)	2σ	± 200	+160 -90	+120 -60
	10^{-6}	<1000 >-400	680 10	520 50
θ_{TD}	μ	5	6.7	3
(deg)	2σ	—	± 1.5	± 2.1
	10^{-6}	<15 >-1	10 3.5	9.4 -0.5
Δh_{window}	μ	0	2	1.5
(ft)	2σ	± 12	± 4	± 3.5

Notes:

1. This table defines landing performance with stochastic disturbances and deterministic wind variations.
2. Deterministic wind disturbances are combined limiting head wind and tail wind levels with appropriate shear.
3. Stochastic disturbances are: limiting turbulence $\sigma_u = 1.92 \text{ m/s (6.3 fps)}$
 $\sigma_w = 0.76 \text{ m/s (2.5 fps)}$
Beam noise $\sigma_{BN} = 0.07^\circ$
4. The specified mean and 2σ requirements are design goals, while the 10^{-6} requirements are based on the safe landing boundaries for the Aug. Wing vehicle.
5. Δh_{window} is vertical tracking error at the 30.5m (100 ft.) approach window.

TABLE B-II. ACTIVITY SUMMARY (RMS)

	<u>CHOKE AUGMENTATION</u>	<u>ELEVATOR AUGMENTATION</u>
$\Delta \dot{h}$, fps	0.8	1.0
$\Delta h/WR$	0.2	0.22
u/U_0	0.036	0.044
θ deg	1.4	1.3
δ_{RPM} , %	0.8	1.0
$\dot{\delta}_{RPM}$, %/sec	0.4	0.7
δ_e , deg	1.2	1.2
$\dot{\delta}_e$, deg/sec	2.0	2.3
δ_{CH} , %	17	0
$\dot{\delta}_{CH}$, %/sec	19	0

NOTES:

1) WR is the 100 ft window requirement, equal to 12 ft.

2) Results shown are in beam tracking, with beam noise and limiting turbulence:

$$\sigma_u = 6.3 \text{ fps}$$

$$\sigma_w = 2.5 \text{ fps}$$

$$\sigma_{BN} = 0.07^\circ$$

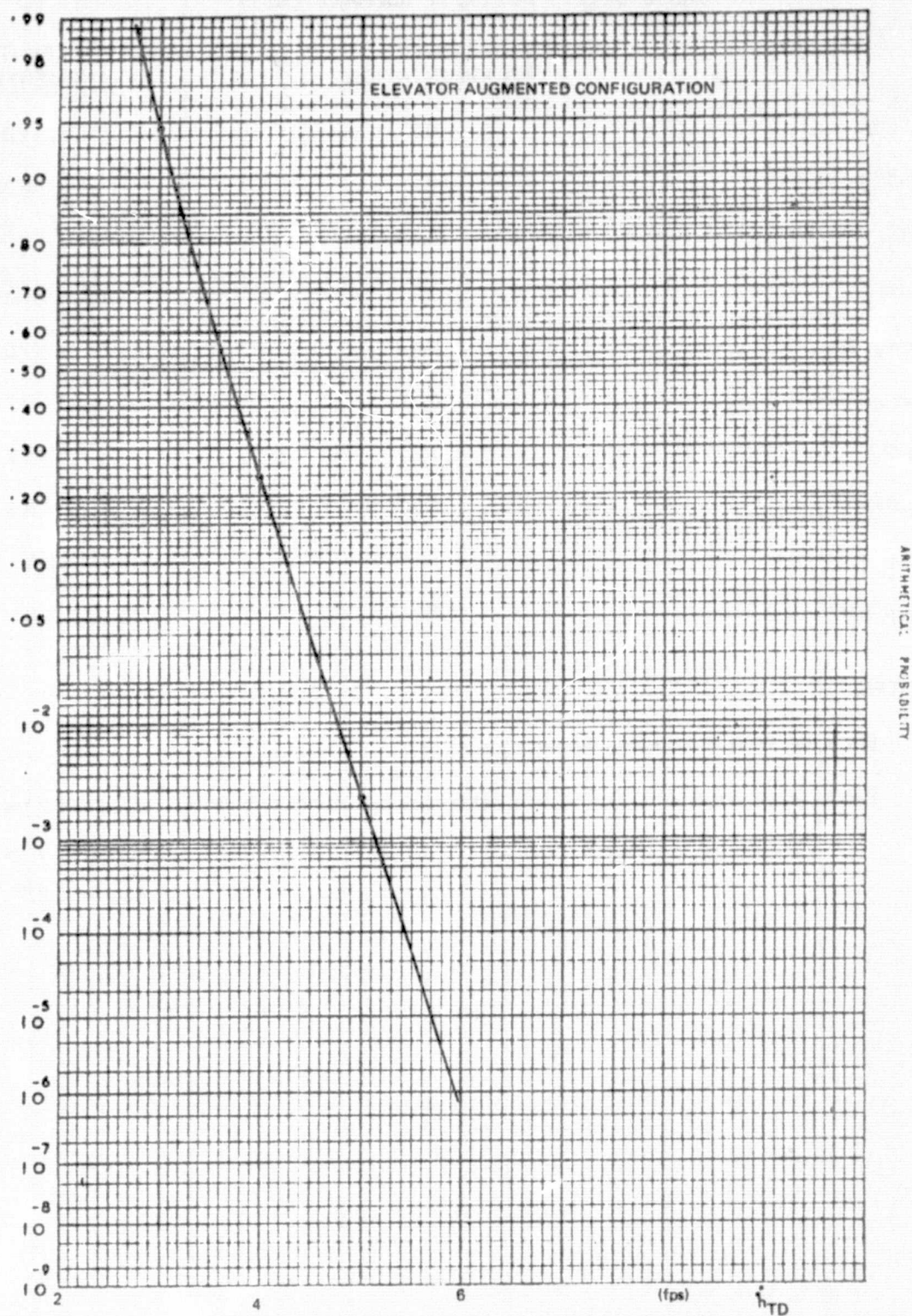


Figure B-4. Touchdown Sink Rate Distribution

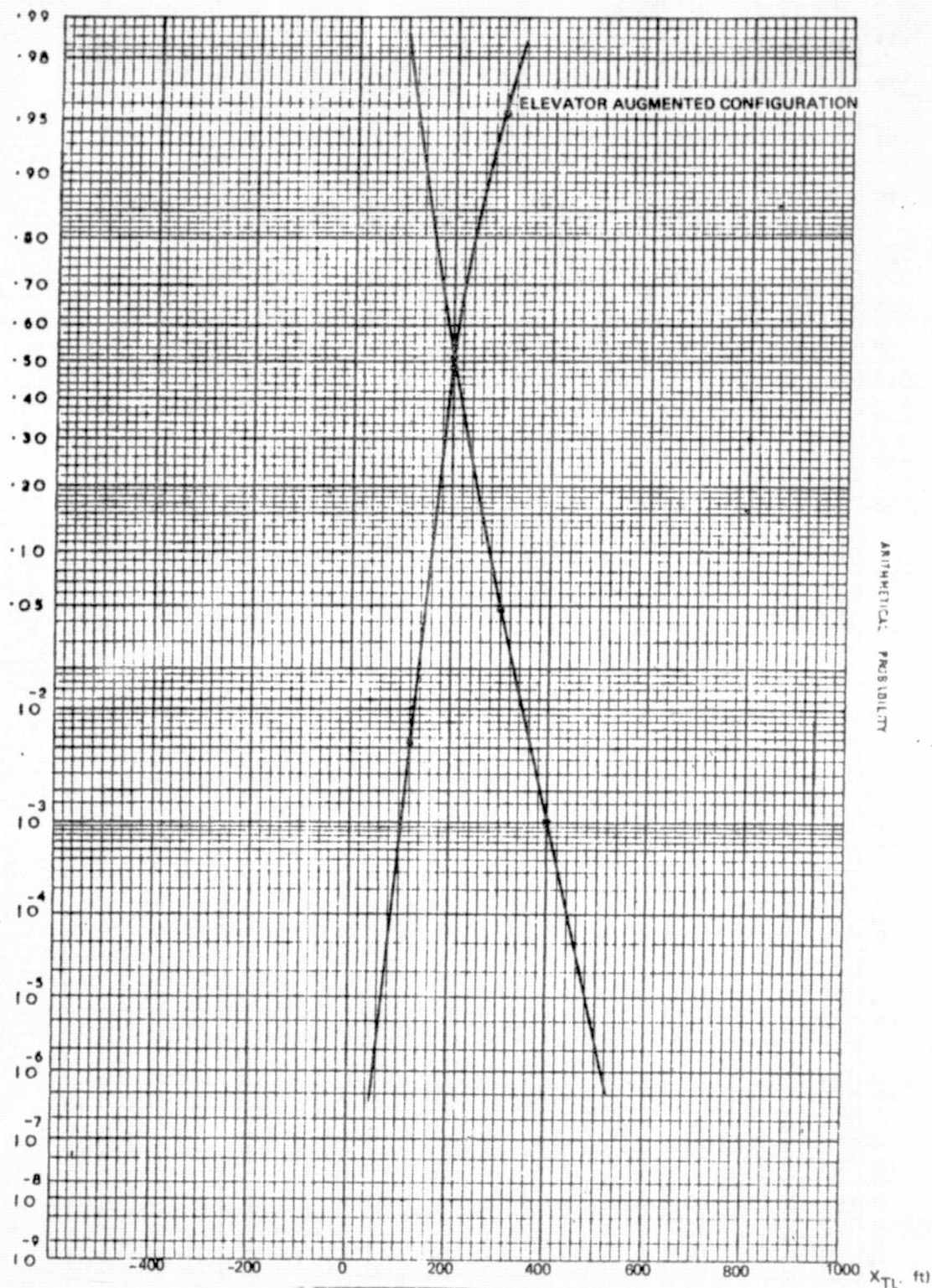


Figure B-5. Touchdown Range Distribution

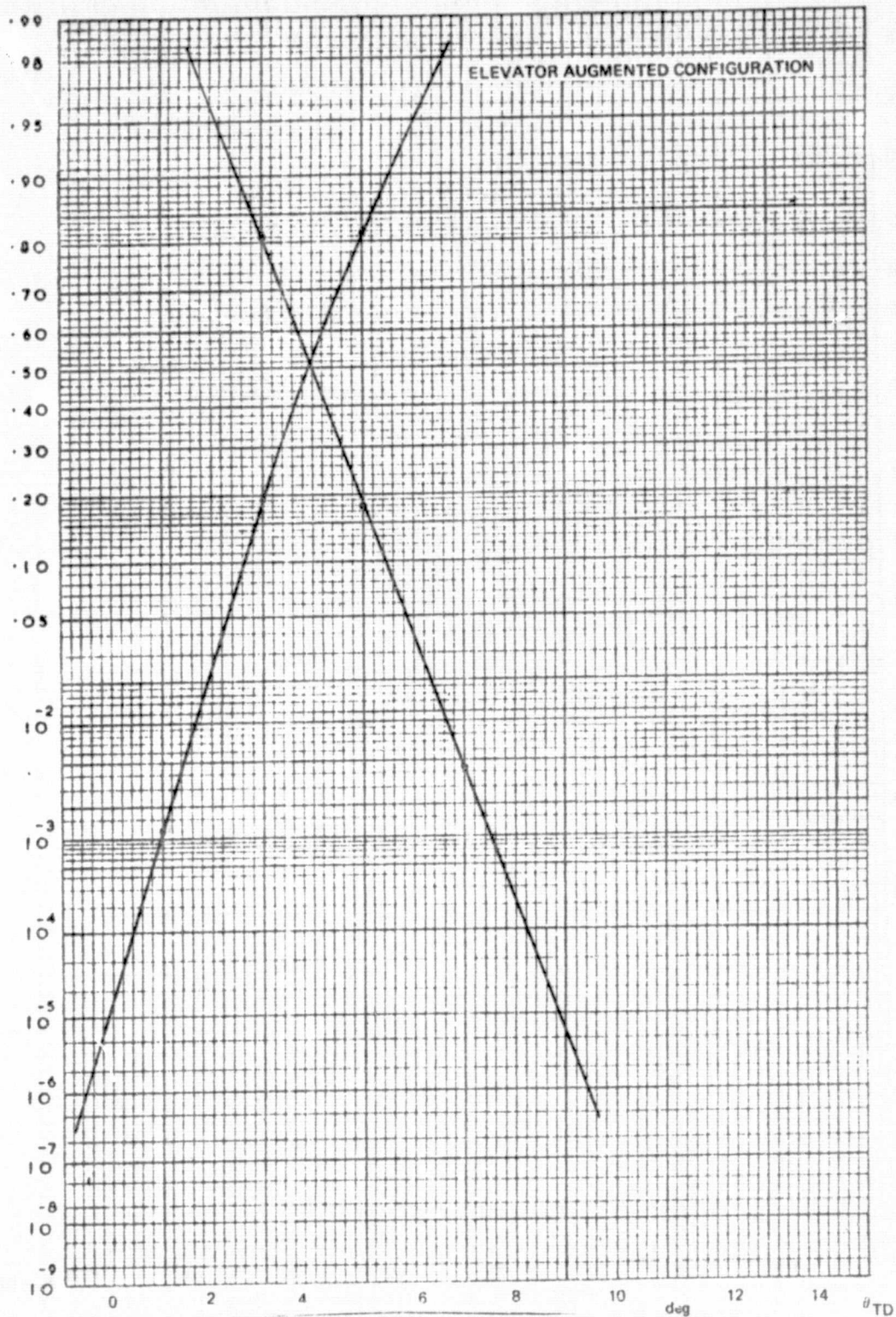


Figure B-6. Touchdown Pitch Attitude Distribution

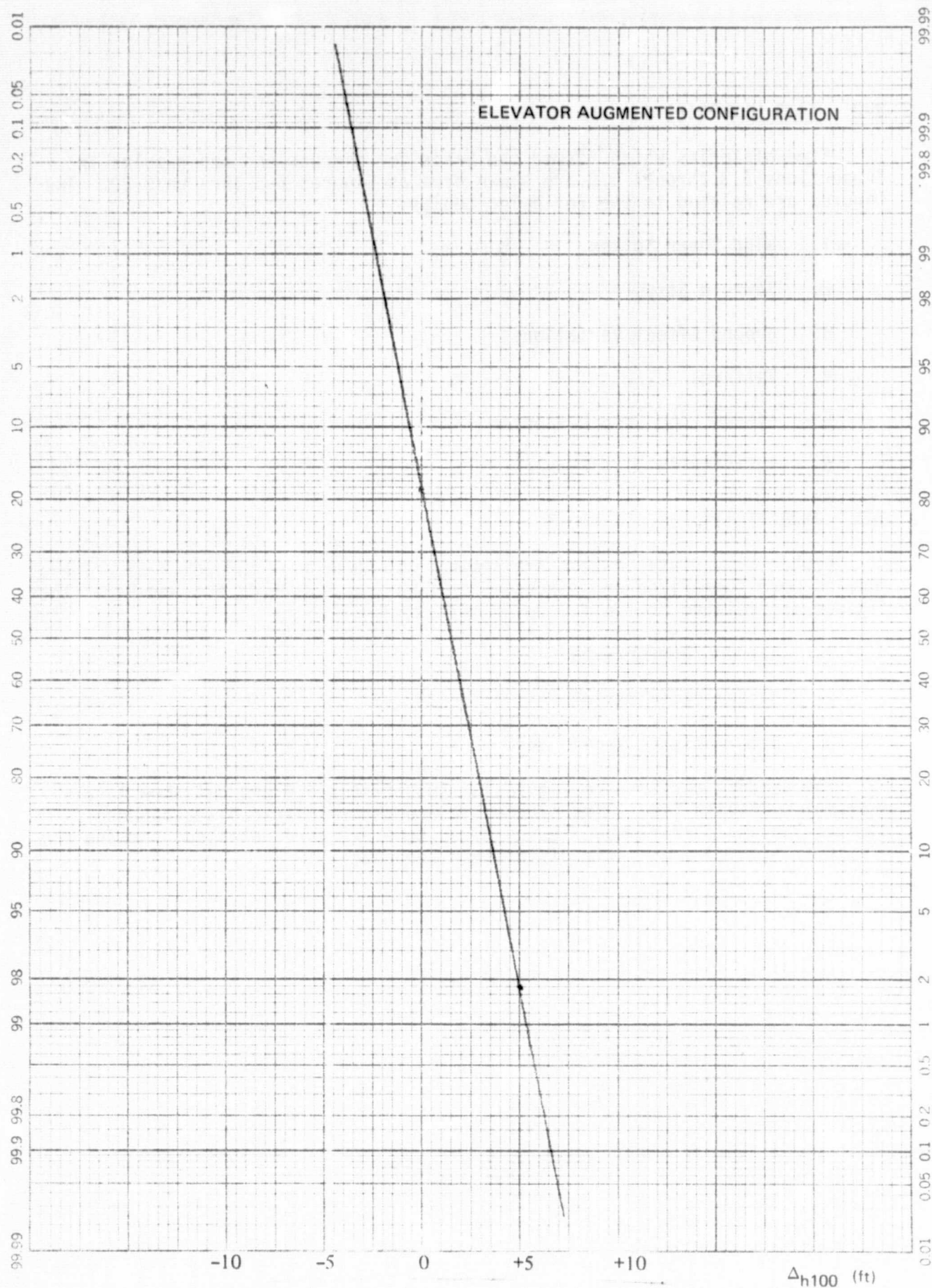


Figure B-7. Vertical Window Deviation Distribution

B-2. TIME HISTORIES

Time histories which formed the basis for discussions and results in Subsections 5.3 through 5.6 are shown here as Figures B-8 through B-32. The figures are related to the following topics:

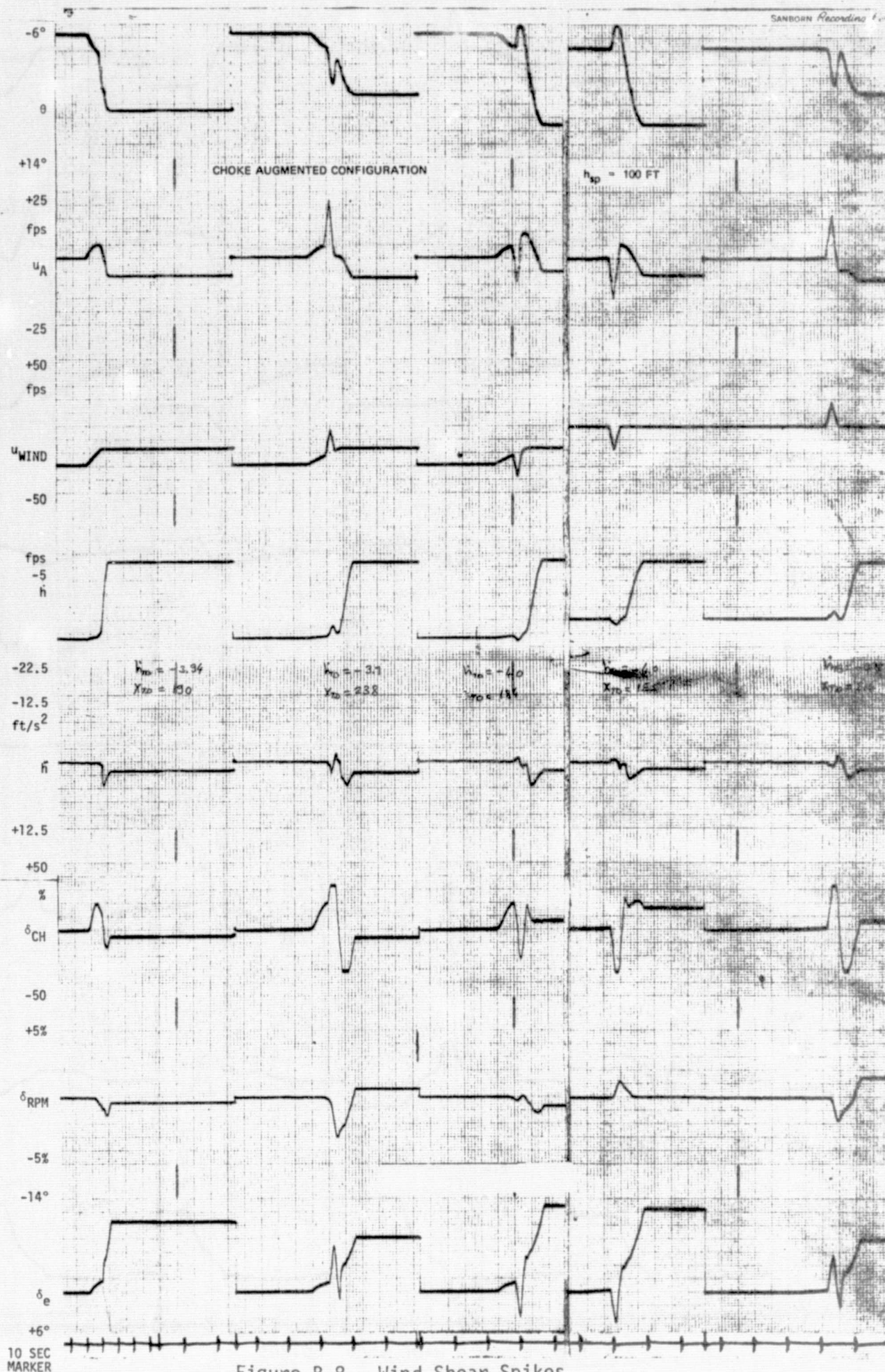
1. Wind Shear Spikes
2. Terrain Steps
3. Ground Effect Variations
4. Failures
5. Closed Loop Step Responses
6. Activity in Disturbances

B-3. PROBABILITY DISTRIBUTIONS

Probability distributions are shown as Figures B-33 through B-69. These results were summarized and discussed in Sections 5.3, 5.4, 5.5 and B-1. The figures are related to the following topics:

1. Landing Performance
2. System Optimization
3. Deterministic Variations

The landing performance figures of Subsections 5.4 and B-1 show total population results (including stochastic and deterministic disturbances) whereas landing performance figures given here are more detailed, showing the effect of each deterministic disturbance separately.



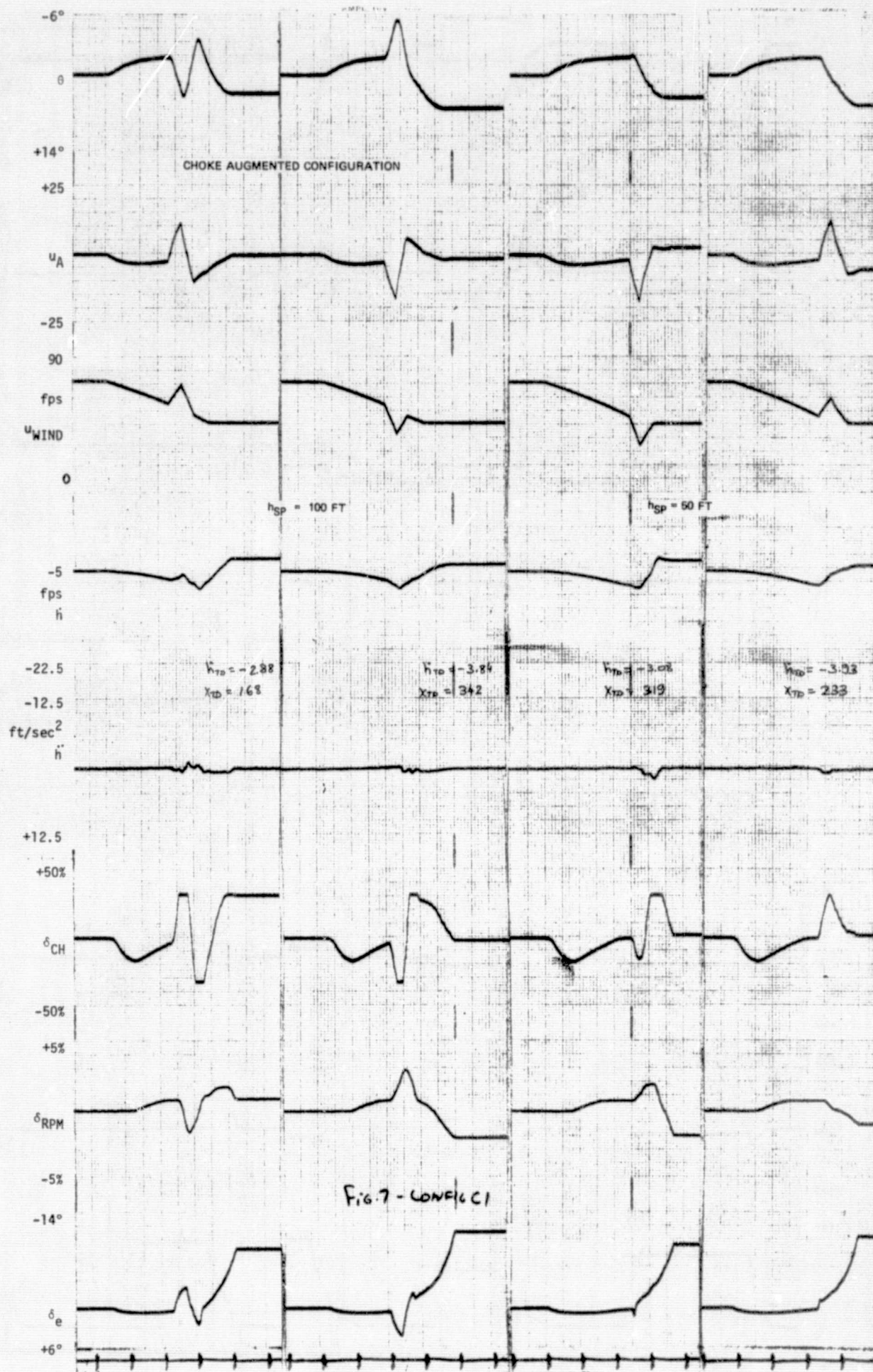


Figure B-9. Wind Shear Spikes

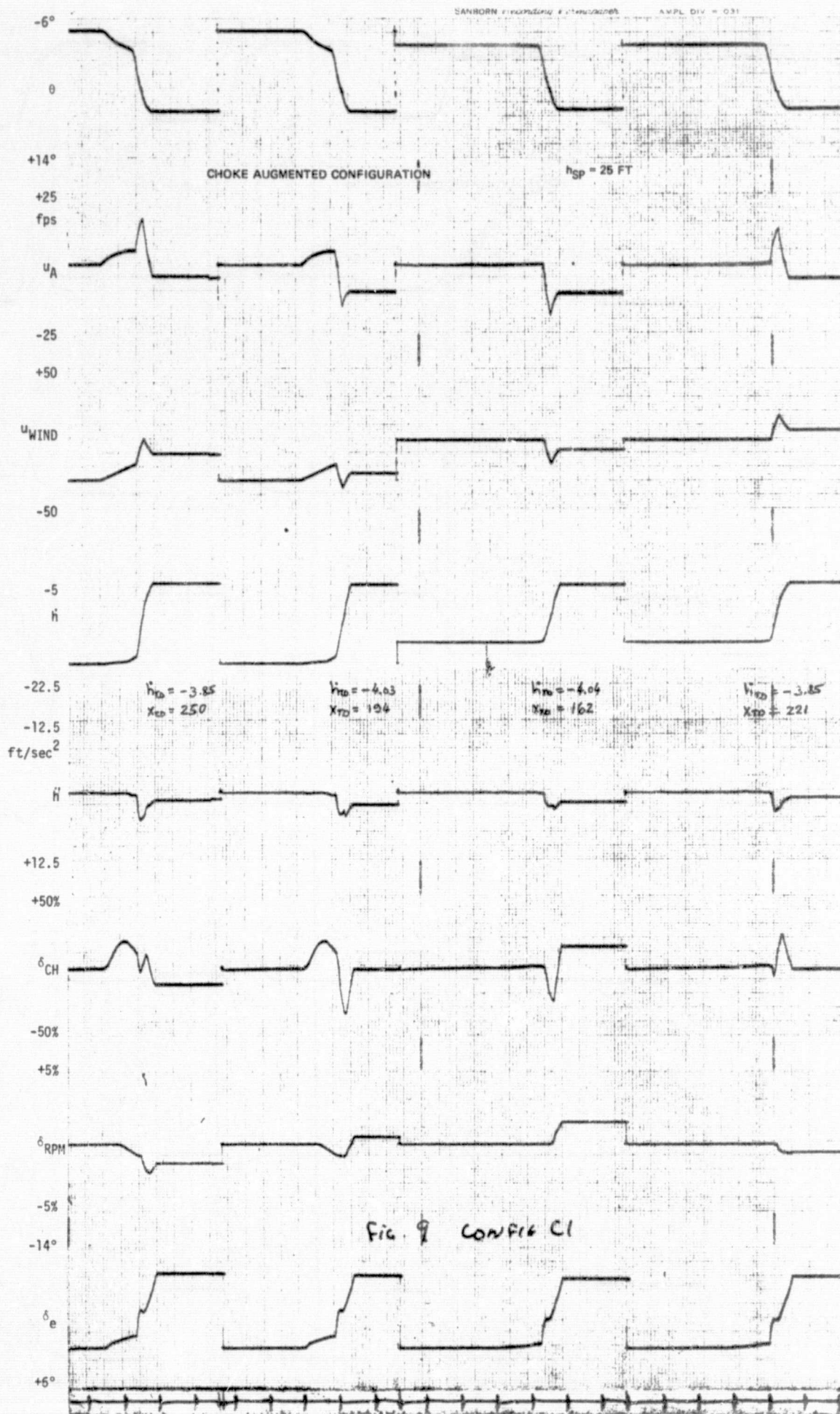


Figure B-11. Wind Shear Spikes

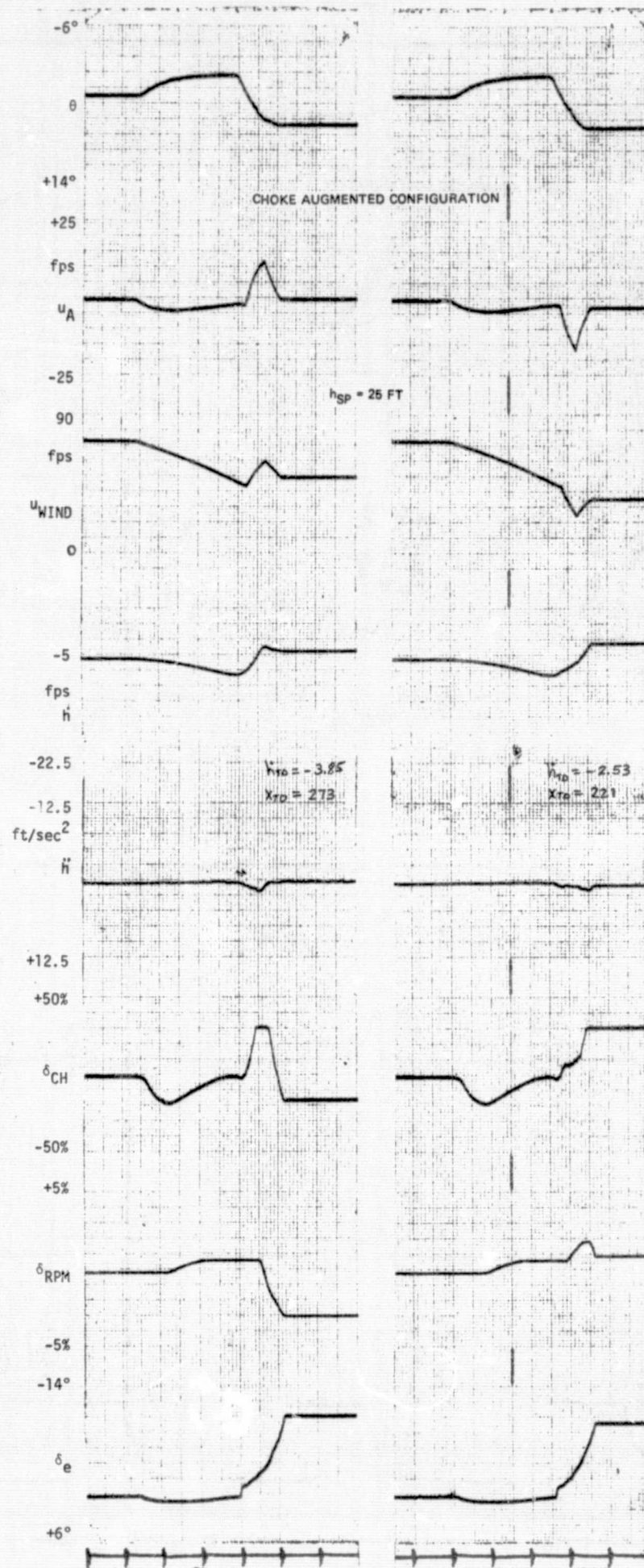


Figure B-12. Wind Shear Spikes



Figure B-13. Terrain Steps

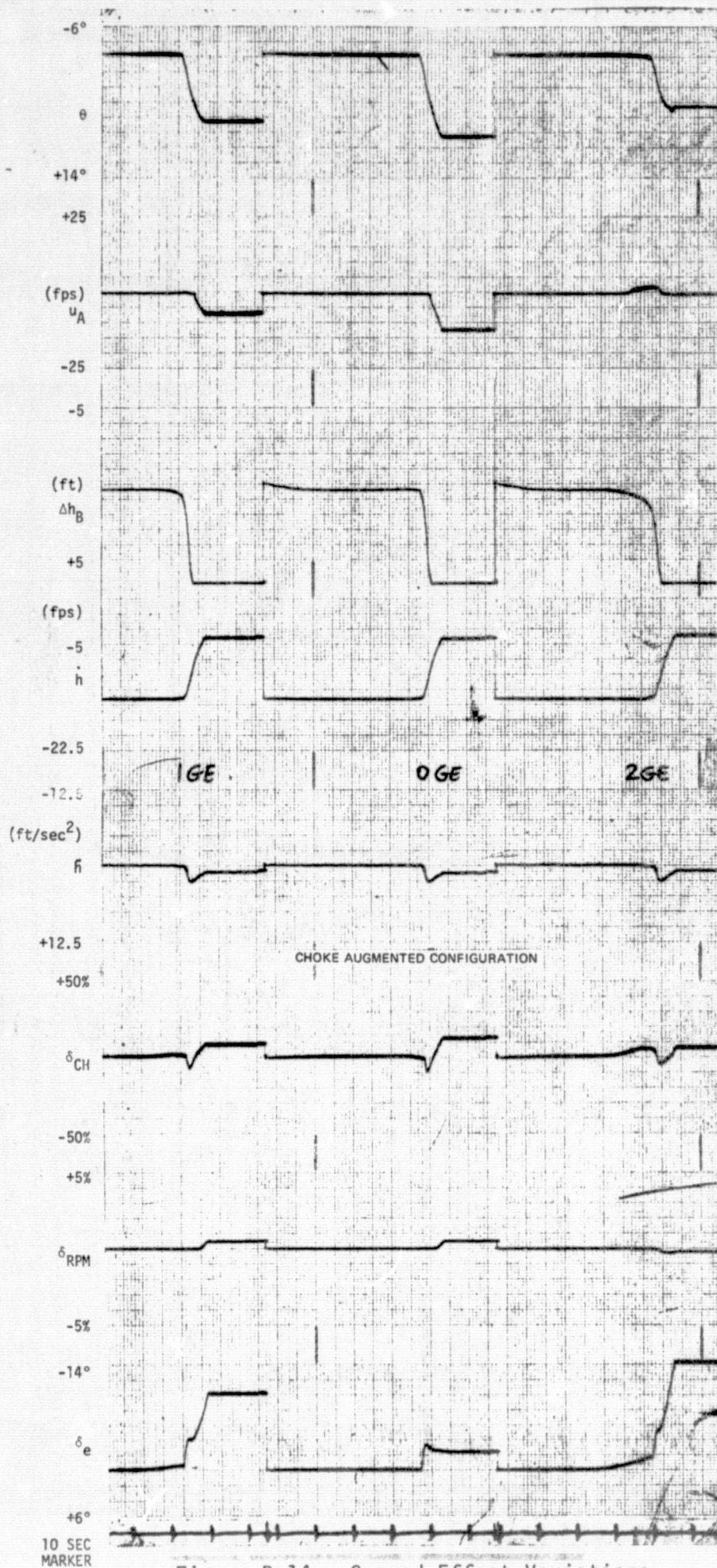


Figure B-14. Ground Effect Variations
B-21

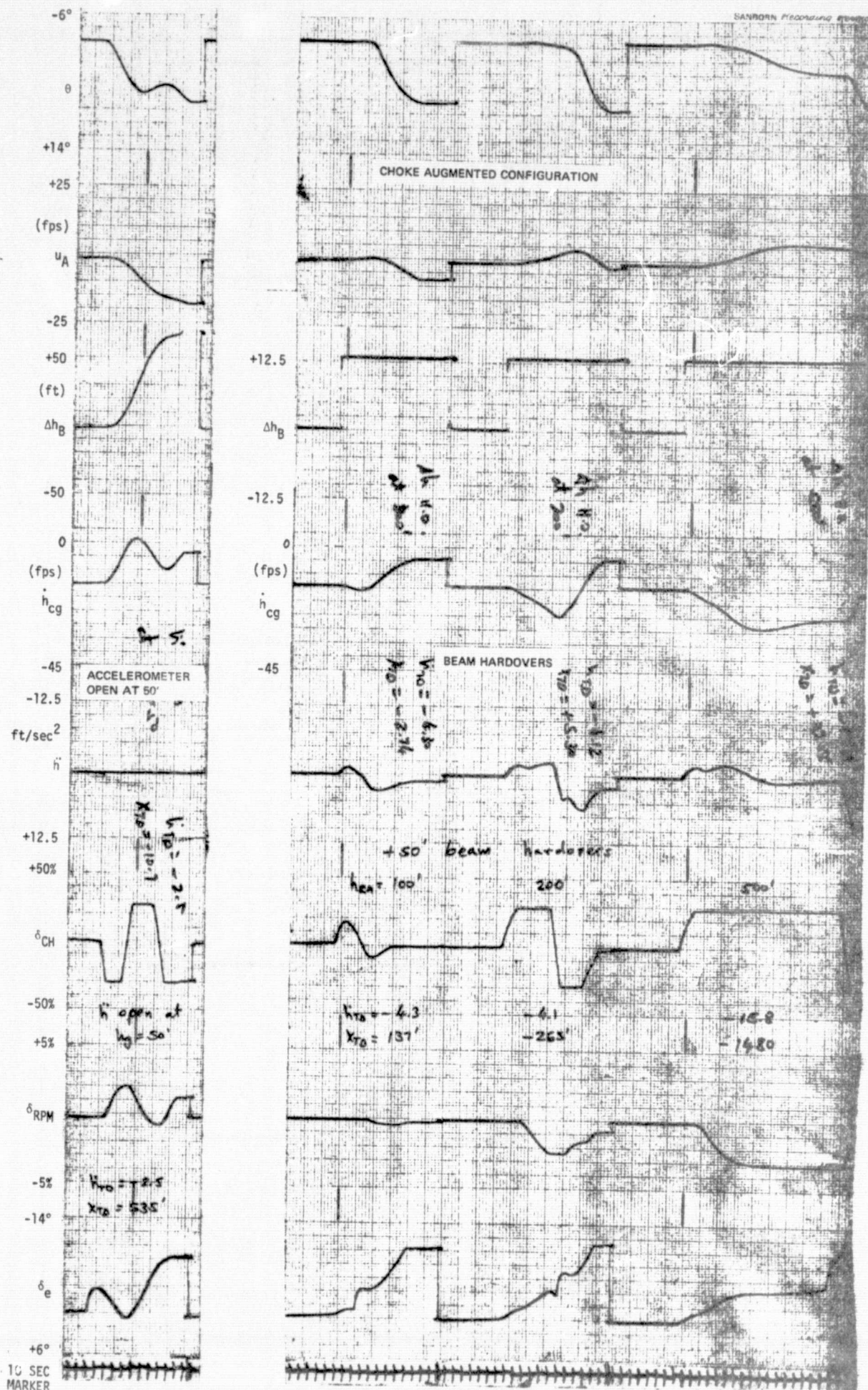


Figure B-15. Failure Time Histories

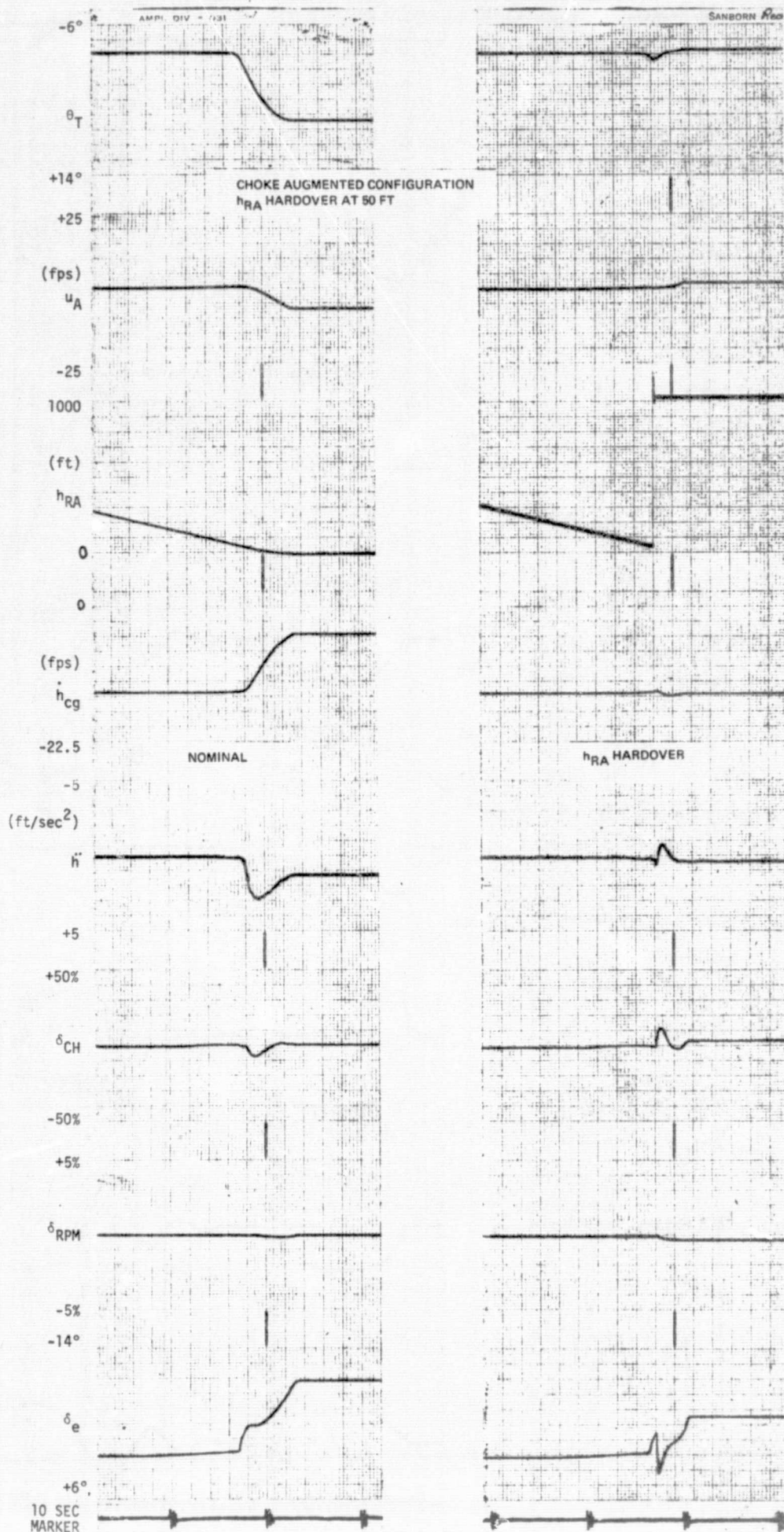


Figure B-16. Failure Time History

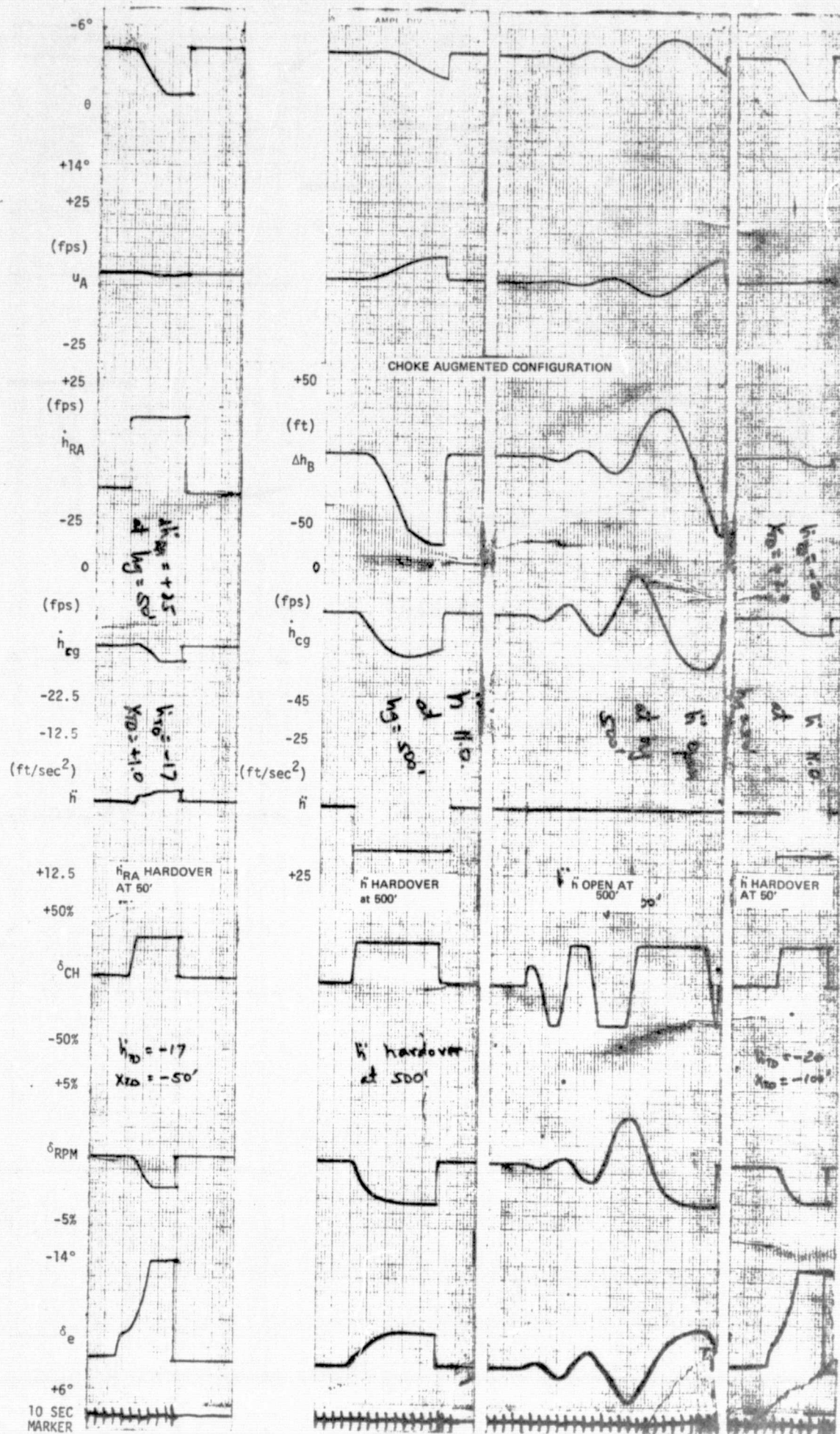


Figure B-17. Failure Time Histories

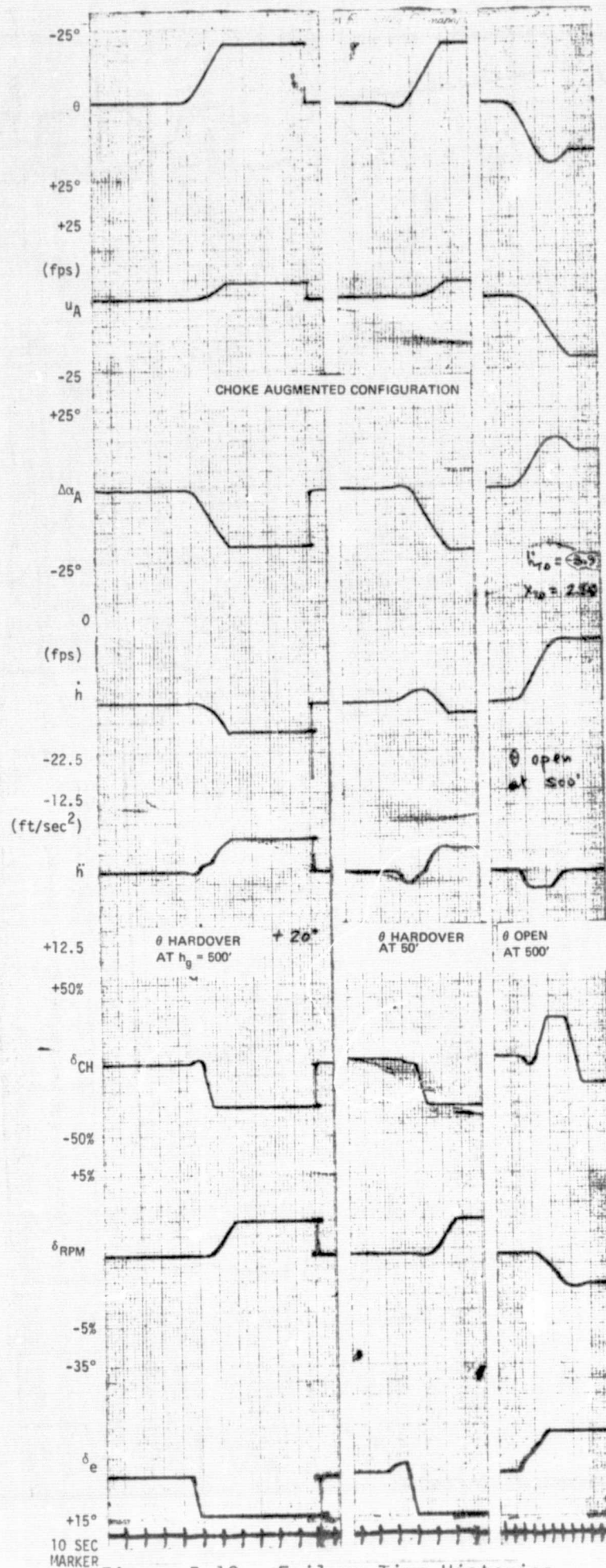


Figure B-18. Failure Time Histories

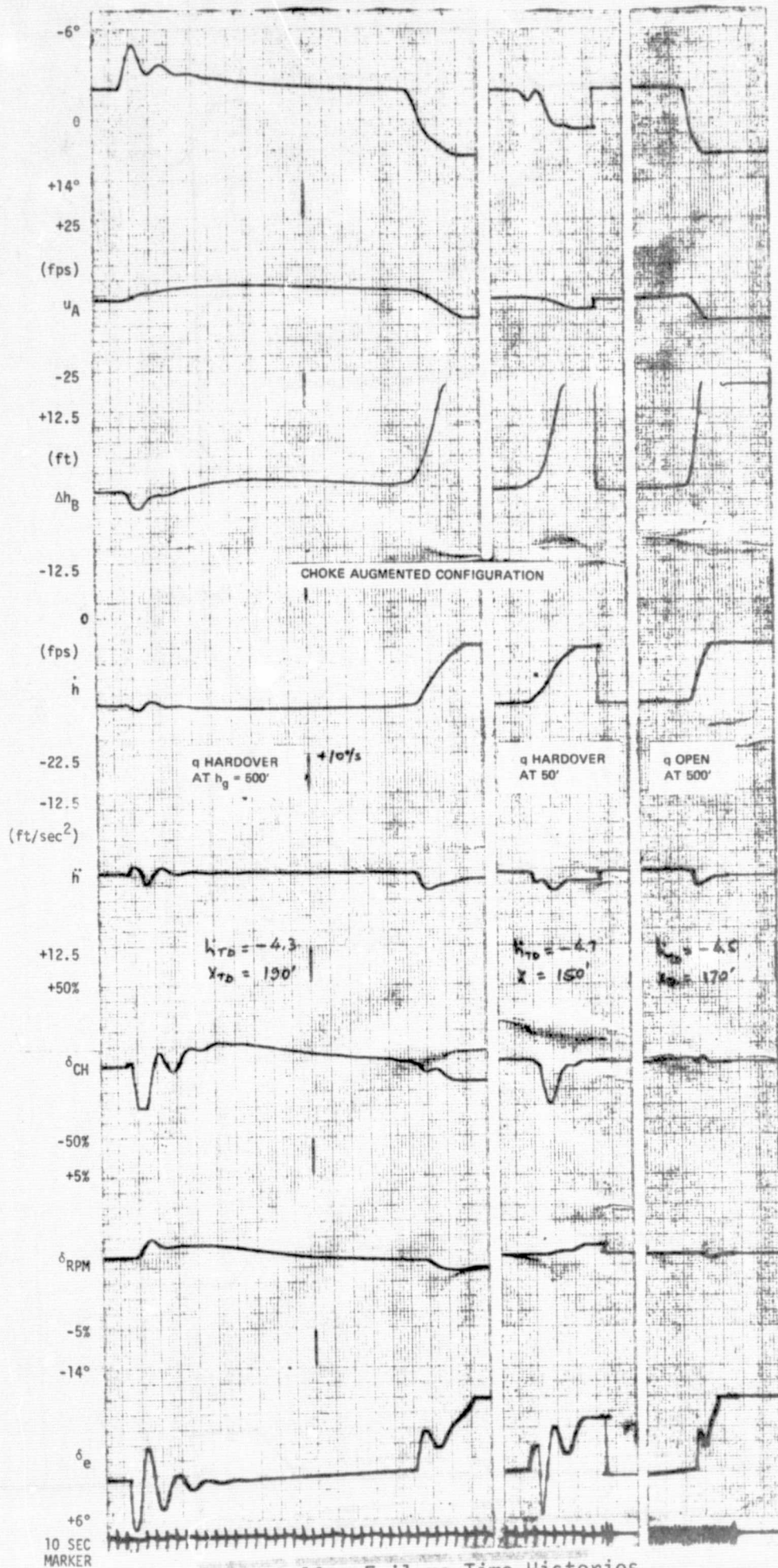


Figure B-19. Failure Time Histories

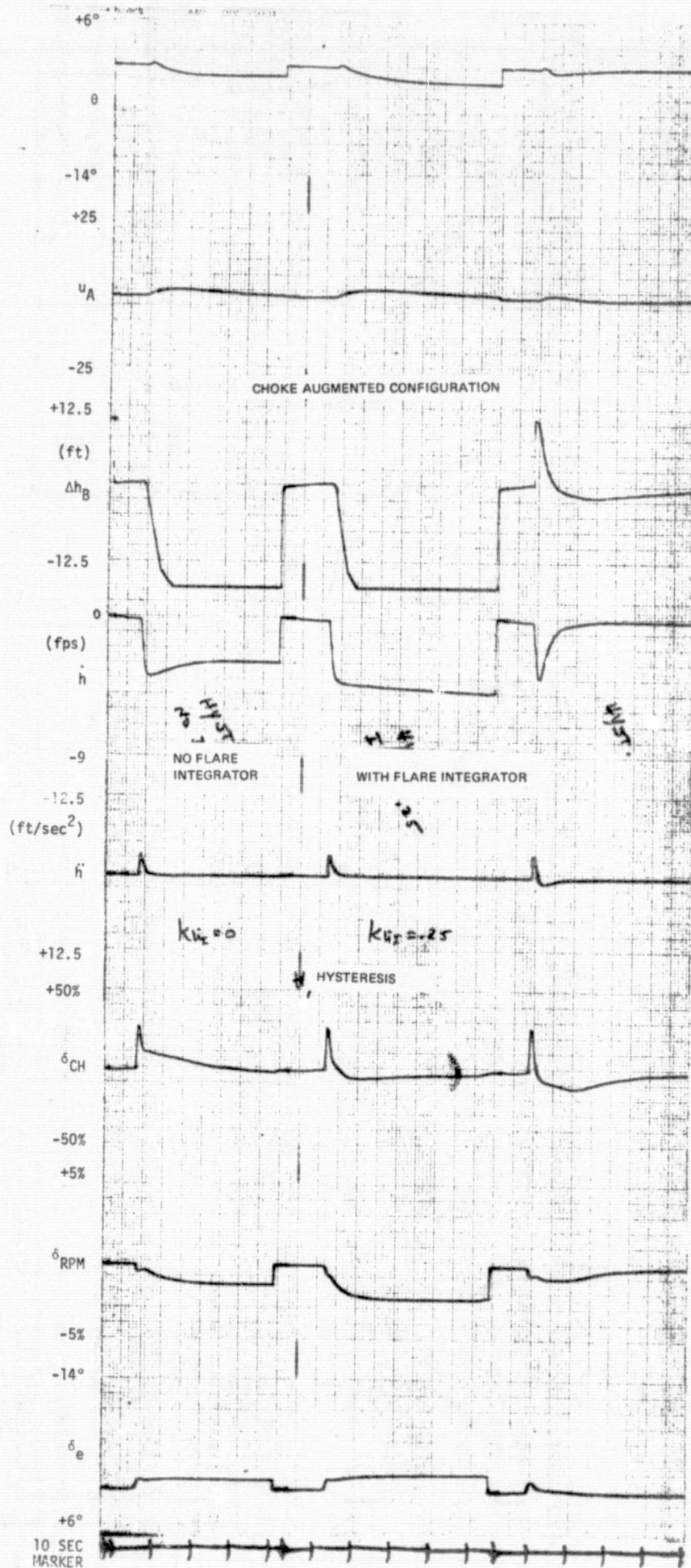


Figure B-20. \dot{h} & Δh Step Responses
B-27

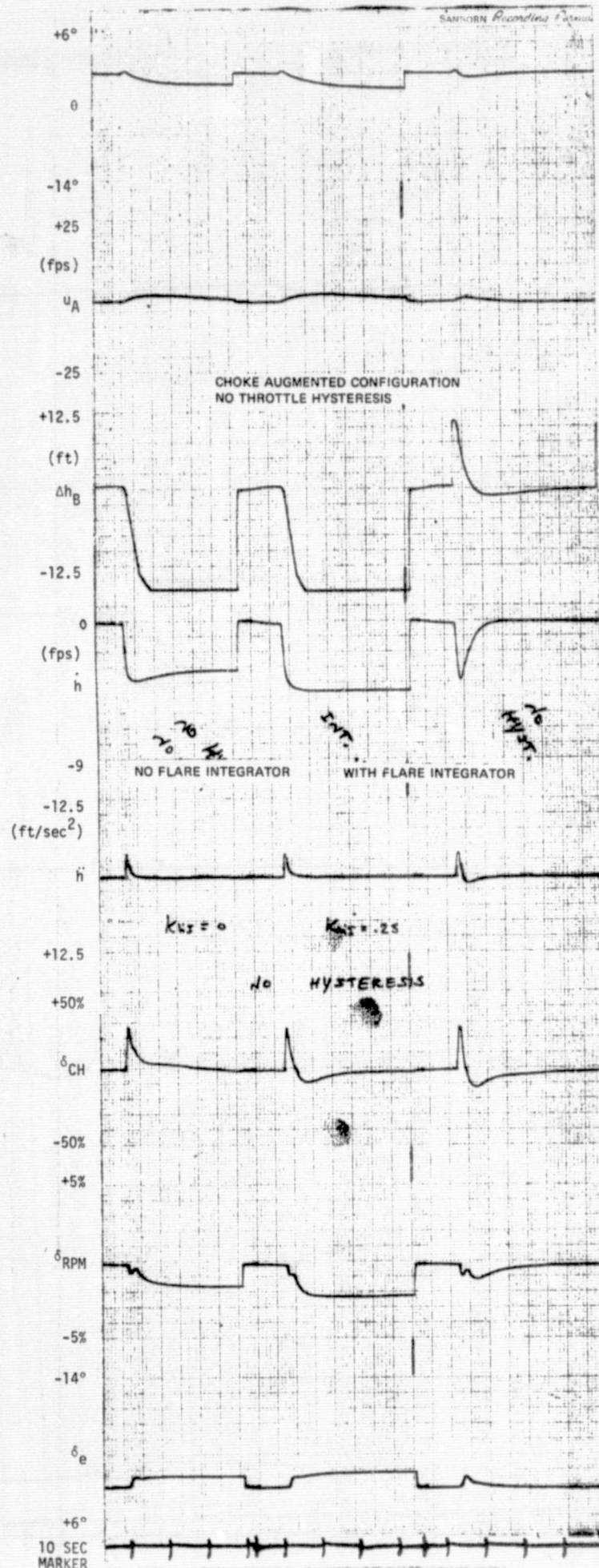


Figure B-21. \dot{h} & Δh Step Responses

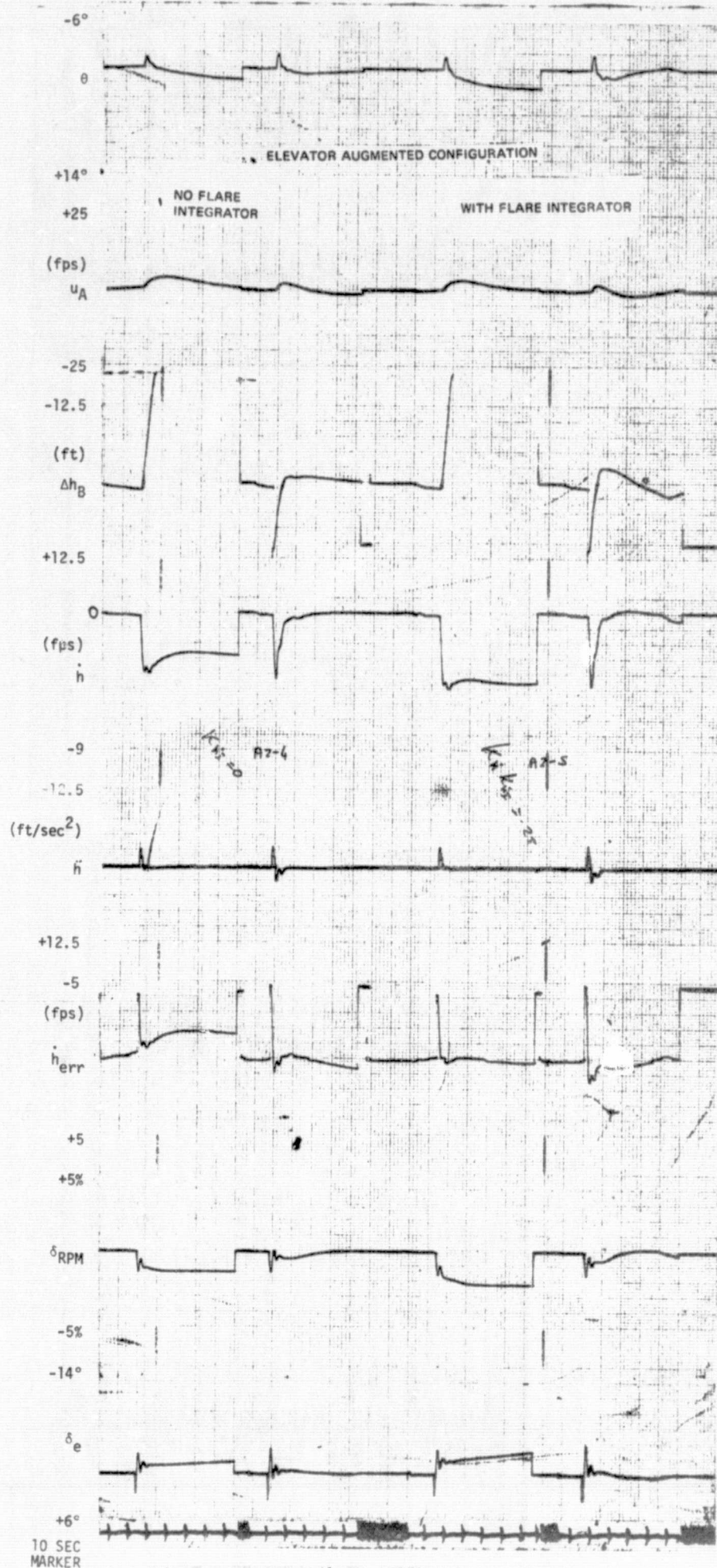


Figure B-22. \dot{h} & Δh Step Responses

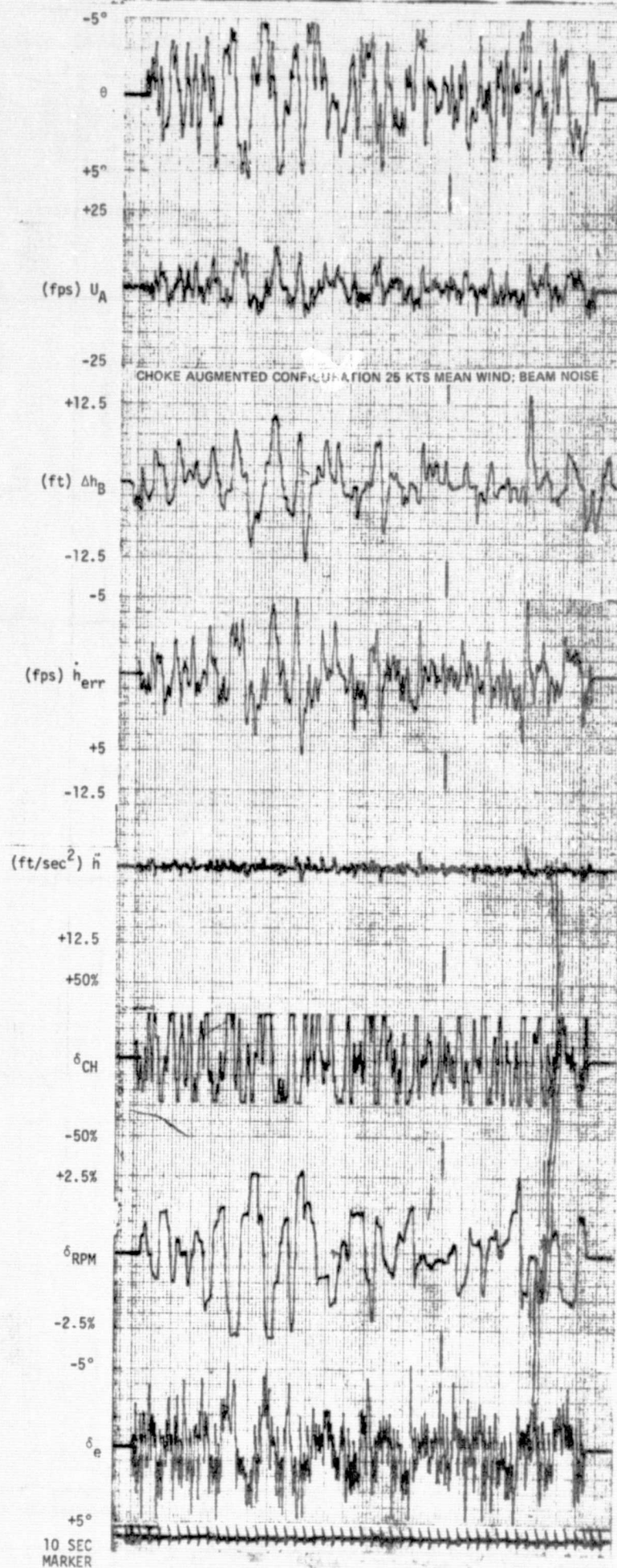


Figure B-23. Activity in Disturbances
B-30

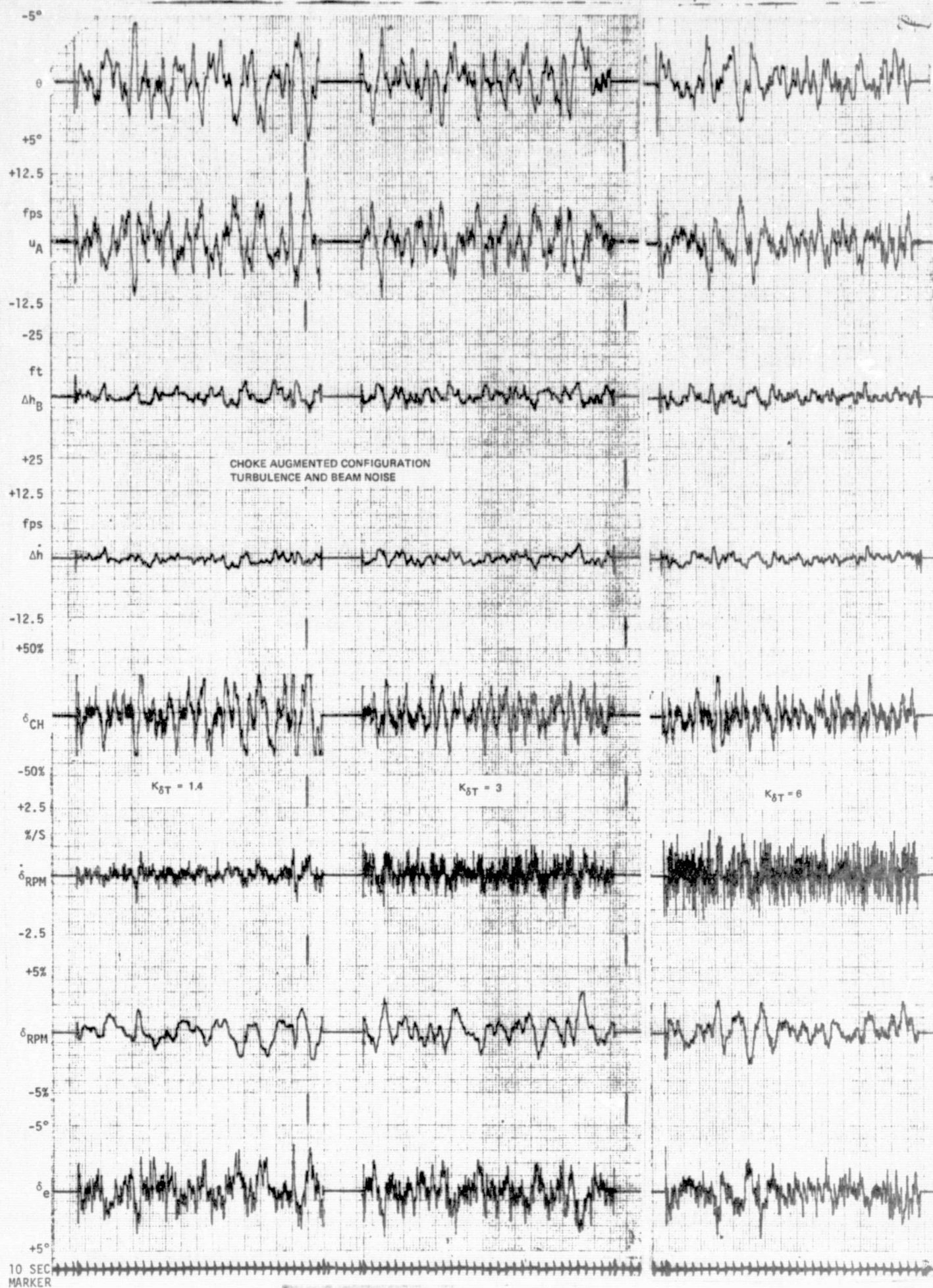


Figure B-24. Activity in Disturbances
R-31

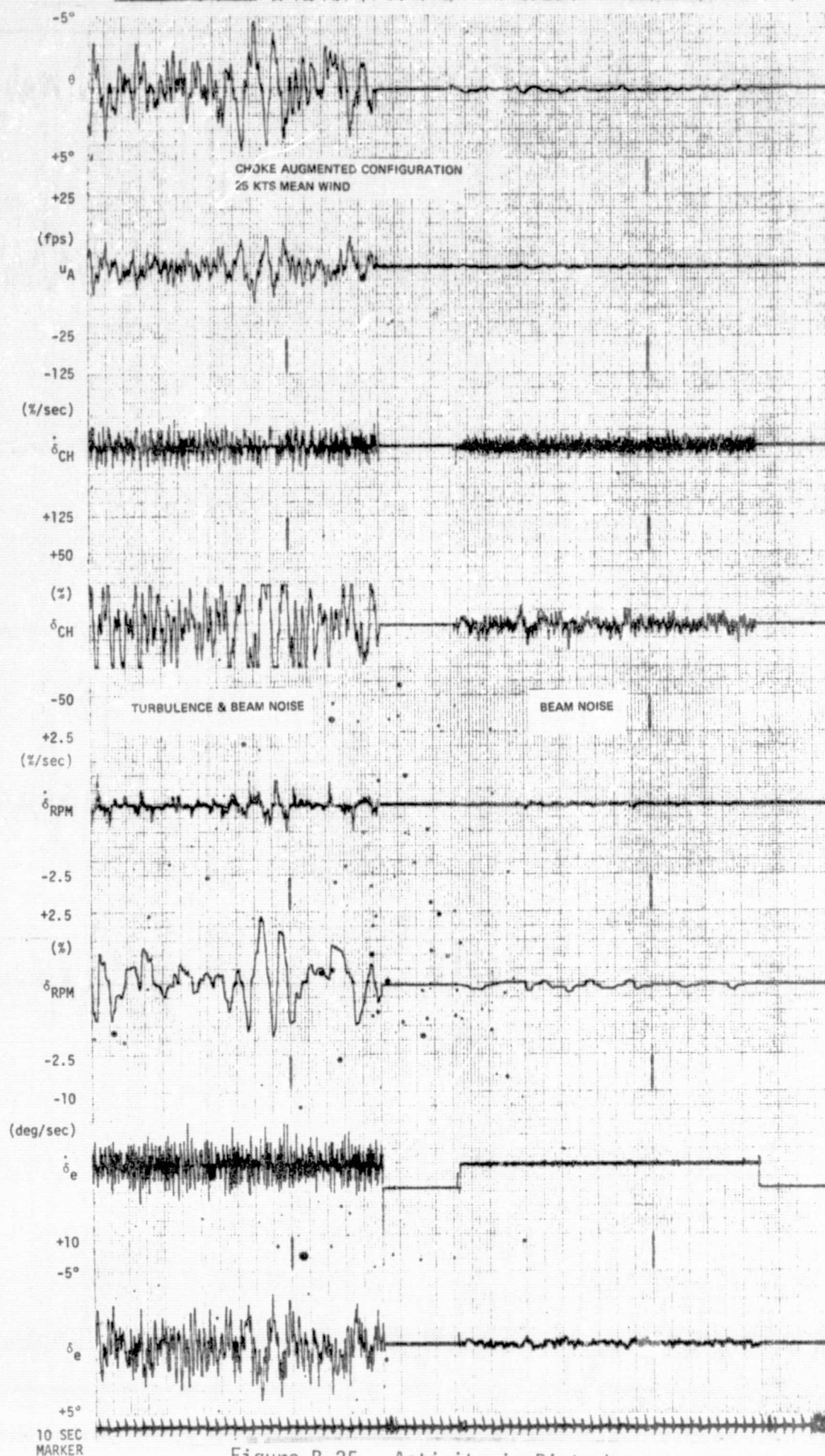


Figure B-25. Activity in Disturbances
B-32

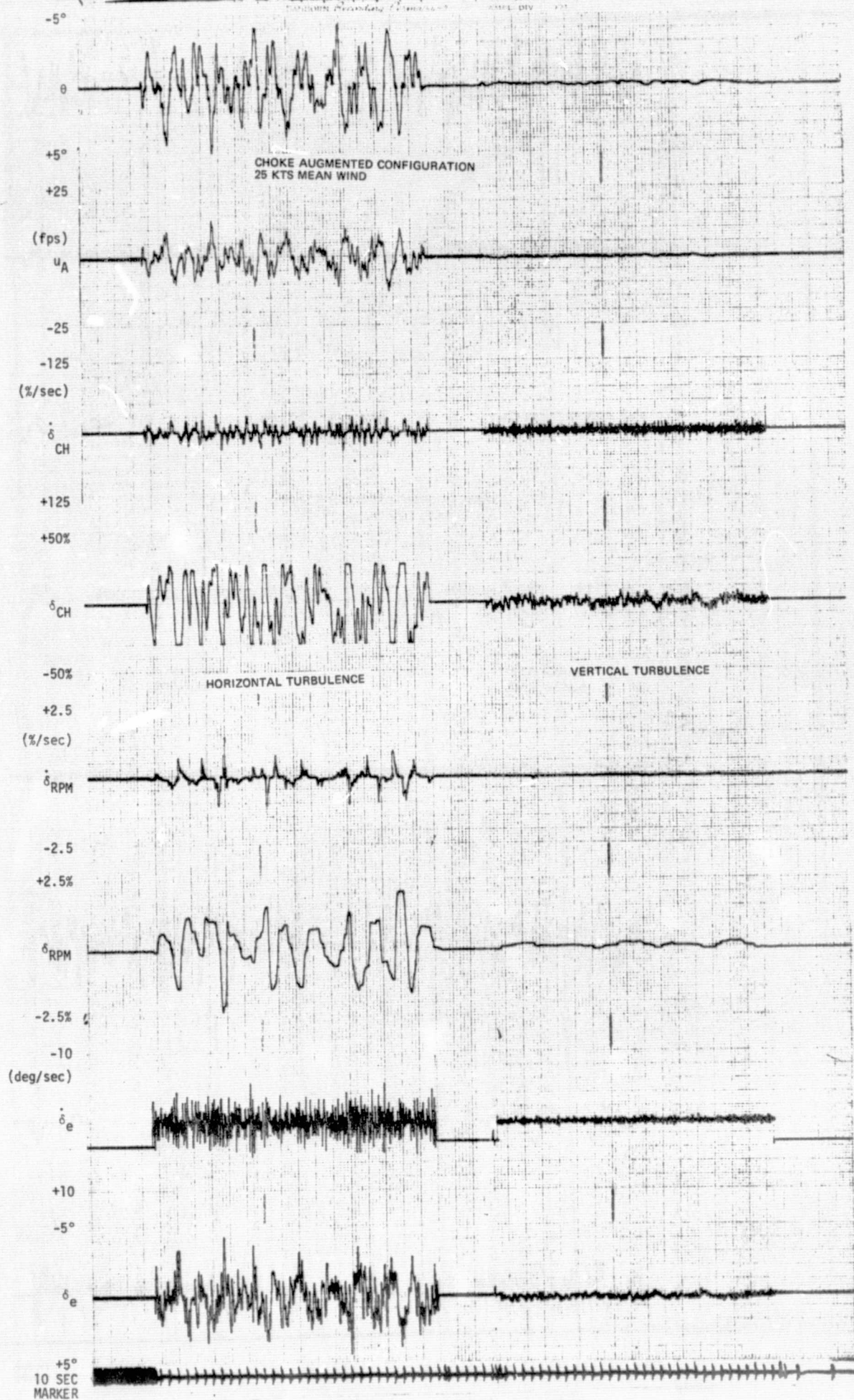


Figure B-26. Activity in Disturbances
B-33

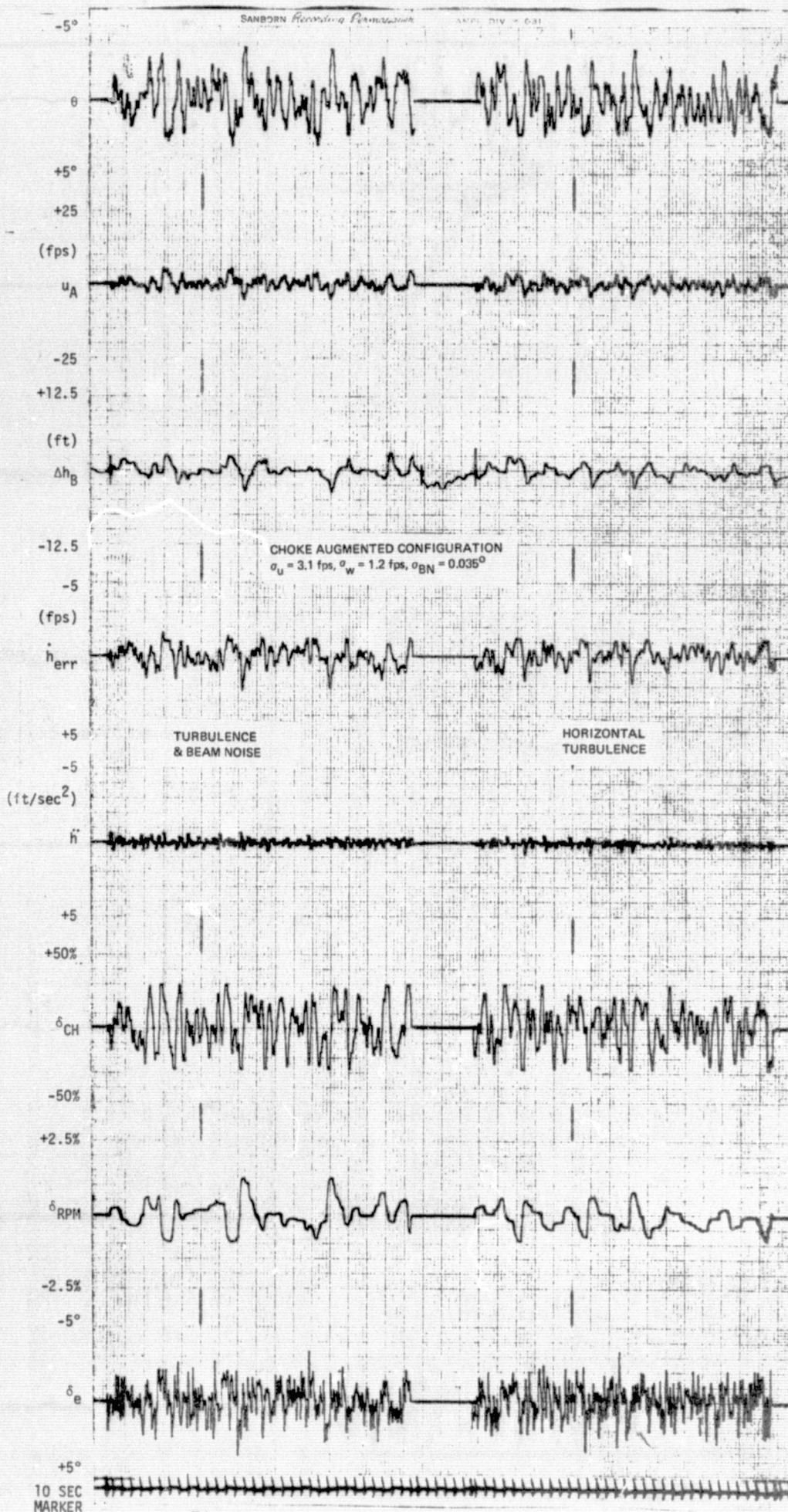


Figure B-27. Activity in Disturbances
 B-34

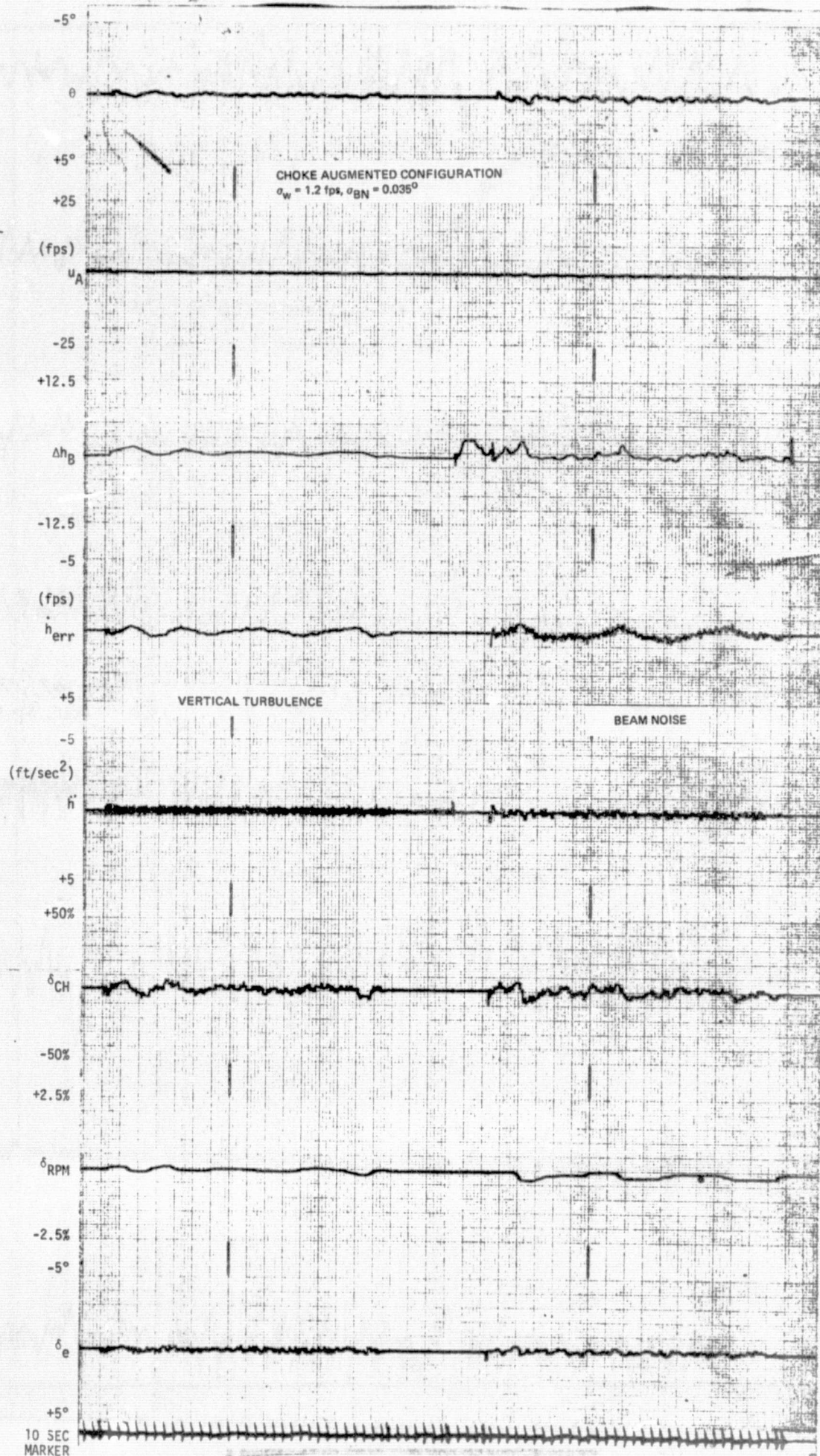


Figure B-28. Activity in Disturbances

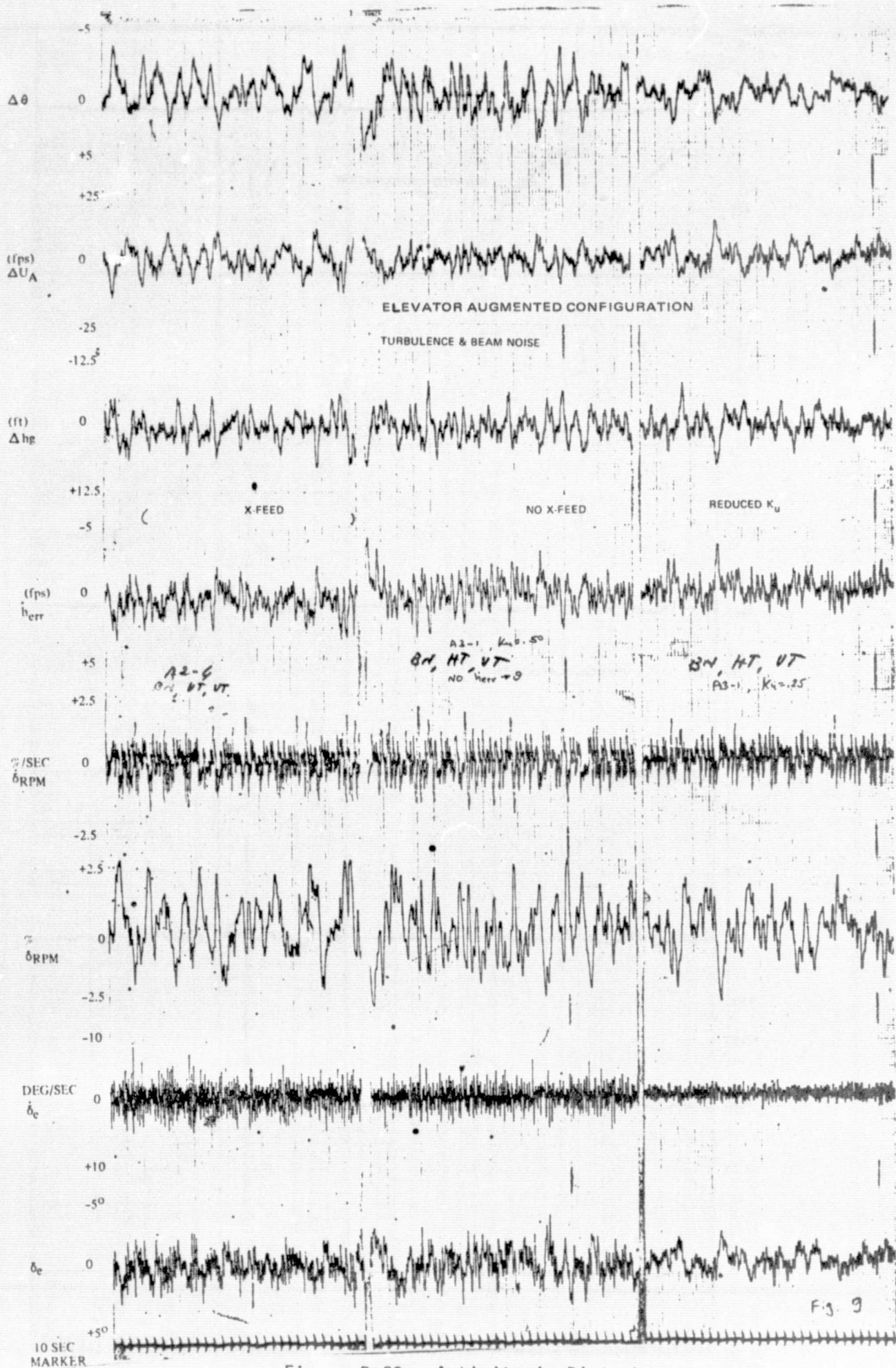
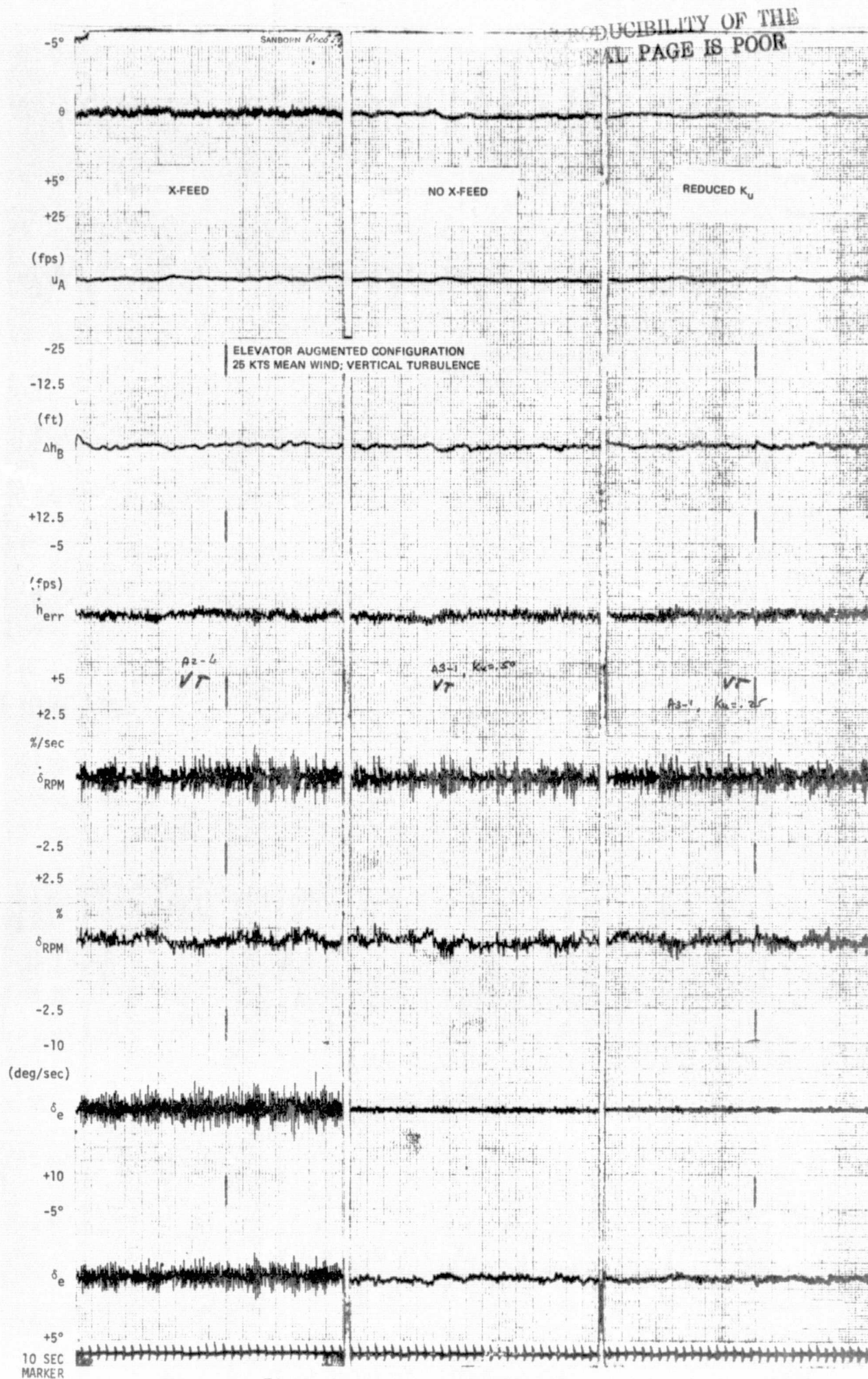


Figure B-29. Activity in Disturbances
B-36



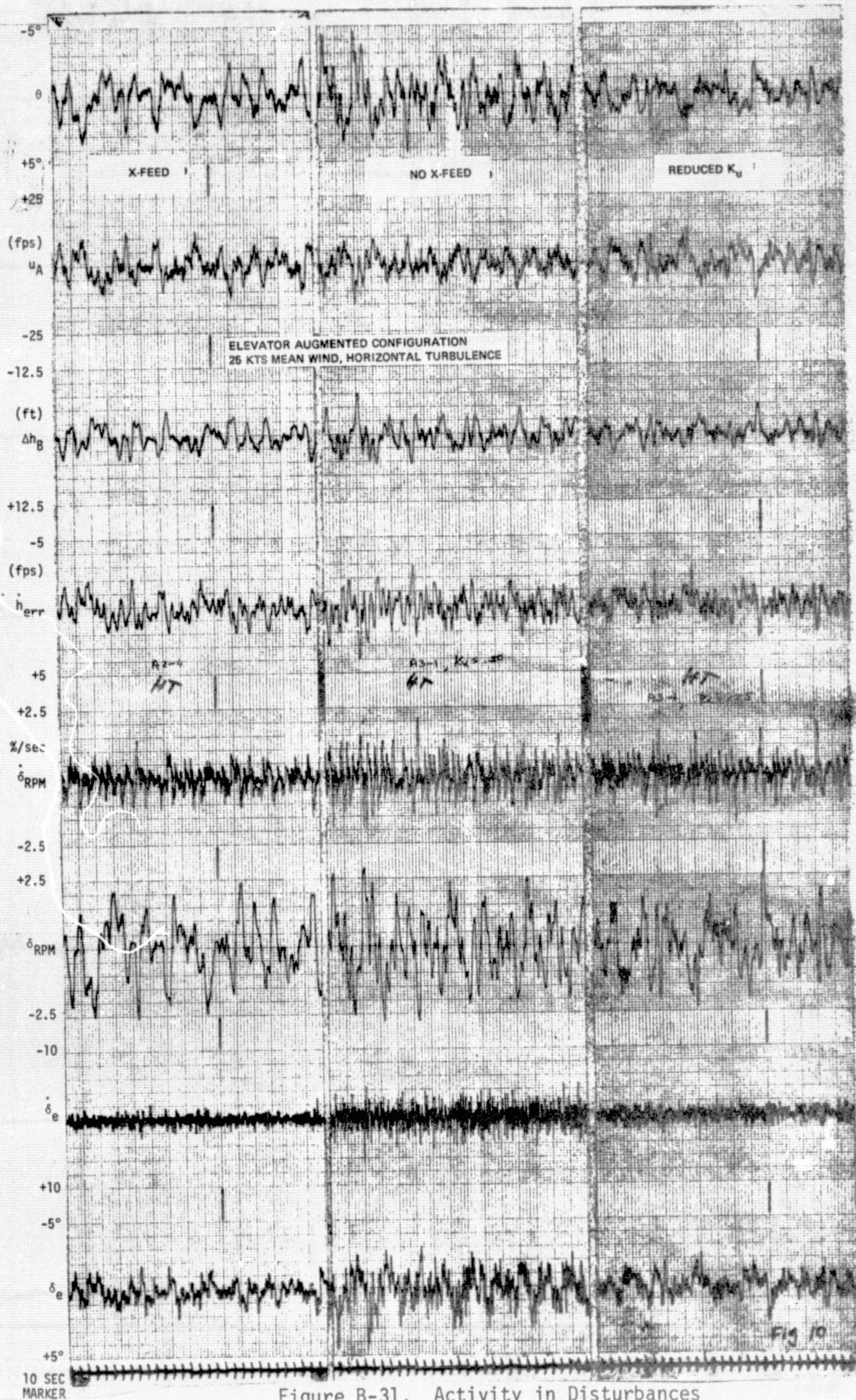


Figure B-31. Activity in Disturbances
B-38

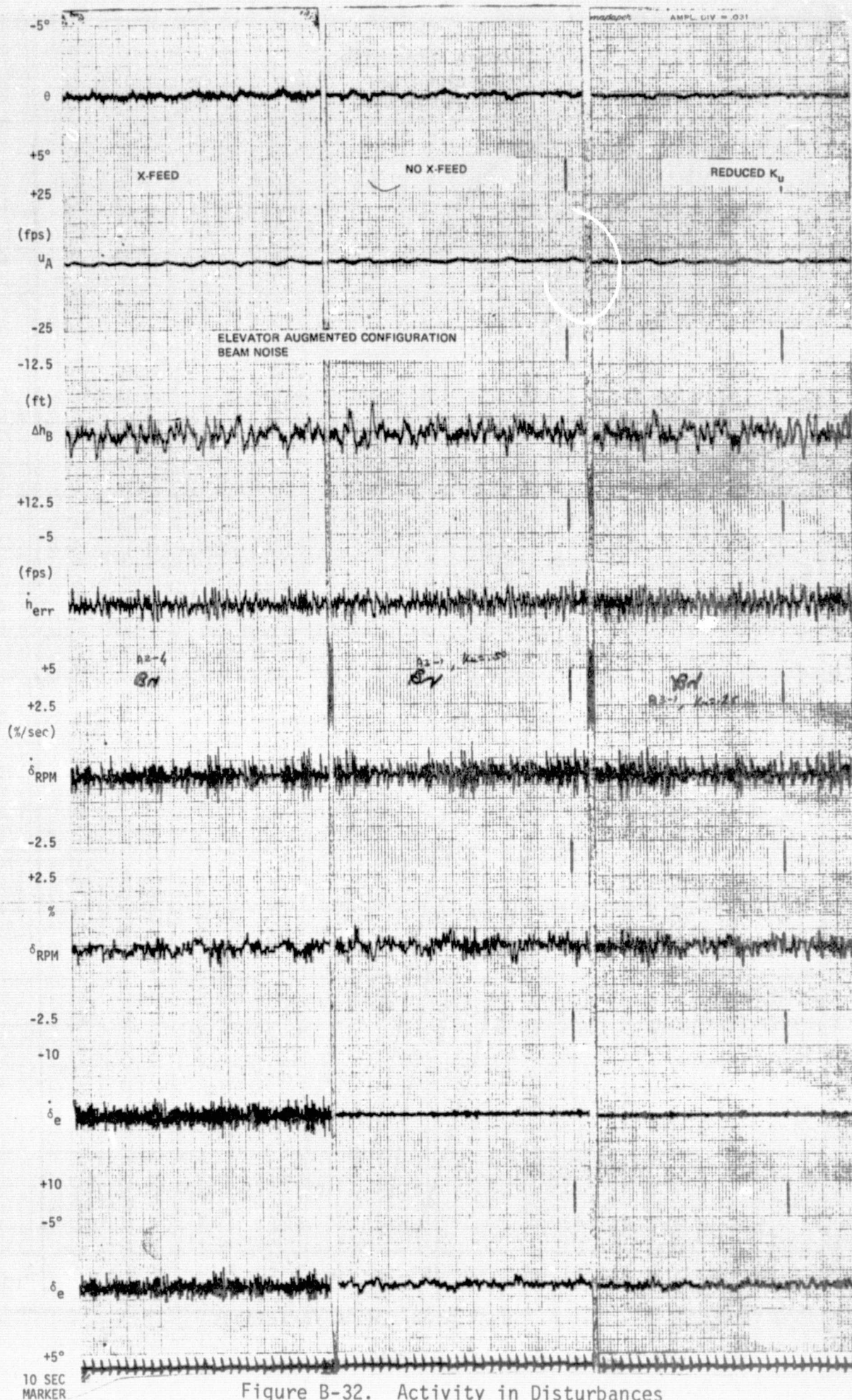


Figure B-32. Activity in Disturbances
R-39

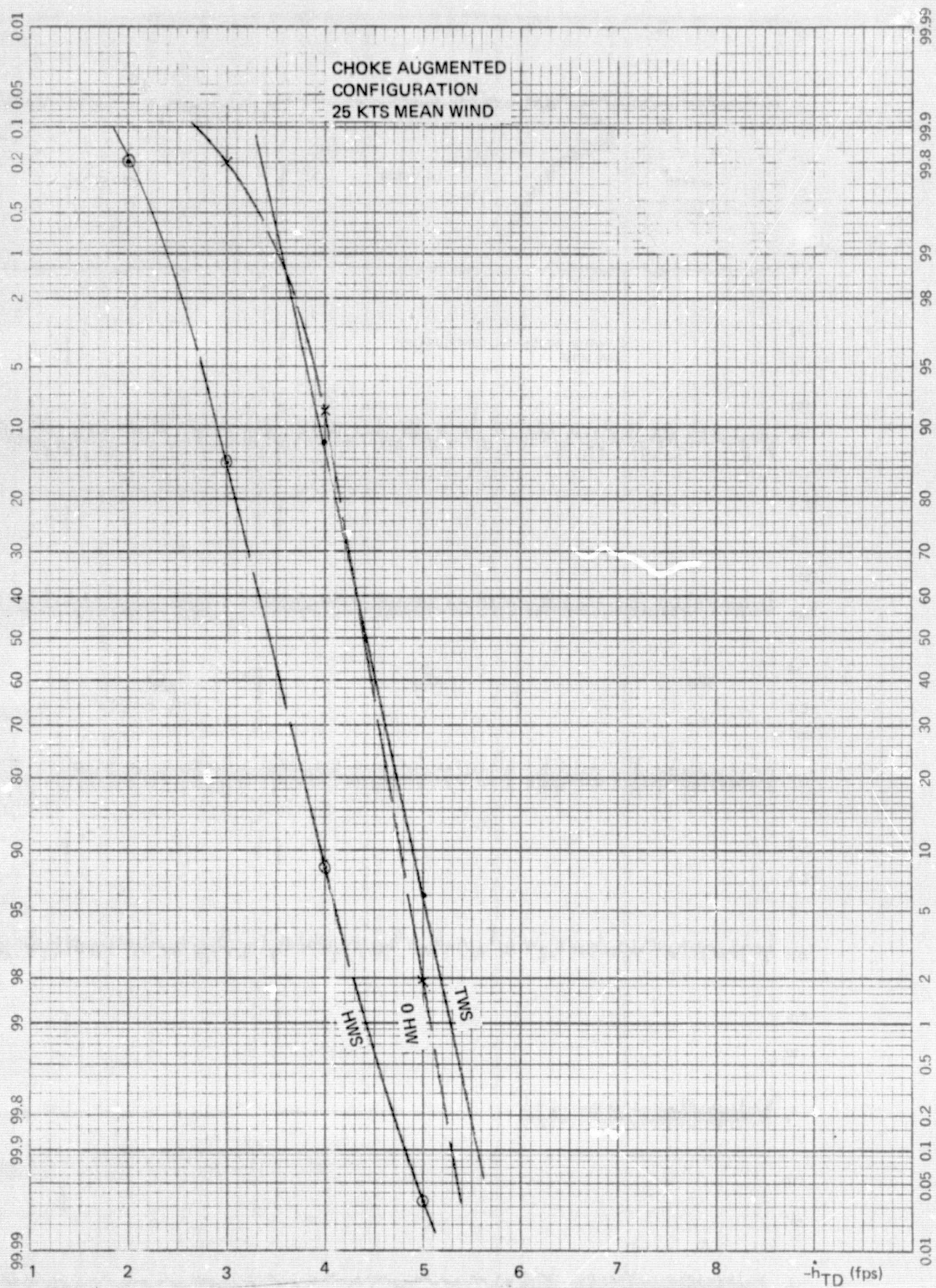


Figure B-33. Wind Variations

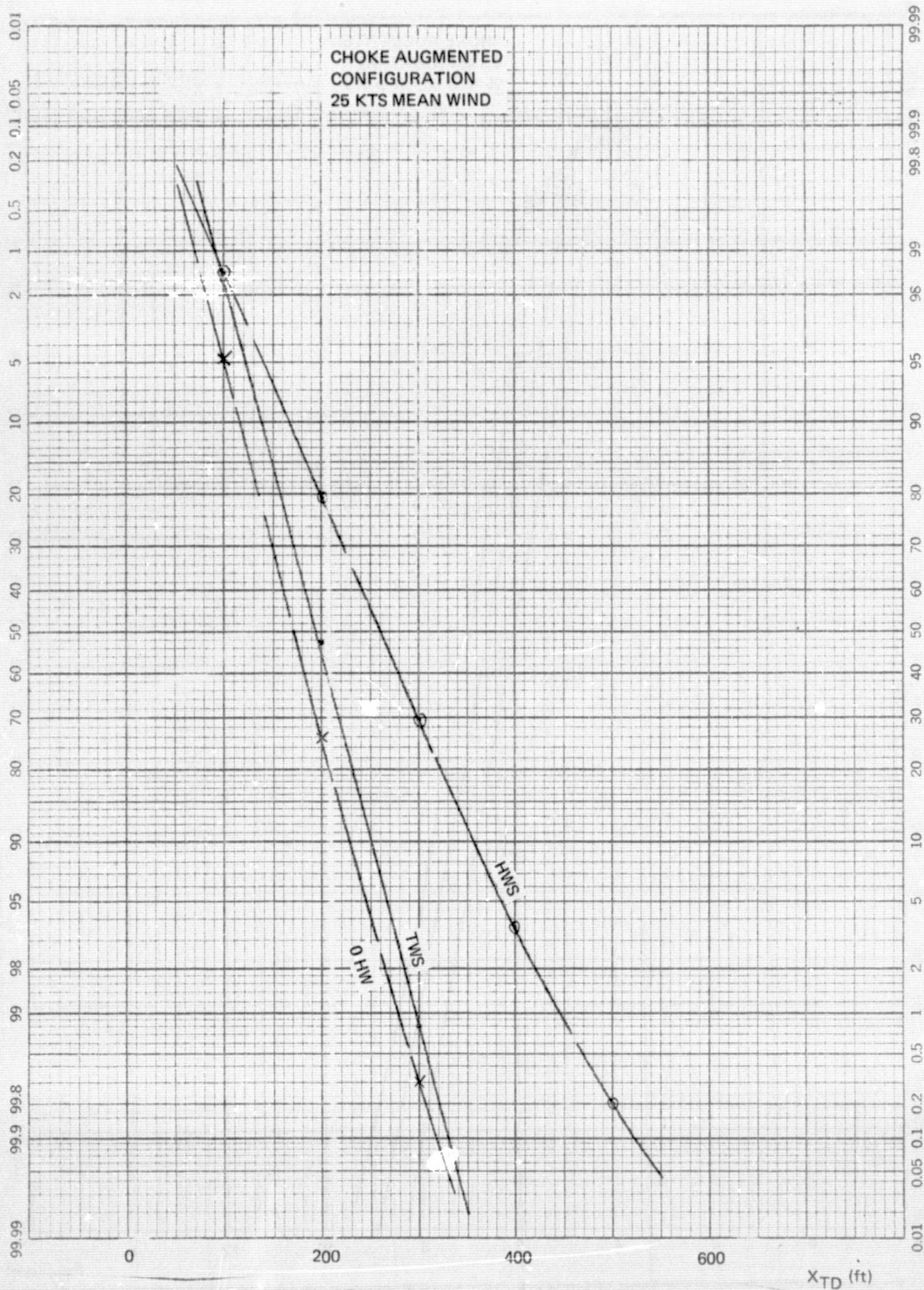


Figure B-34. Wind Variations

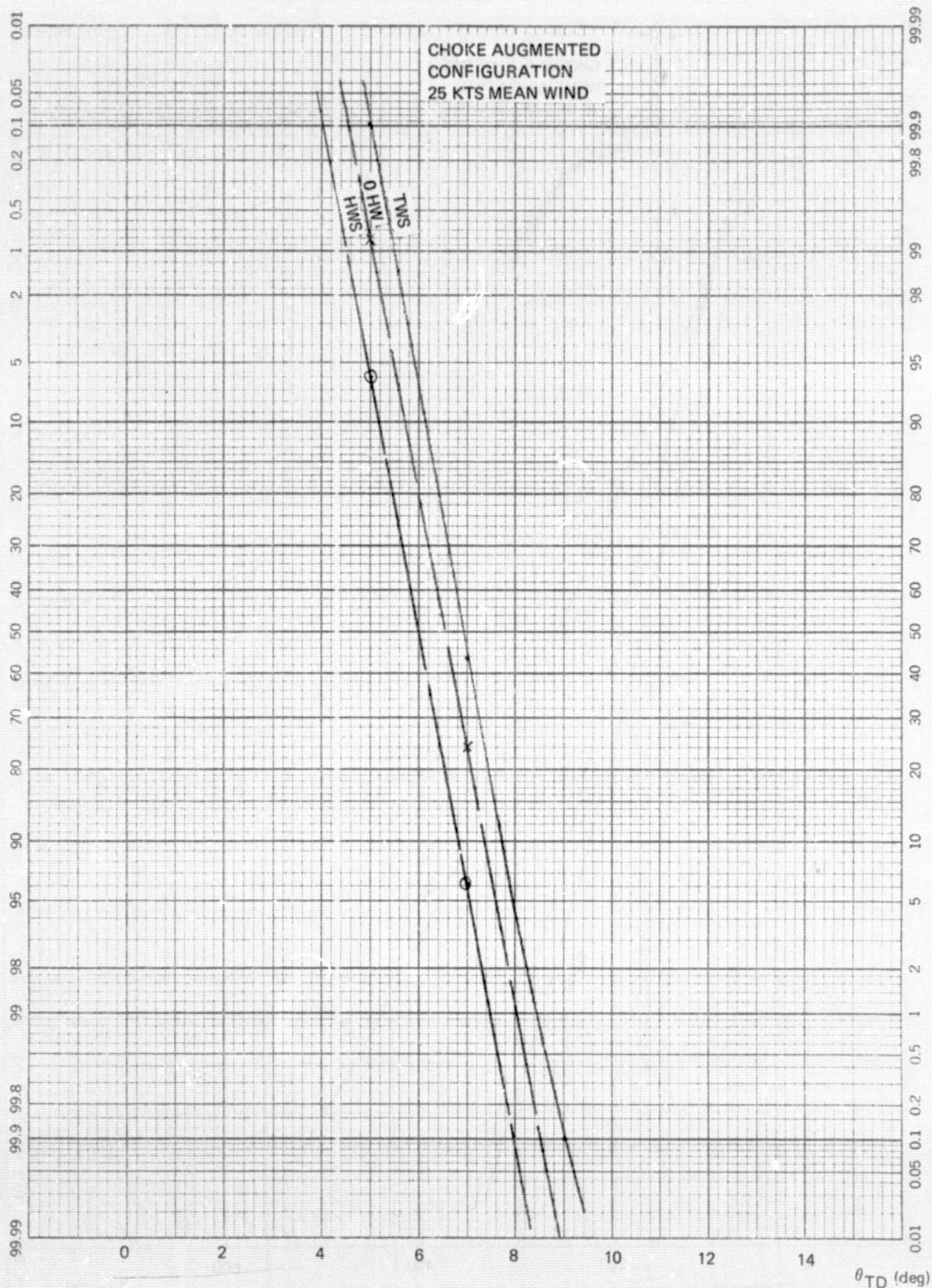


Figure B-35. Wind Variations

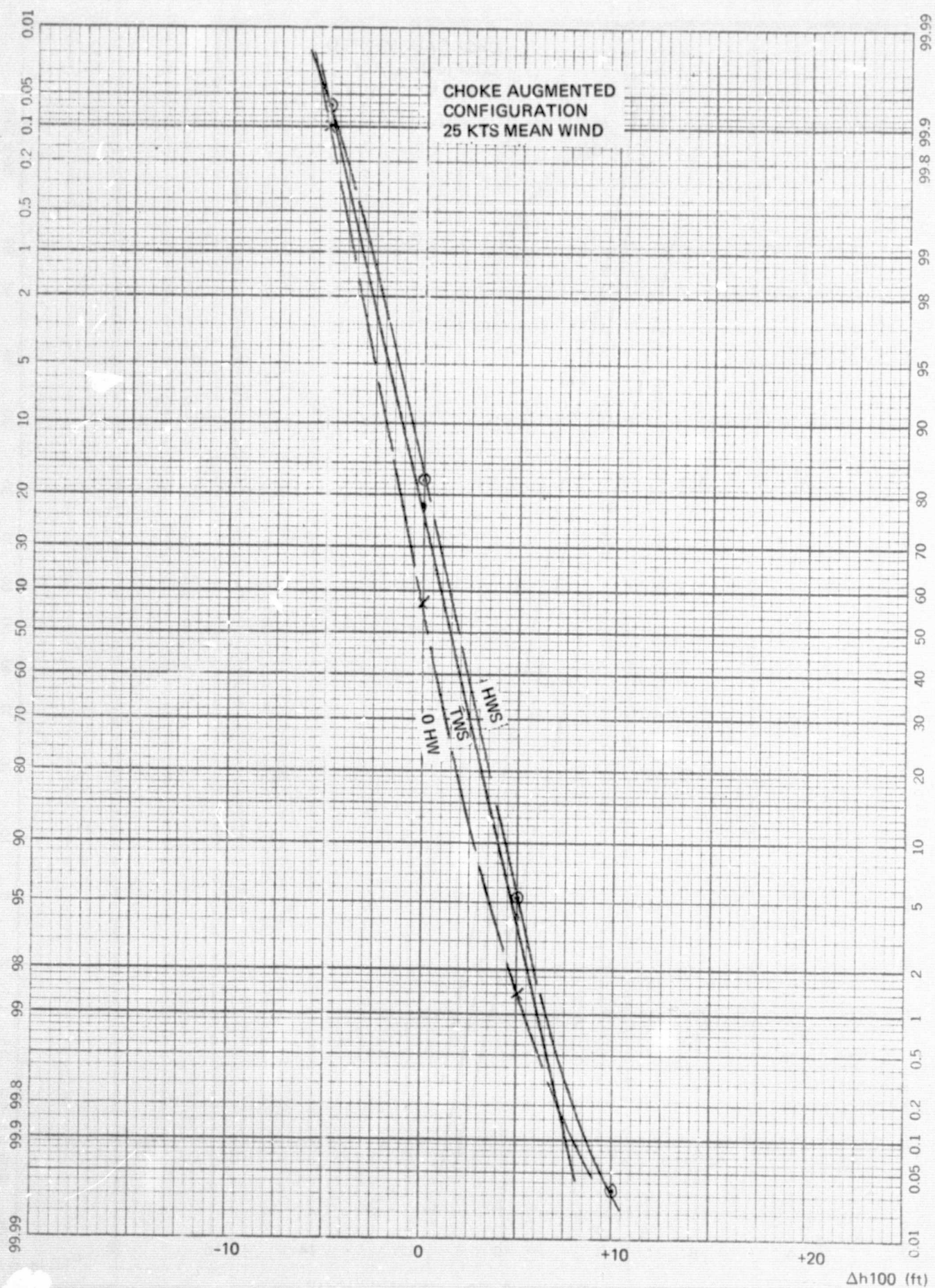


Figure B-36. Wind Variations

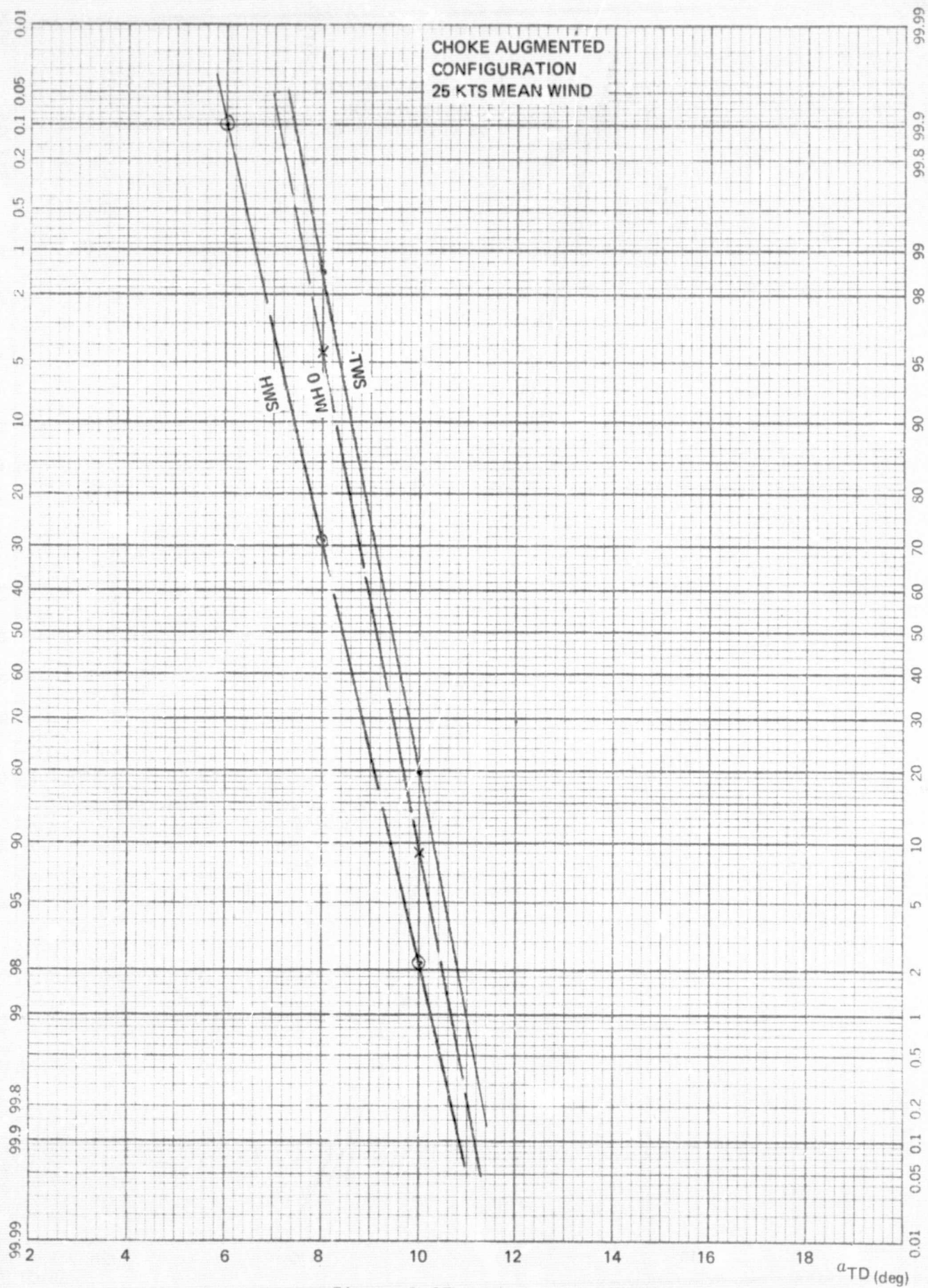


Figure B-37. Wind Variations

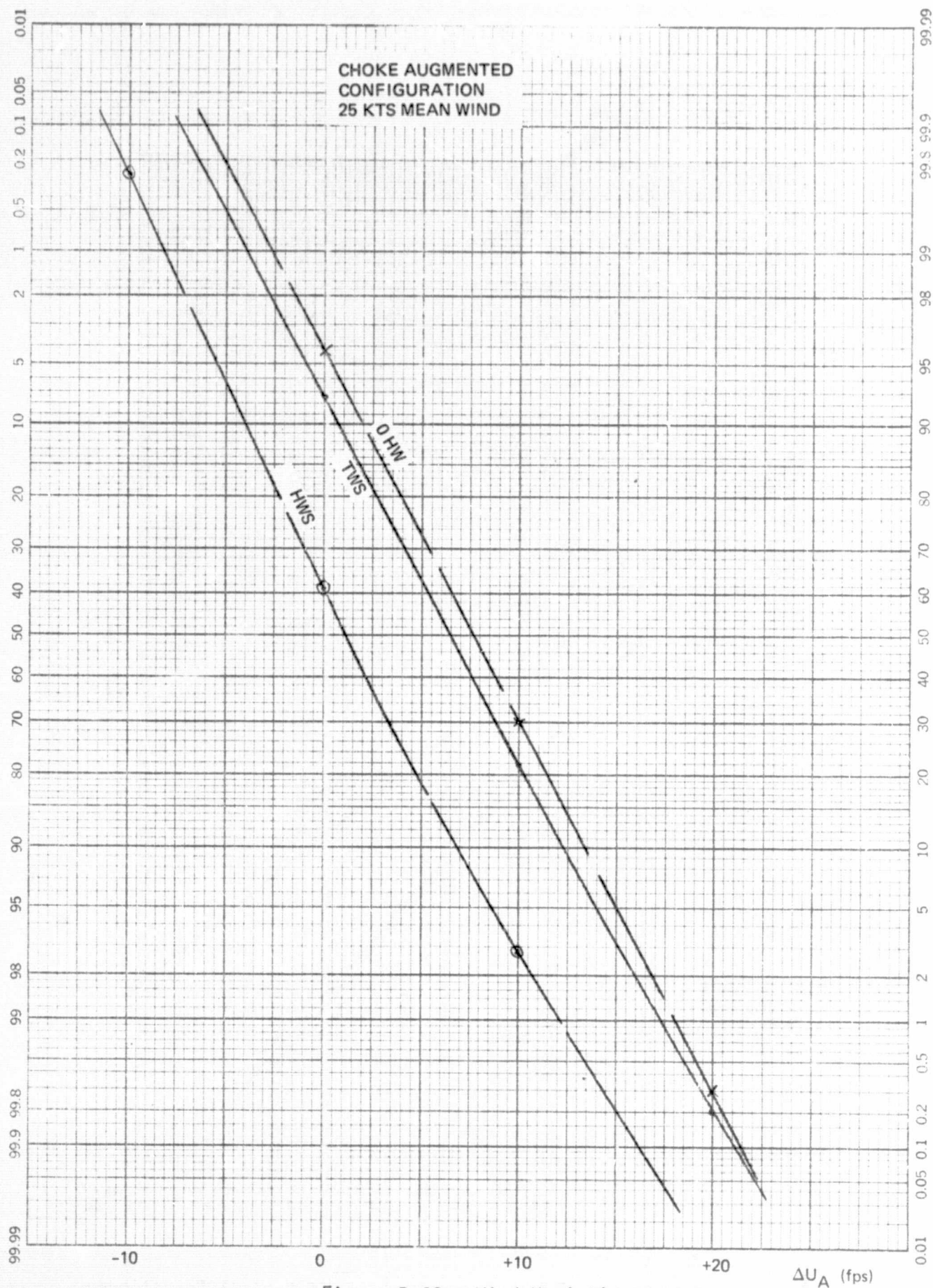


Figure B-38. Wind Variations

REPRODUCIBILITY OF THE
ORIGINAL PAGE IS POOR

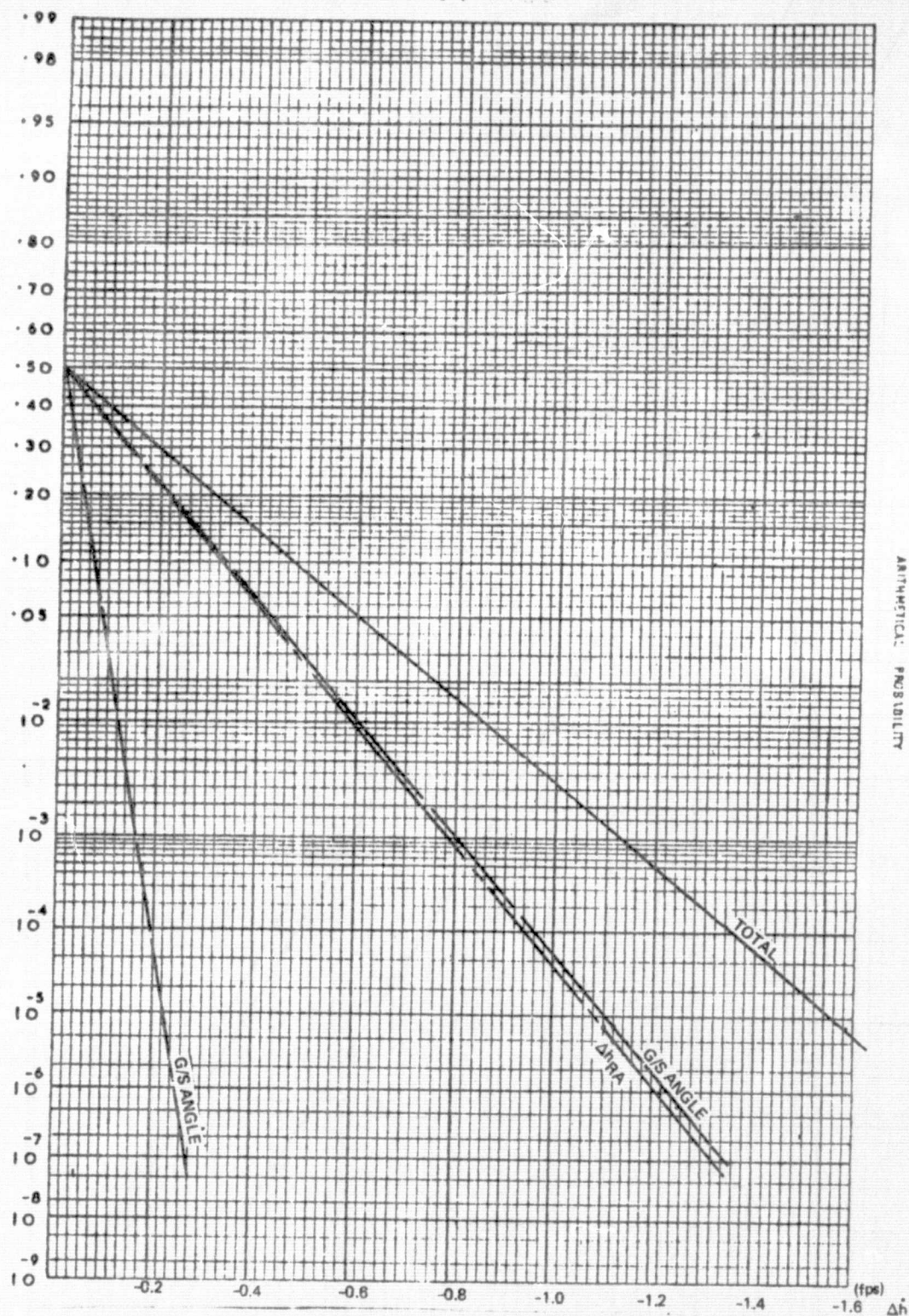


Figure B-39. Sink Rate Dispersion Due to Off-Nominal Conditions

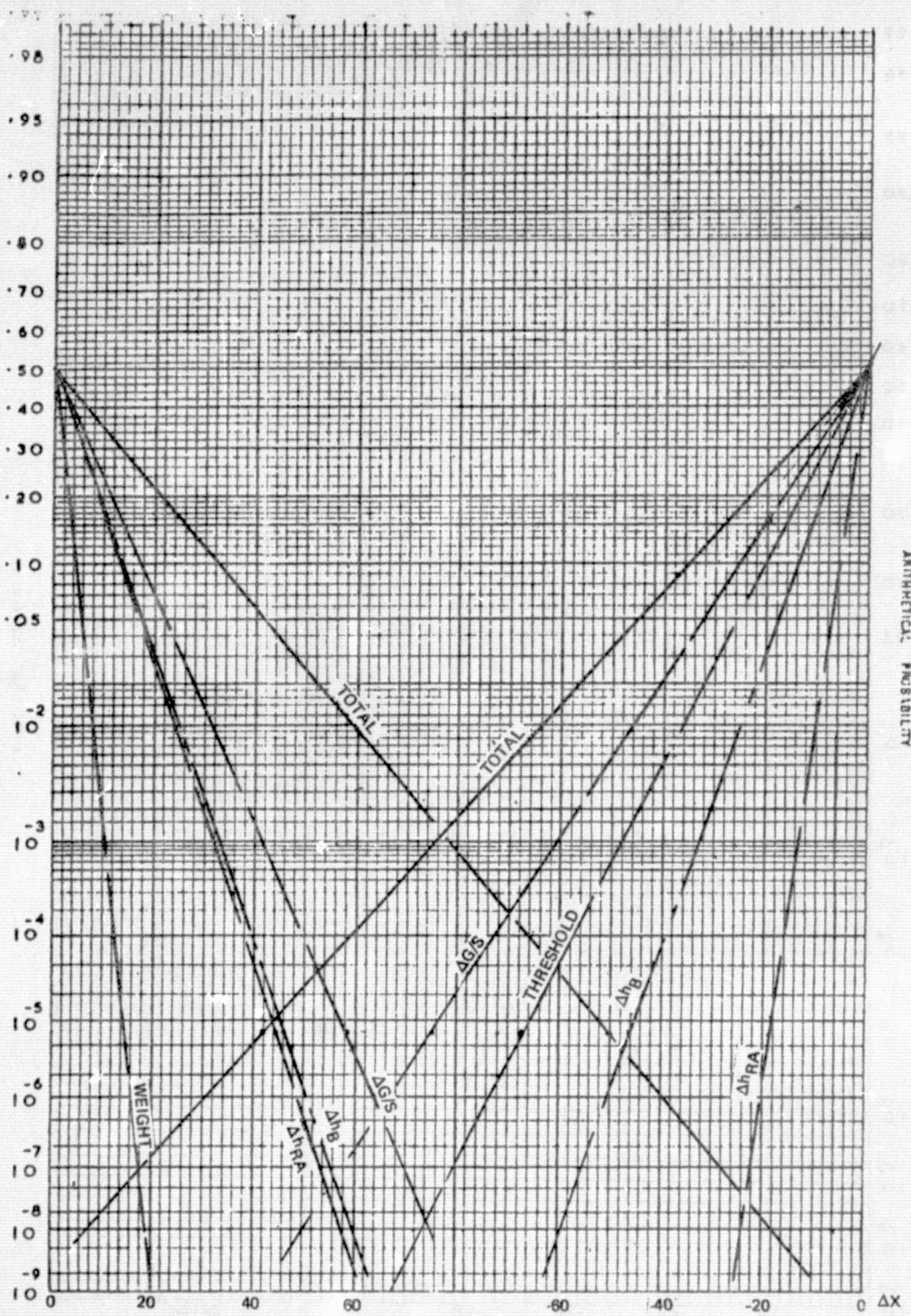


Figure B-40. Range Dispersion Due to Off-Nominal Conditions

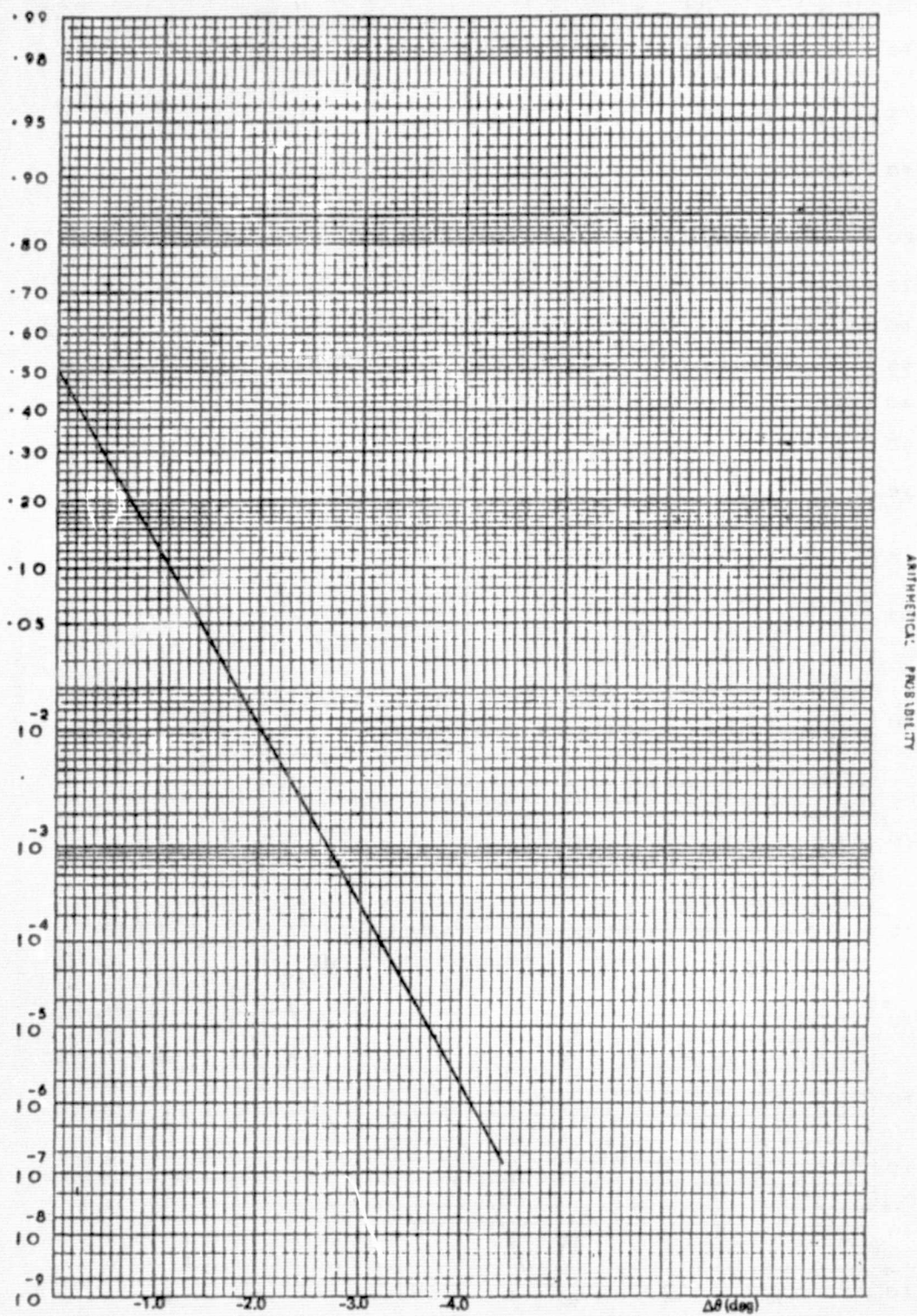


Figure B-41. Pitch Dispersion Due to Glide Slope Angle Variation

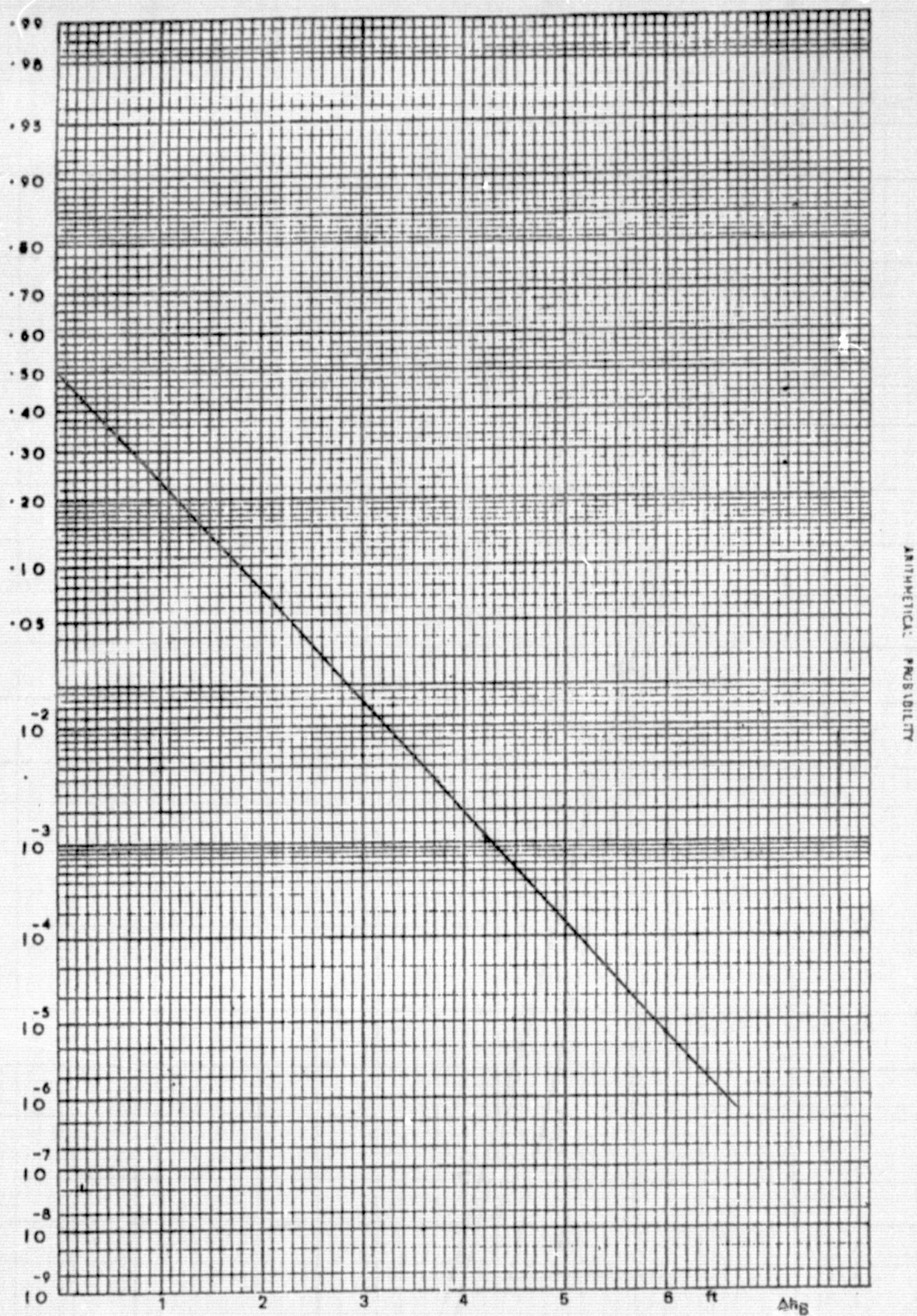


Figure B-42. Effect of Beam Offset on Glide Slope Tracking

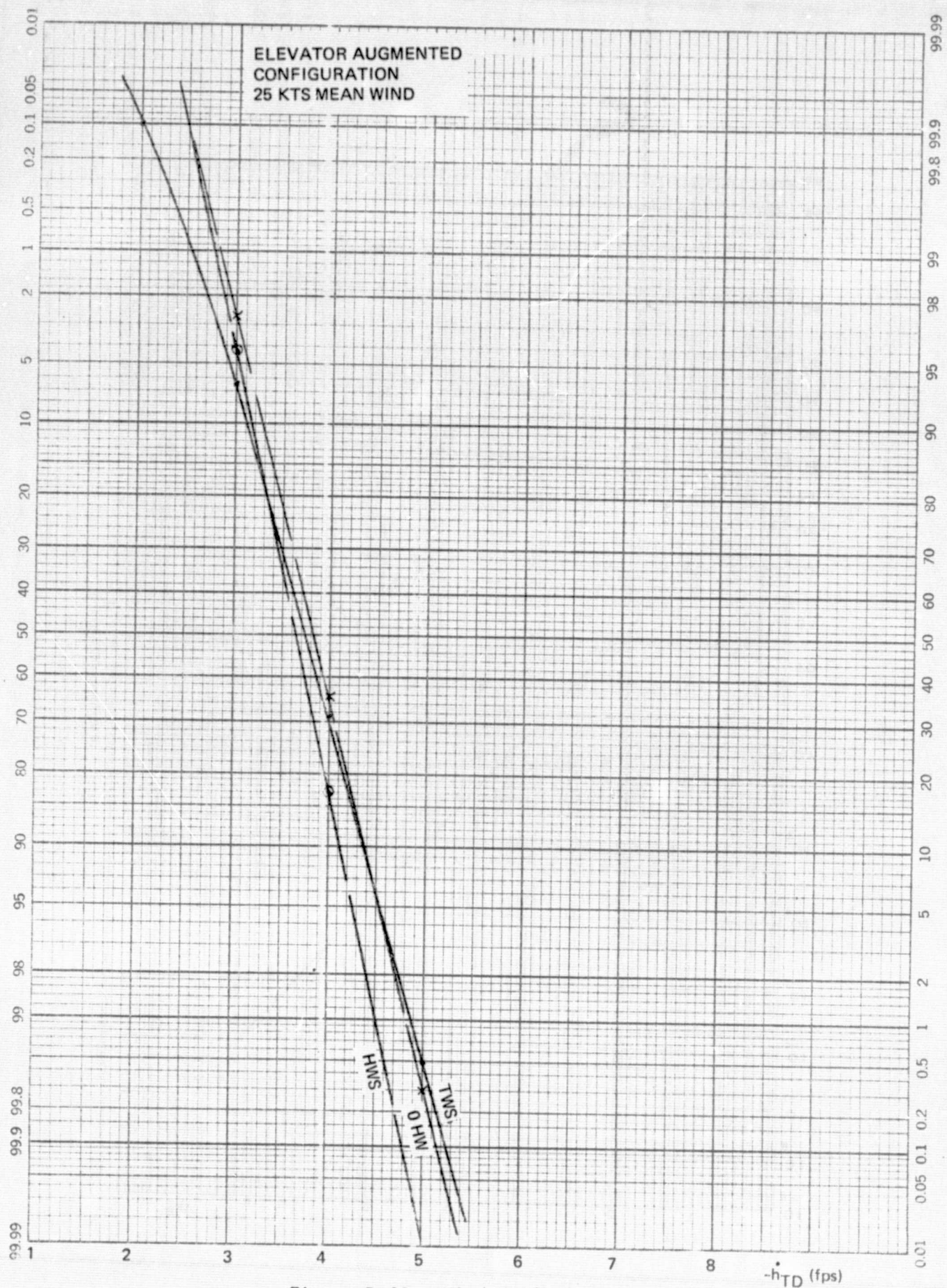


Figure B-43. Wind Variations

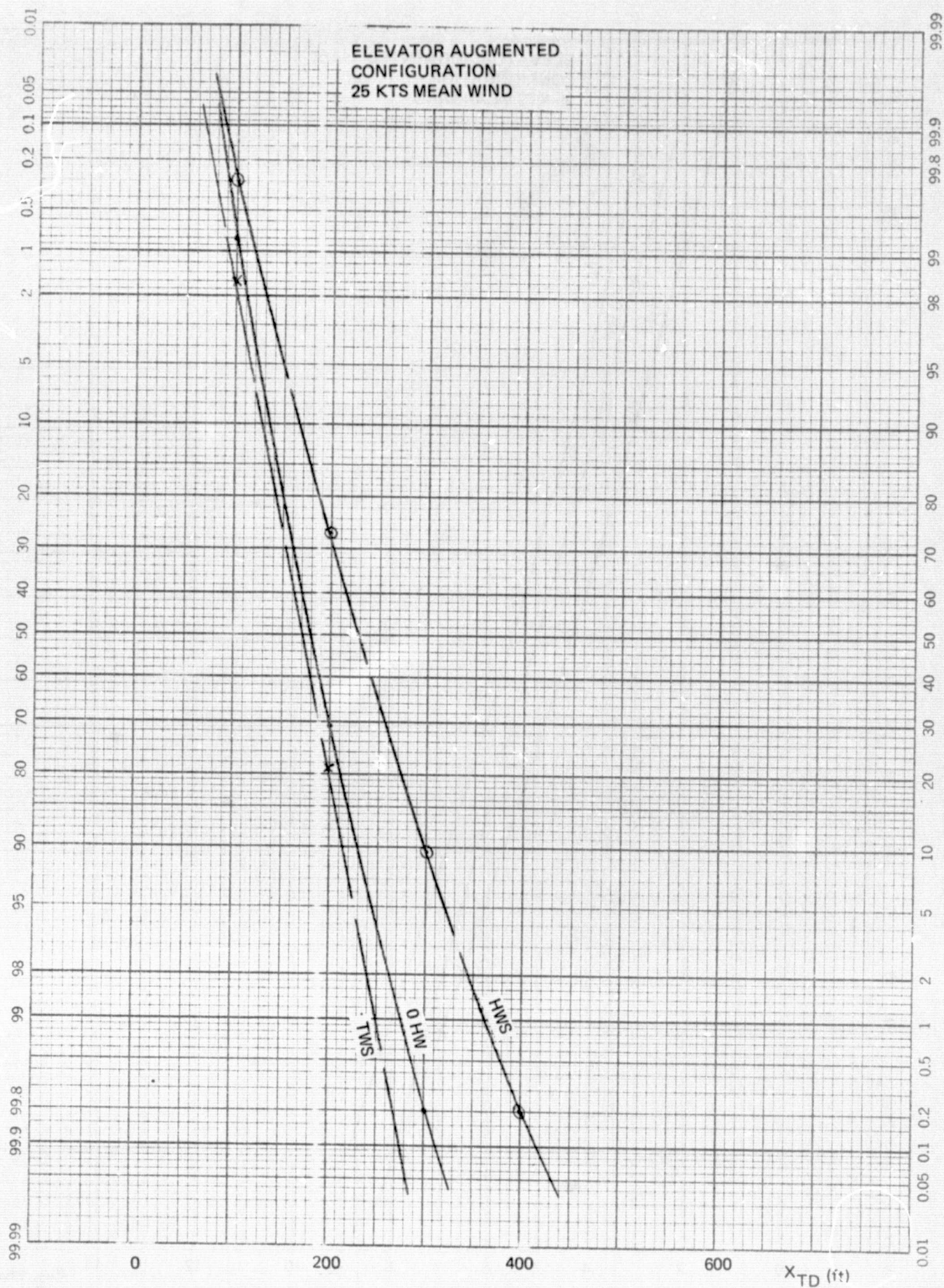


Figure B-44. Wind Variations

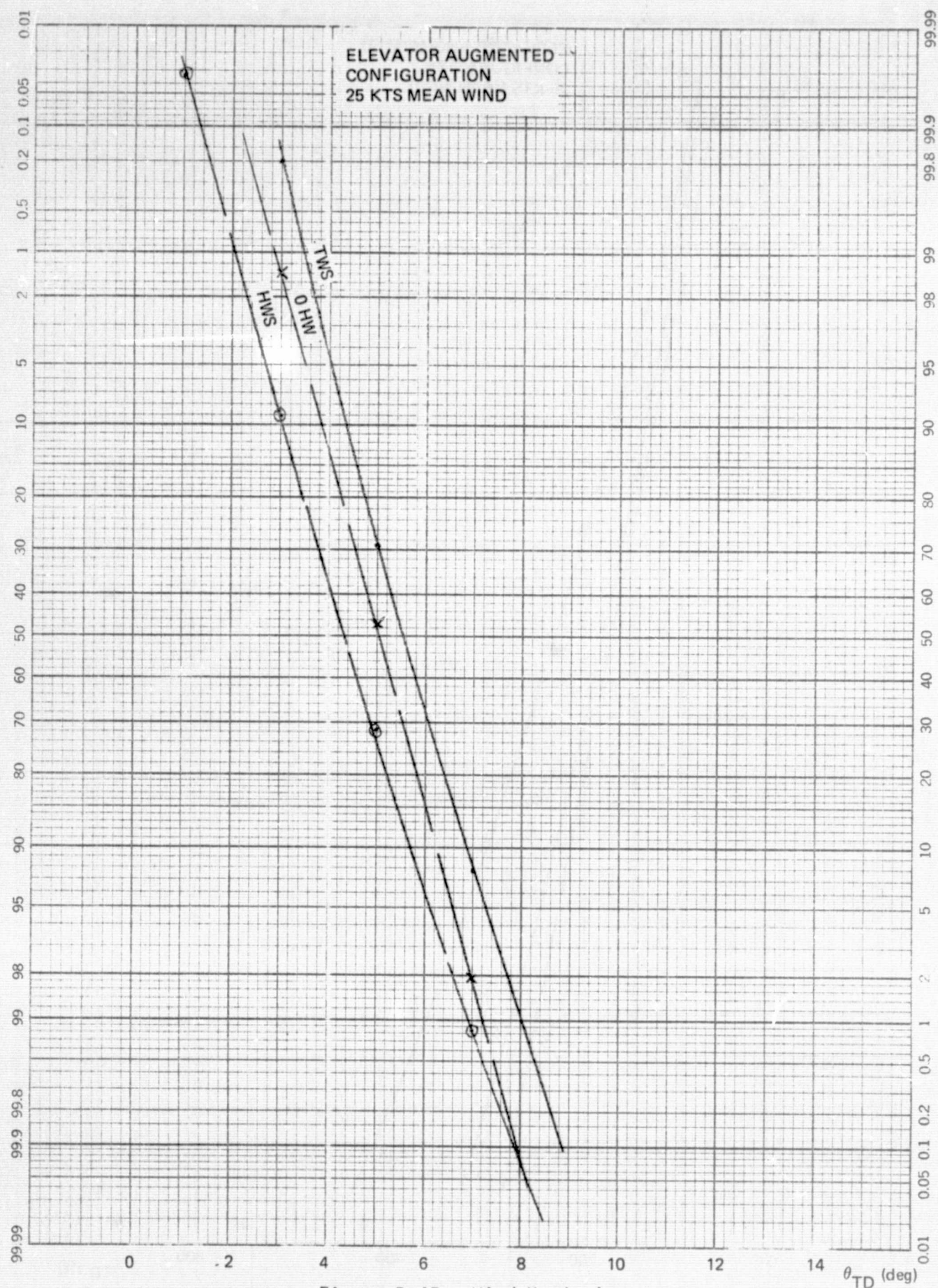


Figure B-45. Wind Variations

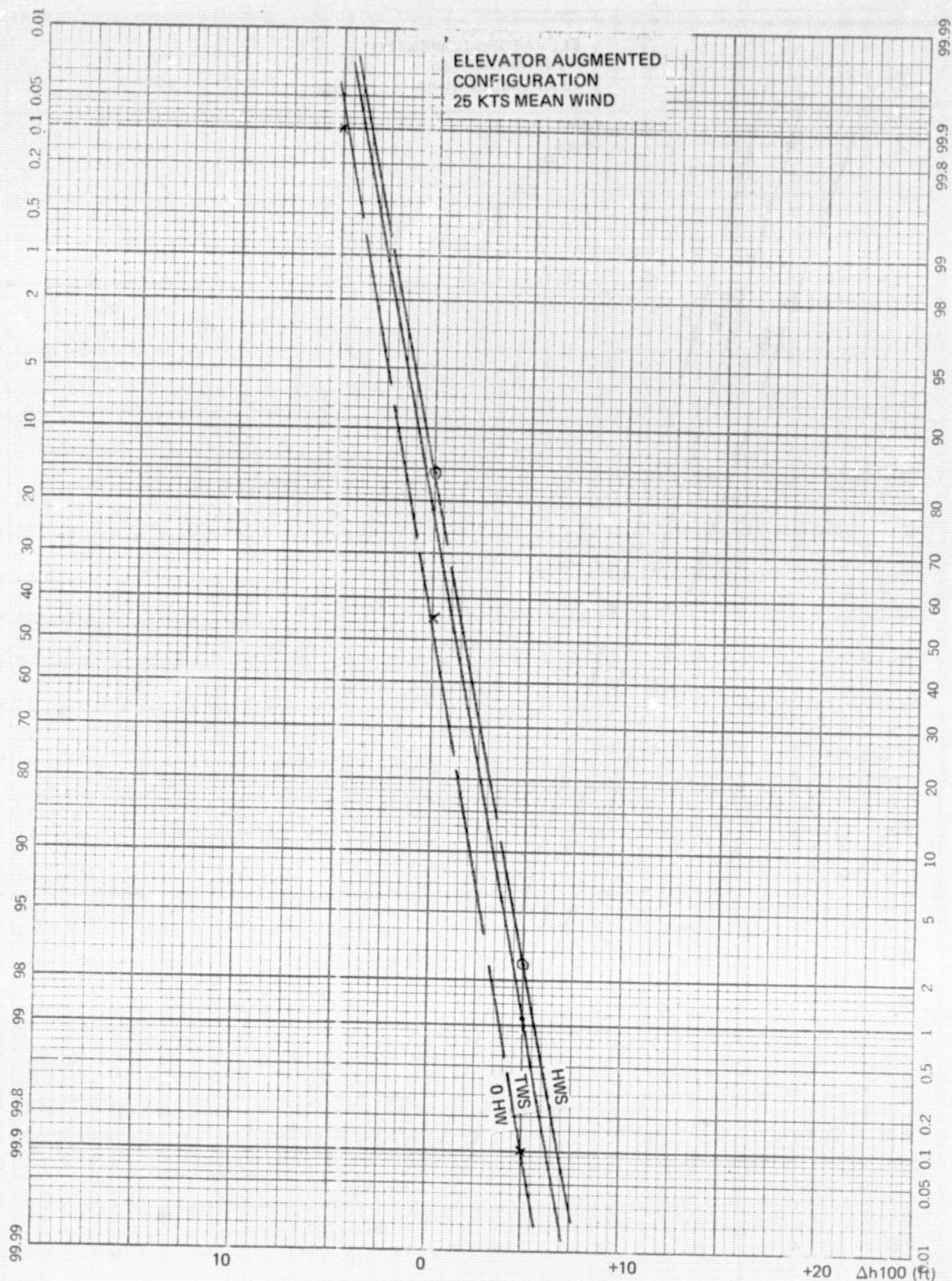


Figure B-46. Wind Variations

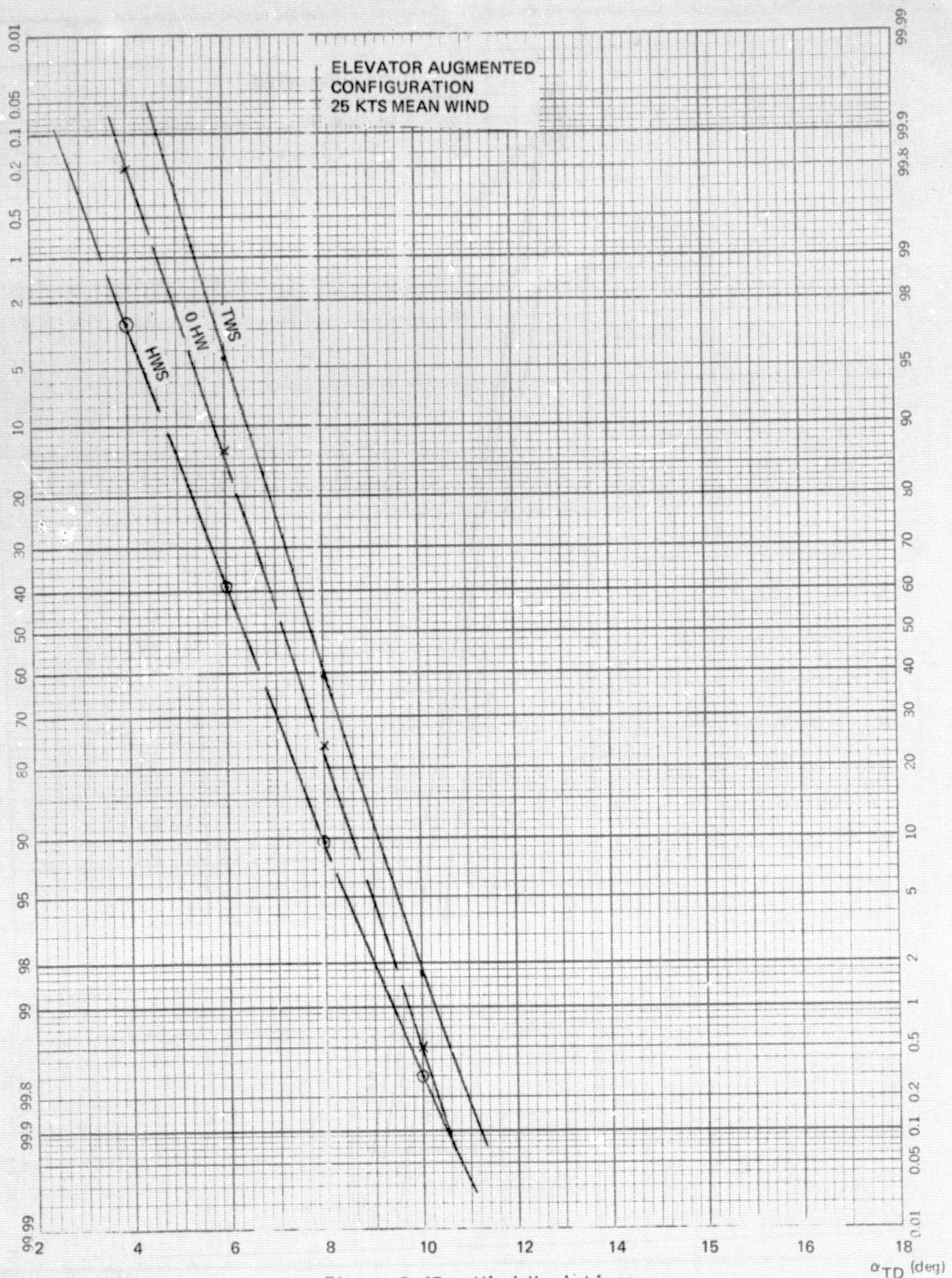


Figure B-47. Wind Variations

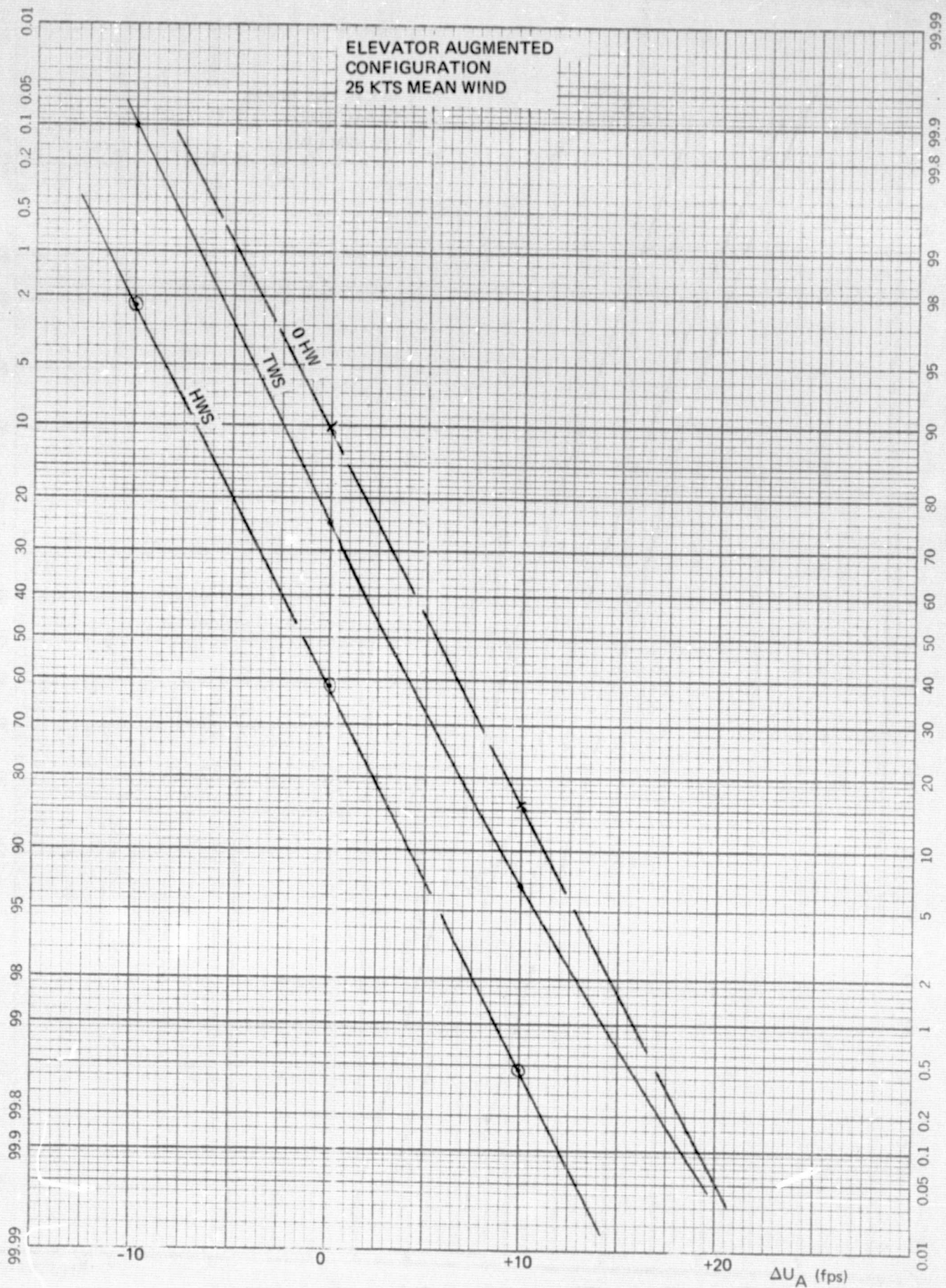


Figure B-48. Wind Variations

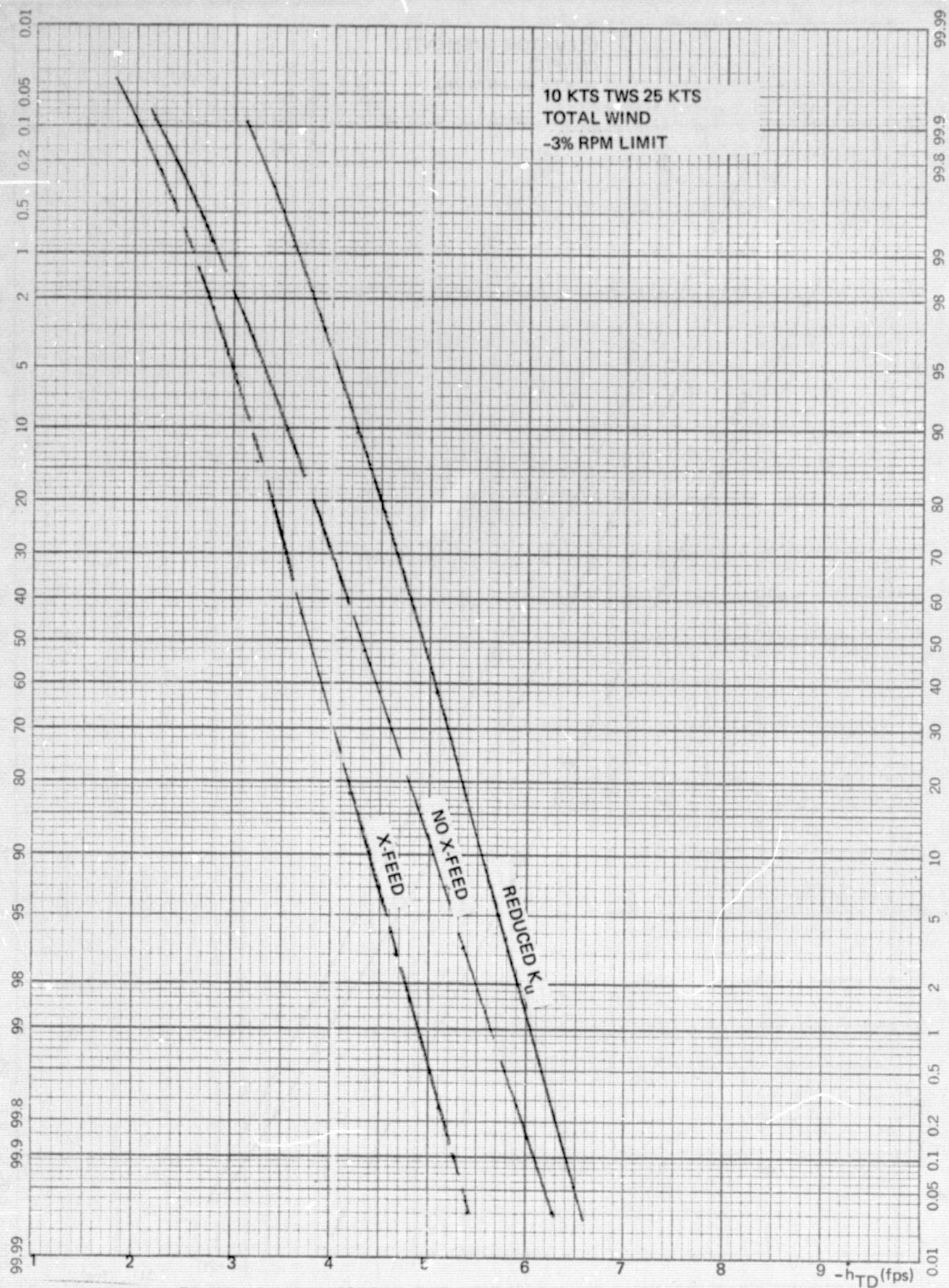


Figure B-49. Elevator Augmentation vs. Reduced K_u

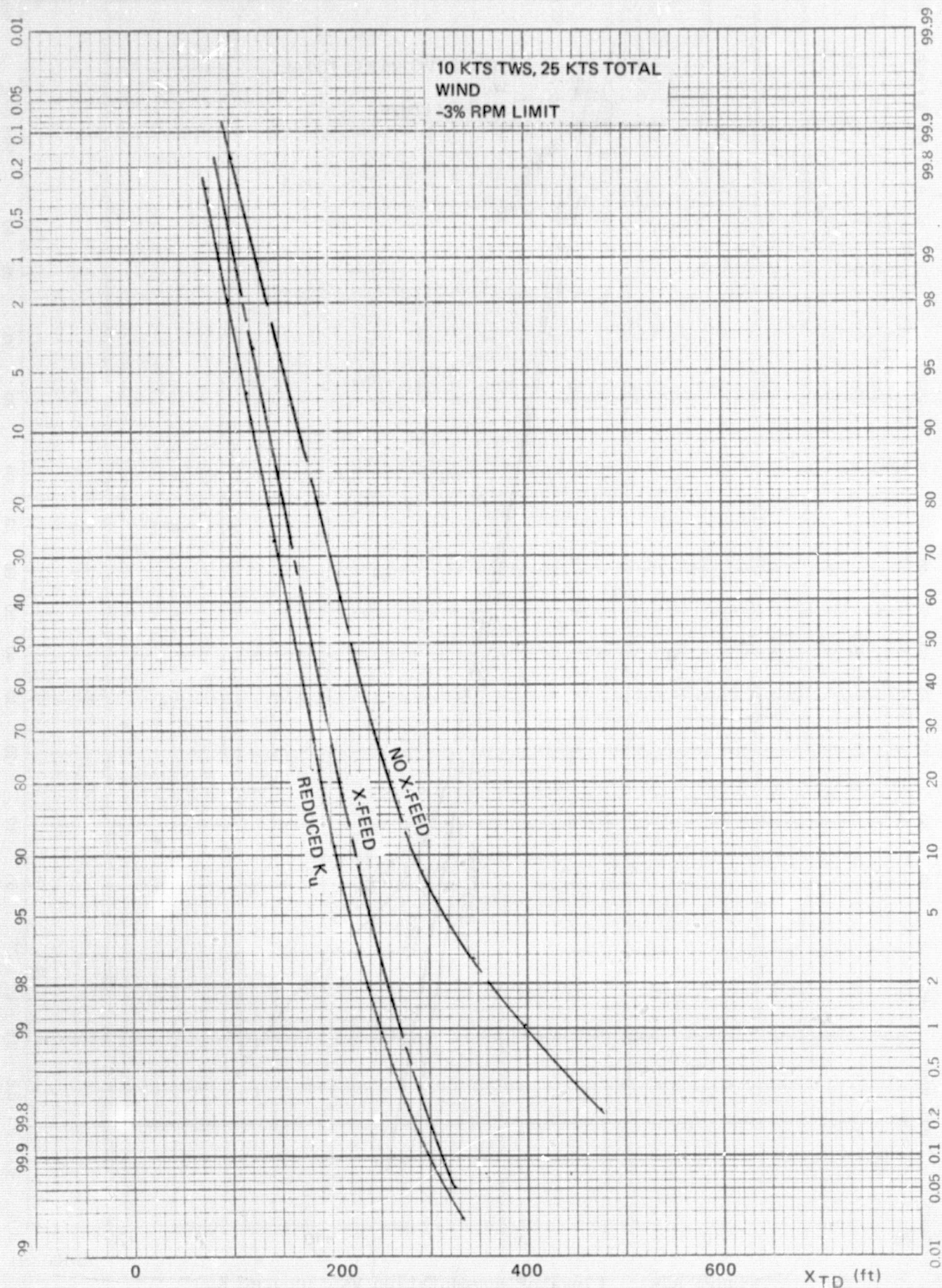


Figure B-50. Elevator Augmentation vs. Reduced K_u

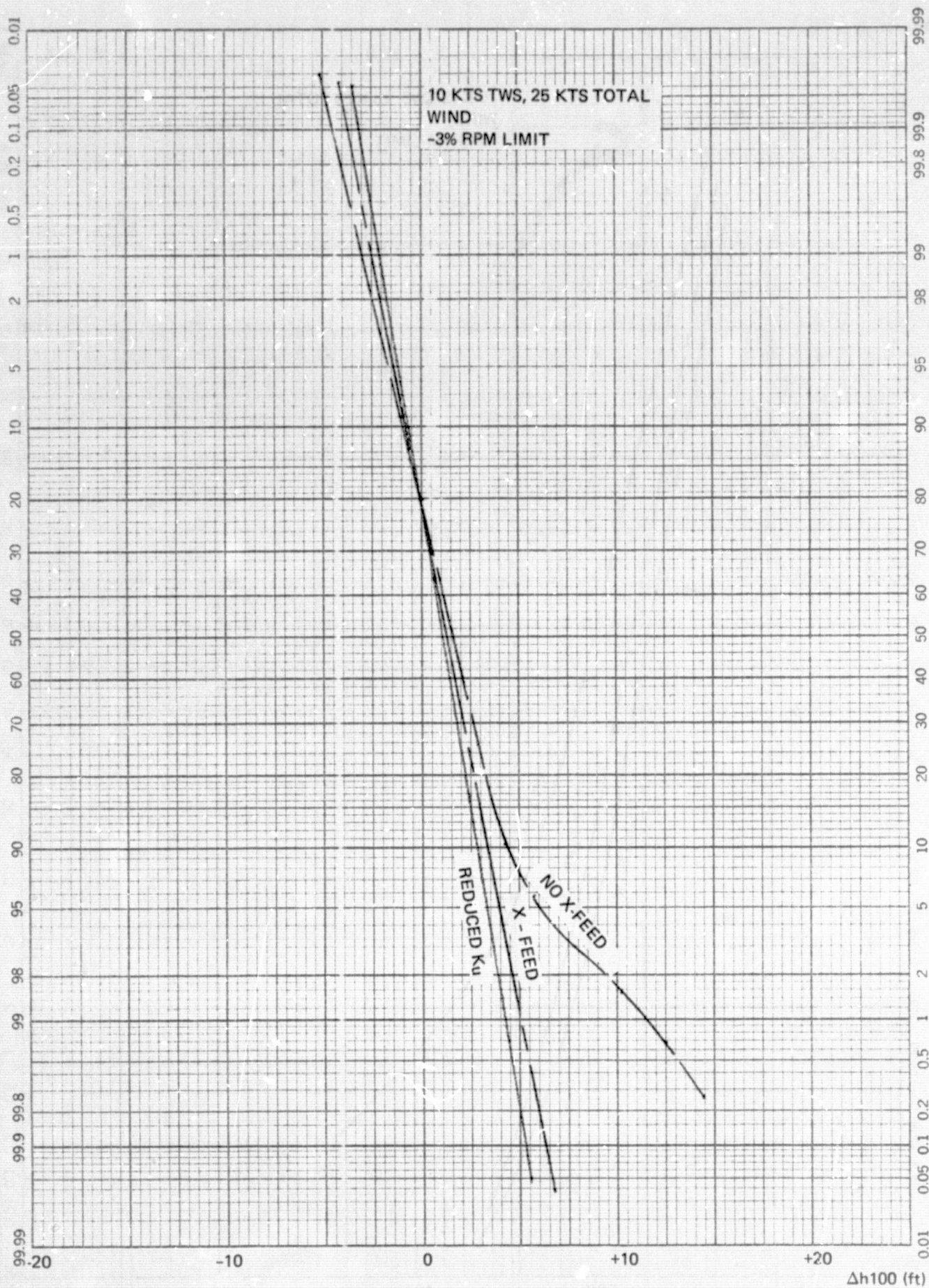
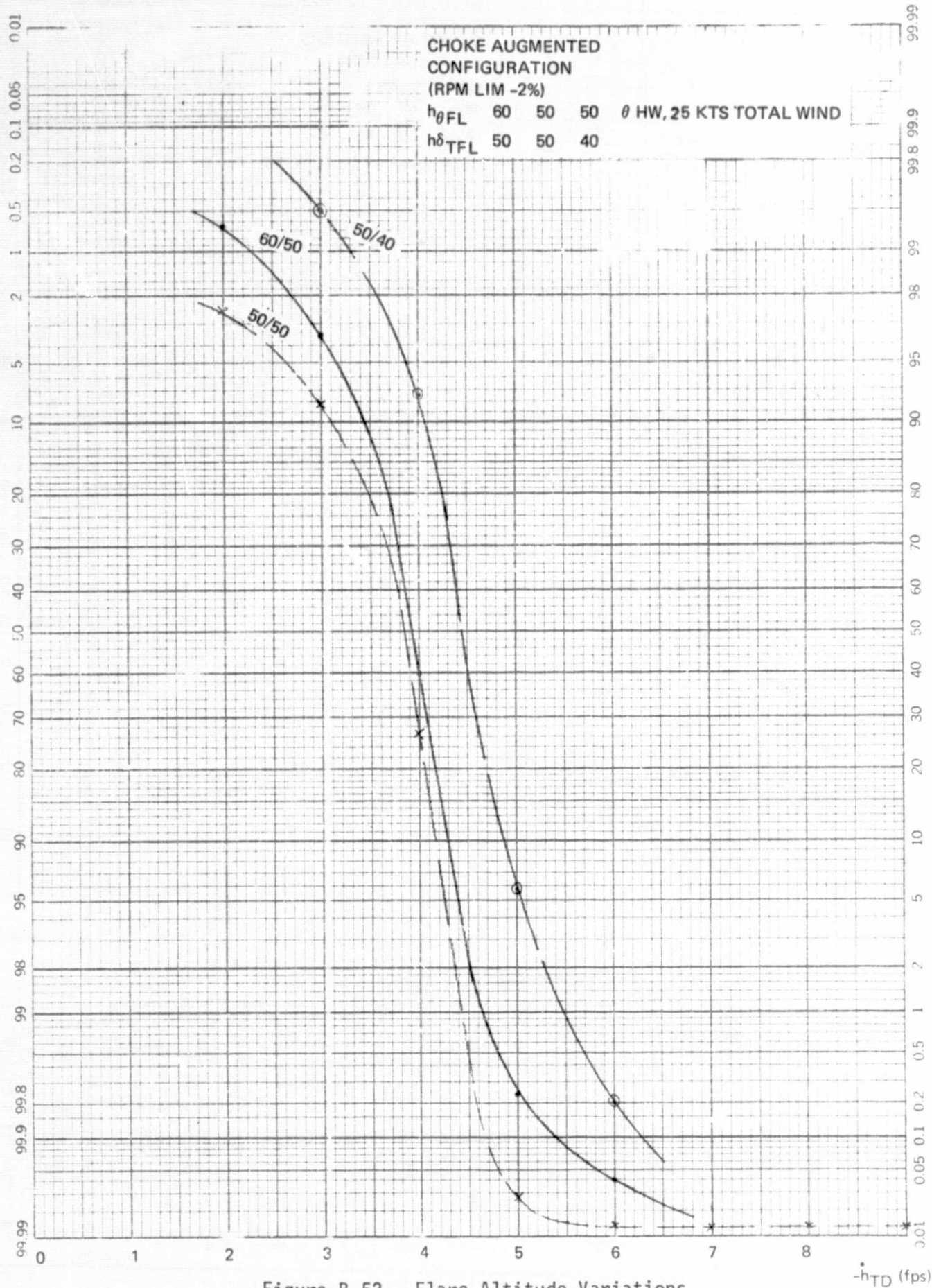


Figure B-51. Elevator Augmentation vs. Reduced K_u



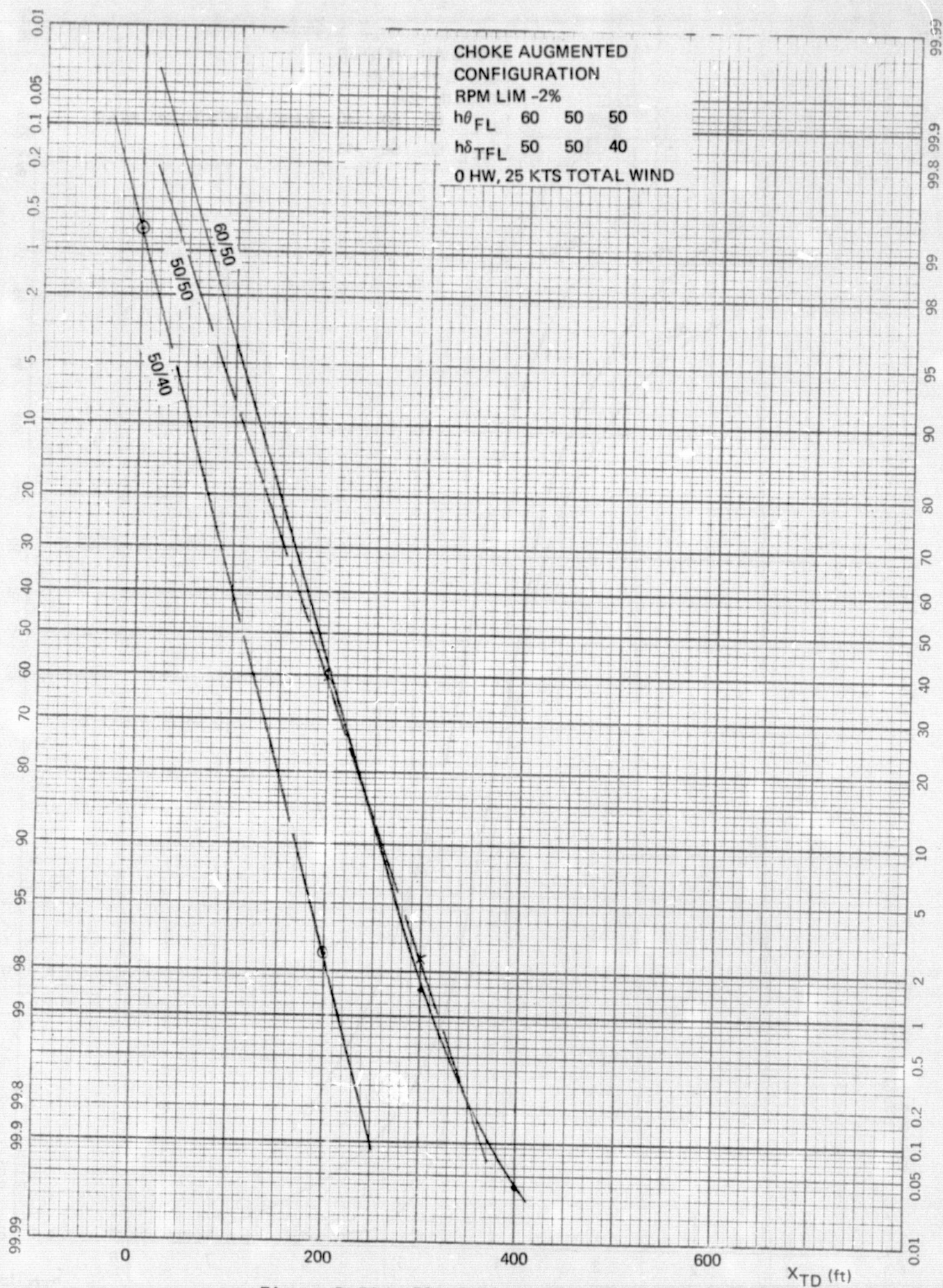


Figure B-53. Flare Altitude Variations

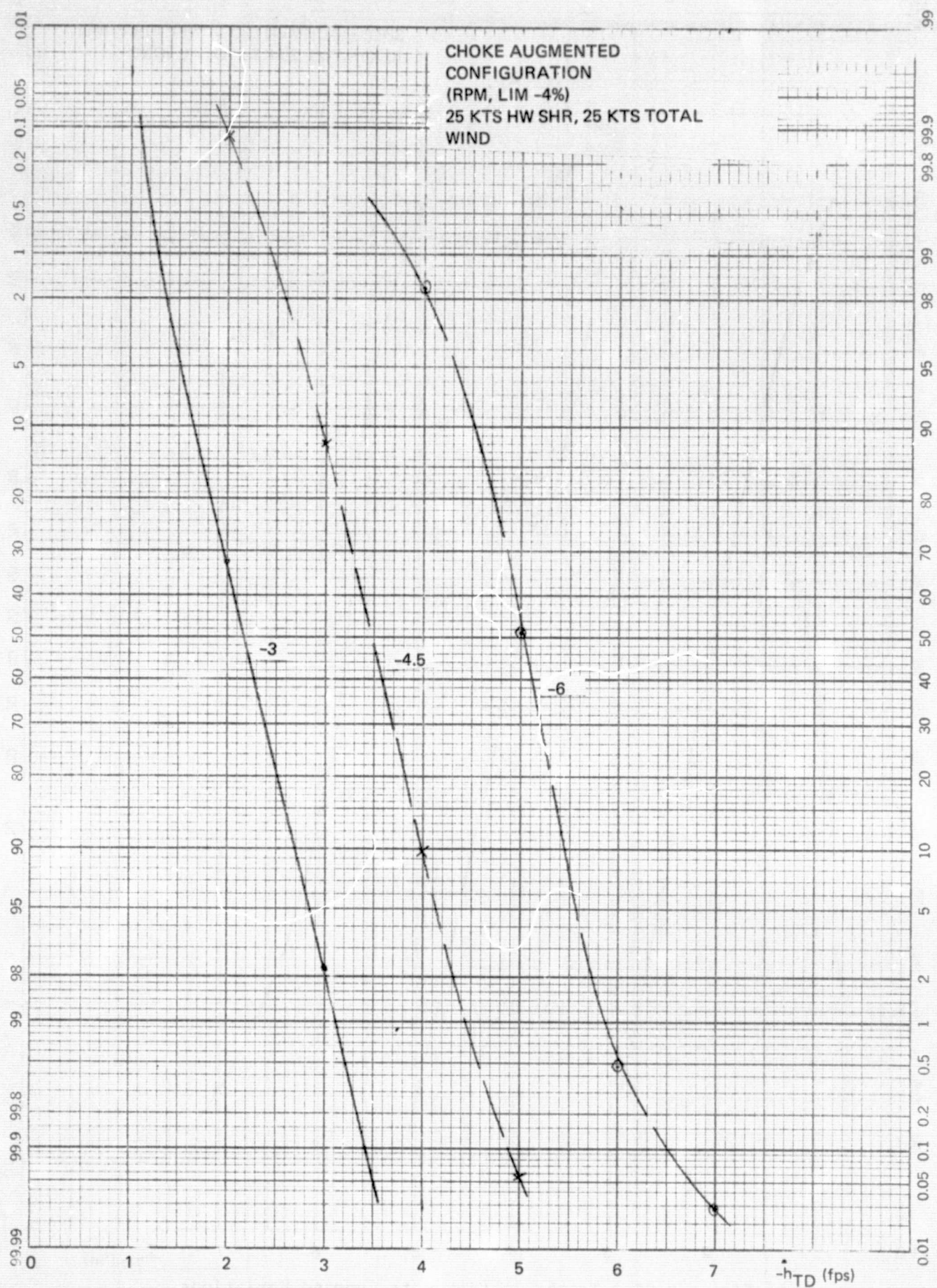


Figure B-54. Touchdown Sink-Rate Command Variations

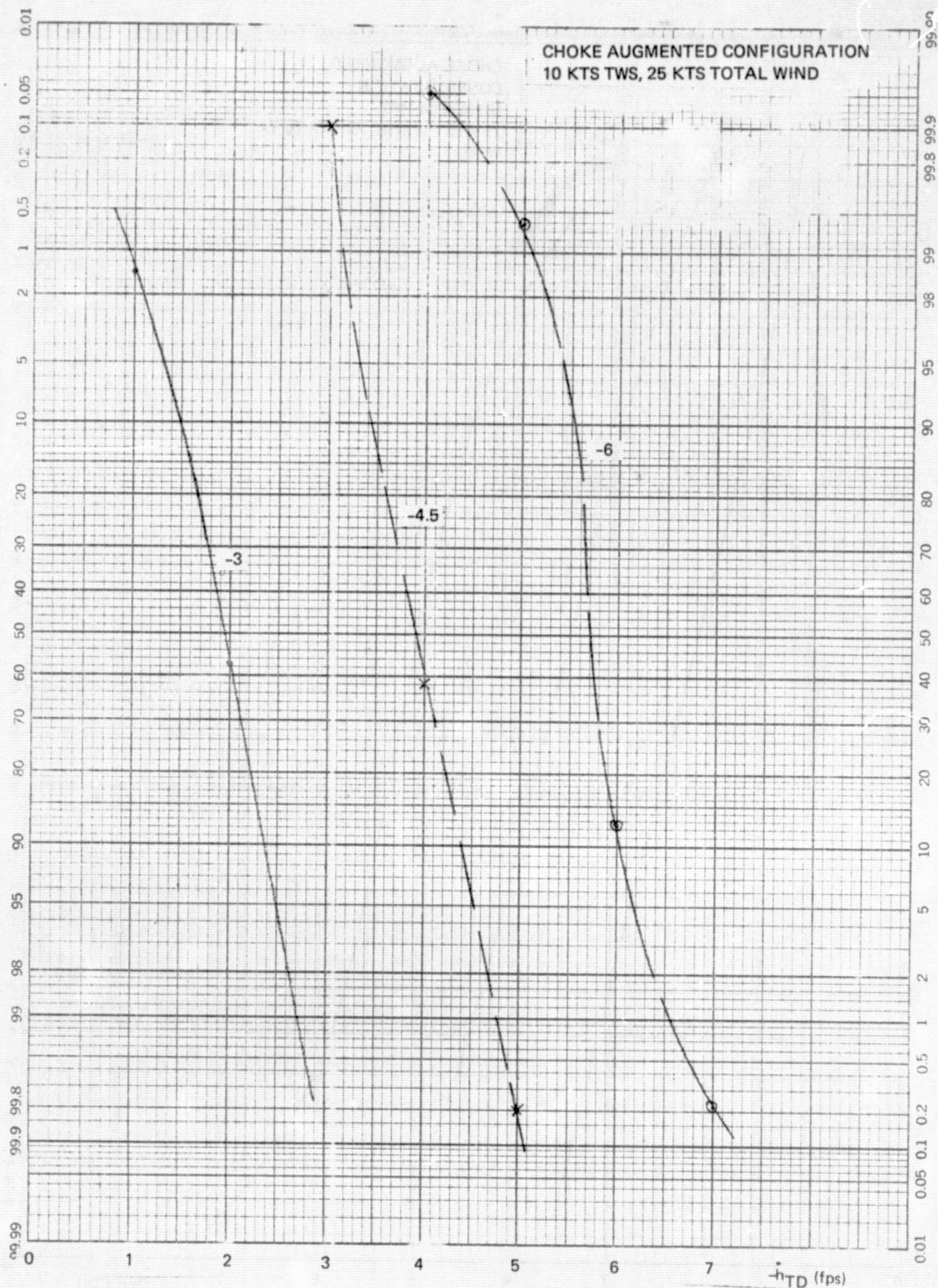


Figure B-55. Touchdown Sink-Rate Command Variations;

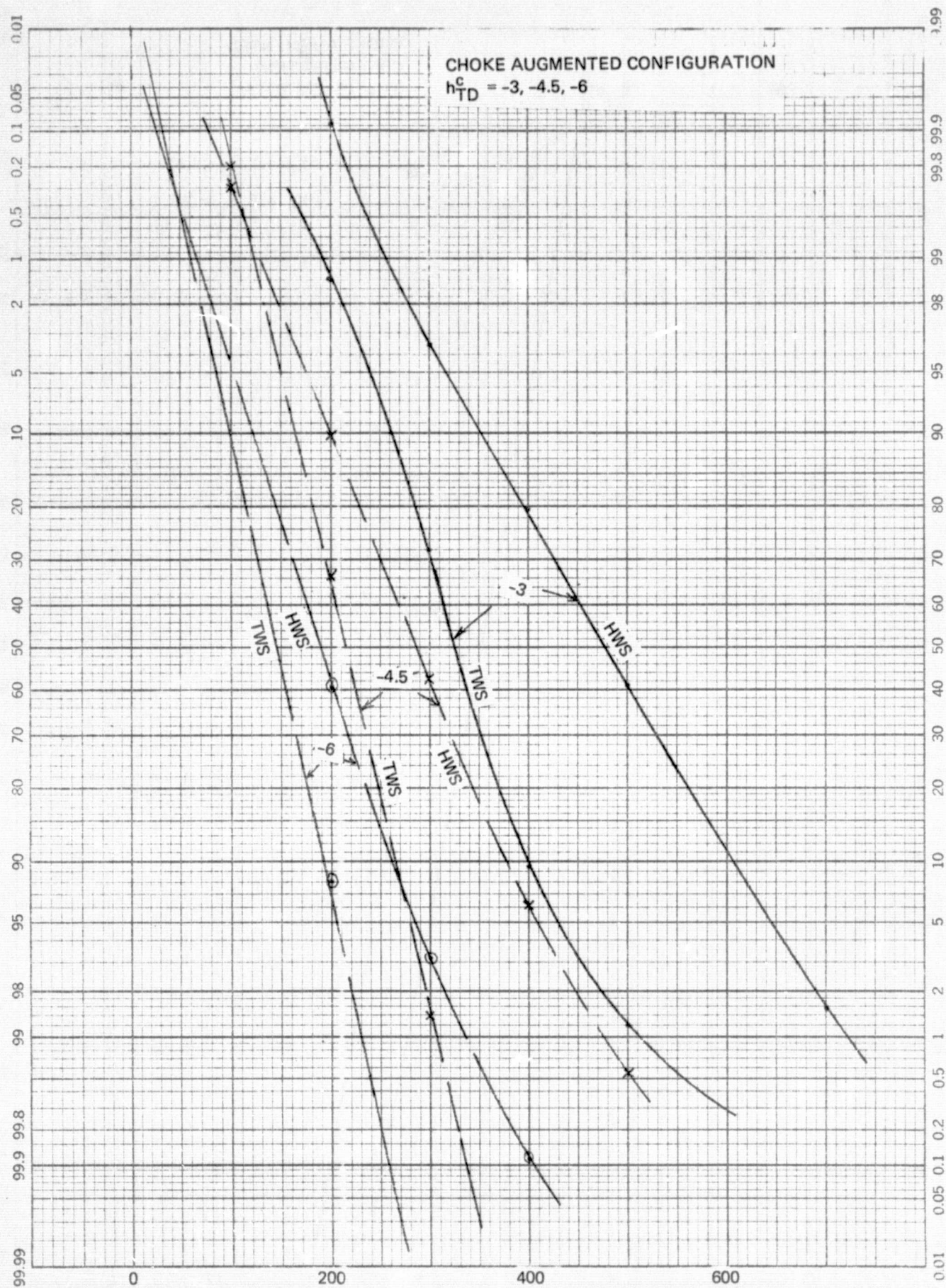


Figure B-56. Touchdown Sink-Rate Command Variations

X_{TD} (ft)

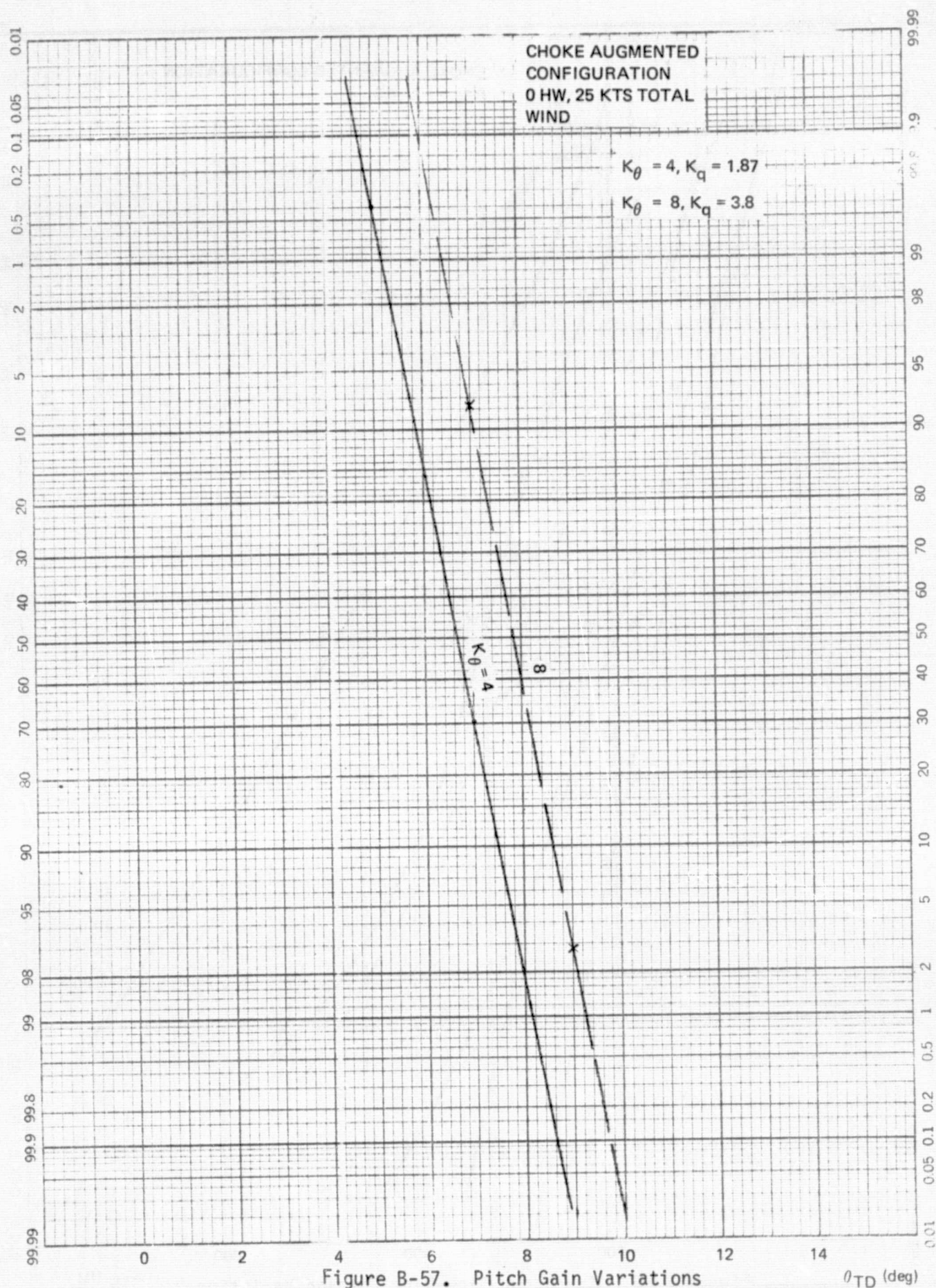


Figure B-57. Pitch Gain Variations

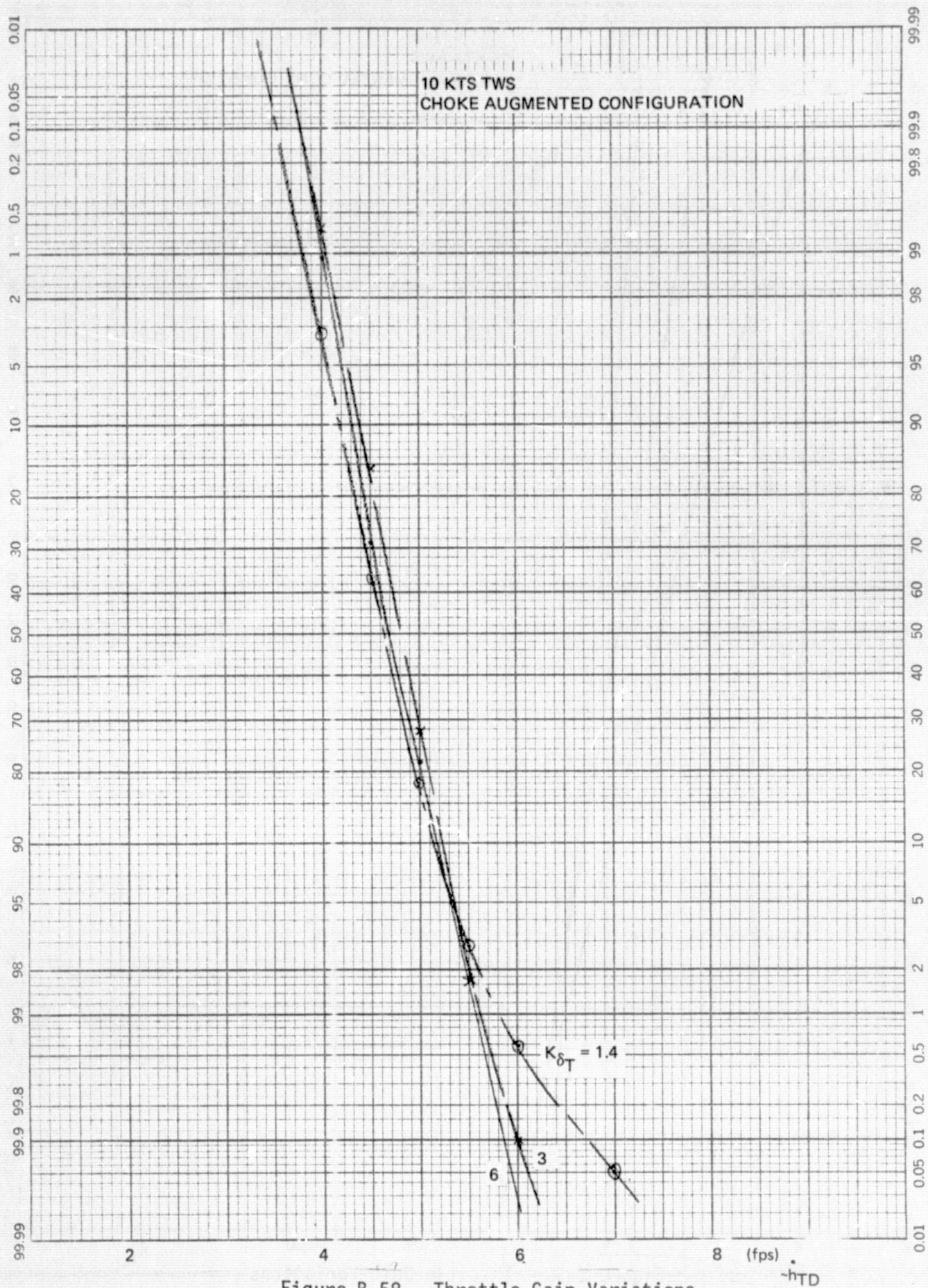


Figure B-58. Throttle Gain Variations

B-65

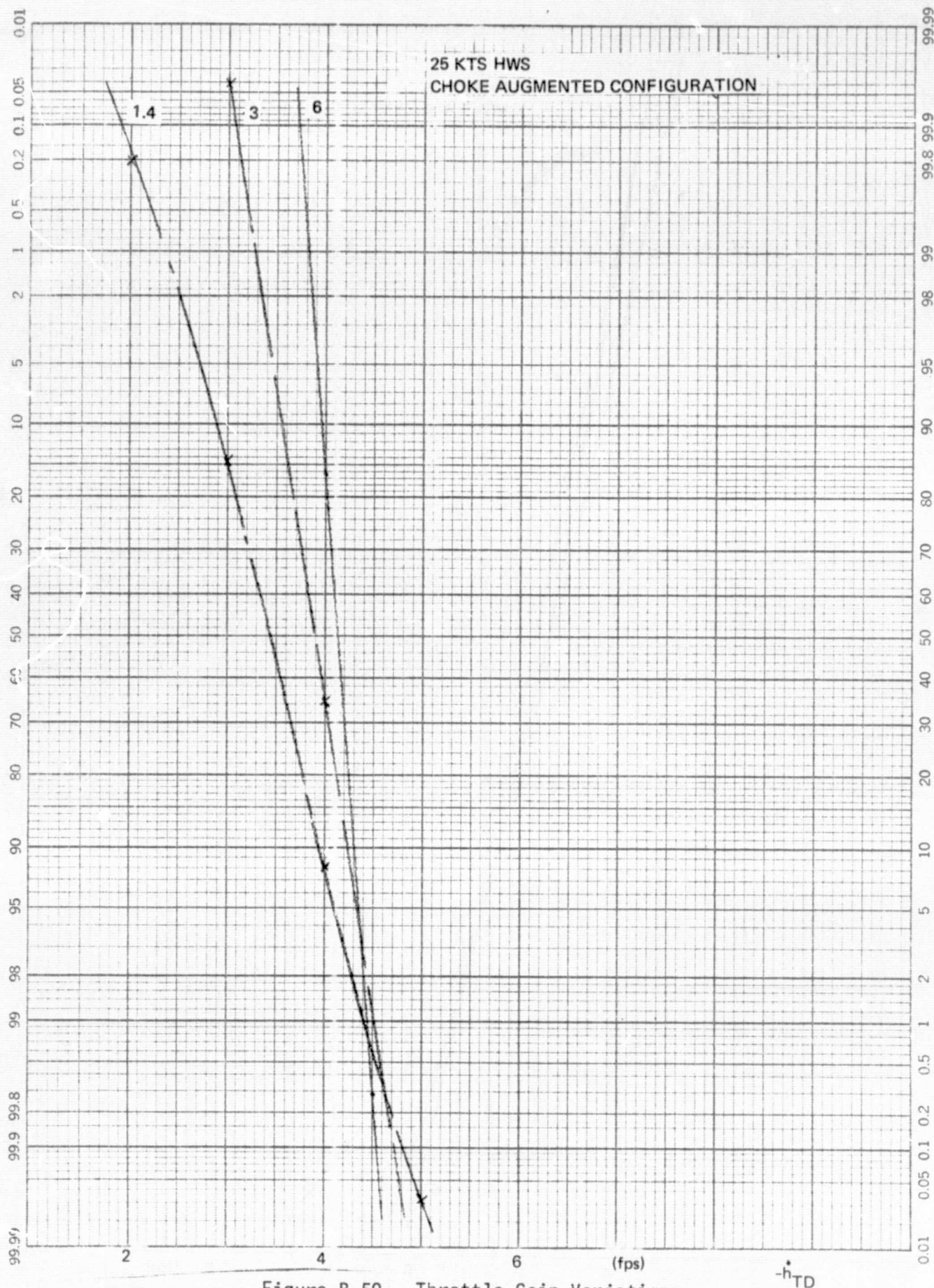


Figure B-59. Throttle Gain Variations

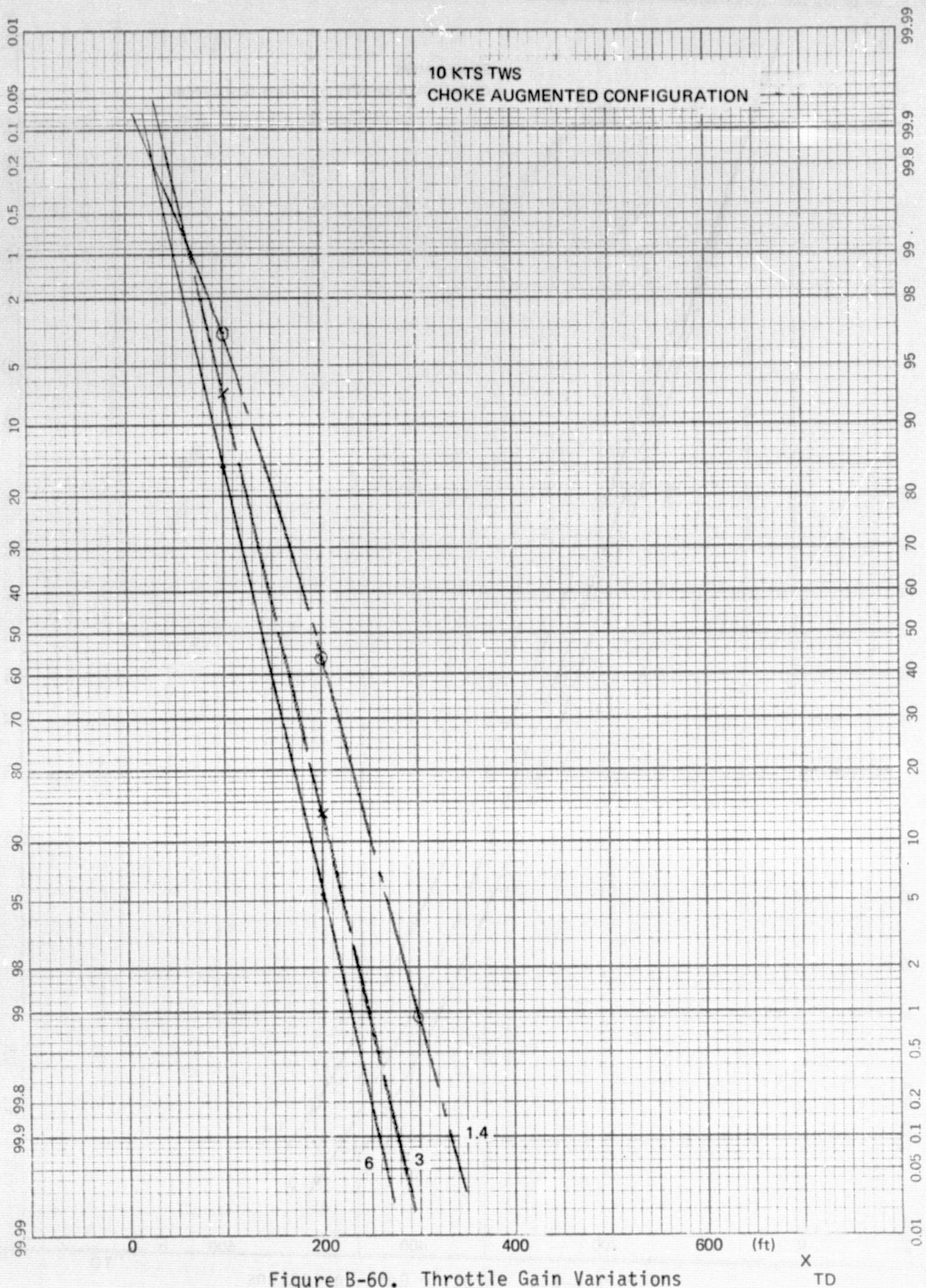


Figure B-60. Throttle Gain Variations

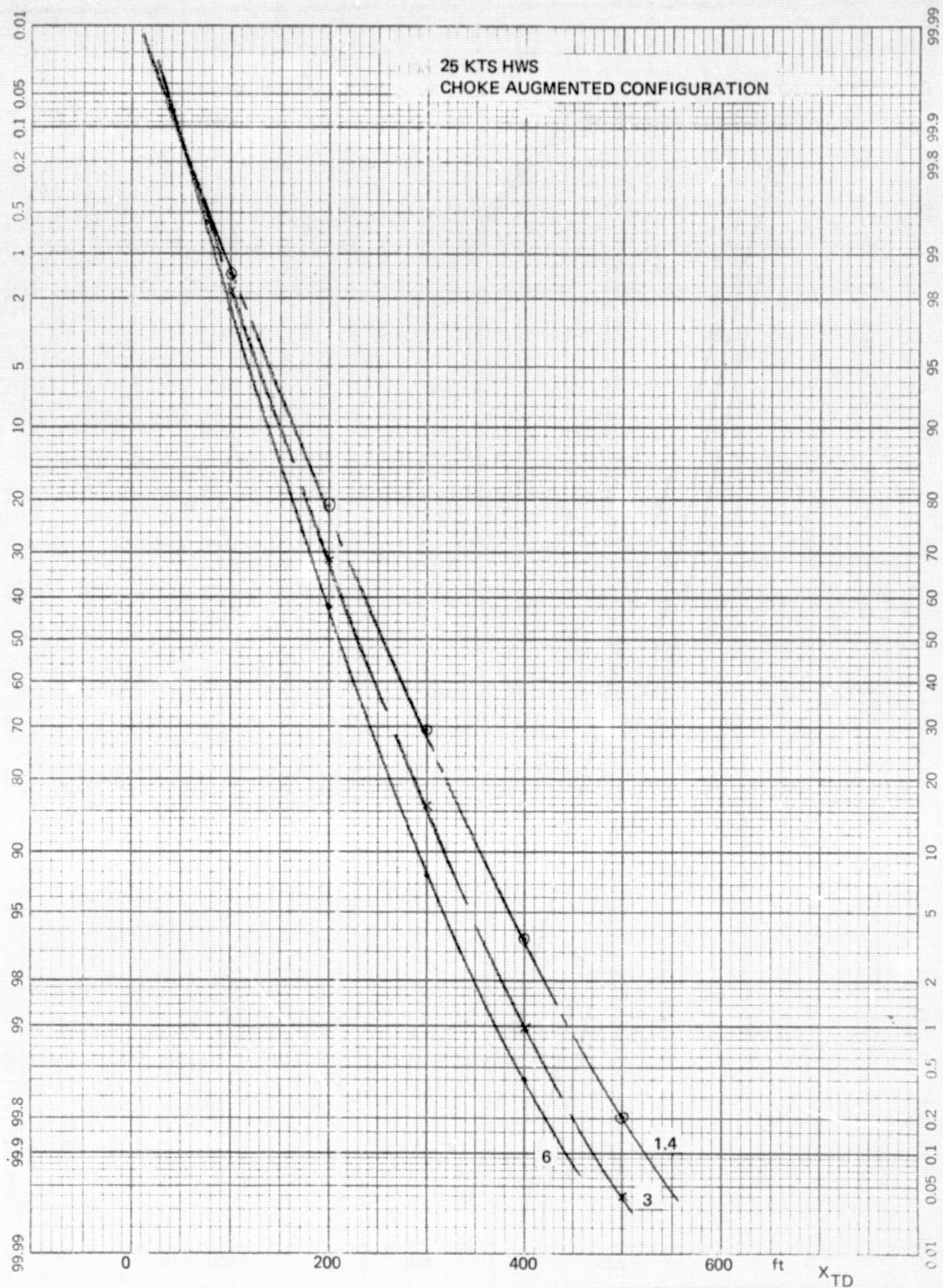


Figure B-61. Throttle Gain Variations
B-68

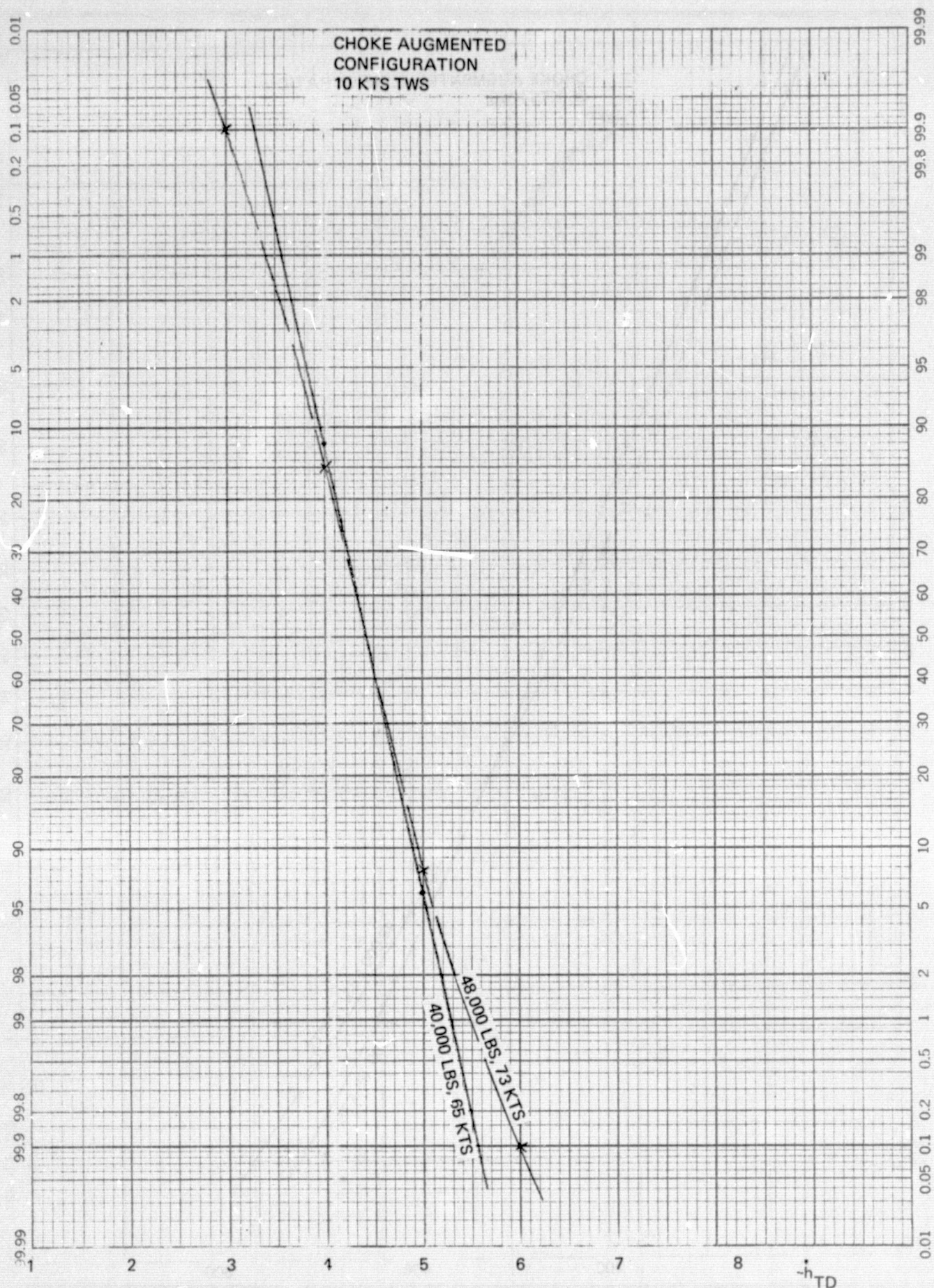


Figure B-62. Aircraft Weight Variations
B-69

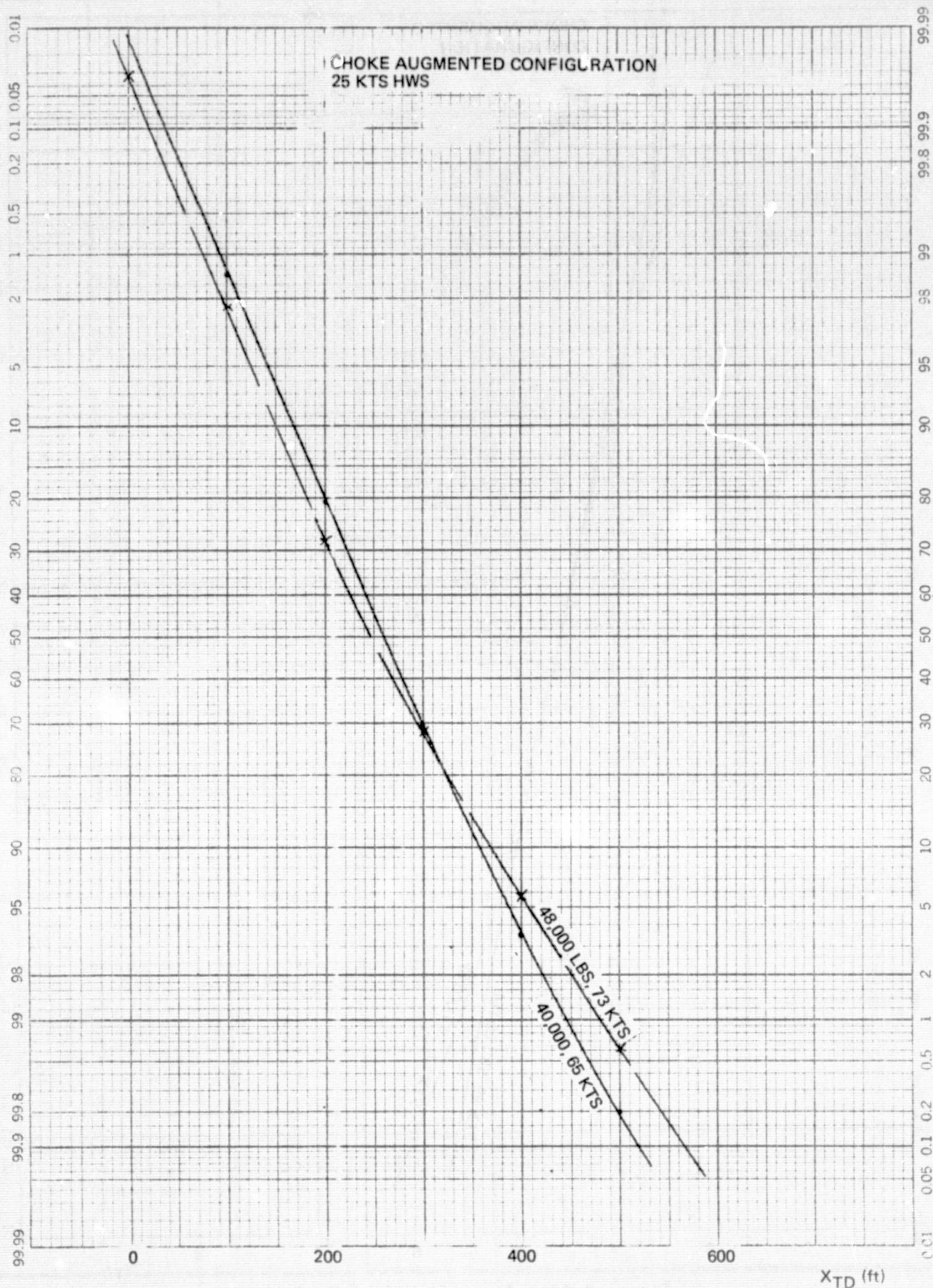


Figure B-63. Aircraft Weight Variation
B-70

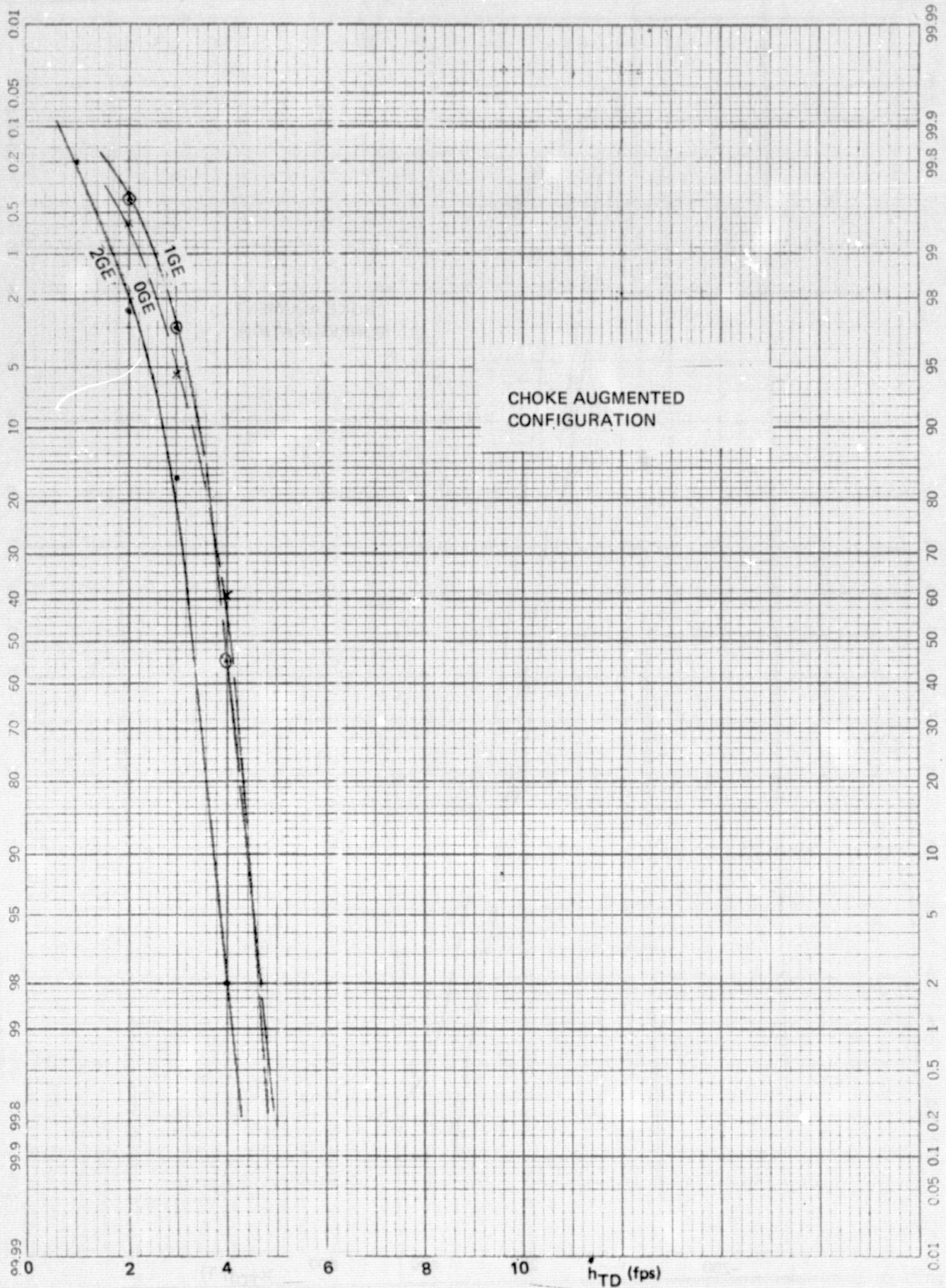


Figure B-64. Ground Effect Variations

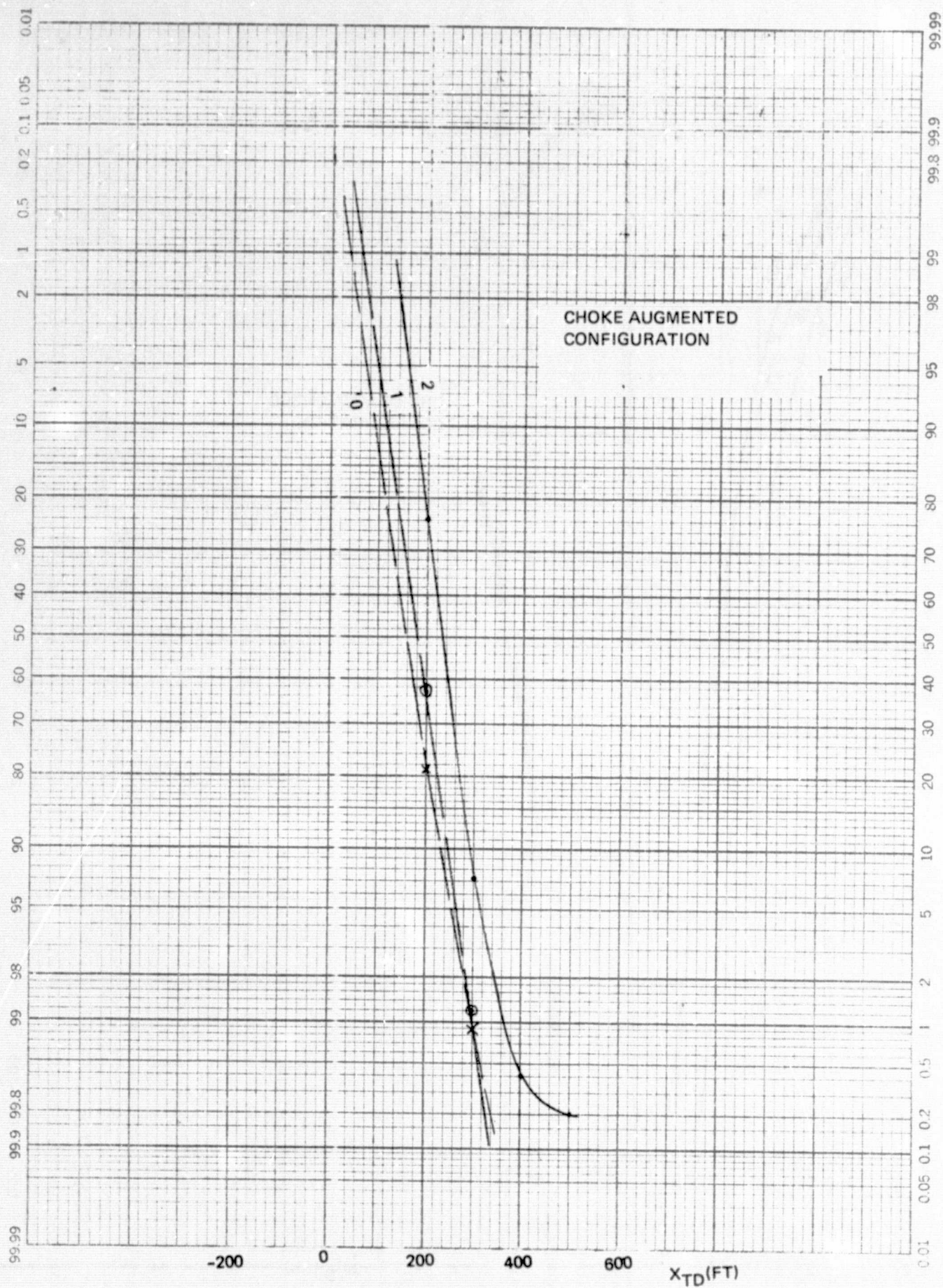


Figure B-65. Ground Effect Variations

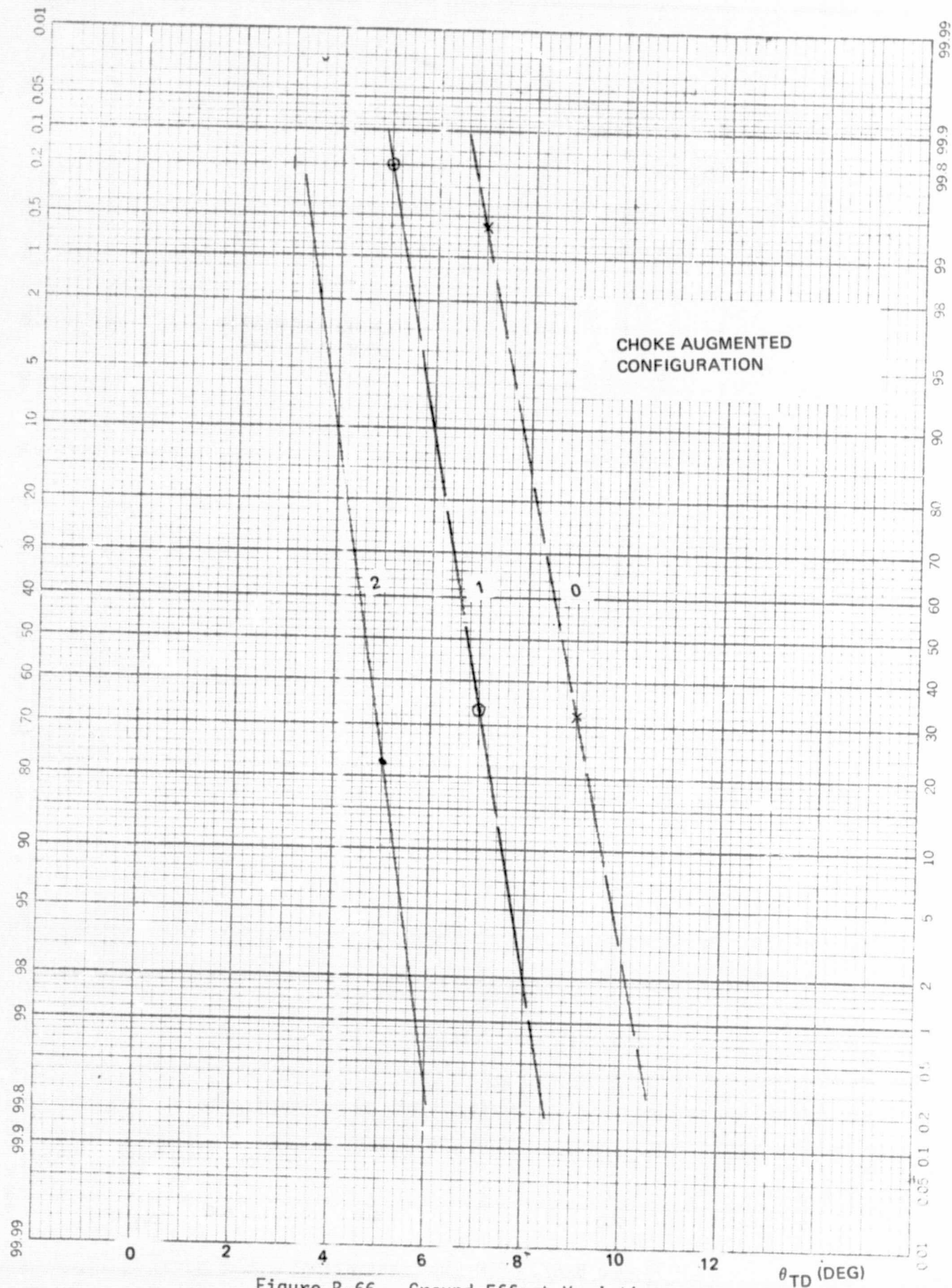


Figure B-66. Ground Effect Variations

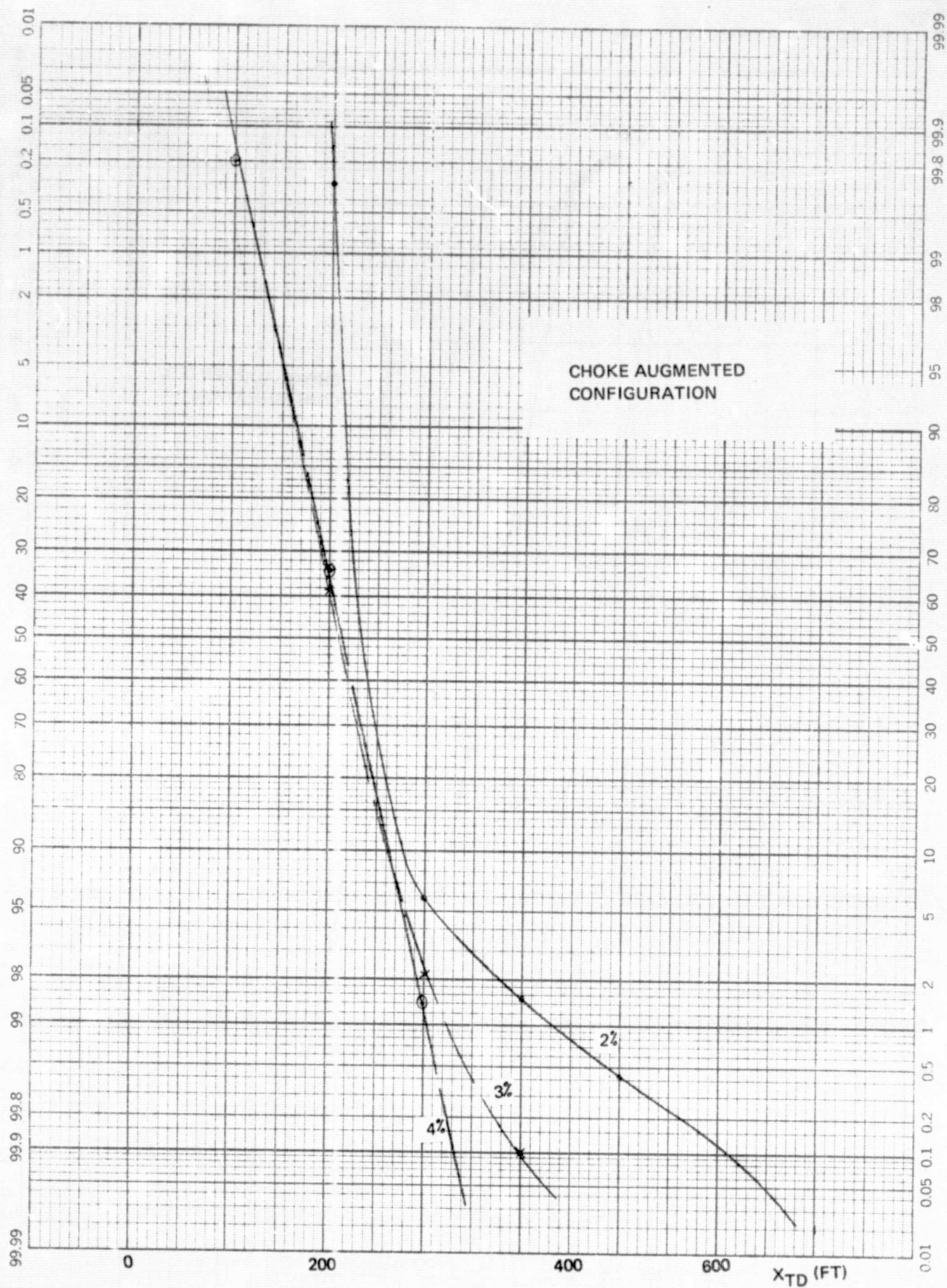


Figure B-67. RPM Limit Variations

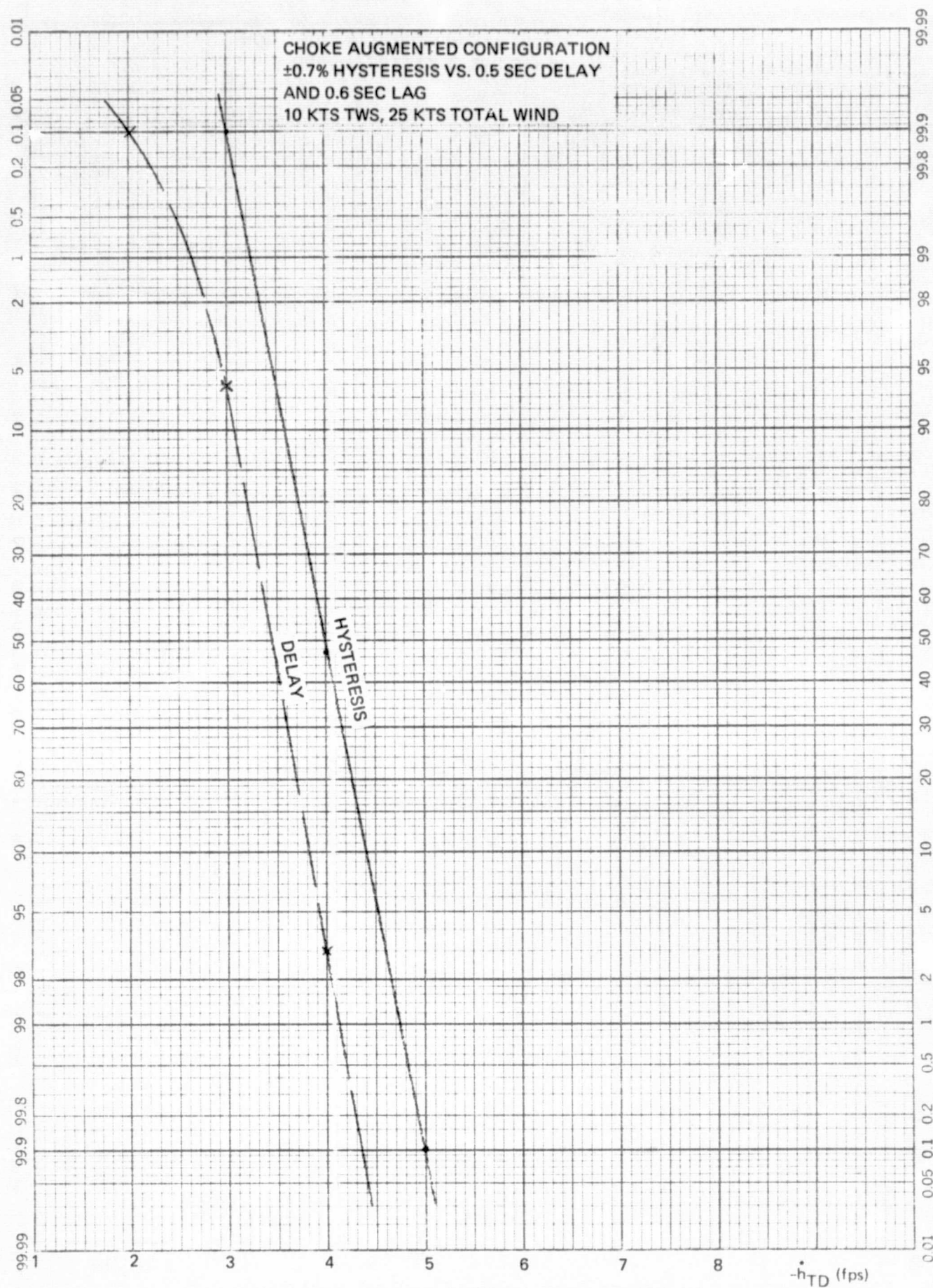


Figure B-68. Throttle Model Variations

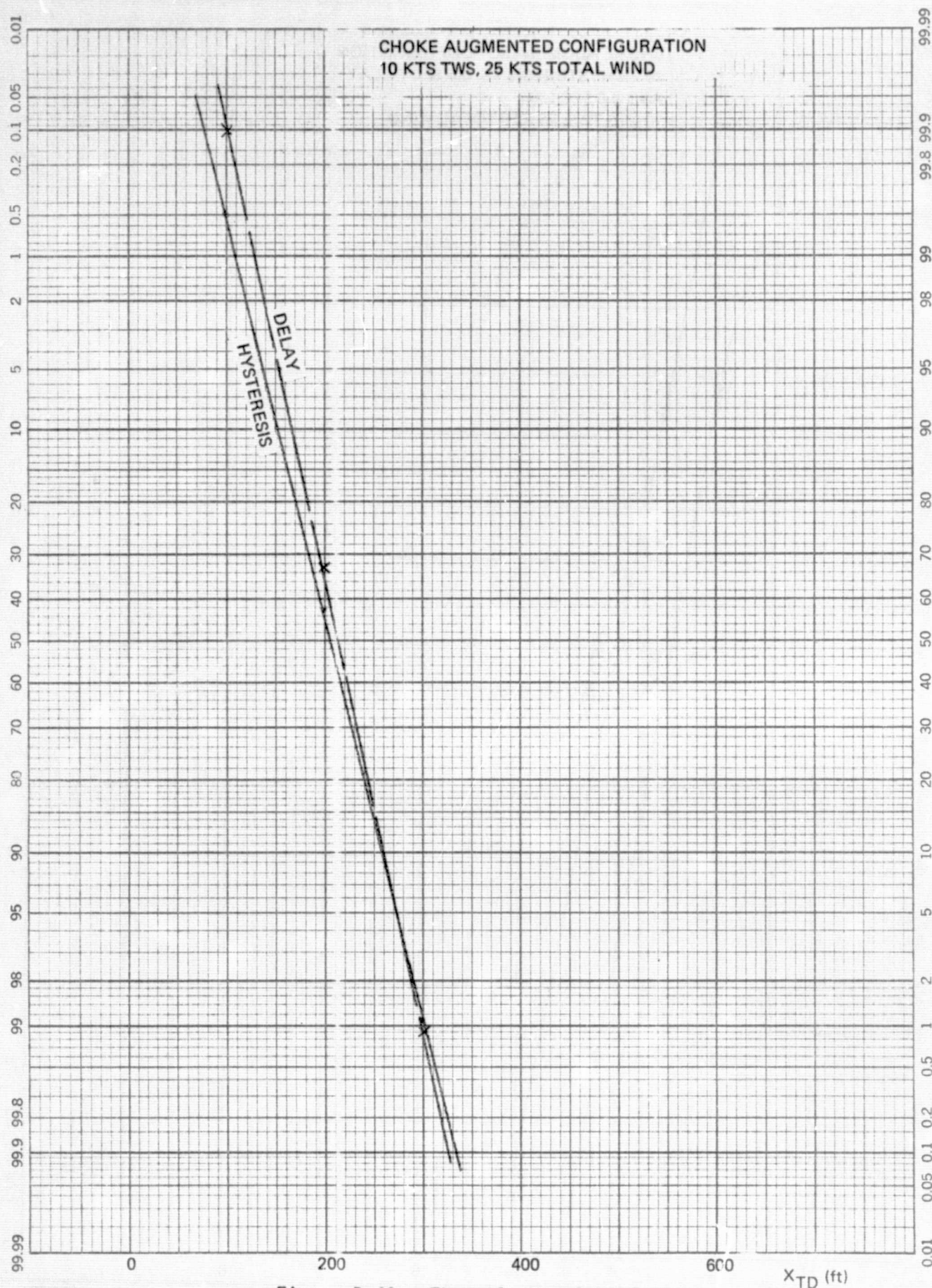


Figure B-69. Throttle Model Variations

APPENDIX C

LOCALIZER TRACK AND ALIGN RESULTS

<u>Figure</u>	<u>Title</u>	<u>Page</u>
C-1	STOLAND Yaw Axis	C-21
C-2	STOLAND Lateral Axis	C-22
C-3	Lateral Position and Derivatives	C-23
C-4	Yaw Axis Rate Limited Forward Slip	C-24
C-5	Lateral Axis - Forward Slip 1	C-25
C-6	Yaw Axis Alt Prog Forward Slip	C-26
C-7	Lateral Axis Forward Slip 2	C-27
C-8	Yaw Axis Closed Loop Forward Slip	C-29
C-9	Roll Axis Closed Loop Forward Slip	C-30
C-10	Probability Distribution Data Collection Implementation	C-31
C-11	Y_{TD} Distribution Comparison - R vs. P	C-32
C-12	\dot{Y}_{TD} Distribution Comparison - R vs. P	C-33
C-13	ψ_{TD} Distribution Comparison - R vs. P	C-34
C-14	ϕ_{TD} Distribution Comparison - R vs. P	C-35
C-15	Y_{100} Distribution Comparison - R vs. P	C-36
C-16	Touchdown Lateral Distance Distribution - Stochastic Disturbances	C-37
C-17	Touchdown Heading Error Distribution - Stochastic Disturbances	C-38
C-18	Y_{TD} Distribution Comparison - C vs. D	C-39
C-19	ψ_{TD} Distribution Comparison - C vs. D	C-40
C-20	ϕ_{TD} Distribution Comparison - C vs. D	C-41
C-21	Y_{TD} and Y_{100} Distributions - Configuration E	C-42
C-22	ψ_{TD} Distribution - Configuration E	C-43

<u>Figure</u>	<u>Title</u>	<u>Page</u>
C-23	ϕ_{TD} Distribution — Configuration E	C-44
C-24	\dot{Y}_{TD} Distribution — Configuration E	C-45
C-25	Effect of Acceleration Washout Time Constant	C-46
C-26	Y_{TD} Distribution Comparison — E, F, N	C-47
C-27	\dot{Y}_{TD} Distribution Comparison — E, F, N	C-48
C-28	ϕ_{TD} Distribution Comparison — E, F, N	C-49
C-29	Y_{100} Distribution Comparison — E, F, N	C-50
C-30	Response to Step $\phi_e = 1.0^\circ$ in Loc Track Mode	C-53
C-31	Nav Filter Response to Step Acceleration Input	C-55
C-32	Response to \ddot{Y}_R Bias in Lateral Axis "Wing Down" Compensation Signal — No Wind	C-56
C-33	Response to \ddot{Y}_R Bias in Lateral Axis "Wing Down" Compensation Signal — With 15 Knot Crosswind	C-57

<u>Table</u>	<u>Title</u>	<u>Page</u>
C-I	Configuration List	C-6
C-II	Log of Statistical Data Runs — Lateral Axis	C-7
C-III	Statistical Performance Data Summary	C-9
C-IV	Noise Response Data	C-11
C-V	Comparative Performance with Rate Damping Term Variations	C-11
	Gain Table C-1	C-12
	Gain Table C-2	C-13
	Gain Table C-3	C-14
	Gain Table C-4	C-15

<u>Table</u>	<u>Title</u>	<u>Page</u>
	Gain Table C-5	C-16
	Gain Table C-6	C-17
	Gain Table C-7	C-18
	Gain Table C-8	C-19
	Gain Table C-9	C-20

APPENDIX C

LOCALIZER TRACK AND ALIGN RESULTS

This appendix presents the detailed results which form the basis of the discussion and conclusions drawn in the body of this report.

CONFIGURATION DESCRIPTION

A number of different possible control law mechanizations for localizer track and runway align have been studied. Statistical data have been accumulated for 17 different configurations. Some of the differences are minor (e.g., gain changes) and some are extensive. In order to clearly define the system configuration under discussion, Table C-I provides identifying configurations by letter designation and references for each the applicable yaw and roll axes diagrams. The gain Tables 1 through 9 are keyed to each diagram C-1 through C-9 and define what parameter values apply to a particular configuration. The Tables C-II and C-III define the 45 statistical sets of runs and a summary of the performance obtained.

RUNWAY ALIGNMENT

Early results established the superiority of the forward slip technique over the flat decrab. Consequently, most of the attention has been given to various performance — related tradeoffs concerning the forward slip maneuver. Of the configurations evaluated, all provide rather similar response under ideal conditions of perfect sensor inputs and steady winds. A set of time history traces for a representative configuration (E) is included in Section 6 of this report.

In order to evaluate the relatively subtle effects of the system differences, it is necessary to examine the response to sensor noise and atmospheric disturbances. Of most value are the distributions for critical performance parameters that are obtained from a statistically significant number of simulated landings. Consequently, most of the evaluation process is related to the statistical landing study results. These results were acquired by connecting the variable of interest to threshold detectors which were gated to drive digital counters at the completion of each landing and at the 100 feet window. By repetitively cycling the simulation through a large number of landings (normally 200), during which random disturbances were applied, the counters accumulated the desired distribution data for a given configuration. Figure C-10 illustrates the arrangement used for this operation.

Initial evaluation of flat decrab versus forward slip compared the performance of configurations A and B. A later set of comparative statistical data has been run (configurations R and P) for a flat decrab system with revised gains and updated aerodynamics versus the recommended forward slip system. Refer to Figures C-11 to C-15 for statistical distribution data. However, the same problem of large scatter in lateral TD deviation due to off nominal time in flare is still present so the earlier conclusion of relative superiority of a forward slip maneuver is reinforced.

For the recommended forward slip configuration (P), only the lateral deviation and heading error at touchdown show a noticeable effect due to longitudinal wind condition variations. The distributions for limiting headwind and tailwind are shown in Figures C-16 and C-17, along with the distribution obtained by combining these curves assuming a 50/50% distribution of headwind and tailwind.

The initial forward slip configuration appears to yield adequate performance; however, improvement was desired in three areas:

1. Overshoot of both zero heading and steady state bank angle occurred on a large percentage of landings.
2. The rate limited align entry resulted in the full crab angle being removed at a relatively high altitude in approaches made with lower than normal sink rate. In so doing, the sideways acceleration due to the influence of gravity in the "wing down" attitude is sustained for up to 10 seconds. This may be undesirable from a ride quality consideration.
3. The implementation utilizes a relatively complex control law in that an estimation of prevailing crosswind is computed and used to bias the rudder command. For aircraft with a large range of landing weights, this computation may require gain scheduling on several parameters.

Configuration C attacks the first two objections by replacing the rate limited align entry with a configuration using an altitude scheduled reference course error trajectory. (Refer to Figure C-6 for the course error profile as implemented.) Typical time history trajectories for roll attitude and course error are nearly identical to those of configuration E.

The next configuration change was to eliminate the computed crosswind term being used to bias the rudder command. Without this term or equivalent, a large heading error would be required to hold the steady state rudder needed to cancel the yawing moment due to sideslip. Configuration D adds an integral $\Delta\psi - \psi_m$ term to provide this function. Essentially the same performance results for a deterministic environment. Comparative data from statistical performance evaluations of configurations C and D are provided by Figures C-18 through C-20, also showing equivalent performance.

In the interest of further simplifying the implementation, it was assumed that no accelerometer data is available, and a configuration using an approximation for \ddot{y}_r (earth axis lateral acceleration) was evaluated. The first attempt used an expression involving ϕ , rudder, and yaw acceleration. Inclusion of the yaw acceleration term (derived from filtered yaw rate), however, caused gross instability to occur in the closed loop control mode. Even without the ψ signal, the approximation appeared sufficiently accurate as utilized in the implementation. In loc track mode, the rudder signal is not really necessary since the aircraft is essentially at zero sideslip angle. During the alignment maneuver, however, the rudder input is necessary to account for the sideways acceleration due to sideslip angle. As a cautionary note, it must be recognized that the adequacy of this approximation is dependent on the magnitude of windshear encountered and the bandwidth of the navigation filter used to produce the lateral rate signal (\dot{y}_f) for path control damping. At the maximum windshear simulated and with the existing nav filter gains (see gain Table C-3), the performance is acceptable as documented by Figures C-21 to C-24 for the standard "maximum wind" environment.

Further minor tradeoffs were evaluated statistically, and the results are briefly described in the following paragraphs. Two sigma variations of the performance indication parameters (y_{TD} , ψ_{TD} , etc.) are listed in Table C-III.

Configuration G — The effect of reduced rate damping in align (i.e., not switching to higher gain) was found to increase the y_{TD} scatter somewhat. (Compare cases 42 and 13.)

Configuration H — Elimination of the heading correction term for the nose-mounted localizer antenna has the effect of shifting the nominal TD point slightly. Of more importance is the extra bit of maneuvering needed to move the aircraft over toward centerline. Since the touchdown statistics are not significantly affected, use of the heading correction does not appear critical. Compare cases 42 and 14.

Configuration I — A reduction in roll attitude loop gain by 50% increases lateral deviation due to disturbances as evidenced by noise response data of Table C-IV and the distribution of the performance parameter y_{100} for case 15. Surprisingly, this additional scatter is not reflected in the y_{TD} statistical data.

Configuration J — Substituting \ddot{y}_r for $g\phi + K\delta_r$ as the \ddot{y} input to the nav filter introduces a slight reduction in lateral deviation scatter at touchdown as compared to Configuration E. (Compare cases 42 and 17.)

Configuration K — The lateral acceleration term input to the roll axis for wing down compensation can be washed out at up to 0.1 radian/sec without significantly degrading performance. However, touchdown statistics (case 19) do show a 5 foot bias in the lateral deviation at touchdown and a higher nominal bank angle (3.7° as compared to 3.0°). Refer to Figure C-25 for time history data with different time constants.

Configuration L — This configuration is the same as C in the yaw axis and E in the roll axis. Again no significant differences in performance were noticed as in the comparison between C and D.

Localizer Track

Several different variations of inertial, beam, and complementary mix techniques of generating the rate damping term are represented by the configurations listed in Table C-1. The resulting performance can probably most easily be assessed by comparing the statistical distribution of the y , \dot{y} , and ϕ performance parameters. Of particular interest is the data tabulated for y deviation at the 100 feet altitude intercept. The configurations of interest in this respect are listed below:

<u>Configuration</u>	<u>Comment</u>
C & D	Rate term is complementary mix of beam deviation and earth axis acceleration.
E	Rate term is complementary mix of beam deviation and acceleration approximated by $g\phi + K \cdot \delta_r$.
F	Rate and position signals are derived from beam deviation data only.
N	Rate term is pure integral of earth axis acceleration, \ddot{y}_r (for reference only).
P	Rate term consists of $1/4 \dot{y}_f + 3/4 \dot{y}_I$ where \dot{y}_f is from standard complementary mix (configuration C & D) and \dot{y}_I is filtered \ddot{y}_r .
Q	Same as P, except \dot{y}_I is derived from $\ddot{y}_2 = g\phi + K \cdot \delta_r$.

Performance of Configurations C, D and E was previously discussed and found to be similar.

Configuration F is of some interest since the advent of the MLS, with its reduced noise content as compared to ILS localizer, offers the potential for greater reliance on unaugmented beam deviation and rate data. Comparative noise response data from Table C-IV does not show any serious amplification of noise for Configuration F as compared to Configuration E, although the change in roll activity and lateral rate excursions is significant. Similarly, increased scatter is evident in the statistical performance data for ϕ_{TD} , ψ_{TD} , and \dot{y}_{TD} .

Although Configuration N is unrealizable (since it assumes perfect lateral rate information), data was obtained as a reference against which to compare

the performance of the other configurations. A comparison of systems E, F and N is provided in the form of statistical distribution curves in Figures C-26 to C-29. One item requiring comment is the increased scatter in y_{100} data for Configuration N as compared with y_{TD} data. This can probably be attributed to the higher rate gain which is used below align altitude. If a pure inertial rate term were indeed to be implemented, the higher gain should be used for the entire loc track mode.

Configurations P and Q, which use a combination of complemented rate and inertial rate, are compared with N and E in the Table C-V, again for the standard max wind environment at nominal airspeed of 70 knots.

The notable statistic from this list is the significantly larger scatter in y_{TD} associated with configuration Q even though y_{100} scatter is no worse than Configuration E. Evidently, the $K \cdot \phi + K \cdot \delta_r$ approximation for \ddot{y} is not adequate when this term (after filtering) is relied on for the low frequency portion of the rate damping term.

TABLE C-I. CONFIGURATION LIST

CONFIG. I.D.	DESCRIPTION	APPLICABLE DIAGRAMS	
		YAW	ROLL
A.	STOLAND control laws with gain set 1.	1	2, 3
B.	Initial forward slip configuration-computed wind for steady state rudder term.	4	5, 3
C.	Rate limited align entry of configuration B is replaced by $\Delta\psi$ model trajectory.	6	7, 3
D.	Same as C except computed wind term is eliminated in favor of integral of $\Delta\psi - \psi_m$.	8	7, 3
D.	Same as D except for finite time constant on \ddot{y}_r washout for wing down compensation signal.	8	7, 3
E.	Yaw as for D. In roll axis, \ddot{y}_R is replaced with pseudo $\ddot{y} = 0.562 \phi + K \cdot \delta_r$.	8	7, 3
F.	Same as E except y_f and \dot{y}_f are derived from loc data only.	8	7, 3
G.	Configuration E with \dot{y} to ϕ_c gain fixed at $0.5^\circ\phi/\text{fps}$.	8	7, 3
H.	Configuration E with no heading correction for nose located antenna.	8	7, 3
I.	Configuration E with K_ϕ gain reduced to 3.5 deg/deg	8	7, 3
J.	Configuration E except \ddot{y}_r is input to nav filter. ($\ddot{y}_2 = 0.562 \phi + K \cdot \delta_r$ is used for wing down compensation.	8	7, 3
K.	Same as D except \ddot{y}_r input to wing down compensation is through a 10 second washout filter	8	7, 3
L.	Same as C in yaw. $\Delta\psi$ model Same as E in roll. $\ddot{y} = 0.56 \phi + K \cdot \delta_R$.	6	7, 3
N.	Same as E except rate damping term consists of integral \ddot{y} instead of \dot{y}_f .	8	9, 3
O.	Configuration E with integral y_f gain doubled	8	7, 3
P.	Same as D except rate damping term is $1/4 \dot{y}_f$ and $3/4$ lagged \dot{y}_r .	8	9, 3
Q.	Same as P except $g/57.3 \phi + K\delta_r$ used in place of \ddot{y}_r .	8	9, 3
R.	Same as A except gains updated and revised.	1	2, 3

TABLE C-II. LOG OF STATISTICAL DATA RUNS - LATERAL AXIS

case	turb P,r, β	y wind	x wind	shear	beam noise	Uo	config.	date
1	x x x -	15 kt.	0	x	x	70 kts.	c	4-30
2	x x x	15	25 HW	x	x	70	c	4-30
3	x x x	15	10 TW	x	x	70	c	4-30
4	x x x	15	0	x	x	70	d	4-30
5	x x x	15	25 HW	x	x	70	d	4-30
6	x x x	15	10 TW	x	x	70	d	4-30
7	x x x	15	0	x	x	65	c	5-4
8	x x x	15	0	x	x	65	d	5-4
9	x x x	15	0	x	x	65	e	5-11
10	x x x	15	0	x	x	70	e	5-11
11	x x x	15	10 TW	x	x	70	e	5-11
12	x x x	15	25 HW	x	x	70	e	5-11
13	x x x	15	0	x	x	70	g	5-11
14	x x x	15	0	x	x	70	h	5-12
15	x x x	15	0	x	x	70	i	5-12
16	x x x	15	0	x	x	70	d	5-12
17	x x x	15	0	x	x	70	j	5-12
18	x x x	15	0	x	x	70	f	5-12
19	x x x	15	0	x	x	70	k	5-12
20	x o o	0	0	-	0	70	e	5-13
21	o x x	0	0	-	0	70	e	5-13
22	o o o	0	0	-	x	70	e	5-13
23	x x x	0	0	-	x	70	e	5-13
24	x x x	15	0	x	x	70	e	5-13
25	x x x	15	25 H	x	x	70	e	5-13

TABLE C-II. LOG OF STATISTICAL DATA RUNS — LATERAL AXIS (continued)

case	turb P, r, β	y wind	x wind	shear	beam noise	Uo	config.	date
23	x x x	0	0	-	x	70 kts.	e	5-13
24	x x x	15 kt	0	x	x	70	e	5-13
25	x x x	15	25H	x	x	70	e	5-13
26	x x x	15	10T	x	x	70	e	5-14
27	x x x	15	0	0	x	70	e	5-14
28	x x x	15	0	x	x +25'IC	70	e	5-14
29	x x x	15	0	x	x	60	e	5-14
30	x x x	15	0	x	x	65	e	5-14
31	x x x	15	25H	x	x	65	e	5-14
32	x x x	15	10T	x	x	65	e	5-14
33	x x x	15	10T	x	x	70	c	5-14
34	x x x	15	10T	x	x	70	l	5-14
35	INVALID DATA							
36	x x x	15	10T	x	x	65	l	5-14
37	x x x	15	10T	x	x	65	r	5-18
38	x x x	15	25H	x	x	65	r	5-18
39	x x x	15	0	x	x	65	r	5-18
40	x x x	15	0	x	x	65	e	5-19
41	x x x	15	0	x	x	70	n	5-24
42	x x x	15	0	x	x	70	e	5-24
43	x x x	15	0	x	x	70	0	5-24
44	x x x	15	0	x	x	70	p	5-25
45	x x x	15	0	x	x	70	q	5-25

TABLE C-III. STATISTICAL PERFORMANCE DATA SUMMARY

CASE	ft		deg		deg		fps		ft	
	y_{TD} mean	2σ	ψ_{TD} mean	2σ	ϕ_{TD} mean	2σ	\dot{y}_{TD} mean	2σ	y_{100} mean	2σ
1	-4.0	9.0	0.8	1.6	3.4	2.0	1.6	2.1	0.5	8.0
2	1.5	6.3	0.4	0.9	3.2	2.4	1.7	1.9	0.0	8.0
3	-5.0	7.6	1.3	2.3	3.5	2.0	0.7	2.6	0.0	7.5
4	-4.2	6.8	0.6	1.5	3.6	1.7	1.6	1.8	1.0	8.5
5	2.0	7.5	0.3	0.8	3.2	1.9	1.4	2.0	-1.5	6.5
6	-4.5	7.4	1.3	2.4	3.4	2.0	1.2	2.0	1.0	8.5
7	-4.0	6.0	1.0	1.7	3.5	2.0	0.5	1.7	1.5	7.5
8	-3.5	5.8	1.0	2.0	3.3	1.6	0.6	1.6	1.5	7.5
9	-1.0	9.0	0.6	2.1	3.4	1.8	-0.6	2.1	0.5	8.5
10	-.5	8.8	0.7	1.4	3.1	1.9	-0.6	2.1	1.0	11.0
11	0.5	8.2	1.8	2.3	3.0	2.0	-0.7	2.3	0.5	9.0
12	-1.0	8.8	0.6	0.9	3.2	2.0	-0.3	2.0	1.5	8.5
13	-1.5	12.5	1.0	2.1	3.2	2.0	-0.3	2.4	1.5	10.5
14	2.0	10.0	1.1	1.8	2.7	2.0	0.5	2.5	-6.5	8.5
15	0.5	8.8	0.8	1.8	3.2	2.5	0.0	3.1	0.5	14.5
16	-4.0	8.5	0.7	1.3	3.3	2.6	0.4	2.3	1.0	14.0
17	-1.5	8.5	0.8	1.6	3.4	2.2	0.2	1.9	1.5	8.0
18	-2.5	9.5	0.8	2.4	3.5	3.4	0.7	3.3	1.5	9.0
19	-5.0	8.5	1.3	2.1	3.7	2.1	0.7	2.1	1.0	9.0
20	-0.6	6.0	0.6	0.8	-0.3	.7	0.0	1.3	-2.0	8.5
21	0.0	2.6	1.0	0.6	-0.1	1.5	0.0	0.9	0.0	4.0
22	0.0	7.0	1.3	0.4	-0.2	1.1	-0.2	1.9	0.0	6.5
23	-0.5	8.5	1.1	0.9	-0.3	2.4	0.2	2.2	-1.0	11.0
24	1.0	8.6	0.7	2.0	3.0	2.1	-0.1	2.3	2.0	11.5
25	-1.0	8.7	0.5	0.9	3.3	2.0	0.0	2.5	2.0	9.0

TABLE C-III. STATISTICAL PERFORMANCE DATA SUMMARY (continued)

CASE	ft		deg		deg		fps		ft	
	y_{TD} mean	2σ	ψ_{TD} mean	2σ	ϕ_{TD} mean	2σ	\dot{y}_{TD} mean	2σ	y_{100} mean	2σ
26	0.4	8.6	1.5	2.3	2.8	2.0	-0.2	2.1	1.5	9.5
27	-1.5	8.5	1.7	0.9	3.2	2.0	0.3	2.1	0.0	11.0
28	4.0	8.5	0.8	1.5	3.0	1.8	-0.3	2.2	6.0	10.0
29	-0.5	8.5	1.5	2.3	3.4	2.0	0.1	2.6	1.0	9.0
30	-1.5	8.7	1.0	1.6	3.4	2.0	-0.1	2.5	0.0	9.5
31	0.5	9.5	0.3	1.1	3.2	2.2	0.3	2.2	1.0	9.5
32	-1.0	9.4	1.8	2.6	3.0	2.4	-0.1	2.2	0.0	9.0
33	-0.5	7.4	0.7	2.8	3.5	2.3	0.3	2.1	0.0	9.5
34	0.5	9.0	1.0	2.6	2.6	1.9	-0.1	2.2	1.0	10.0
35	INVALID DATA									
36	-2.4	9.4	1.4	2.3	3.2	2.1	0.0	2.5	0.0	10.5
37	-4.5	8.5	1.4	2.0	-0.2	3.2	-3.0	4.5	0.5	10.5
38	-11.0	18.0	-1.9	2.3	1.5	4.0	-5.6	8.6	0.0	6.5
39	-5.5	10.5	0.3	1.4	0.1	3.8	-3.8	5.2	0.0	8.5
40	0.0	10.5	1.1	2.2	3.0	2.2	0.0	2.4	0.5	9.5
41	-1.5	4.8	0.9	1.4	3.2	1.4	0.6	0.8	0.5	7.5
42	0.0	8.0	0.8	1.7	3.0	2.3	0.0	2.3	1.5	10.5
43	0.0	10.5	0.9	1.4	2.8	2.4	0.0	2.2	1.5	9.0
44	-4.0	7.0	1.0	1.4	3.2	1.5	0.6	0.9	0.5	7.0
45	5.0	13.0			3.0	1.7	0.7	1.7	2.0	10.5

TABLE C-IV. NOISE RESPONSE DATA

CONFIG.	RMS RESPONSE TO STANDARD TURBULENCE AND BEAM NOISE				
	γ (ft)	ϕ (deg.)	$\dot{\gamma}$ (fps)	δ_R (deg.)	δ_W (deg.)
C	3.8	1.05	1.25	2.0	3.8
D	3.4	1.05	1.05	2.0	3.8
E	5.0	1.2	1.15	1.8	3.6
F	5.4	1.65	2.1	2.1	3.8
G	6.4	0.7	1.5	2.0	3.0
H	4.6	1.3	1.35	2.1	2.8
I	5.4	1.3	1.45	2.1	3.6
J	3.8	1.1	1.05	2.1	3.2
K	4.0	1.0	1.3	1.8	3.4
P	3.1	0.95	0.55	2.0	3.4

TABLE C-V. COMPARATIVE PERFORMANCE WITH
RATE DAMPING TERM VARIATIONS

	γ_{TD}	ψ_{TD}	ϕ_{TD}	$\dot{\gamma}_{TD}$	γ_{100}
E (42)	0 \pm 8 ft	0.8 \pm 1.7 deg	3 \pm 2.3 deg	0 \pm 2.3 fps	1.5 \pm 10.5
N (41)	-1.5 \pm 4.8	0.9 \pm 1.4	3.2 \pm 1.4	0.6 \pm 0.8	0.5 \pm 7.5
P (44)	-4.0 \pm 7.0	1.0 \pm 1.4	3.2 \pm 1.5	0.6 \pm 0.9	0.5 \pm 7.0
Q (45)	5.0 \pm 13.0	Unavailable	3.0 \pm 1.7	0.7 \pm 1.7	2.0 \pm 10.5

GAIN TABLE C-1

PARAMETER	UNITS	VALUE FOR NOTED CONFIG.	
		A	R
$K_2 (\bar{q})$	deg/deg/sec	0.63	0.20
K_R	deg/deg/sec	8.36	1.39
$K_3 (\bar{q})$	deg/fps ²	1.34	
$K_{\psi_{oy}}$	deg/deg	1.83	
K_{RDCB}	deg/deg/sec	1.33	
$K_{\psi DB}$	deg/deg	0.83	
K_{IDCB}	deg/deg-sec	0.3	
τ	sec	0.03	
Position limit	deg	15.0	
Rate limit	deg/sec	35.0	14.0
ALN ALT	ft HRA	16.0	

NOTE: In this and all gain tables, a blank indicates no change from column to the left.

GAIN TABLE C-2

PARAMETER	UNITS	<u>VALUE FOR NOTED CONFIG.</u>	
		A	R
$K_{\dot{\phi}}/\phi$	deg ϕ /deg/sec	0.5	1.0
K_{ϕ}	deg/deg	10.0	3.33
$K_{\dot{y}}$	deg ϕ /fps	0.4	
K_y	deg ϕ /ft	0.03	
K_{IY}	deg ϕ /ft-sec	0.00087	
$K_{\psi OR}$	deg δw /deg $\psi_{\epsilon 0}$	1.0	
K_{PDCB}	deg δw /deg ϕ	3.33	
K_{PCDB}	deg δw /deg/sec	1.66	
ϕ_{cf} rate limit	deg/sec	6.0	3.0
$K_{R\phi}$	deg δw /deg/sec	0.33	2.17
δw position limit	deg	60.0	
δw rate limit	deg/sec	41.6	
τ	sec	0.033	
ALN ALT.	ft. HRA	16.0	

GAIN TABLE C-3

VALUE FOR NOTED CONF'G.

PARAMETER	UNITS	A, B, C, D, K, P, R	E, G, I, L, M, N, O, Q	F	H	J
K_A	ft /deg	0.0	0.436	0.436	0.0	0.432
K_{1y}		0.8	0.8	N/A	same as E	0.8
K_{2y}		0.24	0.24	N/A	" " "	0.24
K_{3y}		0.032	0.032	N/A	" " "	0.032
K_{y1}	fps ² /fps ²	1.0	0.0	N/A	" " "	1.0
K_{y2}	fps ² /fps ²	1.0	0.0	0.0	" " "	0.0
$K_{A\phi}$	fps ² /deg	N/A	0.562	0.562	" " "	0.562
K_{AR}	fps ² /deg	N/A	0.226	0.226	" " "	0.226
τ_y	sec	N/A	N/A	0.5	" " "	N/A
$\tau_{\dot{y}}$	sec	N/A	N/A	0.5	" " "	N/A
\dot{y} limit	fps	N/A	N/A	15.0	" " "	N/A
K_{y3}	fps ² /fps ²	0.0	1.0	1.0	" " "	1.0
K_{y4}	fps ² /fps ²	0.0	1.0	N/A	" " "	0.0

GAIN TABLE C-4

VALUE FOR NOTED CONFIG.

PARAMETER	UNITS	B
K8	deg/deg/sec	8.36
K9	deg/fps ²	1.34
K10	deg/deg/sec	0.53
K11	deg/deg-sec	0.15
K12	deg/deg	3.6
K13	deg/deg/sec	10.0
K14	fps/deg	1.76
K15	fps/fps ²	8.41
K16	fps/fps	1.0
K17	fps/deg	0.82
K18	fps/deg	0.177
K19	deg/fps	0.367
τ_1	sec	1.0
τ_2	sec	5.0
τ_3	sec	50.0
τ_4	sec	0.1
$\Delta\psi$ rate limit	deg δ_R /sec	4.8
YWF rate limit	deg δ_R /sec	1.2
ALN ALT.	ft HRA	150.0

GAIN TABLE C-5

VALUE FOR NOTED CONFIG.		
PARAMETER	UNITS	B
K1	$\text{deg } \phi_c / \text{ft}$	0.06
K2 ^{loc trk} align	$\text{deg } \phi_c / \text{fps}$	0.8 1.6
K3	$\text{deg } \phi_c / \text{ft-s.}$	0.00087
K4	deg / deg	10.0
K5	$\text{deg } \delta_w / \text{deg/sec}$	5.0
K6	$\text{deg } \phi / \text{fps}^2$	1.78
K7.	$\text{deg } \phi / \text{deg } \delta_R$	0.0
ϕ_c position limit	deg	6.0
ϕ_c rate limit	deg/sec	6.0
δ_w position limit	deg.	60.0
δ_w rate limit	deg / sec	42.0
ALN ALT.	ft HRA	150.

GAIN TABLE C-5

PARAMETER	UNITS	VALUE FOR NOTED CONFIG.
		C, L
K_{ψ}	deg / deg	3.0
$K_{\dot{\psi}}$	deg/deg/sec	4.0
$K_{I\psi}$	deg/deg-sec	0.3
$K_{\beta w}$	deg δ_R /deg β_w	0.66
K_{1w}	fps/fps ² a_y	8.23
K_{2w}	fps/deg δ_R	0.935
K_{3w}	fps/deg δ_w	0.174
K_{4w}	fps/deg ψ	1.92
K_R	deg/deg/sec	1.40
K_{a_y}	deg/fps ²	1.34
δ_{RC} position limit	deg	15.0
δ_{RC} rate limit	deg./sec	14.0
ALN limit	deg δ_{RC}	12.5
τ_1	sec	1.0
ALN ALT.	ft.HRA	150.0

GAIN TABLE C-7

PARAMETER	UNITS	C, D, E, F, H, J, L	G	I	K	M	O	D'
K_y	$\text{deg}\phi_c/\text{ft}$	0.06						
$K_{\dot{y}}$	$\text{deg}\phi_c/\text{fps}$	0.5						
K_{yI}	$\text{deg}\phi_c/\text{ft-sec}$	0.001					0.002	0.001
$K_{\dot{y}\Delta}$	$\text{deg}\phi_c/\text{fps}$	0.5	0.0	0.5				
$K_{\dot{\phi}/\phi}$	$\text{deg}\phi/\text{deg/sec}$	1.0						
K_L	rad/sec	10.0						
K_{ϕ}	$\text{deg}\delta_{wc}/\text{deg}$	7.0		3.5	7.0			
$K_{\dot{y}''}$	$\text{deg}\phi/\text{fps}^2$	1.78						
τ_2	sec	1.0						
$\tau_{\dot{y}''}$	sec	00			10.0	00		50.0
$\dot{\phi}_c$ limit	$\text{deg}\phi_c/\text{sec}$	3.0						
ϕ_c limit	$\text{deg}\phi_c$	5.0						
ϕ_{ALN} limit	$\text{deg}\phi_c$	5.0						
δ_{wc} limit	deg	60.0						
$\dot{\delta}_{wc}$ limit	deg/sec	40.0						
ALN ALT.	ft HRA	150				175	150	

GAIN TABLE C-8

PARAMETER	UNITS	VALUE FOR NOTED CONFIG.
		D,E,F,G,H,I,J,K,N,O,P,Q
K_{ψ}	deg/deg	3.0
k_{ψ}	deg/deg/sec	4.0
$K_{I\psi}$	deg/deg-sec	0.3
K_R	deg/deg/sec	1.40
K_{ay}	deg/fps ²	1.34
δR_c limit	deg	15.0
$\dot{\delta R}_c$ limit	deg/sec	14.0
ALN limit	deg δR_c	12.5
ALN ALT	ft HRA	150.0

GAIN TABLE C-9

PARAMETER	UNITS	VALUE FOR NOTED CONFIG.		
		P, Q	N	
K_y	$\text{deg}^\phi/\text{ft}$	0.06		
$K_{\ddot{y}}$	$\text{deg}^\phi/\text{c}/\text{fps}$	0.25	0.0	
K_{yI}	$\text{deg}^\phi/\text{ft-sec}$	0.001		
$K_{\dot{y}L}$	$\text{deg}^\phi/\text{c}/\text{fps}$	0.375	0.5	
$K_{\dot{y}L\Delta}$	$\text{deg}^\phi/\text{c}/\text{fps}$	0.375	0.5	
$K_{\dot{\phi}}/\phi$	$\text{deg}\phi/\text{deg}/\text{sec}$	1.0		
K_L	rad/sec	10.0		
KK_{ϕ}	$\text{deg c}/\text{deg}$	7.0		
$K_{\ddot{y}}$	$\text{deg}\phi/\text{fps}^2$	1.78		
τ_2	sec	1.0		
$\tau_{\dot{y}}$	sec	∞		
$\dot{\phi}_c$ limit	$\text{deg}^\phi/\text{c}/\text{sec}$	3.0		
ϕ_c limit	deg^ϕ/c	5.0		
ϕ_{ALN} limit	deg^ϕ/c	5.0		
δ_{w_c} limit	deg	60.0		
$\dot{\delta}_{w_c}$ limit	deg/sec	40.0		
ALN ALT	ft HRA	150.0		
τ_1	sec	50.0	∞	
τ_3	sec	20.0	∞	

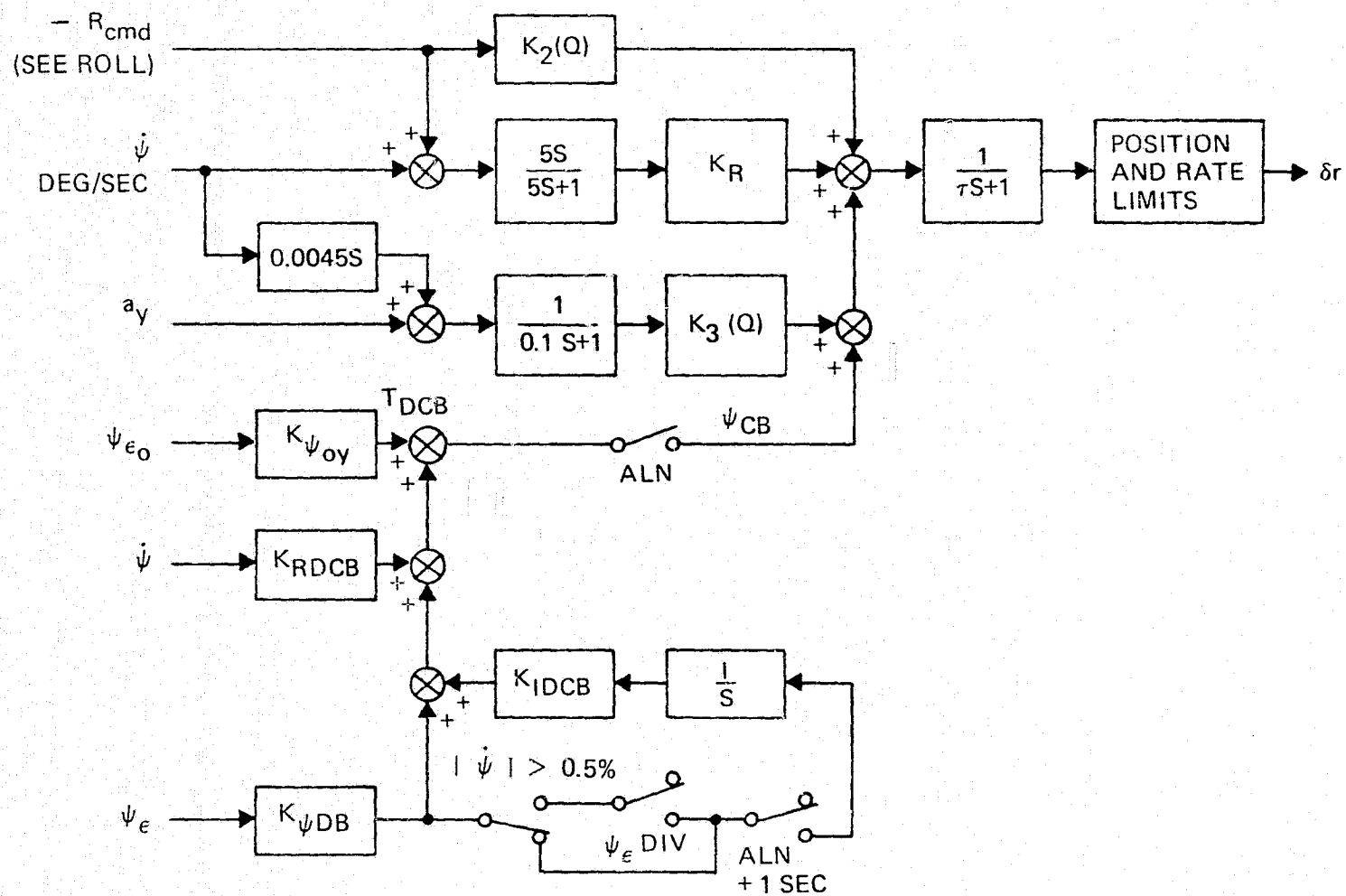


Figure C-1. Stoland Yaw Axis

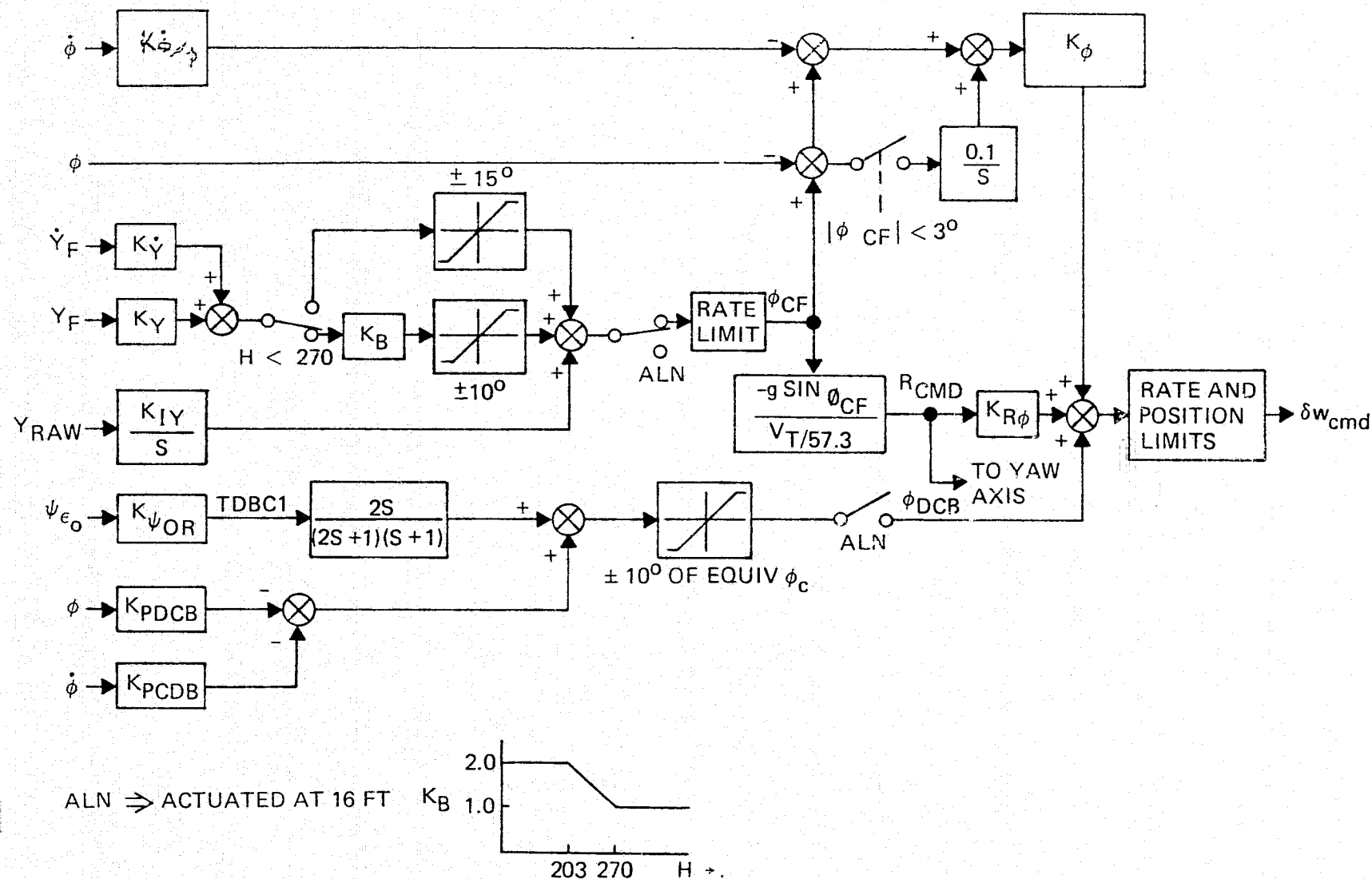


Figure C-2. Stoland Lateral Axis

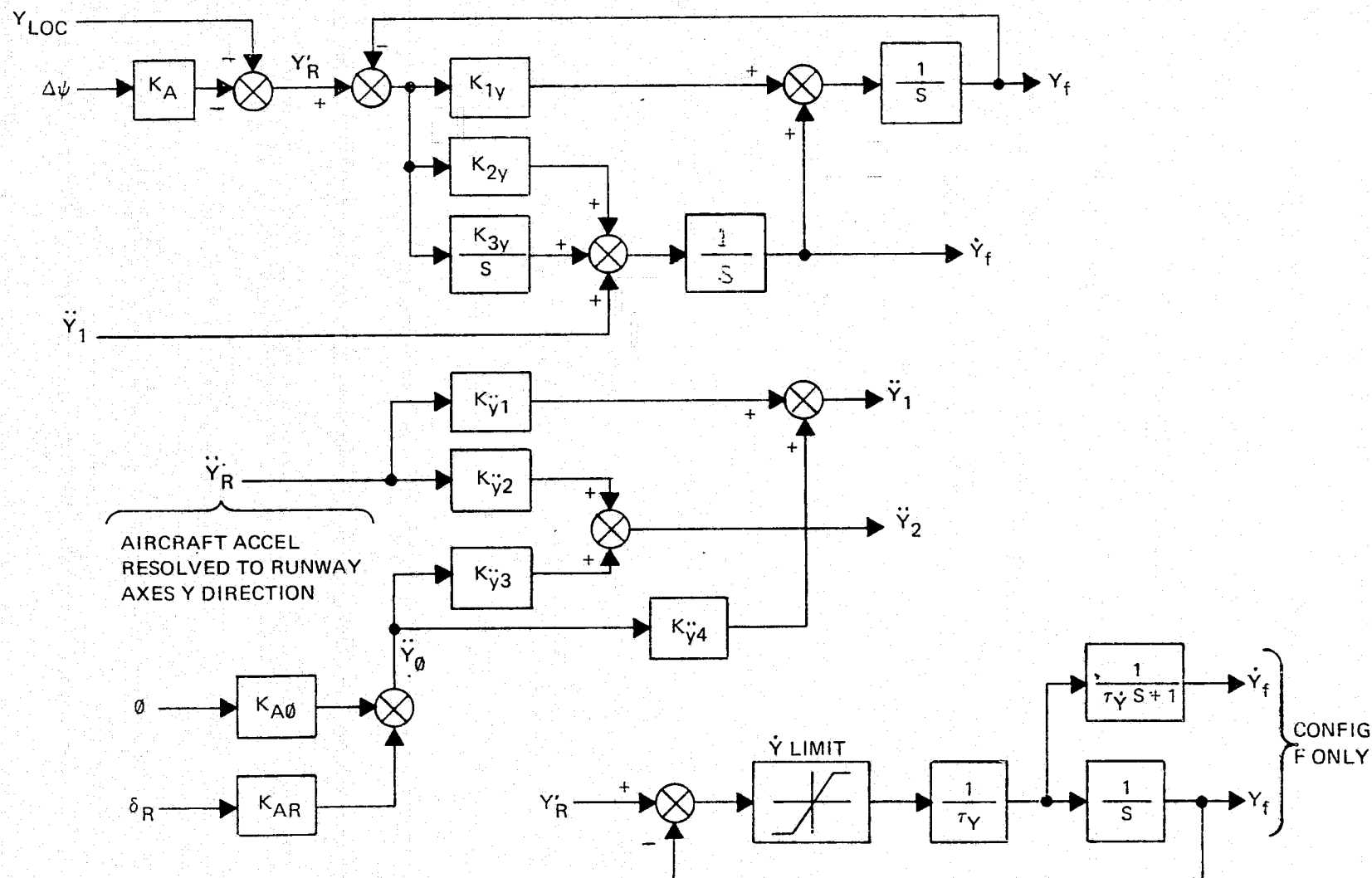
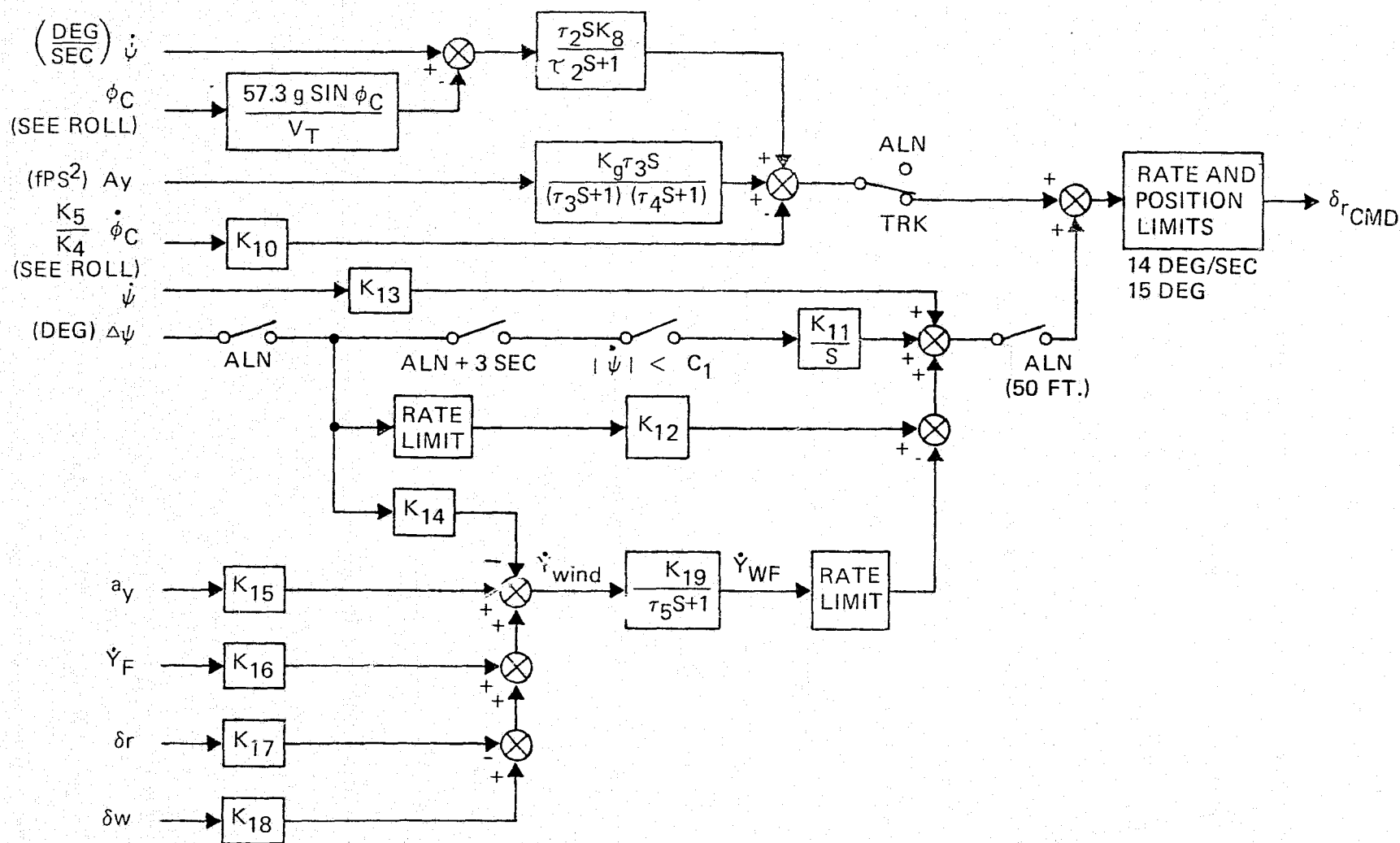


Figure C-3. Lateral Position and Derivatives



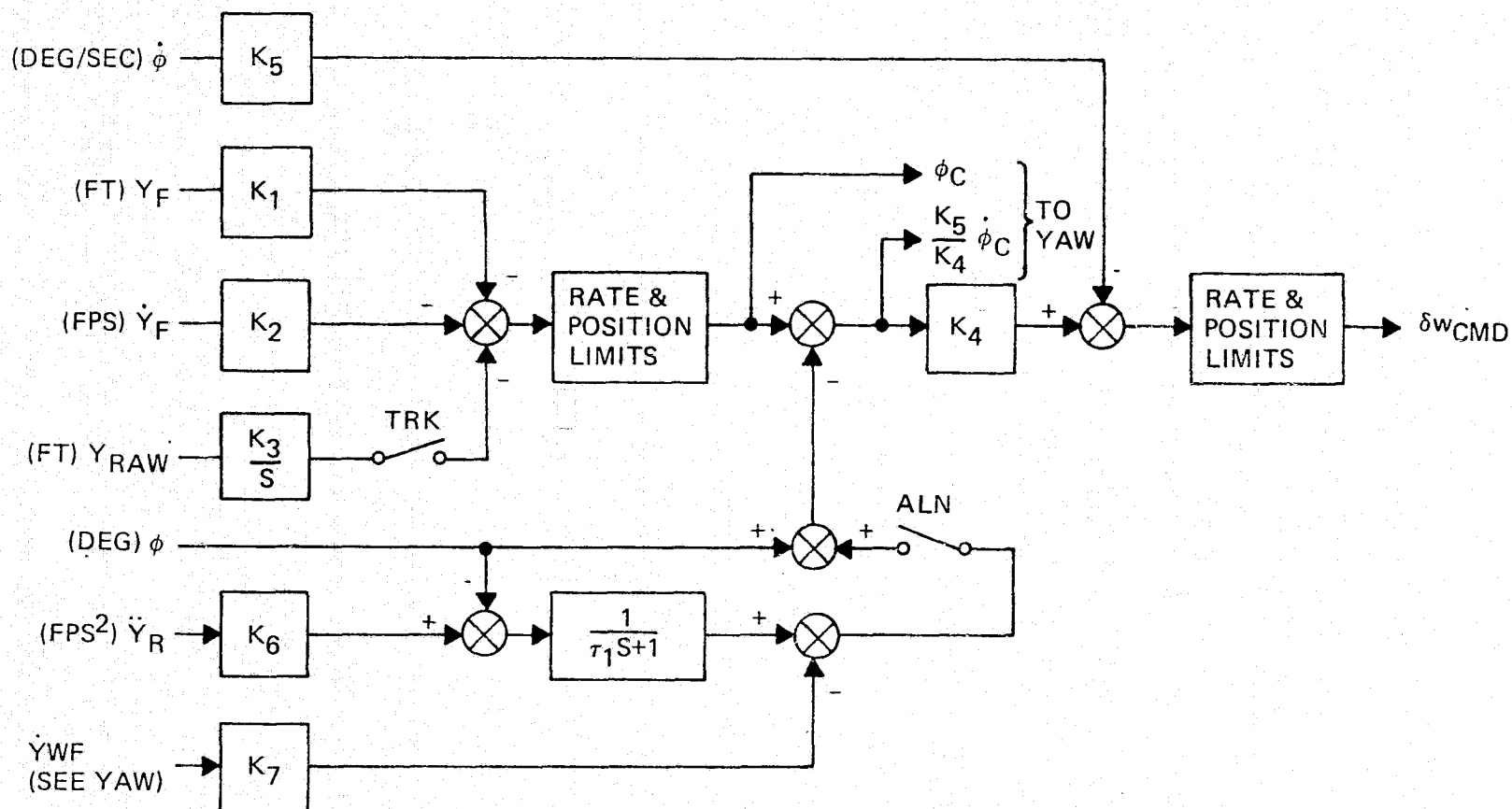


Figure C-5. Lateral Axis-Fwd Slip 1

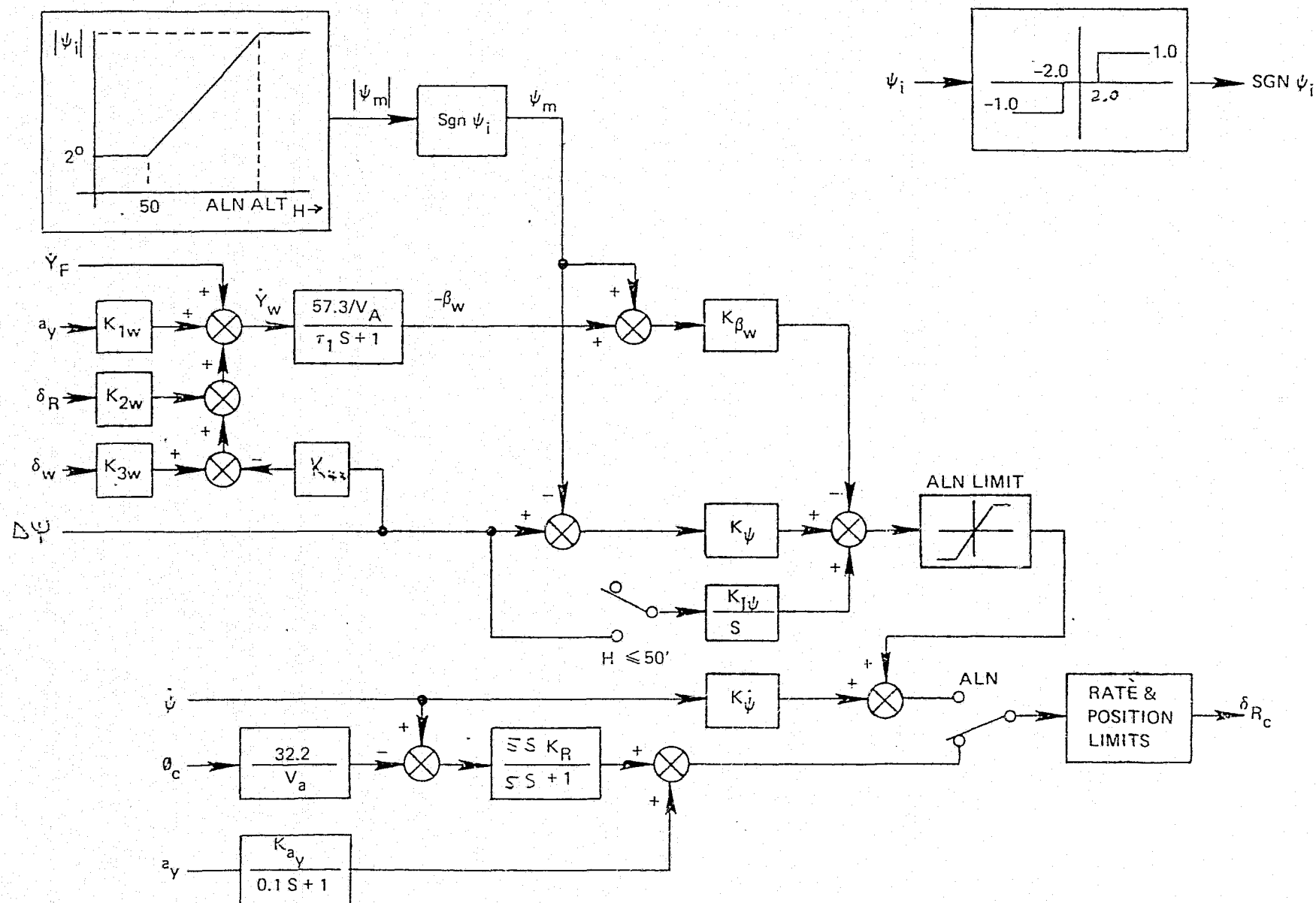


Figure C-6. Yaw Axis Alt Prog Fwd Slip

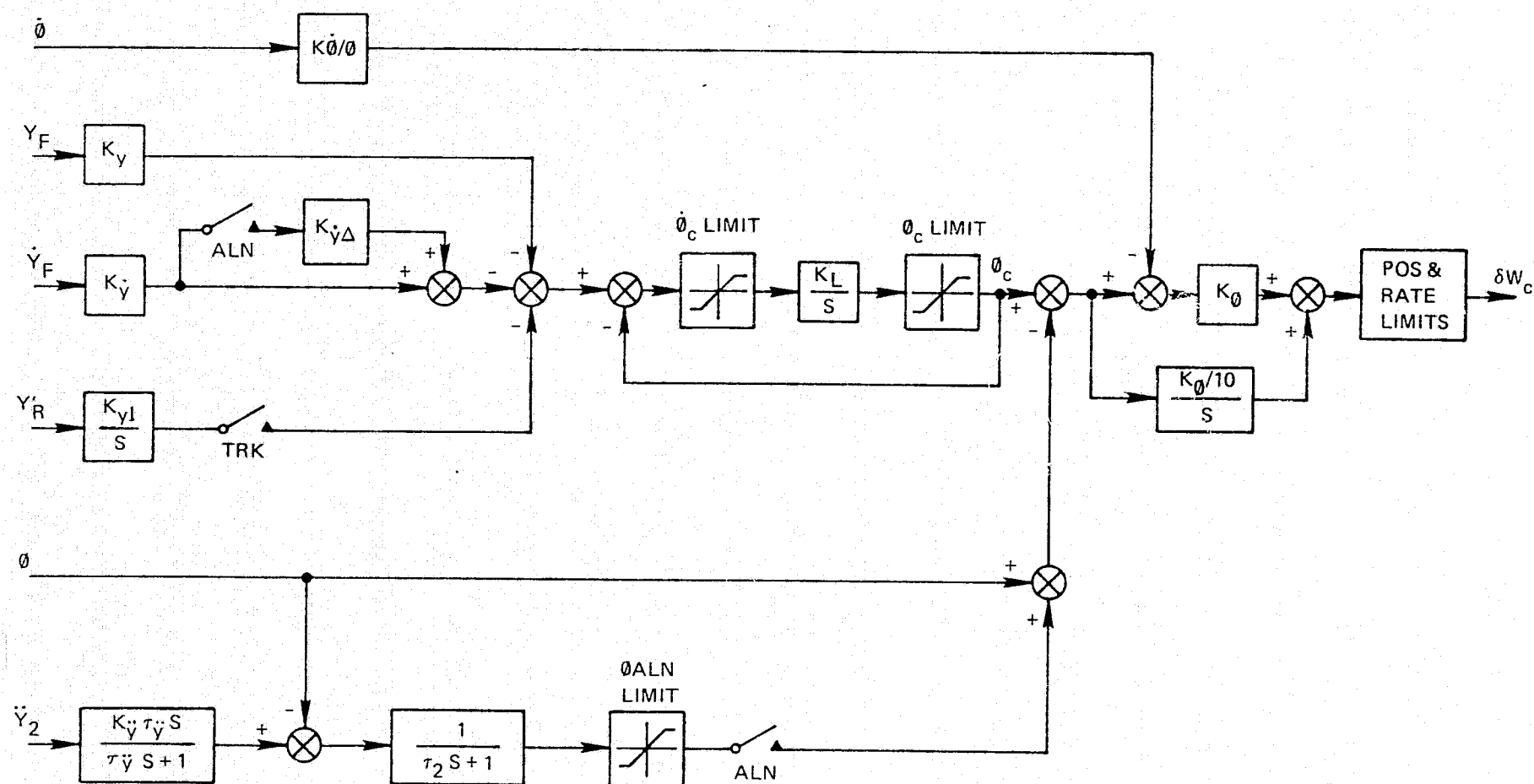


Figure C-7. Lateral Axis Fwd Slip 2

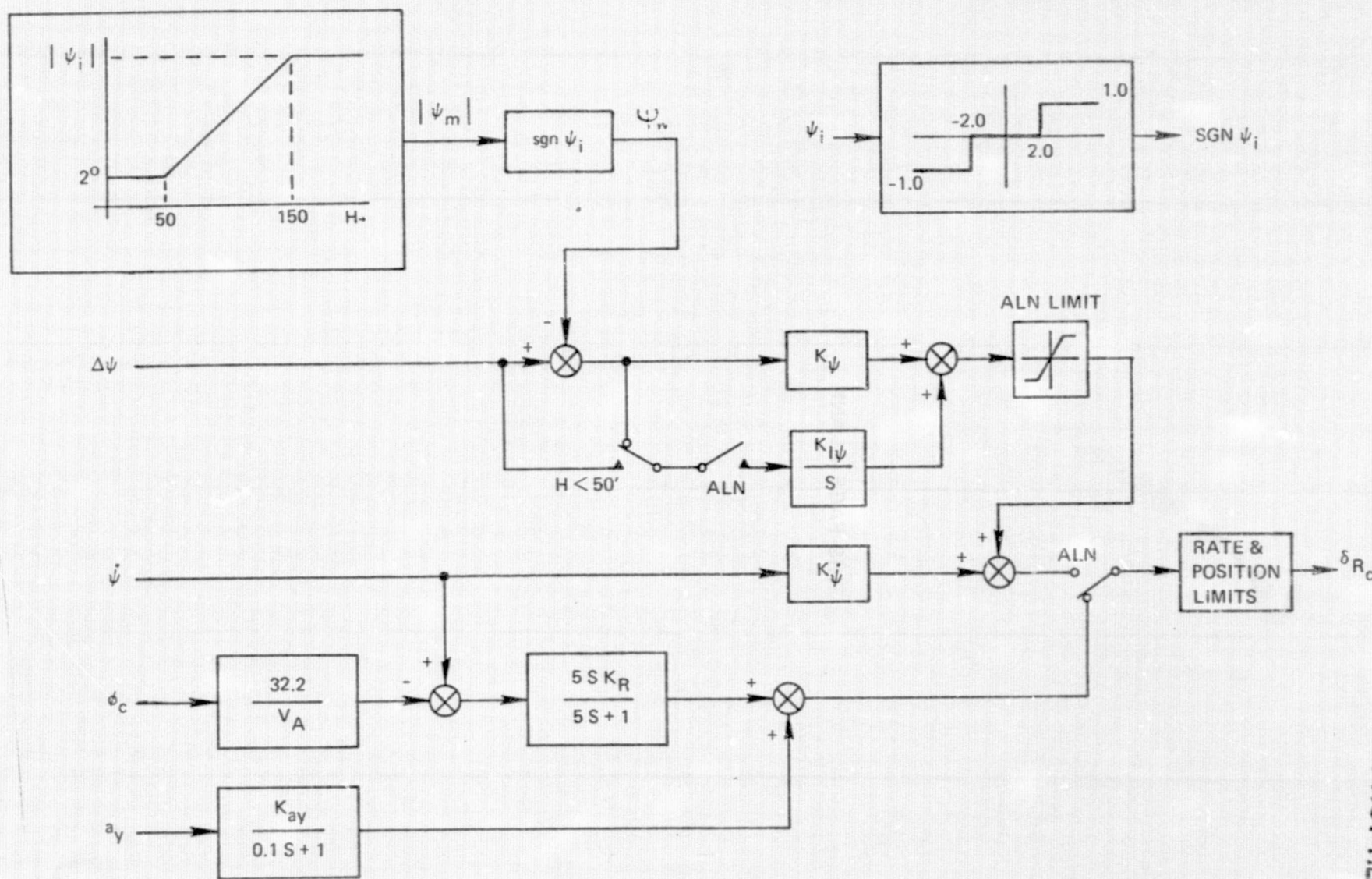


Figure C-8. Yaw Axis Closed Loop Fwd Slip

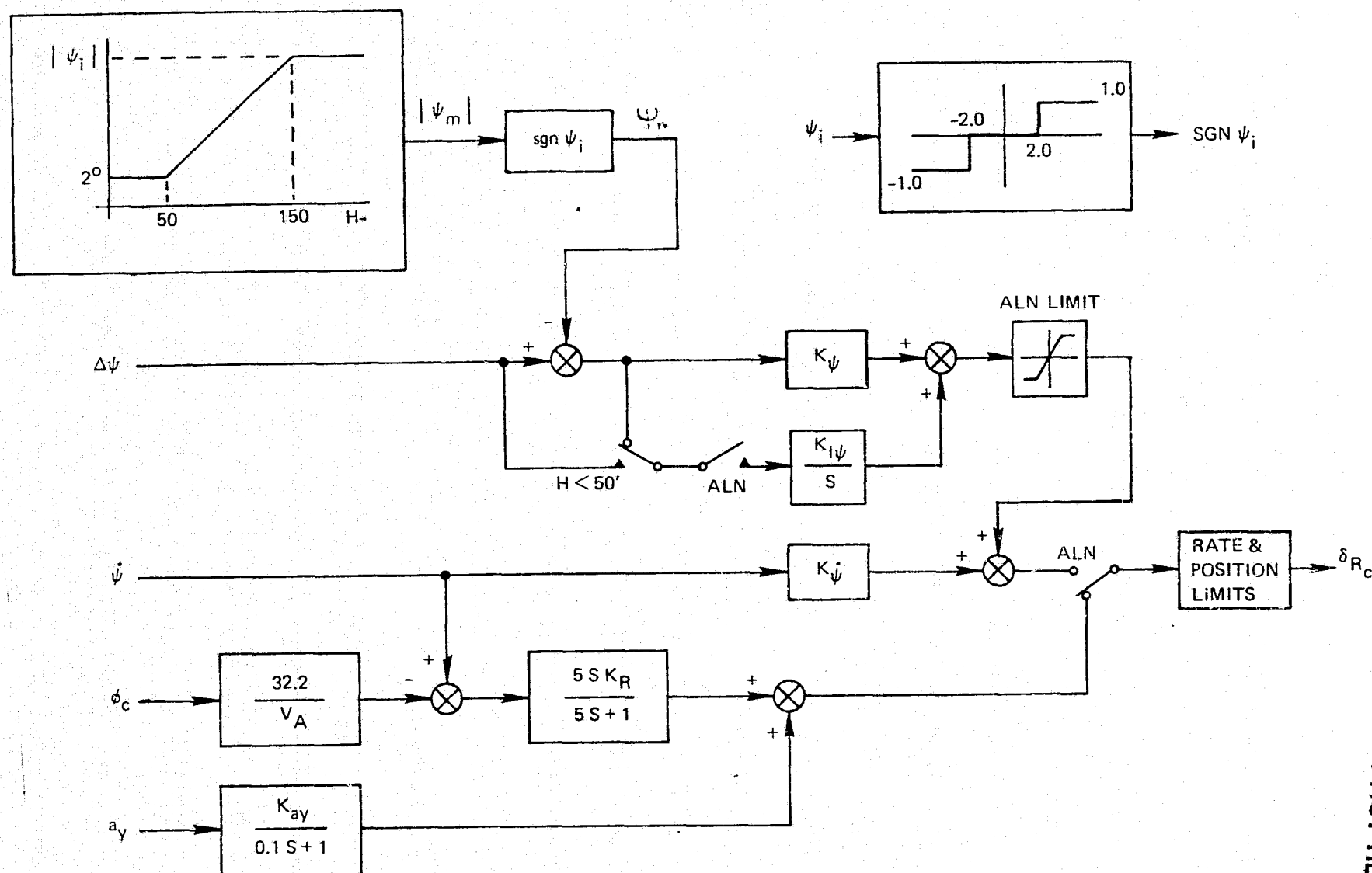


Figure C-8. Yaw Axis Closed Loop Fwd Slip

RECEIVING ROOM BLANK NOT FILMED

C-30

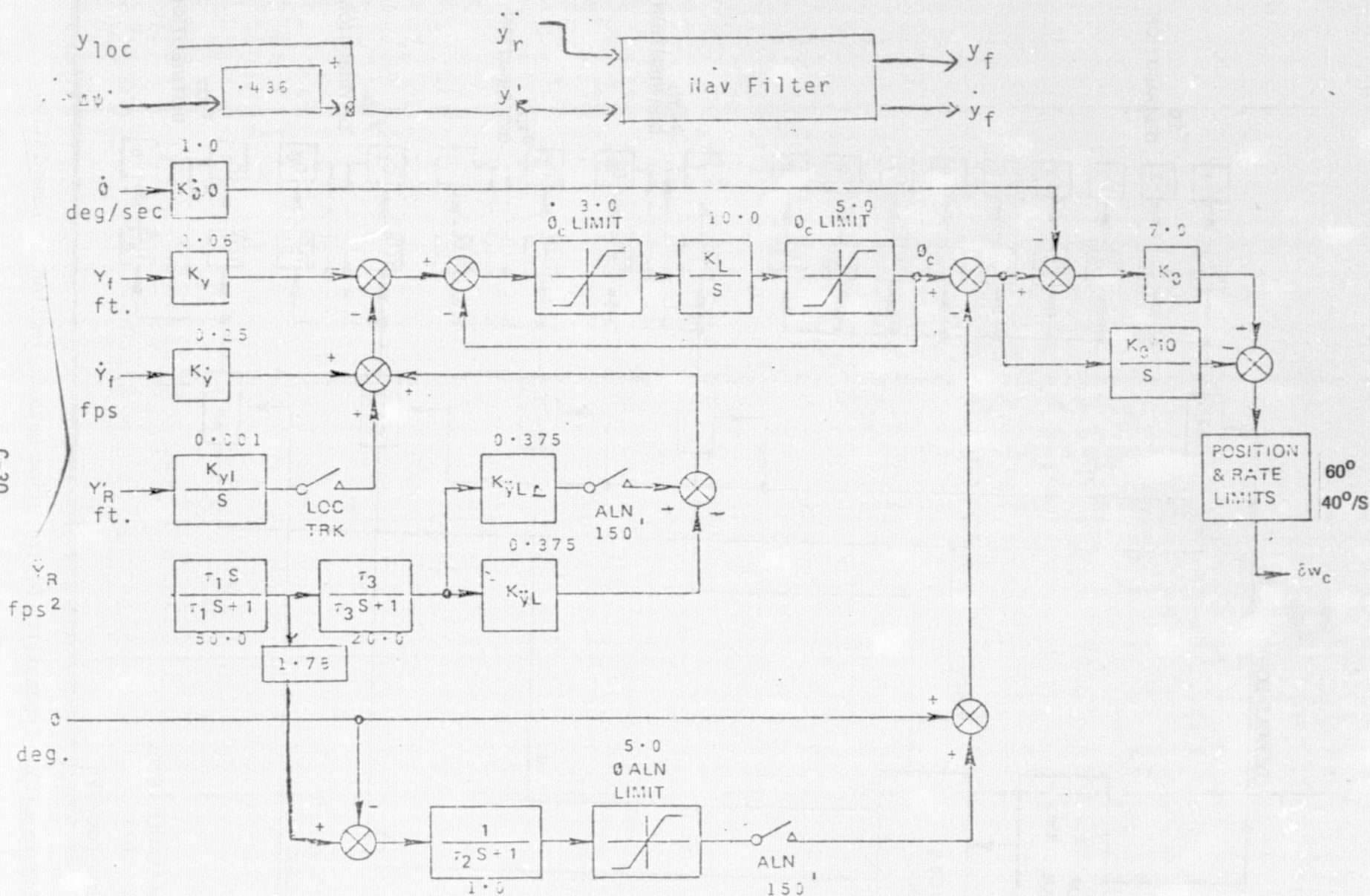


Figure C-9. Roll Axis Closed Loop Forward Slip

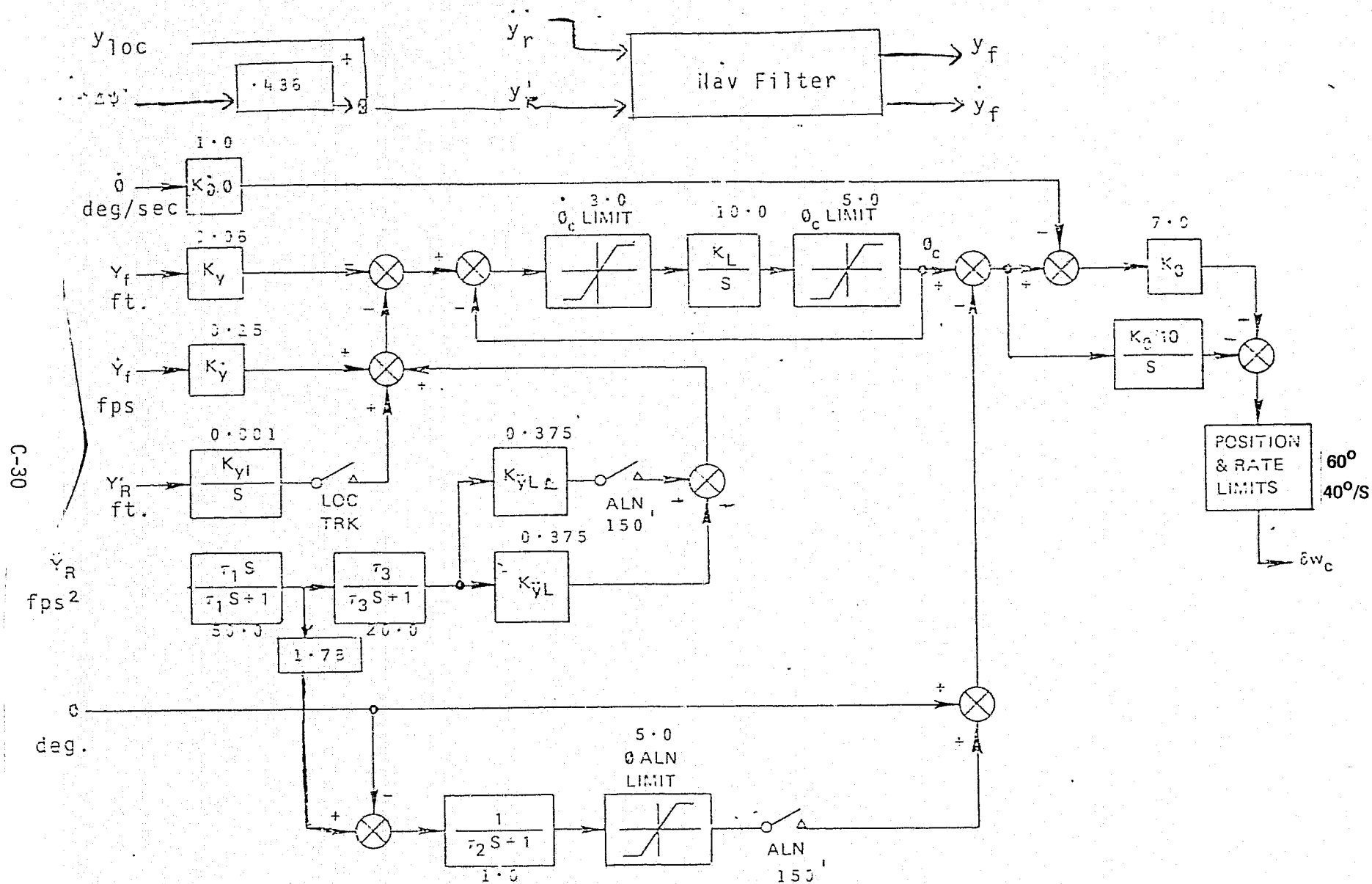


Figure C-9. Roll Axis Closed Loop Forward Slip

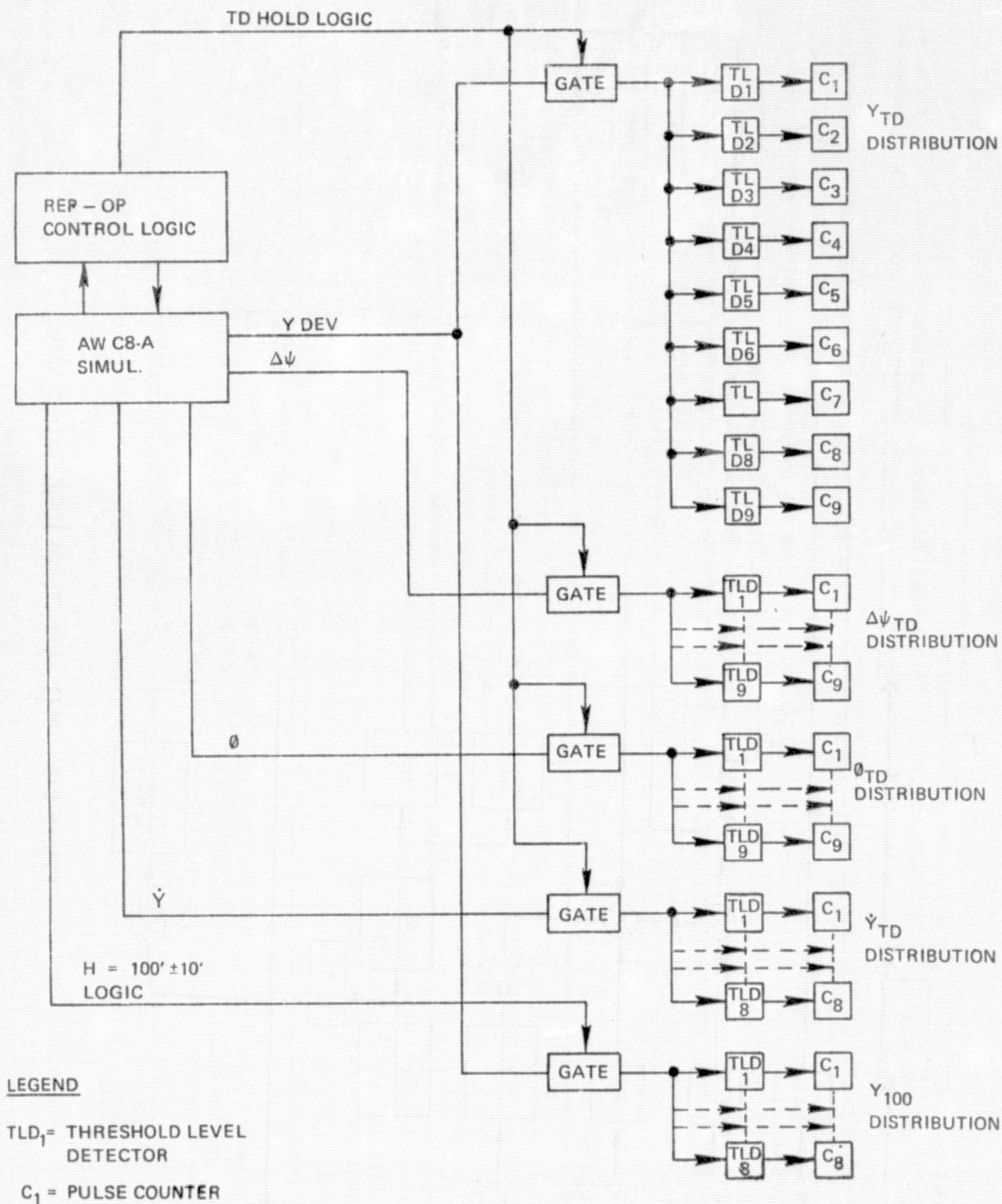


Figure C-10. Probability Distribution Data Collection Implementation

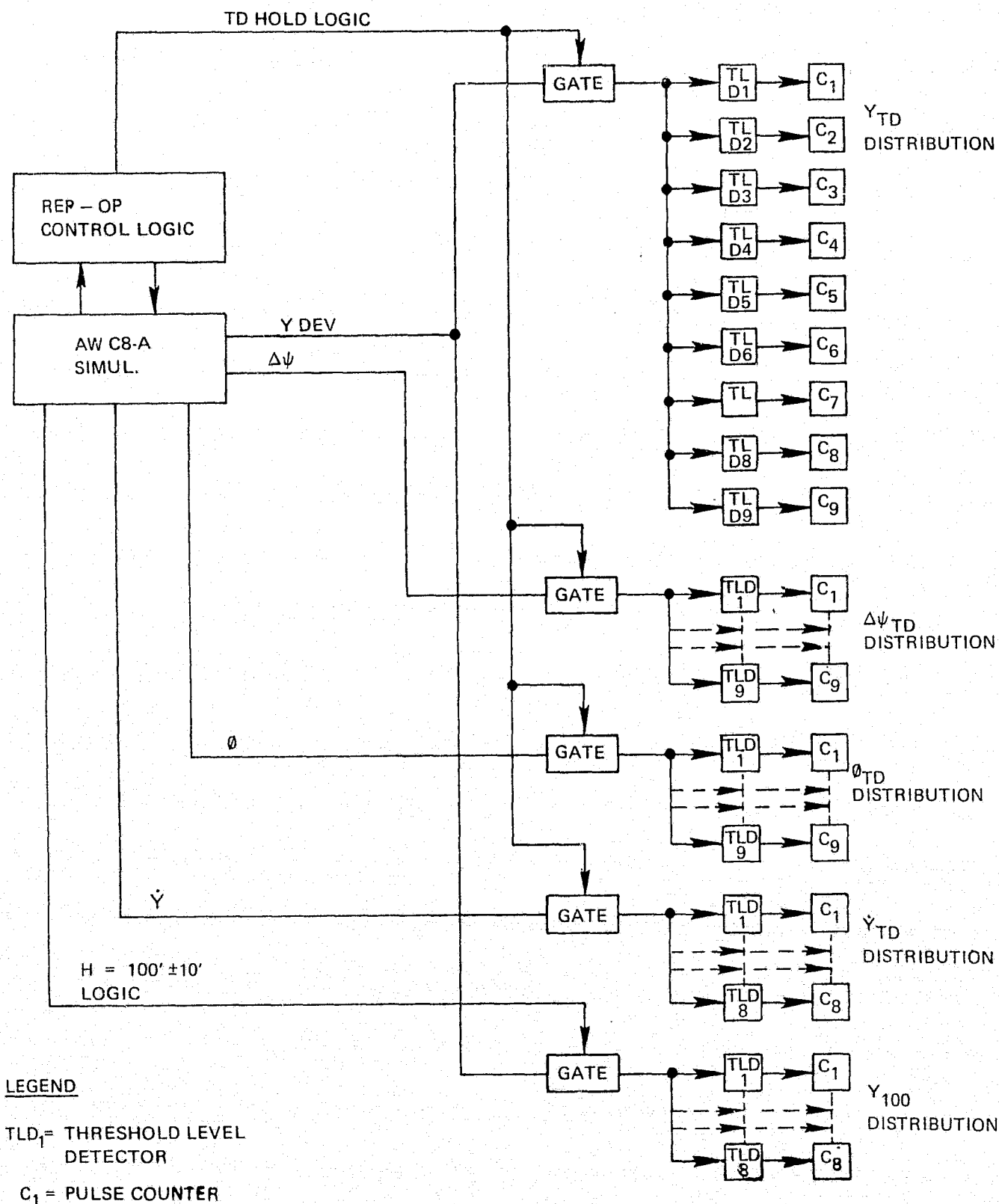


Figure C-10. Probability Distribution Data Collection Implementation

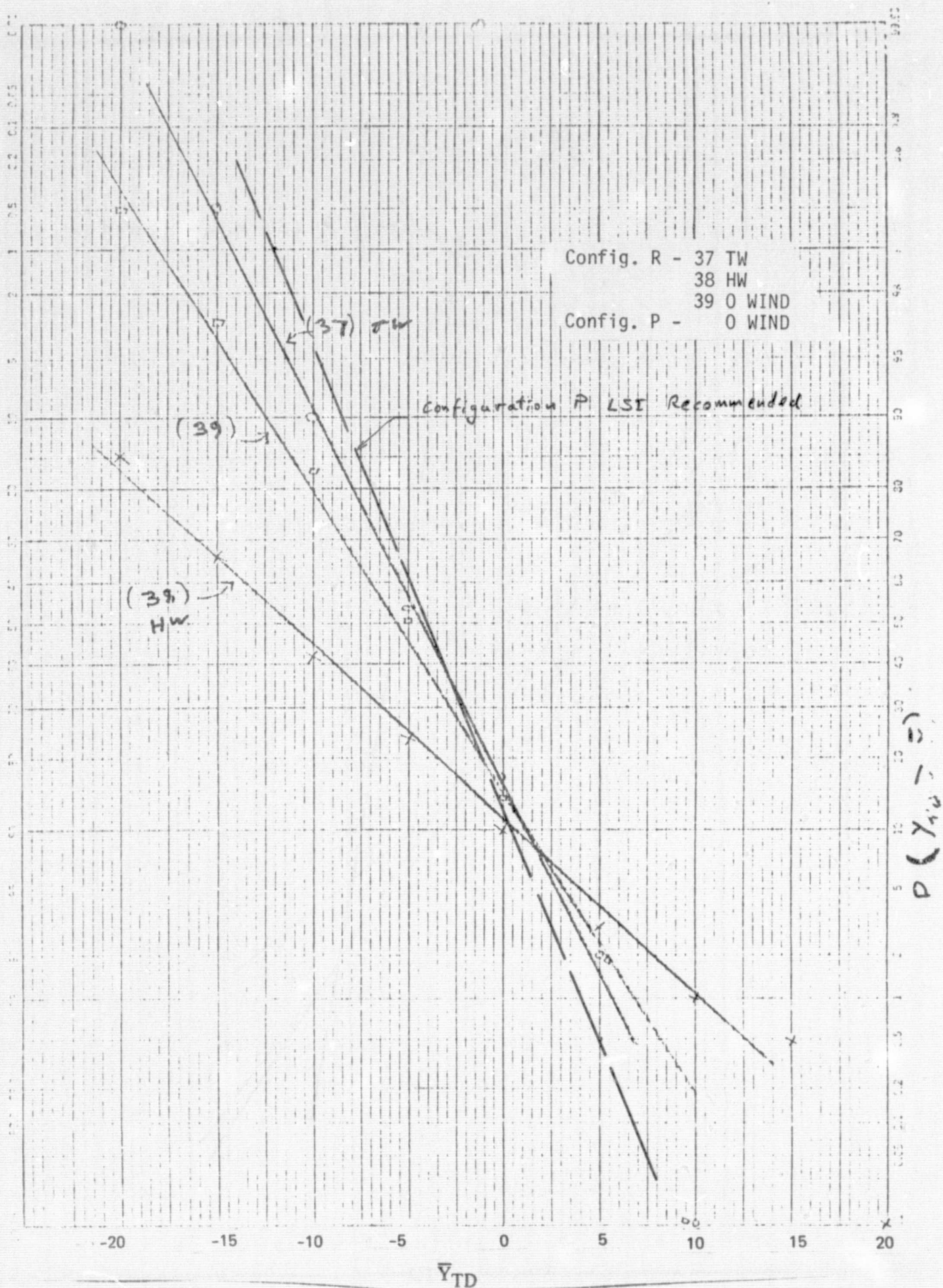


Figure C-11. Y_{TD} Distribution Comparison - R vs. P

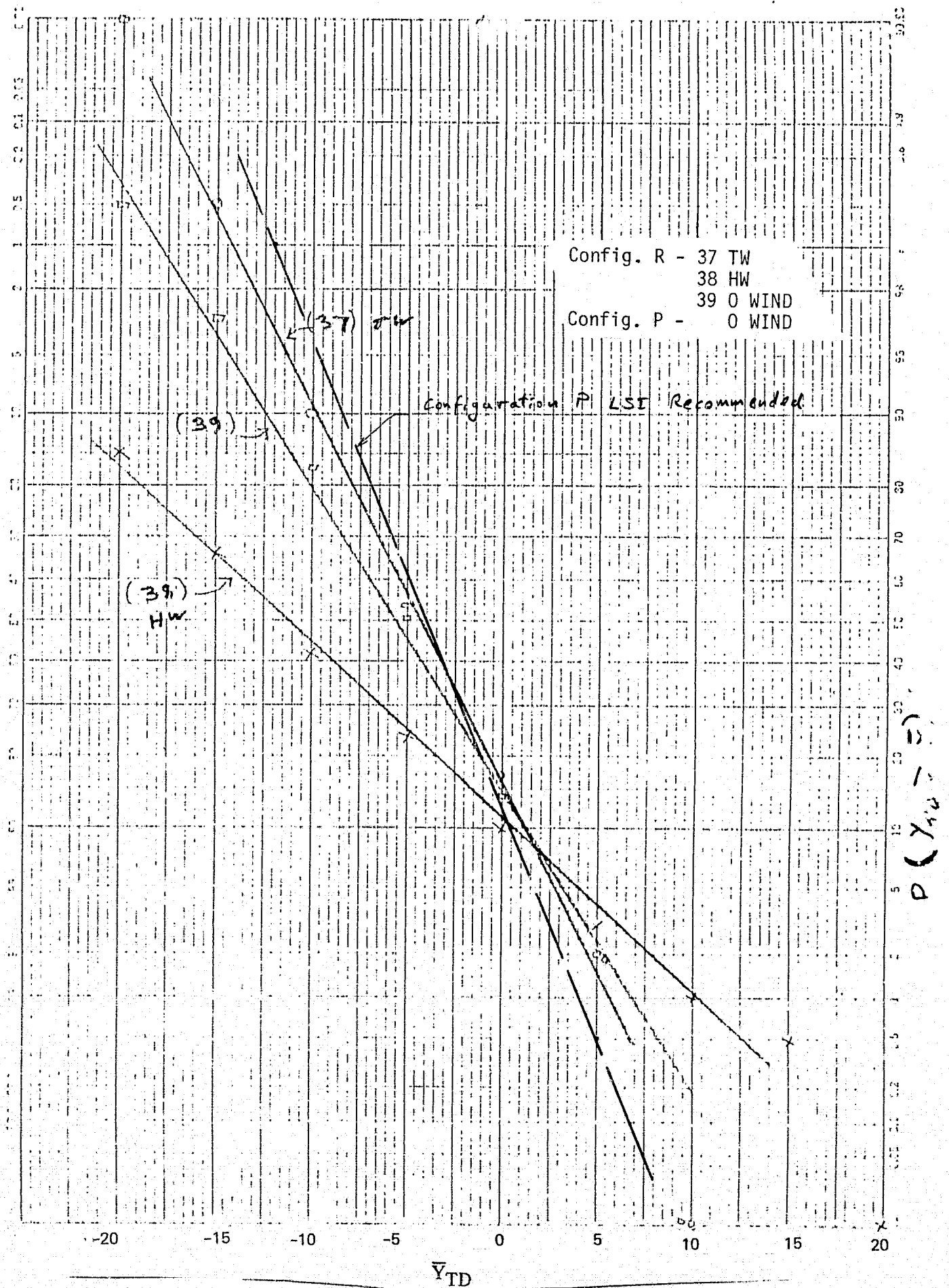


Figure C-11. Y_{TD} Distribution Comparison - R vs. P

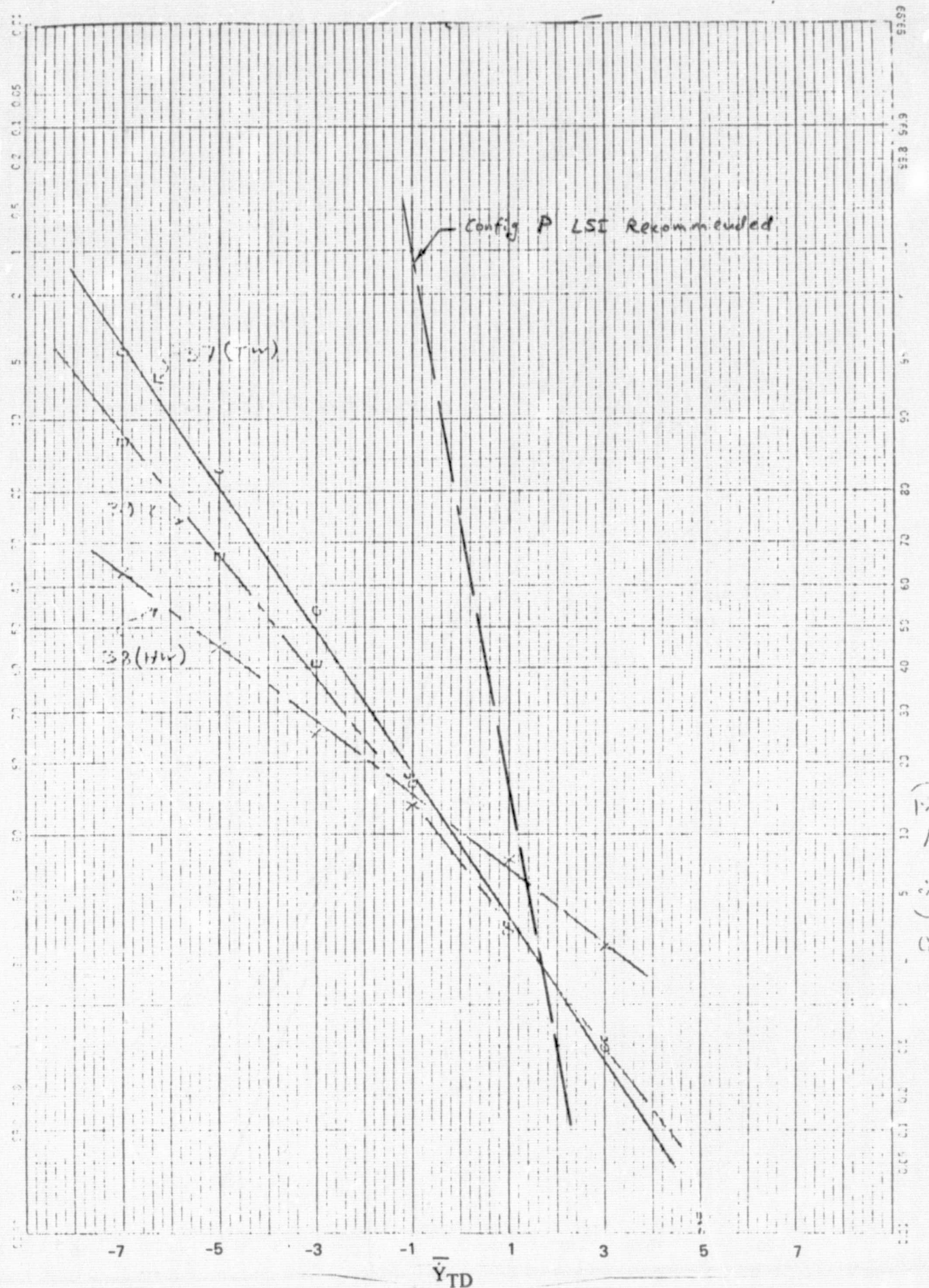


Figure C-12. \bar{Y}_{TD} Distribution Comparison — R vs. P

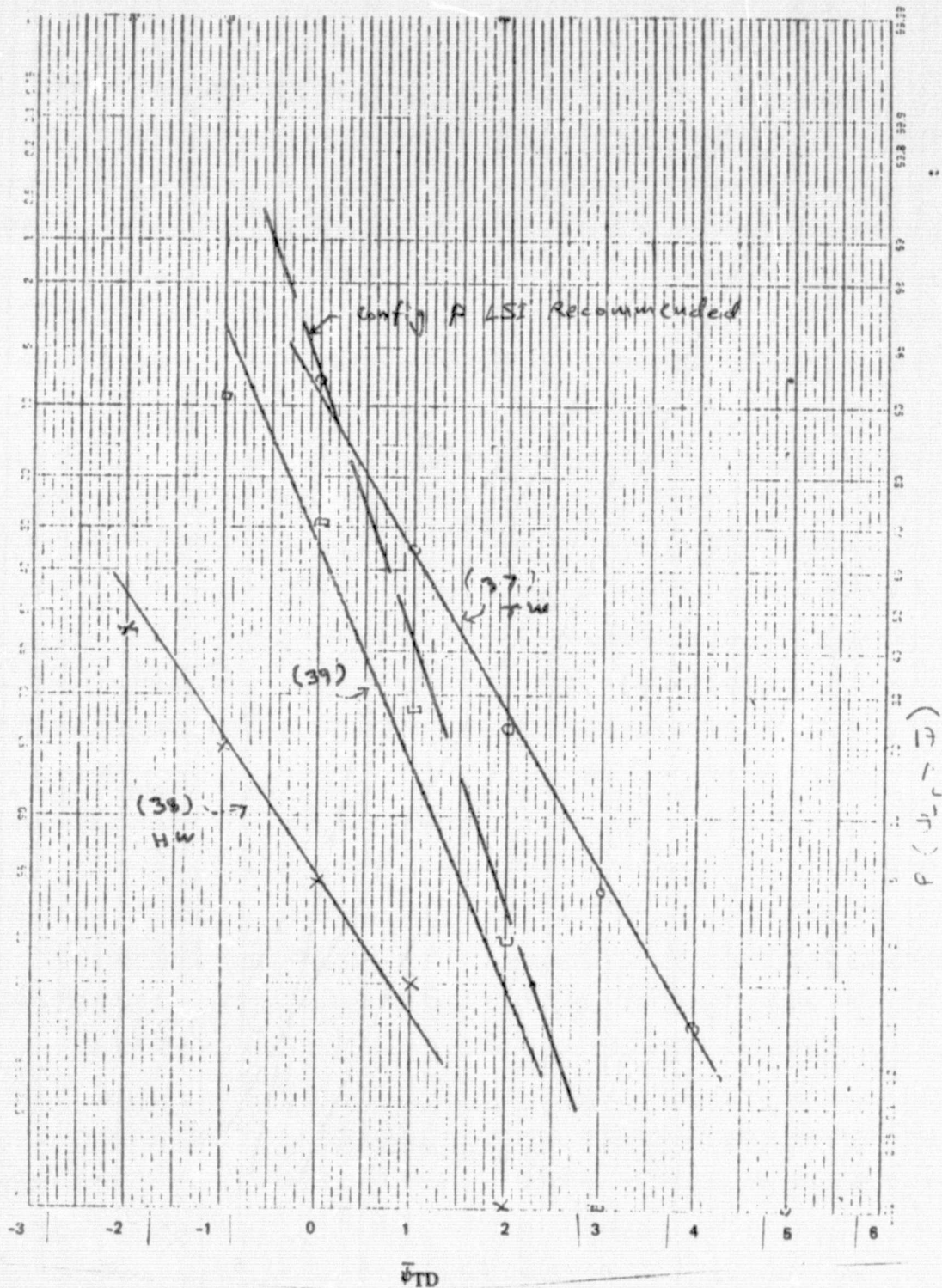


Figure C-13. ψ_{TD} Distribution Comparison R vs. P

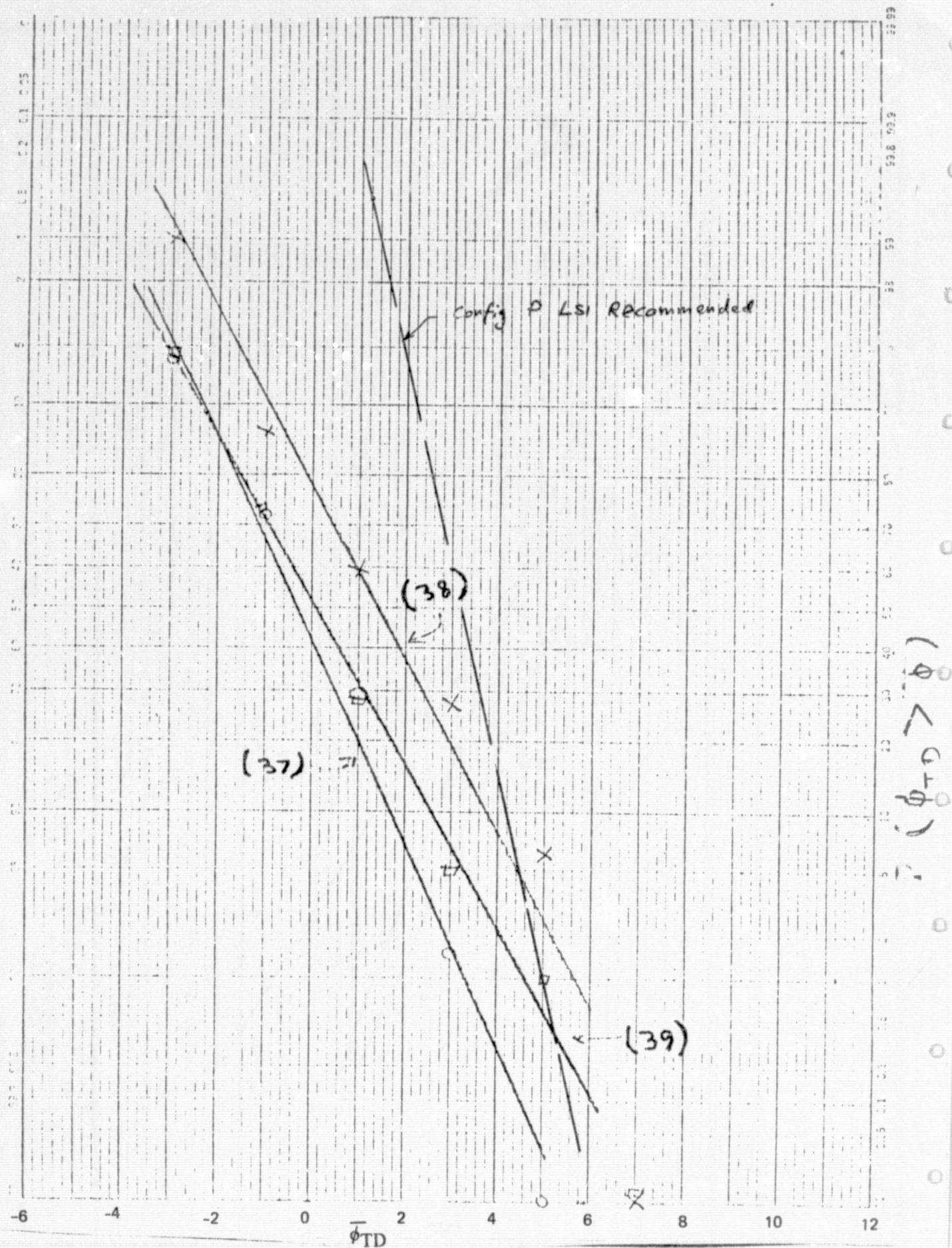


Figure C-14. ϕ_{TD} Distribution Comparison — R vs. P

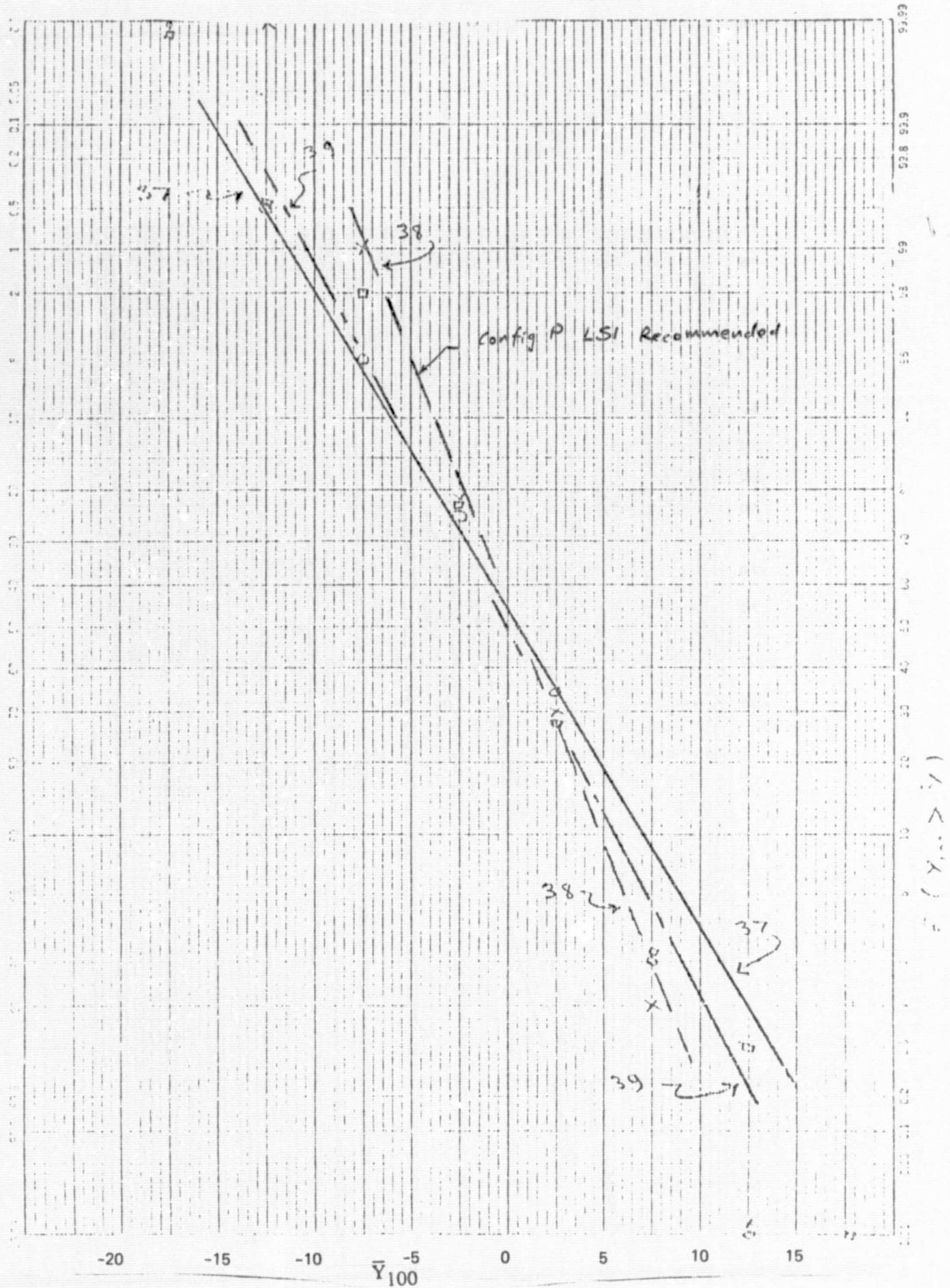


Figure C-15. Y_{100} Distribution Comparison - R vs. P

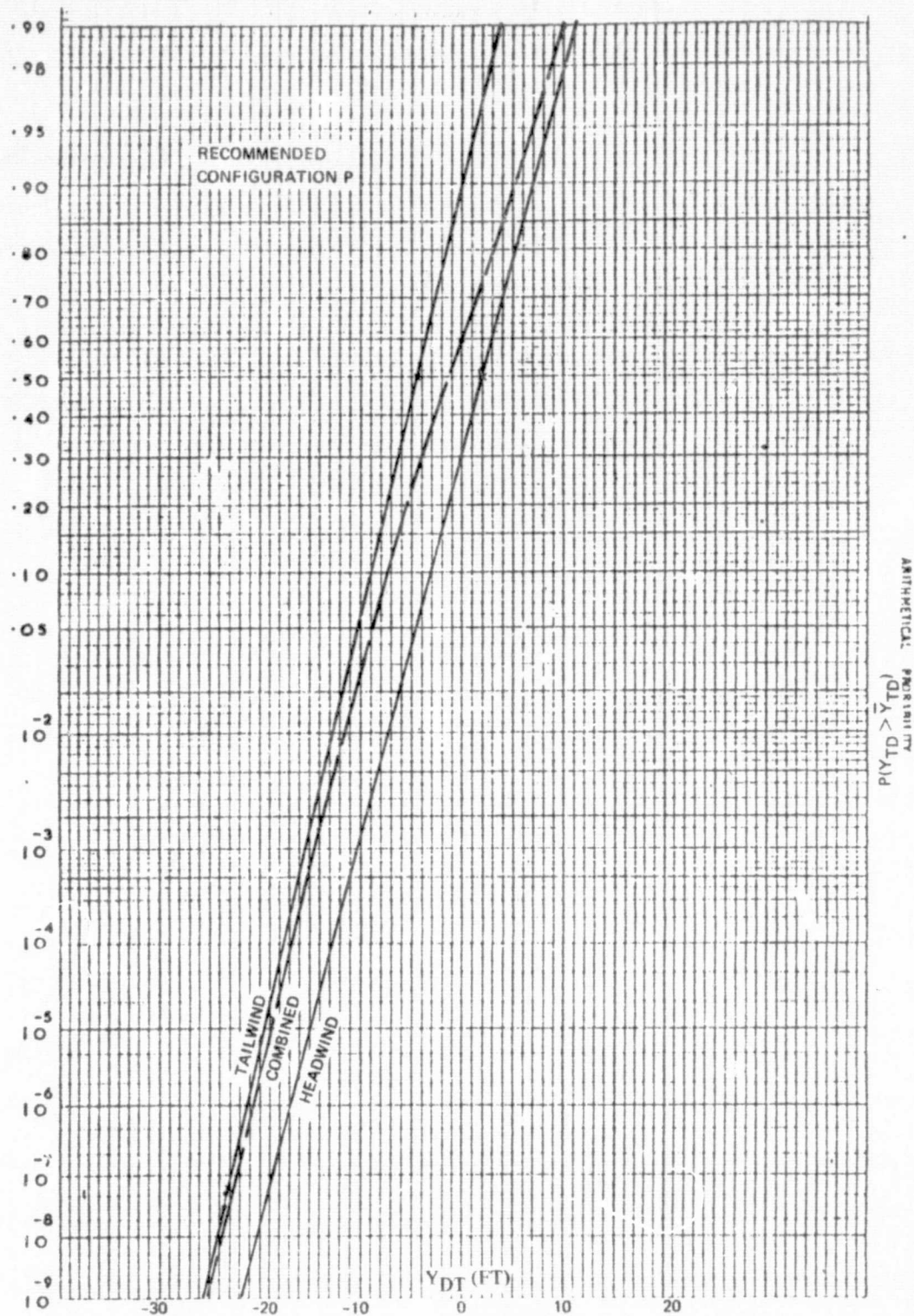


Figure C-16. Touchdown Lateral Distance Distribution — Stochastic Disturbances

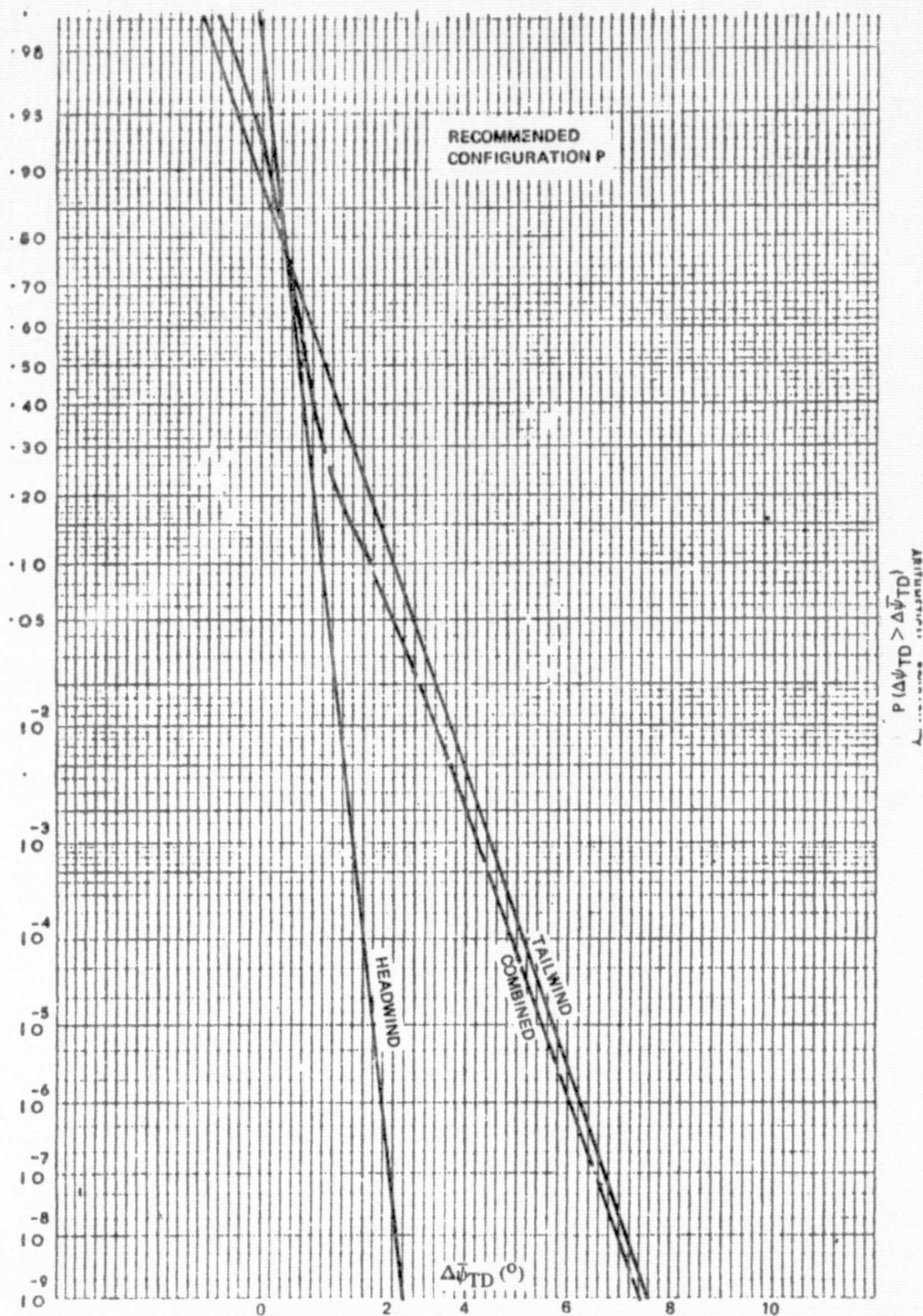


Figure C-17. Touchdown Heading Error Distribution — Stochastic Disturbances

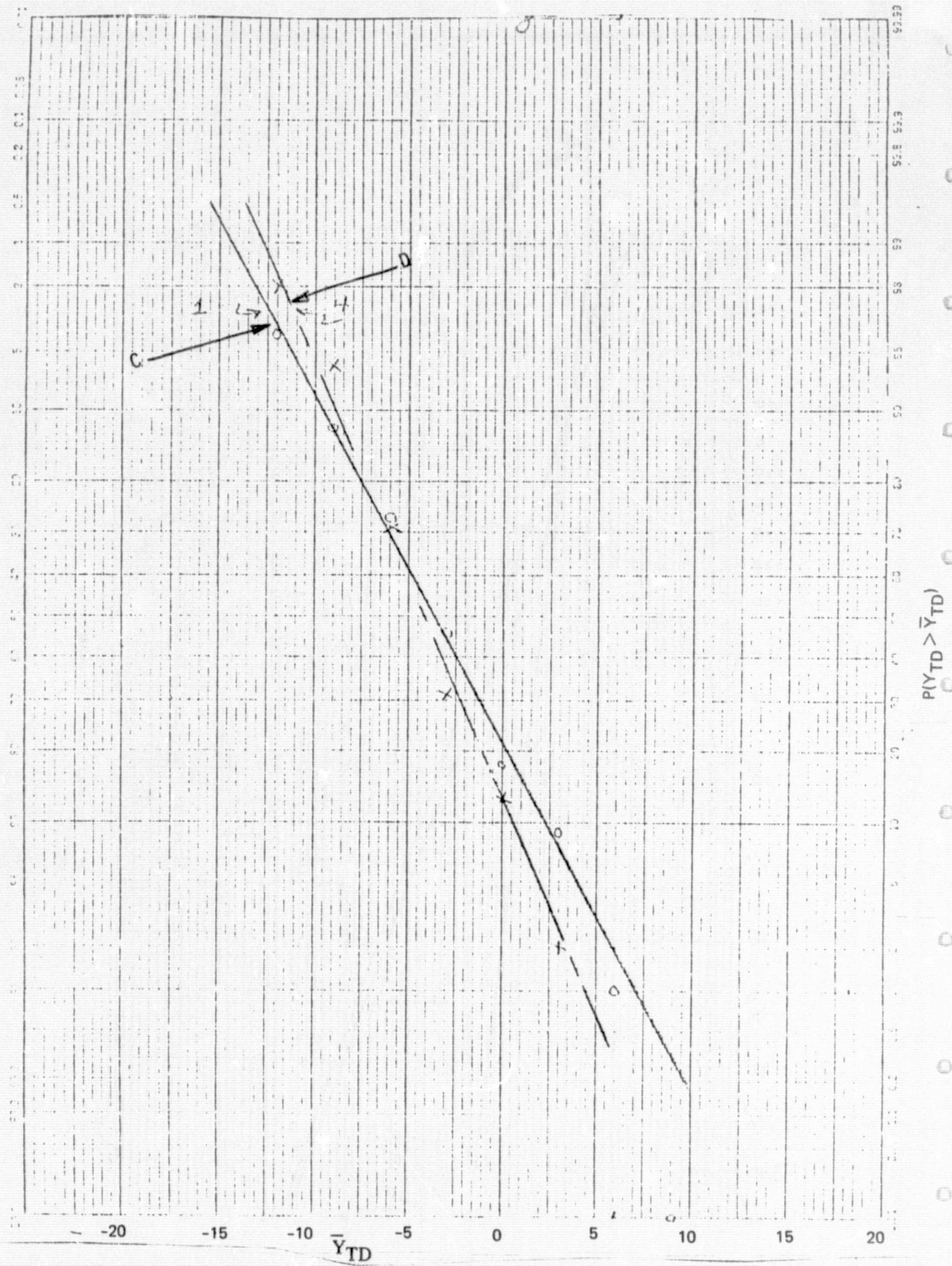


Figure C-18. Y_{TD} Distribution Comparison — C vs. D

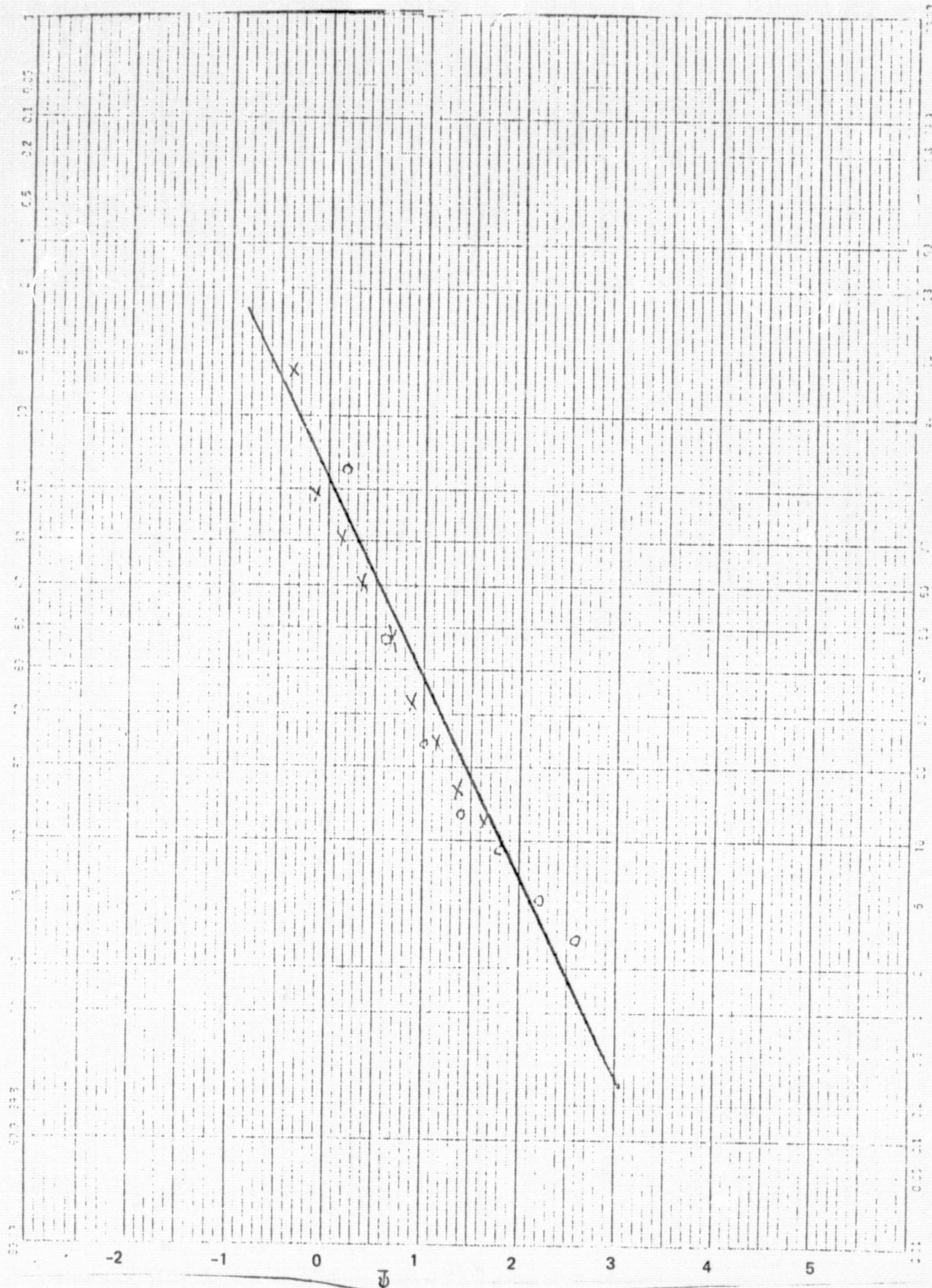


Figure C-19. ψ_{TD} Distribution Comparison - C vs. D

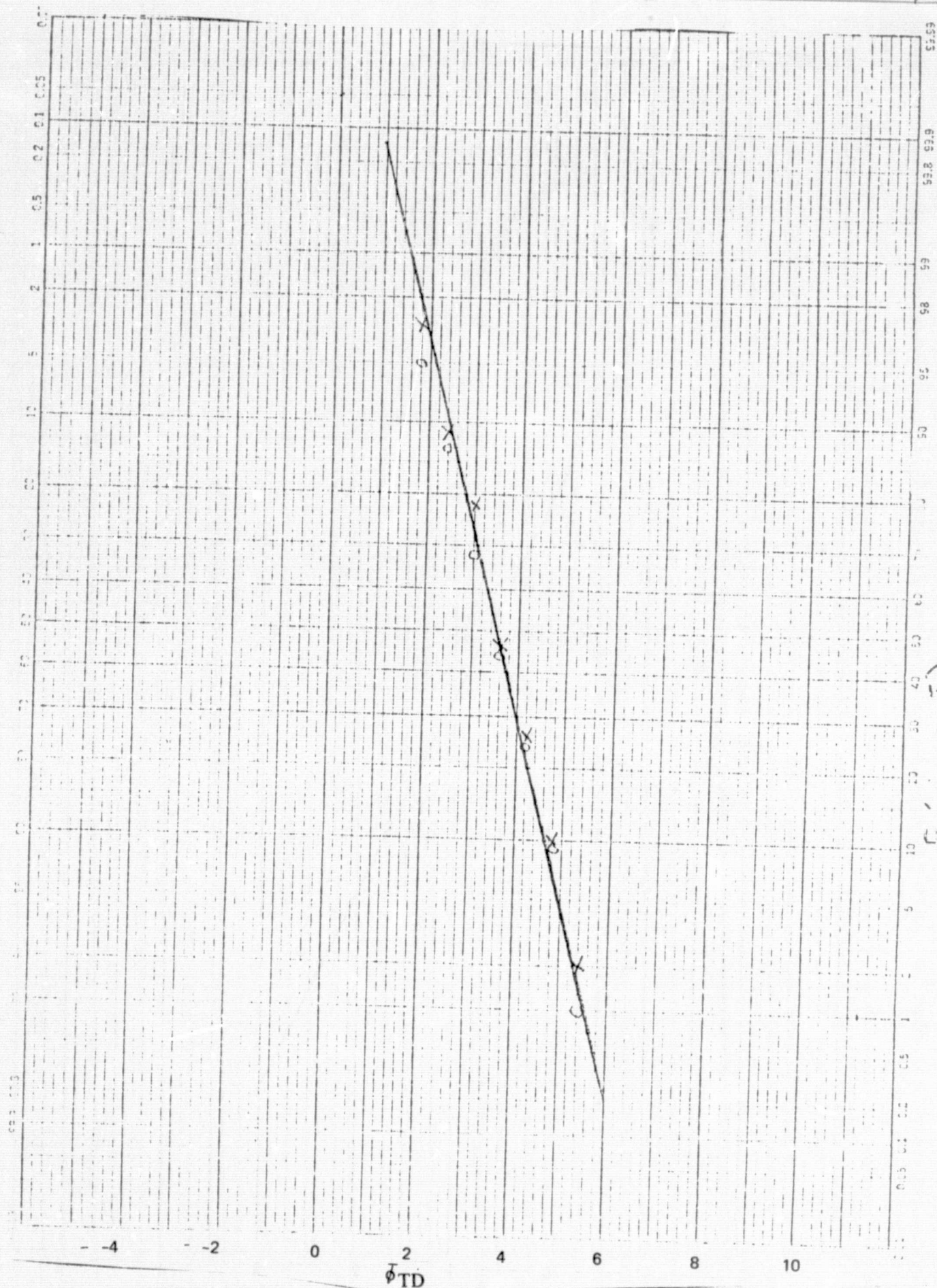


Figure C-20. ϕ_{TD} Distribution Comparison - C vs. D

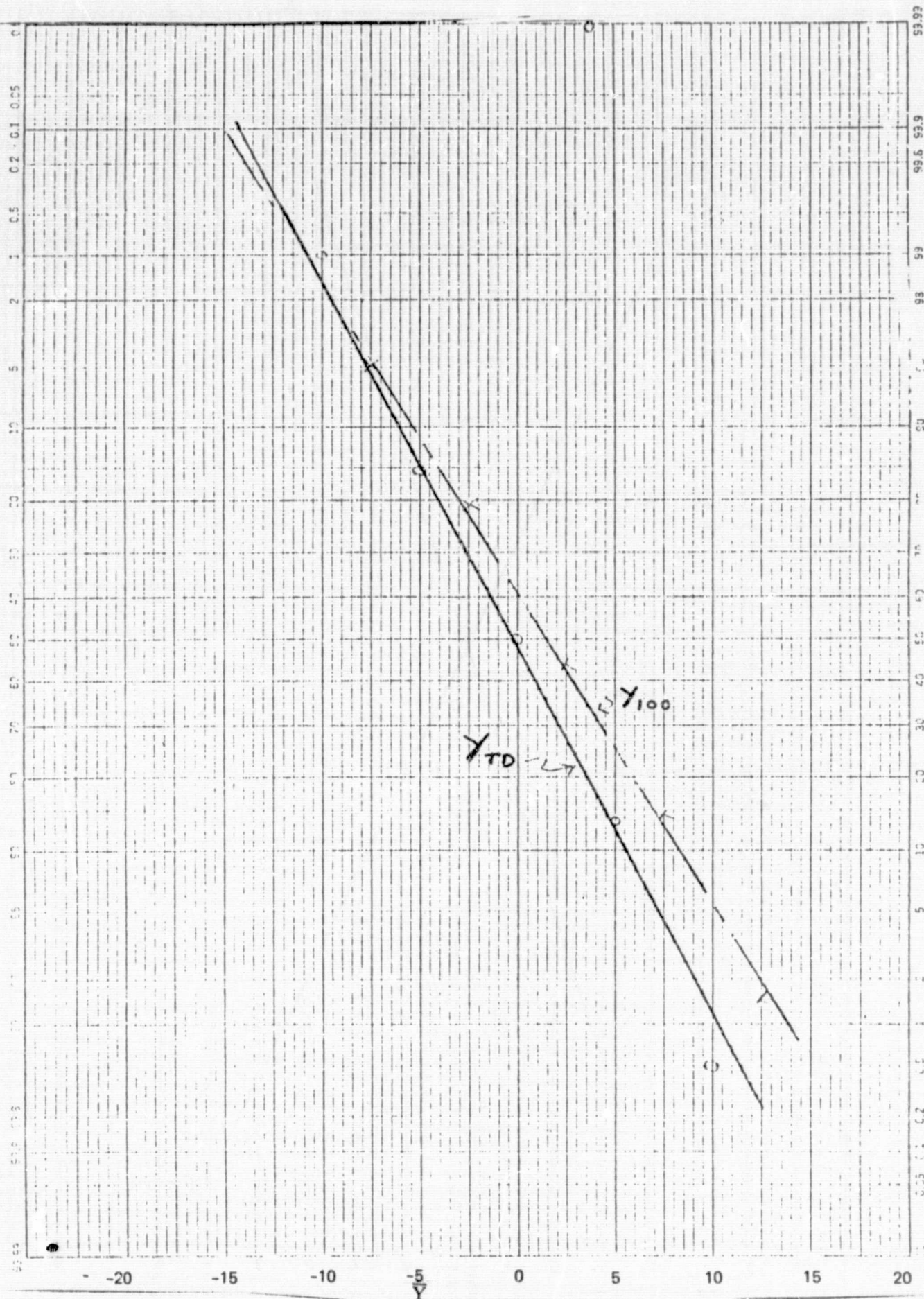


Figure C-21. Y_{TD} and Y_{100} Distributions — Configuration E

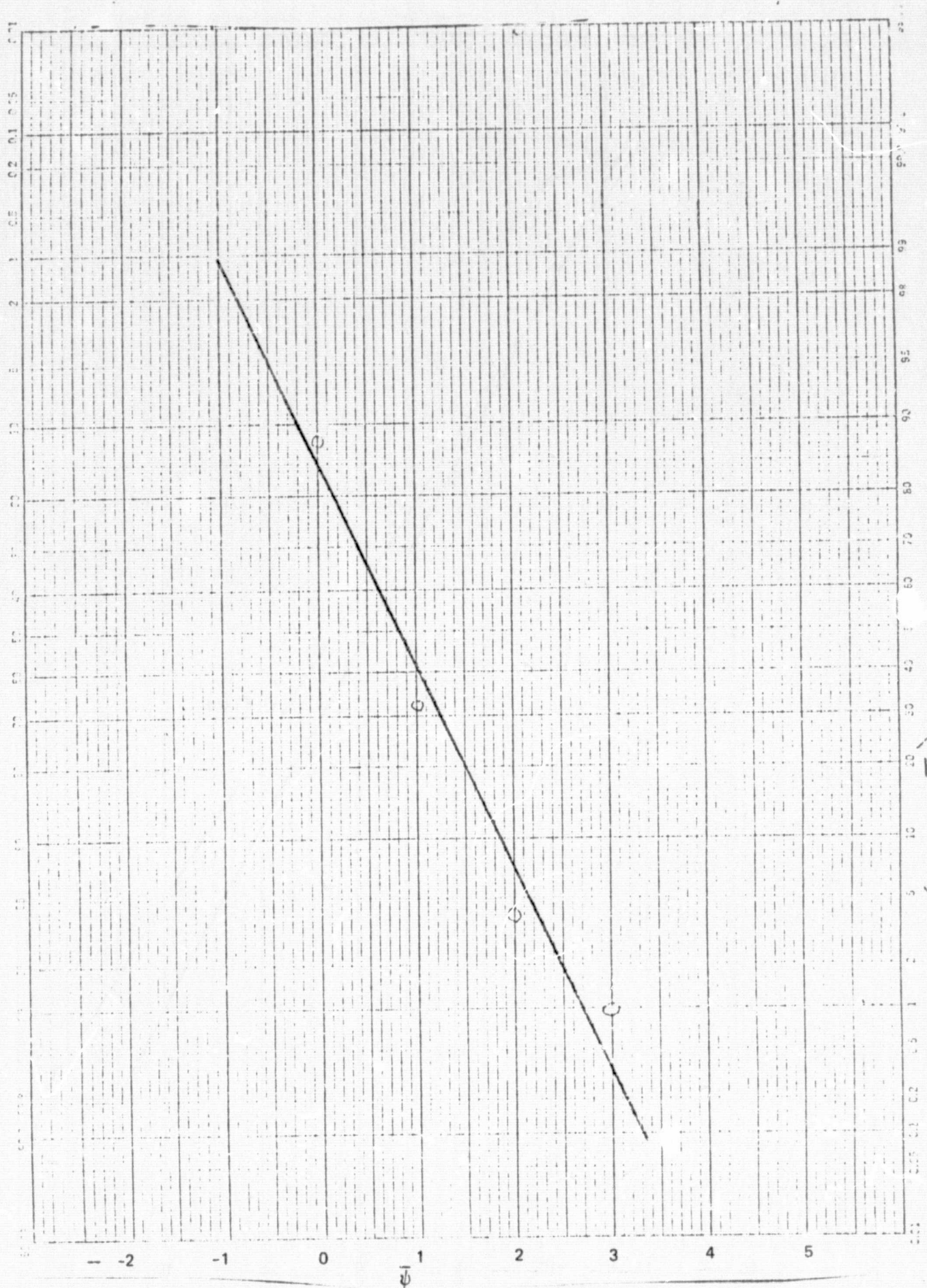


Figure C-22. ψ_{TD} Distribution — Configuration E

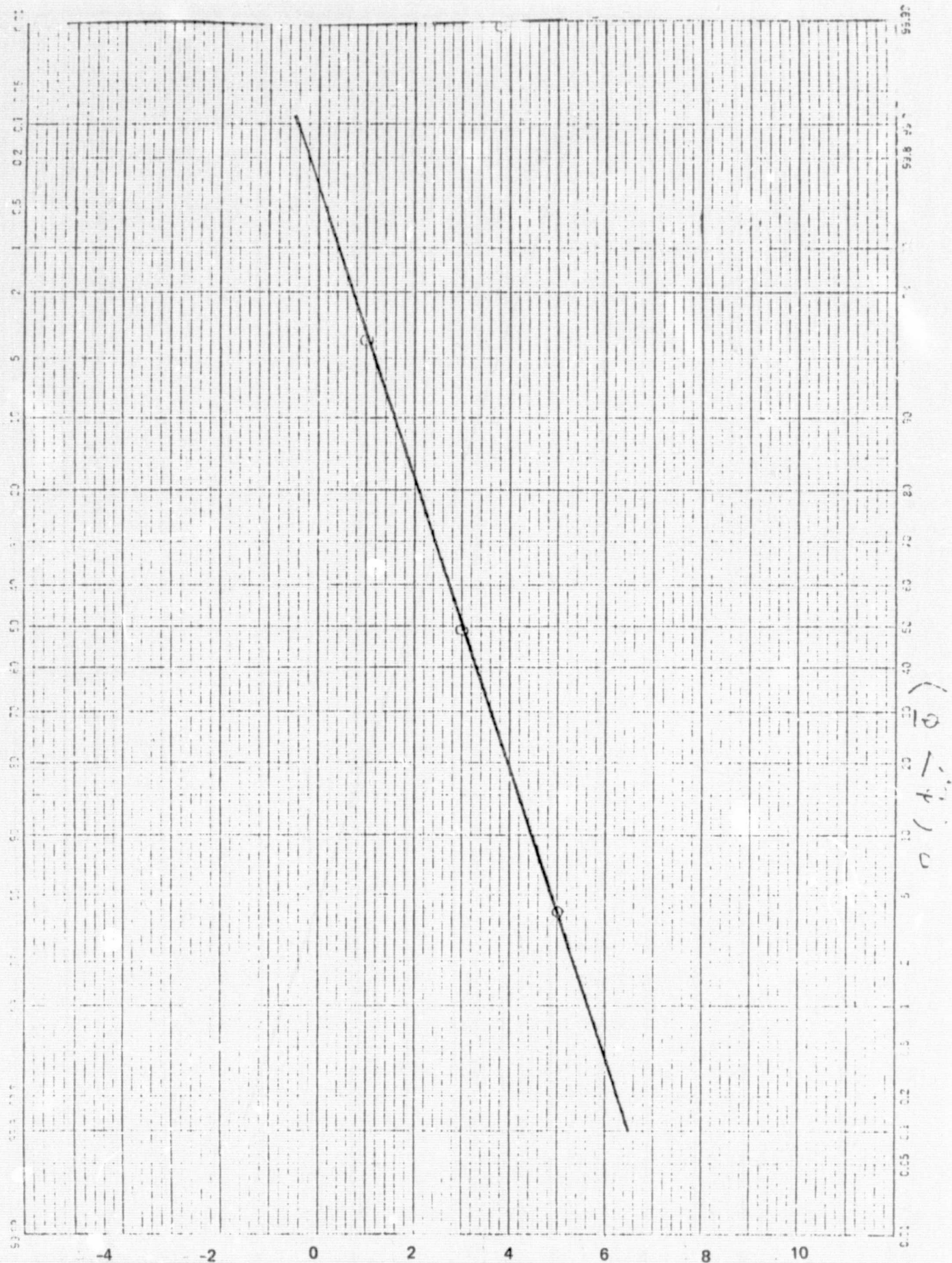


Figure C-23. ϕ_{TD} Distribution — Configuration E

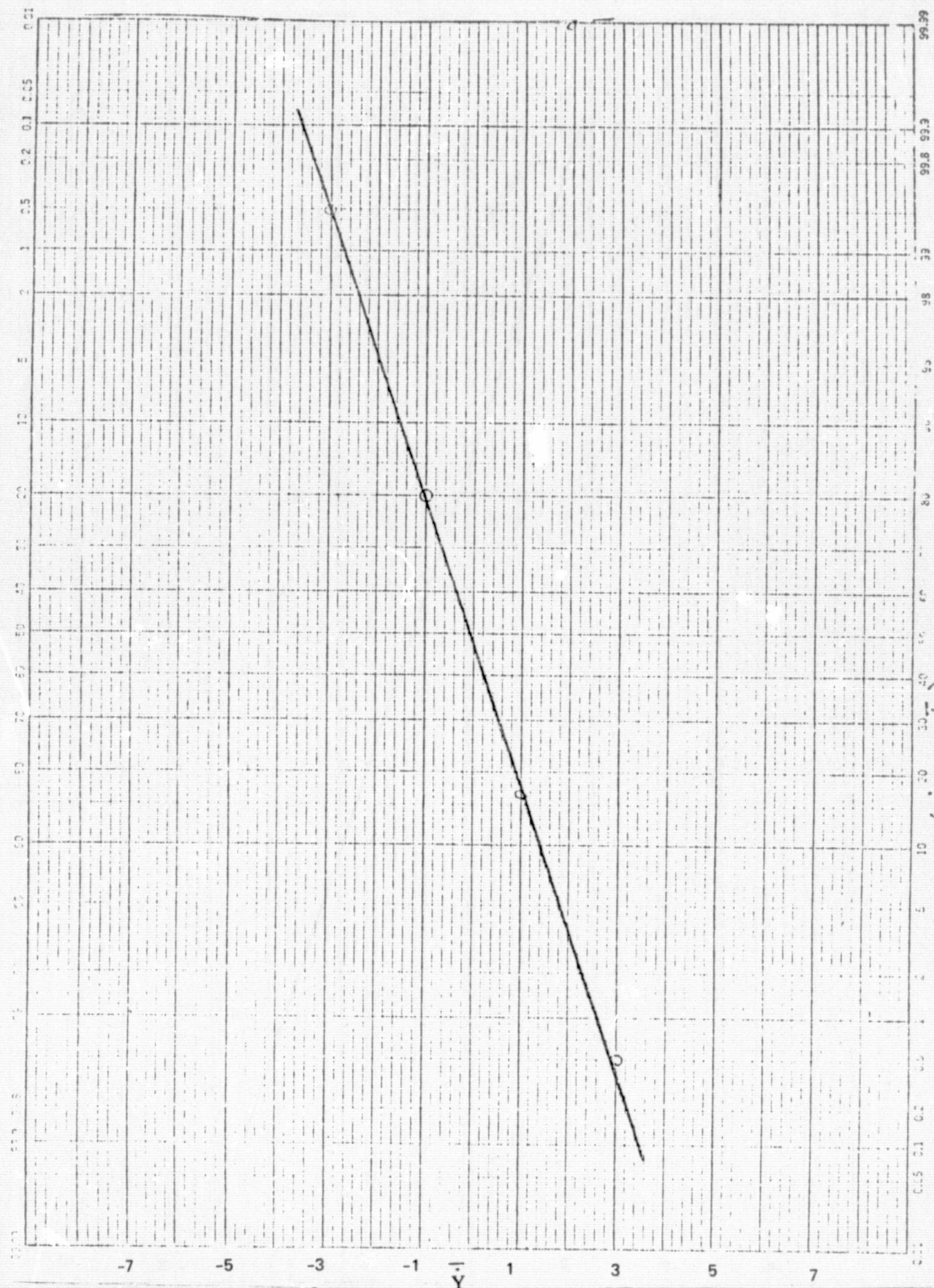


Figure C-24. Y_{TD} Distribution - Configuration E

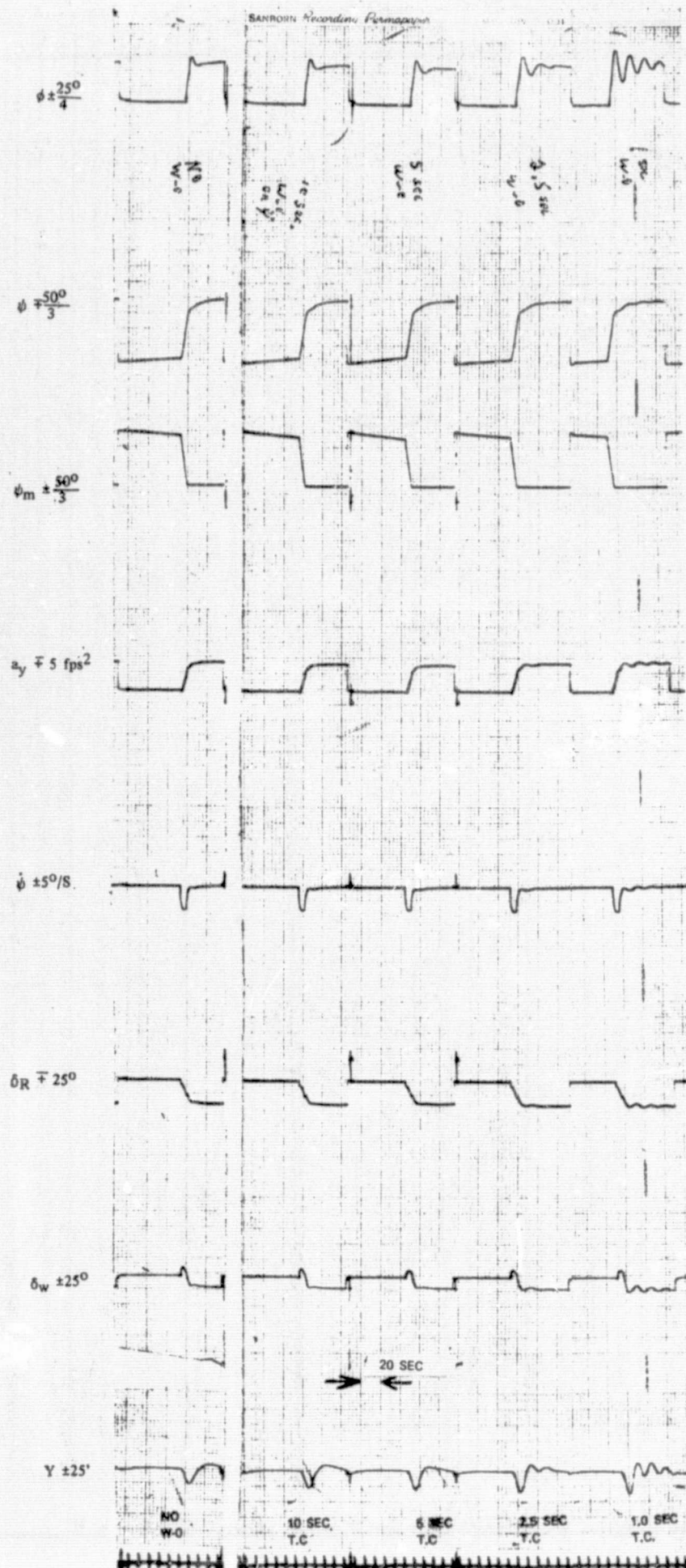


Figure C-25. Effect of Acceleration Washout Time Constant

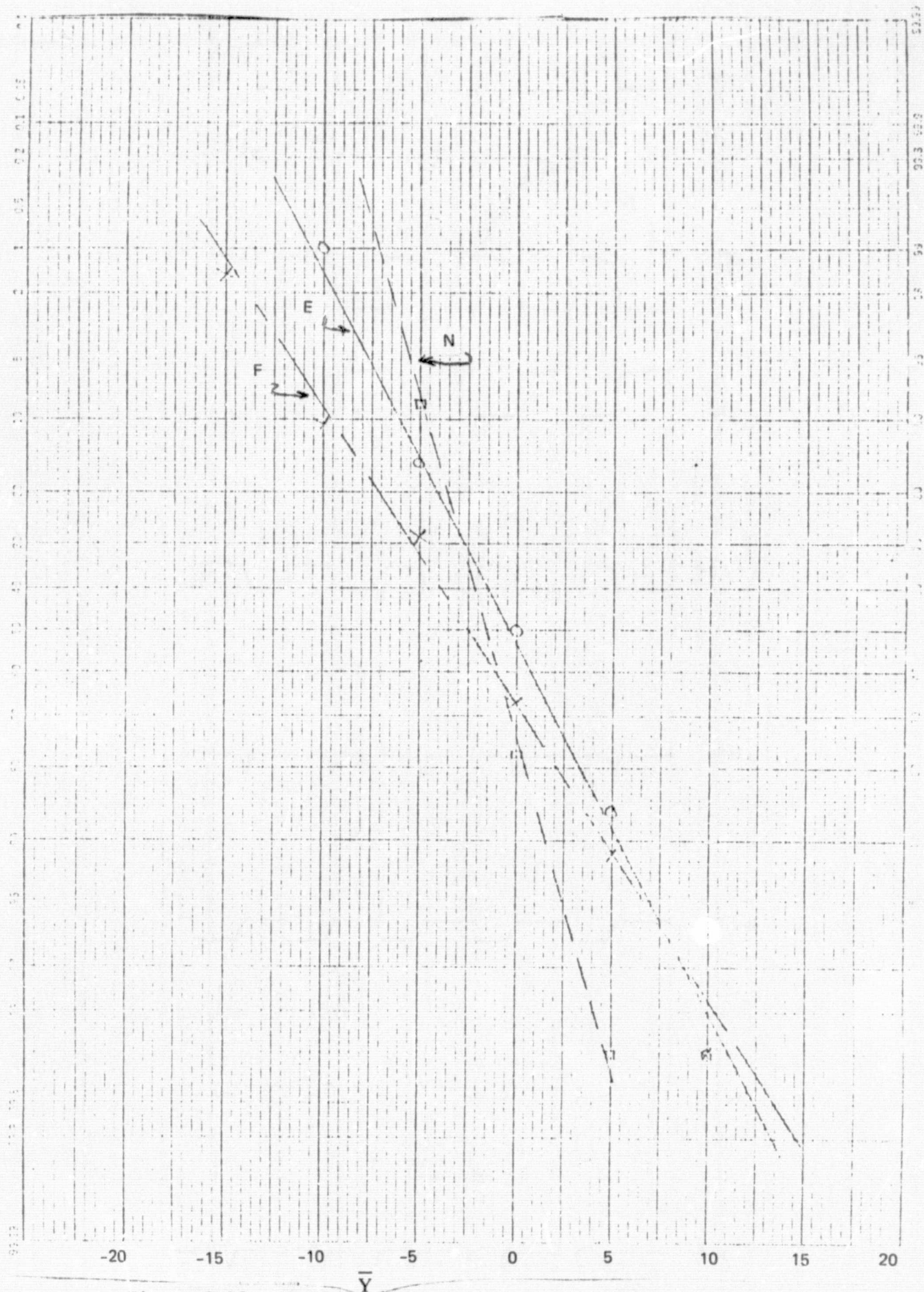


Figure C-26. Y_{TD} Distribution Comparison - E, F, & N

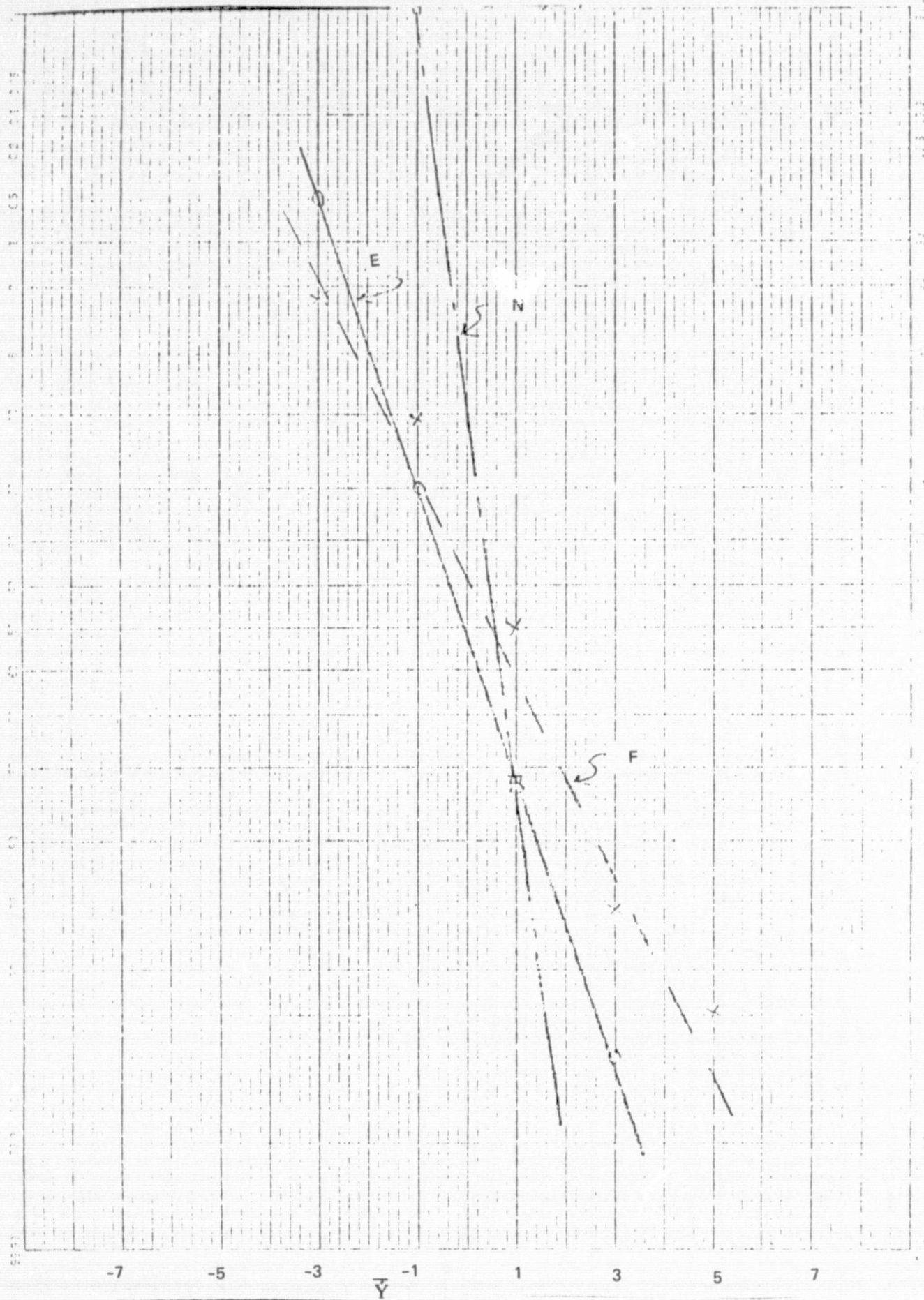


Figure C-27. Y_{TD} Distribution Comparison — E, F, & N

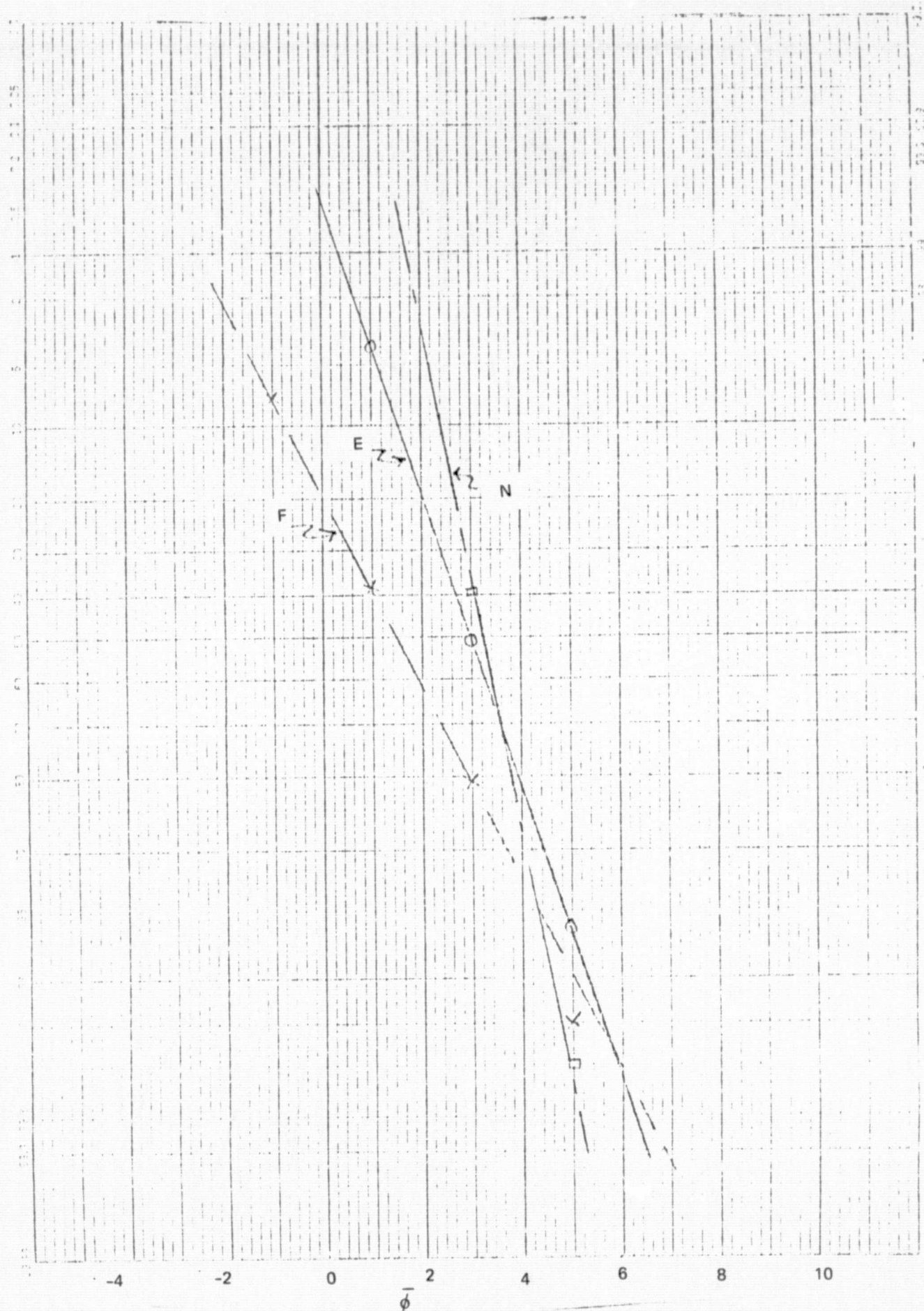


Figure C-28. ϕ_{TD} Distribution Comparison — E, F, & N

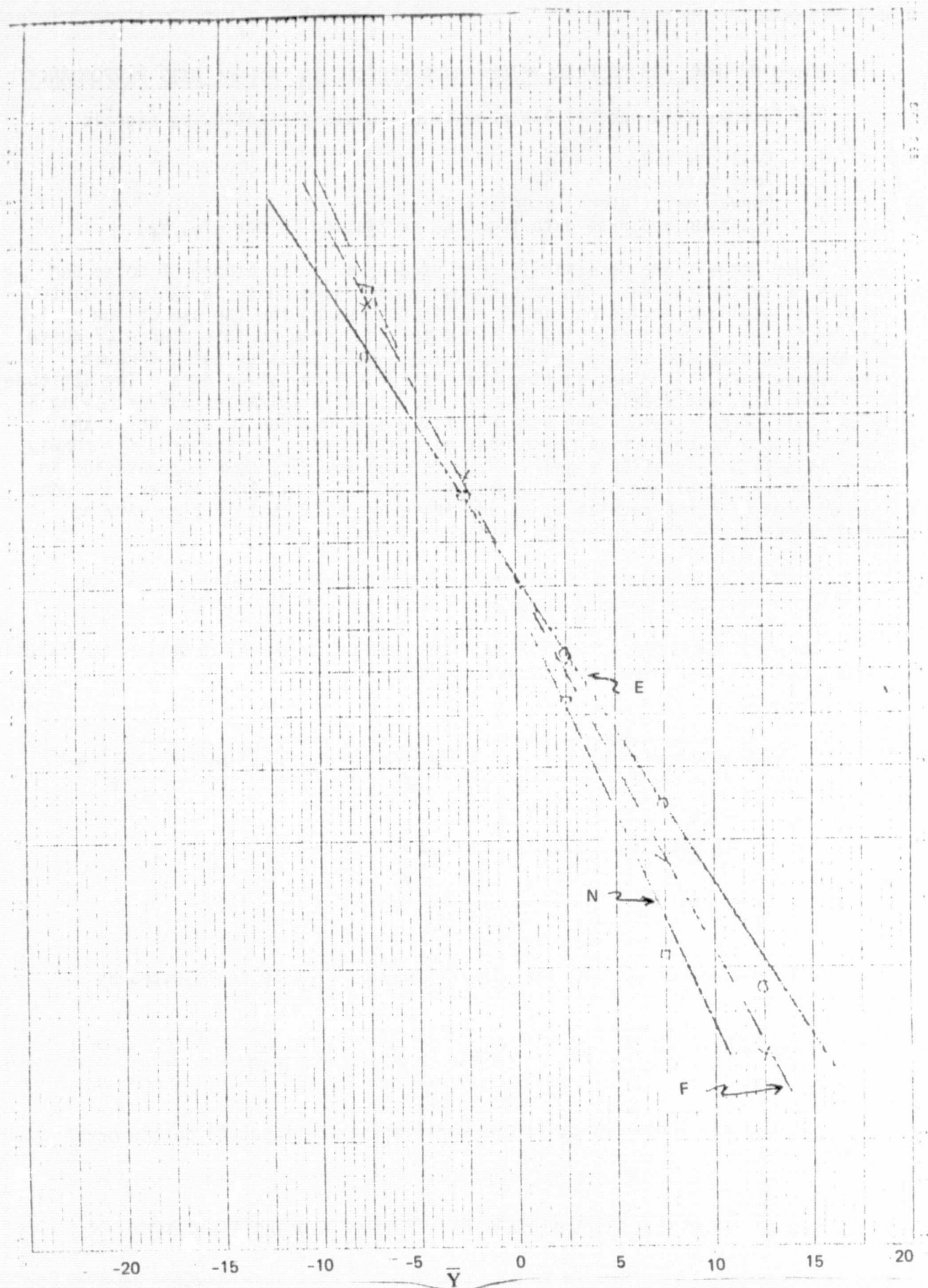


Figure C-29. Y_{100} Distribution Comparison — E, F, & N

DISCUSSION OF GYRO AND ACCELEROMETER ERROR EFFECTS ON LATERAL AXIS PERFORMANCE

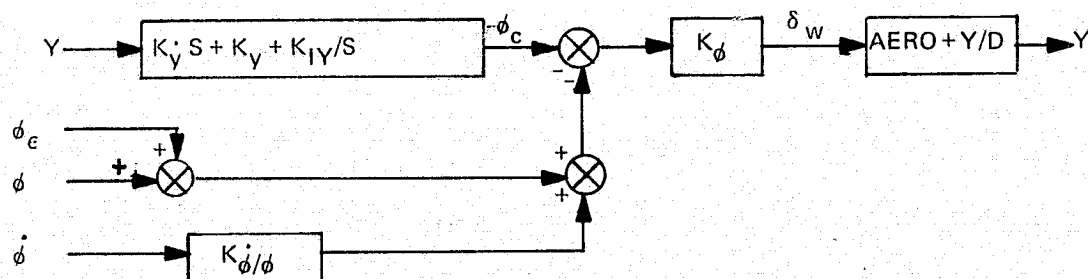
The lateral axis control law accepts as inputs the following signals:

1. Roll attitude
2. Roll rate
3. Runway axis lateral acceleration
4. Position and rate data from the navigation filter (Y_f, \dot{Y}_f)

These signals are necessarily corrupted by a finite amount of noise and errors of various kinds. The most commonly discussed noise is that associated with the localizer deviation signal and is the reason for the use of the navigation filter. The sensitivity of the autoland system to this source of noise is assessed with the simulation by applying random gaussian noise through the appropriate filter and summing this with the Y deviation data. The attitude, attitude rate, and acceleration signals are normally characterized as having a bias (null error). Slow time varying attitude errors due to gyro drift and erection to a false vertical also must be considered. Furthermore, the runway axis lateral acceleration signal, which is used for wing down compensation in align and for localizer signal augmentation in the navigation filter, includes signal product terms such as $a_x \Delta\psi$ and therefore will contain time varying error signals due to bias errors in either signal.

The following material will evaluate these errors quantitatively and a summary of the analysis will be offered at the end of this section.

Consider first the effect of roll gyro errors through the basic stabilization loop. The loc track mode may be described as follows:



With yaw damper active, the aircraft may be closely represented as

$$\delta_w \rightarrow \left[\frac{\phi}{\delta_w} \right] \rightarrow \left[\frac{g}{57.3} \right] \rightarrow \ddot{Y} \quad \text{where} \quad \frac{\dot{\phi}}{\delta_w} = \frac{0.42}{s + 0.612}$$

Closing all loops ($\phi, \dot{\phi}, Y$) and considering the input to be the error signal, ϕ_e :

$$\frac{Y}{\phi_e} = \frac{1.65s}{(s + 0.02)(s + 0.668)(s + 2.5)(s^2 + 0.365s + 0.05)}$$

The signal gains used are:

$$K_{\phi} = 7.0 \text{ deg/deg}$$

$$K_y = 0.06 \text{ deg/ft}$$

$$K_{\dot{y}} = 0.5 \text{ deg/fps}$$

$$K_{Iy} = 0.001$$

The time history for a step input is plotted in Figure C-30. In reality it is more reasonable to assume that the gyro error existed before loc track mode began (i.e., before the integrator is switched on). Assuming a steady state condition has been achieved, the roll error will be cancelled by the Y_f error signal, i.e., $K_y Y_f = \phi_e$, or $Y_f = 16.7\phi_e$.

After loc track is initiated, the error will be removed slowly by the Y integral term. Since the movement is very slow, $\dot{\phi}$ can be assumed to be zero and

$$K_y Y + K_{\dot{y}} \dot{Y} + K_{Iy} \int Y \cdot dt = \phi_e$$

which is equivalent to

$$Y = \frac{SY_0 + 2S\phi_e}{s^2 + 0.12s + 0.002}$$

The corresponding time domain expression for $\phi_e = \text{unit step}$ is

$$Y = \left(20.88e^{-0.02t} - 4.18e^{-0.1t} \right) \phi_e$$

If a minimum time between loc track and touchdown is assumed to be that corresponding to a 10 knot tailwind at $u_0 = 70$ knots and mode initiation at 500 feet altitude, the minimum time is about 30 seconds. At $t = 30$, y in the above expression becomes $11.25\phi_e$.

Available gyro data suggests a worst case (4.5 sigma) number for verticality error of 0.6 degrees and a worst case error of 1.0 degree due to false erection. Assuming half of the erection error will be removed prior to touchdown, the estimated worst case gyro error is found to be 0.78 degrees (by combining the verticality error and erection error on an RSS basis). At 11.25 ft/deg, the resulting 4.5 sigma error in lateral deviation at touchdown is 9.0 feet.

As a point of interest, the frequency response shows a peak gain of 18 to 1 at a frequency of $\omega = 0.071$. Three dB bandwidth is approximately 0.014 rad/sec to 0.15 rad/sec. The lower breakpoint is controlled by the y integrator to y displacement gain ratio of 0.017 and the upper breakpoint

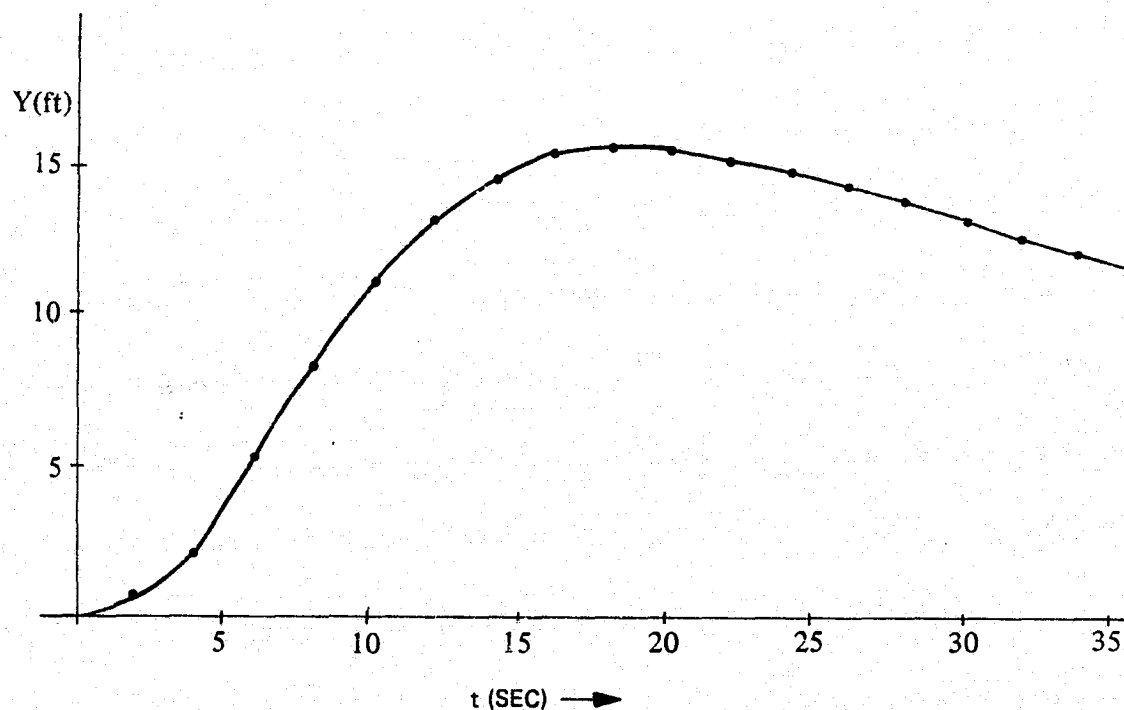


Figure C-30. Response to Step $\phi_E = 1.0^\circ$ in Loc Track Mode

by the ratio $K_y/K_\phi = 0.12$. To attempt to reduce this sensitivity in this frequency range by adding a washout in the roll attitude signal path would require a washout time constant between 0.02 and 0.1. Unfortunately, simulation data indicate this arrangement to significantly reduce the path damping. Similarly, attempting to move the breakpoints by changing the gain ratios undesirably alters the dynamic characteristics of the localizer track performance.

The most likely source of time varying roll attitude error signal is the erection cycle. In loc track mode, there should be no sustained turn to induce false erection. The y offset resulting from a failure-induced erection motion of 2 degrees per minute will introduce approximately 10 feet of error in 30 seconds. This assumes that a potential pitch erection error caused by a decelerating approach does not transfer to roll due to significant, close-in heading changes.

Roll rate gyro nulls will have the same effect as roll gyro offsets and thus can be considered as a component of ϕ_E in the preceding expression. The remaining error source is \dot{Y}_r through its effect on Y_f , \dot{Y}_f and on the align compensation signal.

The effect on the nav filter outputs will be assessed first.

$$\dot{Y}_f = \frac{S(S + K_1) \ddot{Y}_R}{S^3 + K_1 S^2 + K_2 S + K_3} + f_1(S) Y_{Raw}$$

$$Y_f = \frac{S \ddot{Y}_R}{S^3 + K_1 S^2 + K_2 S + K_3} + f_2(S) Y_{Raw}$$

Present values being used for the nav filter coefficients are:

$$K_1 = 0.8$$

$$K_2 = 0.24$$

$$K_3 = 0.032$$

The ϕ command resulting from the \ddot{Y}_r error input through the nav filter is

$$\phi_c = 0.5 \dot{Y}_f + 0.06 Y_f$$

Using the preceding relationships for \dot{Y}_f , and Y_f , roll command error is:

$$\phi_e = \frac{[0.5 S (S + 0.8) + 0.06S] \ddot{Y}_{Re}}{(S + 0.4)(S^2 + 0.4 S + 0.08)}$$

The y response to ϕ_{cmd} has been earlier determined. Combining the two transfer functions:

$$\frac{Y}{\ddot{Y}_{Re}} = \frac{0.825 S^2 (S + 0.92)}{(S + 0.4)(S + 0.02)(S + 0.668)(S + 2.5)(S^2 + 0.365 S + 0.05)(S^2 + 0.4 S + 0.08)}$$

The response to a unit step input is given in Figure C-31. The frequency plot of y/\ddot{y} for the loc track mode indicates that a gain of 30 dB exists between $\omega = 0.1$ and 0.25. This could present a problem if error sources in this frequency range are present. This possibility is considered in a subsequent paragraph.

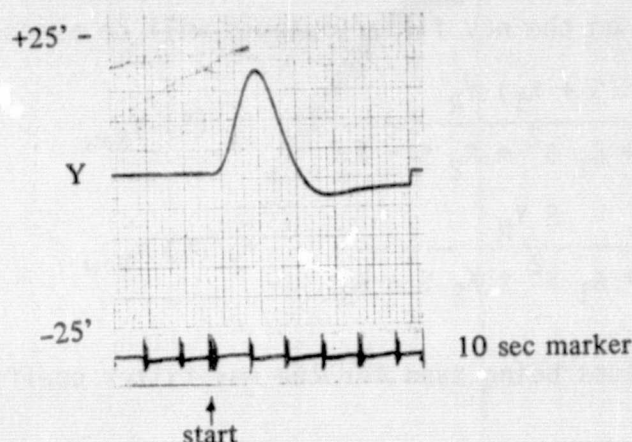


Figure C-31. Nav Filter Response to Step Acceleration Input

The \ddot{Y}_r error also affects the aircraft through the align compensation path.

In this case

$$\phi_c = 1.78 \ddot{Y}_{R_e} / (S + 1)$$

A different relationship for Y/ϕ_c exists in align because the rate gain is increased to $0.95^\circ \phi^c / \text{fps } \dot{Y}$.

Combining the new Y/ϕ_c with ϕ_c/\ddot{Y}_{R_e} from above yields

$$\frac{Y}{\ddot{Y}_{R_e}} = \frac{2.94S}{(S + 1)(S + 2.66)(S^2 + 0.068S + 0.0012)(S^2 + 0.822S + 0.518)}$$

The corresponding step response is shown in Figure C-32. The same upset is recorded in Figure C-33 with 15 knot crosswind. These two figures also indicate the results of using a high pass filter (1st order with $\tau = 10$ sec) in the \ddot{Y}_r signal path. Marked improvement is achieved in this manner and if the filter is upstream of the align switch the bias can be nearly eliminated prior to align.

Figure C-25 provides simulation data of the system response that results when the \ddot{Y}_r align compensation signal is washed out at various time constants. (To allow more time per run for evaluation, the simulation is not stopped when zero altitude is reached.) No performance degradation is apparent for a time constant of 10 seconds or greater.

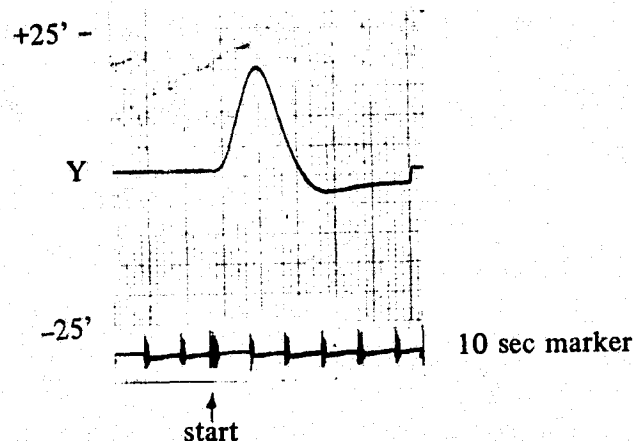


Figure C-31. Nav Filter Response to Step Acceleration Input

The \ddot{Y}_r error also affects the aircraft through the align compensation path.

In this case

$$\phi_C = 1.78 \ddot{Y}_{R_E} / (S + 1)$$

A different relationship for Y/ϕ_E exists in align because the rate gain is increased to $0.95^\circ \phi^C / \text{fps } \dot{Y}$.

Combining the new Y/ϕ_C with ϕ_C/\ddot{Y}_{R_E} from above yields

$$\frac{Y}{\ddot{Y}_{R_E}} = \frac{2.94S}{(S + 1)(S + 2.66)(S^2 + 0.068S + 0.0012)(S^2 + 0.822S + 0.518)}$$

The corresponding step response is shown in Figure C-32. The same upset is recorded in Figure C-33 with 15 knot crosswind. These two figures also indicate the results of using a high pass filter (1st order with $\tau = 10$ sec) in the \ddot{Y}_r signal path. Marked improvement is achieved in this manner and if the filter is upstream of the align switch the bias can be nearly eliminated prior to align.

Figure C-25 provides simulation data of the system response that results when the \ddot{Y}_r align compensation signal is washed out at various time constants. (To allow more time per run for evaluation, the simulation is not stopped when zero altitude is reached.) No performance degradation is apparent for a time constant of 10 seconds or greater.

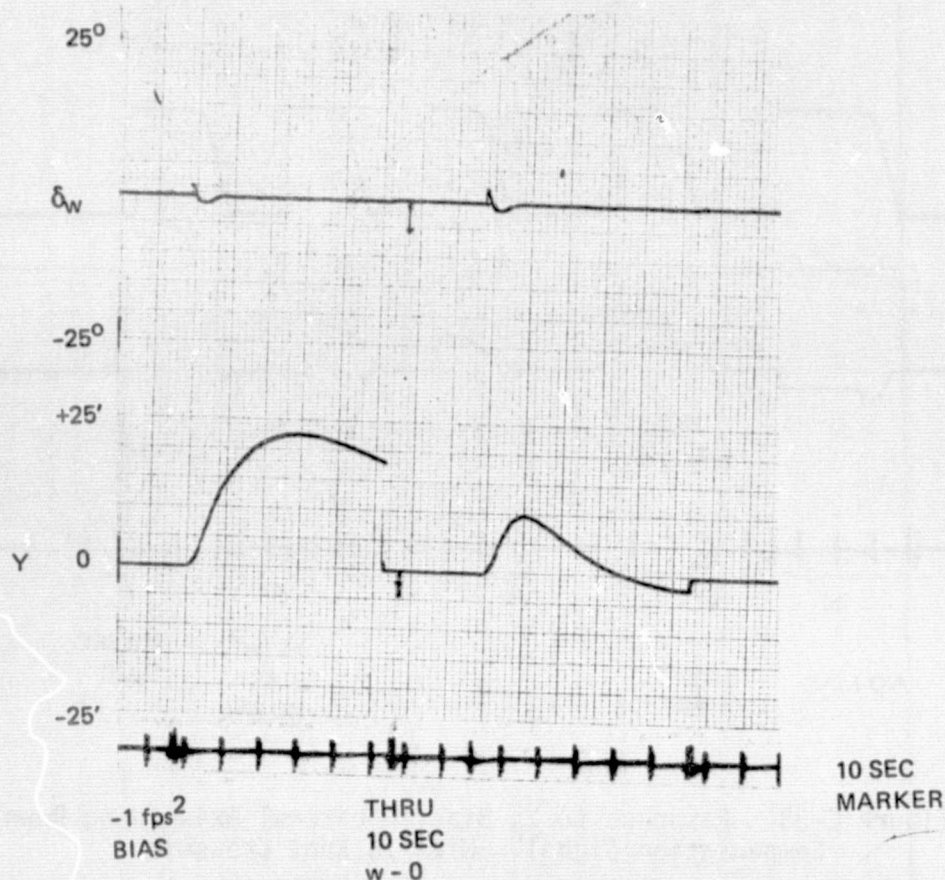


Figure C-32. Response to \ddot{Y}_R Bias in Lateral Axis "Wing Down" Compensation Signal - No Wind

However, if the \ddot{Y}_R signal contains significant error components within the bandpass defined by the 0.1 radian/sec highpass and the 1 radian/sec low pass filters, the response could be unacceptable. The content of the \ddot{Y}_R signal is considered in the following pages:

$$\ddot{Y}_R \cong a_x \cos \theta \sin \Delta\psi + a_y \cos \phi \cos \Delta\psi + a_z (\cos \phi \sin \theta \sin \Delta\psi - \sin \phi \cos \Delta\psi)$$

For small angles (expressed in radians)

$$\ddot{Y}_R \cong a_x \Delta\psi + a_y + a_z \theta \Delta\psi - a_z \phi \cong a_x \Delta\psi + a_y - a_z \phi$$

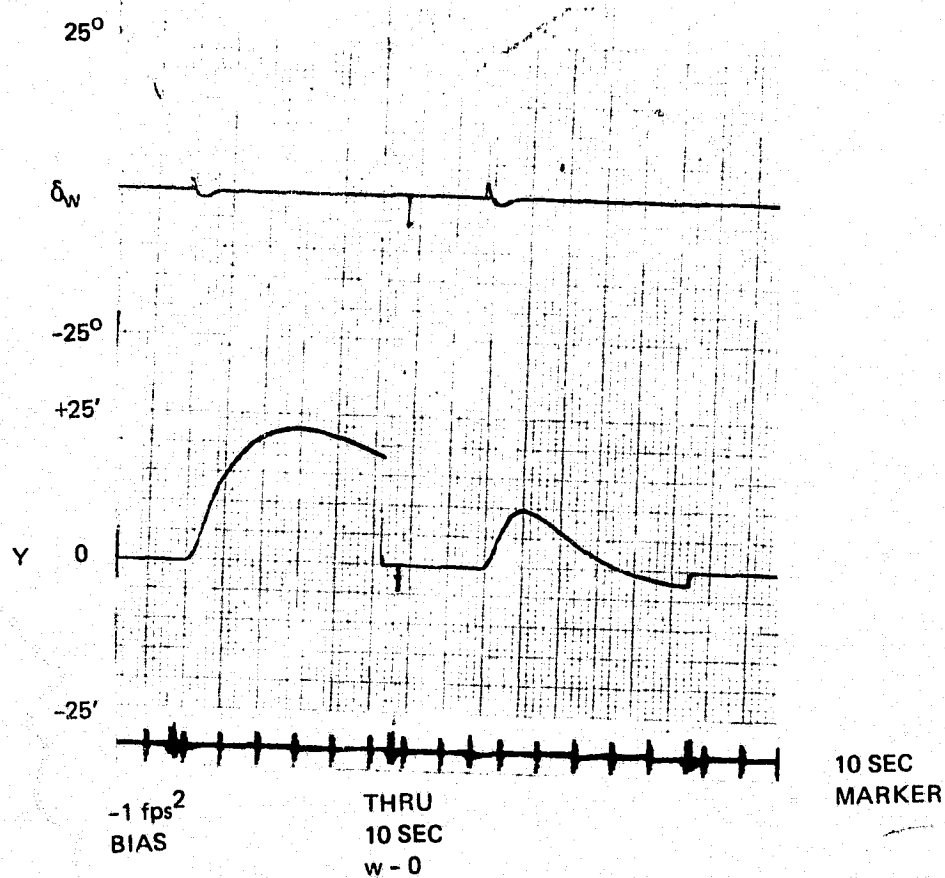


Figure C-32. Response to \ddot{Y}_R Bias in Lateral Axis "Wing Down" Compensation Signal - No Wind

However, if the \ddot{Y}_R signal contains significant error components within the bandpass defined by the 0.1 radian/sec highpass and the 1 radian/sec low pass filters, the response could be unacceptable. The content of the \ddot{Y}_R signal is considered in the following pages:

$$\ddot{Y}_R \cong a_x \cos \theta \sin \Delta\psi + a_y \cos \phi \cos \Delta\psi + a_z (\cos \phi \sin \theta \sin \Delta\psi - \sin \phi \cos \Delta\psi)$$

For small angles (expressed in radians)

$$\ddot{Y}_R \cong a_x \Delta\psi + a_y + a_z \theta \Delta\psi - a_z \phi \cong a_x \Delta\psi + a_y - a_z \phi$$

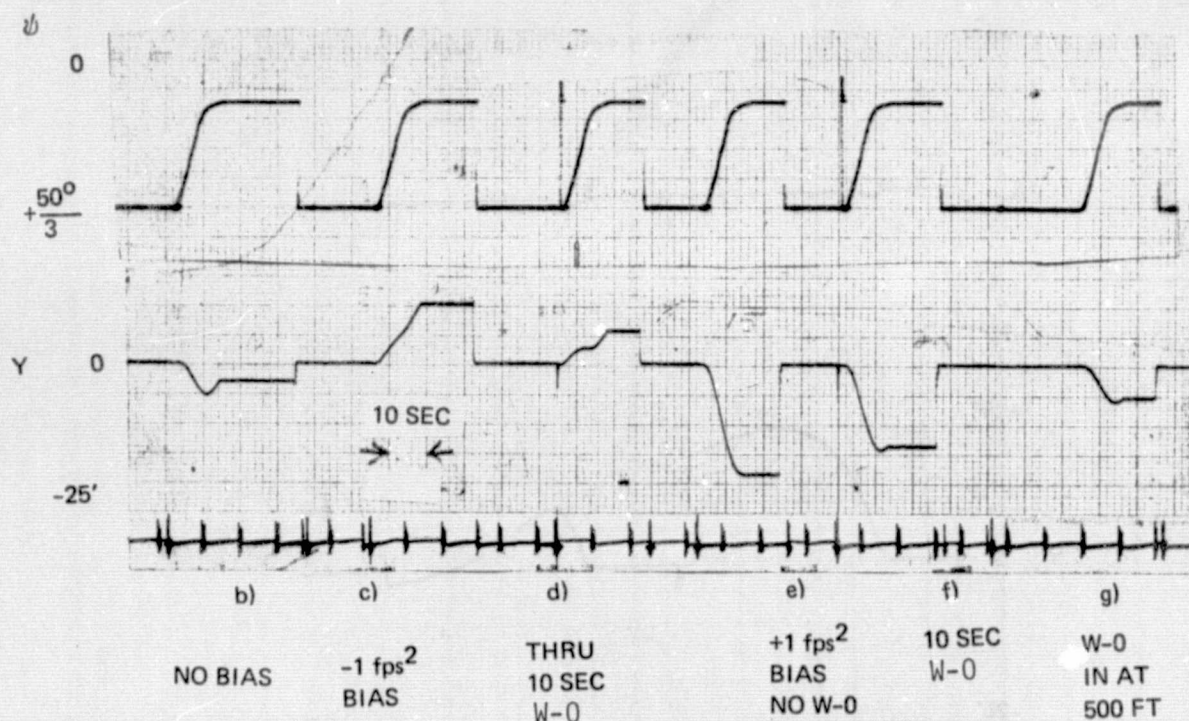


Figure C-33. Response to Y_R Bias in Lateral Axis "Wing Down" Compensation Signal - With 15 Knot Crosswind

Let

$$a_x = a_{x1} + a'_x$$

$$\Delta\psi = \Delta\psi_1 + \Delta\psi'$$

$$a_y = a_{y1} + a'_y$$

$$a_z = a_{z1} + a'_z$$

$$\phi = \phi_1 + \phi'$$

where the 1 subscript indicate the correct value and the prime superscript indicates the error component of the applicable signal.

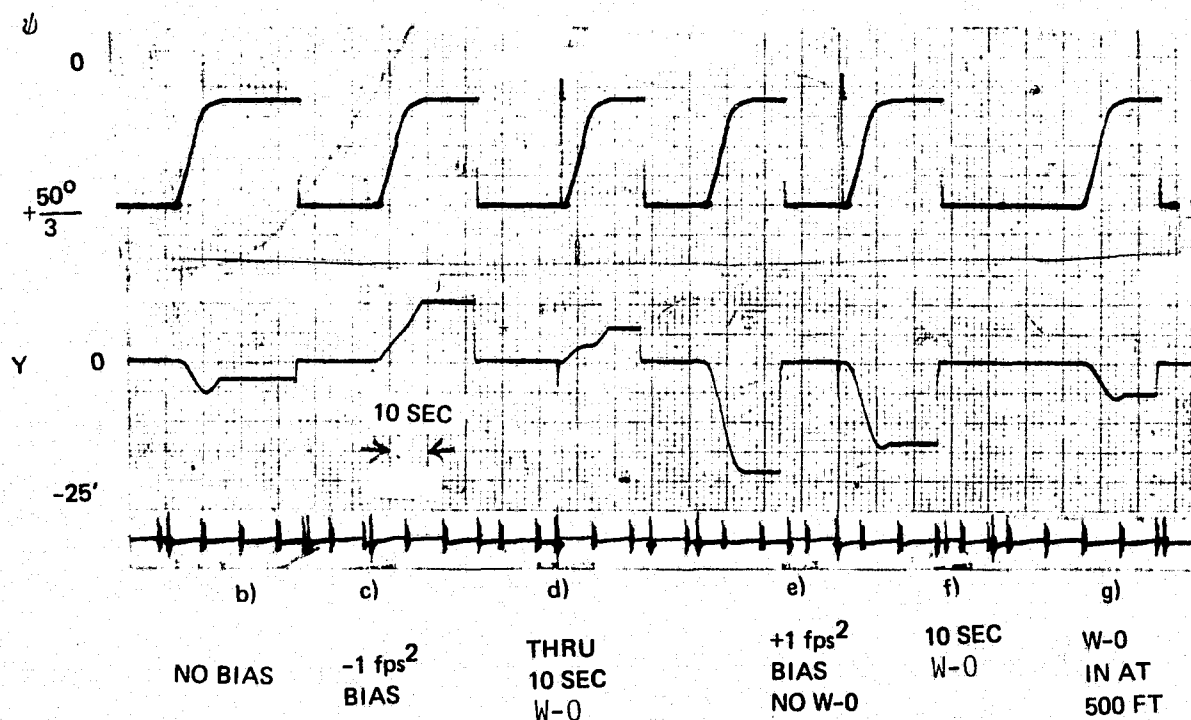


Figure C-33. Response to \dot{Y}_R Bias in Lateral Axis "Wing Down" Compensation Signal_R - With 15 Knot Crosswind

Let

$$a_x = a_{x1} + a'_x$$

$$\Delta\psi = \Delta\psi_1 + \Delta\psi'$$

$$a_y = a_{y1} + a'_y$$

$$a_z = a_{z1} + a'_z$$

$$\phi = \phi_1 + \phi'$$

where the 1 subscript indicate the correct value and the prime superscript indicates the error component of the applicable signal.

Then

$$\begin{aligned}\ddot{Y}_R &= a_{x_1} \Delta\psi_1 + a_{y_1} - a_{z_1} \phi_1 \\ &+ a_{x_1} \Delta\psi' + a_x' \Delta\psi_1 + a_y' - a_{z_1} \phi' - a_z' \phi_1 \\ &+ a_x' \Delta\psi' - a_z' \phi'\end{aligned}$$

Terms on the first line represent the correct value for y_r , whereas those on the 2nd and 3rd lines are the error terms.

Neglecting the product of error terms, the error is

$$\ddot{Y}_{R_e} = a_{x_1} \Delta\psi' + a_x' \Delta\psi_1 + a_y' - a_{z_1} \phi' - a_z' \phi_1$$

The max value of these terms can be expected to be on the order of

$$a_{x_1} \Delta\psi'_{\max} \approx 3 \text{ fps}^2 \times 4 \text{ deg}/57.3 = 0.2 \text{ fps}^2$$

$$a_x' \Delta\psi_{1\max} \approx 0.25 \text{ fps}^2 \times 20 \text{ deg}/57.3 = 0.1 \text{ fps}^2$$

$$a_{y\max}' \approx 0.25 \text{ fps}^2$$

$$a_{z_1} \phi'_{\max} \approx 5.0 \text{ fps}^2 \times 1 \text{ deg}/57.3 = 0.1 \text{ fps}^2$$

$$a_z' \phi_{1\max} \approx 0.5 \text{ fps}^2 \times 5 \text{ deg}/57.3 = 0.05 \text{ fps}^2$$

The two most significant error terms are a_y' and $a_{x_1} \Delta\psi'$.

The error term a_y' is the sum of accelerometer output error (a_y) and roll gyro error $0.562 \phi_e$. Bias error in the a_y signal will be washed out as already noted. The cross axis sensitivity of the accelerometer is estimated to be 0.01 g/g on a 4.5 sigma basis. Allowing for a maximum acceleration of 0.5 g yields the number of 0.005 g for time varying error in a_y' .

The term $a_{x_1} \Delta\psi'$ is the product of a bias ($\Delta\psi$) and the time varying longitudinal acceleration, a_x . To estimate the magnitude of this term, it was assumed that the aircraft is varying in speed ± 5 knots with a 12 second period. The resulting acceleration is $\dot{u} = 4.2 \cos 0.5t$ in fps^2 . Further assuming a

maximum compass system error of four degrees yields an error in \ddot{y}_r of $0.29 \cos 0.5t$. The frequency response plot for Y/Y_r indicates a gain of about 11.8 dB = 3.88 ratio at $\omega = 0.5$ rad/sec. The resulting peak error in Y is 1.13 feet. At a lower frequency around 0.2 radian, the gain is higher (about 25 dB), but the peak acceleration error corresponding to the 5 knot speed variation is reduced by 0.4. The net result is a peak y of 2.0 feet.

Earlier in discussing the response to \ddot{y}_r error through the nav filter, the response to time varying errors was postponed. Using the transfer function developed at that time, the gain at $\omega = 0.5$ is found to be 2.07 for a peak error in y of 0.6 feet with the above mentioned input error signal of $0.29 \cos 0.5t$. At the frequency where the high gain occurs ($\omega = 0.2$ rad/sec), the input error signal would be $0.12 \cos 0.2t$ for a peak y error of 3.55 feet.

Summarizing these worst case acceleration signal errors, the following values apply:

y/\ddot{y} gain through nav filter = 31.6 for $0.1 < \omega < 0.25$

y/\ddot{y} gain through wing down compensation path = 17.8 for $0.05 < \omega < 0.2$

\ddot{y}_R error $\approx a_y'$ error + $a_x \Delta\psi$ error

a_y' error = 0.16 fps^2 (time varying)

$a_x \Delta\psi$ error = 0.29 fps^2

RSS total = 0.33

Nav filter path error = $31.6 \times 0.33 = 10.4 \text{ ft}$

Wing down compensation path error = 5.87 ft

RSS total = 11.94 ft

These numbers are very conservative since the gain values used only apply to a narrow frequency range. Interpreting these worst case values as 4.5 sigma results in a 2σ value of 5.3 feet.

GYRO AND ACCELEROMETER ERROR SUMMARY

1. From roll gyro through stabilization loop.

V.G. roll null error existing prior to loc track results in TD lateral error of about 11.3 ft per degree of gyro error. Thus the estimated two sigma error in touchdown deviation due to gyro error is 4.0 feet.

2. From \ddot{y}_r through the navigation filter.

Resultant y error peaks at 14 seconds at a value 32 times the \ddot{y} error expressed in fps^2 . However, the error is washed out as time elapses. Estimated two sigma error in touchdown deviation due to \ddot{y}_r error through the navigation filter is 4.6 feet.

3. From \ddot{y}_r through the align compensation path.

Without a highpass filter on this signal, a lateral (y) error of over 20 feet per fps^2 of \ddot{y} error could result. A washout filter operating prior to align initiation could minimize this problem without adversely affecting system stability. Thus the estimated two sigma error in touchdown deviation due to \ddot{y}_r error through the wing down compensation path is 2.6 feet.

4. Total

RSS total of all gyro and accelerometer error contributions is 6.6 feet. The effects of these gyro and accelerometer errors on landing performance are included in the "total population" probability distributions.

APPENDIX D

ADVANCED VS CONVENTIONAL CONTROL LAW COMPARISON

<u>Figure</u>	<u>Title</u>	<u>Page</u>
D-1	Pitch Landing System - Control Laws	D-4
D-2	STOLAND Elevator Control Block Diagram	D-5
D-3	STOLAND Throttle Control Block Diagram	D-6
D-4	Sink Rate Distribution Comparison	D-7
D-5	Range Distribution Comparison	D-8
D-6	Pitch Distribution Comparison	D-9
D-7	Beam Deviation Distribution Comparison	D-10
D-8	STOLAND Activity in Turbulence and Beam Noise	D-11
D-9	STOLAND Activity in Turbulence	D-12
D-10	Lateral Landing System - Roll Block Diagram	D-15
D-11	Lateral Landing System - Yaw Block Diagram	D-16
D-12	STOLAND Lateral Axis - Block Diagram	D-17
D-13	STOLAND Yaw Axis - Block Diagram	D-18
D-14	Flat Decrab and Forward Slip Stochastic Performance Summary	D-19

<u>Table</u>	<u>Title</u>	<u>Page</u>
D-I	Throttle Gains Comparison	D-1
D-II	Pitch Statistical Performance Comparison	D-2
D-III	Pitch Activity Comparison	D-3
D-IV	Lateral Autoland Performance Comparison	D-14

APPENDIX D

ADVANCED VERSUS CONVENTIONAL CONTROL LAW COMPARISON

The Augmentor Wing airplane is currently equipped with an experimental digital avionic system having an automatic landing capability, known as the STOLAND system. Its automatic landing control laws are largely based on the application of current CTOL system techniques to the experimental short-haul aircraft.

This appendix compares the implementation and performance of the recommended advanced control laws versus the STOLAND system.

D.1 LONGITUDINAL LANDING SYSTEM

The advanced control laws for the pitch axis were presented in Figure 3-1, which is repeated here for convenience as Figure D-1. STOLAND control laws employ elevator and throttle only, with block diagrams shown in Figure D-2 and D-3.

In the beam track phase, STOLAND and the advanced control laws employ the same feedback paths with differences in some of the gains. Pitch attitude and rate feedbacks to elevator are identical in the two systems, and the feedback of airspeed to elevator is also essentially identical, including gains. Throttle gains are different as compared in Table D-I.

TABLE D-I. THROTTLE GAINS COMPARISON

	<u>STOLAND</u>	<u>Advanced</u>
$\delta_T^c / \ddot{h} \left(\frac{\text{deg}}{\text{ft. sec}} \right)$	-0.72	-3.0
$\delta_T^c / \dot{h} \left(\frac{\text{deg}}{\text{fps}} \right)$	-0.305	-3.0
$\delta_T^c / \Delta h \left(\frac{\text{deg}}{\text{ft}} \right)$	-0.291	-1.5
$\delta_T^c / \left[\int \Delta h \, dt \right] \left(\frac{\text{deg}}{\text{ft. sec}} \right)$	-0.014	-0.075

The difference between STOLAND and the advanced system in the flare are much more substantial. The advanced system utilizes closed loop control of sink rate as described in Subsection 3.1. In STOLAND, essentially open loop throttle and elevator predict commands are inserted at flare to yield the desired flare trajectory for the nominal, no disturbance landing case. Then, closed loop control is added to compensate for disturbances and maintain the aircraft on the desired trajectory. The predict commands are functions of approach speed, weight and path angle to improve performance in those deterministic disturbances.

Performance of the advanced system versus STOLAND in turbulence is compared in Figures D-4 through D-7, and summarized in Table D-II. Statistical runs were performed with zero deterministic headwind and a turbulence level corresponding to 15 kts of total wind, i.e., $\sigma_u = 3.8$ fps, $\sigma_w = 2.5$ fps.

The performance obtained with the advanced control laws is by far superior to STOLAND performance. STOLAND performance is far short of the requirements set forth in Section 4.1.

STOLAND activity traces in turbulence corresponding to 25 kts total wind ($\sigma_u = 6.3$ fps, $\sigma_w = 2.5$ fps) and 0.070 rms beam noise are shown in Figures D-8 and D-9, with a summary and comparison to the recommended system given in Table D-III.

Excursions of controlled variables with STOLAND are much larger than with the advanced configuration. The advanced system obtains its performance advantage through choke activity. Elevator activity is similar for both configurations, as might be expected in view of the similarity in elevator feedbacks in the beam track phase in which activities were recorded.

TABLE D-II. PITCH STATISTICAL PERFORMANCE COMPARISON

		<u>Advanced</u>	<u>STOLAND</u>
$-\dot{h}_{TD}$	(fps)	3.8 ± 0.45	$5.4^{+1.5}_{-2.1}$
X_{TD}	(ft)	180 ± 30	100^{+100}_{-140}
Δh_{100}	(ft)	0 ± 1.5	$3^{+10.5}_{-8.5}$
θ_{TD}	(deg)	6.6 ± 0.5	$3.8^{+1.4}_{-2}$

- NOTES: 1) Zero headwind
 2) Turbulence corresponding to 15 kts total wind
 ($\sigma_u = 3.8$, $\sigma_w = 2.5$ fps)
 3) Performance data give $\mu \pm 1\sigma$ results

TABLE D-III. PITCH ACTIVITY COMPARISON

(rms)

	<u>Advanced</u>	<u>STOLAND</u>
$\Delta \dot{h}$ (fps)	0.8	>4
Δh (ft)	2.4	12
u (fps)	4.0	5.4
θ (deg)	1.4	2
δ_{RPM} (%)	0.8	0.8
$\dot{\delta}_{RPM}$ (%/sec)	0.4	0.4
δ_e (deg)	1.2	1.5
$\dot{\delta}_e$ (deg/sec)	2.2	2.2
δ_{CH} (%)	12	0
$\dot{\delta}_{CH}$ (%/sec)	19	0

Disturbances: Turbulence at 25 kts total wind

($\sigma_u = 6.3$ fps, $\sigma_w = 2.5$ fps)

0.07° rms beam noise

Figure D-1. Pitch Landing System — Control Laws

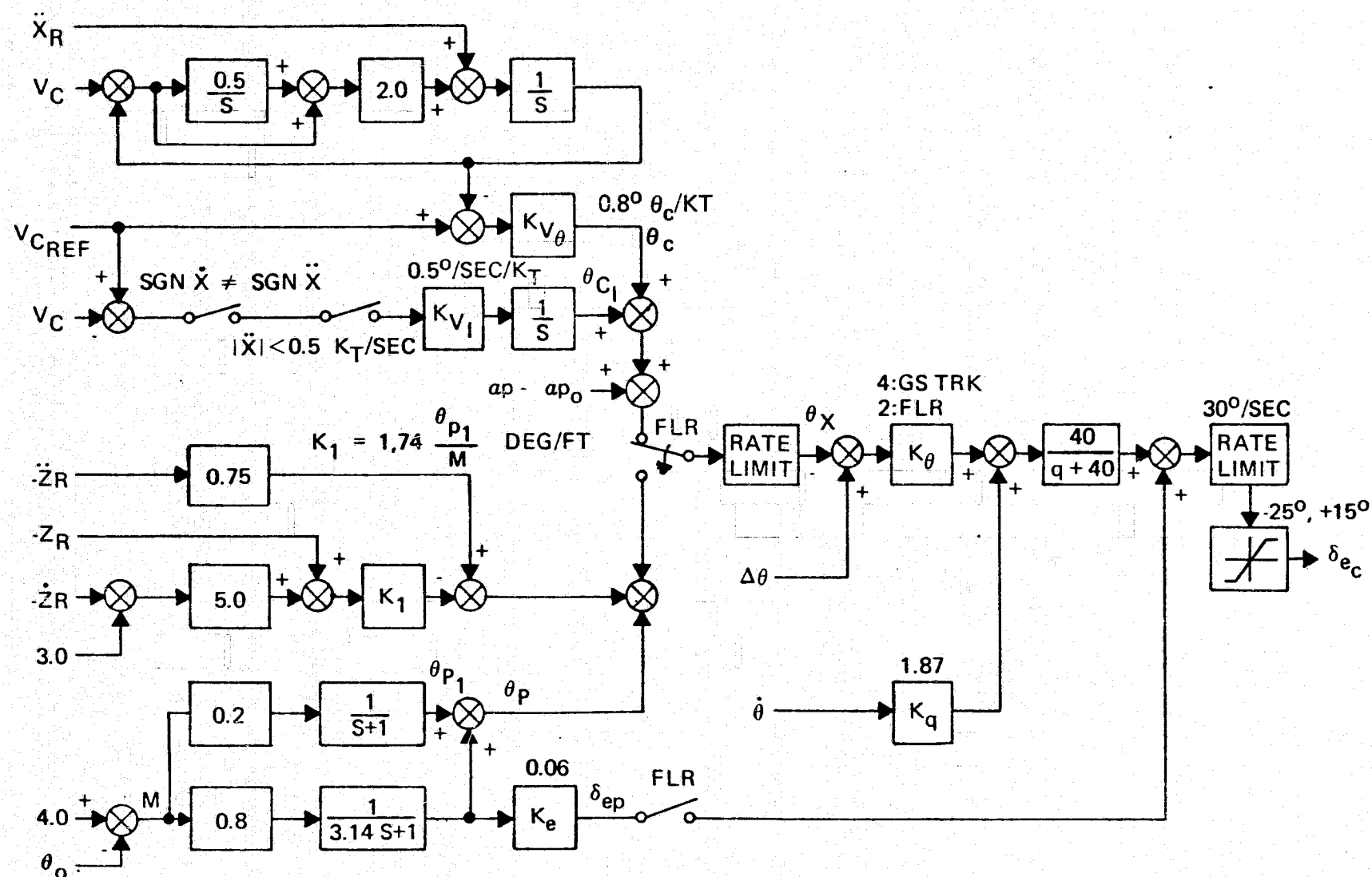


Figure D-2. STOLAND Elevator Control Block Diagram

Figure D-3. STOLAND Throttle Control Block Diagram

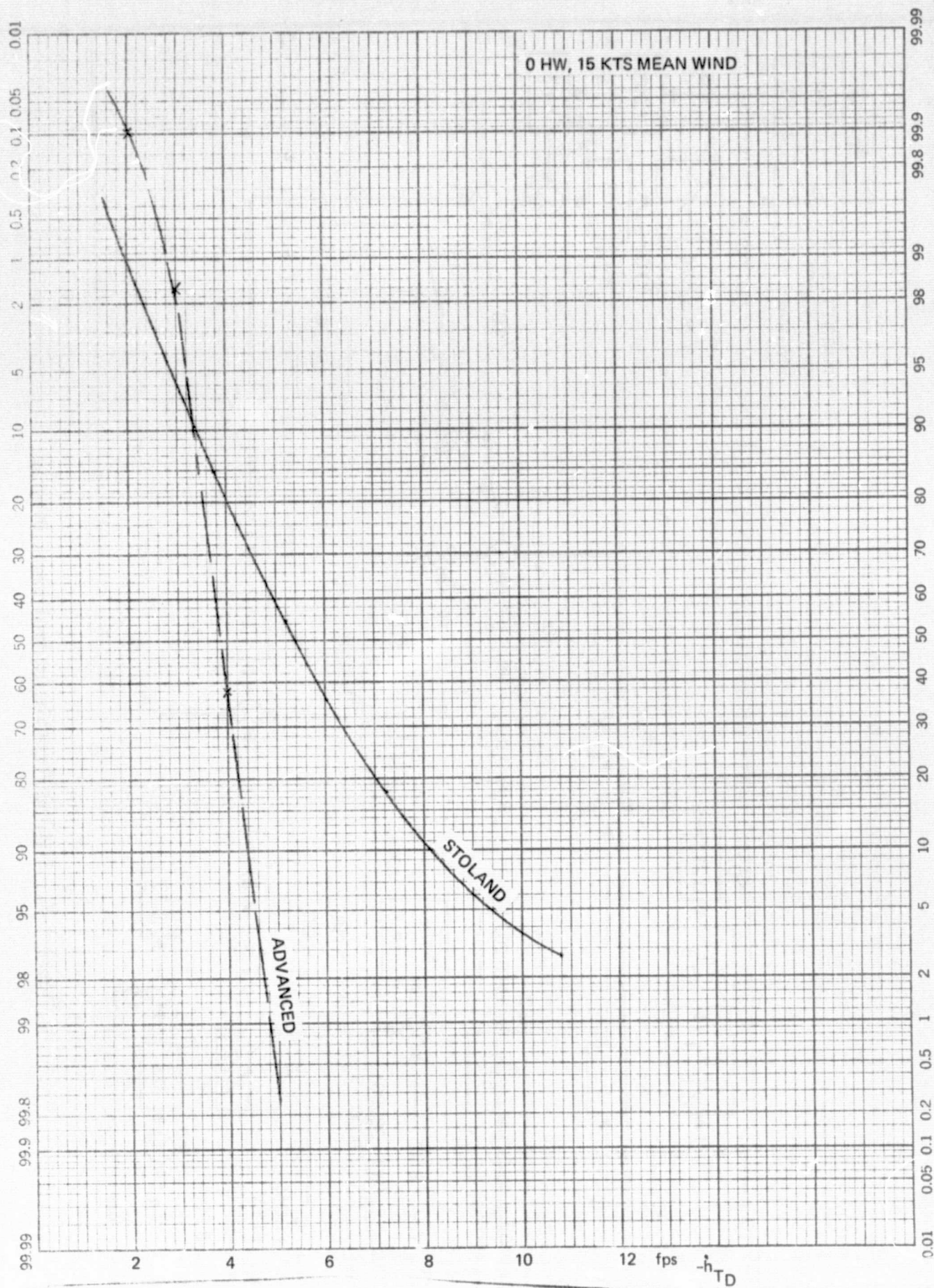


Figure D-4. Sink Rate Distribution Comparison

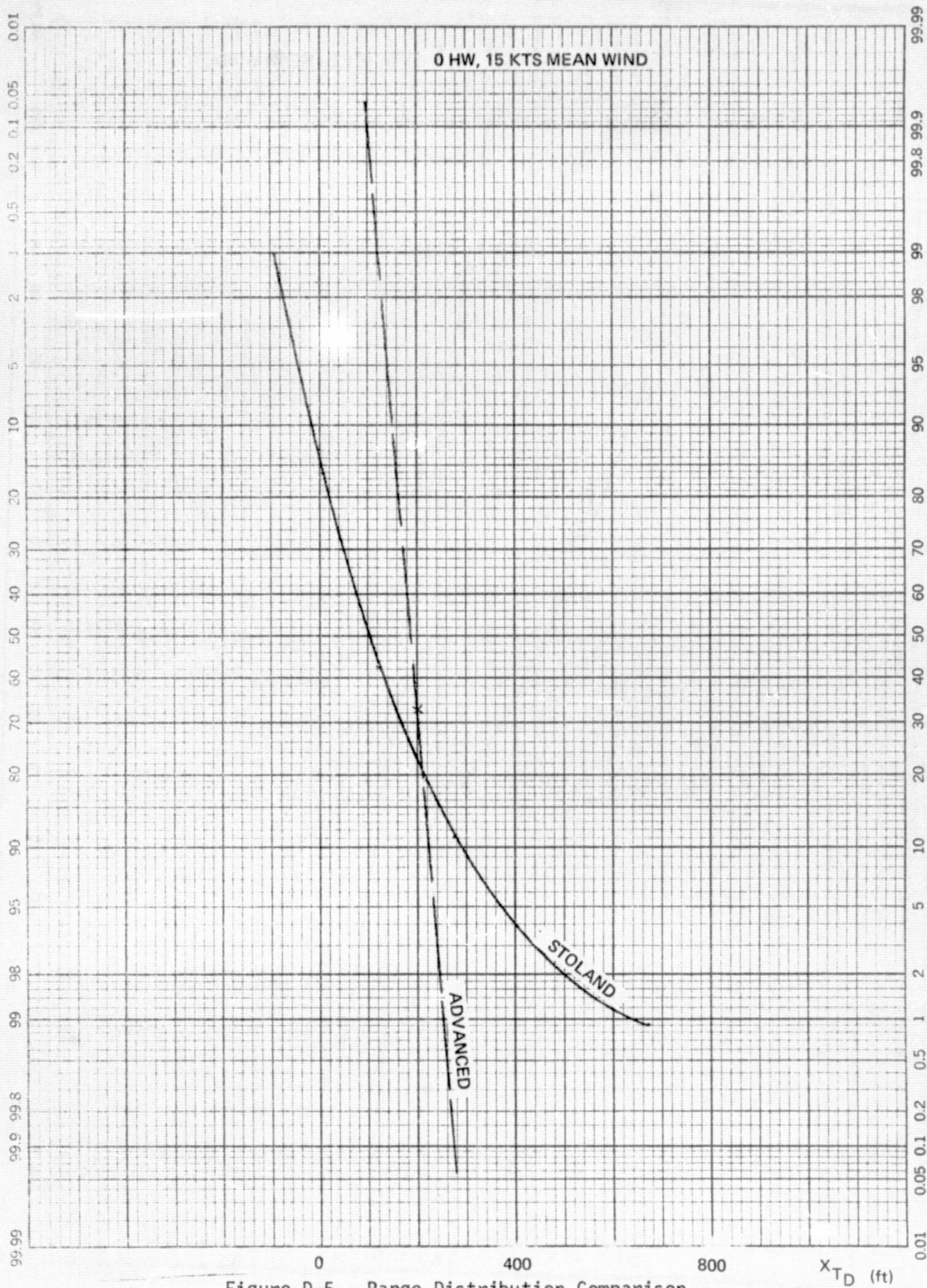


Figure D-5. Range Distribution Comparison

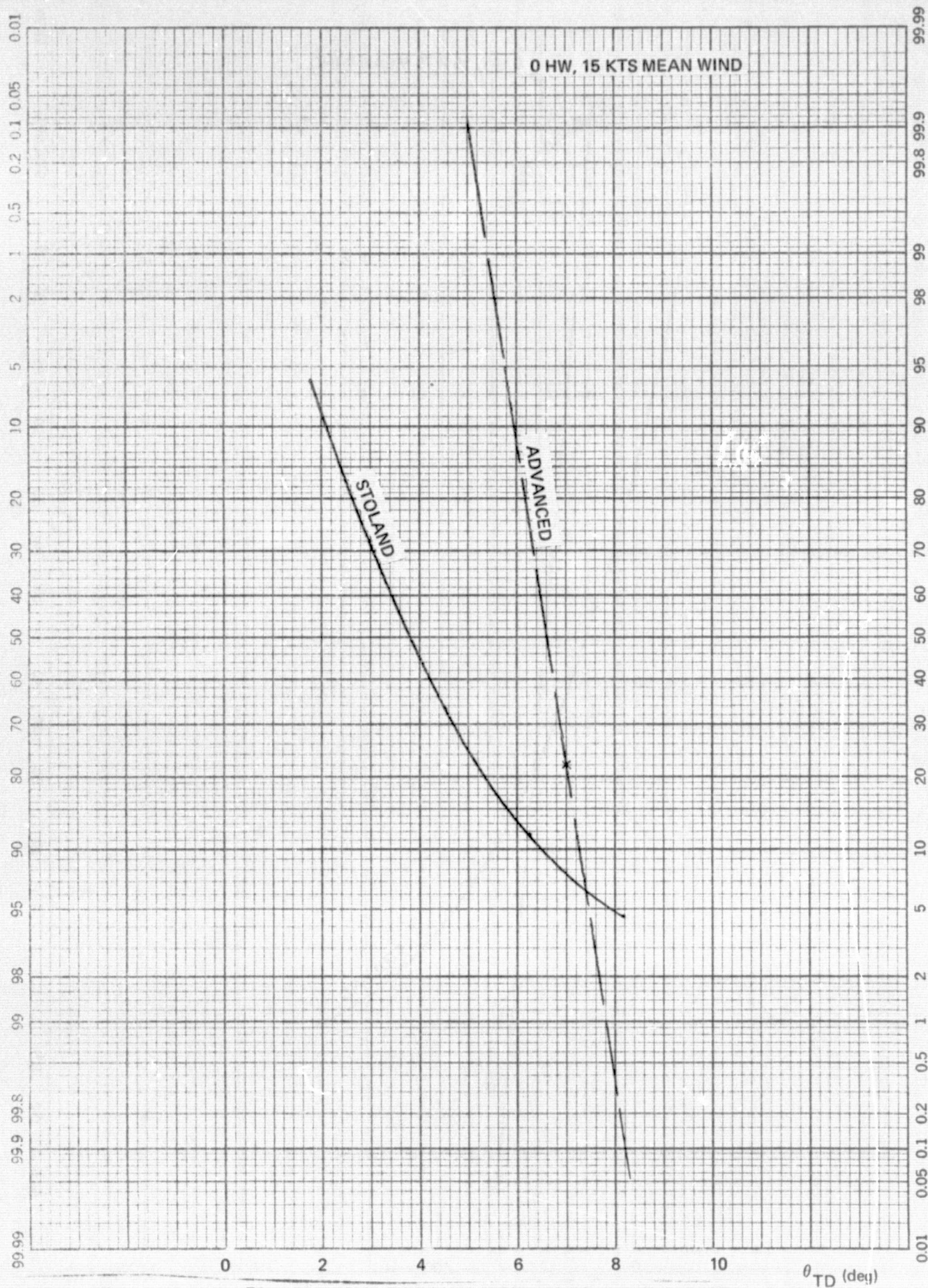


Figure D-6. Pitch Distribution Comparison

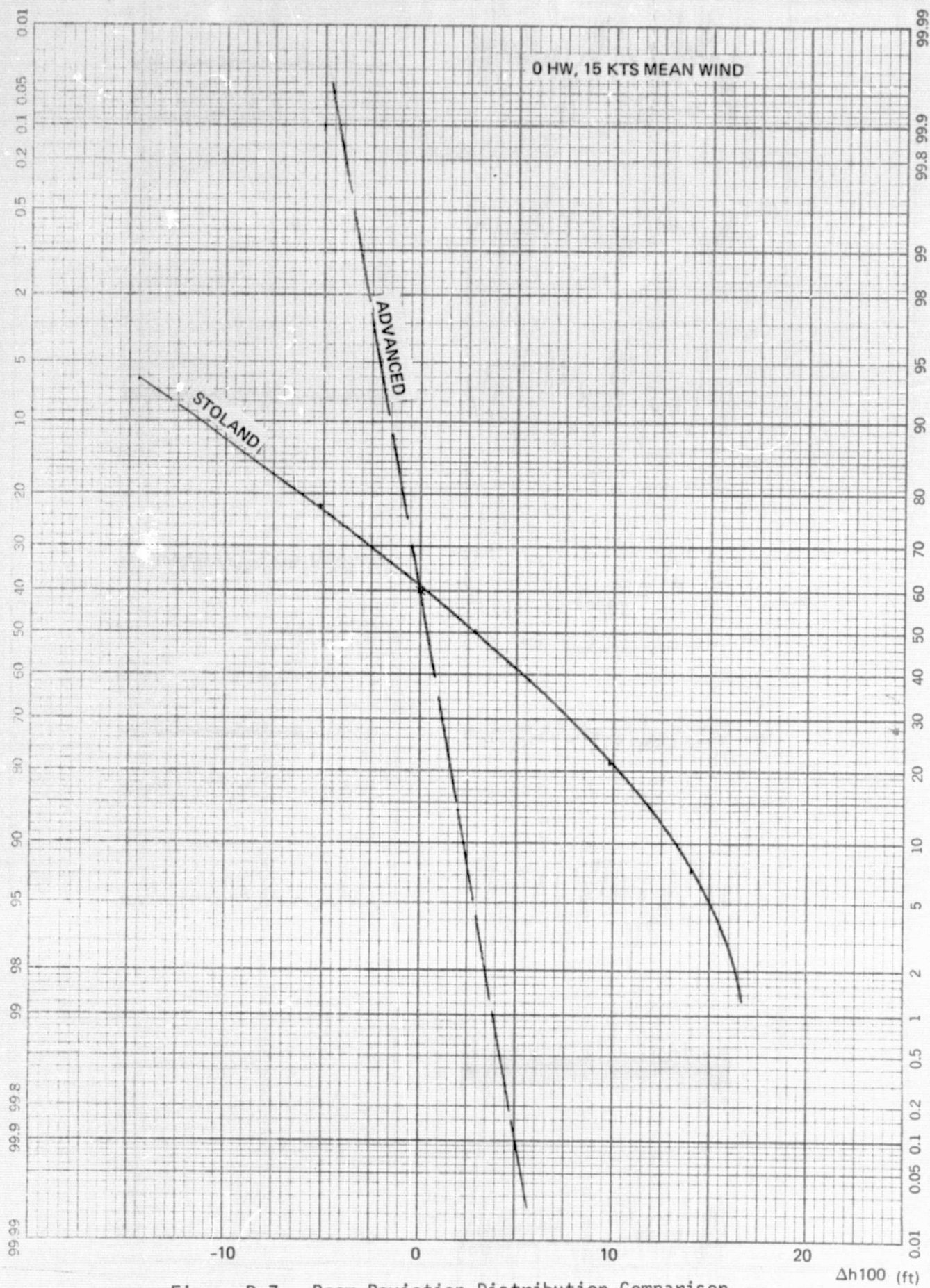


Figure D-7. Beam Deviation Distribution Comparison

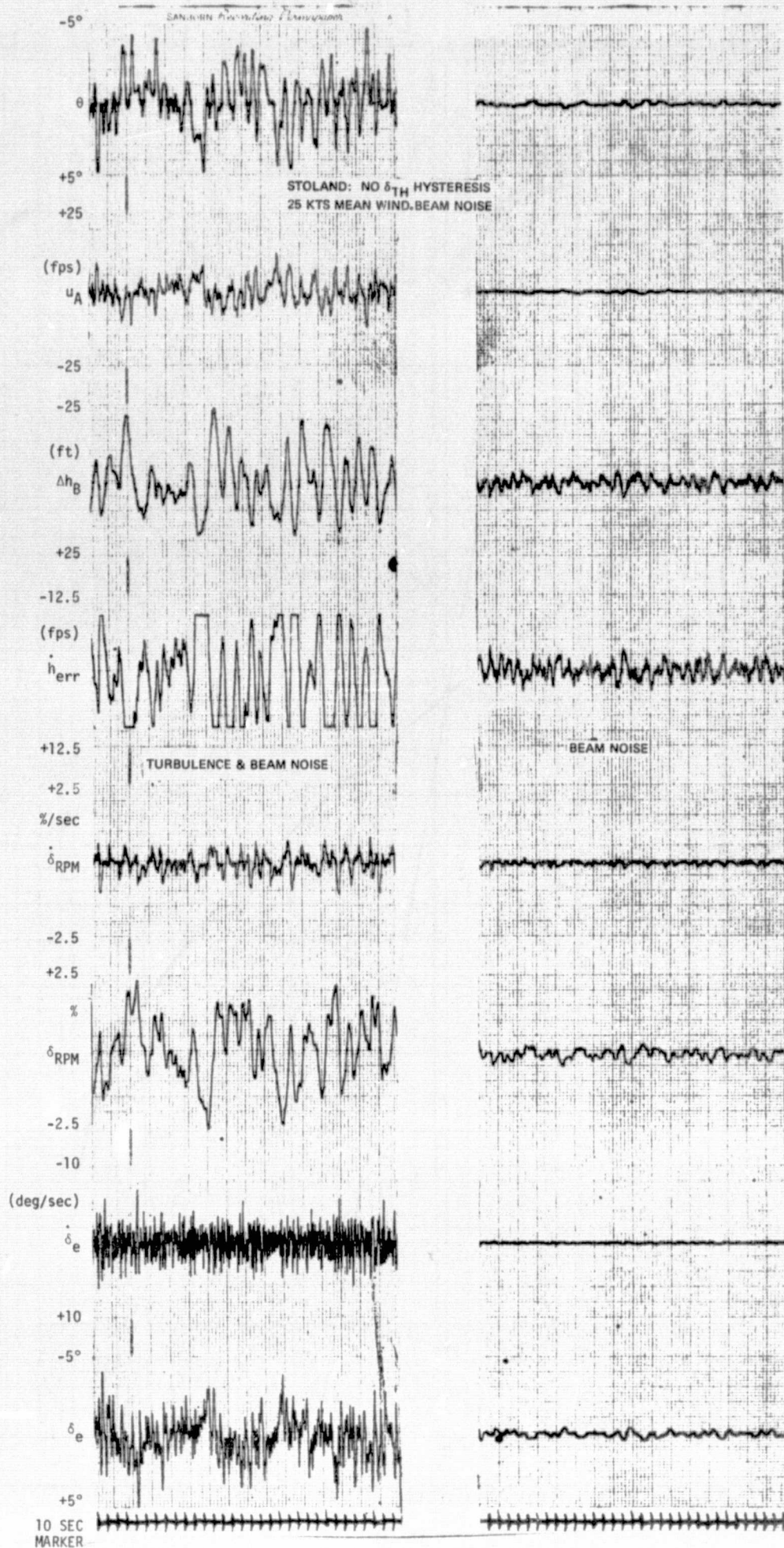


Figure D-8. STOLAND Activity in Turbulence and Beam Noise
D-11

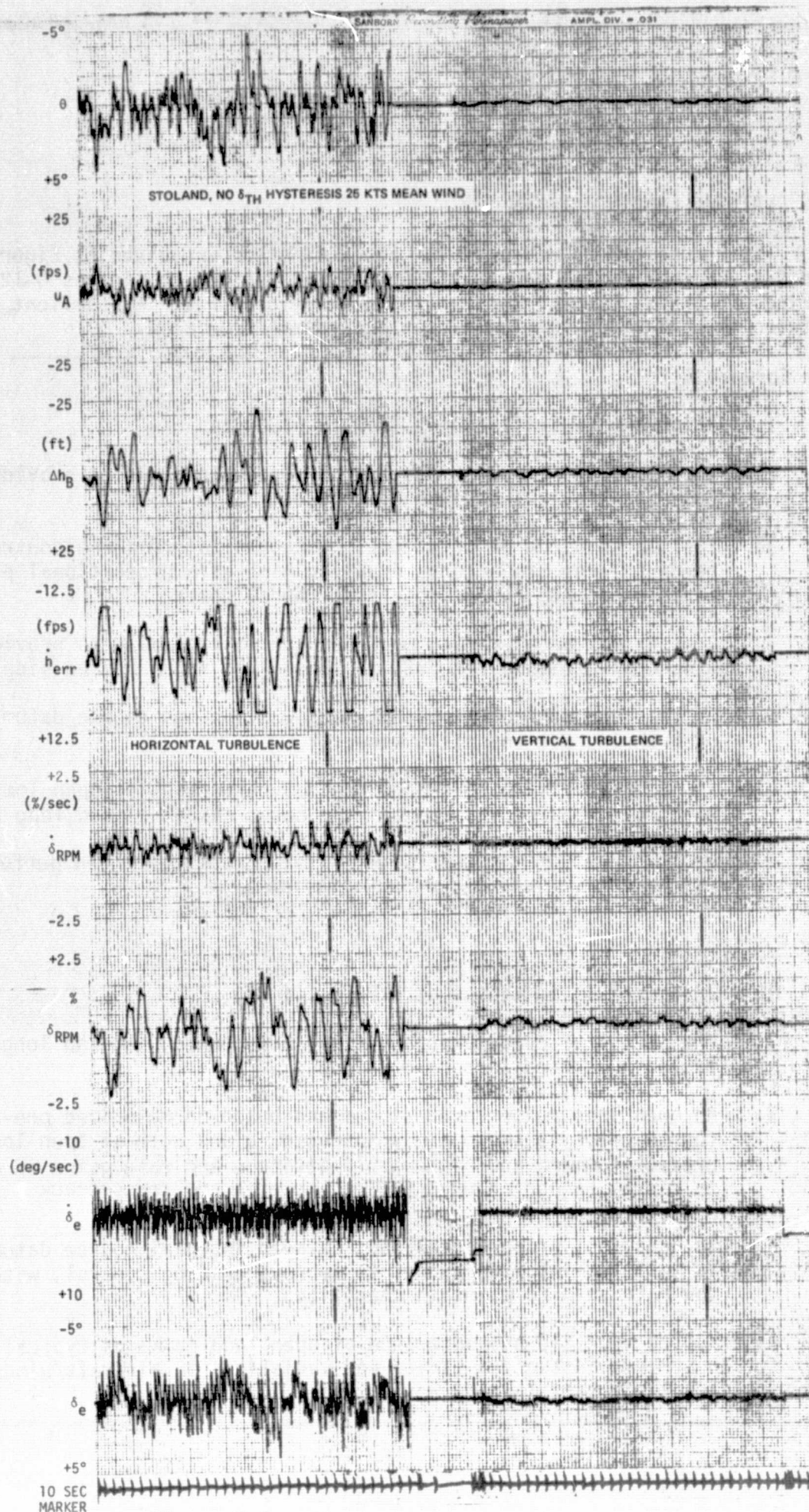


Figure D-9. STOLAND Activity in Turbulence
D-12

D.2 LATERAL LANDING SYSTEM

The recommended landing system block diagrams are given as Figures D-10 and D-11, with the flat decrab STOLAND system defined in Figures D-12 and D-13. During LOC track, the two systems are nearly identical. The salient differences between the two alignment techniques are summarized below.

For Forward Slip

1. Alignment is initiated at 45.72 m (150 ft)
2. The localizer computations to roll are maintained to provide closed loop beam control through touchdown.
3. The course datum error signal, processed to provide a controlled heading error trajectory, provides high gain proportional plus integral commands to the rudder to effect the alignment.
4. Cross-track acceleration modifies the roll command to provide the wing-down attitude required to cancel the wind-induced side force.
5. Closed loop control of both beam deviation and course datum error is used throughout the align maneuver.
6. Since abrupt yaw corrections are not performed, no open loop predict terms are required to augment the basic system closed loop bandwidth.

Thus alignment initiation timing is not critical, and touchdown performance is less dependent on vehicle and wind variations.

For Flat Decrab

1. Alignment is initiated at 4.88 m (16 ft)
2. The localizer computations to roll are opened, thus no longer providing closed loop beam guidance.
3. An open loop rudder predict command based on memorized pre-align course error is immediately inserted, along with an open loop wheel predict command and higher roll attitude and rate gains in an attempt to cancel rudder induced rolling moments and cross-track acceleration.
4. In addition, proportional plus delayed integral course datum error is inserted into the rudder to improve heading control, with increased yaw rate gain to maintain stability.

As expected from the preponderance of open loop commands typical of the flat decrab system, initiation timing and variations in aircraft/wind states can significantly impact landing performance.

A comparison summary of landing performance in zero headwind with limiting lateral disturbances is shown in Table D-IV, based on data presented in Appendix C. This indicates substantial performance degradation with the STOLAND flat decrab system in zero headwind - 50 percent increased \dot{Y}_{TD} variations, 400 percent greater \dot{Y}_{TD} dispersion, more than doubled roll attitude dispersion, and 21 percent greater heading variations.

A further comparison between the STOLAND system and a slightly less refined version of the forward slip configuration (D) is summarized in Figure D-14 for varying longitudinal wind conditions. The significant dependency of the flat decrab system on timing variations induced by longitudinal wind variations is readily apparent in fact, dispersions in headwind are doubled compared to zero wind for the flat decrab, with no increase in dispersion noted for the forward slip system. Thus the flat decrab system will yield about 4 times greater dispersion than the forward slip system over the limiting wind extremes, and will not meet the touchdown accuracy design requirements.

TABLE D-IV. LATERAL AUTOLAND PERFORMANCE COMPARISON

	<u>STOLAND (R)</u>	<u>Recommended (P)</u>
\dot{Y}_{TD} (fps)	(-3.8 ± 5.2)	$(+ .4 \pm 1.25)$
m/sec	-1.158 ± 1.585	$+ .122 \pm .381$
Y_{TD} (ft)	(-5.5 ± 10.5)	(-4.0 ± 7.0)
m	-1.676 ± 3.2	-1.219 ± 2.134
$\phi_{TD} (^{\circ})$	$.1 \pm 3.8$	3.2 ± 1.5
$\psi_{TD} (^{\circ})$	$.3 \pm 1.45$	$.9 \pm 1.2$
Y_{window} (ft)	$(-.1 \pm 8.5)$	$(.5 \pm 6.8)$
m	$-.0305 \pm 2.591$	$.152 \pm 2.073$

NOTE: 1. Data shown for zero headwind, 15 knot crosswind plus limiting turbulence, shear, and beam noise.

2. Data given as $\mu \pm 2\sigma$ values.

3. Data shown for equivalent 65 knot landing speed.

Figure D-10. Lateral Landing System - Roll Block Diagram

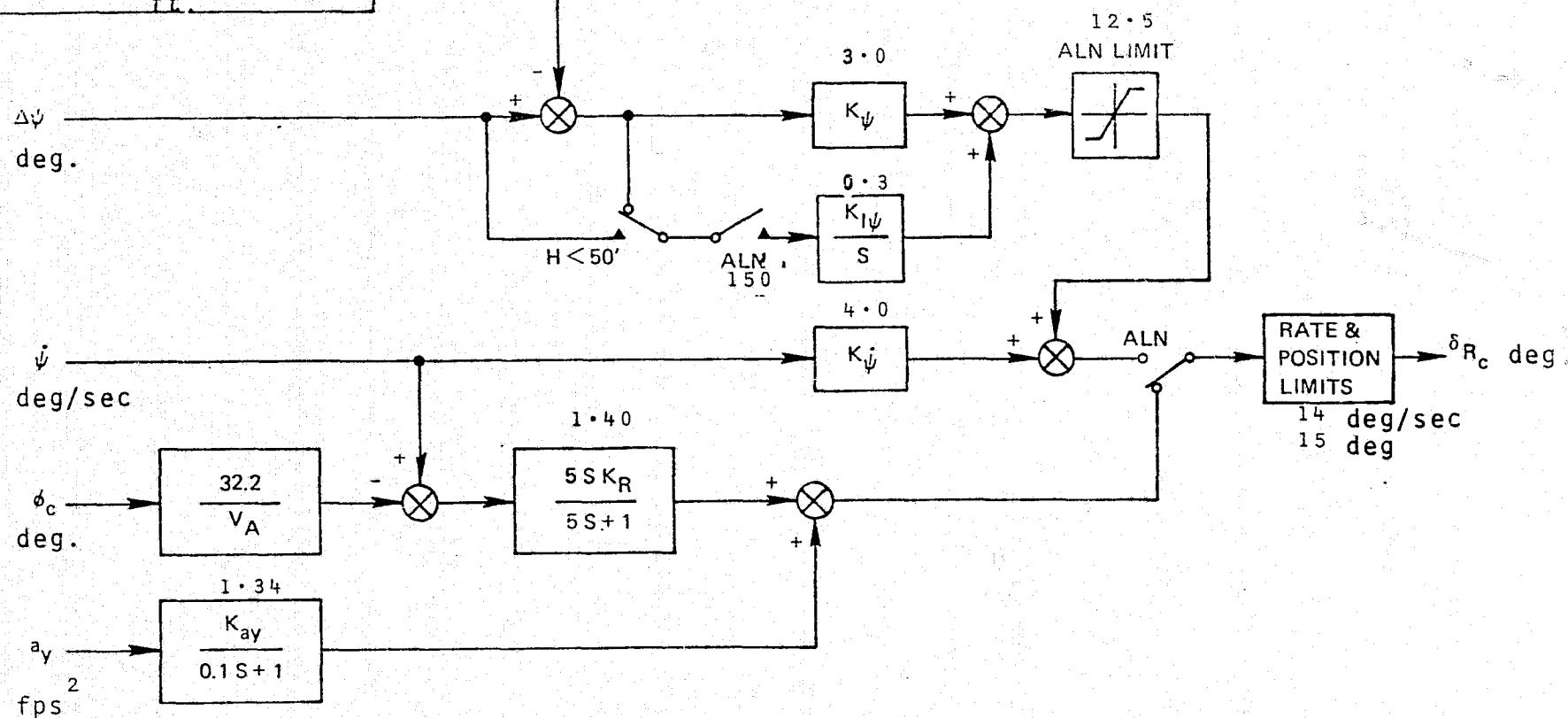
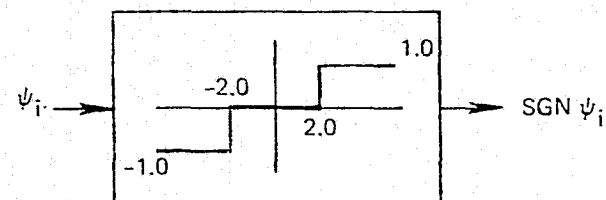
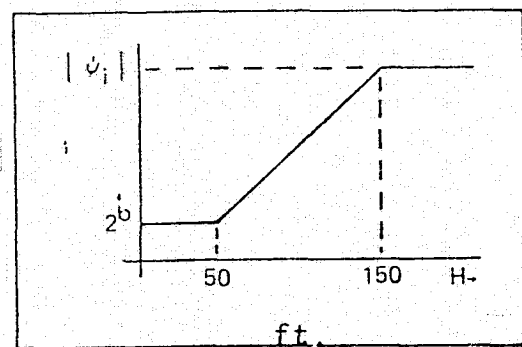


Figure D-11. Lateral Landing System — Yaw Block Diagram

Figure D-12. STOLAND Lateral Axis — Block Diagram

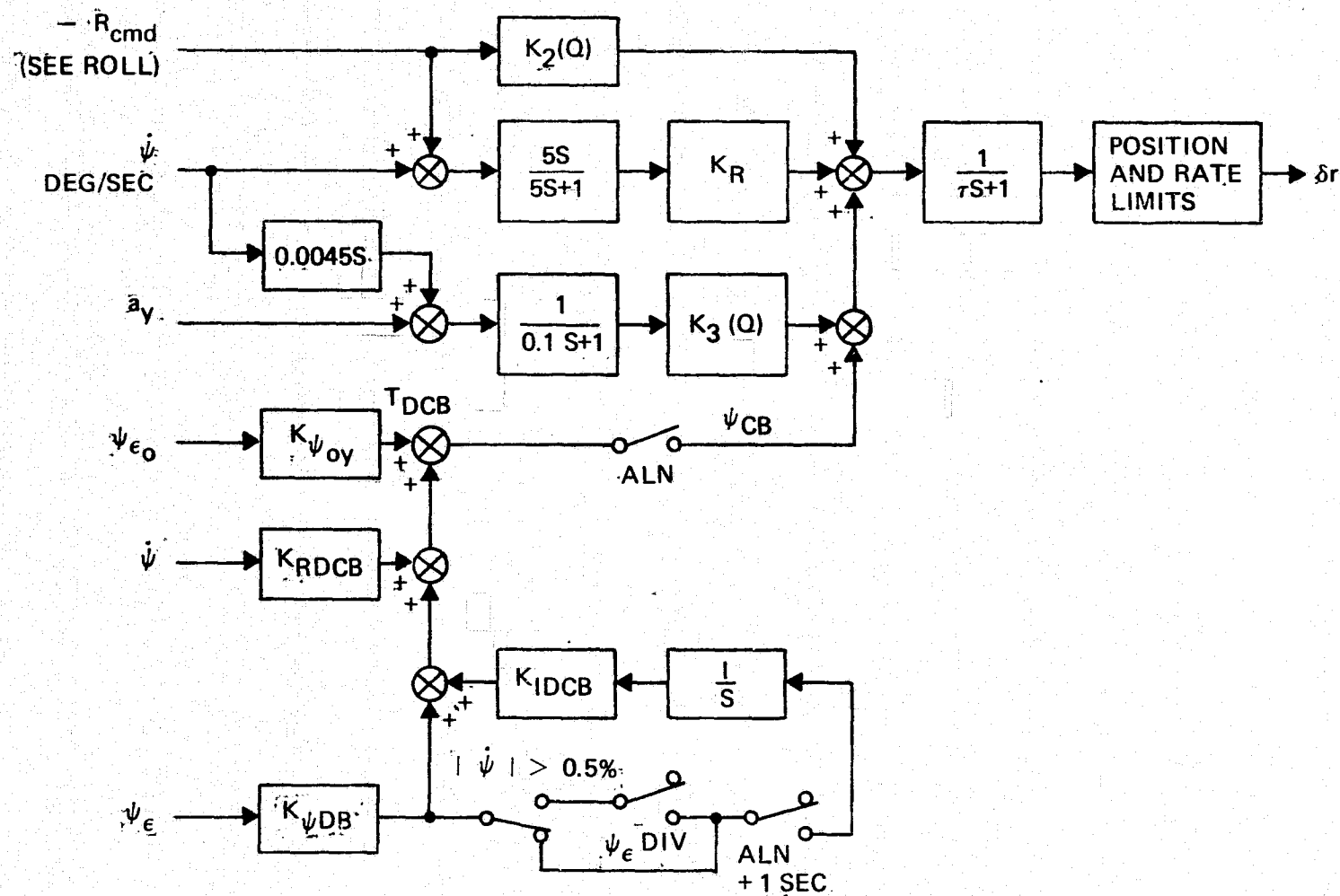


Figure D-13. STOLAND Yaw Axis — Block Diagram

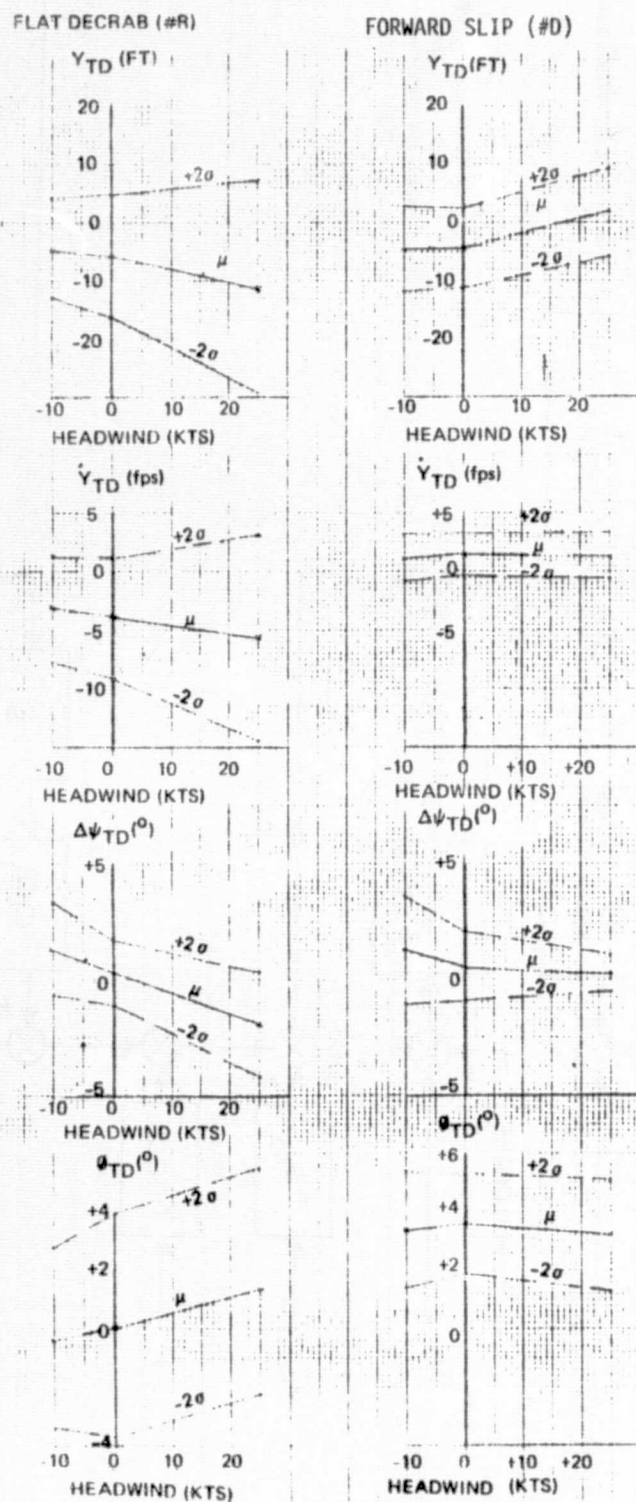


Figure D-14. Flat Decrab & Forward Slip Stochastic Performance Summary

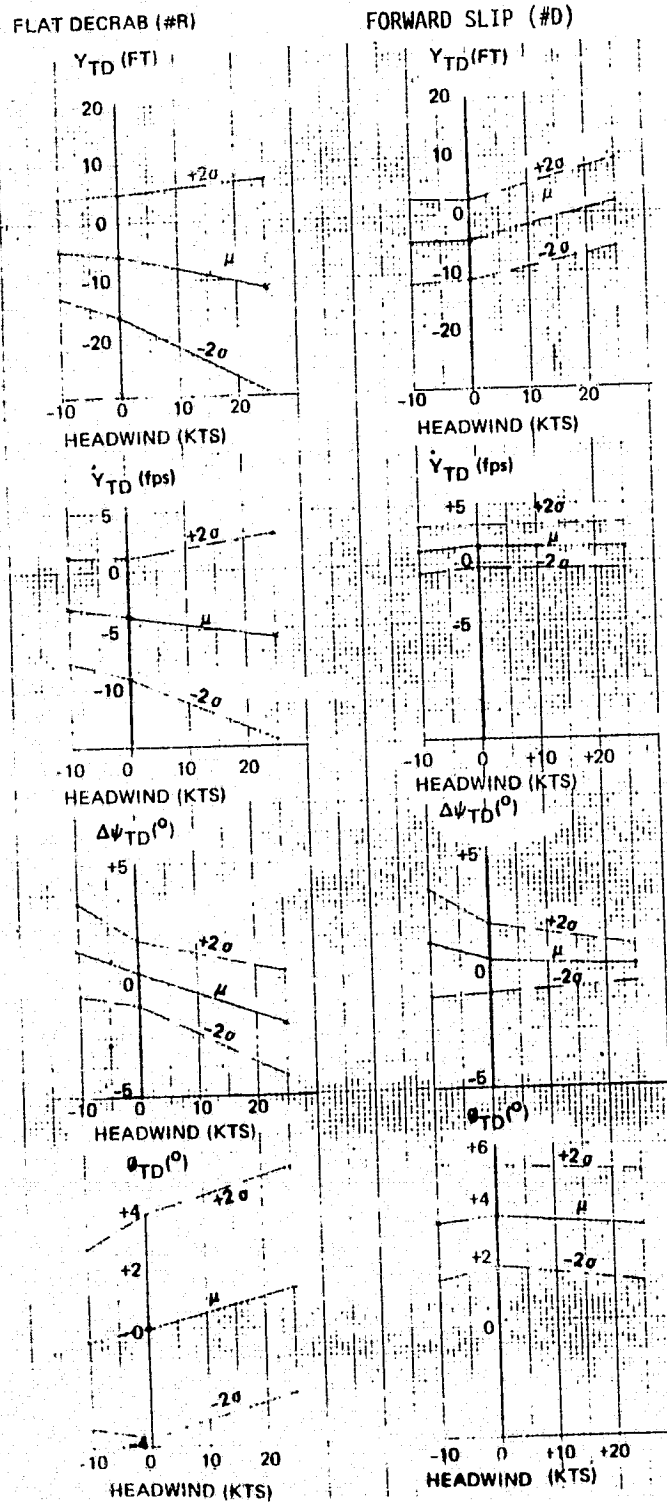


Figure D-14. Flat Decrab & Forward Slip Stochastic Performance Summary